

UNCLASSIFIED

AD NUMBER

AD374199

CLASSIFICATION CHANGES

TO: unclassified

FROM: confidential

LIMITATION CHANGES

TO:

Approved for public release, distribution unlimited

FROM:

Distribution authorized to U.S. Gov't. agencies only; Specific Authority; Nov 65. Other requests shall be referred to Air Force Rocket Propulsion Lab, Air Force Systems Command, Edwards AFB, CA.

AUTHORITY

31 Dec 1972 per GDS; AFRPL ltr dtd 10 Dec 1985

THIS PAGE IS UNCLASSIFIED

# GENERAL DECLASSIFICATION SCHEDULE

IN ACCORDANCE WITH  
DOD 5200.1-R & EXECUTIVE ORDER 11652

## THIS DOCUMENT IS:

Subject to General Declassification Schedule of  
Executive Order 11652-Automatically Downgraded at  
2 Years Intervals DECLASSIFIED ON DECEMBER 31, 1972

BY

Defense Documentation Center  
Defense Supply Agency  
Cameron Station  
Alexandria, Virginia 22314

CONFIDENTIAL

AFRPL - TR-65-209

(UNCLASSIFIED TITLE)

**DUAL-CHAMBER CONTROLLABLE SOLID  
PROPELLANT ROCKET MOTOR**

**THIRD ANNUAL REPORT - FISCAL YEAR 1964  
Volume I - Research and Development Efforts**

**November 1965**

AFSC PROGRAM STRUCTURE NO. 750G  
PROJECT NO. 3059, TASK NO. 305906

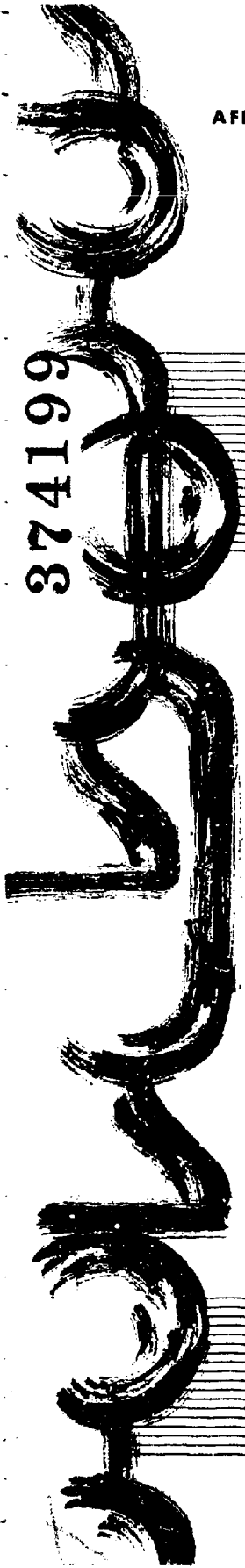
(PREPARED UNDER CONTRACT  
AF 04 (611)-9067 by  
NORTHROP CAROLINA, INC.  
Asheville, N. C.)

DDC  
RECEIVED  
JUL 25 1966  
D

**ROCKET PROPULSION LABORATORY  
AIR FORCE SYSTEMS COMMAND  
Edwards Air Force Base, California**

CONFIDENTIAL

374199



## NOTICES

This document contains information affecting the national defense of the United States within the meaning of the Espionage Laws (Title 18, U.S.C., sections 793 and 794). Transmission or revelation in any manner to an unauthorized person is prohibited by law.

When U. S. Government drawings, specifications, or other data are used for any purpose other than a definitely related government procurement operation, the government thereby incurs no responsibility nor any obligation whatsoever and the fact that the government may have formulated, furnished, or in any way supplied the said drawings, specifications, or other data is not to be regarded by implication or otherwise, as in any manner licensing the holder or any other person or corporation, or conveying any rights or permission to manufacture, use, or sell any patented invention that may in any way be related thereto.

This report is furnished under U.S. Government Contract No. AF 04(611)-9067, and shall not be released outside the Government (except to foreign Governments, subject to these same limitations), nor be disclosed, used, or duplicated, for procurement or manufacturing purposes, except as otherwise authorized by said contract, without the permission of Northrop Carolina, Inc. This legend shall be marked on any reproduction hereof in whole or in part.

DOWNGRADED AT 3 YEAR INTERVALS;  
DECLASSIFIED AFTER 12 YEARS  
DOD DIR 5200.10

AFRPL-TR-65-209, Vol I **CONFIDENTIAL**

Volume I

NC-5025-65

AFR-21-10

Copy No. ~~78~~

(Unclassified Title)

DUAL-CHAMBER

CONTROLLABLE SOLID PROPELLANT ROCKET MOTOR (U)

THIRD ANNUAL REPORT - FISCAL YEAR 1964

Volume I - Research and Development Efforts

Prepared under Contract AF 04(611)-9067

by

Northrop Carolina, Inc., Asheville, North Carolina  
A Subsidiary of Northrop Corporation

November 1965

APPROVED BY:



B. L. Johnson  
Program Manager

**CONFIDENTIAL**

### NOTICE

Northrop Carolina, Inc., has been assigned a patent application by the U. S. Patent Office to cover the Controllable Solid Propellant Rocket Motor invention disclosed in this publication, and the Commissioner of Patents has issued a secrecy order thereon. This secrecy order requires that those who receive a disclosure of the subject matter be informed of the existence of the secrecy order and of the penalties for the violation thereof.

The recipient of this report is accordingly advised that this publication includes information which is now under a secrecy order. It is requested that he notify all persons who will have access to this material of the secrecy order.

Each secrecy order provides that any person who has received a disclosure of the subject matter covered by the secrecy order is

"in nowise to publish or disclose the invention or any material information with respect thereto, including hitherto unpublished details of the subject matter of said application, in any way to any persons not cognizant of the invention prior to the date of the order, including any employee of the principals, but to keep the same secret except by written permission first obtained of the Commissioner of Patents, under the penalties of 35 U. S. C. (1952) 182, 186"

Although the original secrecy order forbids disclosure of the material to persons not cognizant of the invention prior to the date of the order, a supplemental permit attached to each order does permit such disclosures to:

- "(a) Any officer or employee of any department, independent agency or bureau of the Government of the United States.
- (b) Any person designated specifically by the head of any department, independent agency or bureau of the Government of the United States, or by his duly authorized subordinate, as a proper individual to receive the disclosure of the above indicated application.

The principals under the secrecy are further authorized to disclose the subject matter of this application to the minimum necessary number of persons of known loyalty and discretion, employed by or working with the principals or their licensees and whose duties involve cooperation in the development, manufacture or use of the subject matter by or for the Government of the United States, provided such persons are advised of the issuance of the secrecy order. "

No other disclosures are authorized, without written permission from the Commissioner of Patents. Penalties for violation of a secrecy order, include a fine of up to \$10,000 or imprisonment for not more than two years or both.

It must be understood that the requirements of the secrecy order of the Commissioner of Patents are in addition to the usual security regulations which are in force with respect to classified materials in this report. The usual security regulations must still be observed notwithstanding anything set forth in the secrecy order. In the event that this report shall be declassified, the secrecy order remains in full force until it is specifically rescinded.

## FOREWORD

This annual report for the continued development of a dual-chamber controllable solid propellant rocket motor (DCCSR) describes the progress during the third year of this program, which is sponsored by the Air Force Rocket Propulsion Laboratory, Edwards Air Force Base, California. The research and development efforts of the program are being performed by Northrop Carolina, Inc. a Subsidiary of Northrop Corporation, Asheville, North Carolina, under Air Force Contract AF 04(661)-9067. This report is presented in two volumes: Volume I - Research and Development Efforts, and Volume II - Analytical Study. This volume (Volume I) presents results of all research and development efforts during the third year, including development of forward- and aft-grain propellants, results of all development motor firings, and control valve and nozzle development efforts.

# CONFIDENTIAL

(This Abstract is Classified Confidential)

## ABSTRACT

This report presents the results of the third year's development of a dual-chamber controllable solid propellant rocket (DCCSR) motor with stop-restart and thrust modulation capability. The first-year's development was conducted under Air Force Contract AF 04(611)-8175, and the second and third year's efforts under AF 04(611)-9067, both sponsored by the Air Force Rocket Propulsion Laboratory, Edwards Air Force Base, California.

In this year's program the development of propellants for the forward and aft grains was completed by means of laboratory evaluations and subscale motor tests. Present technology was demonstrated by testing full-scale motors containing 300 lb of propellant both at sea-level and altitude. Excellent results were achieved in these tests in which the motors were programmed for both pulse and throttling operation. Thrust ratios as high as 9 to 1 were achieved.

Another full-scale test series was conducted to demonstrate the technology advancements made throughout the entire three-year effort. These motors contained the advanced propellants developed during the program, an improved control valve and control system, and nozzles specifically designed for on-off motor operation. Tests of these 300-lb motors were conducted both at sea level and altitude. One of these motors demonstrated nine stop-restart cycles at altitude conditions.

A full-scale test that fully demonstrated the feasibility of adapting the DCCSR concept to a post-boost propulsion system was also conducted.

# CONFIDENTIAL

TABLE OF CONTENTS

		<u>Page</u>
FOREWORD. . . . .		ii
ABSTRACT . . . . .		iii
LIST OF SYMBOLS . . . . .		xxxix
<u>Section</u>	<u>Title</u>	
I	INTRODUCTION . . . . .	1
	1. General . . . . .	1
	2. Description of DCCSR Concept . . . . .	1
	3. Advantages . . . . .	5
II	PROGRAM OBJECTIVES AND SCOPE . . . . .	7
	1. Phase I - Program Plan . . . . .	7
	2. Phase II - Propellant Development Program . . . . .	7
	<u>a.</u> Forward-Grain Propellant Development . . . . .	9
	<u>b.</u> Aft-Grain Propellant Development . . . . .	10
	3. Phase III - Demonstration of Present Technology . . . . .	10
	4. Phase IV - Nozzle Development . . . . .	10
	5. Phase V - Demonstration of New Technology . . . . .	11
	6. Analytical Study . . . . .	11
III	PROPELLANT DEVELOPMENT . . . . .	13
Subsection 1 - Forward-Grain Propellant Development . . . . .		15
	1. General . . . . .	15
	2. Laboratory Evaluation . . . . .	16
	<u>a.</u> General . . . . .	16
	<u>b.</u> Nitroguanidine . . . . .	16
	<u>c.</u> Ammonium Azide . . . . .	18
	<u>d.</u> Polyethylene Hydrazine Perchlorate . . . . .	19
	<u>e.</u> Triaminoguanidine Azide . . . . .	20

REPRODUCTION OF THIS PAGE WAS BLANK THEREFORE WAS NOT FILMED

TABLE OF CONTENTS (CONT'D)

<u>Section</u>	<u>Title</u>	<u>Page</u>
	<u>f.</u> Potassium Perchlorate . . . . .	20
	<u>g.</u> HMX . . . . .	27
	<u>h.</u> Coolants . . . . .	34
	<u>i.</u> Conclusions . . . . .	34
3.	Motor Testing . . . . .	38
4.	Final Characterization of PPO-90 . . . . .	42
	<u>a.</u> General . . . . .	42
	<u>b.</u> Laboratory Evaluation . . . . .	42
	<u>c.</u> Motor Testing . . . . .	42
	Subsection 2 - Aft-Grain Propellant Development . . . . .	49
1.	General . . . . .	49
2.	Hydrazinium Nitroformate Approach . . . . .	49
	<u>a.</u> General . . . . .	49
	<u>b.</u> Sensitivity and Stability of HNF . . . . .	49
	<u>c.</u> Compatibility Studies with HNF . . . . .	51
	<u>d.</u> Formulation Studies . . . . .	54
3.	Conventional Oxidizer Approach . . . . .	62
	<u>a.</u> Solid-Solution Binders . . . . .	62
	<u>b.</u> Castable Fluorocarbon Binders . . . . .	82
	<u>c.</u> Pressed Grain (OX-5) Modifications . . . . .	144
	<u>d.</u> Carboxy-Terminated Polybutadiene Binder . . . . .	145
4.	Conclusions . . . . .	159
IV	REIGNITION AND INSULATION STUDY . . . . .	161
	1. General . . . . .	161
	2. Insulation Study . . . . .	161

TABLE OF CONTENTS (CONT'D)

<u>Section</u>	<u>Title</u>	<u>Page</u>
	<u>a.</u> General . . . . .	161
	<u>b.</u> Insulation Tests . . . . .	162
	3.    Reignition Study . . . . .	175
	<u>a.</u> General . . . . .	177
	<u>b.</u> Series I Tests . . . . .	177
	<u>c.</u> Chamber Purge Technique . . . . .	182
V	PARAMETRIC STUDY . . . . .	189
	1.    General . . . . .	189
	2.    Scope of Study . . . . .	189
	3.    Summary . . . . .	191
VI	CONCEPT DEMONSTRATION TESTS (SERIES M) . . . . .	193
	1.    General . . . . .	193
	2.    Motor Hardware and Components . . . . .	193
	<u>a.</u> General Description . . . . .	193
	<u>b.</u> Hot-Gas Valves . . . . .	195
	<u>c.</u> Control System . . . . .	203
	<u>d.</u> Nozzle Designs . . . . .	203
	<u>e.</u> Purge System . . . . .	205
	3.    Test M. 1 . . . . .	205
	<u>a.</u> Motor Configuration . . . . .	205
	<u>b.</u> Test Program and Test Conditions . . . . .	206
	<u>c.</u> Test Results . . . . .	206
	4.    Test M. 2 . . . . .	209
	<u>a.</u> Motor Configuration . . . . .	209
	<u>b.</u> Test Program and Test Conditions . . . . .	209
	<u>c.</u> Test Results . . . . .	209

TABLE OF CONTENTS (CONT'D)

<u>Section</u>	<u>Title</u>	<u>Page</u>
5.	Test M. 3 . . . . .	211
	<u>a.</u> Motor Configuration . . . . .	211
	<u>b.</u> Test Program and Test Conditions . . . . .	211
	<u>c.</u> Test Results . . . . .	211
6.	Test M. 4 . . . . .	213
	<u>a.</u> Motor Configuration . . . . .	213
	<u>b.</u> Test Program and Test Conditions . . . . .	215
	<u>c.</u> Test Results . . . . .	215
7.	Test M. 5 . . . . .	222
	<u>a.</u> Motor Configuration . . . . .	222
	<u>b.</u> Test Program and Test Conditions . . . . .	222
	<u>c.</u> Test Results . . . . .	222
8.	Test M. 6 . . . . .	225
	<u>a.</u> Motor Configuration . . . . .	225
	<u>b.</u> Test Program and Test Conditions . . . . .	225
	<u>c.</u> Test Results . . . . .	227
9.	Pyrogen Vacuum Ignition Tests (Test Series K) . . . . .	234
10.	Test M. 7 . . . . .	234
	<u>a.</u> Motor Configuration . . . . .	234
	<u>b.</u> Test Program and Test Conditions . . . . .	237
	<u>c.</u> Test Results . . . . .	238
11.	Test M. 8 . . . . .	242
	<u>a.</u> Motor Configuration . . . . .	242
	<u>b.</u> Test Program and Test Conditions . . . . .	242
	<u>c.</u> Test Results . . . . .	242

TABLE OF CONTENTS (CONT'D)

<u>Section</u>	<u>Title</u>	<u>Page</u>
	12. Data Reduction Parameters . . . . .	249
	<u>a.</u> General . . . . .	249
	<u>b.</u> Forward-Chamber Parameters . . . . .	249
	<u>c.</u> Aft-Chamber Parameters . . . . .	252
	<u>d.</u> Thrust Parameters . . . . .	254
	<u>e.</u> Parameters for Over-all Motor . . . . .	255
	<u>f.</u> Correction Methods . . . . .	256
VII	DEMONSTRATION OF NEW TECHNOLOGY (TEST SERIES N) . . . . .	259
	1. General . . . . .	259
	2. Series N Motor Design . . . . .	259
	3. Series N Test Results . . . . .	266
	<u>a.</u> Sea-Level Tests . . . . .	266
	<u>b.</u> Altitude Tests . . . . .	273
VIII	EVALUATION OF NOZZLE DESIGNS . . . . .	303
	1. General . . . . .	303
	2. Evaluation of Nozzles 1 and 2 . . . . .	303
	3. Evaluation of Nozzle 3 . . . . .	307
	<u>a.</u> General . . . . .	307
	<u>b.</u> Visual Examination . . . . .	307
	<u>c.</u> Dimensional Examination . . . . .	308
	<u>d.</u> Data Analysis and Comparison . . . . .	310
IX	POST-BOOST PROPULSION SYSTEM DEMONSTRATION TESTS . . . . .	317
	1. General . . . . .	317
	2. DCCSR Operation for a PBPS Application . . . . .	318

TABLE OF CONTENTS (CONT'D)

<u>Section</u>	<u>Title</u>	<u>Page</u>
3.	Demonstration Test . . . . .	319
<u>a.</u>	General . . . . .	319
<u>b.</u>	Motor Components . . . . .	322
<u>c.</u>	Propellants . . . . .	322
<u>d.</u>	Attitude Control System. . . . .	322
<u>e.</u>	Test Program and Test Conditions . . . . .	322
<u>f.</u>	Test Results . . . . .	327
X	CONCLUSIONS . . . . .	335
1.	General . . . . .	335
2.	Phase II - Propellant Development Program . . . . .	335
3.	Phase III - Demonstration of Present Technology . . . . .	335
4.	Phase V - Demonstration of New Technology . . . . .	336

LIST OF REFERENCES

APPENDIX

A	DETAILED DESCRIPTION OF SERIES H TESTS H. 1 THROUGH H. 6 . . . . .	A-1
1.	General . . . . .	A-1
2.	Test H. 1 . . . . .	A-1
3.	Test H. 2 . . . . .	A-1
4.	Test H. 3 . . . . .	A-4
5.	Test H. 4 . . . . .	A-4
6.	Test H. 5 . . . . .	A-6
7.	Test H. 6 . . . . .	A-6
B	SYSTEM ANALYSIS AND CONTROL DESIGN FOR PROPORTIONAL HOT-GAS VALVE. . . . .	B-1
1.	Introduction. . . . .	B-1

TABLE OF CONTENTS (CONT'D)

<u>Appendix</u>	<u>Title</u>	<u>Page</u>
	2. Summary of Results . . . . .	B-1
	3. General System Description . . . . .	B-3
	4. System Simulation . . . . .	B-5
	<u>a.</u> Position Loop Simulation . . . . .	B-9
	<u>b.</u> Process and Control Valve Simulation . . . . .	B-22
	<u>c.</u> Frequency Response of Simulated System . . . . .	B-43
	<u>d.</u> Control Design . . . . .	B-49
	<u>e.</u> Control Optimization Studies . . . . .	B-54
	<u>f.</u> Termination Simulation . . . . .	B-57
	5. Recommended Control Operation . . . . .	B-67
	<u>a.</u> Control Configuration . . . . .	B-67
	<u>b.</u> Limits . . . . .	B-70
	<u>c.</u> System Performance . . . . .	B-72
	6. Control Valve Limitations . . . . .	B-74
	7. Frequency Response Data . . . . .	B-76
<b>C</b>	<b>DESIGN ANALYSIS FOR NOZZLE NO. 1 (2-TO-1 EXPANSION)</b> . . . . .	<b>C-1</b>
	1. Introduction . . . . .	C-1
	2. Analyses . . . . .	C-1
	<u>a.</u> Materials Evaluation . . . . .	C-1
	<u>b.</u> Heat Transfer . . . . .	C-17
	3. Design . . . . .	C-18
	4. Fabrication . . . . .	C-20
<b>D</b>	<b>DESIGN ANALYSIS FOR NOZZLES NO. 2 AND 3 (20-TO-1 EXPANSION)</b> . . . . .	
	1. Introduction . . . . .	D-1

TABLE OF CONTENTS (CONT'D)

<u>Appendix</u>	<u>Title</u>	<u>Page</u>
2.	Analyses . . . . .	D-1
	<u>a.</u> Materials Evaluation . . . . .	D-1
	<u>b.</u> Heat Transfer . . . . .	D-1
3.	Design . . . . .	D-3
4.	Fabrication . . . . .	D-5

LIST OF ILLUSTRATIONS

<u>Figure</u>	<u>Title</u>	<u>Page</u>
1	Dual-Chamber Controllable Solid Propellant Rocket Motor . . . . .	3
2	Effect of Nitroguanidine on Strand Burning Rate of PPO-13 Nitroplastisol Propellant . . . . .	17
3	Strand Burning-Rate Data for PPO-88 Propellant . . . . .	17
4	Strand Burning-Rate Data for PPO-89 Propellant . . . . .	18
5	Effect of TAZ on Strand Burning Rate of PPO-13 Nitroplastisol Propellant . . . . .	21
6	Strand Burning-Rate Data for PPO-73 Propellant (50-Micron Potassium Perchlorate) . . . . .	23
7	Strand Burning-Rate Data for PPO-75 Propellant . . . . .	23
8	Strand Burning-rate Data for PPO-76 Propellant . . . . .	24
9	Strand Burning-Rate Data for PPO-72 Propellant . . . . .	24
10	Strand Burning-Rate Data for PPO-71 Propellant . . . . .	25
11	Strand Burning-Rate Data for PPO-74 Propellant . . . . .	25
12	Strand Burning-Rate Data for PPO-77 Propellant . . . . .	26
13	Strand Burning-Rate Data for PPO-73 Propellant (150-Micron Potassium Perchlorate) . . . . .	28
14	Strand Burning-Rate Data for PPO-82 Propellant . . . . .	28
15	Strand Burning-Rate Data for PPO-83 Propellant . . . . .	29
16	Strand Burning-Rate Data for PPO-74 Propellant (100 to 4500 psi) . . . . .	29
17	Strand Burning-Rate Data for PPO-70 Propellant . . . . .	30
18	Strand Burning-Rate Data for PPO-78 Propellant . . . . .	30
19	Strand Burning-Rate Data for PPO-78 Propellant (Six-Micron HMX) . . . . .	31
20	Strand Burning-Rate Data for PPO-78 Propellant (500-Micron HMX) . . . . .	31

LIST OF ILLUSTRATIONS (CONT'D)

<u>Figure</u>	<u>Title</u>	<u>Page</u>
21	Strand Burning-Rate Data for PPO-79 Propellant . . .	32
22	Strand Burning-Rate Data for PPO-80 Propellant . . .	32
23	Strand Burning-Rate Data for PPO-81 Propellant . . .	33
24	Strand Burning-Rate Data for PPO-97 Propellant . . .	33
25	Strand Burning-Rate Data for PPO-90 Propellant . . .	35
26	Strand Burning-Rate Data for PPO-87 Propellant . . .	35
27	Strand Burning-Rate Data for PPO-92 Propellant . . .	36
28	Strand Burning-Rate Data for PPO-91 Propellant . . .	36
29	Strand Burning-Rate Data for PPO-93 Propellant . . .	37
30	Strand Burning-Rate Data for PPO-94 Propellant . . .	37
31	P-K-r Data for PPO-90 Obtained from Motor Tests . .	41
32	Burning Rate Data for PFO-90 Propellant from Series J Tests . . . . .	46
33	Strand Burning-Rate Data for Formulation 8131-46-3 . .	56
34	Pressure- and Thrust-Time Traces for Test H. 13 . .	58
35	Strand Burning-Rate Data for Formulation 8131-39-1 . .	61
36	Effect of Cure Time at 170°F on Mechanical Properties of Formulation 8133-35-6 . . . . .	69
37	Strand Burning-Rate Data for Formulation 8133-35-6 . .	70
38	Strand Burning-Rate Data for Formulation 8133-36-1 . .	70
39	Strand Burning-Rate Data for Formulation 8133-38-3 . .	78
40	Strand Burning-Rate Data for Formulation 8133-38-4 . .	78
41	Strand Burning-Rate Data for Formulation 8983-8-1 . .	85
42	Results of Propellant-to Steel Bond Tests . . . . .	89
43	Extraction of Mandrel from 175-Lb Motor Containing Propellant Formulation 8983-23-2 . . . . .	90

LIST OF ILLUSTRATIONS (CONT'D)

<u>Figure</u>	<u>Title</u>	<u>Page</u>
44	Radiographic Inspection of 175-Lb Motor Containing Propellant Formulation 8983-23-2 . . . . .	90
45	End View of 175-Lb Motor Containing Propellant Formulation 8983-23-2 . . . . .	91
46	Motor Burning-Rate Data for Formulation 8983-23-2 . . . . .	94
47	Pressure- and Thrust-Time Traces for Test H. 9 . . . . .	95
48	Pressure- and Thrust-Time Traces for Test H. 10 . . . . .	96
49	Pressure- and Thrust-Time Traces for Test H. 11 . . . . .	97
50	Pressure- and Thrust-Time Traces for Test H. 12 . . . . .	98
51	Effect of Viton A Concentration on Mechanical Properties of C <sub>7</sub> FA Propellant . . . . .	104
52	Effect of Viton LM Concentration on Mechanical Properties of C <sub>7</sub> FA Propellant Containing Two Percent Viton A . . . . .	104
53	Strand Burning-Rate Data for Formulation 8983-23-2 . . . . .	107
54	Strand Burning-Rate Data for Formulation 8983-33-3 . . . . .	108
55	Strand-Burning-Rate Data for Formulation 8983-30-2 . . . . .	108
56	Strand Burning-Rate Data for Formulation 8983-31-1 . . . . .	109
57	Strand Burning-Rate Data for Formulation 8983-31-2 . . . . .	109
58	Strand Burning-Rate Data for Formulation 8983-31-3 . . . . .	110
59	Strand Burning-Rate Data for Formulation 8983-33-4 . . . . .	111
60	Strand Burning-Rate Data for Formulation 8983-33-5 . . . . .	111
61	Strand Burning-Rate Data for Formulation 8983-37-1 . . . . .	112
62	Strand Burning-Rate Data for Formulation 8983-38-1 . . . . .	113
63	Strand Burning-Rate Data for Formulation 8983-38-3 . . . . .	114
64	Strand Burning-Rate Data for Formulation 8983-38-4 . . . . .	115
65	Strand Burning-Rate Data for Formulation 8983-39-4 . . . . .	115

LIST OF ILLUSTRATIONS (CONT'D)

<u>Figure</u>	<u>Title</u>	<u>Page</u>
66	Strand Burning-Rate Data for Formulation 8983-39-3 .	116
67	Strand Burning-Rate Data for Formulation 8983-38-5 .	116
68	Strand Burning-Rate Data for Formulation 8983-38-7 .	117
69	Strand Burning-Rate Data for Formulation 8983-43-1 .	118
70	Strand Burning-Rate Data for Formulation 8983-44-1 .	118
71	Strand Burning-Rate Data for Formulation 8983-40-1 .	120
72	Strand Burning-Rate Data for Formulation 8983-39-4 .	120
73	Strand Burning-Rate Data for Formulation 8983-34-3 .	121
74	Strand Burning-Rate Data for Formulation 8983-38-6 .	121
75	Strand Burning-Rate Data for Formulation 8983-35-2 .	122
76	Strand Burning-Rate Data for Formulation 8983-43-1 .	122
77	Strand Burning-Rate Data for Formulation 8983-45-6 .	123
78	Strand Burning-Rate Data for Formulation 8983-45-7 .	123
79	Strand Burning-Rate Data for Formulation 8983-41-6 .	125
80	Strand Burning-Rate Data for Formulation 8983-45-1 .	125
81	Strand Burning-Rate Data for Formulation 8983-23-2 with Two Percent Oxamide . . . . .	126
82	Strand Burning-Rate Data for Formulation 8983-45-2 .	126
83	Strand Burning-Rate Data for Formulation 8983-45-4 .	127
84	Strand Burning-Rate Data for Formulation 8983-44-2 .	127
85	Strand Burning-Rate Data for Formulation 8983-45-3 .	128
86	Strand Burning-Rate Data for Formulation 8983-44-6 .	128
87	Strand Burning-Rate Data for Formulation 8983-41-7 .	129
88	Strand Burning-Rate Data for Formulation 8983-41-3 .	129
89	Strand Burning-Rate Data for Formulation 8983-41-8 .	130

LIST OF ILLUSTRATIONS (CONT'D)

<u>Figure</u>	<u>Title</u>	<u>Page</u>
90	Strand Burning-Rate Data for Formulation 8983-41-5 .	130
91	Strand Burning-Rate Data for Formulation 8983-41-2 .	131
92	Strand Burning-Rate Data for Formulation 8983-33-1 .	132
93	Strand Burning-Rate Data for Formulation 8983-44-4 .	132
94	Strand Burning-Rate Data for Formulation 8983-44-3 .	133
95	Strand Burning-Rate Data for Formulation 8983-49-8 .	134
96	Strand Burning-Rate Data for Formulation 8983-33-2 .	137
97	Strand Burning-Rate Data for Formulation 8983-42-2 .	141
98	Strand Burning-Rate Data for Formulation 8983-39-6 .	141
99	Strand Burning-Rate Data for Formulation 8983-39-1 .	142
100	Strand Burning-Rate Data for Formulation 8983-43-4 .	142
101	Strand Burning-Rate Data for Formulation 8983-42-1 .	143
102	Strand Burning-Rate Data for Formulation 8982-1-10 .	143
103	Strand Burning-Rate Data for C-445 Propellant, Modified by Northrop Carolina . . . . .	148
104	Strand Burning-Rate Data for C-430 Propellant, Modified by Northrop Carolina . . . . .	149
105	Burning-Rate Data for C-445 Propellant Obtained from Subscale Motor Tests . . . . .	153
106	Burning-Rate Data for C-430 Propellant Obtained from Subscale Motor Tests . . . . .	156
107	Aft- to Forward-Chamber Mixture Ratio as a Function of $K_n$ at 100 Psia for C-430 Propellant . . . . .	160
108	Insulation Samples after 6-Second Torch Test . . . . .	165
109	Insulation Samples after 9-Second Torch Test . . . . .	166
110	Insulation Samples after 30-Second Torch Test . . . . .	167

LIST OF ILLUSTRATIONS (CONT'D)

<u>Figure</u>	<u>Title</u>	<u>Page</u>
111	Pancake Motor Assembly Used for Insulation Study . . .	171
112	Interior View of Pancake Motor Aft Closure Before Test I. 1. 1 . . . . .	172
113	Pancake Motor Mounted on Test Stand (Test I. 1) . . . . .	173
114	Interior View of Pancake Motor Aft Closure After Test I. 1 . . . . .	173
115	Insulation Samples after Test I. 1 . . . . .	176
116	Temperature versus Time for Two Insulation Materials (Tests I. 1. 1 and I. 1. 2) . . . . .	176
117	Pancake Test Motor Assembly Used in Tests I. 2 through I. 14 . . . . .	178
118	Pressure and Temperature versus Time for Test I. 2 . . . . .	181
119	$V_f/S_p$ versus Termination Pressure for Series I Tests I. 2 through I. 14 . . . . .	181
120	Nitrogen Coolant Characteristics at Various Storage Pressures . . . . .	184
121	Diagram of Nitrogen Purge System . . . . .	185
122	Motor Assembly Used in Test M. 1 . . . . .	196
123	Motor Assembly Used in Test M. 2 . . . . .	197
124	Motor Assembly Used in Test M. 3 . . . . .	198
125	Motor Assembly Used in Tests M. 4, M. 5 and M. 6 . . . . .	199
126	Northrop Carolina - Designed On-Off Hot-Gas Valve . . . . .	201
127	Pressure-Time Trace for Valve Checkout Test I. 19B . . . . .	202
128	Cross-Section of Proportional Hot-Gas Valve . . . . .	204
129	Pressure- and Thrust-Time Traces for Test M. 1 . . . . .	207
130	Pressure- and Thrust-Time Traces for Test M. 2 . . . . .	210
131	Pressure- and Thrust-Time Traces for Test M. 3 . . . . .	212

LIST OF ILLUSTRATIONS (CONT'D)

<u>Figure</u>	<u>Title</u>	<u>Page</u>
132	Pressure- and Thrust-Time Traces for Test M. 4 . . .	216
133	Steady-State Aft-Chamber Pressure and Vacuum Thrust Values as a Function of Steady-State Forward-Chamber Pressure for Tests M. 4 and M. 5 . . . . .	220
134	Post-Test View of Forward End of Hot-Gas Valve Used in Test M. 4 . . . . .	221
135	Post-Test View of Aft End of Hot-Gas Valve Used in Test M. 4, Showing Cracks 180° Apart . . . . .	221
136	Pressure- and Thrust-Time Traces for Test M. 5 . . .	223
137	Pressure- and Thrust-Time Traces for Tests M. 6. 1, M. 6. 2, and Reignition Following M. 6. 2 . . . . .	228
138	Pressure- and Thrust-Time Traces for Tests M. 6. 3 and M. 6. 4 . . . . .	230
139	Pressure- and Thrust-Time Traces for Test M. 6. 5 . .	231
140	Shut-Down Impulse as a Function of Web Fraction Consumed for Tests M. 4, M. 5, and M. 6 . . . . .	233
141	Pressure-Time Traces for Pyrogen Vacuum Ignition Tests . . . . .	236
142	Motor for Test M. 7 Mounted in Altitude Chamber at OAL	237
143	Pressure- and Thrust-Time Traces for Test M. 7 . . .	239
144	End View of Aft Grains after Test M. 7 . . . . .	240
145	Three-Quarter Side View of Aft Grains after Test M. 7	240
146	Pressure- and Thrust-Time Traces for Test M. 8 . . .	245
147	End View of Aft Grains after Test M. 8 . . . . .	246
148	Three-Quarter Side View of Aft Grains after Test M. 8 .	246
149	Representative DCCSR Pressure and Thrust-Time Traces	250

LIST OF ILLUSTRATIONS (CONT'D)

<u>Figure</u>	<u>Title</u>	<u>Page</u>
150	Motor Assembly for Test Series N . . . . .	260
151	Calculated Burning Surface Area as a Function of Web Burned for Series N Aft Grain . . . . .	263
152	Aft-Chamber Pressure versus Forward-Chamber Pressure for Series N Aft Grain. . . . .	264
153	Aft Case and Insulation Design for Series N Motor . . . . .	265
154	Valve Stroke-Area Relationship for Various Motor Configurations . . . . .	267
155	Pressure- and Thrust-Time Traces for Test N. 1. . . . .	269
156	Pressure- and Thrust-Time Traces for Test N. 2. . . . .	270
157	Pressure-Time Traces for Test N. 3 . . . . .	272
158	Diagram Showing Installation of Motor in Test Cell T-3 . . . . .	274
159	Photograph of Motor Installed in Test Cell . . . . .	275
160	Traces for Test N. 4. 1. . . . .	277
161	Traces for Test N. 4. 2. . . . .	278
162	Traces for Test N. 4. 3 . . . . .	279
163	Traces for Test N. 4. 4 . . . . .	280
164	Traces for Test N. 4. 5 . . . . .	281
165	Traces for Test N. 4. 6 (First 2-sec of Operation). . . . .	282
166	Traces for Test N. 4. 6 (t + 2-sec to Burnout). . . . .	283
167	Traces for Test N. 5. 1. . . . .	289
168	Traces for Test N. 5. 2 . . . . .	290
169	Traces for Test N. 5. 3 . . . . .	291
170	Traces for Test N. 5. 4 . . . . .	292
171	Traces for Test N. 5. 5 . . . . .	293
172	Traces for Test N. 5. 6 . . . . .	294
173	Traces for Test N. 5. 7 . . . . .	295

LIST OF ILLUSTRATIONS (CONT'D)

<u>Figure</u>	<u>Title</u>	<u>Page</u>
174	Traces for Test N. 5. 8. . . . .	296
175	Traces for Test N. 5. 9. . . . .	297
176	Traces for Test N. 5. 10 (First 2-sec of Operation) . .	298
177	Traces for Test n. 5. 10 (t + 2-sec to Burnout) . . . .	299
178	Sketch of Nozzle No. 2 after Series M Tests, Showing Erosion Profile. . . . .	305
179	Dimensional Variations at Nozzle Throat and Exit Cone (Series N) . . . . .	309
180	Sketch of Nozzle Cross Section, Showing Thermocouple Locations . . . . .	311
181	Temperature Rise Data for Series N Tests . . . . .	312
182	Temperature Gradients Occurring at Throat and Throat Extension . . . . .	313
183	Comparison of Predicted and Measured Temperature Gradient for a 1. 5-sec Pulse . . . . .	315
184	Comparison of Predicted and Measured Surface Tem- perature for Long-Duration Pulses . . . . .	316
185	Schematic Diagram of DCCSR Motor of PBPS Application	320
186	PBPS Demonstration Motor Mounted on Test Stand . .	321
187	Close-up of PBPS Demonstration Motor, Showing Attitude Control System Valving . . . . .	321
188	Programmed Duty Cycle for PBPS Demonstration Test	326
189	Typical Pressure-Time Trace for Axial Pulse Cycle (PBPS Demonstration Test). . . . .	328
190	Typical Pressure-Time Trace for Attitude Control System Cycle (PBPS Demonstration Test) . . . . .	329
191	Typical Pressure-Time Trace for 10-Cps Cycle of Attitude Control System (PBPS Demonstration Test) .	330
192	Pressure-Time Trace for Entire PBPS Demonstration Test. . . . .	331

LIST OF ILLUSTRATIONS (CONT'D)

<u>Figure</u>	<u>Title</u>	<u>Page</u>
A-1	Traces for Test H. 1 . . . . .	A-2
A-2	Traces for Test H. 2 . . . . .	A-3
A-3	Traces for Test H. 3 . . . . .	A-5
A-4	Traces for Tests H. 4. 1 and H. 4. 2 . . . . .	A-7
A-5	Traces for Test H. 5 . . . . .	A-8
A-6	Traces for Tests H. 6. 1 and H. 6. 2 . . . . .	A-10
B-1	Basic Block Diagram of Controlled System . . . . .	B-4
B-2	Basic Block Diagram of Position Loop . . . . .	B-6
B-3	Major Analog Computer Elements . . . . .	B-8
B-4	Position Loop Pictorial Diagram . . . . .	B-10
B-5	Actuator Block Diagram and Computer Diagram . . . . .	B-13
B-6	Hydraulic Block Diagram and Computer Diagram . . . . .	B-18
B-7	Servo valve Block Diagram and Computer Diagram . . . . .	B-21
B-8	Position Loop Response, $P_A = 0$ . . . . .	B-23
B-9	Position Loop Response, $P_A = 0$ . . . . .	B-24
B-10	Position Loop Response, $P_A = 1500$ psi . . . . .	B-25
B-11	Position Loop Response, $P_A = 1500$ psi . . . . .	B-26
B-12	Process Block Diagram and Computer Diagram . . . . .	B-31
B-13	Computer Approximation of $P^{.672}$ . . . . .	B-32
B-14	Desired and Actual Control Valve Area Versus Displacement . . . . .	B-34
B-15	Computer Approximation of Control Valve Area Versus Displacement . . . . .	B-35
B-16	Steady-State Forward Pressure Versus Displacement . . . . .	B-37
B-17	Process Response to Step Change in Displacement, Initial Free Volume . . . . .	B-38

LIST OF ILLUSTRATIONS (CONT'D)

<u>Figure</u>	<u>Title</u>	<u>Page</u>
B-18	Process Response to Step Change in Displacement, Final Free Volume . . . . .	B-39
B-19	Process Response to Step Change in Displacement, Final Free Volume . . . . .	B-40
B-20	Process Response to Step Change in Displacement, Final Free Volume . . . . .	B-41
B-21	Process Response to Step Change in Displacement, Final Free Volume . . . . .	B-42
B-22	Frequency Response Characteristics of Position Loop Obtained from Computer Simulation . . . . .	B-45
B-23	Frequency Response of Process for Initial Conditions.	B-46
B-24	Frequency Response Characteristics of Process for Final Conditions . . . . .	B-47
B-25	Frequency Response Characteristics of Combined Position Loop and Process. . . . .	B-48
B-26	Frequency Response Characteristics of Position Loop Determined from System and Process Response.	B-50
B-27	Normalized Frequency Response of Proportional Plus Integral Controller . . . . .	B-53
B-28	Controller Block Diagram and Computer Diagram . .	B-55
B-29	Controlled System Response to Small Step Input . . .	B-58
B-30	Controlled System Response to Small Step Input . . .	B-59
B-31	Controlled System Response to Small Step Input . . .	B-60
B-32	Controlled System Response to Small Step Input . . .	B-61
B-33	Controlled System Response to Small Ramp Input. . .	B-62
B-34	Controlled System Response to Small Ramp Input. . .	B-63
B-35	Controlled System Response to Large Step Input . . .	B-64
B-36	Controlled System Response to Large Step Input . . .	B-65
B-37	Complete Computer Diagram for Controlled System .	B-66

LIST OF ILLUSTRATIONS (CONT'D)

<u>Figure</u>	<u>Title</u>	<u>Page</u>
B-38	Control Valve Termination. . . . .	B-68
B-39	TR-10 Computer Diagram for Actual System. . . . .	B-69
B-40	Servo Valve Drive and Termination Circuitry . . . . .	B-71
B-41	Computer Amplifier Limiting Circuitry . . . . .	B-73
B-42	Example of Frequency Response Data Reduction . . . . .	B-77
C-1	Schematic Diagram of Equipment Used for Low Cycle Thermal Fatigue Evaluation . . . . .	C-4
C-2	Relationship between Number of Thermal Cycles and Maximum Temperature Required to Produce Exaggerated Grain Growth in Unalloyed Tungsten Rod . . . . .	C-11
C-3	Influence of Exposure Temperature on the Average Grain Size Produced in Unalloyed Tungsten Subjected to Temperature Cycling (10 to 17-Cycles) . . . . .	C-12
C-4	Bend Transition Temperatures for Sheet Specimens of Unalloyed Tungsten . . . . .	C-15
C-5	Bend Transition Temperatures for Rod Specimens of Unalloyed 1% Th O <sub>2</sub> Tungsten . . . . .	C-15
C-6	Design for Nozzle No. 1 (2-to-1 Expansion) . . . . .	C-19
D-1	Design for Nozzles No. 2 and 3 (20-to-1 Expansion) . . . . .	D-4

LIST OF TABLES

<u>Table</u>	<u>Title</u>	<u>Page</u>
I	CSR Test Plan . . . . .	8
II	Results of Stability and Sensitivity Tests of Candidate Additives for Forward-Grain Propellant . . . . .	19
III	Effect of Additives to Nitroplastisol Binder on Burning-Rate Pressure Exponent . . . . .	22
IV	Summary of Initial Series J Termination Tests . . . . .	39
V	Summary of Series J Tests (J. 1 through J. 11) . . . . .	40
VI	Properties of PPO-13 and PPO-90 Propellants . . . . .	43
VII	Comparison of PPO-90 Propellant Properties with Forward Propellant Goals . . . . .	44
VIII	Summary of Series J Burning-Rate Tests with PPO-90 Propellant . . . . .	45
IX	Summary of Series J Reignition Tests with PPO-90 Propellant . . . . .	48
X	Drop Sensitivity of HNF and other Propellant Ingredients . . . . .	50
XI	Summary of Compatibility Studies of HNF with Binder Constituents and Oxidizers . . . . .	52
XII	Summary of Compatibility Studies of HNF with Solid-Solution Binder Ingredients . . . . .	53
XIII	Summary of Ballistic Data for Test H. 13 . . . . .	59
XIV	Results of Process Studies with Solid-Solution Propellants in Two-Pound Batches . . . . .	64
XV	Results of Process Studies with Solid-Solution Propellants in 10- to 14-Lb Batches . . . . .	65
XVI	Mechanical Properties of Formulation 8133-35-6 at 74°F . . . . .	68
XVII	Effect of Cure Temperature on Mechanical Properties of Formulation 8133-35-5 at 74°F . . . . .	68

LIST OF TABLES (CONT'D)

<u>Table</u>	<u>Title</u>	<u>Page</u>
XVIII	Reduced Ballistic Data for Tests H. 2, H. 3, H. 4, and H. 6	72
XIX	Effect of Carbon Black and Ferric Oxide on Properties of Solid-Solution Propellants . . . . .	74
XX	Properties of Acrylamide Solid-Solution Formulations Containing HMX . . . . .	76
XXI	Summary of Formulation Studies of Acrylonitrile/ Ammonium Perchlorate System . . . . .	79
XXII	Properties of Acrylonitrile Solid-Solution Formulations Containing HMX . . . . .	81
XXIII	Results of Differential Thermal Analysis to Determine Lithium Perchlorate Purity . . . . .	83
XXIV	Results of Mechanical Properties Improvement Studies of C <sub>7</sub> Fluorocarbon Acrylate Propellant System . . . . .	86
XXV	Effect of Cure Time on Mechanical Properties of Formulation 8983-23-3 Cured at 120°F . . . . .	87
XXVI	Effect of Binder Modification on Mechanical Properties of C <sub>7</sub> FA Propellant (12-Lb Batch Size) . . . . .	88
XXVII	Reproducibility of Mechanical Properties of Formulation 8983-23-2 (12 Lb Batch Size) . . . . .	88
XXVIII	Mechanical Properties of 200-Lb Batch of Propellant Formulation 8983-23-2 . . . . .	91
XXIX	Summary of Ballistic Data for Tests H. 9 through H. 12	93
XXX	Comparison of Properties of Northrop Carolina Fluorocarbon Formulations with State-of the Art Composite Propellant . . . . .	101
XXXI	Effect of Additives on Mechanical Properties of C <sub>7</sub> FA Propellant . . . . .	106
XXXII	Results of Mechanical Properties Improvement Studies of Fluorocarbon Monomer Propellant System . . . . .	136

LIST OF TABLES (CONT'D)

<u>Table</u>	<u>Title</u>	<u>Page</u>
XXXIII	Effect of Binder Modification and Cure Time on Mechanical Properties of FX-189 Propellant . . . . .	138
XXXIV	Effect of TAC on Mechanical Properties of FX-189 Propellant . . . . .	139
XXXV	Reduced Ballistic Data for Modified OX-5 Propellant Tests . . . . .	146
XXXVI	Composition and Properties of C-445 and C-430 Propellants . . . . .	147
XXXVII	Summary of Termination Tests (C-445 Aft Propellant)	151
XXXVIII	Summary of Termination Tests (C-430 Aft Propellant)	155
XXXIX	Insulation Materials Selected for Study . . . . .	163
XL	Torch Test Results . . . . .	168
XLI	Results of Insulation-to-Metal Bond Tests . . . . .	169
XLII	Results of Insulation-to-Propellant Bond Tests . . . . .	170
XLIII	Results of Pancake Motor Insulation Tests . . . . .	174
XLIV	Summary of Data for Series I Tests . . . . .	180
XLV	Summary of Data for Tests I. 15 through I. 18 . . . . .	187
XLVI	Total Impulse and Thrust Range for Parametric Analysis	190
XLVII	Summary of Series M Motor Configurations . . . . .	194
XLVIII	Summary of Data for Tests M. 1 and M. 2 . . . . .	208
XLIX	Reduced Ballistic Data for Test M. 3 . . . . .	214
L	Reduced Ballistic Data for Pulse Cycles of Test M. 4 . . . . .	217
LI	Reduced Ballistic Data for Throttling Cycle of Test M. 4 . . . . .	219
LII	Reduced Ballistic Data for Pulse Cycles of Test M. 5 . . . . .	224
LIII	Reduced Ballistic Data for Throttling Cycle of Test M. 5 . . . . .	226
LIV	Reduced Ballistic Data for Pulse Cycles of Test M. 6 . . . . .	232

LIST OF TABLES (CONT'D)

<u>Table</u>	<u>Title</u>	<u>Page</u>
LV	Reduced Ballistic Data for Throttling Cycle of Test M. 6	235
LVI	Reduced Ballistic Data for Pulse Cycles of Test M. 7 . .	241
LVII	Reduced Ballistic Data for Throttling Cycle of Test M. 7	243
LVIII	Reduced Ballistic Data for Pulse Cycles of Test M. 8 . .	247
LIX	Reduced Ballistic Data for Throttling Cycle of Test M. 8	248
LX	Ballistic Design for Series N Motor . . . . .	262
LXI	Motor Summary for Test N. 4 . . . . .	284
LXII	Summary of Reduced Ballistic Data for Test N. 4 . . . .	285
LXIII	Motor Termination Summary for Test N. 4. . . . .	286
LXIV	Motor Summary for Test N. 5 . . . . .	300
LXV	Summary of Reduced Ballistic Data for Test N. 5 . . . .	301
LXVI	Termination Summary for Test N. 5. . . . .	302
LXVII	Formulation of Gas Generator Propellant Used in . . . . PBPS Demonstration Test . . . . .	323
LXVIII	Formulation of Aft Propellant Used in PBPS Demon- stration Test . . . . .	324
LXIX	Attitude Control System Valve Characteristics . . . . .	325
B-I	Position Loop Component Specifications . . . . .	B-11
B-II	Process Equation Constants . . . . .	B-29
C-I	Effect of Time and Temperatures on the Grain Size of Tungsten Sheet (AS-Received, Recrystallized Condition). . . . .	C-7
C-II	Effect of Time and Temperature on the Grain Size of Tungsten Sheet (Hot-Cold Worked 75% at 2300 <sup>o</sup> F). . . .	C-7
C-III	Effect of Time and Temperature on the Grain Size of 1/4-Inch Tungsten - 1% Th O <sub>2</sub> Rod (70-90% Reduction) .	C-9

LIST OF TABLES (CONT'D)

<u>Table</u>	<u>Title</u>	<u>Page</u>
C-IV	Effect of Time, Temperature, and Thermal Cycling on the Grain Size of 1/8-Inch Tungsten Rod . . . . .	C-10
C-V	Effect of Time, Temperature, and Thermal Cycling on the Grain Size of 1/8-Inch Tungsten - 1% Th O <sub>2</sub> . .	C-13

LIST OF SYMBOLS

Ballistic symbols are listed in Section VI, paragraph 12.

<u>Symbol</u>	<u>Definition</u>
$a$	= Burning rate constant (in./sec)
$A_b$	= Burning surface area (sq in.)
$A_m$	= Exposed metal surface area (sq in.)
$C_D$	= Discharge coefficient ( $\text{sec}^{-1}$ )
$E_o$	= Modulus of elasticity (psi)
$\bar{F}_b$	= Average thrust over thrust burning time ( $\text{lb}_f$ )
$J$	= Mechanical equivalent of heat (joules/gm-cal)
$k$	= Propellant thermal conductivity ( $\text{cal/cm-sec}^\circ\text{C}$ )
$K_n$	= Aft chamber burning area to throat area ratio
$\dot{m}_g$	= Gas generator mass flow rate (lb/sec)
$\dot{m}_o$	= Mass flow rate through a choked nozzle (lb/sec)
$M$	= Gas molecular weight (lb/lb-mole)
$n$	= Pressure exponent
$P$	= Chamber pressure (psi)
$q$	= Expression for the propellant preheat (cal)
$\bar{R}$	= Universal gas constant $\left(\frac{\text{psi-cu in.}}{\text{lb/lb mol-}^\circ\text{R}}\right)$
$S_b$	= Propellant surface area (sq in.)
$S_m$	= Stress (psi)
$T_s$	= Propellant flash temperature ( $^\circ\text{F}$ )
$T_u$	= Propellant initial temperature ( $^\circ\text{F}$ )
$V_f$	= Chamber free volume (cu in.)
$W_g$	= Gas weight (lb)

LIST OF SYMBOLS (CONT'D)

<u>Symbol</u>	<u>Definition</u>
$\gamma$	= Specific heat ratio of gas
$\Delta_{T_g}$	= Temperature drop of the gases ( $^{\circ}F$ )
$E_m$	= Elongation (in. /in.)
$\theta$	= Aft to forward chamber mixture ratio
$\rho$	= Propellant density (lb/cu in.)
$\tau$	= Time for termination to reignition (sec)

LIST OF SYMBOLS (CONT'D)

<u>Symbol</u>	<u>Definition</u>
$\gamma$	= Specific heat ratio of gas
$\Delta_{T_g}$	= Temperature drop of the gases ( $^{\circ}\text{F}$ )
$E_m$	= Elongation (in. /in. )
$\theta$	= Aft to forward chamber mixture ratio
$\rho$	= Propellant density (lb/cu in. )
$\tau$	= Time for termination to reignition (sec)

SECTION I - INTRODUCTION

1. GENERAL

Northrop Carolina, Inc., a subsidiary of Northrop Corporation, Asheville, North Carolina, has completed the third year of development of a command controllable dual-chamber solid propellant rocket motor (DCCSR). This report describes the work conducted during the third year of development, under Air Force Contract AF 04(611)-9067, for the Air Force Rocket Propulsion Laboratory (AFRPL), Edwards Air Force Base, California.

The first year's efforts from 15 April 1962 through 14 April 1963, were conducted under Air Force Contract AF 04(611)-8175 and are reported in References 1 through 4. The second year's efforts (15 March 1963 through 14 March 1964) were conducted under Contract AF 04(611)-9067, awarded on 15 March 1963, and reported in References 5 through 8. The third year's efforts, which were continued under Contract AF 04(611)-9067, awarded on 10 February 1964, are reported in References 9 through 13, respectively. This report along with Reference 8 provides a complete summary of all efforts under Contract AF 04(611)-9067.

This report is presented in two volumes. Volume I presents the program objectives, results of the propellant development work, results of the studies and tests conducted during the program, and conclusions. Volume II presents the results of an analytical study to determine the effect of various parameters on performance of the DCCSR motor.

2. DESCRIPTION OF DCCSR CONCEPT

A basic necessity for space and re-entry maneuvering on advanced scientific and military missions as well as terminal guidance for advanced weapon systems is a rocket propulsion system capable of stop-restart functions and thrust magnitude control. It is highly desirable to combine these features with the inherent advantages of simplicity and increased state of readiness found in solid propellant rocket motors.

---

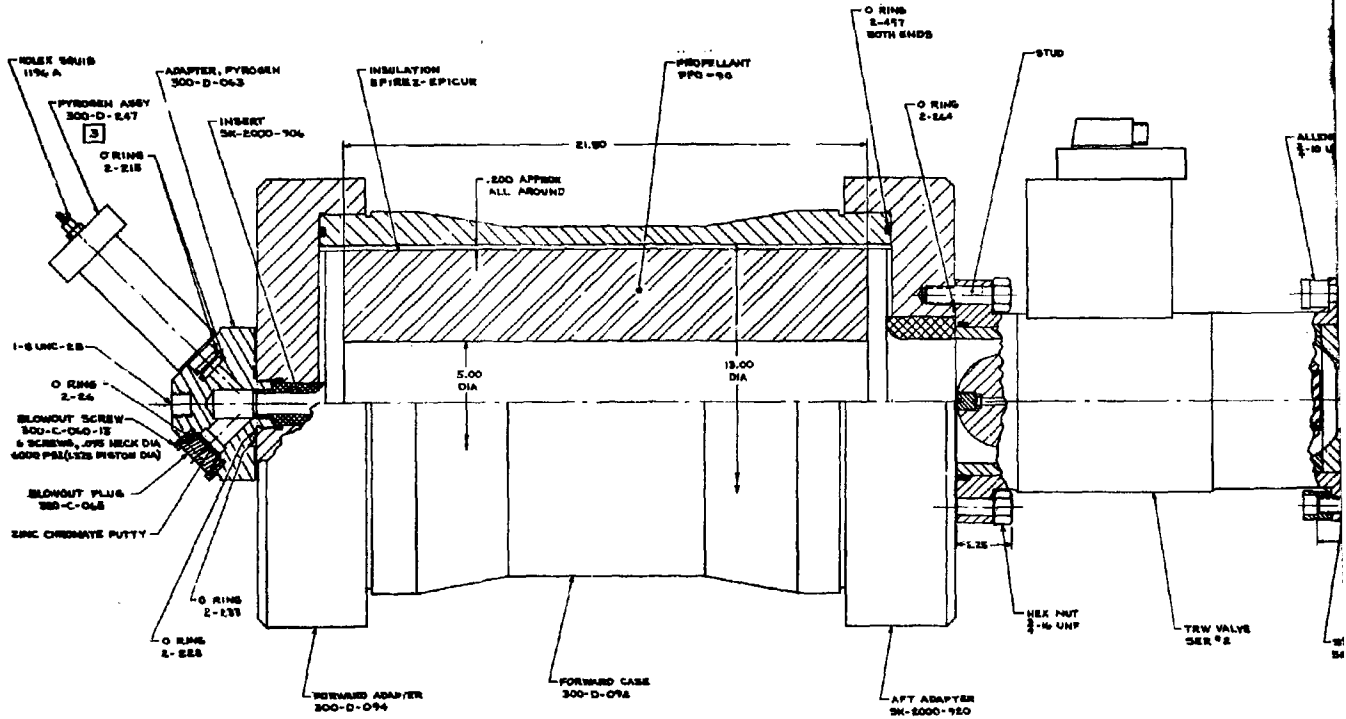
\* Formerly Amcel Propulsion Company.

The most direct method by which these desirable aspects can be provided in a solid propellant rocket motor is through use of a variable throat area instead of the standard fixed nozzle in a single-chamber motor. Changing the throat area would thus produce variable thrust due to changes in the motor mass flow and the expansion ratio of the nozzle. The propellant grain could be extinguished by suddenly increasing the throat area, resulting in a rapid chamber pressure decay. Reignition could be accomplished by multiple igniter units that exhaust directly into the forward end of the chamber.

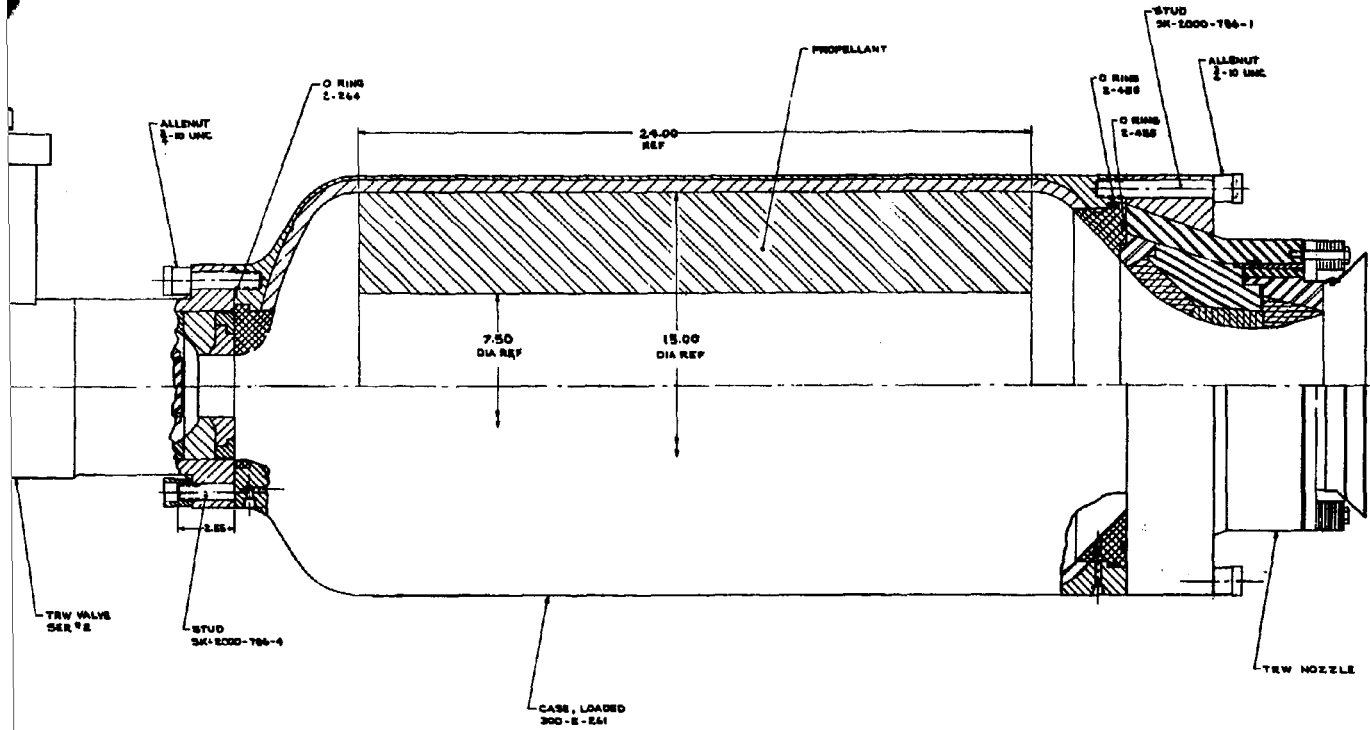
The principal problems that must be overcome to achieve the above approach are associated with the design of a throttle valve that will operate reliably in a hot gas environment. With current state-of-the-art propellants, the valve will be subjected to a hot (5500°F), corrosive gas stream containing erosive condensed particles. Adjusting the propellant formulation for combustion gases which are compatible with a mechanical valve normally reduces the performance of the propellant. Considerable progress has been made in the development of hot-gas valves for thrust vector control using solid propellant combustion products. However, the development of these valves is not sufficiently advanced to provide precise throttling area control for prolonged periods nor to withstand the temperature cycling effects introduced by on-off operation with high-energy metallized solid propellants. (Confidential)

The dual-chamber controllable solid rocket motor concept utilizes fuel-rich (forward) and oxidizer-rich (aft) propellant chambers separated by a throttle valve (see Figure 1). The fact that the fuel-rich combustion products are relatively cool burning (2800°F) permits the use of state-of-the-art materials in the valve construction. A conventional high-temperature nozzle is used on the aft chamber where high-temperature combustion takes place. A multiple pyrogen unit ignition system is included as an integral part of the forward chamber. (Confidential)

Thrust is initiated by igniting the forward propellant with a single pyrogen unit. The relatively cool combustion products from the forward chamber are throttled through the control valve into the aft chamber where additional reaction occurs, resulting in more energy release. The aft propellant will not sustain combustion in the absence of heat supplied by the forward propellant. Therefore, throttleability is achieved by varying the forward chamber pressure (and burning rate) through valve position control. The aft propellant burns when the combustion gases from the forward propellant pass over it. (Confidential)



**CONFIDENTIAL**



(Confidential)

Figure 1 - Dual-Chamber Controllable Solid Propellant Rocket Motor

**CONFIDENTIAL**

2

Thrust can be terminated at any time during the burning period by suddenly increasing the valve flow area, which produces a rarefaction wave that extinguishes combustion of the forward propellant. Since the aft propellant will not sustain combustion alone, it too is extinguished. (Confidential)

Repeated on-off cycle operation is achieved by reignition of the forward propellant using another pyrogen igniter of the multiple ignition system for each restart. During motor operation, the unused igniters are protected against autoignition from the forward propellant combustion products by means of individual burst diaphragms that are fractured as each igniter is fired. (Confidential)

### 3. ADVANTAGES

Some of the advantages of the unique concept over other approaches to a variable-thrust, on-off system include:

1. No pressurization or gravity force feed systems are required at start-up, since an all solid-propellant system is used.
2. Thrust termination and throttleability are achieved by a single controlling element (system simplicity).
3. The exposure of the throttling element to an extremely high-temperature environment is eliminated.
4. The dual-chamber concept provides an excellent mechanism for using high-energy propellant ingredients that may not be compatible in a conventional system.

(Confidential)

THIS PAGE WAS BLANK THROUGHOUT AND NOT FILLED

SECTION II - PROGRAM OBJECTIVES AND SCOPE

The scope of the program, originally scheduled to cover 15 months, encompassed five Phases:

- Phase I - Prepare and Maintain a Program Plan
- Phase II - Propellant Development Program
- Phase III - Demonstration of Present Technology
- Phase IV - Nozzle Development
- Phase V - Demonstration of New Technology

The development tests planned to be conducted during these phases is presented in Table I.

1. PHASE I - PROGRAM PLAN

The requirements of this phase were fulfilled by preparing a detailed program plan (Reference 14) and updating the plan on a monthly basis.

2. PHASE II - PROPELLANT DEVELOPMENT PROGRAM

This phase was subdivided into the development of forward- and aft-grain propellants. The primary objective of the over-all propellant development effort (forward and aft) was to further develop the propellant system for use in the DCCSR motor, which would be demonstrated subsequently in Phase V tests (Test Series N). The effort was to be directed generally toward achieving the following:

1. Improved termination capability
2. Delivered vacuum specific impulse of  $280 \text{ lb}_f\text{-sec}/\text{lb}_m$  at 20-to-1 expansion ratio
3. 10-to-1 throttleability
4. Space storability (desirable, not mandatory)

(Confidential)

THIS PAGE WAS BLANK THEREFORE WAS NOT FILLED

TABLE I - CSR TEST PLAN

Test Series	Number of Tests	Number of Cycles per Test	Type of Hardware	Propellant		Test Objective
				Forward	Aft	
H	20	2	Subscale	PPO-13	Aft	Aft propellant development Reignition and insulation study Forward propellant development Demonstration of present technology Demonstration of new technology
I	18	4	Subscale	PPO-13	Candidate propellants OX-1	
J	20	2	Subscale	PPO-80 & PPO-90		
M	8	5, 4, 2 <sup>†</sup>	Full scale	PPO-13	OX-1, OX-5 <sup>*</sup>	
N	5	11	Full scale	PPO-90	C-430	

<sup>†</sup> Two tests consisted of 5 cycles each; two tests, 4 cycles; and four tests, 2 cycles.

\* OX-1 was used in six tests; OX-5, in the remainder.

a. Forward-Grain Propellant Development

The objective of this portion of Phase II was to develop a propellant, or propellants, for use in the forward chamber, which would meet the following requirements in the relative order of importance:

1. Combustion of the propellant should be capable of being extinguished without subsequent reignition, at sea level, by pressure decay rates comparable to those necessary for extinguishing PPO-13 (Reference 7).
2. The propellant flame temperature should be less than 3000°F.
3. The percentage of liquid and/or solid combustion products of the propellant should be very low, and preferably none at all.
4. The burning-rate pressure index should be between 0.7 and 0.9 over the wide pressure range of 100 to 4500 psi; the motor should operate stably at this range.
5. The propellant should be castable and have mechanical properties comparable to state-of-the-art formulations.
6. The propellant should be capable of a delivered vacuum specific impulse of  $280 \text{ lb}_f\text{-sec}/\text{lb}_m$ , in combination with the aft propellant. (Confidential)

In addition to these major requirements, it is desirable that the propellant be space storable.

The requirements of this phase were to be met by conducting laboratory evaluations of (1) a nitroplastisol binder system and (2) a composite binder system, and by conducting propellant development tests (Test Series J, as shown in Table I).

The results of this development program are presented in Section III, Subsection 1.

b. Aft-Grain Propellant Development

The objective of this investigation was to develop a propellant, or propellants, for use in the aft chamber, which would meet the following requirements in the relative order of importance:

1. The propellant should terminate without reignition at decay rates compatible with those achieved previously in test firings.
2. The mechanical properties should be comparable to those of state-of-the-art propellants, and the propellant should be castable and case bondable.
3. The slope (n) of the P-r curve should approach unity.  
(Confidential)

In addition to these primary requirements, the propellant should, in combination with the forward propellant, deliver 280 lb<sub>f</sub>-sec/lb<sub>m</sub> specific impulse, have low sensitivity and high stability, and be space storable. These requirements were to be achieved by conducting a comprehensive laboratory evaluation and by conducting propellant development tests (Test Series H, as shown in Table I). (Confidential)

The results of this development program are presented in Section III, Subsection 2.

3. PHASE III - DEMONSTRATION OF PRESENT TECHNOLOGY

The objective of Phase III was to establish the mechanism of operation and performance envelope of the DCCSR concept. This phase was to consist of a reignition study (Test Series I), an insulation evaluation, development of a control valve for the full-scale motors, and full-scale motor tests (Test Series M). The results of this phase are presented in Sections IV and VI.

4. PHASE IV - NOZZLE DEVELOPMENT

The objective of this phase was to demonstrate technology for the design of a nozzle that is capable of surviving cycle firings of the DCCSR motor. The final nozzle design was to be used in the latter Series M firings and all the Series N firings. The efforts of this phase are described in Section VI and in Appendixes C and D. The evaluation of the nozzle design is presented in Section VIII.

5. PHASE V - DEMONSTRATION OF NEW TECHNOLOGY

The objective of this phase was to demonstrate the mechanism of operation and performance envelope of the DCCSR motor with the new forward and aft propellants developed during Phase II. This phase was to consist of Test Series N, which would utilize full-scale motors consisting of (1) a spherical forward chamber containing propellant developed during Phase II, a proportional hot-gas valve developed during Phase III, a new cylindrical aft-chamber containing propellant developed during Phase II, and the nozzle developed during Phase IV.

The results of this phase of effort are presented in Section VII.

6. ANALYTICAL STUDY

In addition to the five separate program phases described above, a comprehensive analytical study was conducted in order to determine the effects of scaling on internal ballistics, physical properties, and general operating and control characteristics of the DCCSR motor. The study was programmed for Northrop Carolina's IBM 1620 Computer, and the results presented in the form of charts and graphs. A summary of this effort is presented in Section V herein; the detailed results are presented in Volume II.

SECTION III - PROPELLANT DEVELOPMENT

The development of improved forward- and aft-grain propellants, in accordance with the objectives outlined in Section II, is described in detail in this section. The forward-grain development effort was completed mid-way through the program, with the primary objectives having been achieved. The aft-grain development, however, was more extensive, and continued throughout the course of the program. Because of the length and complexity of the propellant development work, this section has been divided into subsections. Forward grain development results are presented in Subsection I, beginning on the following page, and aft-grain propellant development in Subsection 2, beginning on page 49.

PREVIOUS PAGE WAS BLANK THEREFORE WAS NOT FILLED

THIS PAGE WAS BLANK THROUGHOUT THE ENTIRE PERIOD

SECTION III - PROPELLANT DEVELOPMENT

Subsection 1 - Forward-Grain Propellant Development

I. GENERAL

The forward-grain development effort was confined exclusively to the nitroplastisol binder system, which, on the basis of previous experience, offered the following advantages over the composite systems:

1. An essentially constant slope over a wide pressure range; composite propellants generally exhibit an increased slope between 1000 and 2000 psi.
2. High-pressure operation; composite systems are generally operated below 1500 psi, since some composites are thought to burn in micropores at high pressures.
3. Termination under sea-level conditions; propellants containing large amounts of aluminum and/or ammonium perchlorate with hydrocarbon binders have been observed to reignite following termination at sea level.

(Confidential)

The effect of additives (burning-rate modifiers) on the basic nitroplastisol propellant system was evaluated; additives included the following conventional and high-energy oxidizers as well as coolants:

1. Nitroguanidine
2. Ammonium azide
3. Polyethylene hydrazine perchlorate
4. Triaminoguanidine azide
5. Potassium perchlorate
6. HMX
7. Coolants (oxamide, ammonium oxalate, triacetin).

(Confidential)

Initially, these additives were evaluated in the laboratory over pressure ranges of 50 to 2000 psi, and compared with formulation PPO-13, the basic forward-grain propellant used during the first two years of the DCCSR program. The more promising formulations were then evaluated more thoroughly in the laboratory and in motor tests. The selected propellant was then thoroughly characterized in the laboratory and in motor firings. The details of this evaluation are presented below. (Confidential)

2. LABORATORY EVALUATION

a. General

The nine candidate additives listed above were incorporated into a nitroplastisol binder consisting of a 1 : 1 ratio of nitro-cellulose ball powder and triethylene glycol dinitrate (TEGDN), with one percent resorcinol, a stabilizer. Twenty-three formulations were evaluated.

b. Nitroguanidine

To compare the effect of various additives in the nitroplastisol binder, burning rates of the binder alone were measured in the strand bomb. Then, to determine the effect of nitroguanidine on the binder, these results were compared with those previously obtained with PPO-13 nitroplastisol propellant, which contains 12 percent nitroguanidine. Figure 2 presents this comparison. Above 500 psi, the burning rates of the binder and PPO-13 are nearly identical. However, at lower pressures, the slope of the burning-rate curve for the binder decreases, whereas the slope for PPO-13 remains identical to that at high pressures. Burning-rate data obtained from motor tests with PPO-13 are almost identical to the strand data. Higher concentrations of nitroguanidine (19 and 24 percent) in formulations PPO-88 and -89, respectively, had little, if any, effect on pressure exponent (see Figures 3 and 4). (Confidential)

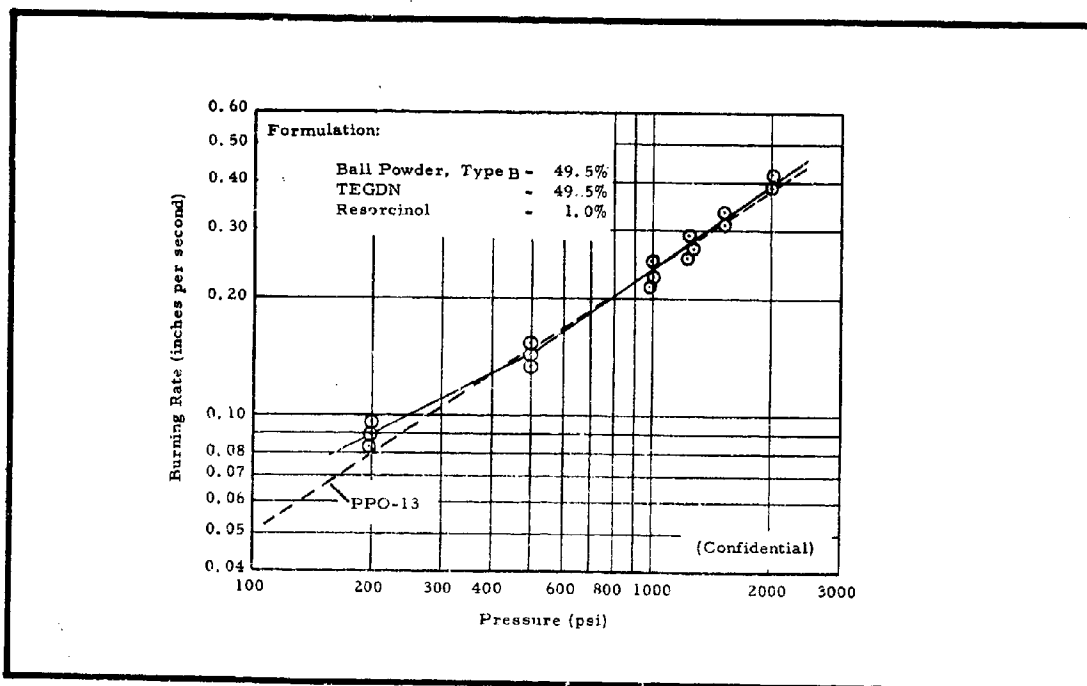


Figure 2 - Effect of Nitroguanidine on Strand Burning Rate of PPO-13 Nitroplastisol Propellant

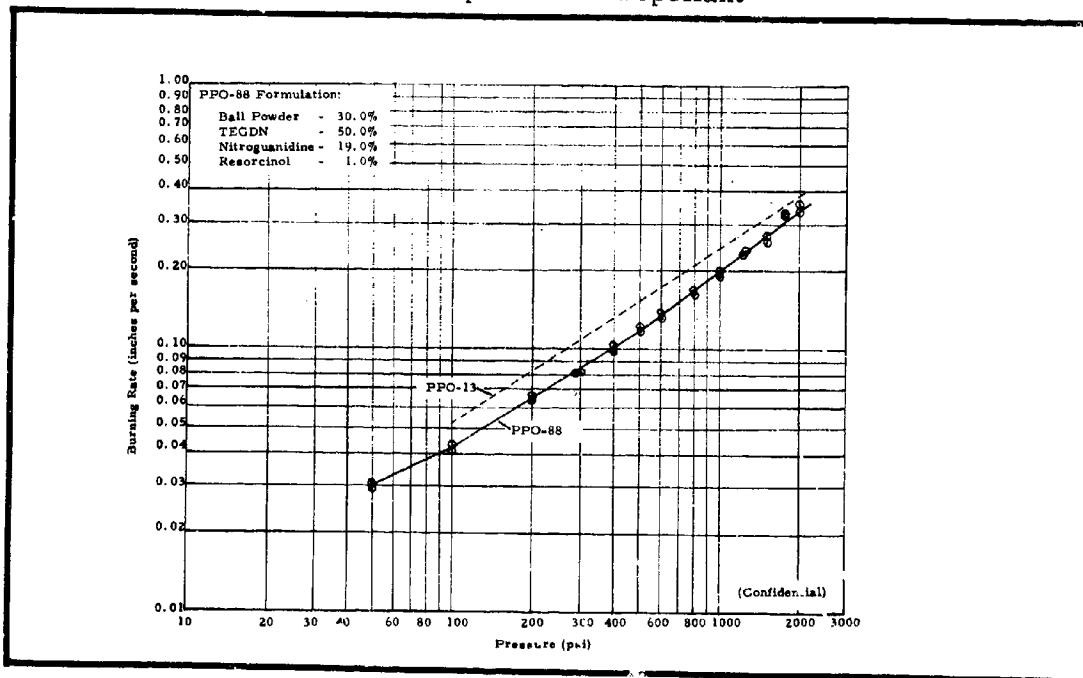


Figure 3 - Strand Burning-Rate Data for PPO-88 Propellant

# CONFIDENTIAL

AFRPL-TR-65-209, Vol I

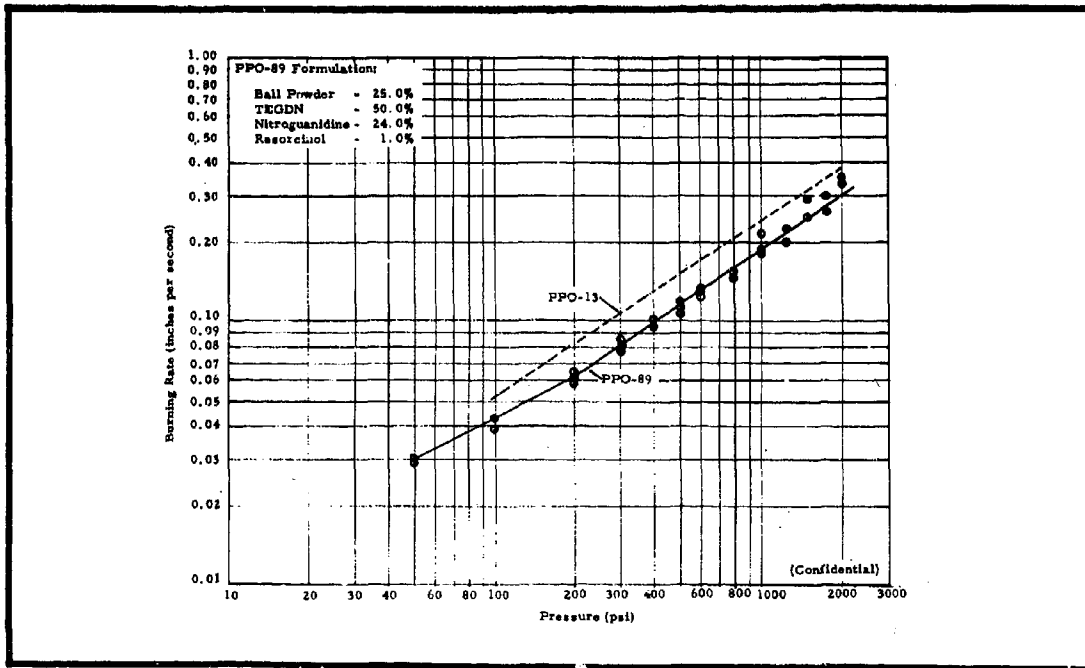
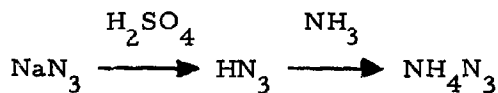


Figure 4 - Strand Burning-Rate Data for PPO-89 Propellant

## c. Ammonium Azide

Ammonium azide ( $\text{NH}_4\text{N}_3$ ) was selected for evaluation because of its high working fluid content, which contributes to a low flame temperature. Since ammonium azide is not commercially available because of a lack of demand, a small quantity was synthesized by the following sequence:



Ammonium azide has a density of 1.35 and sublimates at  $134^\circ\text{C}$ . Vacuum thermal stability and explosion temperature test results are given in Table II. Considerable decomposition occurred with the azide mixed with nitrocellulose at  $120^\circ\text{C}$ . Even when cured at  $50^\circ\text{C}$  in the nitroplastisol binder, "gassing" occurred. Because of this incompatibility of the  $\text{NH}_4\text{N}_3$  with the binder, further evaluation of this additive was discontinued. (Confidential)

TABLE II - RESULTS OF STABILITY AND SENSITIVITY TESTS  
OF CANDIDATE ADDITIVES FOR FORWARD-GRAIN PROPELLANT

Additive	Drop Sensitivity (Drop height, with 2-kg weight 50% fire) (cm)	Vacuum Stability (Gas liberated at 120°C) (cc/gm/hr)	Five-Second Autoignition Temperature (°C)
NH <sub>4</sub> N <sub>3</sub>	...	0.15* (in 44 hr)	238
TAZ	42	0.52* (in 44 hr)	...
PEHP	26	...	235
HMX	42	0.01 (in 40 hr)	327
1:1 TAZ-Type B Ball Powder	...	23.5 (in 1 hr)	...
1:1 NH <sub>4</sub> N <sub>3</sub> -Type B Ball Powder	...	>25	...
2% TAZ; 98% B Ball Powder	...	...	206
2% NH <sub>4</sub> N <sub>3</sub> ; 98% B Ball Powder	...	...	210

\*Material sublimed, as well as decomposed.

(Confidential)

d. Polyethylene Hydrazine Perchlorate

Polyethylene hydrazine perchlorate (PEHP) was evaluated for sensitivity, compatibility, and strand burning-rate properties in the nitroplastisol binder. The pure PEHP was found to have a somewhat greater sensitivity than HMX, as shown in Table II. It had no effect on the burning rate of nitroplastisol in concentrations up to two percent. The slope and burning rates were

identical to those of the pure binder. On the basis of these preliminary results, the evaluation of PEHP was discontinued. (Confidential)

e. Triaminoguanidine Azide

One pound of triaminoguanidine azide (TAZ) was obtained from Dow Chemical Company and evaluated in the nitroplastisol system. Tests indicated that the drop sensitivity of TAZ was similar to that of HMX, but its stability at elevated temperatures was far inferior. Considerable decomposition occurred at 120°C in vacuum stability tests with Type B ball powder. (Confidential)

In preliminary formulation studies with TAZ, there was some evidence of "gassing" when cured at 50°C. The cure temperature was therefore lowered to 40°C to obtain strands for burning-rate studies. Strand burning-rate data, shown in Figure 5, indicate that at the two-percent and eight-percent levels, TAZ increases the burning rate, but does not affect the slope significantly. (Confidential)

f. Potassium Perchlorate

Table III presents a summary of the potassium perchlorate ( $KClO_4$ ) and HMX formulations studied, and gives the measured pressure exponents up to 2000 psi for all formulations, and up to 4500 psi for the most promising formulations. PPO-13 data are given for comparison. The strand burning rates for the potassium perchlorate formulations are plotted as a function of pressure in Figures 6 through 12. As indicated in Table III, each formulation, except PPO-76, gave higher pressure exponents than PPO-13. Since a break occurs in most of the burning-rate curves in the range from 300 to 600 psi, two exponents are given: (1) an over-all exponent between 100 and 2000 psi, and (2) the exponent between 600 and 2000 psi. The latter values give an indication of the exponent to be expected at the higher pressures of the pressure range of interest (100 to 4500 psi), over which the five most promising formulations were subsequently investigated. (Confidential)

The addition of potassium perchlorate to the nitroplastisol binder increased pressure exponent at both the low and high pressures as shown in Figure 6 for formulation PPO-73. The extremely high exponent, 0.95, of this formulation at high pressures is

**CONFIDENTIAL**

AFRPL-TR-65-209, Vol I

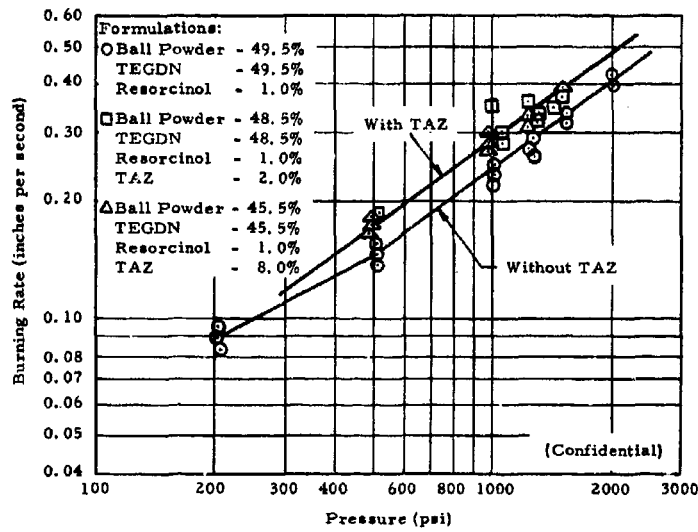


Figure 5 - Effect of TAZ on Strand Burning Rate of PPO-13 Nitroplastisol Propellant

**CONFIDENTIAL**

**CONFIDENTIAL**

AFRPL-TR-65-209, Vol I

TABLE III - EFFECT OF ADDITIVES TO NITROPLASTISOL BINDER ON BURNING-RATE PRESSURE EXPONENT

Formulation	Binder #	Nitro-guanidine	Constituents (percent by weight)				Mean Exponent		
			Potassium Perchlorate	Guanidine Carbonate	HMX	Ammonium Oxalate	100 to 2000 psi	100 to 4500 psi	600 to 2000 psi
PPO-13	88.0	12.0	.	.	.	.	0.67	0.67	0.95
PPO-73	95.0	.	5.0**	.	.	.	0.77	.	.
PPO-73	95.0	.	5.0††	.	.	.	0.84	.	.
PPO-74	90.0	.	5.0	5.0	.	.	0.76	0.77	0.81
PPO-75	90.0	5.0	5.0	.	.	.	0.70	.	0.86
PPO-76	88.0	9.0	3.0	.	.	.	0.64	.	0.78
PPO-72	90.0	.	5.0	.	.	5.0	0.74	.	0.90
PPO-71	90.0	.	5.0	.	.	.	0.76	.	0.88
PPO-77	88.0	6.0	3.0	.	.	5.0	0.67	.	0.74
PPO-83	85.0	10.0	5.0	.	.	.	0.81	.	.
PPO-82	80.0	10.0	5.0	.	.	5.0†	0.71	.	.
PPO-70	95.0	.	.	.	.	.	0.69	.	0.77
PPO-78	80.0	7.0	.	.	.	5.0†	0.74	.	0.78
PPO-78	88.0	7.0	.	.	.	.	0.69	.	.
PPO-78	88.0	7.0	.	.	.	5.0‡	0.70	.	.
PPO-79	80.0	10.0	.	.	.	5.0†	0.80	.	.
PPO-80	80.0	10.0	.	.	.	5.0†	0.75	0.77	.
PPO-81	90.0	.	.	.	.	5.0†	0.71	.	.
PPO-97	85.0	.	.	.	.	5.0†	0.70	.	.
PPO-88	81.0	19.0	.	.	.	5.0†	0.69	.	.
PPO-89	76.0	24.0	.	.	.	.	0.65	.	.
PPO-90	95.0	.	.	.	.	.	0.82	0.82	.
PPO-87	90.0	.	.	.	.	.	0.83	.	.
PPO-92	95.0	.	.	.	.	.	0.70	0.71	.
PPO-91	90.0	.	.	.	.	5.0	0.83	.	.
PPO-93	95.0	.	.	.	.	10.0	0.70	0.69	.
PPO-94	90.0	.	.	.	.	.	0.70	.	.

\*Binder consists of a 1.-to-1 ratio of Type B Ball Powder and TECDN, plus one percent resorcinol, based on total formulation.

\*\* 50-micron particle size

†† 150-micron particle size

† 200-micron particle size

# 500-micron particle size

‡ 600-micron particle size

(Confidential)

**CONFIDENTIAL**

# CONFIDENTIAL

AFRPL-TR-65-209, Vol I

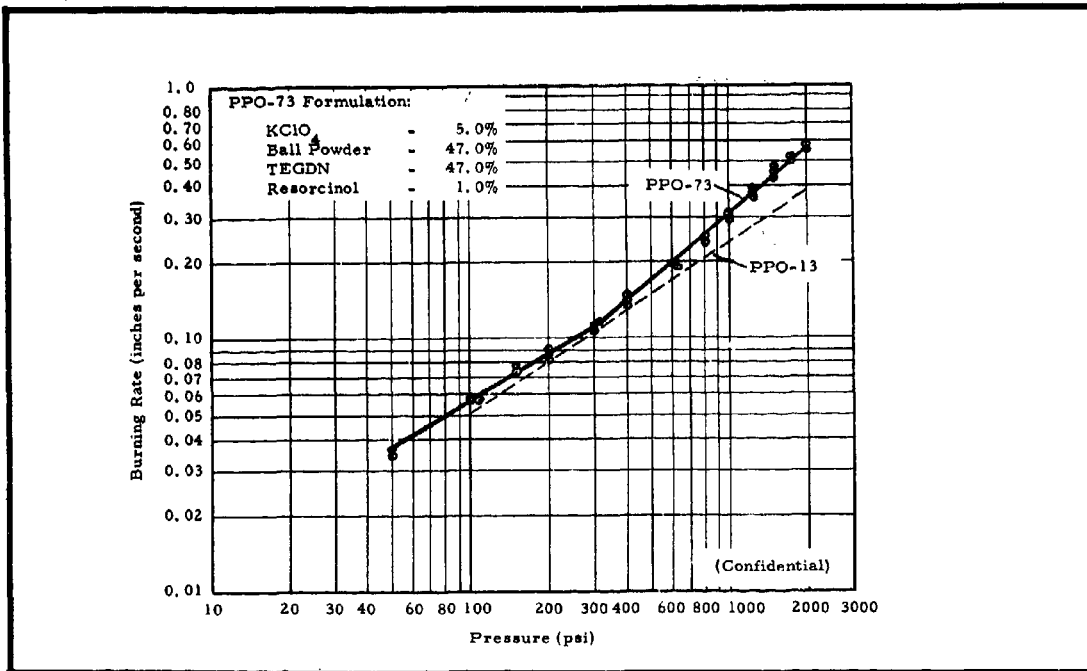


Figure 6 - Strand Burning-Rate Data for PPO-73 Propellant (50-Micron Potassium Perchlorate)

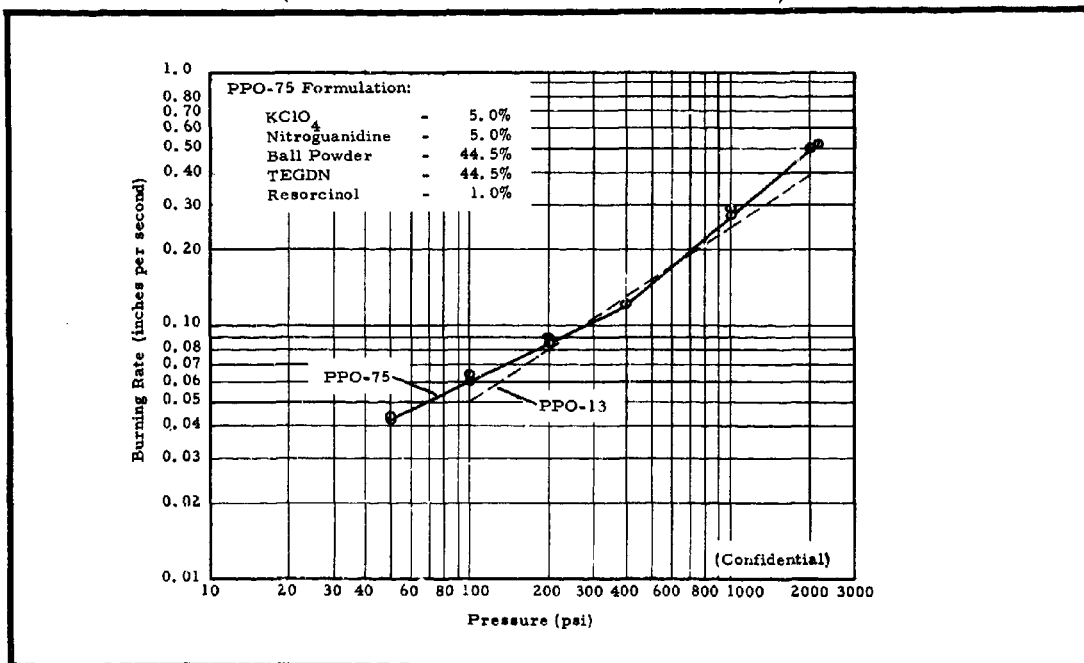


Figure 7 - Strand Burning-Rate Data for PPO-75 Propellant

# CONFIDENTIAL

# CONFIDENTIAL

AFRPL-TR-65-209, Vol I

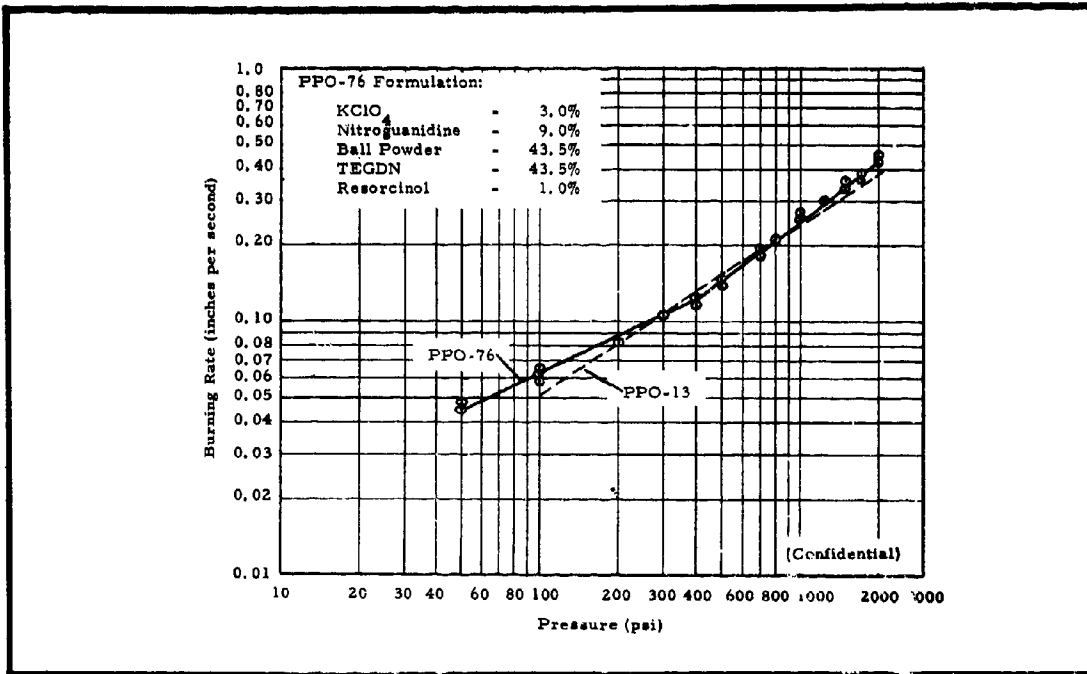


Figure 8 - Strand Burning-Rate Data for PPO-76 Propellant

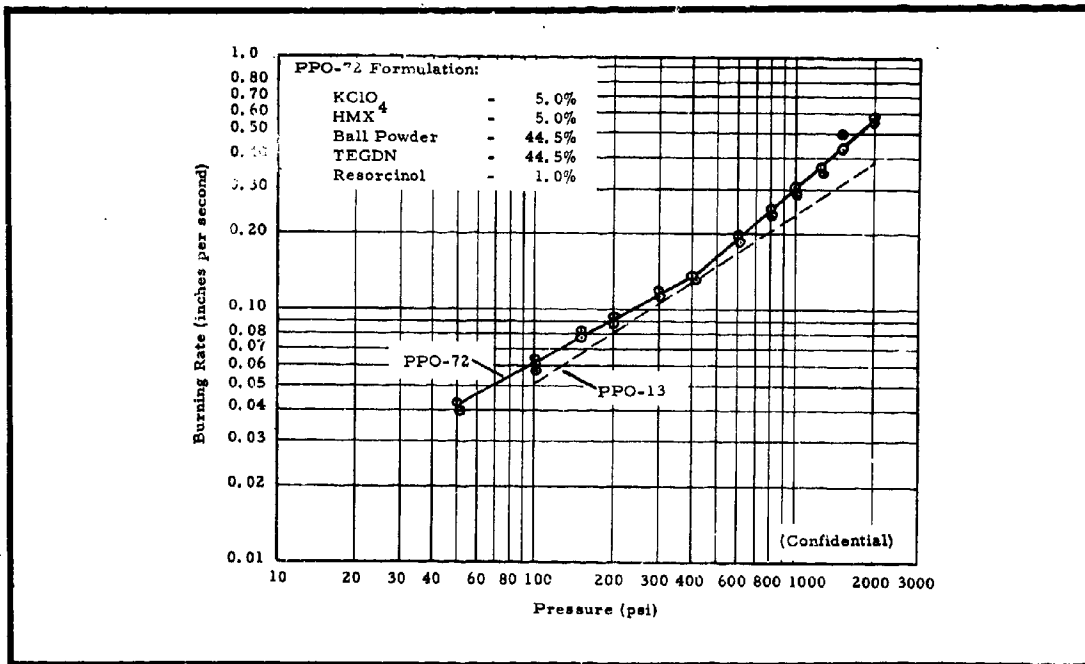


Figure 9 - Strand Burning-Rate Data for PPO-72 Propellant

# CONFIDENTIAL

AFRPL-TR-65-209, Vol I

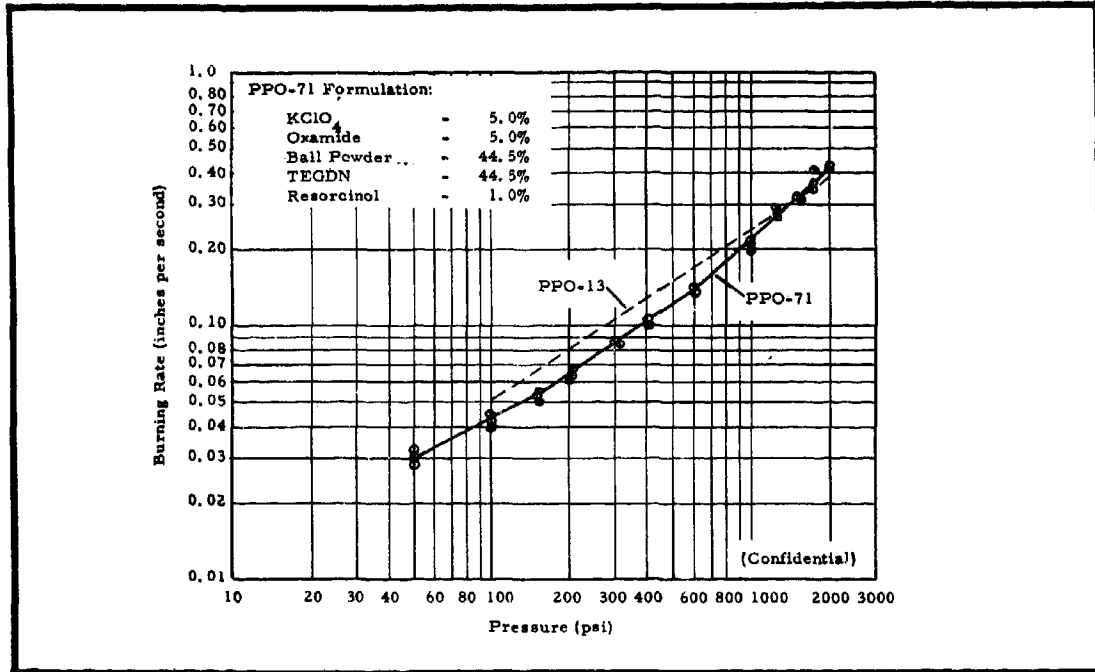


Figure 10 - Strand Burning-Rate Data for PPO-71 Propellant

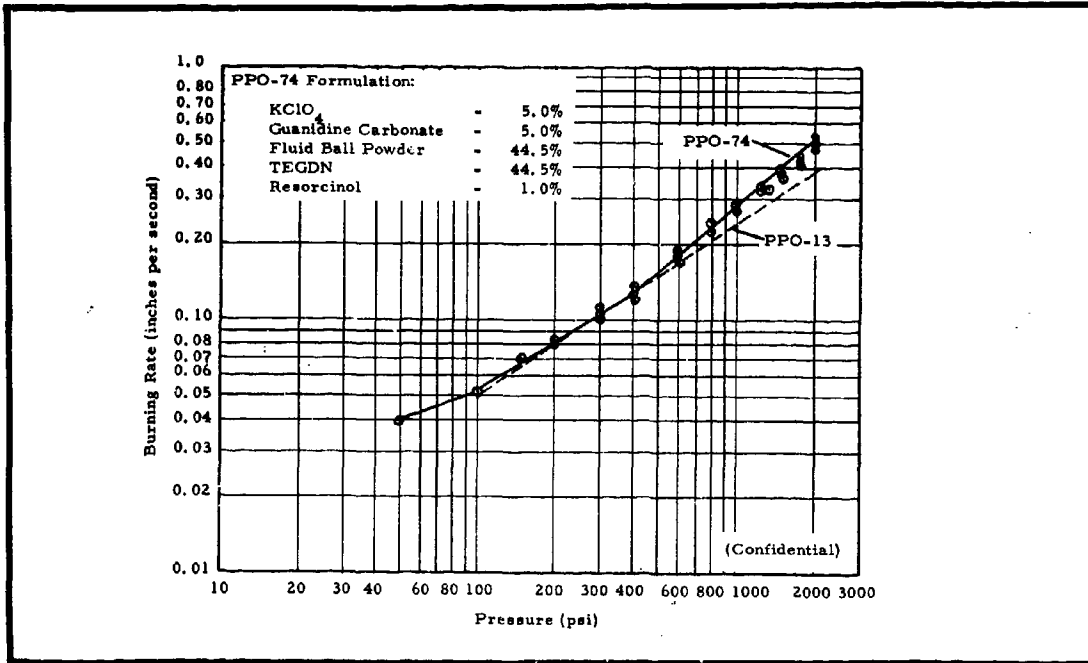


Figure 11 - Strand Burning-Rate Data for PPO-74 Propellant

# CONFIDENTIAL

**CONFIDENTIAL**

AFRPL-TR-65-209, Vol I

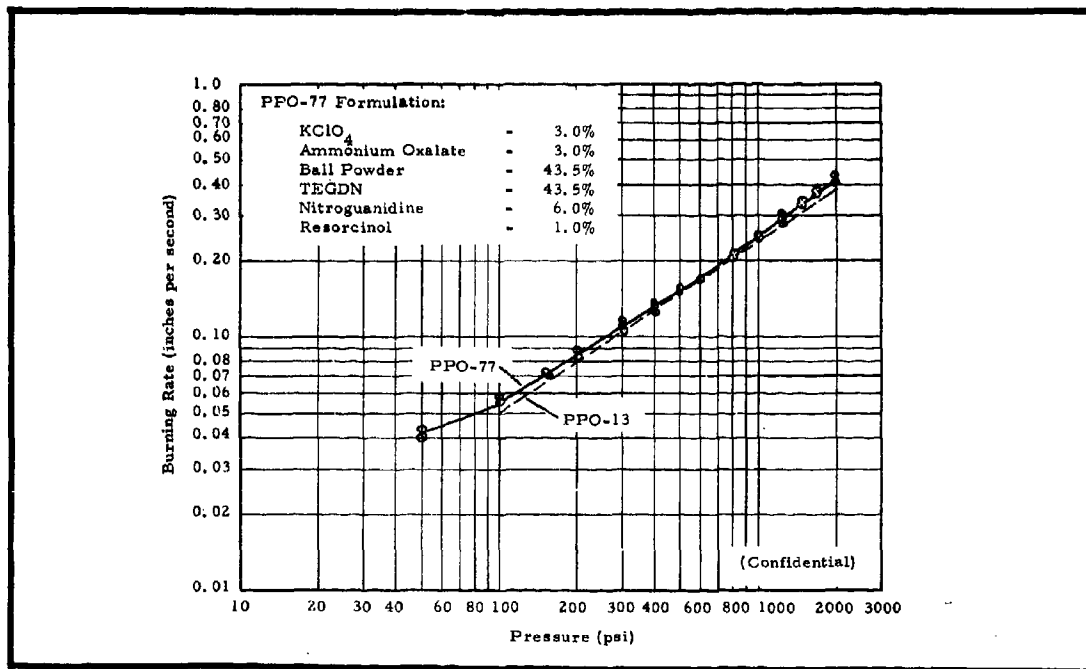


Figure 12 - Strand Burning-Rate Data for PPO-77 Propellant

undesirable, however. The addition of nitroguanidine to the potassium perchlorate in formulations PPO-75 and PPO-76 lowered the exponent at both high and low pressures as shown in Figures 7 and 8. The addition of HMX to the potassium perchlorate in formulation PPO-72 lowered the burning-rate slope slightly (see Figure 9). The effects of three coolants, oxamide, guanidine carbonate, and ammonium oxalate, were studied in potassium perchlorate formulations PPO-71, -74, and -77, respectively; the results are shown in Figures 10 through 12. The first two coolants decreased the undesirably high pressure exponent at high pressures without appreciably affecting the slope in the low-pressure range (see Figures 10 and 11). These results were very encouraging since coolants must be used with potassium perchlorate to keep the flame temperature below 3000°F. (Confidential)

The potassium perchlorate used in the preceding formulations had an average particle size of 50 microns. To determine the effect of particle size, 150-micron potassium perchlorate was used in formulations PPO-73, -82, and -83

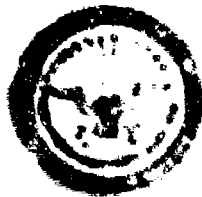
**CONFIDENTIAL**

AD 374 199

AUTHORITY:

AERPL

100 10 DEC 85



(Figures 13, 14, and 15). The exponent of 0.84 achieved for PPO-73 with 150-micron potassium perchlorate (Figure 13) is considerably higher than the exponent of 0.77 achieved previously for PPO-73 with 50-micron oxidizer (Figure 6 and Table III). However, extremely high exponents were achieved for both particle sizes at pressures above 600 psi, i. e., 1.0 and 0.95, respectively. (Confidential)

The coolant guanidine carbonate was again incorporated into the propellant (formulation PPO-74) and evaluated over the pressure range from 100 to 4500 psi. A constant exponent of 0.76 to 0.77 was achieved over this range (Figure 16). (Confidential)

g. HMX

The addition of HMX to the nitroplastisol binder in formulation PPO-70 increased the pressure exponent above 600 psi, as shown in Figure 17. However, the pressure exponent below 600 psi was slightly less than that of PPO-13. The addition of nitroguanidine as well as HMX, in formulation PPO-78, also produced a higher burning-rate slope in the low-pressure range (see Figure 18). This formulation had a mean slope of 0.74 between 100 and 2000 psi. (Confidential)

The effect of HMX particle size was studied by incorporating, separately, 6- and 500-micron HMX in the PPO-78 formulation. PPO-82, a formulation with 200-micron HMX, had previously been evaluated and found to have a 0.74 exponent between 100 and 2000 psi (Figure 14). Both the smaller and larger particle size HMX decreased the exponent (Figures 19 and 20). (Confidential)

The addition of ammonium oxalate (PPO-79) increased the exponent of HMX propellants, whereas triacetin had little effect (PPO-80, -81, and -97), as shown in Figures 21 through 24. PPO-80, with five percent triacetin, had an exponent of 0.75 (Figure 22) up to 2000 psi, compared with 0.74 for PPO-78, with 200-micron HMX but no triacetin. Nitroguanidine increased slightly the exponent of HMX formulations in the low-pressure range, as shown by a comparison of PPO-80 with PPO-81 (Figures 22 and 23). (Confidential)

# CONFIDENTIAL

AFRPL-TR-65-209, Vol I

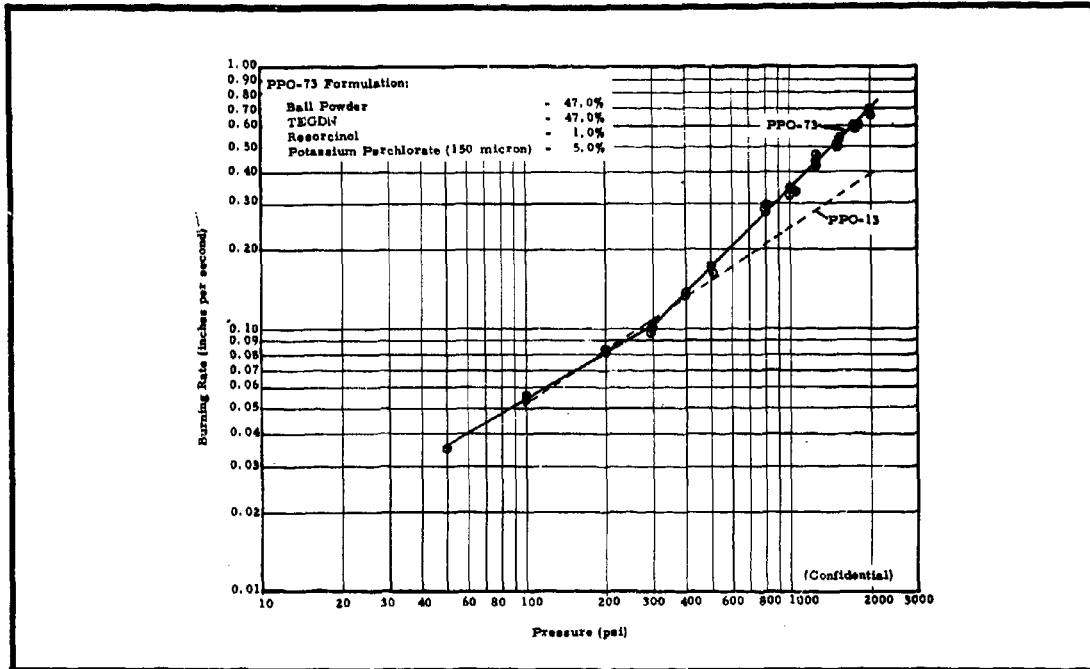


Figure 13 - Strand Burning-Rate Data for PPO-73 Propellant (150-Micron Potassium Perchlorate)

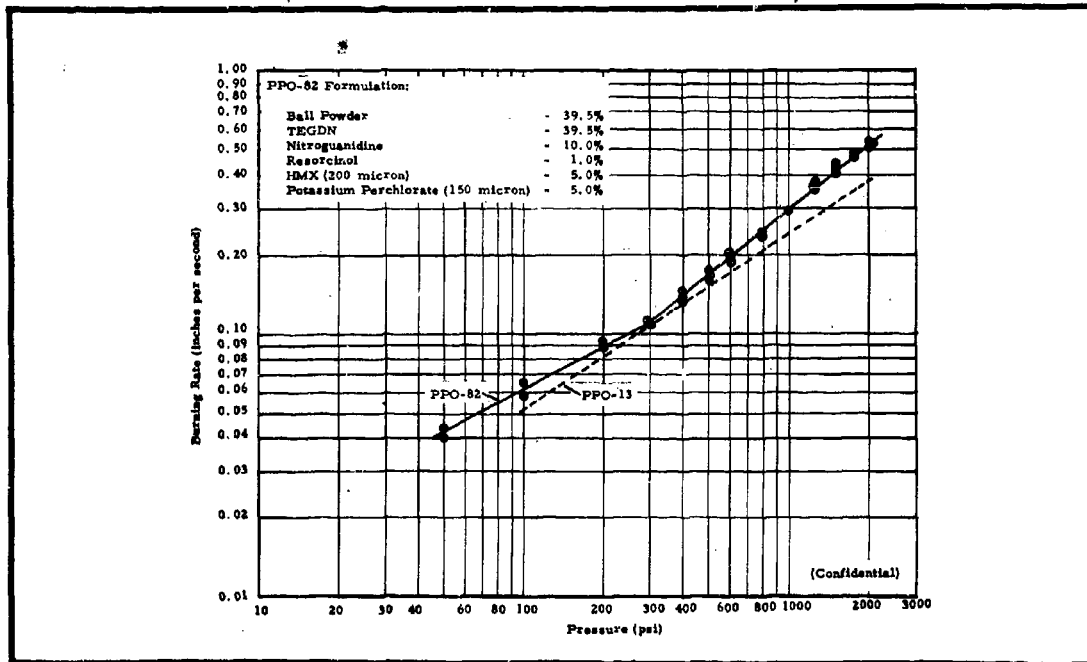


Figure 14 - Strand Burning-Rate Data for PPO-82 Propellant

# CONFIDENTIAL

AFRPL-TR-65-209, Vol I

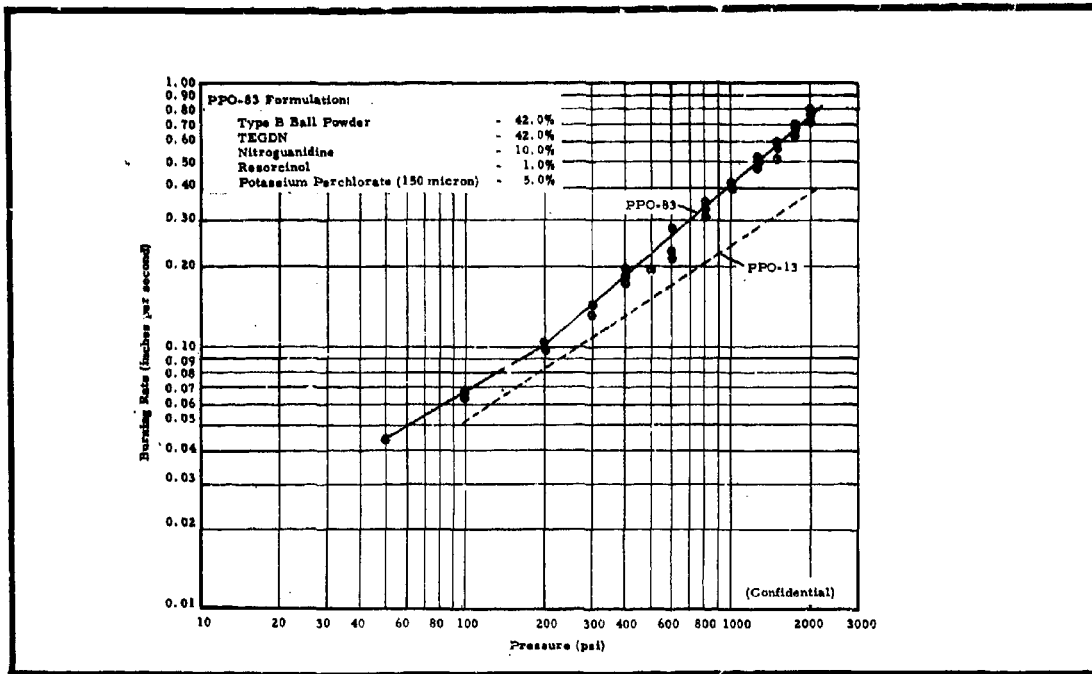


Figure 15 - Strand Burning-Rate Data for PPO-83 Propellant

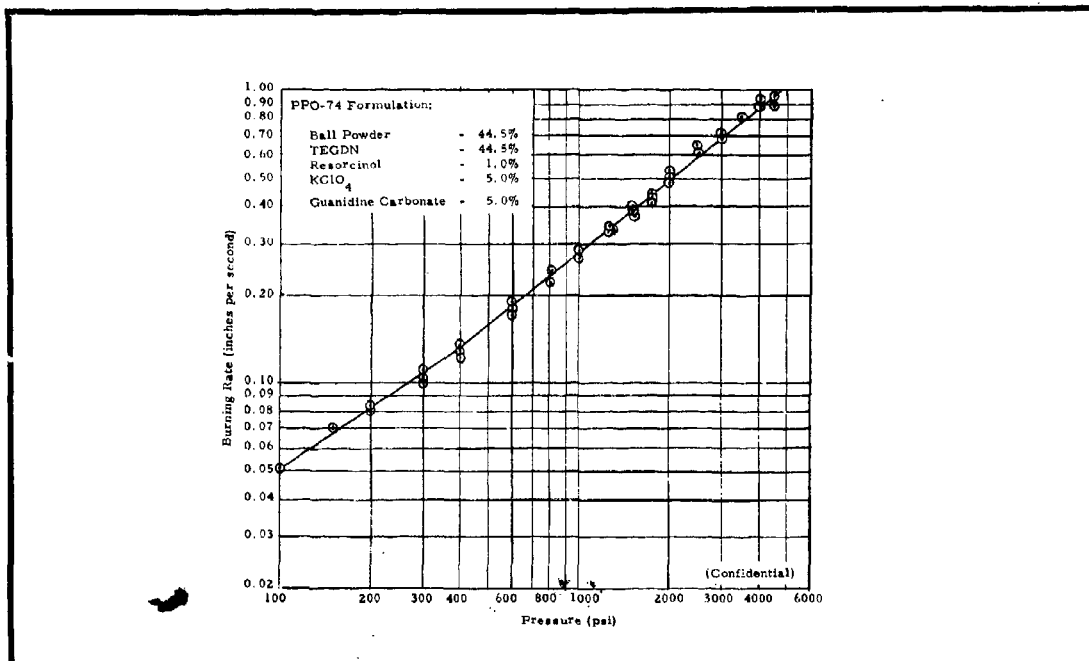


Figure 16 - Strand Burning-Rate Data for PPO-74 Propellant  
(100 to 4500 psi)

# CONFIDENTIAL

# CONFIDENTIAL

AFRPL-TR-65-209, Vol I

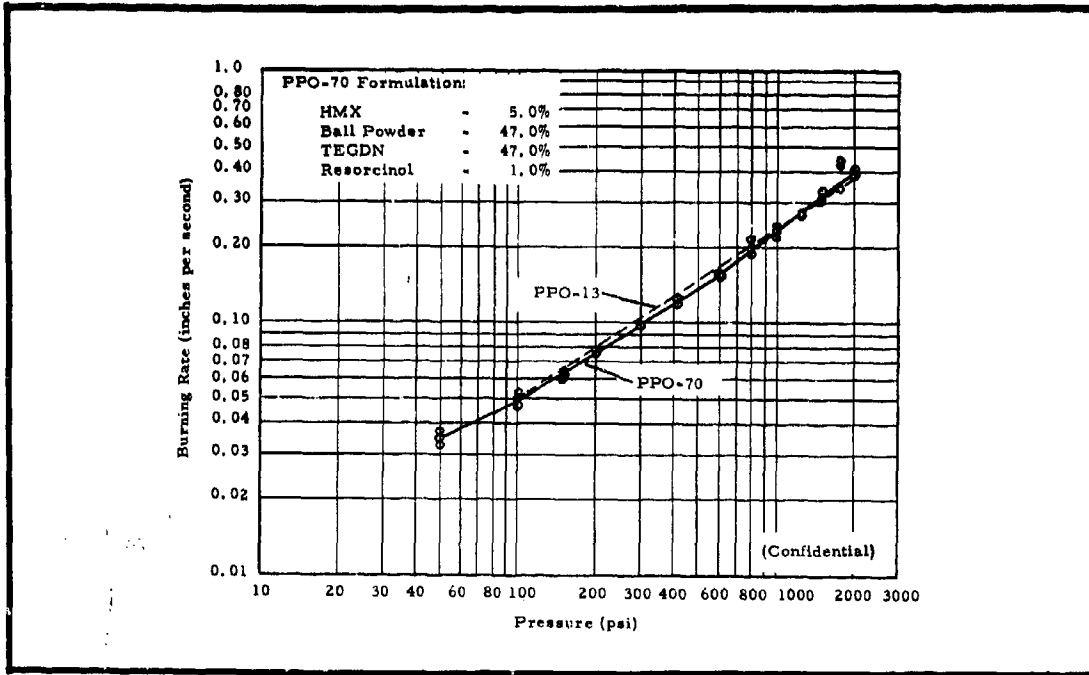


Figure 17 - Strand Burning-Rate Data for PPO-70 Propellant

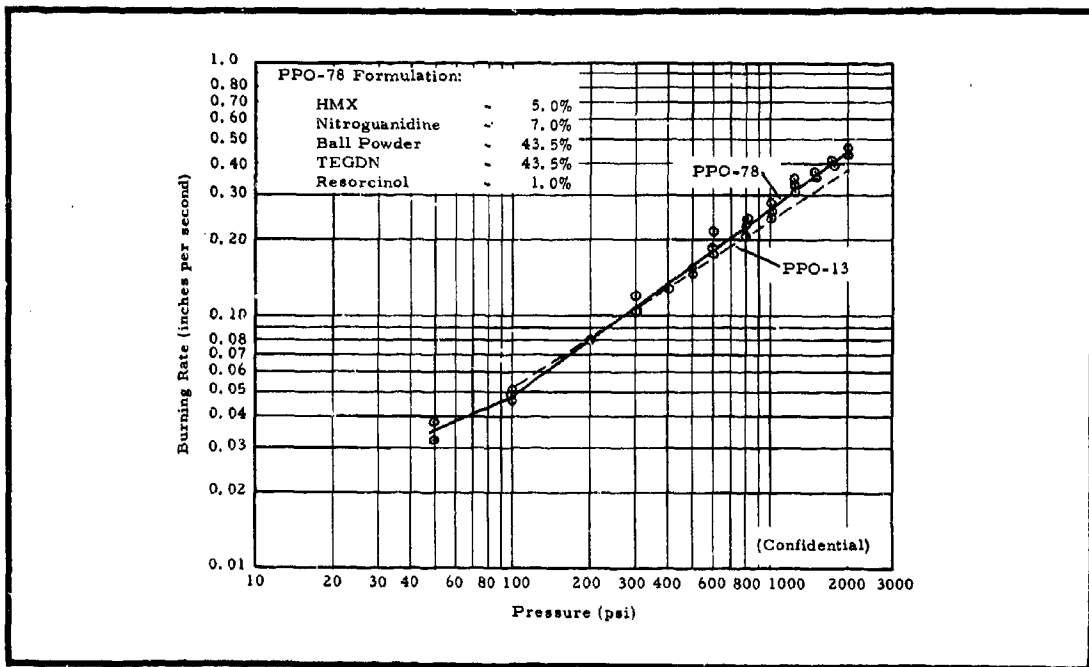


Figure 18 - Strand Burning-Rate Data for PPO-78 Propellant

# CONFIDENTIAL

AFRPL-TR-65-209, Vol I

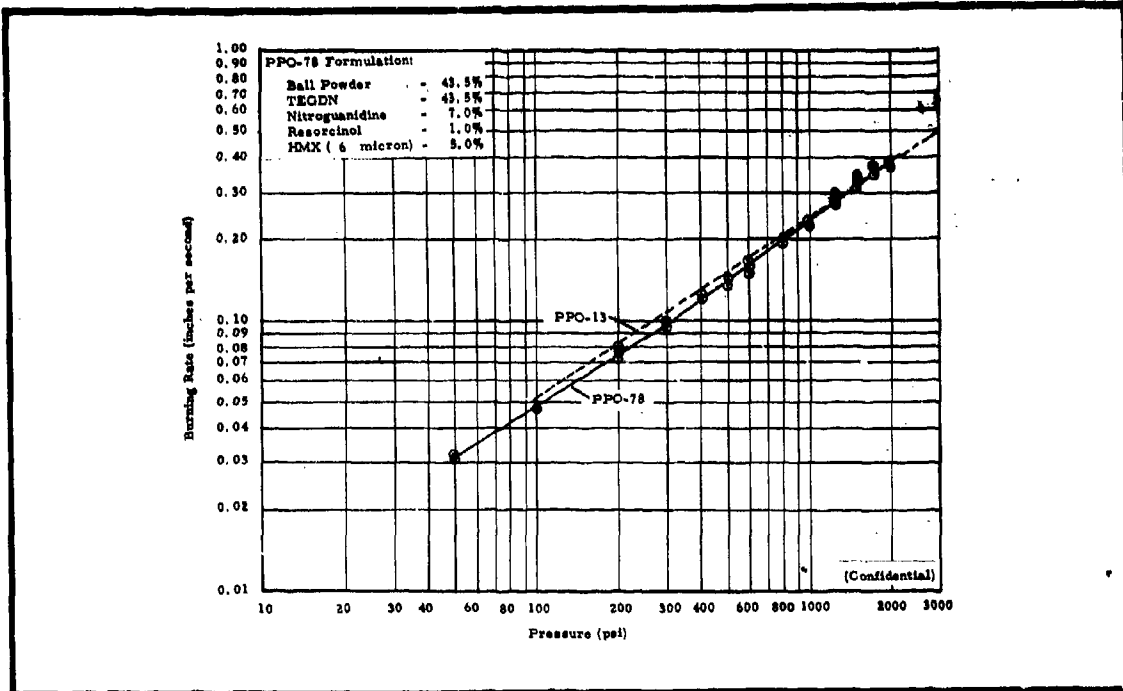


Figure 19 - Strand Burning-Rate Data for PPO-78 Propellant (Six-Micron HMX)

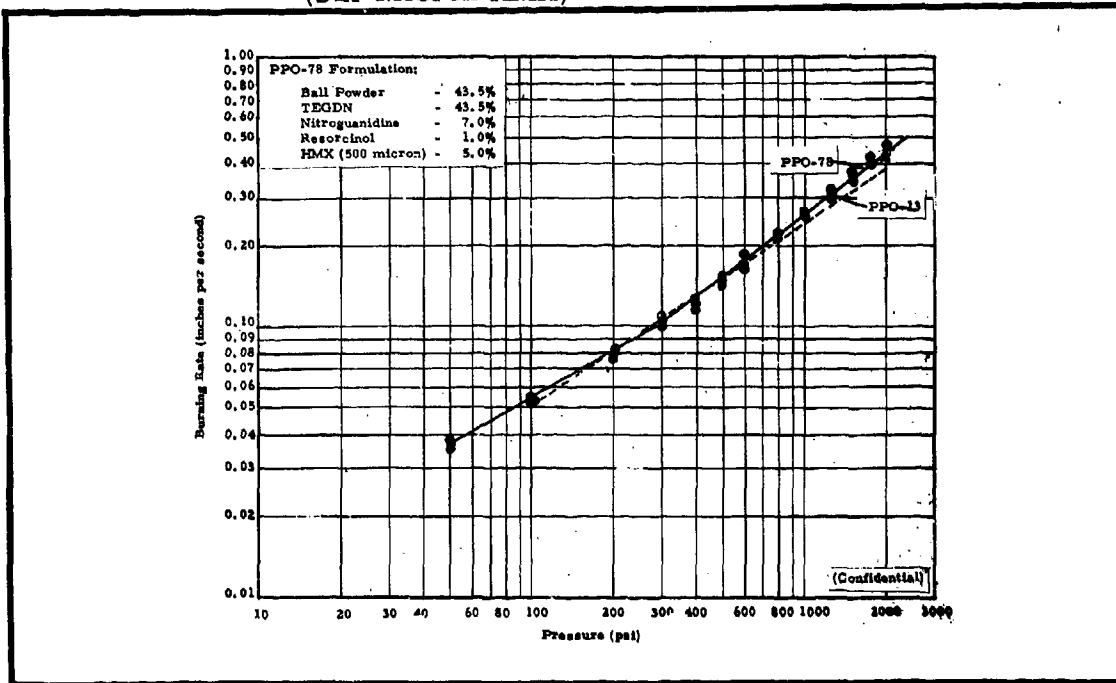


Figure 20 - Strand Burning-Rate Data for PPO-78 Propellant (500-Micron HMX)

CONFIDENTIAL

**CONFIDENTIAL**

AFRPL-TR-65-209, Vol I

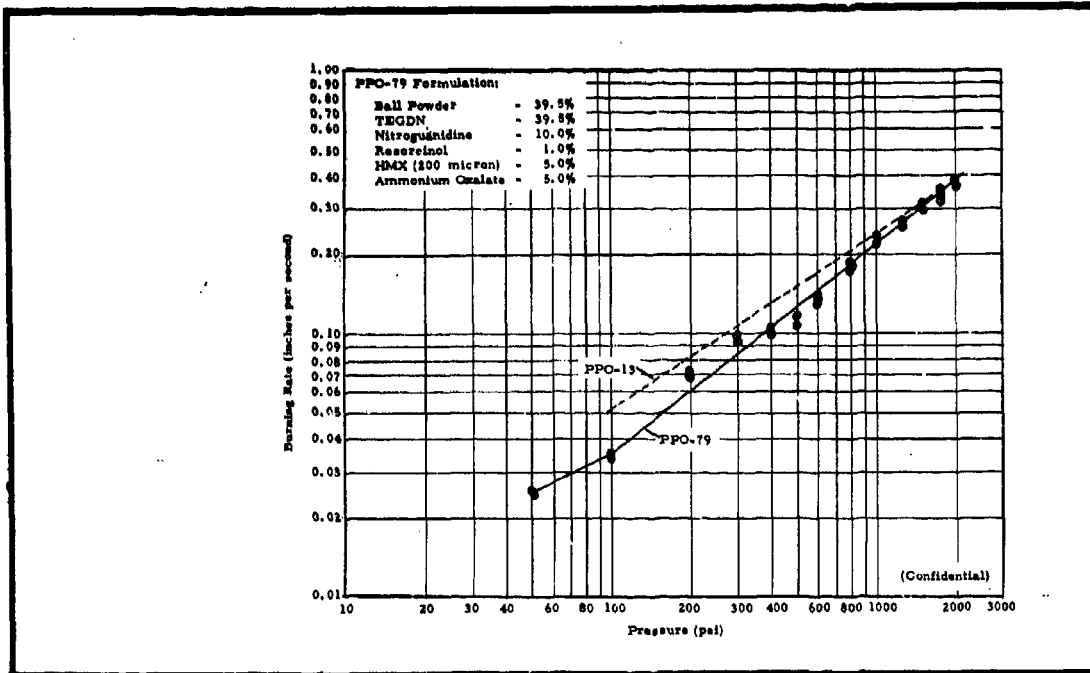


Figure 21 - Strand Burning-Rate Data for PPO-79 Propellant

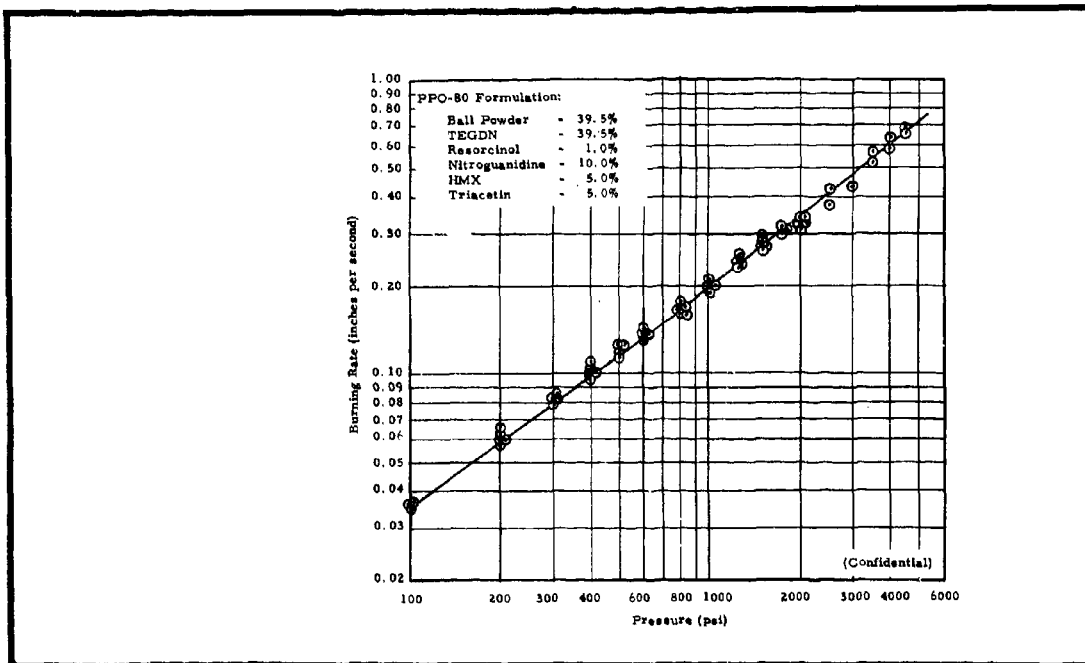


Figure 22 - Strand Burning-Rate Data for PPO-80 Propellant

**CONFIDENTIAL**

# CONFIDENTIAL

AFRPL-TR-65-209, Vol I

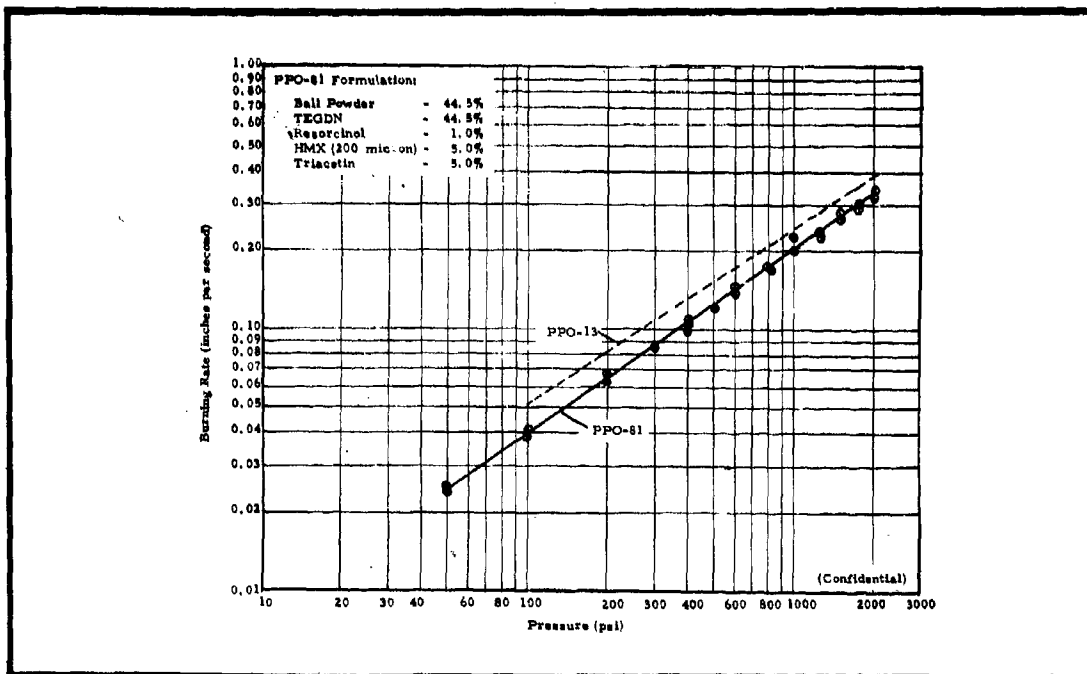


Figure 23 - Strand Burning Rate Data for PPO-81 Propellant

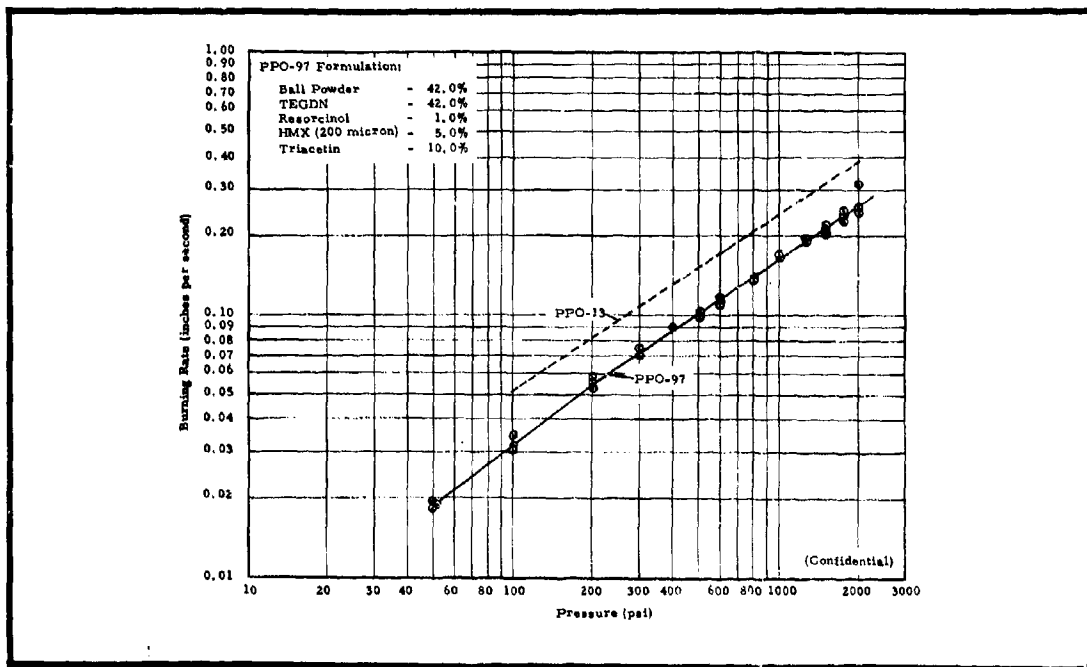


Figure 24 - Strand Burning-Rate Data for PPO-97 Propellant

CONFIDENTIAL

On the basis of the favorable results obtained with PPO-80, it was evaluated over the range from 100 to 4500 psi. The exponent increased from 0.75, for the 100- to 2000-psi range, to 0.77 for the entire pressure range. (Confidential)

Of the two additives, HMX and potassium perchlorate, HMX is much preferred from the standpoint of specific impulse and the desirability of solid-free exhaust. Each of the formulations was burned at pressures down to 50 psi to evaluate the low-pressure combustion properties, and each formulation produced less residual char at low pressures than PPO-13. (Confidential)

h. Coolants

The addition of oxamide to the nitroplastisol binder significantly increased the pressure exponent, which increased with increasing concentration of oxamide (Figures 25 and 26). The amount of residue at low pressures increased with oxamide content, although with five percent oxamide (PPO-90), the residue at 50 psi was very small. The addition of oxamide as well as the other coolants, ammonium oxalate and triacetin, reduced the burning rate compared to that of the binder alone or to PPO-13. (Confidential)

The addition of 10 percent ammonium oxalate increased the pressure exponent to 0.83 (PPO-91), whereas at the 5 percent level (PPO-92), little effect was observed (Figures 27 and 28). For the 10 percent ammonium oxalate formulation, the strand inhibitor apparently lowered the measured burning rate below 400 psi. Uninhibited strands gave a better fit with the data at higher pressures (Figure 28). (Confidential)

The addition of triacetin at the 5 and 10 percent levels lowered the overall burning rate compared to binder alone, but had little effect on pressure exponent (Figures 29 and 30). (Confidential)

i. Conclusions

Note that formulations PPO-90, PPO-92, and PPO-93 were evaluated up to 4500 psi. These three formulations, along with PPO-80, PPO-74, and the basic PPO-13 formulation, were the ones evaluated over the full 100- to 4500-psi pressure range.

**CONFIDENTIAL**

AFRPL-TR-65-209, Vol I

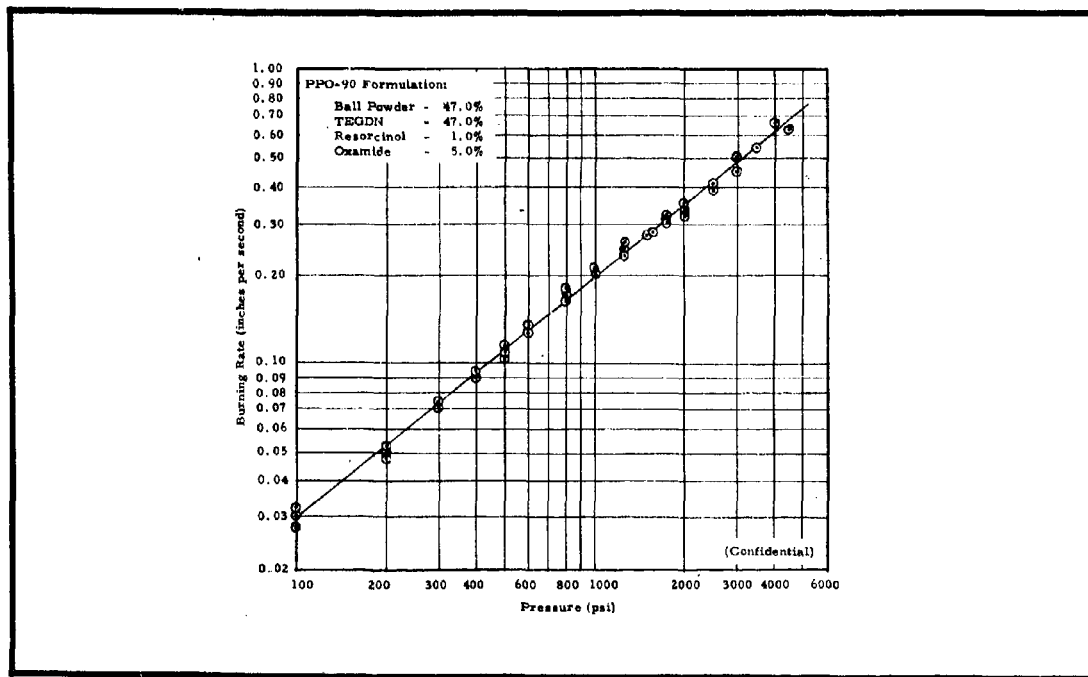


Figure 25 - Strand Burning-Rate Data for PPO-90 Propellant

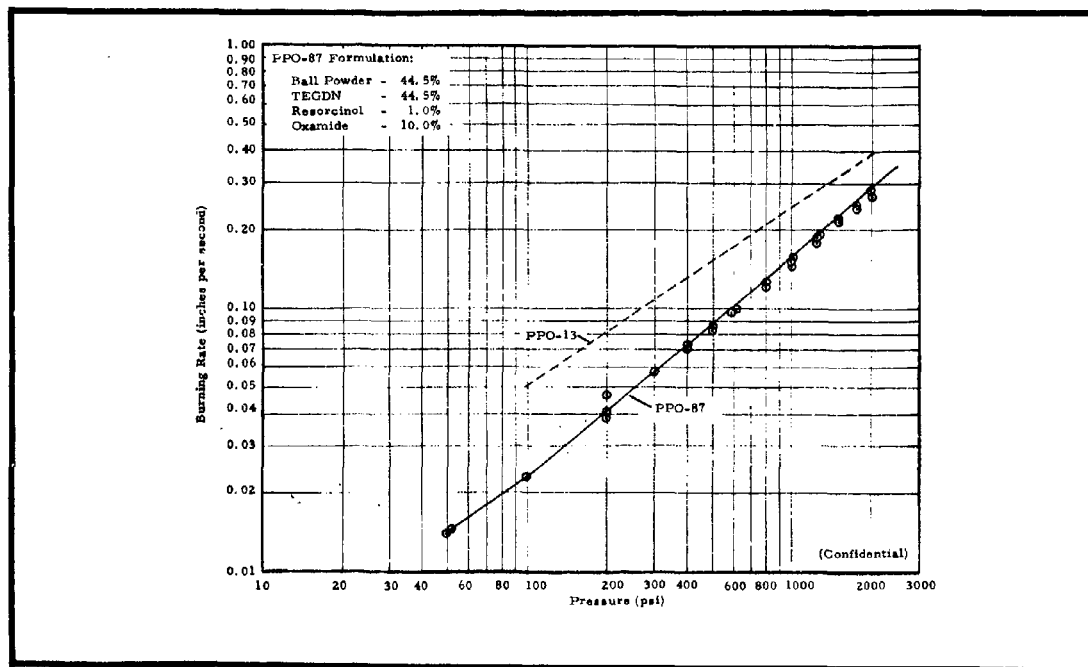


Figure 26 - Strand Burning-Rate Data for PPO-87 Propellant

**CONFIDENTIAL**

# CONFIDENTIAL

AFRPL-TR-65-209, Vol I

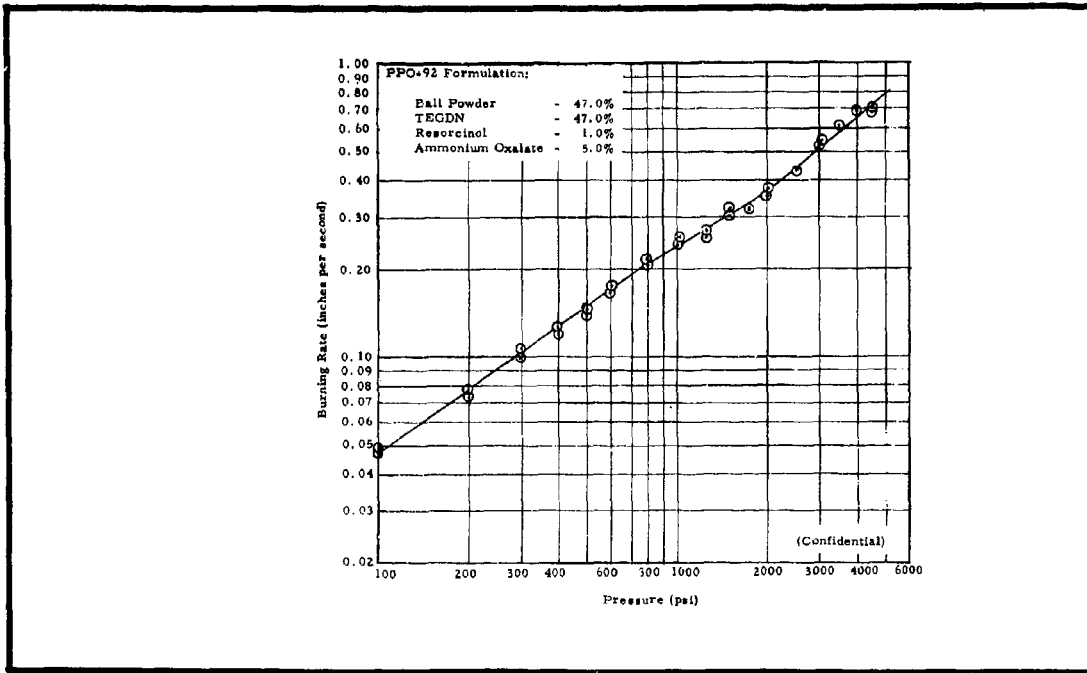


Figure 27 - Strand Burning-Rate Data for PPO-92 Propellant

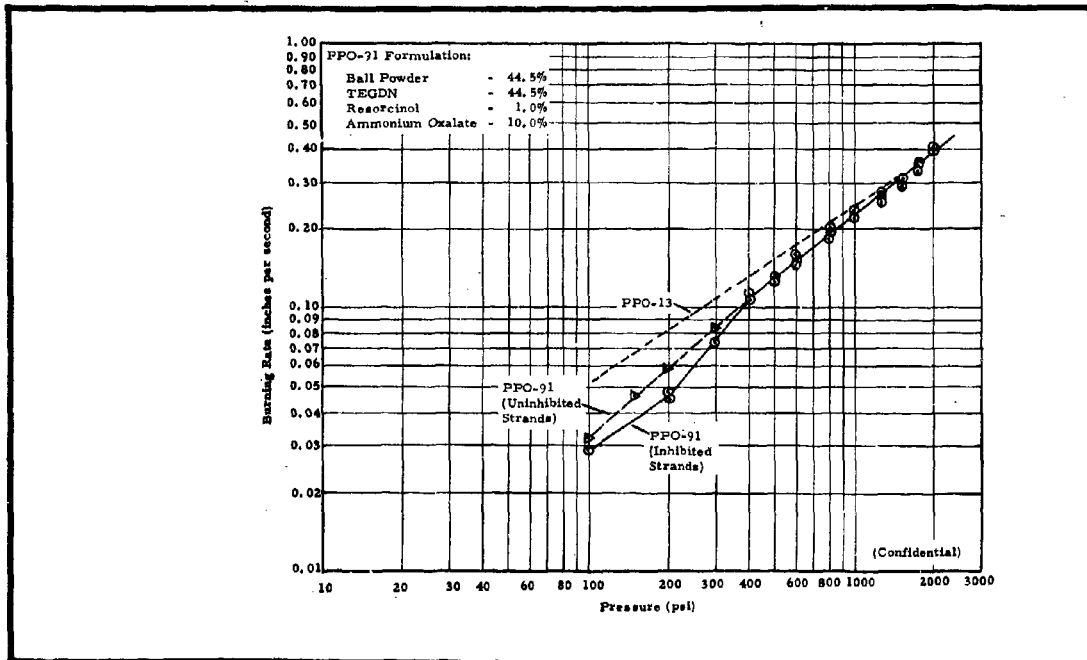


Figure 28 - Strand Burning-Rate Data for PPO-91 Propellant

# CONFIDENTIAL

# CONFIDENTIAL

AFRPL-TR-65-209, Vol I

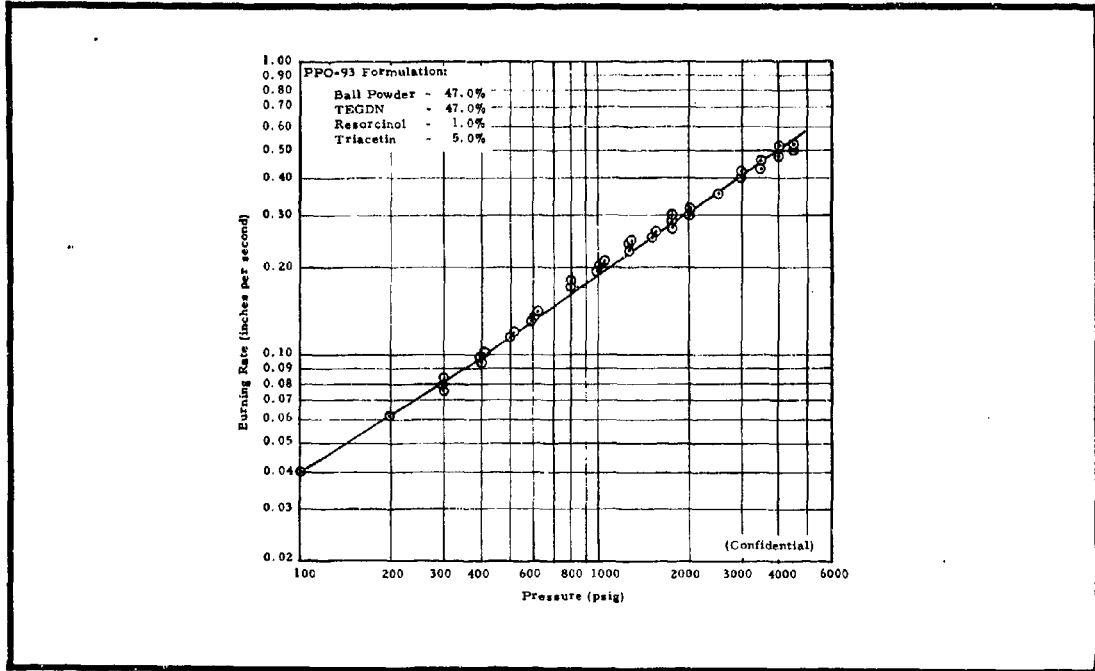


Figure 29 - Strand Burning-Rate Data for PPO-93 Propellant

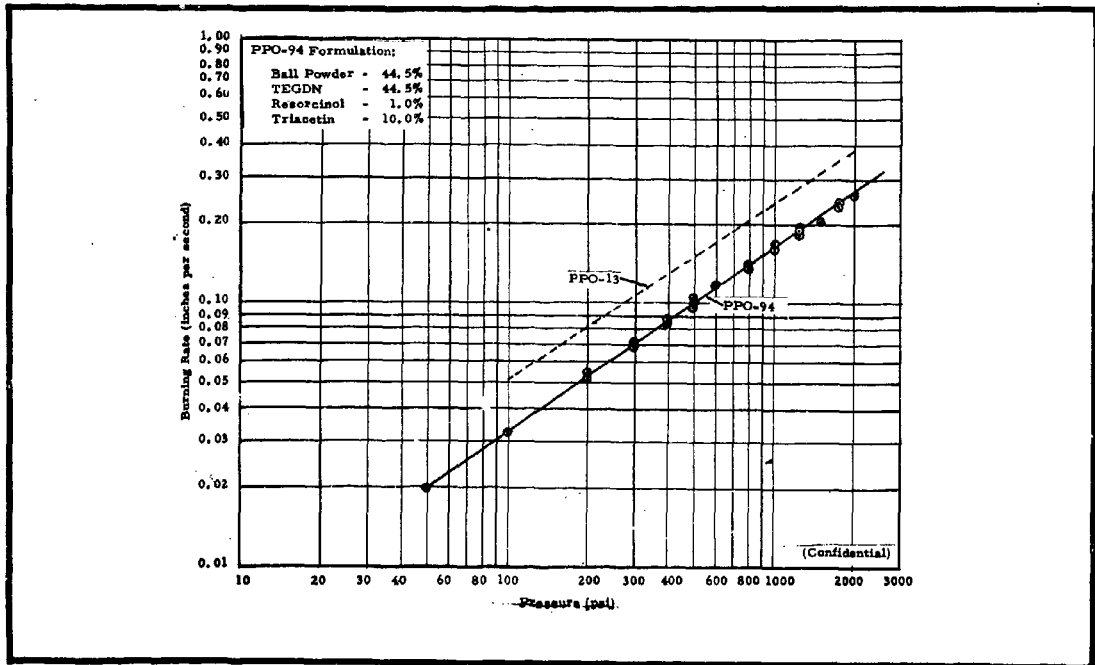


Figure 30 - Strand Burning-Rate Data for PPO-94 Propellant

# CONFIDENTIAL

On the basis of the results of the foregoing evaluation, formulations PPO-80 and PPO-90 were selected for further evaluation in motor tests. These formulations exhibited constant pressure exponents of 0.77 and 0.82, respectively, over the range of 100 to 4500 psi. The tests are described in 3, below. (Confidential)

### 3. MOTOR TESTING

The forward-grain formulations (PPO-80 and PPO-90) were evaluated in two types of test motors: a 4.25-in. -diameter "pancake" motor and a 2-in. -diameter test motor. The pancake motor, which had an end-burning grain 4.25-in. in diameter, was used primarily for termination studies since the ratio of free volume to burning surface area could be varied over a wide range. Burning rates could also be obtained from this motor. The 2-in. test motor had an internal-burning cylindrical grain, 7-in. long, with a 1.5-in. I.D. and a 1.94-in. O.D. This motor was used to obtain P-K-r and  $C^*$  data.

Table IV presents termination data for the first three Series J termination tests, J. 1 through J. 3, for which the pancake motor was used. A PPO-90 grain was extinguished five consecutive times without reignition in Test J. 1. A PPO-80 grain reignited after the second termination in Test J. 2. In Test J. 3, also with PPO-80, the chamber pressure was increased and two successful terminations were achieved. From these tests, PPO-90 appeared to be superior to PPO-80 in termination capability since the latter reignited more readily. (Confidential)

Table V summarizes all Series J test data for both propellant formulations, and includes the termination tests. The motor burning rates for both formulations agreed closely with the rates determined in strand tests. In Figure 31, the motor burning-rate data for PPO-90 are plotted as a function of pressure. The pressure exponent, based on these data, using least squares, was 0.81. The strand burning rate is shown as a dashed line. The burning rate point in greatest disagreement with strand data was for Test J. 11 in which the mandrel was off-center at one end of the motor. This condition caused premature burnout on one side of the case and a long tailoff, resulting in an erroneously high burning-rate measurement. (Confidential)

Since the motor burning rate for PPO-90 correlated with strand data, giving a pressure exponent in the desired range (0.80 to 0.82), it was selected as the forward-grain propellant. This formulation was completely characterized, as described in 4, below. (Confidential)

**CONFIDENTIAL**

AFRPL-TR-65-209, Vol I

TABLE IV - SUMMARY OF INITIAL SERIES J TERMINATION TESTS†

Test # No.	Propellant Formulation	$V_f/S_b$	$L^*$ ( $V_f/A_t$ )	Termination Pressure, $P_c^{term}$ (psia)	Pressure Decay Rate, ( $dp/dt$ ), 75% (psia/sec)	Reignition
J. 1. 1	PPO-90	0. 823	25. 4	1277	445, 000	No
J. 1. 2	PPO-90	0. 930	28. 6	542	199, 000	No
J. 1. 3	PPO-90	0. 995	30. 8	522	198, 000	No
J. 1. 4	PPO-90	1. 110	34. 3	736	248, 000	No
J. 1. 5	PPO-90	1. 250	38. 4	529	123, 000	No
J. 2. 1	PPO-80	0. 755	23. 3	757	363, 000	No
J. 2. 2	PPO-80	0. 920	28. 3	683	271, 000	Yes
J. 3. 1	PPO-80	0. 805	25. 0	1090	550, 000	No
J. 3. 2	PPO-80	1. 082	33. 7	1871	713, 000	No

† Symbols are defined as follows:  $V_f$  = Chamber free volume;  $S_b$  = Propellant surface area; and  $A_t$  = Throat area.

‡ Ballistic data for these tests are given in Table V.

(Confidential)

**CONFIDENTIAL**

**CONFIDENTIAL**

AFRPL-TR-65-209, Vol I

TABLE V - SUMMARY OF SERIES J TESTS (J.1 THROUGH J.11)

Test No.	Type Motor	Date Fired	Propellant Formulation	A <sub>t</sub> (sq in.)	K <sub>n</sub>	t <sub>b</sub> (sec)	T <sub>b</sub> (in. sec)	P <sub>b</sub> (psia)	P <sub>k</sub> (psia)	C* (fps)
J. 1.1 <sup>‡</sup>	Pancake	7/16/64	PPO-90	0.0176	..	0.924	0.204	974	..	..
J. 1.2 <sup>‡</sup>	Pancake	7/17/64	PPO-90	0.0188	..	0.940	0.095	411	..	..
J. 1.3 <sup>‡</sup>	Pancake	7/17/64	PPO-90	0.0165	..	0.549	0.090	412	..	..
J. 1.4 <sup>‡</sup>	Pancake	7/17/64	PPO-90	0.0175	..	0.768	0.129	597	..	..
J. 1.5 <sup>‡</sup>	Pancake	7/17/64	PPO-90	0.0196	..	0.970	0.111	517	..	..
J. 1.6 <sup>‡</sup>	Pancake	7/20/64	PPO-90	0.0190	..	2.329	0.118	477	..	..
J. 2.1 <sup>‡</sup>	Pancake	7/17/64	PPO-80	0.0171	..	0.947	0.141	669	..	..
J. 2.2 <sup>‡</sup>	Pancake	7/17/64	PPO-80	0.0186	..	0.986	..	680	..	..
J. 3.1 <sup>‡</sup>	Pancake	7/20/64	PPO-80	0.0157	..	1.068	0.163	846	..	..
J. 3.2 <sup>‡</sup>	Pancake	7/20/64	PPO-80	0.0142	..	1.057	0.214	1173	..	..
J. 4	2 in.	7/24/64	PPO-90	0.0527	713	1.146	0.192	846	780	4051
J. 5	2 in.	7/24/64	PPO-90	0.0460	815	0.709	0.310	1609	1545	4342
J. 6	2 in.	7/24/64	PPO-90	0.0426	878	0.637	0.345	2006	2030	2155
J. 7	2 in.	7/24/64	PPO-90	0.0403	931	0.537	0.375	2320	2390	4446
J. 8 <sup>•</sup>	2 in.	7/30/64	PPO-90	0.0661	567	..	..	..	..	..
J. 9	2 in.	7/30/64	PPO-90	0.0558	672	1.070	0.210	894	..	4206
J. 10	2 in.	7/30/64	PPO-90	0.0373	1005	0.423	0.532	3353	..	4273
J. 11 <sup>§</sup>	2 in.	7/30/64	PPO-90	0.0558	672	0.956	0.235	869	..	4183

<sup>†</sup>The pancake motor was a propellant termination evaluation motor (Reference 7, Figure 18); the two-inch motor was a standard ballistic evaluation motor.

<sup>‡</sup>A small leak occurred, making it impossible to determine A<sub>t</sub>. Therefore, K<sub>n</sub> and C\* could not be calculated from acquired data.

<sup>•</sup>Motor reignited following termination.

<sup>•</sup>Two unsuccessful ignition attempts were made.

<sup>§</sup>Data for remaining Series J tests are given in Tables VIII and IX.

(Confidential)

**CONFIDENTIAL**

AFRPL-TR-65-209, Vol I

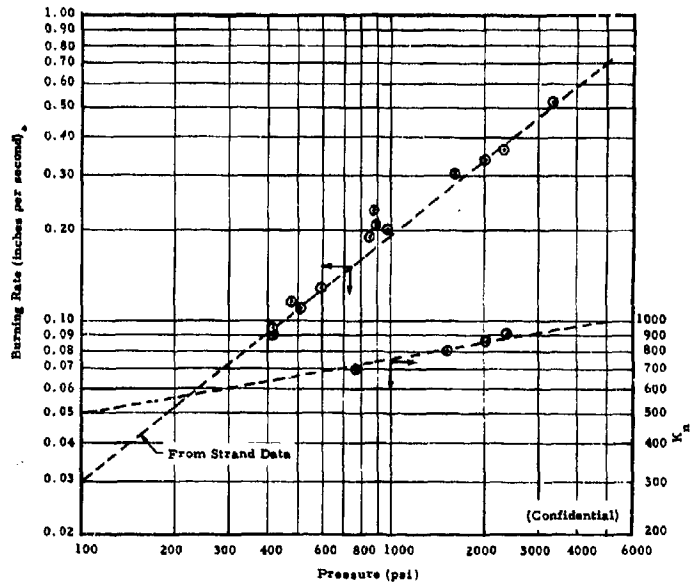


Figure 31 - P-K-r Data for PPO-90 Obtained from Motor Tests

**CONFIDENTIAL**

4. FINAL CHARACTERIZATION OF PPO-90

a. General

As indicated in paragraph 3, above, forward-grain propellant formulation PPO-90 was selected for use in the Series N motors (see Section VII) on the basis of its desirable pressure exponent and other characteristics. The characterization of PPO-90 was then completed through continued laboratory evaluation and subscale motor tests.

b. Laboratory Evaluation

The characterization of PPO-90 in the laboratory was completed by obtaining strand burning rates and measuring the physical properties at  $-40^{\circ}$ ,  $77^{\circ}$ , and  $140^{\circ}$ F. The results of these studies are presented in Table VI, which also presents the properties of PPO-13 for comparison; the composition of both formulations is also given. As shown, burning-rate characteristics, mechanical properties, and flame temperature of PPO-90 are superior to those of PPO-13. (Confidential)

The program goals for the forward-grain propellant are given in Table VII, along with the corresponding characteristics of PPO-90. Note that PPO-90 meets or exceeds all program goals except space storability, which was considered to be a desirable characteristic rather than a requirement. (Confidential)

c. Motor Testing

Four burning-rate motors containing PPO-90 propellant were fired; two of these were pancake motors, and two were six-inch test motors. The results of these tests are presented in Table VIII. The two pancake motors were used to obtain data at low pressures since these motors, which have a large (10 to 1) ratio of free chamber volume to propellant surface area, permit ignition at low pressures. The two six-inch motors were also tested primarily to obtain P-k data. However, propellant batch N-77, from which these motors were loaded, exhibited a lower strand burning rate than previous PPO-90 batches. The motor burning rates obtained from this batch (Tests J. 16 and J. 17) were also low, as shown in Figure 32.

TABLE VI-PROPERTIES OF PPO-13 AND PPO-90 PROPELLANTS

Parameter	Formulation	
	PPO-13	PPO-90
Composition (percent by weight)		
Fluid ball powder	43.5	47.0
TEGDN	43.5	47.0
Resorcinol	1.0	1.0
Nitroguanidine	12.0	...
Oxamide	...	5.0
Burning rate data		
Burning rate at 1000 psi (in./sec)	0.25	0.20
Pressure index (100 psi to 4500 psi)	0.67	0.82
Temperature coefficient of rate (%/°F)	0.35	0.27
Mechanical properties		
140°F		
Maximum stress (psi)	93	113
Strain at maximum stress (in./in.)	0.50	1.09
Modulus (psi)	6.60	501
77°F		
Maximum stress (psi)	164	177
Strain at maximum stress (in./in.)	0.52	1.00
Modulus (psi)	1230	760
-40°F		
Maximum stress (psi)	2070	1890
Strain at maximum stress (in./in.)	0.08	0.19
Modulus (psi)	10,300	9920
Density (lb/cu in.)	0.0535	0.0530
Shore A hardness	56	50
Five-second autoignition temperature (°F)	400	401
Drop sensitivity with 2-kg weight, 50% fire (cm)	80.6	77.7
Flame temperature (°F)	2980	2700

(Confidential)

**CONFIDENTIAL**

TABLE VII-COMPARISON OF PPO-90 PROPELLANT PROPERTIES WITH  
FORWARD PROPELLANT GOALS

Program Goals for Forward Propellant	PPO-90 Properties
Capable of being extinguished by rapid pressure decay at sea level	Extinguishment characteristics are similar to those of PPO-13
Flame temperature less than 3000° F	Flame temperature of 2700° F
Low percentage of solids in combustion products	No solids or liquids exist in combustion products at either chamber or throat conditions
Burning-rate pressure index between 0.7 and 0.9 over pressure range from 100 to 4500 psi	Pressure index of 0.82 from 100 psi to 4500 psi measured with strands; index of 0.81 from 150 psi to 3350 psi measured in test motors
Castable propellant, with mechanical properties comparable to state-of-the-art formulations	Castable propellant with superior mechanical properties (see Table VI)
Delivered vacuum specific impulse of 280 lb-sec/lb in combination with aft propellant	Theoretically capable of delivering 280 lb-sec/lb in combination with an aft propellant containing HNF, with 93% efficiency
Space storable	Propellant is not space storable

(Confidential)

**CONFIDENTIAL**

**CONFIDENTIAL**

AFRPL-TR-65-209, Vol I

TABIE VIII-SUMMARY OF SERIES J. BURNING-RATE TESTS WITH PPO-90 PROPELLANT

Test No. <sup>†</sup>	Date Fired	Motor Type	Batch Number	Throat Area, $A_t$ (in. <sup>2</sup> )	$K_n$	$t_b$ (sec)	$\bar{r}_b$ (in./sec)	$\bar{P}_b$ (psia)	$\bar{P}_k$ (psia)	$C^*$ (fps)
J. 12	8/8/64	Pancake	E-106	0.0215	660	6.514	0.139	577	602	3922
J. 13	8/8/64	Pancake	E-108	0.0255	554	19.824	0.0438	151	134	3495
J. 16	8/13/64	6-inch	N-77	0.2376	799	8.939	0.0610	306	313	3545
J. 17	8/12/64	6-inch	N-77	0.1886	1010	2.026	0.259	1698	1778	4045

<sup>†</sup>Data for Tests J. 14 and J. 15 are presented in Table IX.

(Confidential)

**CONFIDENTIAL**

# CONFIDENTIAL

AFRPL-TR-65-209, Vol I

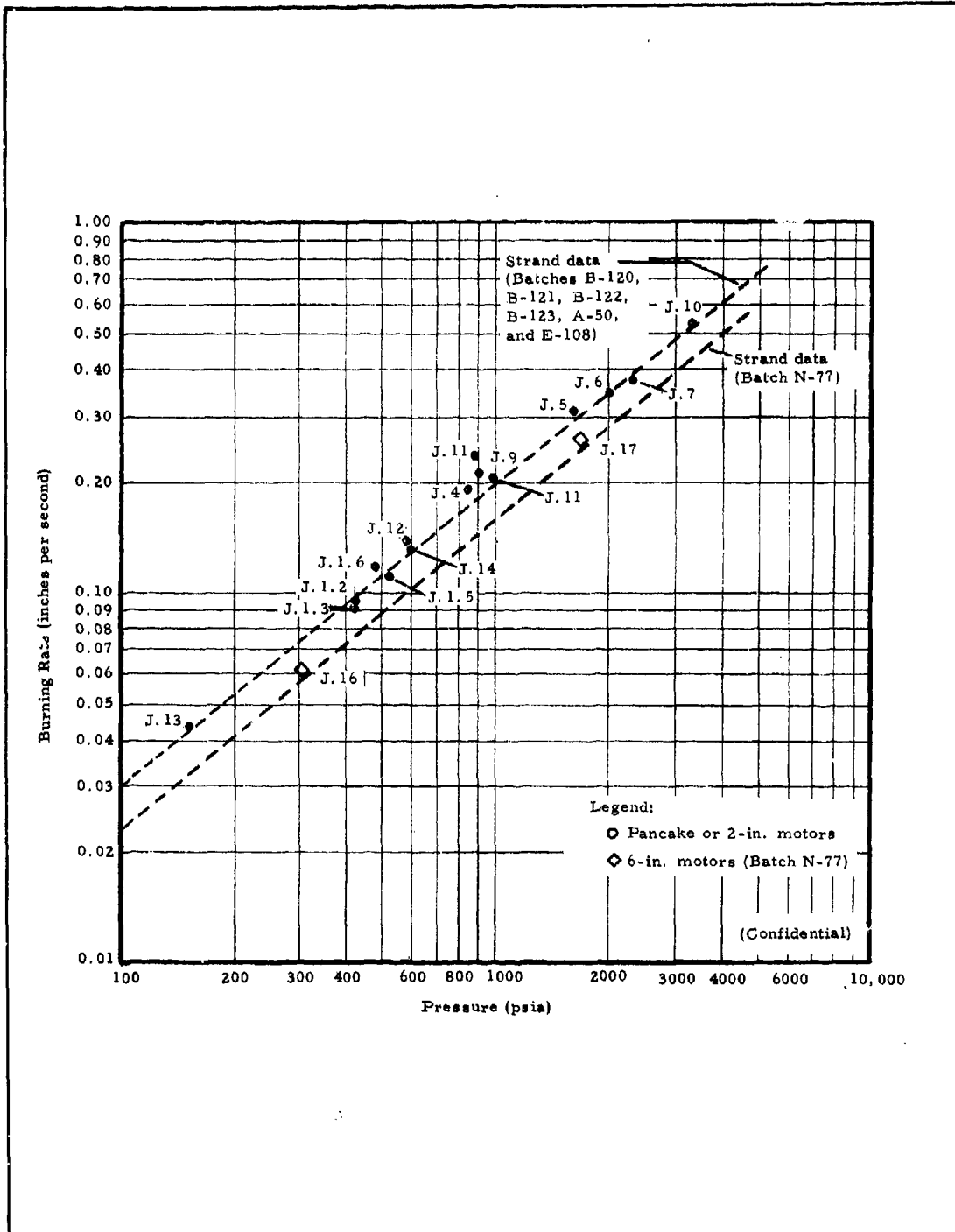


Figure 32 - Burning Rate Data for PPO-90 Propellant from Series J Tests

# CONFIDENTIAL

Table IX summarizes the reignition tests using PPO-90 propellant (J. 14 and J. 15). The ratio of free chamber volume to propellant surface area was progressively increased from cycle to cycle until reignition occurred spontaneously. Since the motor used in Test J. 14 contained a batch of normal PPO-90, whereas the motor used in J. 15 contained propellant from Batch N-77 with low burning rate, the data are not consistent. However, they show that PPO-90 reignites at a slightly higher free-volume-to-surface-area ratio, at a given termination pressure, than PPO-13 propellant. (Confidential)

**CONFIDENTIAL**

AFRPL-TR-65-209, Vol I

TABLE IX - SUMMARY OF SERIES J REIGNITION TESTS WITH PPO-90 PROPELLANT\*

Test No.	Date Fired	Batch Number	$V_f/S_b$ (in.)	$V_f/A_t$ (in.)	Termination Pressure, $P_c$ term (psia)	Pressure Decay Rate, (dp/dt), 75% (psi/sec)	Reignition Occurred
J. 14.1 <sup>†</sup>	8/17/64	N-77	...	...	...	...	...
J. 14.2	8/27/64	A-50	2.40	74.0	1125	162,000	No
J. 14.3	8/27/64	A-50	2.54	78.3	1248	170,000	No
J. 14.4	8/27/64	A-50	2.67	82.5	1262	167,000	Yes
J. 15.1	8/12/64	N-77	1.77	54.6	357	94,900	No
J. 15.2	8/12/64	N-77	1.84	56.9	419	103,000	No
J. 15.3	8/14/64	N-77	1.95	60.1	203	44,500	No
J. 15.4	8/14/64	N-77	2.08	64.1	360	75,000	Yes

\* Symbols are defined as follows:  $V_f$  = chamber free volume;  $S_b$  = propellant surface area; and  $A_t$  = throat area.

<sup>†</sup> Termination port failed to actuate; combustion continued to web burnout. A new propellant cup was installed for subsequent J. 14 firings.

(Confidential)

SECTION III - PROPELLANT DEVELOPMENT

Subsection 2 - Aft-Grain Propellant Development

1. GENERAL

To meet the objectives for the aft-grain propellant, as outlined in Section II, Northrop Carolina pursued two approaches: (1) the incorporation of a high-energy oxidizer (hydrazinium nitroformate) and (2) the use of conventional oxidizers in the aft-grain propellant. The high-energy oxidizer was selected for investigation in order to meet the program specific impulse requirements without the use of metal additives. This effort is reported in detail in 2, below. (Confidential)

The conventional oxidizer approach encompassed the investigation of several binder systems: (1) solid-solution binders (acrylamide and acrylonitrile), (2) castable fluorocarbon binders (C<sub>7</sub> fluoroacrylate and FX-189 fluorocarbon monomers), (3) modifications to the pressed aft grain, and (4) carboxy-terminated polybutadiene binders. The details of this investigation are given in paragraph 3, below.

2. HYDRAZINIUM NITROFORMATE APPROACH

a. General

To meet the specific impulse requirements for the program without using metal additives, hydrazinium nitroformate (HNF) was selected for incorporation in the aft-grain propellant. The work on HNF consisted of sensitivity and compatibility studies and evaluation of various HNF/binder formulations. (Confidential)

b. Sensitivity and Stability of HNF

The drop sensitivity of HNF dried with a stream of dry air for 72 hours was found to be less than that of HNF wet with carbon tetrachloride, as shown in Table X. However, HNF is considerably more sensitive than RDX or HMX. (Confidential)

TABLE X - DROP SENSITIVITY OF HNF AND OTHER  
PROPELLANT INGREDIENTS

Material	Drop Height* (cm)
HNF (dried for 72 hr)	14.7
HNF (moist with $\text{CCl}_4$ )	
Run No. 1	9.0
Run No. 2	10.9
RDX	44.6
HMX	34.5
Lead azide	19.5
Nitroglycerin <sup>†</sup>	5.9 to 14.7

\* 50-percent fire with 2-kg weight and #12 (sandpaper) tooling.

† Same as above, but without sandpaper.

(Confidential)

The thermal stability of HNF was determined using a Du Pont Model 900 differential thermal analyzer. A heating rate of 20°C per minute was used, and the 0.7-mg samples were tested under air or dry nitrogen. The degree to which HNF is dried was found to have considerable effect on its thermal stability. HNF dried with dry air for 24 hours began to decompose at 100°C, whereas HNF dried for 72 hours underwent a melting endotherm beginning at 125°C and began a decomposition exotherm at 130 to 132°C. (Confidential)

c. Compatibility Studies with HNF

The compatibility of HNF with other oxidizers and various binder constituents was studied using the differential thermal analyzer. Table XI summarizes the results of this study. The temperatures of the HNF melt endotherm are given. In some cases, decomposition occurred at a temperature below the melting point of HNF. Endotherms occurring below 123 to 130°C are characteristic of the materials being evaluated with HNF. (Confidential)

HMX was found to be compatible with HNF since the decomposition temperature of the mixture corresponded to that of pure HNF. The mixture of lithium perchlorate and HNF exhibited an endotherm at 80°C and began to decompose at 98°C, however. Other components of the solid-solution binder system were found to be compatible with HNF up to 90°C. (Confidential)

The polymerizable fluorocarbon monomers and their cure catalyst,  $\alpha, \alpha'$  azobis-isobutyl nitrile (VAZO), were found to be compatible with HNF up to 100°C, the decomposition temperature of VAZO. Ethyl acetate, a solvent for the C<sub>9</sub> fluoroalkyl methacrylate(FMA)/VAZO system, was also compatible. The endotherm of this mixture at 76°C corresponds to the boiling point of ethyl acetate. (Confidential)

Additional tests were conducted to ascertain the thermal compatibility of solid-solution binder components with HNF; the results are given in Table XII. These tests indicated that acrylonitrile alone is incompatible with HNF above 50°C. However, with lithium perchlorate added, an exotherm did not occur until 74°C. The addition of lithium perchlorate to the acrylonitrile/HNF mixture lowered the pH from 4.5 to 3.5, which possibly

**CONFIDENTIAL**

AFRPL-TR-65-209, Vol I

**TABLE XI - SUMMARY OF COMPATIBILITY STUDIES OF HNF WITH BINDER CONSTITUENTS AND OXIDIZERS**

Material or Mixture	Atmosphere	Endotherm Inflection Temperature (°C)	Temperature at Endotherm Peak (°C)	Exotherm Inflection Temperature (°C)	Temperature at Exotherm Peak (°C)
HNF (dried 24 hr)	N <sub>2</sub>	---	---	100	141
HNF (dried 72 hr)	Air	125	131	131	132-140
HNF (dried 72 hr)	N <sub>2</sub>	120	123	123	132-140
HNF/HMX	Air	125	131	131	132-140
HNF/LiClO <sub>4</sub>	Air	73	80	98	145
HNF/Acrylonitrile	Air	---	---	100	127
HNF/Ethylene Glycol	N <sub>2</sub>	---	---	121	149
HNF/Ammonium Persulfate	N <sub>2</sub>	---	---	98	114
HNF/Ferric Acetylacetonate	N <sub>2</sub>	---	---	94	---
HNF/Benzoyl Peroxide	N <sub>2</sub>	100	105	105	115
HNF/Solid-Solution Binder *	Air	---	---	121	125
HNF/Fluorocarbon Monomer	N <sub>2</sub>	---	---	117	137
HNF/C9 Fluoroalkyl methacrylate	N <sub>2</sub>	124	129	129	142
HNF/C <sub>8</sub> Fluoroalkyl acrylate	N <sub>2</sub>	---	---	117	138
VAZO †	N <sub>2</sub>	97	102	102	127
HNF/VAZO	N <sub>2</sub>	88	97	97	121
HNF/C <sub>9</sub> FMA, Viton A, VAZO	Air	---	---	131	---
HNF/Ethyl Acetate	Air	71	76	131	---

(Confidential)

\* Acrylonitrile, formamide, ammonium persulfate, n-NDA, and lithium perchlorate.

† α, α', azobis-isobutyl nitrile.

**CONFIDENTIAL**

AFRPL-TR-65-209, Vol I

**TABLE XII - SUMMARY OF COMPATIBILITY STUDIES OF HNF WITH  
SOLID-SOLUTION BINDER INGREDIENTS**

Ingredients	Endotherm Peak (°C)	Exotherm Inflection (°C)	Exotherm Peak (°C)
HNF	131	131	...
Acrylonitrile (distilled)	...	50	106
HNF + acrylonitrile	74	...	...
HNF, acrylonitrile, n-NDA	...	50	107
HNF, acrylonitrile, n-NDA, lithium perchlorate	...	74	125
Methyl ethyl hydroquinone	55	...	...
HNF + methyl ethyl hydroquinone	54	131	...
Dichlorobenzoyl peroxide	...	82	...
HNF + dichlorobenzoyl peroxide	...	72	140
Lauryl peroxide	42	60	123
HNF + lauryl peroxide	42	60	130
HNF + trimethylol propane diallyl ether	127	127	...

(Confidential)

**CONFIDENTIAL**

accounts for the higher compatible range, since HNF is most stable in the 3 to 4 pH range. These studies also indicate no compatibility problems with the low-temperature free-radical initiators, lauryl peroxide and dichlorobenzoyl peroxide (DCBP), and the stabilizer, methyl ethyl hydroquinone (MEHQ). A possible cross-linking agent for acrylonitrile, trimethylol propane diallyl ether, was also compatible. (Confidential)

d. Formulation Studies

(1) Solid-Solution Binder System

Preliminary small-scale mixes of HNF in the acrylonitrile system were evaluated, but the results obtained were inconclusive. Processing was limited to 10-gram batches processed in a remote handling facility. (Confidential)

Solid-solution systems containing up to 76 percent by weight of HNF and 14-percent lithium perchlorate were evaluated. Batch sizes ranging from 25 to 50 grams were processed in a glass mixer under nitrogen. (Confidential)

Three initiators (dichlorobenzoyl peroxide, azobisisobutyl nitrile, and ammonium persulfate) were evaluated in these propellant formulations, but a cure could not be achieved with any of the three. For the latter two catalysts, considerable HNF decomposition was evident at 100 to 120°F, but no decomposition occurred with the dichlorobenzoyl peroxide below 140°F. (Confidential)

(2) Fluorocarbon Systems

Studies were conducted to achieve a satisfactory low-temperature cure of fluoroalkylacrylate monomers. The most promising system studied was a mixture of fluoroalkyl acrylates (40-percent C<sub>5</sub>FA, 30-percent C<sub>7</sub>FA, 20-percent C<sub>9</sub>FA, and 10-percent C<sub>11</sub>FA), which cures in three days at 120°F using dichlorobenzoyl peroxide.

Preliminary process studies indicated that it is feasible to press a highly loaded HNF propellant. A system consisting of C<sub>9</sub>FMA/VAZO dissolved in ethyl acetate and potassium perchlorate, rather than HNF, was slurried in a turbine mixer. The solvent was then stripped at ambient temperature

with vacuum. Samples were pressed in a laboratory-scale hydraulic press at 1000, 2000, 4000, and 20,000 psi, and then cured at 120°F to polymerize the fluoroalkyl methacrylate monomer. High-tensile-strength samples were obtained from the 1000-psi pressings. Although this processing procedure is not considered ideal, it does offer a direct approach toward obtaining highly loaded HNF grains. (Confidential)

Several batches of HNF in fluoroacrylates and fluoromethacrylates were processed and evaluated. With the available HNF particle size, solid loading was limited to 70 percent. The catalysts that functioned best in the unloaded binder (that is, VAZO, benzoyl peroxide, and dichlorobenzoyl peroxide) were used. However, these HNF formulations, like the solid-solution system (see (1), above), would not cure at 100, 120, or 140°F. (Confidential)

(3) Siloxane System

The evaluation of a siloxane monomer binder for HNF propellants was conducted. Differential thermal analysis studies indicated that both the siloxane monomer and curing agent are compatible with HNF. A solid loading of 75 percent was obtained in the binder using ammonium perchlorate. (Confidential)

A dimethyl siloxane binder, Q93-029, manufactured by Dow Corning, was successfully cured in the presence of HNF, producing grains with acceptable mechanical properties. Differential thermal analysis studies showed that HNF is thermally stable in the presence of this siloxane binder. The addition of a cure catalyst lowered the decomposition temperature slightly, from 129°C to 118°C. Twenty-grain batches of a formulation with 70-percent HNF were processed and cured in 48 hours at 80°F. This propellant was castable and had good physical properties, but burned readily at ambient pressure. The solid loading could possibly be increased by using bimodal or trimodal blends of HNF particles. (Confidential)

This system was further characterized in 30- to 50-gram batches. Formulation 8131-46-3 was selected from these preliminary studies for motor loading and test firings.

# CONFIDENTIAL

AFRPL-TR-65-209, Vol I

This formulation contained 68-percent HNF, which was near the limit of processability due to the particle-size distribution of the available HNF. The strand burning-rate curve for this formulation is given in Figure 33. Drop sensitivity tests showed that formulation 8131-46-3 was less sensitive than HNF alone; that is, using a two-kilogram weight, all-fire occurred above a 14-cm drop height for HNF alone and above 28 cm for formulation 8131-46-3. The vacuum stability at 120°F for formulation 8131-46-3 approximated that of HNF. For HNF alone, 0.79 milliliter of gas was liberated per gram of sample during a 40-hour period, compared with 1.00 milliliter for formulation 8131-46-3. (Confidential)

Five two-inch pipe motors were loaded with this formulation from batches ranging from 700 to 1500 grams. The propellant was mixed remotely in a humidity-controlled (30 percent, maximum) area. The propellant was processed at 75°F and cured in 96 hours at 75°F.

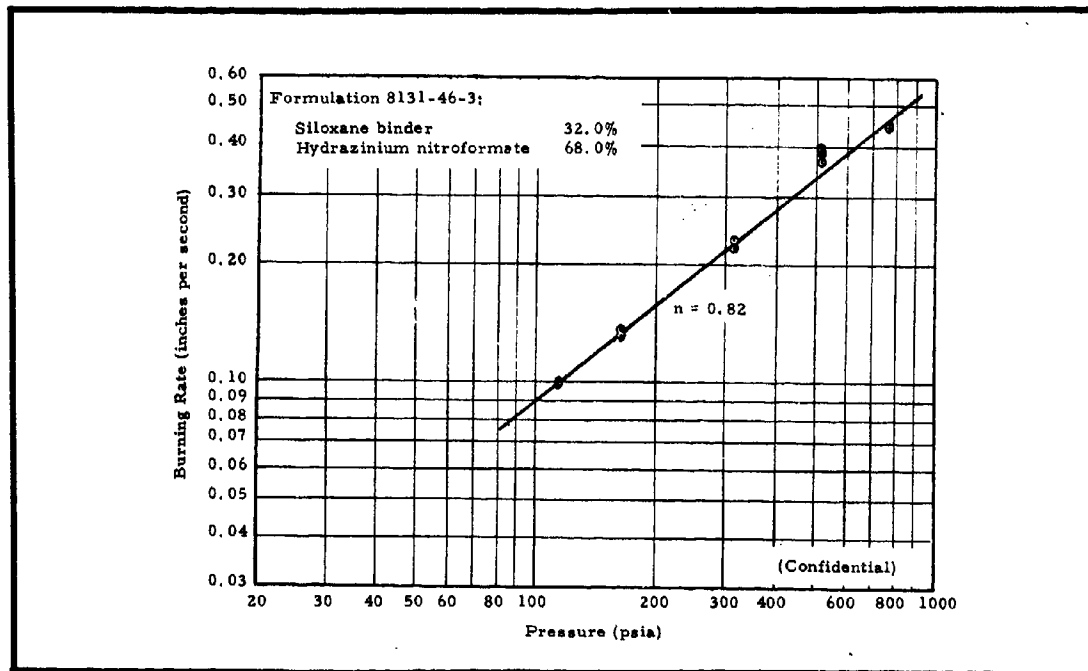


Figure 33 - Strand Burning-Rate Data for Formulation 8131-46-3

In addition, three dual-chamber motor tests (H. 8, H. 14, and H. 13) were conducted; PPO-13 was used in the forward chamber and formulation 8131-46-3 in the aft. A ball valve was not used between chambers in these tests since the forward and aft grains were designed to burn out simultaneously. In the first two tests, H. 8 and H. 14, the aft nozzle was oversized, causing very low pressure in the aft chamber. In the third test, H. 13, the forward and aft grains burned out almost simultaneously; the pressure- and thrust-time traces are shown in Figure 34. The forward grain, an end-burner, did not burn out uniformly, causing a long tail-off, as shown. The cause of the small aft pressure pip that occurred midway through the test is unknown. Table XIII summarizes the ballistic data for this test. Although the measured performance from this test is low, it is probably reasonable in view of the relatively low oxidizer loading in the aft grain. Theoretical performance could not be calculated because information on the binder was not available. If a high solid loading of 85 to 90 percent could be achieved, this system might be promising. Since it is doubtful that a solid loading in this range could be achieved, based on the previous work, the investigation of this siloxane system was discontinued. (Confidential)

(4) Nitroplastisol Binder System

Because of the difficulty experienced in curing the vinyl monomer binders in the presence of HNF, it was decided to investigate other binder systems. The nitroplastisol binder system was evaluated first since HNF is compatible with this system. (Confidential)

First, the nitroplastisol binder was loaded with 60-percent HNF, producing a mix that was quite viscous but processable. This formulation cured in 16 hours at 85° F followed by 18 hours at 120° F. (Confidential)

To improve the termination capability, an attempt was made to incorporate lithium perchlorate. Lithium perchlorate was found to be soluble, up to 24 percent by weight, in the plasticizer, TEGDN. A differential thermal analysis indicated that the solution of HNF in TEGDN began to decompose at 60°C. However, the addition of one percent

**CONFIDENTIAL**

AFRPL-TR-65-209, Vol I

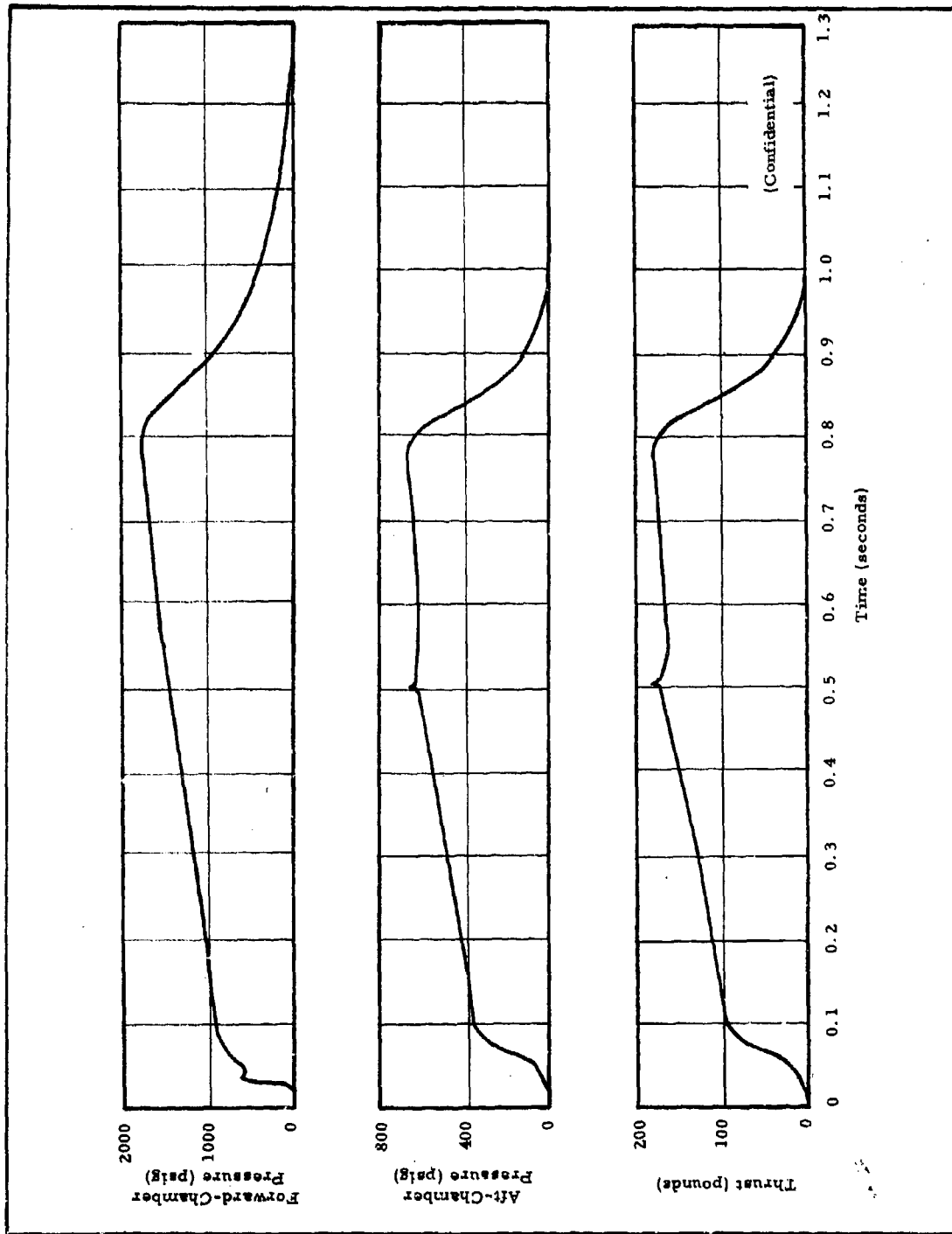


Figure 34 - Pressure- and Thrust- Time Traces for Test H. 13

**CONFIDENTIAL**

# CONFIDENTIAL

AFRPL-TR-65-209, Vol I

TABLE XIII - SUMMARY OF BALLISTIC DATA FOR TEST H<sub>13</sub>

Parameter	Value
<b>Forward chamber (PPO-13)</b>	
Weight burned (lb)	0.1746
Web burned (in.)	0.24
Burn time (sec)	0.781
Burn rate (in./sec)	0.31
$\int P dt_p$ (psig-sec)	1300.9
$\bar{P}_b$ (psia)	1348.4
Throat area (sq in.)	0.0177
Characteristic velocity (fps)	4240
<b>Aft chamber (8131-46-3)</b>	
Weight burned (lb)	0.4674
Web burned (in.)	0.235
Burn time (sec)	0.750
Burn rate (in./sec)	0.313
$\int P dt_p$ (psig-sec)	438.2
$\bar{P}_b$ (psia)	543.8
<b>Total motor</b>	
Weight burned (lb)	0.6420
Weight <sub>aft</sub> /weight <sub>fwd</sub>	2.677
Throat area (sq in.)	0.183
Expansion ratio	3.07
Characteristic velocity (fps)	4020
$\int F dt_f$ (lb <sub>f</sub> -sec)	116.4
$I_{sp_{meas}}$ (lb-sec/lb)	181.3
Ratio of specific heats, $\gamma$	1.24
$C_{f_{theo}}$ (measured conditions)	1.438
$I_{sp_{1000/14.7}}$ (lb-sec/lb)	198.3

(Confidential)

# CONFIDENTIAL

resorcinol raised the decomposition temperature to 140°C. The mixture of HNF and this solution was stable up to 118°C, which was slightly lower than the 128°C at which HNF alone begins to decompose. (Confidential)

The introduction of lithium perchlorate into the propellant hindered cure, however. Formulations with very low solid loadings cured, whereas those with 60 percent or more solids cured incompletely. Although these propellants were fairly stable, one formulation did ignite after 18 hours at 140°F.

(5) Viton Binder System

The development of a method to compression mold HNF with a thermoplastic polymer was carried out in a parallel effort with the castable siloxane investigation reported in (3), above. Mixes were prepared by dissolving Viton A, the selected binder, in ethyl acetate and adding HNF to the solution. The mixture was slurried with a propeller-type agitator until the HNF was well dispersed. Normal hexane was then added to force the Viton A out of solution. The solvent was decanted and the mixture of Viton A and HNF vacuum dried. (Confidential)

Formulation 8131-39-1, made by this procedure, contained 90-percent HNF and 10-percent Viton A. The drop sensitivity of this formulation was less than that of pure HNF; that is, 16 cm for the mixture compared to 12 cm for HNF above. (Confidential)

This formulation has been molded into a 0.25-in. - diameter cylinder 1.2-in. long by pressing at 75°F and 35,000 psi with a 10-minute dwell time. The physical properties of this pressed propellant appear to be slightly superior to those of the OX-1 and OX-5 formulations. The pressed density of formulation 8131-39-1 was 98.5 percent of theoretical. (Confidential)

# CONFIDENTIAL

AFRPL-TR-65-209, Vol I

The strand burning-rate data of this formulation, presented in Figure 35, show that the pressure exponent increases with pressure from 0.6 at 50 psi to 1.44 at 700 psi. The propellant burned readily at atmospheric pressure. Even when modified with 5 percent and 20 percent binder, this formulation gave almost identical results at ambient pressure. (Confidential)

This propellant bonded well to EC-1838 epoxy. When samples of this propellant were bonded to steel with EC-1838, failure occurred in the propellant grain rather than at the bond. This epoxy, when filled with an inert salt, also inhibited combustion on the bonded face.

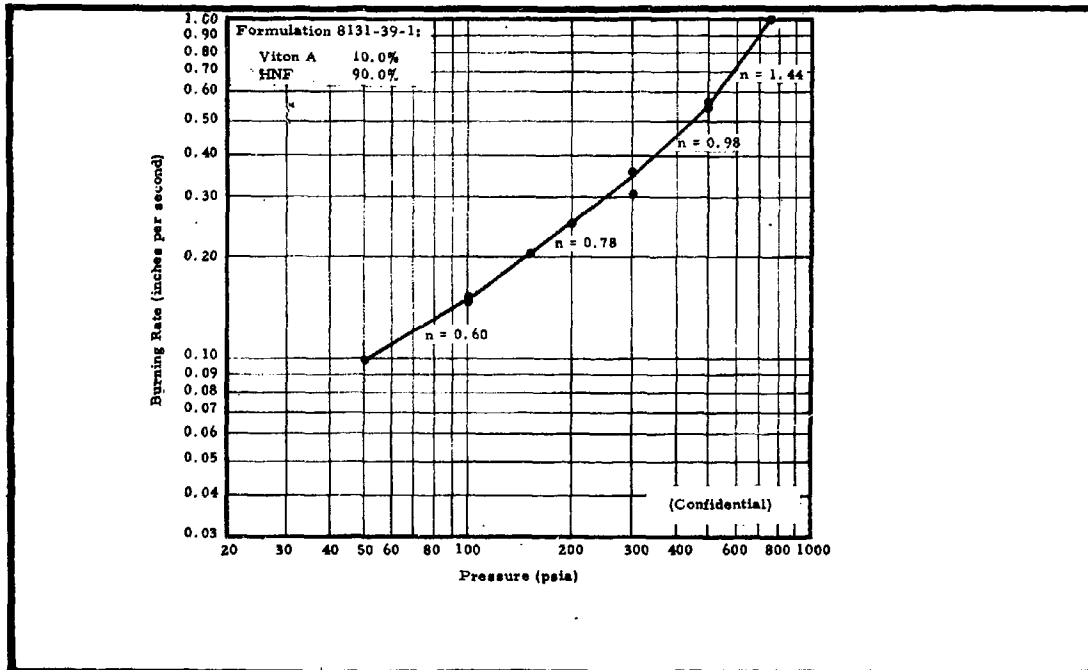


Figure 35 - Strand Burning-Rate Data for Formulation 8131-39-1

-61-

# CONFIDENTIAL

3. CONVENTIONAL OXIDIZER APPROACH

a. Solid-Solution Binders

(1) General

Two solid-solution binders were evaluated in the development of a castable aft-grain propellant; these were the polymerizable vinyl monomers acrylamide and acrylonitrile, which are also solvents for lithium perchlorate. The encouraging results previously obtained (Reference 8) indicated that solid-solution compositions with 90 percent oxidizer are readily extinguished upon termination of the forward grain and also have acceptable physical properties. (Confidential)

(2) Acrylamide

(a) General

An 89- to 91-percent solid loaded solid-solution propellant system with a polyacrylamide binder was thoroughly evaluated for the aft-grain propellant. This system was selected for the following reasons:

1. A high solid loading can be achieved with this propellant; that is, a 90 percent loading can be achieved without using high-density metal additives such as aluminum.
2. These propellants possess acceptable physical properties with a tensile strength of 130 psi and an elongation of 11 percent at 70°F.
3. The termination capabilities of these propellants appear to be far superior to those of other castable propellants investigated. (Confidential)

The development effort consisted of initial process studies, mechanical property studies, strand burning-rate studies, and motor tests, followed by more thorough evaluation of ammonium perchlorate and HMX in acrylamide binders.

(b) Process Studies

Numerous problems were encountered in processing the solid-solution propellants when the batch sizes were increased from 2 to 10 lb. Formulations processed in 10- to 14-lb mixes exhibited short pot life, and even cured rapidly in the mixer. Also, the mixes underwent a considerable volume change during cure as a result of internal "gassing." These problems were attributed to the combined effects of:

1. High processing temperature, resulting in precure
2. High-shear mixing, resulting from the addition of solids to the mix too quickly
3. The volatilization, decomposition, and/or reactivity of the polymerization catalyst (a boron trifluoride-etherate complex) at the mix temperatures. (Confidential)

Tables XIV and XV summarize the results of processing mixes in 2-lb and 10- to 14-lb batches, respectively. To alleviate the problems mentioned above, for batches D-190 through D-198 (Table XIV) and E-64 through E-78 (Table XV), the following changes were made in the process procedure:

1. The acrylamide was melted at 180°F. Ethylene glycol, lithium perchlorate, and 2-NDA were added and the temperature reduced to 140°F. As ammonium perchlorate and aluminum were added, the temperature was gradually increased until a final mix temperature of 160 to 170°F was attained. This procedure was designed to minimize the mix temperature and reduce the possibility of precure.
2. The trimodal ammonium perchlorate system was preblended and added over a 45-minute period to reduce shear, which causes internal heating of the mix. The total mix time was one hour.

TABLE XIV - RESULTS OF PROCESS STUDIES WITH SOLID-SOLUTION PROPELLANTS IN TWO-POUND BATCHES

Formulation	Batch No.	Purpose of Mix	Constituents (percent by weight)										BF <sub>3</sub> etherate	Total S <sub>2</sub> O <sub>8</sub> (M)	Total S <sub>2</sub> O <sub>8</sub> (M)	Kin-Viscosity (cP)	Pot Life	Remarks
			AA	EG	γ-NDA	LP	Al	Ammonium Perchlorate	Al	Ammonium Perchlorate	Al	Ammonium Perchlorate						
8133-19-4	D-189	Process at 140-160°F to increase pot life	4.40	4.40	0.10	12.0	10.0	15.0	35.0	19.0	0.10	91	0.10	91	6.2/145	> 40 min at 140°F	AA melted at 160°F; EG, γ-NDA added and temperature reduced to 150°F; mixed at 150°F; no crystallization of AA on LP; increase pot life compared to normal firing on case. No internal gassing on firing at 160°F.	
8133-19-4	D-190	Ammonium persulfate initiator, low process temperature, internal gassing	4.40	4.40	0.10	12.0	10.0	15.0	35.0	19.0	0.10	91	0.10	91	9/148	> 2 hr at 160°F	160°F temperature maintained throughout mix. Fired well with vibration.	
8133-19-4	D-191	Process at 160°F, add (NH <sub>4</sub> ) <sub>2</sub> C <sub>2</sub> O <sub>4</sub> dissolved in EG	4.40	4.40	0.10	12.0	10.0	15.0	35.0	19.0	0.10	91	0.10	91	9/167	> 30 min at 160°F	Practiced to mix when (NH <sub>4</sub> ) <sub>2</sub> C <sub>2</sub> O <sub>4</sub> was added, process temperature, 165°F. Unstable, extremely thixotropic. Very thick, marginal castability.	
8133-15-1	D-192	Evaluate (NH <sub>4</sub> ) <sub>2</sub> C <sub>2</sub> O <sub>4</sub> initiator in AN system	4.48	4.48	0.02	12.0	10.0	15.0	35.0	19.0	0.22	91	0.48	91	.....	> 3 hr at room temp.	Very thick, marginal castability.	
8133-15-2	D-193	Mix loading with no Al, 12% LP	4.90	4.90	0.10	12.0	.....	19.5	39.0	19.5	0.10	90	0.10	90	13/160	> 3 hr at room temp.	Unstable, extremely thixotropic. Very thick, marginal castability.	
8133-15-3	D-194	Improve processability of 90% solids formulation with no Al and 12% LP by changing AP loading	4.90	4.90	0.10	12.0	.....	15.5	41.0	21.5	0.10	90	0.10	90	11/116	> 3 hr at room temp.	Very thick, marginal castability.	
8133-15-4	D-195	Change AP classification from 12% to 15% loading with 12% LP, no Al	4.90	4.90	0.10	12.0	.....	17.5	41.0	19.5	0.10	90	0.10	90	12/167	> 3 hr at room temp.	Very thick, marginal castability.	
8133-15-5	D-196	90% loading with 12% LP, processability study	5.40	5.40	0.10	12.0	.....	17.28	40.5	19.28	0.10	89	0.10	89	12.5/140	> 3 hr at room temp.	Very fluid, excellent pot life.	
8133-15-4	D-197	Mix loading with 14% LP, no Al	4.90	4.90	0.10	14.0	.....	17.0	40.0	19.0	0.10	90	0.10	90	7.5/176	> 2 hr	Fired well with vibration, no gassing on case. Unstable, very thick.	
8133-15-7	D-198	Determine maximum loading with 12% LP, no Al	5.15	5.15	0.10	12.0	.....	17.35	46.75	19.40	0.10	89.5	0.10	89.5	14/162	> 2 hr	Unstable, very thick.	

[Confidential]

Legend:  
 AA - Polyacrylamide  
 EG - Ethylene glycol  
 γ-NDA - N-methylololamine  
 LP - Lithium perchlorate  
 Al - Aluminum (15-18)  
 AP - Ammonium perchlorate  
 BF<sub>3</sub> etherate - Boron trifluoride etherate complex  
 AN<sup>+</sup> - Acrylonitrile  
 (NH<sub>4</sub>)<sub>2</sub>C<sub>2</sub>O<sub>4</sub> - Ammonium persulfate

TABLE XV - RESULTS OF PROCESS STUDIES WITH SOLID-SOLUTION PROPELLANTS IN 10 TO 14-LB BATCHES

Formulation No.	Batch No.	Purpose of Mfr	Constituents (percent by weight)										Total (NH <sub>4</sub> ) <sub>2</sub> SO <sub>4</sub> (wt %)	Tensile Strength (psi)	Elongation (%)	Molecular Weight (psi)	Brookfield Viscosity (poise/cm <sup>2</sup> )	Pot Life	Remarks	
			AA	EG	nDA	LP	Al	Al	Al	Al	Al	Al								
8133-19-4	E-62	Lead 6 lb. motor for combustion termination firing	4.40	4.40	0.10	12.0	10.0	15.0	35.0	19.0	0.10	.....	91	Propellant processed in miller.	20 min					
			4.40	4.40	0.10	12.0	10.0	15.0	35.0	19.0	0.10	.....	91							
8133-19-4	E-63	Same as above	4.40	4.40	0.10	12.0	10.0	15.0	35.0	19.0	0.10	.....	91	Appeared to be starting to cure while loading into motor; ammonia (ammonia) "leaking" in propellant. Motor scrapped.	2 hr	2.4/122				
8133-19-4	E-64	Processability at reduced temperature	4.40	4.40	0.10	12.0	10.0	15.0	35.0	19.0	0.10	.....	91	Same procedure as for batch E-199 (Table III); very good pot life. Ammonia very low; propellant slight increase in viscosity when cured under 25-psi N <sub>2</sub> pressure.	2 hr	8/67				
8133-35-6	E-65	12-lb mix with 90% solids, no Al, using (NH <sub>4</sub> ) <sub>2</sub> SO <sub>4</sub> as initiator.	4.90	4.90	0.10	14.0	.....	17.0	40.0	19.0	.....	98	At 70°F: 120 At 100°F: 64 At 160°F: 64	Physical properties characterized at 70 and 160°F.	2 hr	6/67				
8133-35-6	E-70	Same as for batch E-64	4.90	4.90	0.10	14.0	.....	17.0	40.0	19.0	.....	98	Miller loaded so phos; cured under 25-psi N <sub>2</sub> at 160°F.	2 hr	6.5/78					
8133-35-5	E-74	Processed at 180°F	5.40	5.40	0.10	12.0	.....	17.25	40.5	19.25	.....	98		2 hr	6.5/78					
8133-36-1	E-75	Processed at 180°F	4.90	4.90	0.10	14.0	2.0	16.40	39.0	18.40	.....	98		2 hr	6.5/109					
8133-35-5	E-76	Processed at 140°F	5.40	5.40	0.10	12.0	.....	17.25	40.5	19.25	.....	98		2 hr	1.8/131					
8133-36-1	E-77	Processed at 140°F	4.90	4.90	0.10	14.0	2.0	16.40	39.0	18.40	.....	98		> 4 hr	1.8/131					
8133-35-5	E-78	Processed at 140°F	5.40	5.40	0.10	12.0	.....	17.25	40.5	19.25	.....	98		> 4 hr	2.0/132					

Legend:  
 AA - Polyacrylamide  
 EG - Ethylene Glycol  
 nDA - Nitrocellulose  
 LP - Lithium Perchlorate  
 Al - Aluminum (E-10)  
 p/AP - Average particle size of ammonium perchlorate  
 BP - Barium Perchlorate  
 (NH<sub>4</sub>)<sub>2</sub>SO<sub>4</sub> - Ammonium persulfate

3. The benzoyl peroxide and boron trifluoride etherate complex, which provided free-radical initiation for polymerization, were replaced with ammonium persulfate ( $(\text{NH}_4)_2\text{S}_2\text{O}_8$ ). The ammonium persulfate was first dissolved in a small amount of ethylene glycol and added prior to the final vacuum mix cycle. More consistent cures were obtained with this procedure than by adding the persulfate directly to the mix as a solid. The internal "gassing" experienced with benzoyl peroxide and boron trifluoride catalyst was completely eliminated when ammonium persulfate was used.

(Confidential)

The maximum solid loading attainable prior to this year's effort (Reference 8) in a processable, non-metallized solid-solution system with 12 percent lithium perchlorate was 89 percent. Formulation 8133-35-5 (see Table XV) was quite processable, having a Brookfield viscosity of 3 kilopoises, which is comparable to mixes of conventional composite propellants. The mechanical properties of this formulation, 137-psi tensile strength and 12.5 percent elongation at 70°F, are quite acceptable. Efforts to increase the solid loading above 89 percent with 12-percent lithium perchlorate produced propellants that were very viscous and virtually uncastable (formulations 8133-35-2, -3, -4, and -7 in Table XIV). (Confidential)

By increasing the lithium perchlorate content to 14 percent, a solid loading of 90 percent was achieved with a castable formulation (8133-35-6 in Table XIV). The viscosity of this formulation was somewhat higher than desired (7.5 kilopoises), but the propellant was quite thixotropic and flowed well when vibrated. The mechanical properties of this formulation were close to those for the 89-percent loaded propellant. The pot life of this formulation, when scaled up to a 12-lb mix in the one-gallon vertical mixer (Batch E-66, Table XV), was greater than two hours. (Confidential)

To further evaluate the effect of reduced mix temperature on the processability of these formulations, 12-lb batches E-74 through -78 (Table XV) were processed. The results are illustrated by the data in Table XV for formulations 8133-35-5 (89 percent solids, 12 percent LP) and 8133-36-1 (90 percent solids, 14 percent LP, 2 percent Al). The batches processed at 140°F had viscosities of 1.8 to 2.0 kilopoises, whereas batches E-74 and E-75, processed at 180°F, had viscosities of 6.5 kilopoises. The higher viscosities for the batches processed at 180°F are obviously caused by a greater degree of precure during mixing. The pot life of the formulations processed at 140°F was greater than four hours. (Confidential)

(c) Mechanical Property Studies

The mechanical properties of the solid-solution formulations have been very reproducible, as evidenced by the data for two separate batches of formulation 8133-35-6, presented in Table XVI. The effect of cure temperature on the properties of formulation 8133-35-5 was very slight, as shown in Table XVII. (Confidential)

Since the solid-solution cure mechanism involves polymerization of a vinyl monomer, the effect of post-cure is of interest. To determine the effect of long exposure at elevated temperature, samples of formulation 8133-35-6 (90 percent solids, 14 percent LP) propellant were cured at 172°F for as long as 100 hr. These samples were then pulled at 74°F. The results shown in Figure 36 indicate that little, if any, postcure occurred after 25 hr. (Confidential)

(d) Strand Burning-Rate Studies

Preliminary results of strand burning-rate studies indicate that the pressure exponents for formulations 8133-35-5 and 8133-35-6 were above unity. However, these data were obtained with polyethylene strands. It was found that, by changing

**CONFIDENTIAL**TABLE XVI-MECHANICAL PROPERTIES OF FORMULATION8133-35-6\* AT 74°F

Batch	Cure Temperature (°F)	Cure Time (hr)	Maximum Stress (psi)	Strain (in./in.)
E-66	165	24.0	130	0.11
E-71	172	27.5	129	0.12

\*90 Percent solids, 14 percent LP (see Table XV).

(Confidential)

TABLE XVII-EFFECT OF CURE TEMPERATURE ON MECHANICALPROPERTIES OF FORMULATION 8133-35-5 AT 74°F

Batch	Cure Temperature (°F)	Cure Time (hr)	Maximum Stress (psi)	Strain (in./in.)
E-76	180	24	154	0.11
E-76	160	24	140	0.12

\*89 Percent solids, 12 percent LP (see Table XV).

(Confidential)

**CONFIDENTIAL**

# CONFIDENTIAL

AFRPL-TR-65-209, Vol I

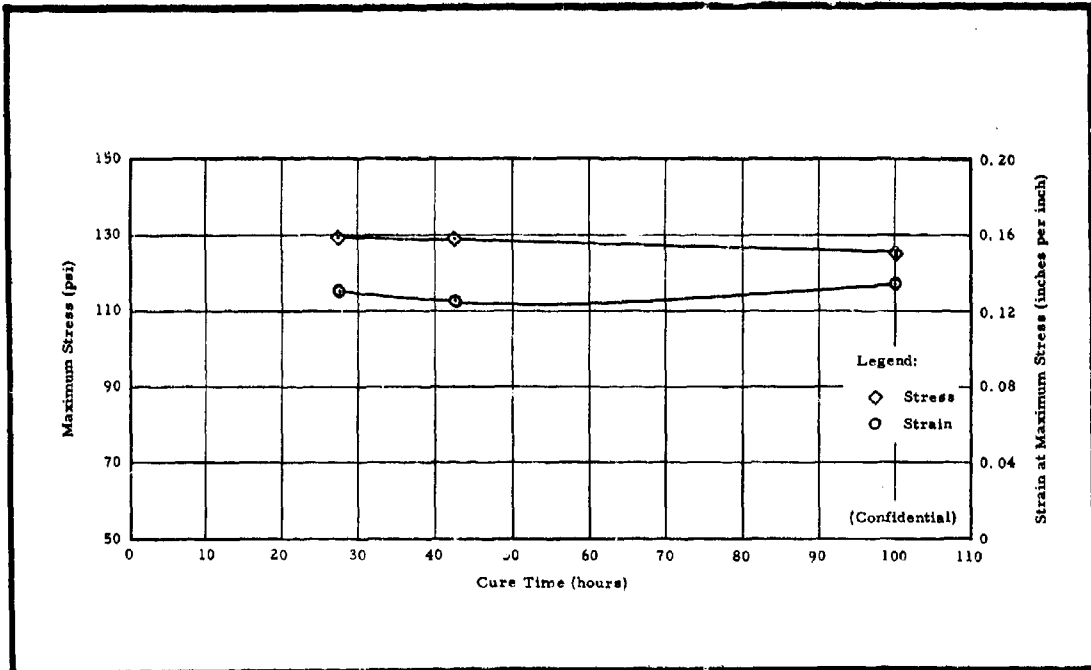


Figure 36 - Effect of Cure Time at 170°F on Mechanical Properties of Formulation 8133-35-6

to an epoxy inhibitor, both the burning rates and pressure exponents at high pressures (above 500 psi), were reduced. The exponents with the epoxy inhibitor were 0.75 to 0.77. It has been concluded that the strands with polyethylene inhibitor flashed between the propellant and inhibitor at higher pressures, thus giving erroneous burning rates and exponents. (Confidential)

Tests in which the epoxy inhibitor was used have given more reproducible results, which agree with motor data. Figure 37 presents burning-rate data for formulation 8133-35-6 (90 percent solids, 14 percent LP); the slope is 0.67 below 350 psi and 0.83 above-350 psi. (Confidential)

In Figure 38, burning-rate data for formulation 8133-36-1 (90 percent solids, 14 percent LP, 2 percent Al) are given. This formulation had a higher burning rate than the non-aluminized

**CONFIDENTIAL**

AFRPL-TR-65-209, Vol I

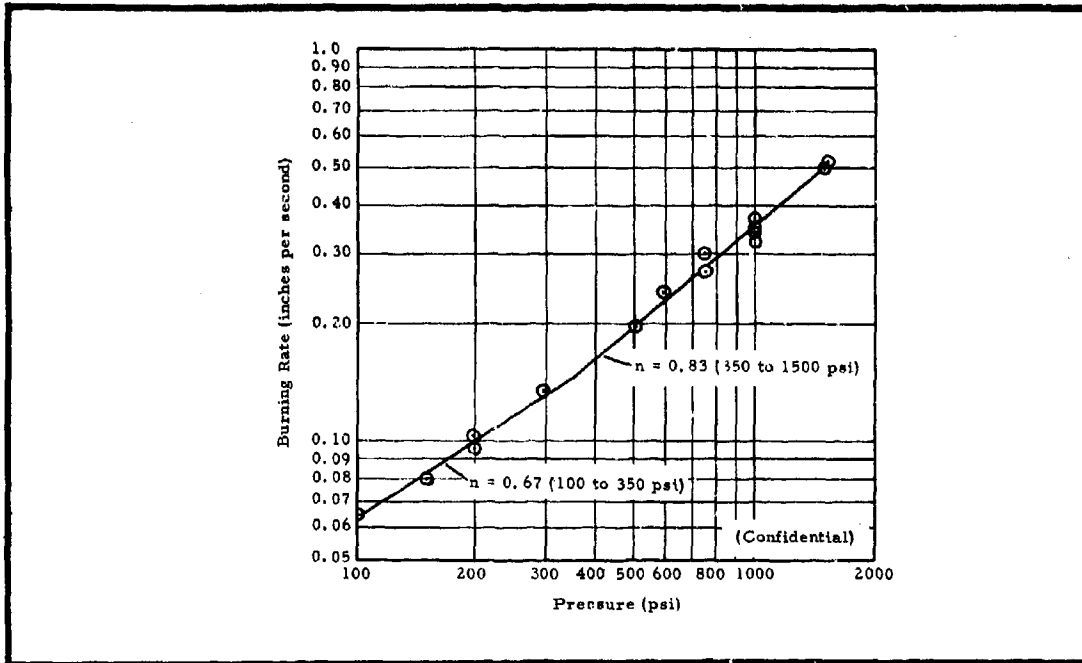


Figure 37 - Strand Burning-Rate Data for Formulation 8133-35-6

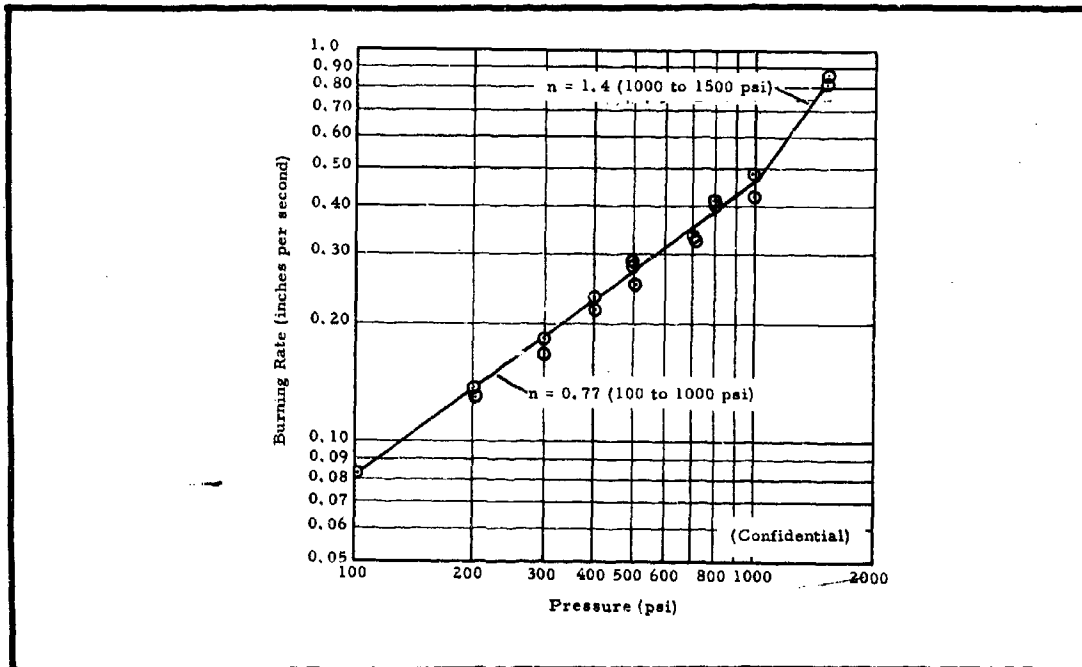


Figure 38 - Strand Burning-Rate Data for Formulation 8133-36-1

**CONFIDENTIAL**

formulation, 8133-35-6, and a constant slope of 0.77 up to 1000 psi. The slope increased sharply above 1000 psi; however, this pressure region is not of particular interest. (Confidential)

(e) Motor Test Results

Six 20-lb motor tests (Tests H. 1 through H. 6) were conducted as part of aft propellant development Test Series H. Two of these were multi-cycle tests, with two cycles each. The reduced ballistic data obtained from these tests, in which reignition did not occur, are presented in Table XVIII. A detailed discussion of these tests is presented in Appendix A, along with the pressure- and thrust-time traces for each, and the propellant formulation used in each.

From these initial motor tests, utilizing castable solid-solution propellants, several characteristics were evident:

1. Formulations containing 10 percent binder and 14 percent lithium perchlorate can be terminated reproducibly in the DCCSR motor, based on the results of Tests H. 2, H. 4. 1, H. 4. 2, H. 6. 1 and H. 6. 2. In tests H. 1 and H. 3, however, the aft grain reignited, but the formulations used in these tests contained only 12 percent lithium perchlorate, along with 10 percent aluminum (Test H. 1) and 11 percent binder (Test H. 3). The reignition observed in these tests is characteristic of formulations containing a reduced percentage of lithium perchlorate.
2. Low-frequency oscillations occurred in all the tests conducted. These oscillations, which were a strong function of chamber pressure, were just detectable above 300 psi, but were quite severe below 150 psi. The addition of aluminum had no apparent effect on this instability, which verified the observations of others as a characteristic of low-frequency instability. (Reference 15).

# CONFIDENTIAL

AFRPL-TR-65-209, Vol I

TABLE XVIII - REDUCED BALLISTIC DATA FOR TESTS H. 2, H. 3, H. 4, and H. 6

Parameter	Test Number					
	H. 2	H. 3	H. 4			H. 6
			First Cycle	Second Cycle	Total	First Cycle
<b>Forward Chamber</b>						
Weight burned (lb)	8.02	3.64	3.15	2.53	5.68	2.29
Web burned (in.)	1.01	0.400*	0.414	0.294	0.708	0.290
Burn time (sec)	2.419	0.974*	0.946	0.960	1.906	0.959
Pressure time (sec)	3.000	1.089	1.063	1.065	2.128	1.034
Burn rate (in./sec)	0.418	0.411*	0.438	0.306	0.371	0.302
$\int P dt_p$ (psig-sec)	5513	2310*	2269	1278	3547	1293
$\bar{P}_b$ (psia)	2200	2339*	2370	1312	1844	1343
$\dot{m}_b$ (lb/sec)	3.18	3.50*	3.27	2.60	2.93	2.35
Throat area (sq in.)	0.196	0.197	0.194	0.251	....	0.238
Characteristic velocity (ft/sec)	4350	4020	4500	4080	....	4320
$P_{term}$ (psia)	....	2414	2395	1178	....	1424
$dp/dt_{term}$ (psi/sec)	....	110,000	110,000	52,500	....	81,000
<b>Aft Chamber</b>						
Weight burned (lb)	5.07	10.40	1.75	1.44	3.19	1.56
Web burned (in.)	0.41	0.92*	0.088	0.095	0.183	0.130
Burn time (sec)	2.370	0.926*	0.902	0.921	1.823	0.955
Pressure time (sec)	3.009	1.176*	1.086	1.037	2.123	1.016
Burn rate (in./sec)	0.173	....*	0.097	0.103	0.100	0.136
$\int P dt_p$ (psig-sec)	688.6	242.7*	272.8	198.3	471.1	150.3
$\bar{P}_b$ (psia)	292	258.5*	291.6	216.3	253.6	162.5
$\dot{m}_b$ (lb/sec)	2.05	....	1.78	1.47	1.62	1.54
$P_{prior}$ (psia)	....	264	299	176	....	196
$P_{max}$ (psia)	....	719	946	588	....	492
$dp/dt_{term}$ (psi/sec)	....	31,800	38,100	28,300	....	31,900
<b>Overall Motor</b>						
Weight burned (lb)	13.09	14.04	4.90	3.97	8.87	3.85
$Wt_{aft}/Wt_{fwd}$	0.632	....	0.556	0.569	0.562	0.655
$\gamma$ (at $Wt_{aft}/Wt_{fwd}$ )	1.24	....	1.24	1.24	1.24	1.24
$\int F dt_f$ (lb-sec)	2550	1088	1050.4	764.8	1815.2	710.2
$\bar{F}_b$ (lb <sub>f</sub> )	1032	1082	1060	781.2	919.8	701.8
Throat area (sq in.)	2.528	....	2.53	2.53	2.53	3.299
Expansion ratio ( $A_e/A_t$ )	2.99	2.90	2.98	2.98	2.98	1.50
Specific impulse measured (lb-sec/lb)	194.8	....	214.5	192.6	204.5	185
Specific impulse corrected 1000/14.7 (lb-sec/lb)	221.1	....	240	223	232	230
Specific impulse corrected vac, 20/1 (lb-sec/lb)	251.5	....	273	254	264	261
Characteristic velocity (ft/sec)	4280	....	4530	4070	4320	4150

\*Values measured prior to termination.

3. Each propellant formulation evaluated to date has exhibited, to varying degrees, erosive burning at initial port-to-throat ratios of 4 to 5. The aft ends of these grains burned faster than the forward ends. This increase in burning rate appears to be a linear relationship, progressing down the grain. In Test H. 6, the aft grain was turned end for end between cycles in order to eliminate the possibility that the settling of the solids during propellant cure could be the cause. However, the results of the second cycle in Test H. 6 showed that erosive burning was responsible. (Confidential)

(f) Solid-Solution System with Ammonium Perchlorate and HMX

Acrylamide/Ammonium Perchlorate System

The solid-solution propellant formulations in which ammonium perchlorate is used as the oxidizer have exhibited burning-rate pressure exponents of 0.7 to 0.8, as measured in the strand bomb and motor firings. Since it is desirable that the aft propellant pressure exponent be nearer unity, two additives to increase the pressure exponent were evaluated: ferric oxide and carbon black. Ferric oxide, a well-known combustion catalyst for ammonium perchlorate, increases the pressure exponent of some ammonium perchlorate propellants. (Confidential)

Table XIX gives the composition, process parameters, mechanical properties, and burning-rate pressure exponent for the formulations containing ferric oxide and carbon black (formulations 8133-41-1 and 8133-41-2, respectively, as well as the basic propellant with no additives, formulation 8133-35-6. Both additives increased the burning-rate pressure exponent of the propellant, with ferric oxide increasing the pressure exponent over the entire pressure range (100 to 1000 psi) to 0.96. (Confidential)

The use of both carbon black and ferric oxide, like aluminum, eliminated the uncured surface layer

**CONFIDENTIAL**

TABLE XIX-EFFECT OF CARBON BLACK AND FERRIC OXIDE ON  
PROPERTIES OF SOLID-SOLUTION PROPELLANTS

Property	Formulation		
	8133-35-6 (Batch E-66)	8133-41-1 (Batch D-205)	8133-41-2 (Batch D-204)
<b>Composition (percent by weight)</b>			
Acrylamide	4.90	4.90	4.90
Ethylene glycol	4.90	4.90	4.90
Lithium perchlorate	14.00	14.00	14.00
Ammonium perchlorate	76.00	75.00	75.00
Ammonium persulfate	0.10	0.10	0.10
n-Nitrosodiphenylamine	0.10	0.10	0.10
Carbon black	. . . .	1.00	. . . .
Ferric oxide	. . . .	. . . .	1.00
<b>Process parameters</b>			
Mix temperature (°F)	180*	130 to 145	130 to 145
Mix viscosity (kilopoises)	8.0*	1.6	7.0
Cure temperature (°F)	165	180	180
Cure time (hr)	24	24	24
<b>Mechanical properties</b>			
Maximum stress (psi)	130	123	107
Strain (in./in.)	0.11	0.12	0.09
Pressure exponent, n (100 to 1000 psi)	0.75	0.96	0.96

\* The high viscosity of this batch is attributed to the high mix temperature of 180° F.

(Confidential)

**CONFIDENTIAL**

previously observed on acrylamide propellants. The ferric oxide apparently catalyzed the propellant cure to some degree, as evidenced by the relatively high viscosity (7 kilopoises) of the mix. The tensile strength for both formulations was above 100 psi, and the elongation of the carbon black formulation was 12 percent. (Confidential)

#### Acrylamide/HMX System

Although HMX is compatible with the solid-solution propellant ingredients, formulation studies have shown that the HMX interferes with the free-radical-initiated polymerization so that very long cure times are required. Since ammonium persulfate will not initiate the polymerization in the presence of HMX, ferric acetylacetonate was used exclusively in the four formulations studied (see Table XX).

All four formulations had viscosities of less than one kilopoise, and were easily processed. The formulations contained various ratios of ammonium perchlorate to HMX, as well as all HMX. These propellants exhibited low tensile strengths and high elongations, probably as a result of incomplete cure. As in the ammonium perchlorate system, the incorporation of aluminum powder (formulation 8133-38-4) improved the curing of the surface layer. However, all formulations showed some degree of decomposition, evidenced by internal "gassing" during cure. In an attempt to reduce this decomposition during cure, n-nitrosodiphenylamine was eliminated so that, hopefully, the HMX alone would retard polymerization during mixing and casting, but the mix cured in the mixer. Reducing the n-nitrosodiphenylamine content in formulations 8133-38-3 and 8133-38-4 did not improve "gassing" during cure. (Confidential)

The drop sensitivity of the 90-percent loaded formulation, 8133-38-4, was comparable to that of pure HMX, and the five-second autoignition temperature was 495°F. (Confidential)

**CONFIDENTIAL**

**TABLE XX- PROPERTIES OF ACRYLAMIDE SOLID-SOLUTION  
FORMULATIONS CONTAINING HMX**

Property	Formulation			
	8133-38-1 (Batch D-202)	8133-38-2 (Batch D-203)	8133-38-3 (Batch D-206)	8133-38-4 (Batch D-207)
Composition (percent by weight)				
Acrylamide	5.40	5.40	5.40	5.00
Ethylene glycol	5.40	5.40	5.40	4.88
Lithium perchlorate	14.00	14.00	12.00	14.00
Ammonium perchlorate	55.00	10.00	57.00	.. .
HMX	20.00	65.00	20.00	74.00
Aluminum	.. .	.. .	.. .	2.00
n-Nitrosodiphenylamine	0.10	0.10	0.05	0.02
Ferric acetylacetonate	0.10	0.10	0.10	0.10
Process parameters				
Mix temperature (°F)	120 to 130	120 to 130	130 to 145	130 to 145
Mix viscosity (kilopoises)	0.64	0.68	.. .	0.88
Cure temperature (°F)	180	180	180	185
Cure time (hr)	24	71	170	16
Five-second autoignition temperature (°F)	.. .	.. .	.. .	495
Drop-hammer sensitivity, 2 kg (cm)	.. .	.. .	.. .	39
Pressure exponent, n (100 to 1000 psi)	0.5*	0.6*	0.56	0.88

\* Approximate values.

(Confidential)

**CONFIDENTIAL**

Strand burning-rate data for formulations 8133-38-1 and 8133-38-2 were erratic; their measured pressure exponent was approximately 0.6. More reproducible rate data were obtained for formulations 8133-38-3 and 8133-38-4, as plotted in Figures 39 and 40, respectively. The latter formulations, containing all HMX, gave a constant slope of 0.88 from 100 to 1000 psi. (Confidential)

(3) Acrylonitrile

(a) General

Acrylonitrile offers an advantage over acrylamide binder because of its improved processability. This improvement results from the fact that (1) lithium perchlorate is more soluble in acrylonitrile than acrylamide and (2) acrylonitrile has a lower density than acrylamide.

(b) Acrylonitrile/Ammonium Perchlorate System

Small laboratory batches (50 grams) of acrylonitrile in ethylene glycol were cured, using dichlorobenzoyl peroxide catalyst with methyl ether hydroquinone at 140°F in 24 to 48 hours. The process was subsequently scaled up to 2000 grams and four batches were processed; the formulations are given in Table XXI. Each batch was easily processed at 70°F. Scaling to 2000 grams required an increased percentage of catalyst so that the batch would cure in a reasonable length of time. No "gassing" was observed during cure. (Confidential)

(c) Acrylonitrile/HMX System

The acrylonitrile approach offers an advantage over the acrylamide approach from the standpoint of processability because of the combined effects of (1) the increased solubility of lithium perchlorate in the acrylonitrile system and (2) the lower density of acrylonitrile. Monsanto personnel have indicated that improved mechanical properties and lower cure temperatures are achieved with acrylonitrile. (Confidential)

# CONFIDENTIAL

AFRPL-TR-65-209, Vol I

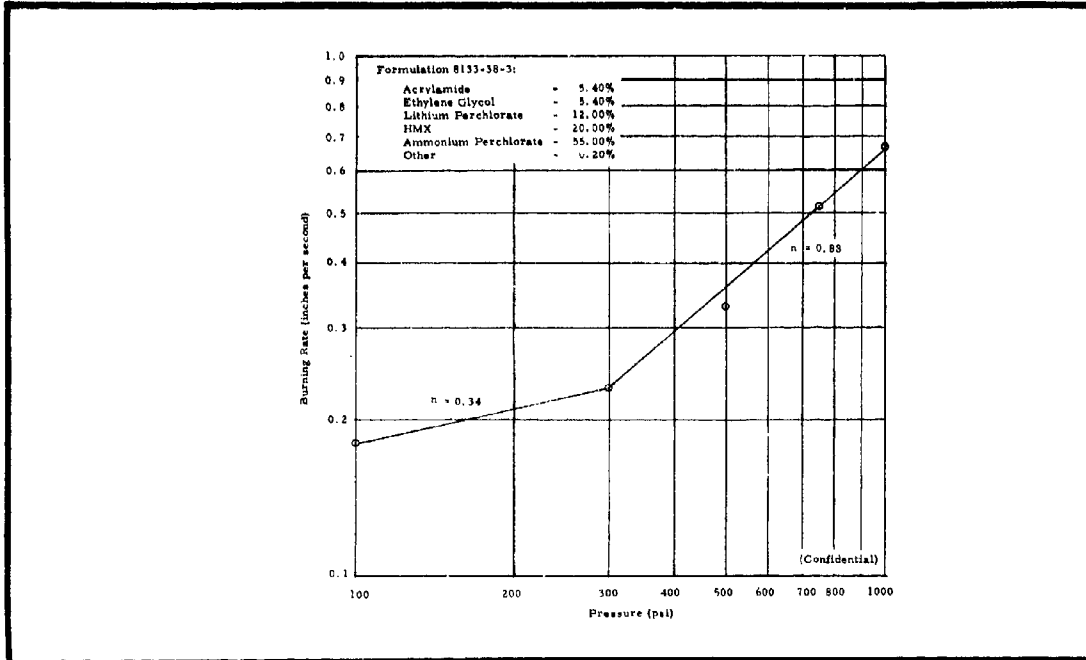


Figure 39 - Strand Burning-Rate Data for Formulation 8133-38-3

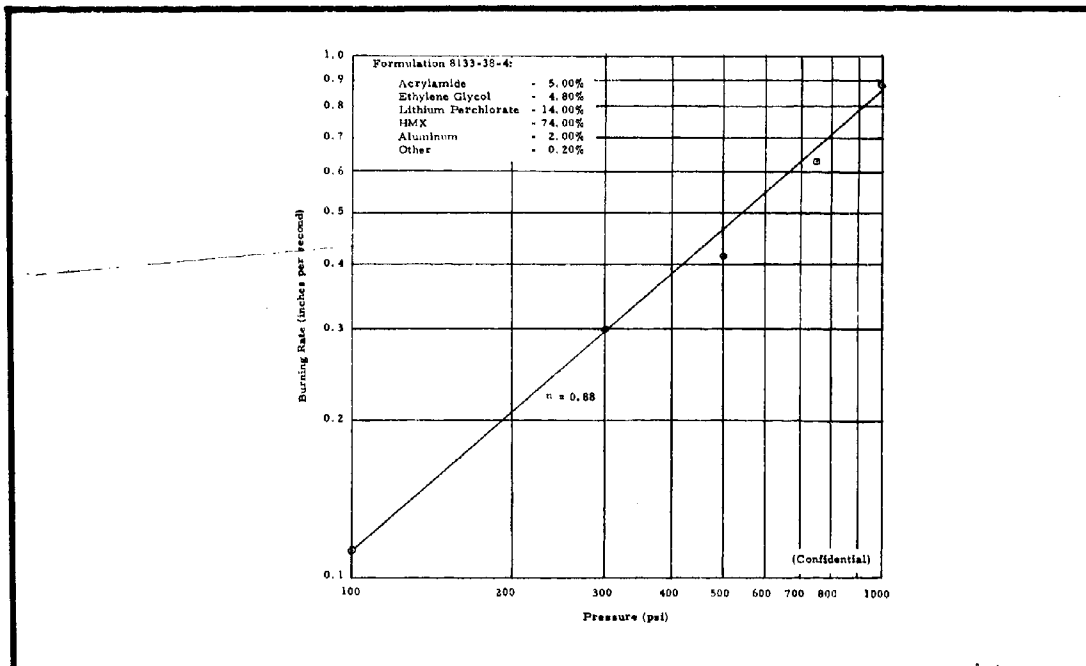


Figure 40 - Strand Burning-Rate Data for Formulation 8133-38-4

TABLE XXI- SUMMARY OF FORMULATION STUDIES OF ACRYLONITRILE/AMMONIUM  
PERCHLORATE SYSTEM

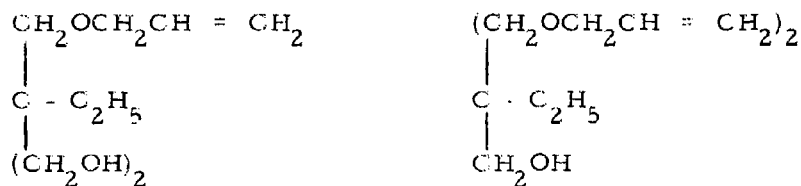
Property	Batch Number			
	9002-30-7	9002-31-9	9002-31-10	9002-31-11
Composition (percent by weight)				
Acrylonitrile	4.990	4.987	4.982	4.975
Ethylene glycol	4.990	4.987	4.982	4.975
Methyl ether hydroquinone	500 ppm AN	500 ppm AN	500 ppm AN	500 ppm AN
Dichlorobenzoyl peroxide	0.020	0.025	0.035	0.050
Lithium perchlorate	14.000	14.000	14.000	14.000
Ammonium perchlorate	76.000	74.000	74.000	76.000
Aluminum	. . .	2.000	2.000	2.000
Mix viscosity at 70° F (kilopoises)	1.76	1.80	1.60	1.60
Cure characteristic at 140° F	Partially cured in 10 days	Partially cured in 9 days	Partially cured in 5 days	Approached full cure in 3 days

(Confidential)

Two 90-percent solid loaded formulations (8133-38-5 and 8133-38-6) with 14-percent lithium perchlorate, 2-percent aluminum, and 74-percent HMX were processed (see Table XXII). The plasticizer used in formulations 8133-38-5 and -6 was ethylene glycol and formamide, respectively. Both formulations contained 0.1-percent ferric acetylacetonate to catalyze the polymerization and a small amount (0.02 percent) of a retardant, n-nitrosodiphenylamine. The viscosity of both mixes was low at 70°F, but neither cured at 165°F in 18 hours. An extremely thermoplastic solid was achieved, however, when the mixes were cured at 185°F for four days. Both formulations produced gas during cure, as observed previously with other compositions containing HMX. (Confidential)

(4) Chain Branching and Cross-Linking

Since both acrylamide and acrylonitrile propellants are somewhat thermoplastic when cured due to the linear nature of the polymers, methods of branching and cross-linking the polymers were investigated. Two compounds were investigated for this purpose: trimethylol propane monoallyl ether and trimethylol propane diallyl ether, shown below, from left to right.



The first compound is a monofunctional olefin with a side chain to act, in essence, as a "reactive" plasticizer. The other compound, trimethylol propane diallyl ether, is a true diene cross-linking agent. Lithium perchlorate was found to be compatible and actually soluble in both compounds up to approximately 20 percent by weight at 125°F. Another propellant formulation, 8133-38-7, was processed with 0.44 percent of the monoallyl ether (see Table XXII). Although the viscosity of this batch was quite high, the

**CONFIDENTIAL**

AFRPL-TR-65-209, Vol I

TABLE XXII- PROPERTIES OF ACRYLONITRILE SOLID-SOLUTION  
FORMULATIONS CONTAINING HMX

Property	Formulation		
	8133-38-5 (Batch D-208)	8133-38-6 (Batch D-209)	8133-38-7 (Batch D-210)
Composition (percent by weight)			
Acrylonitrile	4.94	4.94	4.72
Ethylene glycol	4.94	. . .	. . .
Lithium perchlorate	14.00	14.00	14.00
HMX	74.00	74.00	74.00
n-Nitrosodiphenylamine	0.02	0.02	0.02
Aluminum	2.00	2.00	2.00
Ferric acetylactonate	0.10	0.10	0.10
Formamide	. . .	4.94	4.72
Trimethylol propane monoallyl ether	. . .	. . .	0.44
Process parameters			
Mix temperature (°F)	70	70	70
Mix viscosity (kilopoises)	3.1	1.8	> 20
Cure temperature (°F)	185	185	185
Cure time (days)	4	4	4
Five-second autoignition temperature (°F)	485	480	500

(Confidential)

propellant cure was superior to previous acrylonitrile formulations. An initial laboratory evaluation indicated that the use of diallyl ether in the acrylamide/ethylene glycol binder improved the mechanical properties. This compound has not been incorporated in a propellant formulation, however. (Confidential)

(5) Determination of Degree of Hydration of Lithium Perchlorate

The anhydrous lithium perchlorate used for the foregoing evaluations was found to exhibit only a small endotherm at 145°C, the decomposition temperature of the tightly bound third hydrate, thus indicating only a small amount of water present. The melt endotherm at 236°C was quite large and sharp, indicating high-purity material. However, after a can of lithium perchlorate is opened, the material picks up water quickly.

Table XXIII presents the results of differential thermal analyzer runs for five samples of lithium perchlorate, including four samples from previously opened cans and one sample from a new can. As shown, drying lithium perchlorate from a can previously opened and resealed for 18 hours at 120 or 160°C did not eliminate the third hydrate. However, when dried at 180°C for 18 hours, the purity of the old material was equal to that of the new material. These results indicate that a higher temperature, 180°C, should be used for drying lithium perchlorate.

b. Castable Fluorocarbon Binders

(1) General

A comprehensive evaluation of castable fluorocarbon binders for the conventional oxidizers was conducted. This investigation consisted of the parallel evaluations of a fluoroalkyl acrylate binder and a fluorocarbon monomer binder.

(2) Fluoroalkyl Acrylate Binder

(a) Preliminary Investigation

TABLE XXIII - RESULTS OF DIFFERENTIAL THERMAL ANALYSIS TO  
DETERMINE LITHIUM PERCHLORATE PURITY

Lithium Perchlorate Sample	Atmosphere	Third Hydrate Decomposition Endotherm at 145°C	Melt Endotherm at 236°C
Fresh from new can	Air	Very small	Large
Previously opened can (vacuum dried 18 hr at 120°C)	Air	Large	Small
Previously opened can (vacuum dried 18 hr at 160°C)	Air	Intermediate	Small
Previously opened can (vacuum dried 18 hr at 180°C)	N <sub>2</sub>	Very small	Large
Previously opened can (opened 45 min at 57-percent R. H.)	N <sub>2</sub>	Large	Small

General

Previous work with fluoroacrylates, reported in Reference 8, involved a comonomer system of C<sub>9</sub> fluoroalkyl methacrylate and C<sub>5</sub> fluoroalkyl acrylate. Because these monomers are not as readily available as C<sub>7</sub> fluoroalkyl acrylate (C<sub>7</sub>FA), the latter was selected for evaluation.

Preliminary cure studies indicated that C<sub>7</sub>FA with benzoyl peroxide, which has a 10-hour half-life at 162°F, and dichlorobenzoyl peroxide, which has a 10-hour half-life at 129°F, produced the best results. Formulations with benzoyl catalyst cured to rubbery solids in 24 to 36 hours at 185°F, whereas those with dichlorobenzoyl peroxide catalyst cured in 24 to 36 hours at 120°F. The pot life of these small-scale formulations was also good. Solid loadings of 79 percent, including 15 percent aluminum, were quite processable at 120 to 125°F. The use of plasticizers such as Viton A and Viton LM were observed to aid processability. (Confidential)

Formulation 8983-8-1, which did not contain a plasticizer, gave promising strand-burning rates, as shown in Figure 41. This 79-percent solid loaded formulation, which contained a trimodal aggregate of ammonium perchlorate, barely sustained combustion at ambient pressure, and combustion could be extinguished easily by blowing on the flame. (Confidential)

Processability and Mechanical Property Improvement

Preliminary processing and cure studies were conducted with 100-gram batches of propellant, which were cured for 24 hours at 120°F. Table XXIV presents a summary of the formulation modifications, and the mechanical properties obtained for each. The 79-percent solid loaded formulation with no binder modifications (formulation 8983-16-1) had a very low (i. e., 16 psi) tensile strength. The

# CONFIDENTIAL

AFRPL-TR-65-209, Vol I

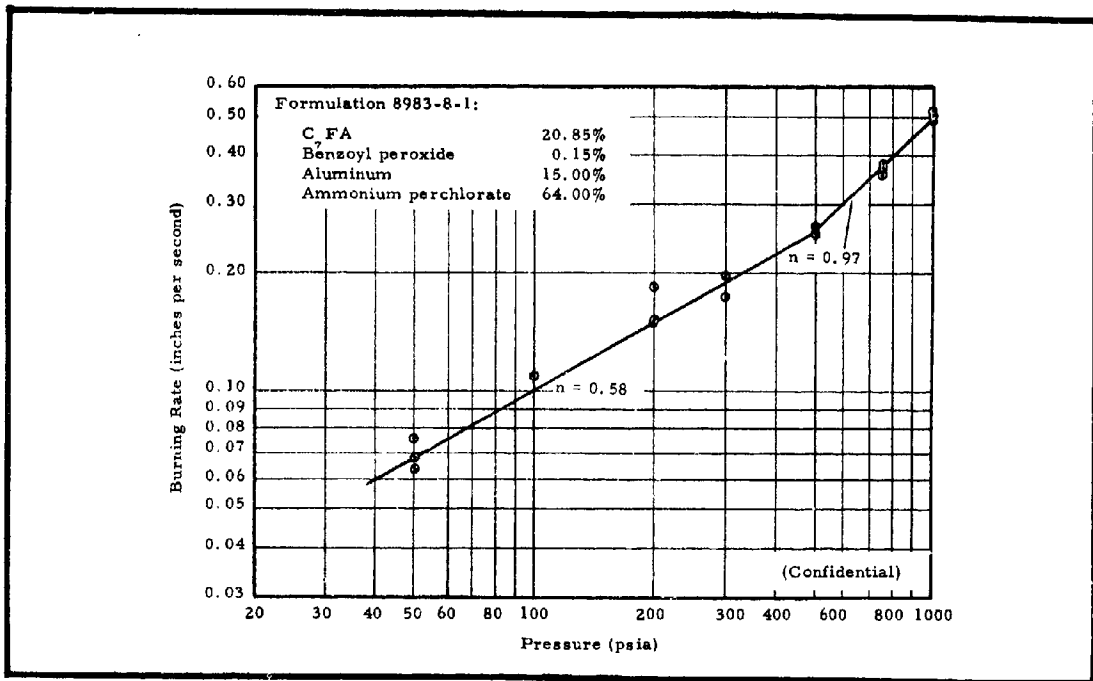


Figure 41 - Strand Burning-Rate Data for Formulation 8983-8-1

addition of 0.1 percent triallylcyanurate (TAC), a trifunctional cross-linking agent, increased the tensile strength to 54 psi in formulation 8983-18-2, but was accompanied by a decrease in elongation from 17 percent to 11 percent.  
(Confidential)

The addition of plasticizers Viton A and Viton LM had little effect on the mechanical properties of this batch size of propellant. The formulations without Viton A were very thixotropic, but would flow at 75°F when vibrated. In formulation 8983-23-2, Viton A was dissolved in the C<sub>7</sub>FA monomer; the resulting mixture was no longer thixotropic. The viscosity of this propellant mix at 75°F was only 2.5 kilopoises.  
(Confidential)

**TABLE XXIV - RESULTS OF MECHANICAL PROPERTIES IMPROVEMENT STUDIES OF  
C<sub>7</sub> FLUOROALKYL ACRYLATE PROPELLANT SYSTEM**

Property	Formulation									
	8983-16-1	8983-18-2	8983-20-5	8983-24-1	8983-24-2	8983-24-3	8983-23-3	8983-23-2		
Composition (percent by weight)										
C <sub>7</sub> FA	20.00	20.90	17.01	18.92	23.65	23.92	20.90	18.80		
2,4 DCBP*	1.00	1.00	1.00	1.00	1.25	1.00	1.00	1.00		
TAC	. . .	0.10	0.10	0.08	0.10	0.08	0.10	0.10		
Viton A	. . .	. . .	. . .	. . .	. . .	. . .	. . .	2.10		
Viton LM	. . .	. . .	1.89	. . .	. . .	. . .	. . .	. . .		
Ammonium perchlorate	67.00	67.00	68.00	65.00	60.00	60.00	63.00	63.00		
Aluminum	10.00	10.00	10.00	15.00	15.00	15.00	15.00	15.00		
Carbon black	1.00	1.00	1.00	. . .	. . .	. . .	. . .	. . .		
Iron oxide	1.00	1.00	1.00	. . .	. . .	. . .	. . .	. . .		
Cure data										
Time (hr)	24	24	24	24	24	24	24	24		
Temperature (°F)	120	120	120	120	120	120	120	120		
Mechanical properties										
Tensile strength (psi)	16	54	55	45	40	35	52	41		
Elongation (%)	17	11	9	8	10	15	5	8		

\* A mixture of 50 percent 2,4 dichlorobenzoyl peroxide and 50 percent dibutylphthalate.

(Confidential)

The effect of cure time on the mechanical properties of formulation 8983-23-3 is shown in Table XXV. Both the tensile strength and elongation were increased considerably by extending the cure time from 24 to 48 hours. Little additional improvement was observed by increasing the cure time to 72 hours. (Confidential)

TABLE XXV - EFFECT OF CURE TIME ON  
MECHANICAL PROPERTIES OF  
FORMULATION 8983-23-3 CURED AT 120°F

Cure Time (hr)	Stress, $S_m$ (psi)	Elongation, $\epsilon_m$ (in./in.)
24	52	0.05
48	64	0.08
72	67	0.08

(Confidential)

This C<sub>7</sub>FA propellant system was scaled up to 12-lb batch sizes and evaluated; the effect of Viton A on mechanical properties for this batch size is shown in Table XXVI. These data indicate that Viton A at the 2.1-percent level increases both tensile strength and elongation. This increase can be explained by assuming that the long-chain unsaturated elastomer acts as a plasticizer as well as taking part in the vinyl polymerization. Increasing the Viton A concentration to 3.3 percent, in formulation 8983-32-2, lowered the stress, but did not improve strain. Moreover, the mix viscosity was increased considerably at this greater Viton A concentration. The reproducibility of mechanical properties for four 12-lb batches of formulation 8983-23-2 is shown in Table XXVII. (Confidential)

TABLE XXVI - EFFECT OF BINDER MODIFICATION ON MECHANICAL  
PROPERTIES OF C<sub>7</sub>FA PROPELLANT (12-LB BATCH SIZE)

Batch No.	Formulation	Composition (percent by weight)				Stress, S <sub>m</sub> (psi)	Elongation, ε <sub>m</sub> (in./in.)
		C <sub>7</sub> FA	2, 4 DCBP	TAC	Viton A		
E-125	8983-23-3	20.9	1.0	0.10	. . .	64	0.08
E-127	8983-23-2	18.8	1.0	0.10	2.1	89	0.12
E-131	8983-32-1	18.8	1.0	0.05	2.1	61	0.16
E-132	8983-32-2	17.6	1.0	0.10	3.3	68	0.12

(Confidential)

TABLE XXVII - REPRODUCIBILITY OF MECHANICAL  
PROPERTIES OF FORMULATION 8983-23-2  
(12-LB BATCH SIZE)

Batch No.	Stress, S <sub>m</sub> (psi)	Elongation, ε <sub>m</sub> (in./in.)
E-127	89	0.12
E-128	88	0.11
E-129	87	0.11
E-130	97	0.11

(Confidential)

The C<sub>7</sub>FA propellants, as well as those with the fluorocarbon monomer (see (3), below), bond very well to steel. Figure 42 shows broken bond specimens for both systems; note that failure occurred in the propellant. (Confidential)

# CONFIDENTIAL

AFRPL-TR-65-209, Vol I

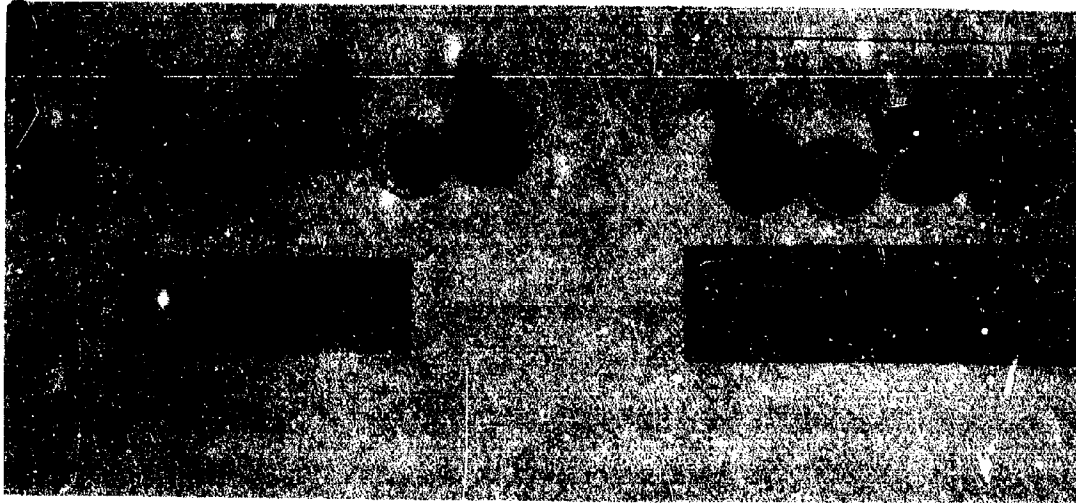


Figure 42 - Results of Propellant-to-Steel Bond Tests

(b) Process Scaling to 200-Lb Batch Size

Since the cure characteristics of this propellant system are based upon the bulk polymerization of a monomer, the problems associated with scaling up to large batch sizes was of concern. Therefore, a 200-lb mix of formulation 8983-23-2 was made. The propellant processed well and was pressure-bayonet cast into a 13-in. -diameter motor case with a 5-in. -diameter mandrel; the center-perforated grain was 22 in. long. The grain was cured for 48 hours at 120°F, and then radiographically inspected; its integrity was good. The largest internal void on the X-ray was 0.1 in. Photographs of this motor taken during processing and X-ray, are presented in Figures 43, 44, and 45.

The mechanical properties of the propellant processed in this batch (R-17) are presented in Table XXVIII. These properties are comparable

# CONFIDENTIAL

**CONFIDENTIAL**

AFRPL-TR-65-209, Vol I

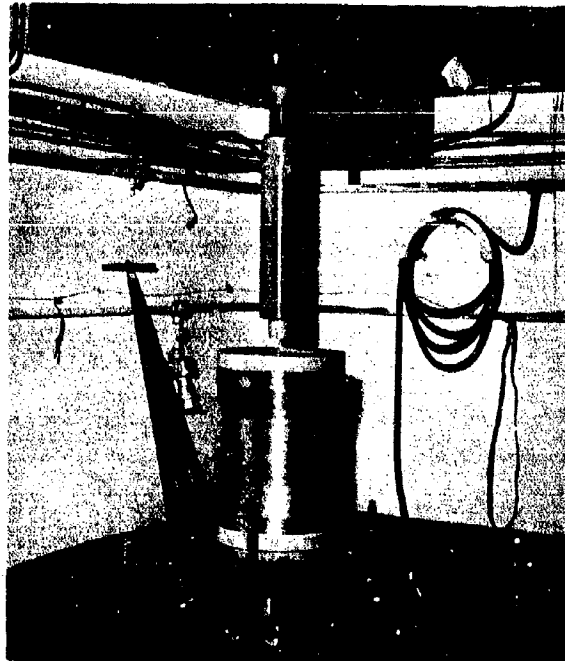


Figure 43 - Extraction of Mandrel from 175-Lb Motor Containing Propellant Formulation 8983-23-2

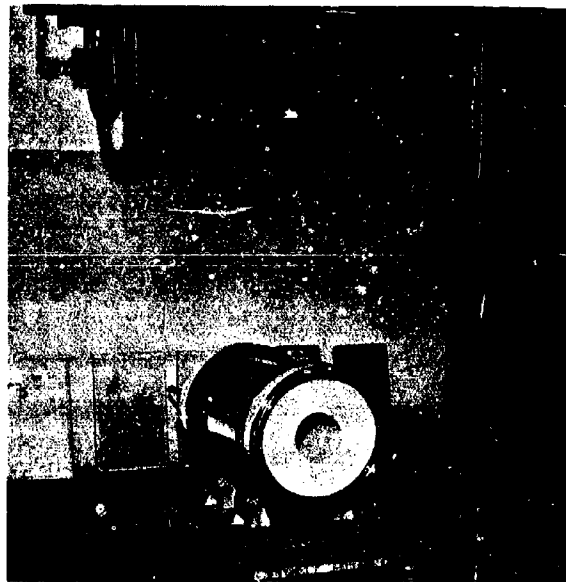


Figure 44 - Radiographic Inspection of 175-Lb Motor Containing Propellant Formulation 8983-23-2

-90-

**CONFIDENTIAL**

**CONFIDENTIAL**

AFRPL-TR-65-209, Vol I

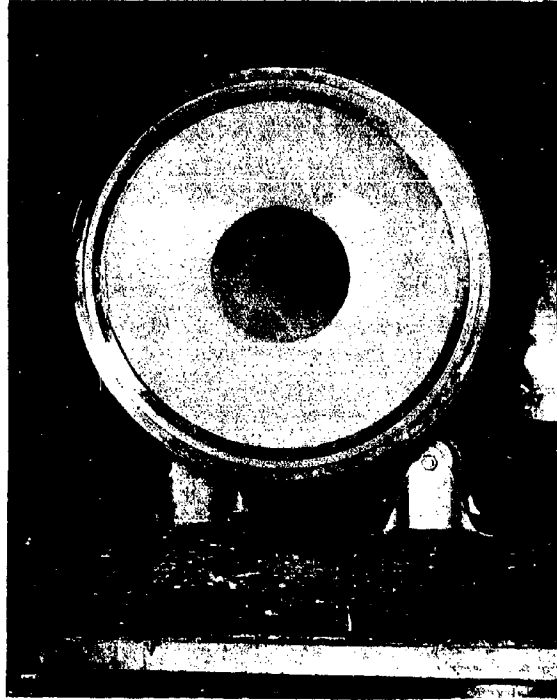


Figure 45 - End View of 175-Lb Motor Containing Propellant Formulation 8983-23-2

TABLE XXVIII - MECHANICAL PROPERTIES OF 200-LB BATCH OF FORMULATION 8983-23-2

Temperature (°F)	Stress, $S_m$ (psi)	Elongation, $\epsilon_m$ (in./in.)
+140	45	0.08
+ 75	89	0.10
- 40	982	0.03

(Confidential)

**CONFIDENTIAL**

to those for the 12-lb batches. The density of this batch of propellant was 0.0695 lb/cu in. (Confidential)

(c) **Subscale Motor Tests with Propellant Formulation 8983-23-2**

To evaluate the combustion characteristics of C<sub>7</sub>FA propellants during motor operation, four six-inch grains were cast with formulation 8983-23-2. The propellant was mixed and cast at 75°F. The viscosities ranged from 2.0 to 2.8 kilopoises, and pot-life was greater than 3 hours at 75°F. The grains were cured for 48 hours at 120°F, and case-bonded directly to the steel chamber walls. (Confidential)

These six-inch aft grains were fired in dual-chamber motors, with six-inch forward chambers containing PPO-13 propellant. A Jamesbury ball valve was used between chambers. The motors were purged with nitrogen gas after each termination.

The reduced ballistic data for these four dual-chamber tests (Test H. 9 through H. 12) are given in Table XXIX. For Tests H. 9 and H. 11, two successful start-stop cycles were achieved. In Test H. 10, low decay rates were experienced at termination due to the valve's overshooting its termination position; the aft grain reignited before the nitrogen purge started and was completely consumed. In Test H. 12, a higher aft-chamber burning-surface-to-throat-area ratio of 69.3 was used to increase the aft-to-forward mixture ratio, but the aft grains (two aft chambers were used in tandem in this test) did not extinguish at termination and burned out. The forward grains were extinguished without reignition in each test. (Confidential)

The aft-chamber characteristic velocity values for Tests H. 9 and H. 11 are believed to be low because of the position of the pressure port in the aft chamber. These ports were located in the forward end of the chamber where high-velocity gas from the forward chamber enters. In Tests H. 10 and H. 12, the

# CONFIDENTIAL

AFRPL-TR-65-209, Vol I

TABLE XXIX - SUMMARY OF BALLISTIC DATA FOR TESTS H.9 THROUGH H.12

Parameter	Test H.9		Test H.10	Test H.11		Test H.12
	First Cycle	Second Cycle		First Cycle	Second Cycle	
<b>Forward chamber (PPO-13)</b>						
Weight burned (lb)	2.391	2.102	1.80	2.664	1.468	2.868
Web burned (in.)	...	...	0.254	0.345	0.198	0.284
Burn time (sec)	1.075	1.066	1.232	0.832	0.880	0.986
Burn rate (in./sec)	...	...	0.206	0.417	0.225	0.288
$\int P dt_p$ (psig-sec)	1212	1160	855.5	1723	679.7	1191
$\bar{P}_b$ (psia)	1139	1089	629.4	2043	766.4	1203
Throat area (sq in.)	0.232	0.232	0.258	0.189	0.258	0.303
$P_{term}$ (psia)	1089	1124	425	2184	687	1244
$dp/dt_{term}$ (psi/sec)	47,100	37,900	7660	89,600	21,800	52,700
Characteristic velocity (fps)	3780	4110	3950	3930	3840	4089
<b>Aft chamber (8983-23-2)</b>						
Weight burned (lb)	1.598	1.483	7.62	1.570	1.080	14.72
Web burned (in.)	...	...	0.710	0.130	0.103	0.606
Burn time (sec)	1.029	1.055	8.475	0.824	0.876	4.390
Burn rate (in./sec)	...	...	0.0838	0.158	0.118	0.138
$\int P dt_p$ (psig-sec)	155.5	151.3	475.7	174.8	103.5	575.8
$\bar{P}_b$ (psia)	153.3	146.9	117.9/65.7*	206.9	121.6	188.6/137.9*
$P_{prior}$ (psia)	161	153	97	212	119	202
$P_{max}$ (psia)	294	278	144	443	192	306
$dp/dt_{term}$ (psi/sec)	4420	4810	1950	12,700	2940	6530
$K_{aft} (S_b/A_t)$	52.6	52.6	52.5	51.8	51.8	69.3
<b>Total motor</b>						
Weight burned (lb)	3.989	3.585	9.42	4.234	2.548	17.59
$Weight_{aft}/Weight_{fwd}$	0.668	0.706	0.74/4.24*	0.589	0.736	1.20/5.13*
Ratio of specific heats, $\gamma$	1.24	1.24	1.24/1.20*	1.24	1.24	1.23/1.20*
$\int F dt_f$ (lb <sub>f</sub> -sec)	646.9	623.7	1655.3	765.2	403.5	3296.6
$\bar{F}_b$ (lb <sub>f</sub> )	563.7	543.0	415/192*	834.0	425.3	1105/573*
Throat area (sq in.)	2.889	2.889	2.894	2.894	2.894	4.300
Expansion ratio ( $A_e/A_t$ )	2.801	2.801	2.807	2.796	2.797	1.996
$I_{sp_{meas}}$ (lb-sec/lb)	162.2	174.0	176 <sup>†</sup>	180.7	158.4	187.4
$I_{sp_{1000/14.7}}$ (lb-sec/lb)	201.7	216.4	... <sup>†</sup>	212.1	206.2	237.5
$I_{sp_{vac, 20/1}}$ (lb-sec/lb)	229.4	246.1	... <sup>†</sup>	241.2	234.5	270.7
$I_{sp_{eff}}$ (%)	82.9	88.6	... <sup>†</sup>	88.2	84.2	93.2
Characteristic velocity (fps)	3490	3930	4560	3844	3782	4529

\*These values are pretermination and total firing data (pretermination/total firing).

<sup>†</sup>The nozzle was greatly overexpanded during the reignition portion of this test.

(Confidential)

# CONFIDENTIAL

AFRPL-TR-65-209, Vol I

location of the ports was identical to that for Tests H. 9 and H. 11, but no gas was produced in the forward chamber over most of the aft pressure-time integral since the forward grains permanently extinguished at termination. Thus, the characteristic velocities for Tests H. 10 and H. 12 are reasonably high, as expected. (Confidential)

Figure 46 shows the burning-rate data for formulation 8983-23-2 plotted as a function of pressure for Tests H. 9 through H. 12. The strand burning-rate curve for this propellant is also shown for comparison.

The pressure- and thrust-time traces for these tests are shown in Figures 47, 48, 49, and 50, respectively. The first cycles of Tests H. 9, H. 10, and H. 12 show aft-chamber ignition peaks. No ignition peaks occurred during the second cycle of Test H. 9 and both cycles of H. 11 in which the aft grain was the same as that used in H. 9. Since the peaks occurred

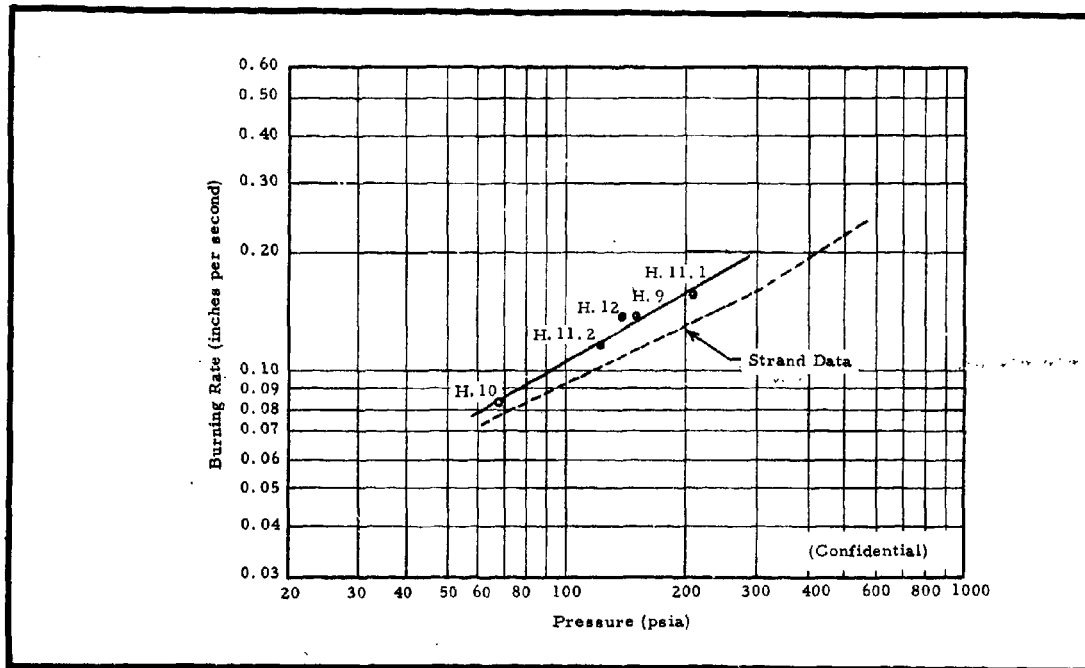


Figure 46 - Motor Burning-Rate Data for Formulation 8983-23-2

-94-

# CONFIDENTIAL

**CONFIDENTIAL**

AFRPL-TR-65-209, Vol I

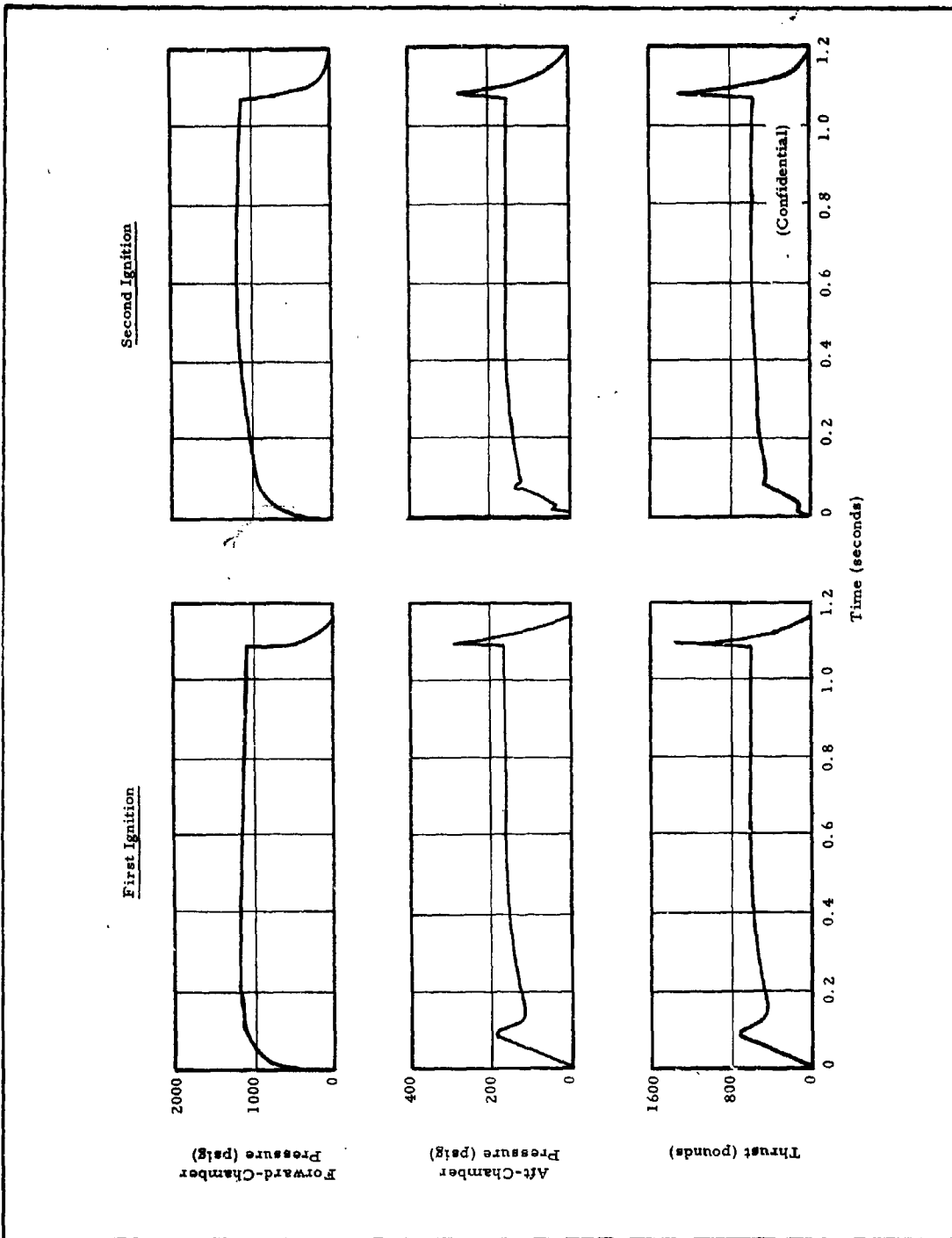


Figure 47 - Pressure- and Thrust-Time Traces for Test H.9

**CONFIDENTIAL**

**CONFIDENTIAL**

AFRPL-TR-65-209, Vol I

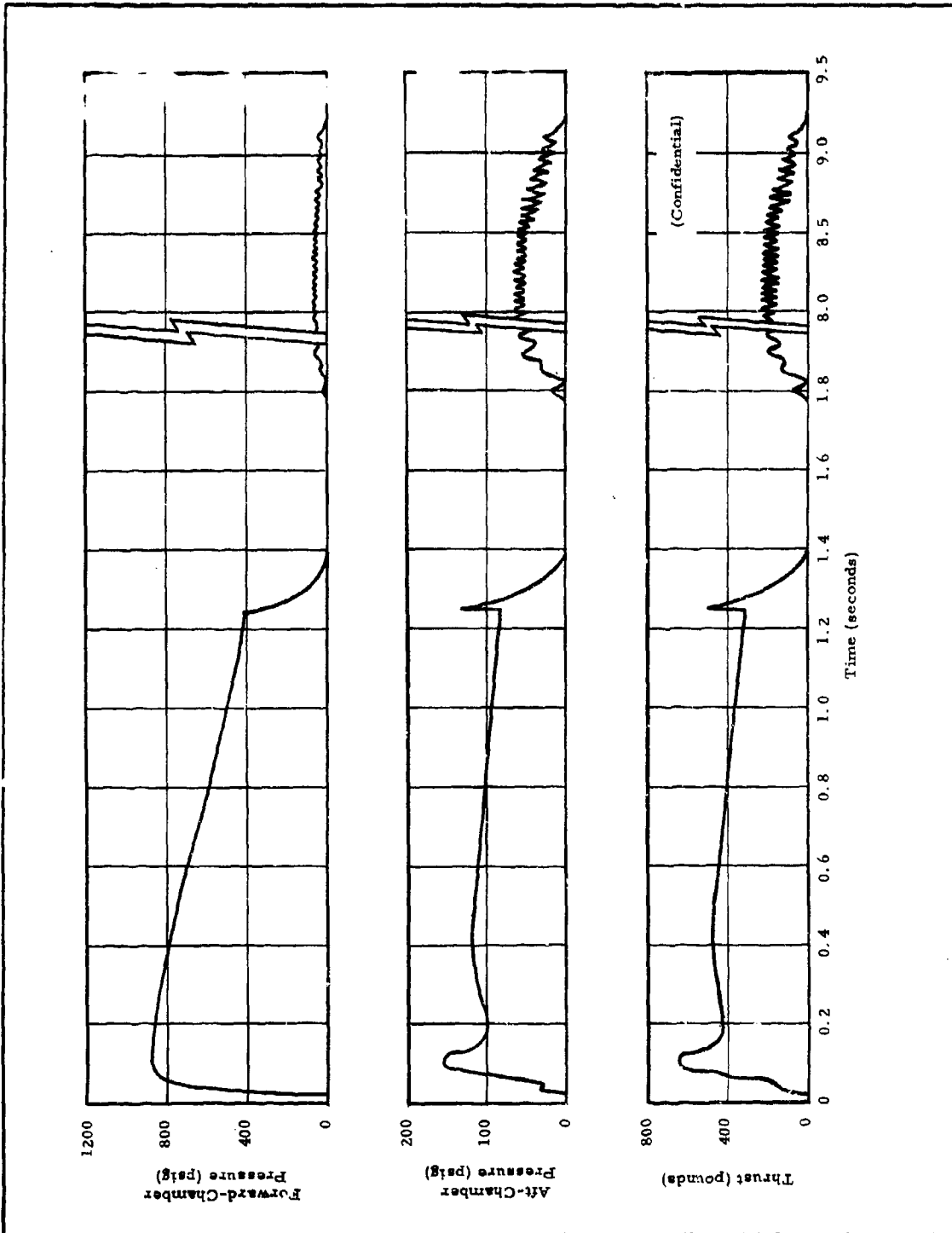


Figure 48 - Pressure- and Thrust-Time Traces for Test H. 10

**CONFIDENTIAL**

# CONFIDENTIAL

AFRPL-TR-65-209, Vol I

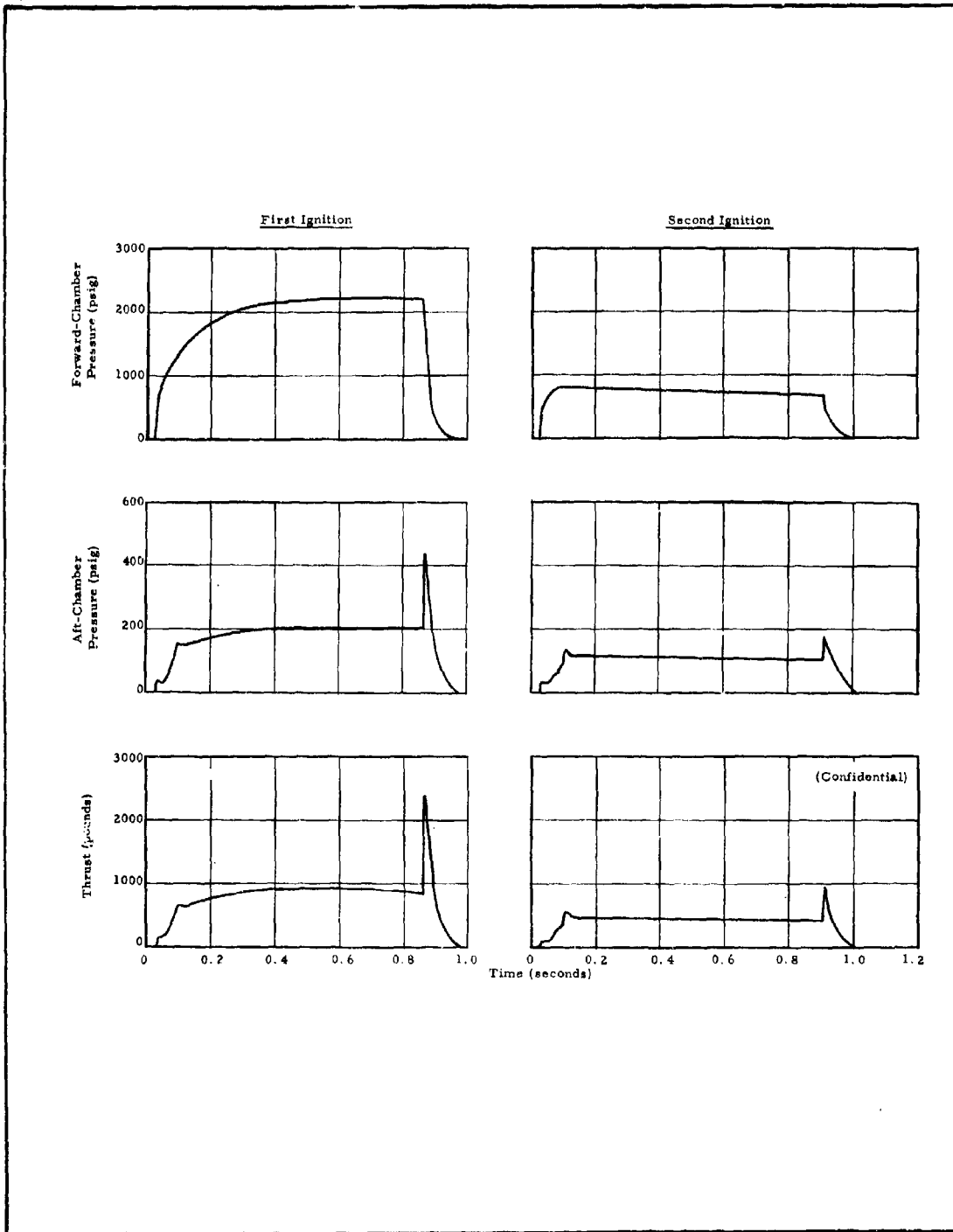


Figure 49 - Pressure- and Thrust-Time Traces for Test H. 11

CONFIDENTIAL

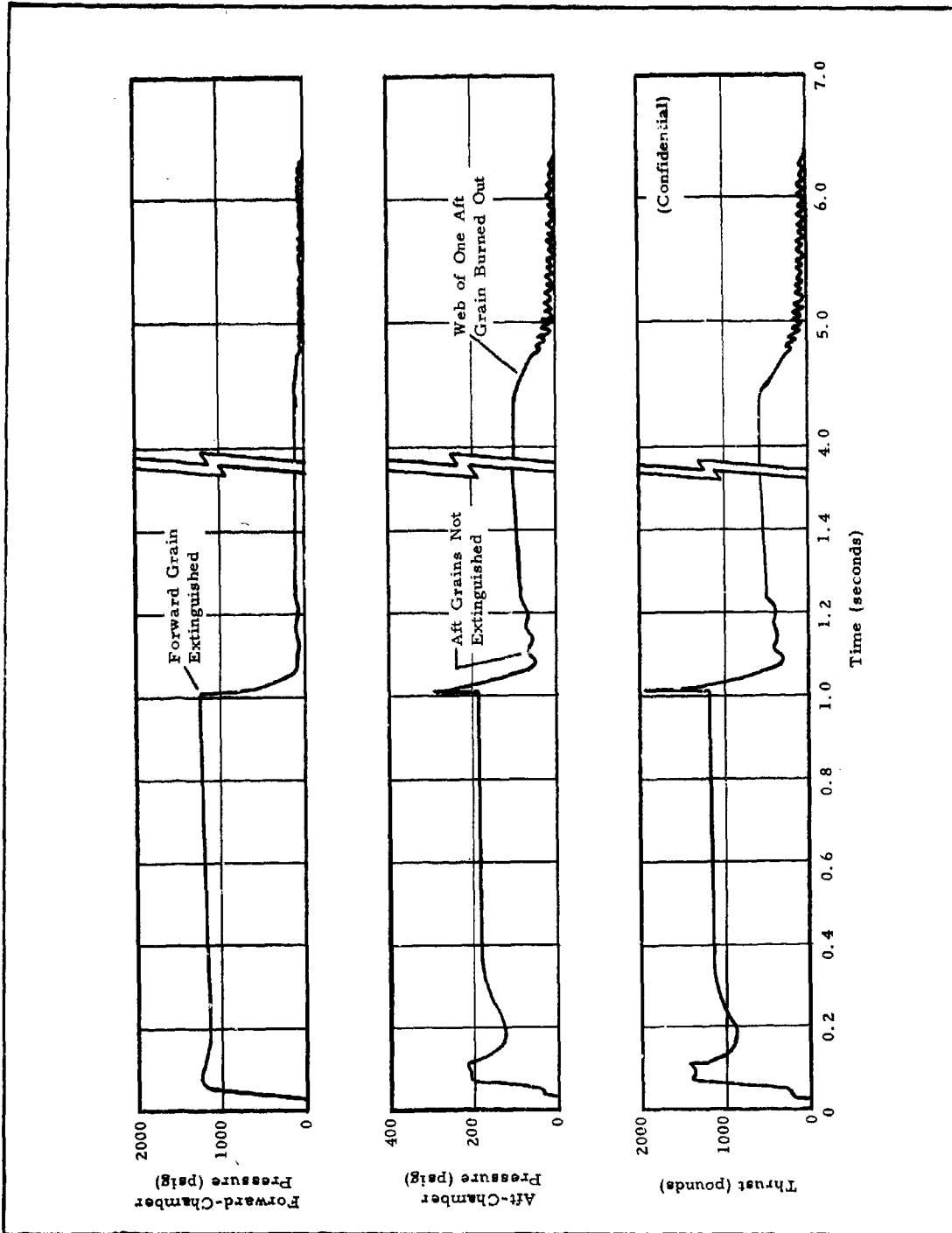


Figure 50 - Pressure- and Thrust-Time Traces for Test H. 12

during the first ignition of a grain but not thereafter, the peaks were attributed to a surface condition probably produced by the mandrel during casting and curing. (Confidential)

The post-termination combustion of the aft grains in Tests H. 10 and H. 12 shows that the propellant itself will burn stably above 50 psi, but instability occurs below this pressure. (Confidential)

(d) Processability and Mechanical Property Improvement

General

On the basis of the promising results obtained with C<sub>7</sub>FA propellant in the subscale motor tests and the successful scaling up to a 200-lb batch sizes, described in the preceding paragraphs, additional evaluation was conducted. The chief disadvantages of this propellant were its undesirably low pressure exponent (0.5 to 0.6) and elongation (10 to 12 percent). The additional effort was directed toward improving these characteristics by increasing the burning-rate pressure exponent and improving the processability and mechanical properties. (Confidential)

Effect of Increased Solid Loading

Attempts to improve processability and mechanical properties were conducted, using two approaches: (1) increasing the process temperature and (2) changing plasticizers.

In the first of these studies, the viscosity of formulation 8983-23-2, which contains 78 percent solids, was evaluated at various process temperatures. This formulation, which had previously been characterized (page 87 ), has a mix viscosity of 3.1 kilopoises (Brookfield) when processed at 75°F. Increasing the process temperature to 120°F decreased the viscosity to 1.5 kilopoises. (Confidential)

**CONFIDENTIAL**

By increasing the total solids to 79.5 percent, at 120°F, the viscosity increased to 2.6 kilopoises. Then, by further increasing the process temperature to 135°F, at this same loading, the viscosity was reduced to 2.1 kilopoises. Further increases in the solid loading, at 135°F, increased the viscosity as follows:

<u>Solid Loading</u> (percent)	<u>Viscosity</u> (kilopoises)
80.0	2.4
80.5	2.5
80.8	3.3

The final value of 3.3 kilopoises is near the maximum processable mix viscosity. Moreover, increasing the process temperature to 120 or 135°F requires the addition of a cure inhibitor. (Confidential)

Since increasing the total solids to 80 percent produced only a slight increase in the burning-rate pressure exponent, it was decided not to pursue this approach any further. Significantly, the solid loading of formulations under development by Northrop Carolina approached that of highly loaded state-of-the-art composite propellants, as shown in Table XXX. (Confidential)

After the investigation of the effect of process temperature on solids loading was completed, the effect of changing plasticizers was investigated. By substituting Viton LM for Viton A, the solid loading of C<sub>7</sub>FA propellant was generally increased from 78 to 83 percent without affecting the processability. Viton LM, which has a lower molecular weight than Viton A, is a wax at room temperature. As mentioned above, formulation 8983-23-2, which contains Viton A, had a viscosity of 3.1 kilopoises at 75°F, but with Viton LM substituted for Viton A, the viscosity dropped to 0.4 kilopoises at 75°F. The 83-percent solid loaded propellant containing Viton LM had a viscosity of 2.1 kilopoises. (Confidential)

**CONFIDENTIAL**

CONFIDENTIAL

AFRPL-TR-65-209, Vol I

TABLE XXX - COMPARISON OF PROPERTIES OF NORTHROP CAROLINA FLUOROCARBON FORMULATIONS WITH STATE-OF-THE-ART COMPOSITE PROPELLANT

Property	Formulation		
	TP-H-1001*	8983-23-2†	8983-30-2‡
Composition (percent by weight)			8983-33-2
PBAA binder	14.0	...	...
C <sub>7</sub> FA binder	...	22.0	...
FX-189 binder	...	...	22.0
Ammonium perchlorate	70.0	63.0	75.0
Aluminum	16.0	15.0	3.0
Solid loading			
Percent by weight	86.0	78.0	78.0
Percent by volume	75.6	72.9	73.8
Density, theoretical (lb/cu in.)	0.0653	0.0696	0.0674

(Confidential)

\* State-of-the art composite propellant.

† Described in Table XXIV.

‡ Described on page 107.

§ Described on page 135.

CONFIDENTIAL

However, the substitution of Viton LM for Viton A adversely affected the mechanical properties (see following paragraph). At a 78-percent solid loading, the tensile strength was reduced from 85 to 51 psi and elongation at maximum stress from 10 to 6 percent. Apparently, then, the Viton LM, with its lower molecular weight, improves binder mobility in the uncured condition while Viton A has a reinforcing, rather than diluting, effect on the cured polymer. (Confidential)

The above formulations with Viton A and LM contained a trimodal blend of ammonium perchlorate, with 600 micron/200 micron/10 micron particle sizes in a 25/50/25 percent distribution, respectively. The effect of the 600-micron particle size on processability was determined by preparing a batch without this large particle size. This batch, with 78 percent solids, had a viscosity of 6.0 kilopoises, compared to 3.1 kilopoises for the trimodal blend. (Confidential)

#### Effect of Binder Modifications

The low elongation of the C<sub>7</sub>FA propellant is probably caused by the lack of unsaturation in the polymeric backbone and the bulky side groups attached to the chain. The addition of Viton A, a gum rubber fluorocarbon, to the C<sub>7</sub>FA propellants increased elongation slightly, and tensile strength was increased by the addition of TAC, a cross-linking agent (see page 85). Formulation 8983-23-2, which contains Viton A and TAC, was cast into a full-scale motor, as described on page 89. This batch exhibited a tensile strength of 88 psi and an elongation of 11 percent. After the grain cured, its integrity was good. However, after storage for three weeks at temperatures ranging from 45 to 80°F, X-rays indicated that a small crack had developed in the web. (Confidential)

An evaluation of catalyst and catalyst concentration on the cure of unloaded C<sub>7</sub>FA binder was also conducted. The catalysts evaluated were 2.4 dichlorobenzoyl peroxide, benzoyl peroxide, lauryl peroxide,

methyl ethyl ketone peroxide, ammonium persulfate, and VAZO. The cures obtained with 2.4 dichlorobenzoyl peroxide, benzoyl peroxide, and VAZO were superior to those obtained with the other catalysts; no cure was obtained with ammonium persulfate and methyl ethyl ketone peroxide. For the C<sub>7</sub>FA/Viton A system, a concentration of 2.4 dichlorobenzoyl peroxide equal to 1.75 percent of the binder produced the best cure. (Confidential)

The effect of plasticizer was also evaluated with C<sub>7</sub>FA gumstock. The substitution of Viton LM for Viton A did not affect the cure, but reduced the tensile strength, as mentioned above. The most promising binder contained a 2-to-1 ratio of Viton LM to Viton A. The mechanical properties of this binder were equal to or superior to those of Viton A alone, and processability was improved. (Confidential)

Additional binder studies were conducted, with a 78-percent solid loaded system, to ascertain the relationship of Viton A and Viton A/Viton LM on mechanical properties. Figure 51 presents the effect of Viton A concentration on mechanical properties, showing that elongation increases and tensile strength decreases as Viton A concentration increases. The effect of Viton LM concentration on mechanical properties, with Viton A concentration constant at two percent, is shown in Figure 52. Here, both tensile strength and elongation increase with increased Viton LM concentration up to four percent. Thus, the use of combined plasticizers improves the properties of the C<sub>7</sub>FA system somewhat. (Confidential)

#### Effect of Additives

The effect of additives on the mechanical properties of C<sub>7</sub>FA propellant was investigated; the additives used were MgO (in aluminum), aluminum, tricalcium phosphate (in ammonium perchlorate), and hydroquinone (in C<sub>7</sub>FA). Batches of a standard formulation containing 18.7 percent C<sub>7</sub>FA and 2.75 percent Viton A were used, with the above additives varied in

**CONFIDENTIAL**

AFRPL-TR-65-209, Vol I

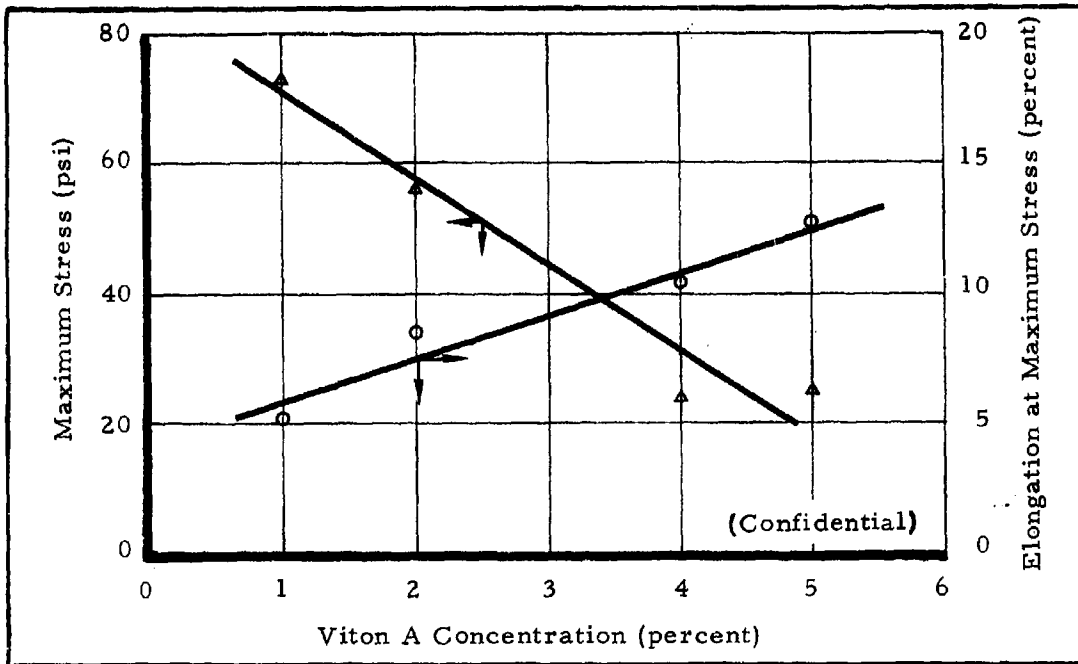


Figure 51- Effect of Viton A Concentration on Mechanical Properties of C<sub>7</sub>FA Propellant

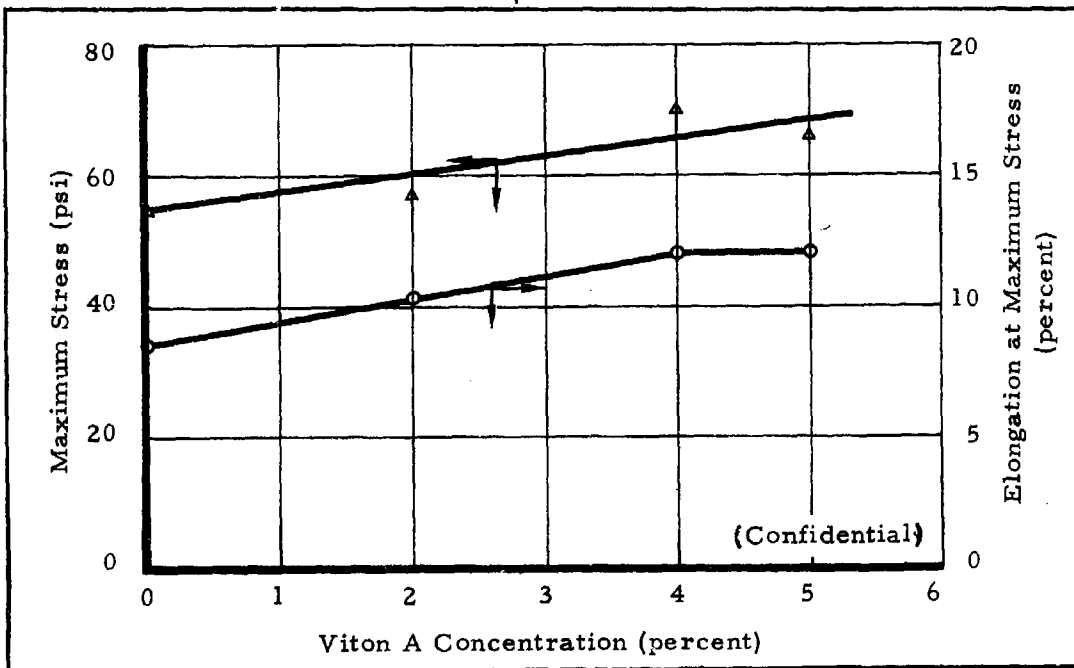


Figure 52- Effect of Viton LM Concentration on Mechanical Properties of C<sub>7</sub>FA Propellant Containing Two Percent Viton A

**CONFIDENTIAL**

the pattern shown in Table XXXI. The mechanical properties were then measured, yielding the results given in the table. (Confidential)

Hydroquinone was added by using the unwashed C<sub>7</sub>FA binder, which contains hydroquinone as an inhibitor. To obtain batches without hydroquinone, the hydroquinone was simply removed by washing. The effect of aluminum was evaluated by comparing batches containing Reynolds 400 aluminum (which contained MgO), high-purity H-5 aluminum, and no aluminum.

The presence of hydroquinone (unwashed C<sub>7</sub>FA) had little effect on the mechanical properties. Likewise, the addition of tricalcium phosphate had little effect. The addition of high-purity H-5 aluminum reduced the tensile strength, while the addition of Reynolds 400 aluminum generally resulted in slightly superior properties than batches without aluminum. (Confidential)

(e) Modification of Burning-Rate Pressure Exponent

General

The pressure exponent for formulation 8983-23-2, obtained from strand burning-rate data, was 0.49 below 300 psi, as shown in Figure 53. Since a pressure exponent near unity is desired for the aft-grain propellant, an effort to increase the exponent by modifying the formulation was begun. Two approaches were used to increase the burning-rate pressure exponent: (1) incorporating burning-rate additives and secondary oxidizers, and (2) increasing the solid loading. These burning-rate evaluations were conducted in Northrop Carolina's Crawford-type strand bomb at 75°F under nitrogen pressurization. (Confidential)

Initial Studies

Initially, Sylon "S," a very small particle size silica, was added to formulation 8983-23-2. This

**TABLE XXXI-EFFECT OF ADDITIVES ON MECHANICAL PROPERTIES OF  
C<sub>7</sub>FA PROPELLANT**

Aluminum	Additive Used		TCP*	Mechanical Properties		
	Hydroquinone			Maximum Stress (psi)	Elongation at Maximum Stress, $\epsilon_m$ (%)	Modulus of Elasticity, $E_o$ (psi)
R-400	X		X	94.9	8.3	1500
R-400	X		.	91.6	9.1	1300
H-5	X		.	68.6	7.5	1300
.	X		X	73.0	7.3	1250
R-400	.	.	X	89.2	9.7	1164
R-400	.	.	.	101.9	8.8	1365
H-5	.	.	.	67.5	9.1	1000
.	.	.	X	93.2	6.5	2000

\*The tricalcium phosphate (0.2 percent) was added to ground ammonium perchlorate.  
(Confidential)

# CONFIDENTIAL

AFRPL-TR-65-209, Vol I

additive increased the exponent to 0.64 below 500 psi, as shown in Figure 54, which also presents the composition of this formulation (8983-33-3). (Confidential)

Next, the aluminum content was decreased to three percent. Figure 55 shows that the burning rate for this formulation (8983-30-2) below 300 psi is slightly higher than that of formulation 8983-23-2, which contained 15 percent aluminum. However, the pressure exponents for both formulations below 300 psi were identical. (Confidential)

The addition of Sylon "S" to the three-percent aluminum formulation had very little effect on the pressure exponent, as shown in Figure 56. (Confidential)

Iron oxide increased the pressure exponent slightly (see Figure 57), whereas carbon black

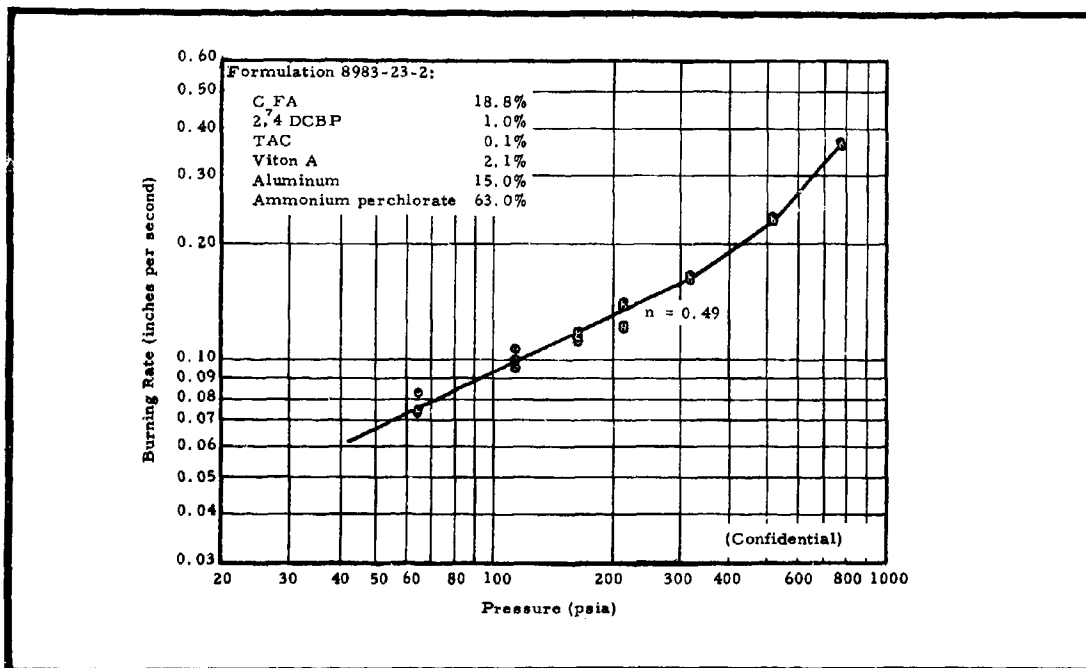


Figure 53 - Strand Burning-Rate Data for Formulation 8983-23-2

-107-

# CONFIDENTIAL

**CONFIDENTIAL**

AFRPL-TR-65-209, Vol I

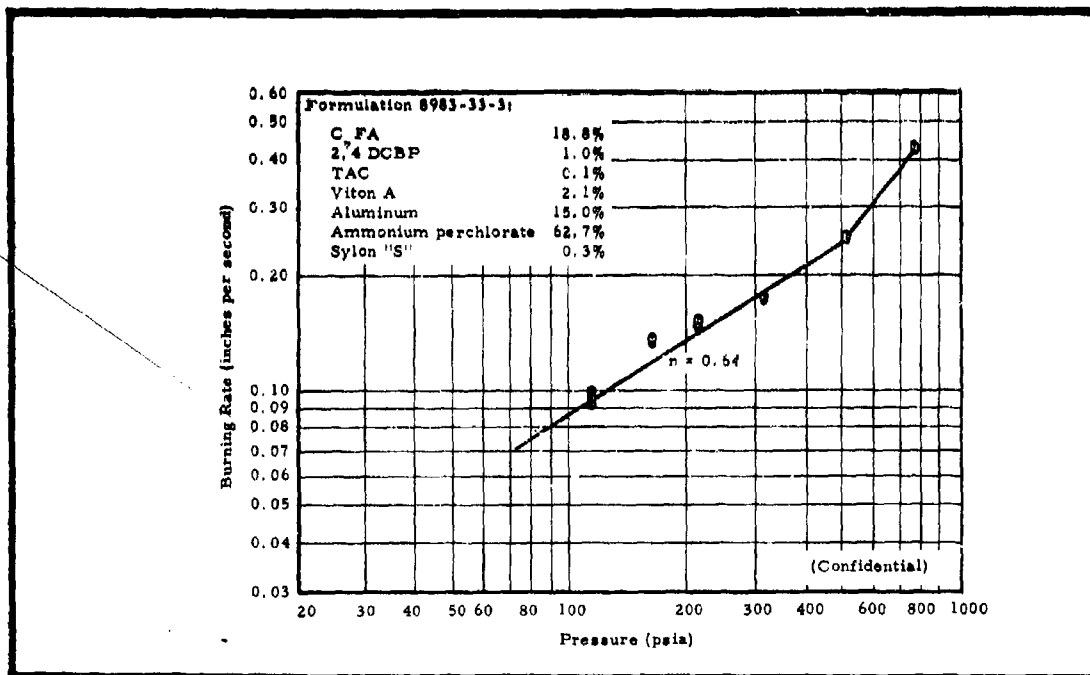


Figure 54 - Strand Burning-Rate Data for Formulation 8983-33-3

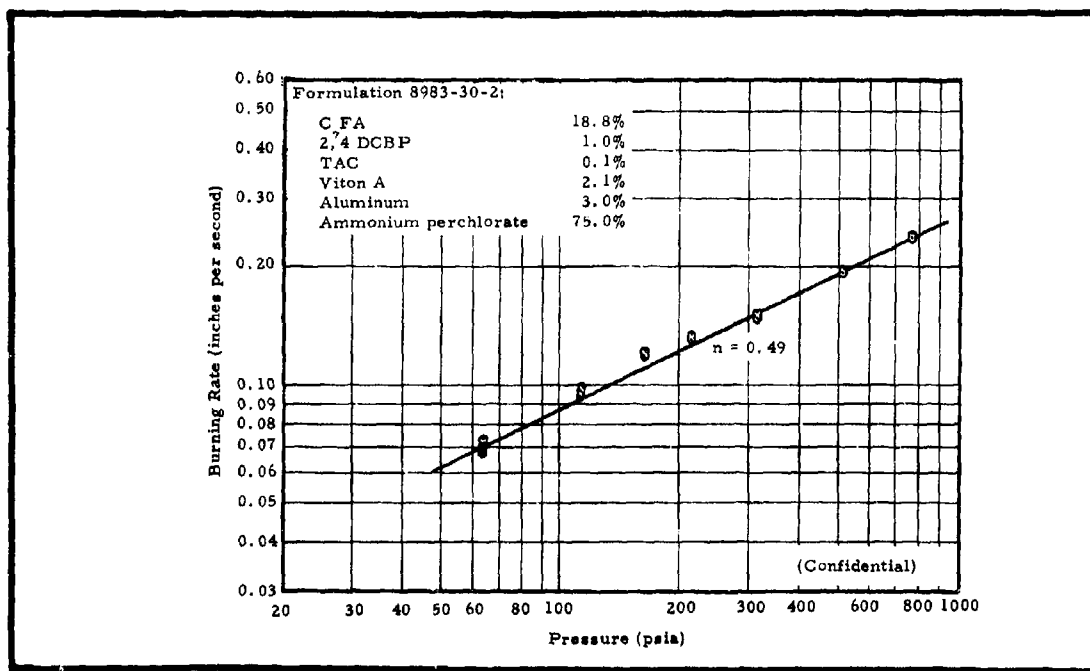


Figure 55 - Strand Burning-Rate Data for Formulation 8983-30-2

**CONFIDENTIAL**

# CONFIDENTIAL

AFRPL-TR-65-209, Vol I

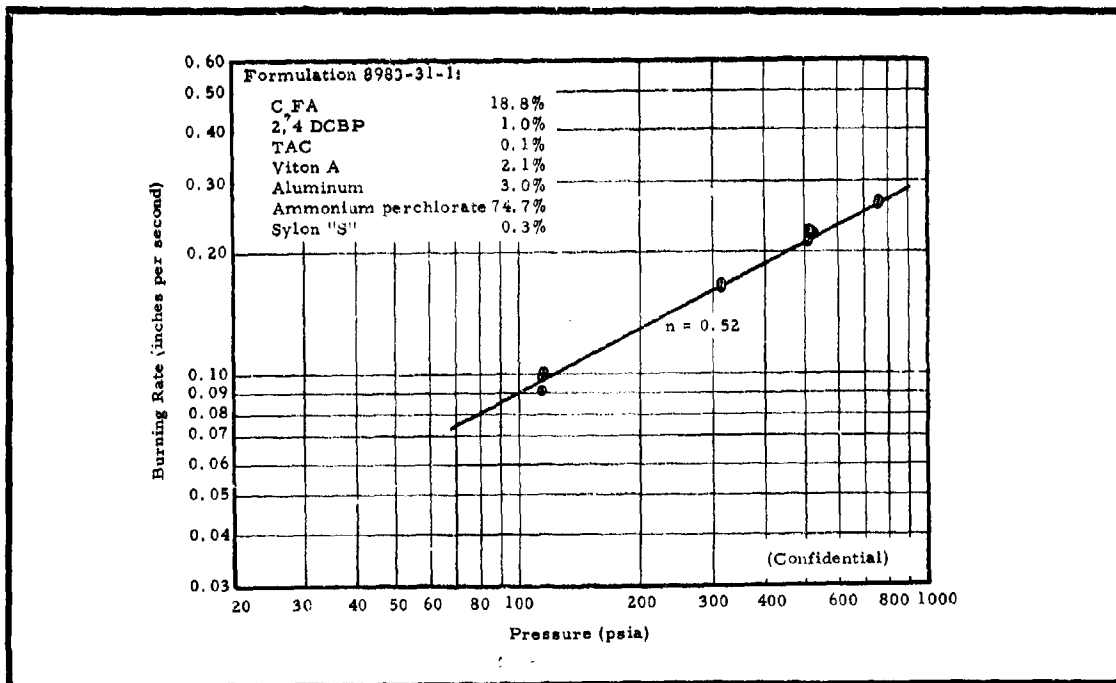


Figure 56 - Strand Burning-Rate Data for Formulation 8983-31-1

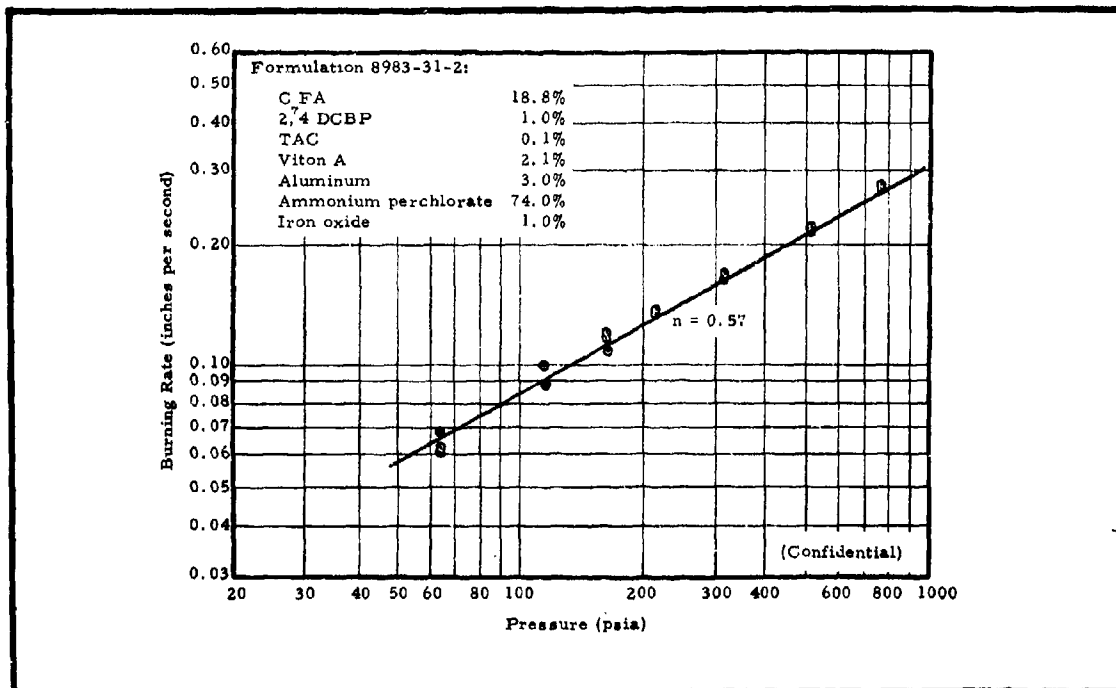


Figure 57 - Strand Burning-Rate Data for Formulation 8983-31-2

# CONFIDENTIAL

AFRPL-TR-65-209, Vol I

produced about the same effect as Sylon "S" (see Figure 58). (Confidential)

In Formulation 8983-33-4, 20 percent potassium perchlorate was substituted for ammonium perchlorate. The pressure exponent of this formulation was less than that of the formulation without potassium perchlorate (8983-30-2) below 300 psi, as shown in Figure 59. (Confidential)

The highest pressure exponent obtained for the  $C_7FA$  system was achieved by the substitution of 20 percent HMX for ammonium perchlorate. A pressure exponent of 0.81 was obtained, as shown in Figure 60. (Confidential)

## Effect of Additives

Polyethylene Hydrazine Perchlorate-The  
strand burning-rate data for formulation 8983-37-1,

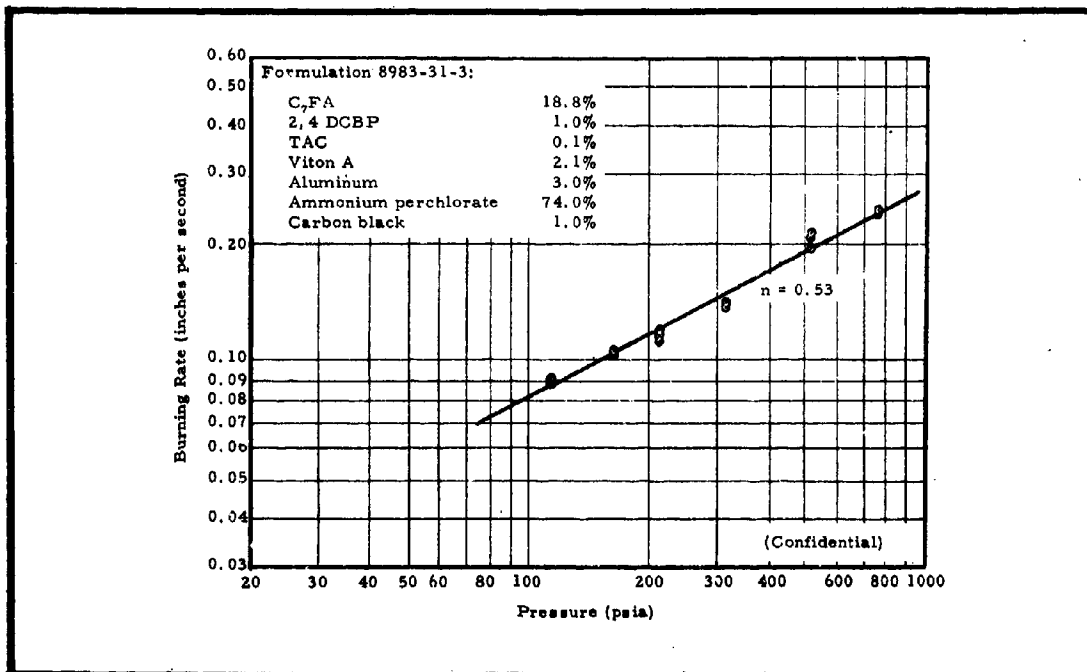


Figure 58 - Strand Burning-Rate Data for Formulation 8983-31-3

-110-

# CONFIDENTIAL

# CONFIDENTIAL

AFRPL-TR-65-209, Vol I

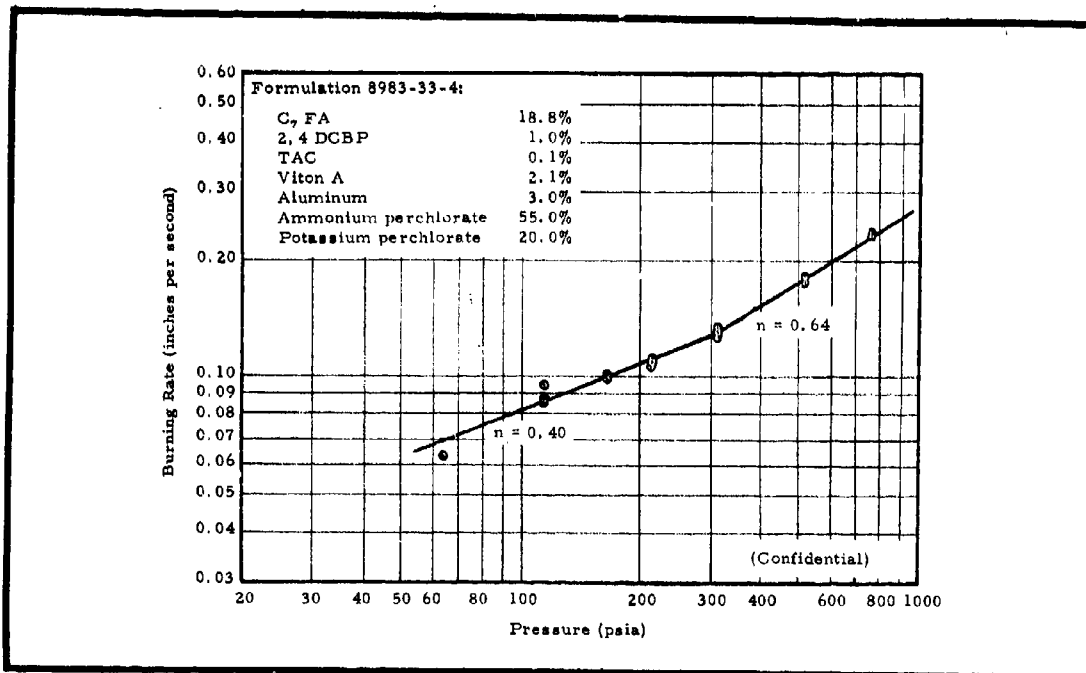


Figure 59 - Strand Burning-Rate Data for Formulation 8983-33-4

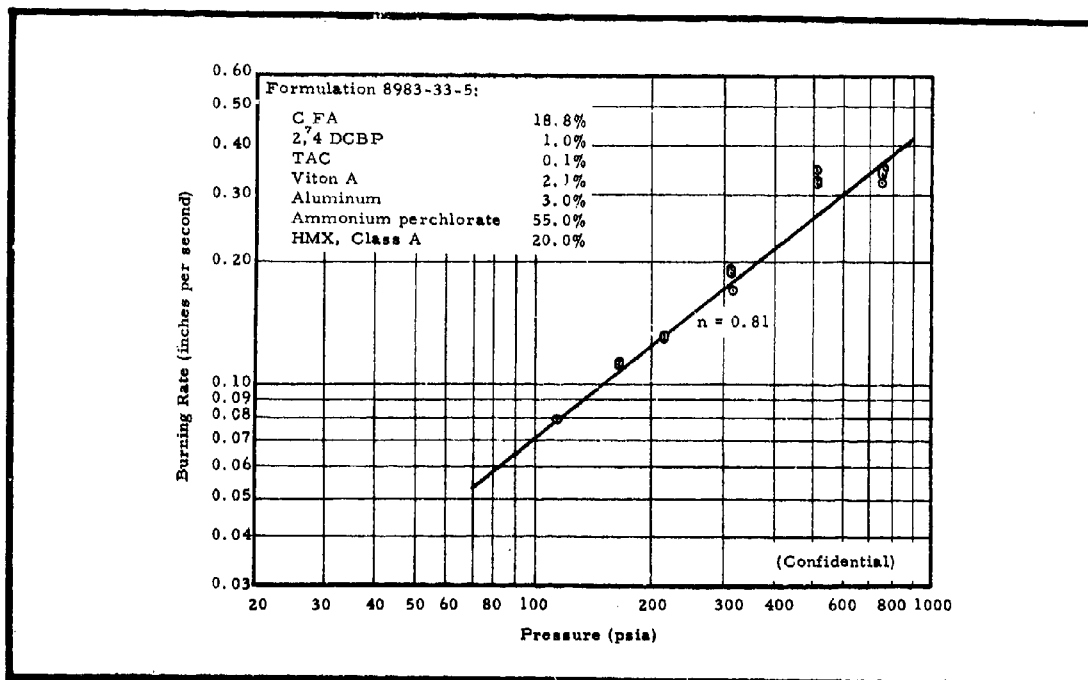


Figure 60 - Strand Burning-Rate Data for Formulation 8983-33-5

# CONFIDENTIAL

AFRPL-TR-65-209, Vol I

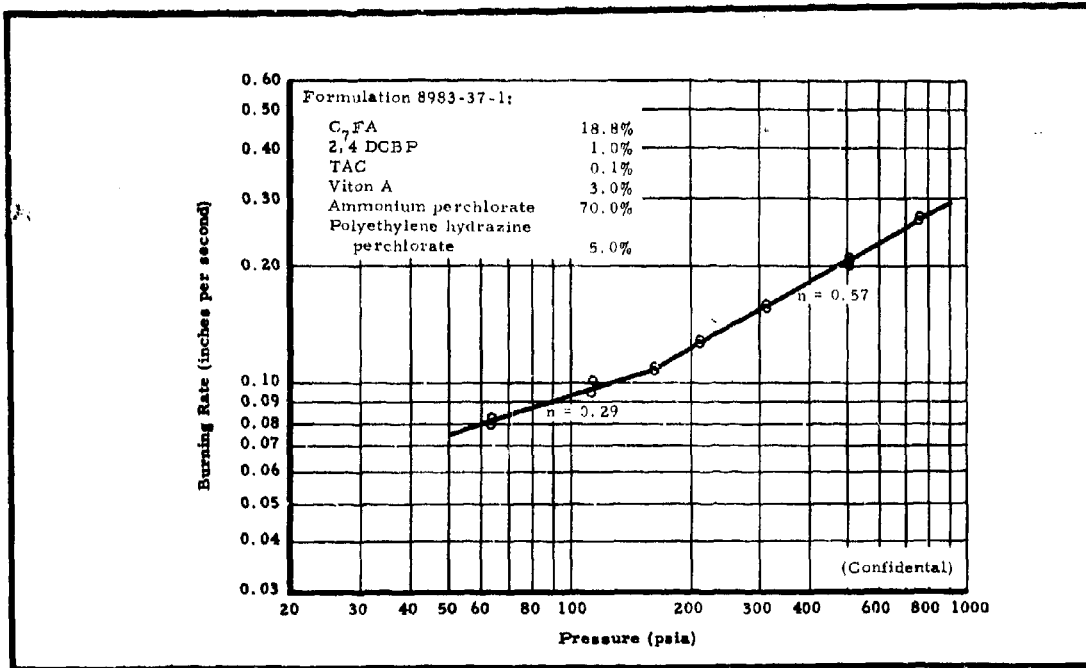


Figure 61 - Strand Burning-Rate Data for Formulation 8983-37-1

which contained five percent of the additive polyethylene hydrazine perchlorate, are given in Figure 61. The low pressure exponent of 0.29 below 200 psi was lower than that obtained with formulation 8983-30-2, which was similar but contained no polyethylene hydrazine perchlorate. Data for the latter formulation were given on page 107 (Confidential)

TEGDN-The effect of adding TEGDN to the basic formulation (8983-30-2) is shown in Figure 62, for formulation 8983-38-1. The overall pressure exponent over the range from 50 to 750 psi was near that obtained for formulation 8983-30-2 (page 107), which contained no TEGDN. Moreover, the addition of TEGDN produced a propellant that was crumbly and had very poor physical properties. (Confidential)

# CONFIDENTIAL

AFRPL-TR-65-209, Vol I

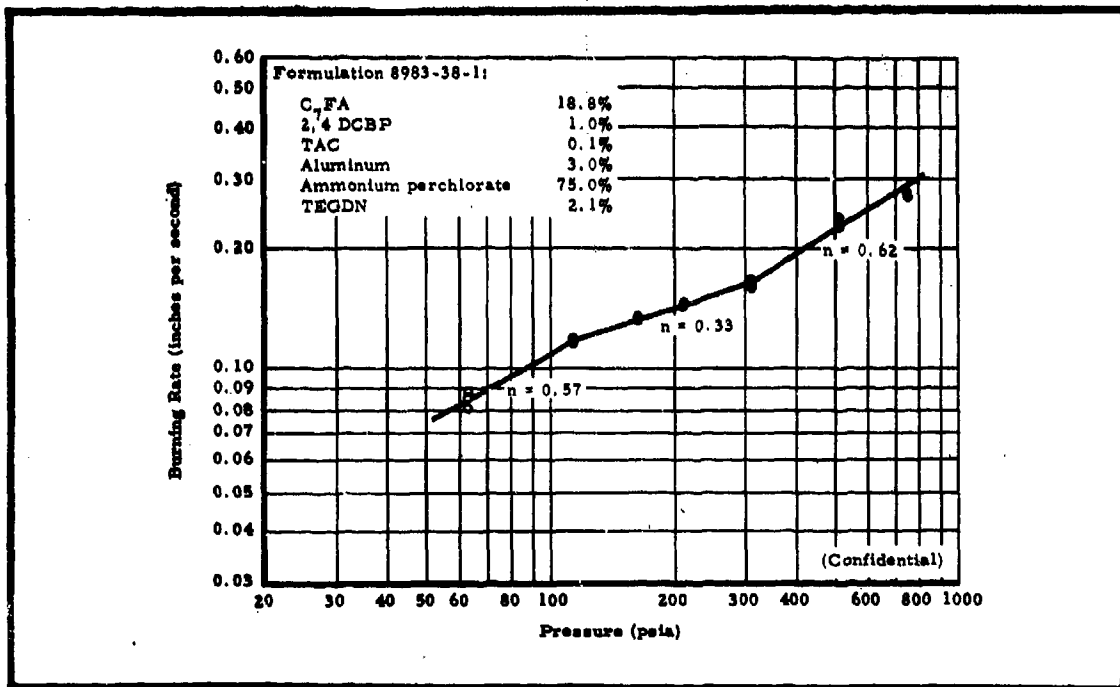


Figure 62 - Strand Burning-Rate Data for Formulation 8983-38-1

Nitroguanidine-The addition of 2.2 percent nitroguanidine, in formulation 8983-38-3, increased the slope to 0.64 below 100 psi, as shown in Figure 63. However, as with TEGDN, the overall slope was not increased. (Confidential)

Copper Chromite-The effect of adding two percent copper chromite on burning rate is shown in Figure 64. For this formulation (8933-38-4), the pressure exponent was increased to 0.65 above 100 psi; but below 100 psi, the slope was very low (0.25). Increasing the concentration of copper chromite to five percent did not significantly affect the exponents, as shown in Figure 65 for formulation 8983-39-4. Formulation 8983-39-3, in which copper chromite and Sylon "S" were combined, yielded a burning rate similar to the formulations with copper chromite alone, as shown in Figure 66. (Confidential)

# CONFIDENTIAL

AFRPL-TR-65-209, Vol I

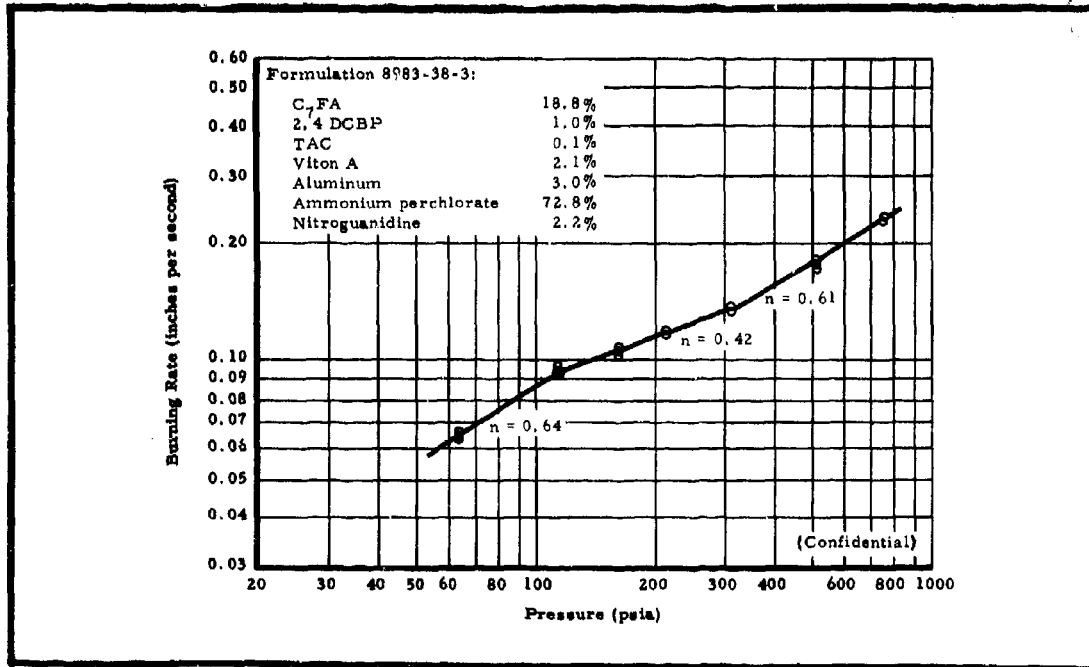


Figure 63 - Strand Burning-Rate Data for Formulation 8983-38-3

Iron Oxide-It was learned that the addition of one percent iron oxide increased the exponent of the basic three-percent aluminum formulation from 0.49 to 0.57 (page 107). The concentration of iron oxide was increased to three percent in formulation 8983-38-5, but no further increase in pressure exponent below 500 psi was achieved (Figure 67). (Confidential)

HMX-The addition of 20 percent HMX (in formulation 8983-33-5) increased the pressure exponent to 0.81, above 100 psi. However, these results were not duplicated in subsequent batches of this same formulation; an exponent of 0.73, above 100 psi, was achieved in preliminary tests. Below 100 psi, the burning rate tended to plateau. When a smaller particle size HMX (Class E; less than 10 micron) was used in the same basic formulation, the exponent was reduced below that obtained with the larger particle size Class A HMX, as

# CONFIDENTIAL

AFRPL-TR-65-209, Vol I

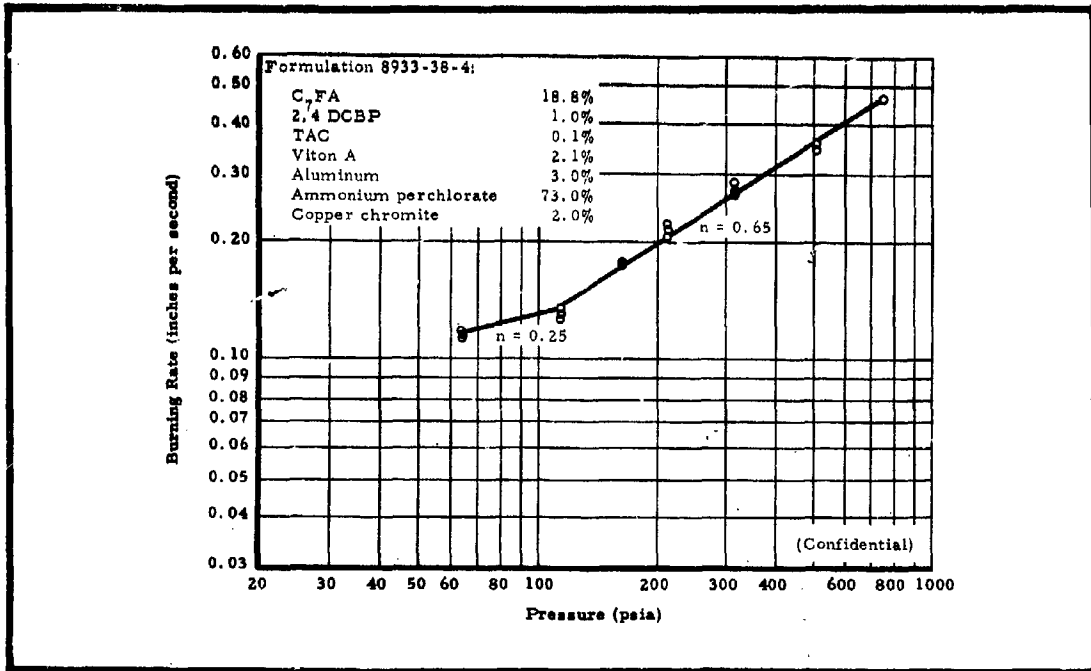


Figure 64 - Strand Burning-Rate Data for Formulation 8933-38-4

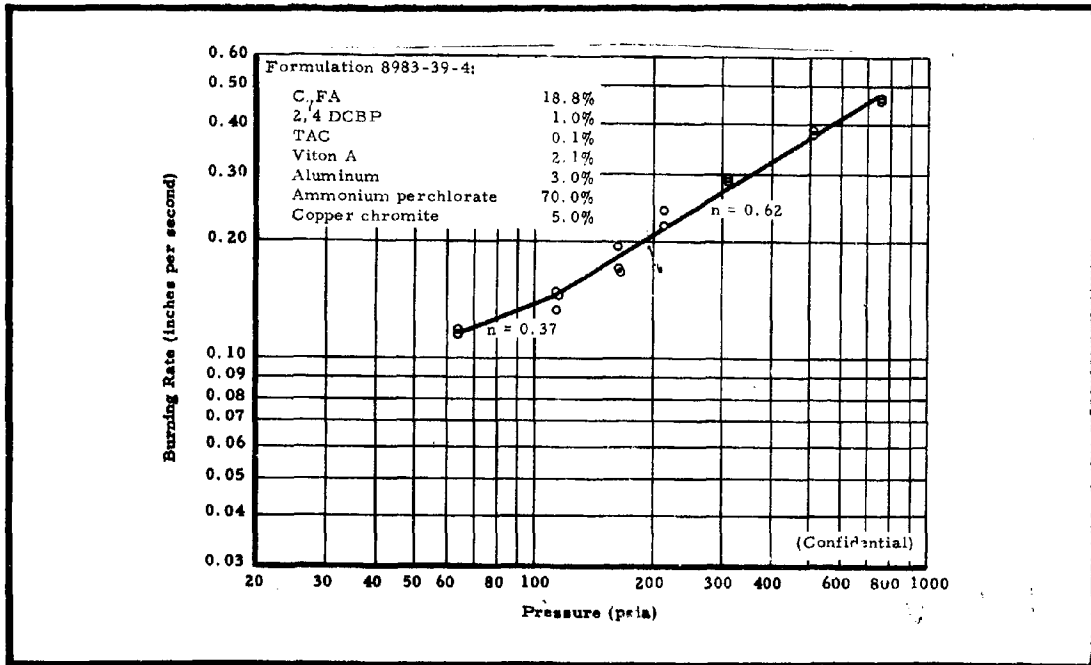


Figure 65 - Strand Burning-Rate Data for Formulation 8983-39-4

# CONFIDENTIAL

**CONFIDENTIAL**

AFRPL-TR-65-209, Vol I

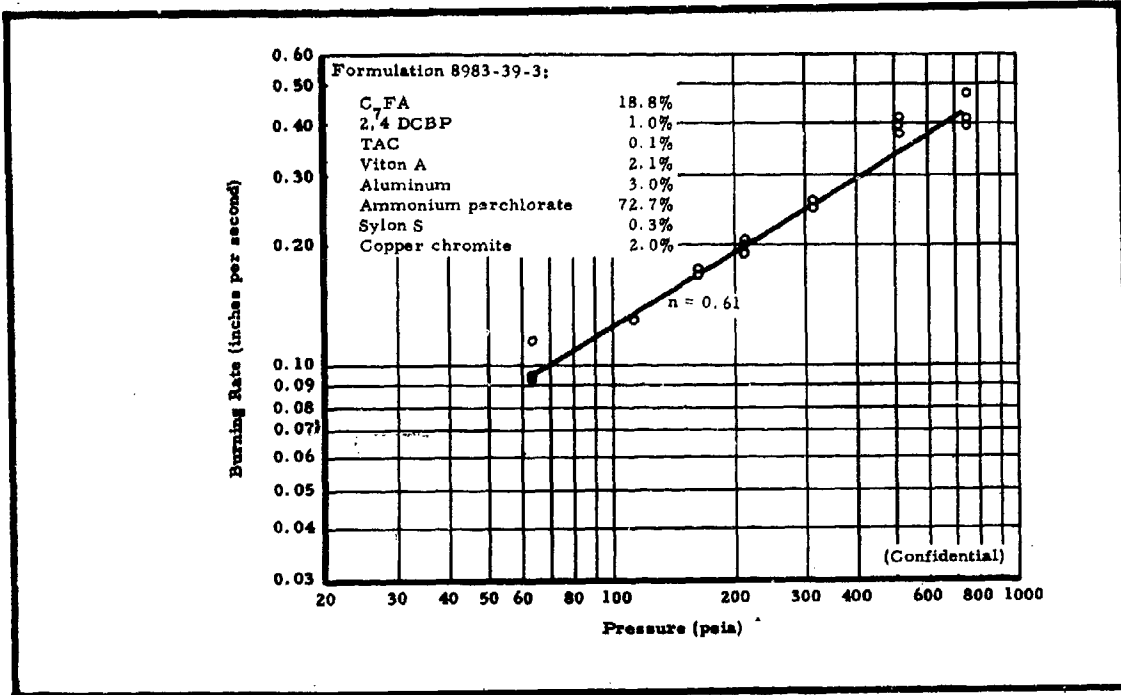


Figure 66 - Strand Burning-Rate Data for Formulation 8983-39-3

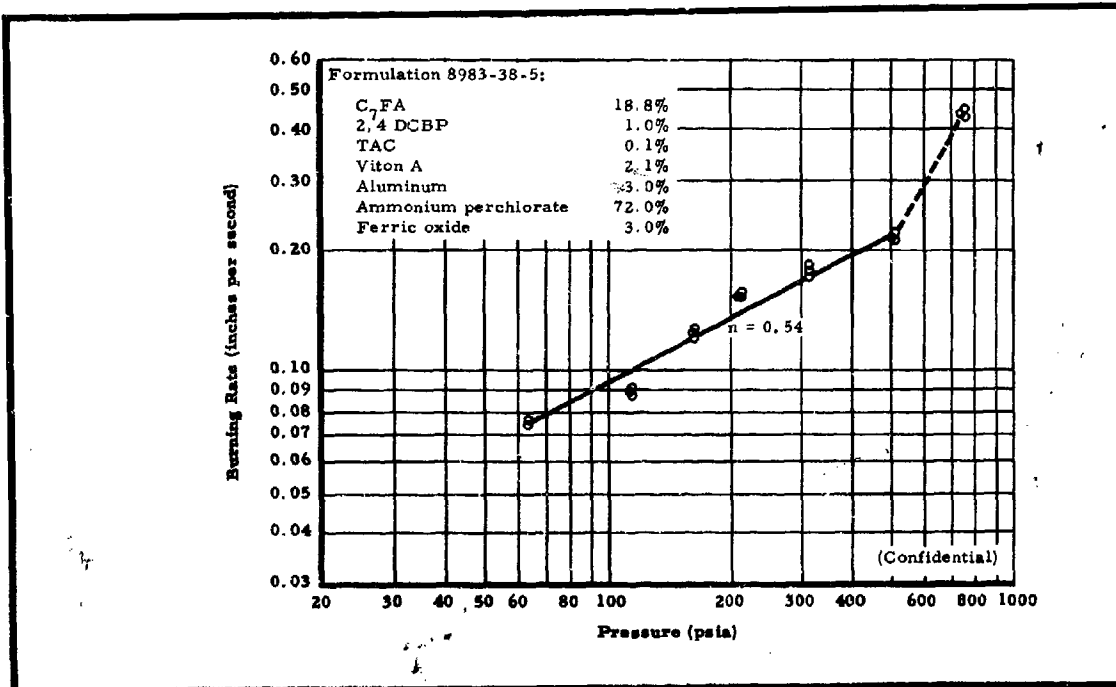


Figure 67 - Strand Burning-Rate Data for Formulation 8983-38-5

**CONFIDENTIAL**

# CONFIDENTIAL

AFRPL-TR-65-209, Vol I

shown in Figure 68. To investigate further the inconsistent results obtained with HMX as an additive, a more thorough pressure burning-rate profile was conducted using formulation 8983-43-1, which contained 20 percent Class A HMX and 3 percent aluminum. The resulting burning-rate curve, shown in Figure 69, had two slight breaks in it, with the exponent in each region being lower than desired. (Confidential)

The effect of adding two percent oxamide to formulation 8983-43-1 was investigated. Although the strand burning-rate data for this formulation (8983-44-1), shown in Figure 70, formed a straight line, the burning rates were very close to those achieved previously without oxamide, and the overall slope was nearly the same for both. (Confidential)

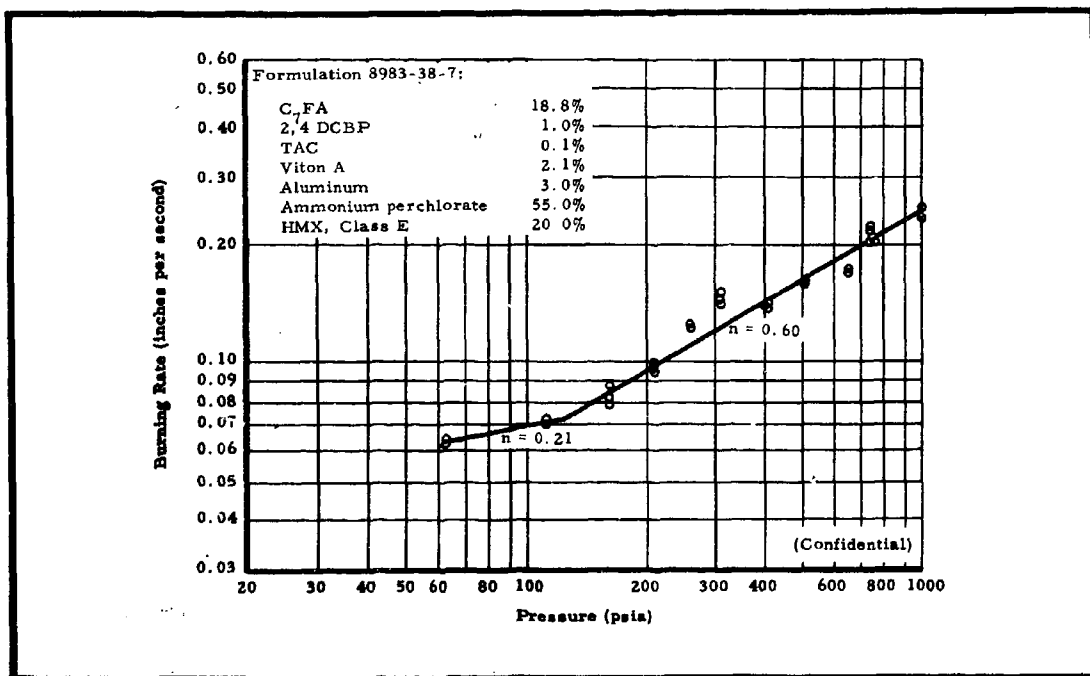


Figure 68 - Strand Burning-Rate Data for Formulation 8983-38-7

# CONFIDENTIAL

**CONFIDENTIAL**

AFRPL-TR-65-209, Vol I

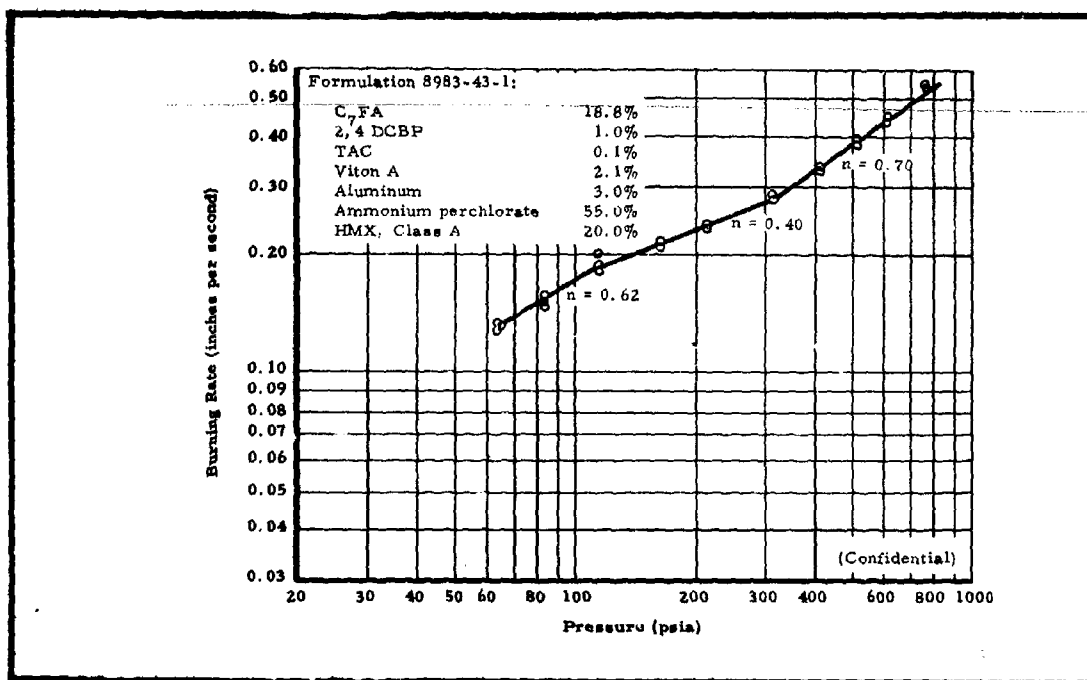


Figure 69 - Strand Burning-Rate Data for Formulation 8983-43-1

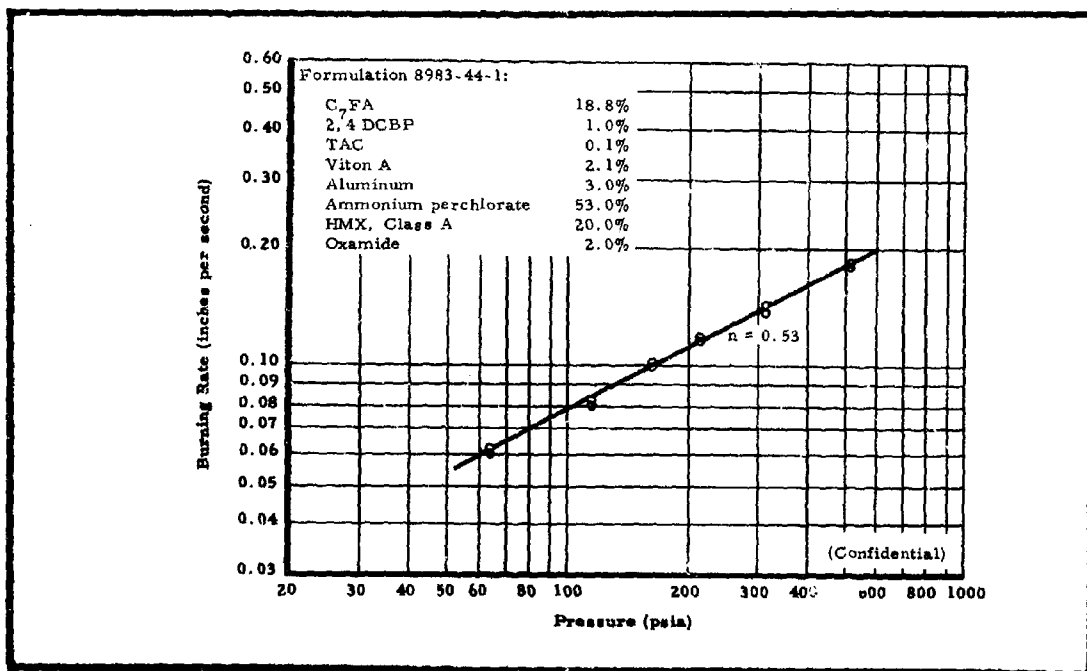


Figure 70 - Strand Burning-Rate Data for Formulation 8983-44-1

**CONFIDENTIAL**

**CONFIDENTIAL**

Additional evaluations were conducted in which HMX was combined with the additives copper chromite, nitroguanidine, ferric oxide, and ferric oxide and Sylon "S" in the C<sub>7</sub>FA system. The results of these tests are shown in Figures 71 through 74, respectively. None of these additives with HMX improved the burning-rate pressure exponent; instead, the formulation containing HMX alone (Figure 68) produced a higher exponent above 100 psi than HMX combined with the other additives. (Confidential)

The preceding formulations incorporating HMX contained three percent aluminum. HMX was also evaluated in a 15-percent aluminum formulation (8983-35-2), giving the results shown in Figure 75. A pressure exponent of 0.73 was obtained above 100 psi, but below this pressure, the exponent dropped to 0.21. (Confidential)

A further evaluation of the effect of HMX was conducted on a 78-percent solid loaded formulation containing a larger ammonium perchlorate particle size; that is, a 70/30 ratio of unground (500 to 1200 micron) to ground. The burning-rate curve for this formulation (8983-43-1), shown in Figure 76, is similar to that obtained with the smaller ammonium perchlorate particle size in that the pressure exponent decreased sharply at pressures below 100 psi. (Confidential)

Ethyl Ortho Silicate-Of the available ortho silicates, ethyl ortho silicate was the only one found to be miscible with the C<sub>7</sub>FA binder. Incorporating three percent ethyl ortho silicate increased the burning rate, but did not increase pressure exponent, as shown in Figure 77. By adding both ethyl ortho silicate and ferric oxide, burning rate was further increased, and the exponent was increased slightly (from 0.50 to 0.56), as shown in Figure 78. (Confidential)

Coolants-The effects of several coolants on burning rate were evaluated, including oxamide, oxamide and copper chromite, guanidine carbonate,

**CONFIDENTIAL**

**CONFIDENTIAL**

AFRPL-TR-65-209, Vol I

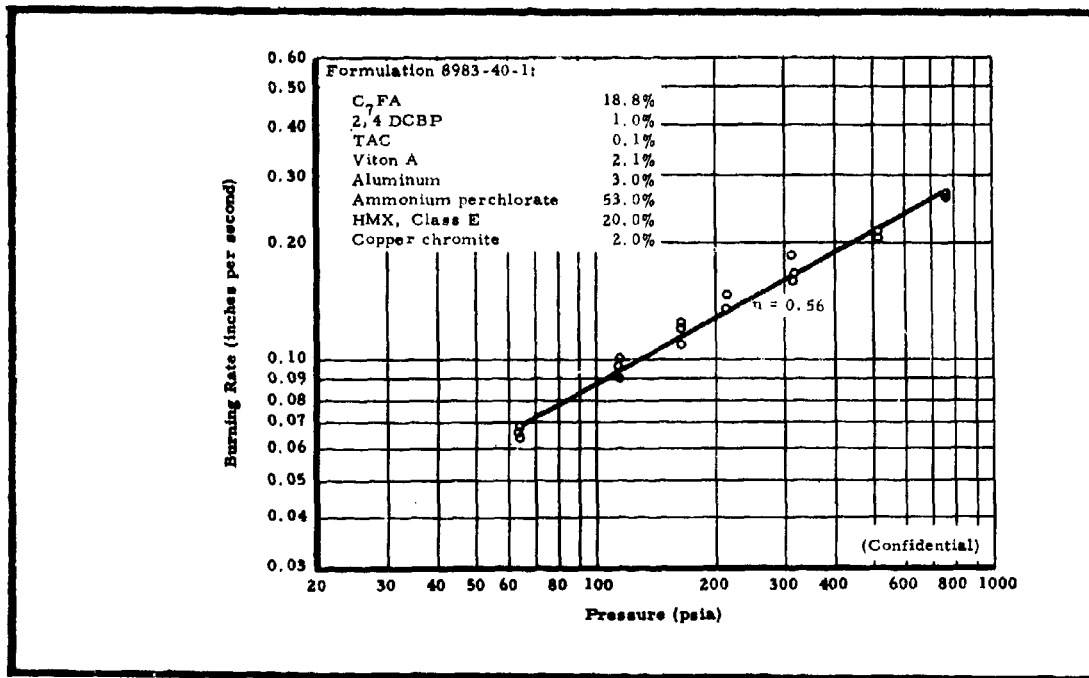


Figure 71 - Strand Burning-Rate Data for Formulation 8983-40-1

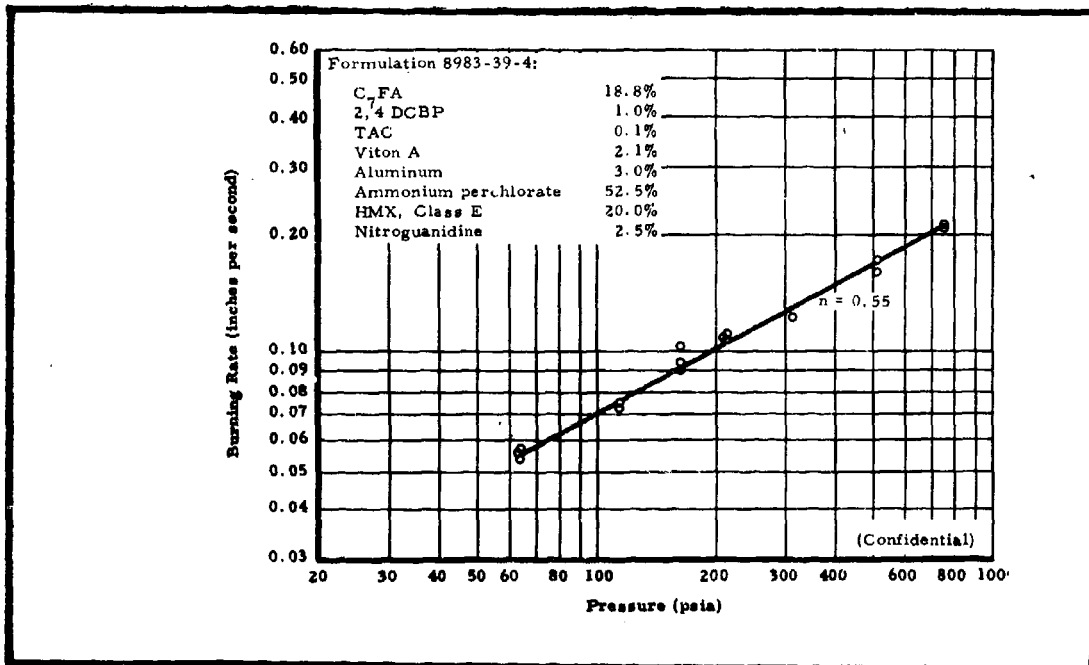


Figure 72 - Strand Burning-Rate Data for Formulation 8983-39-4

**CONFIDENTIAL**

**CONFIDENTIAL**

AFRPL-TR-65-209, Vol I

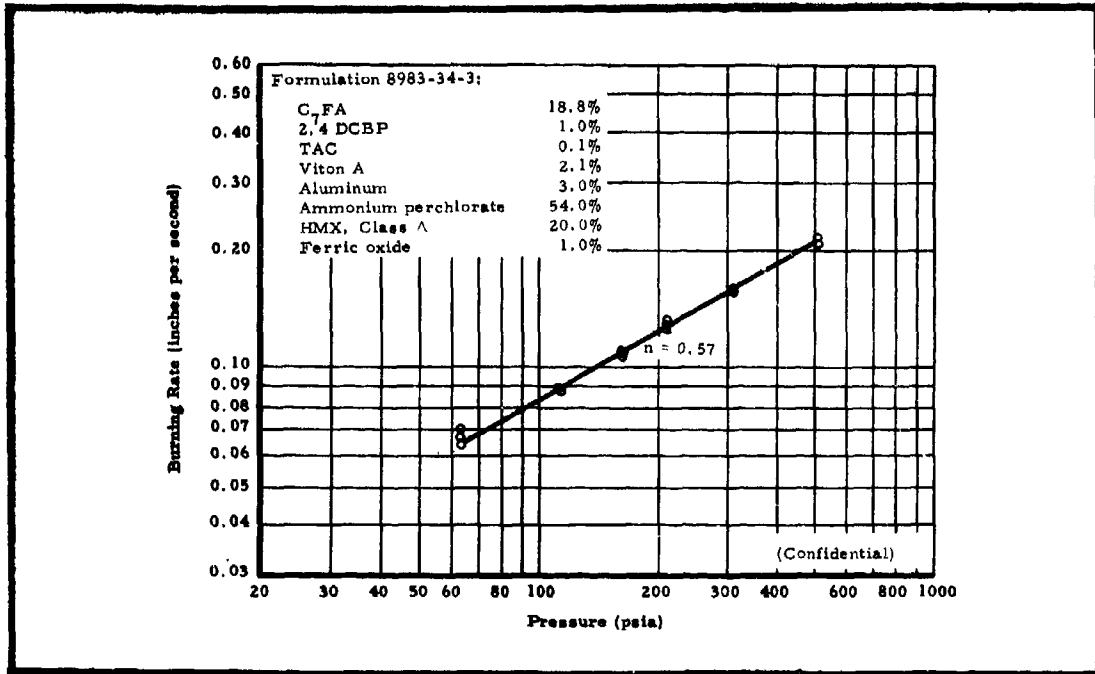


Figure 73 - Strand Burning-Rate Data for Formulation 8983-34-3

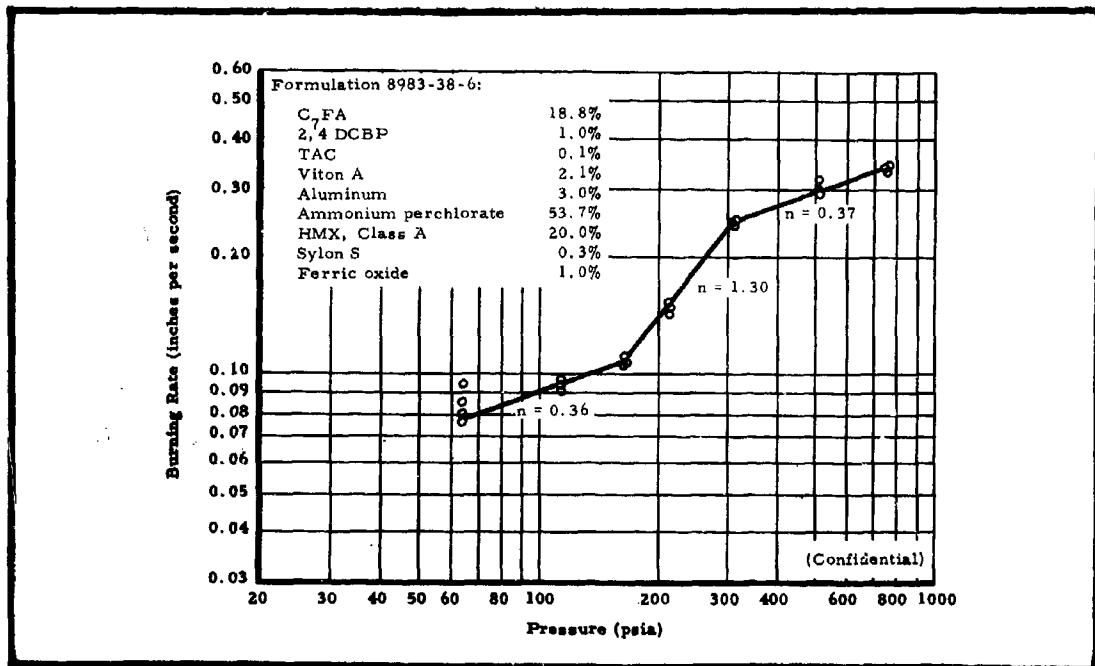


Figure 74 - Strand Burning-Rate Data for Formulation 8983-38-6

**CONFIDENTIAL**

# CONFIDENTIAL

AFRPL-TR-65-209, Vol I

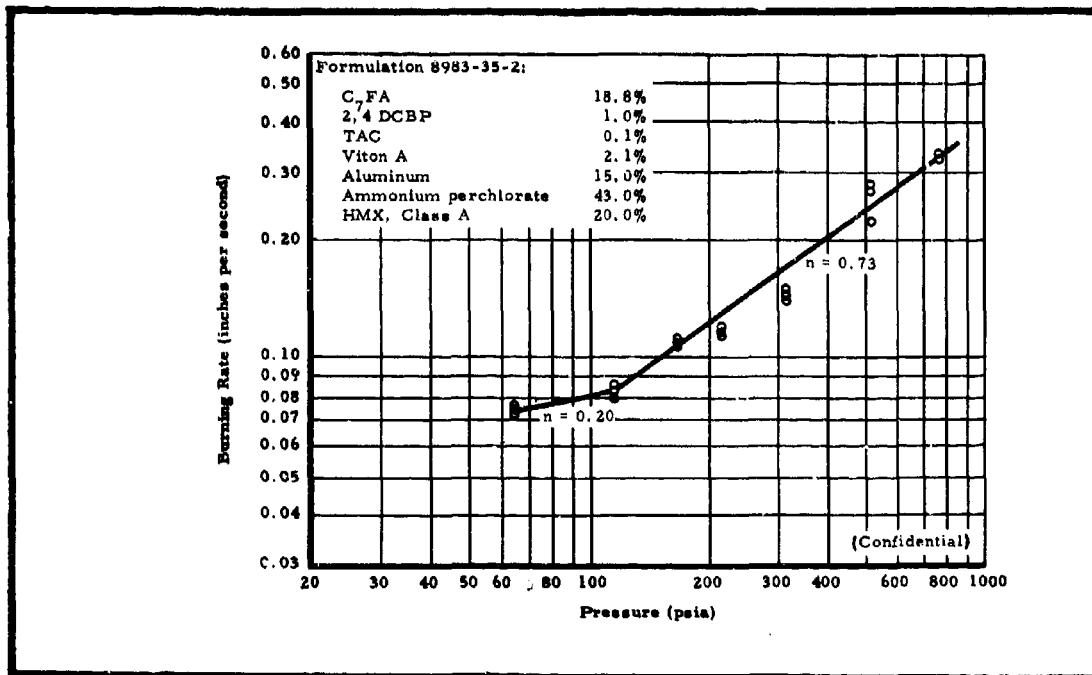


Figure 75 - Strand Burning-Rate Data for Formulation 8983-35-2

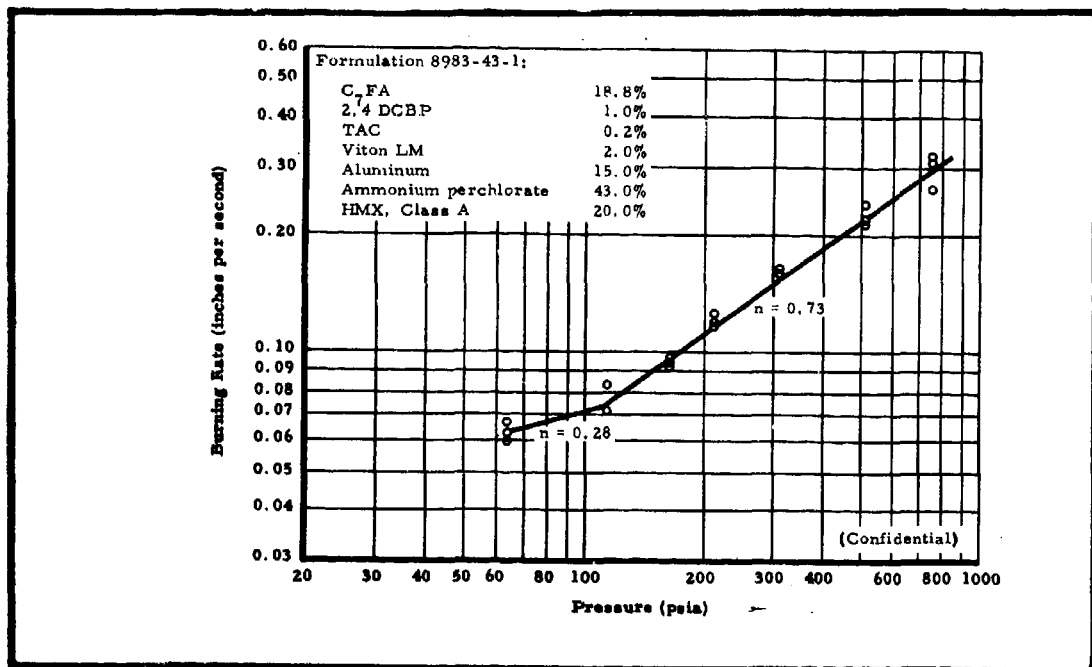


Figure 76 - Strand Burning-Rate Data for Formulation 8983-43-1

**CONFIDENTIAL**

AFRPL-TR-65-209, Vol I

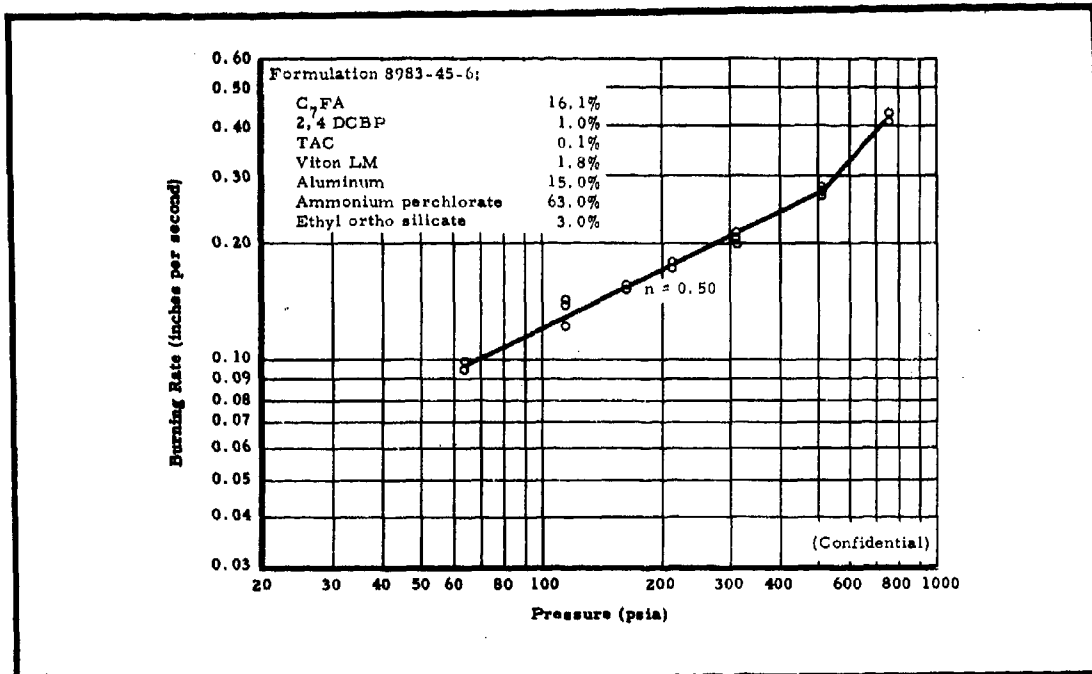


Figure 77 - Strand Burning-Rate Data for Formulation 8983-45-6

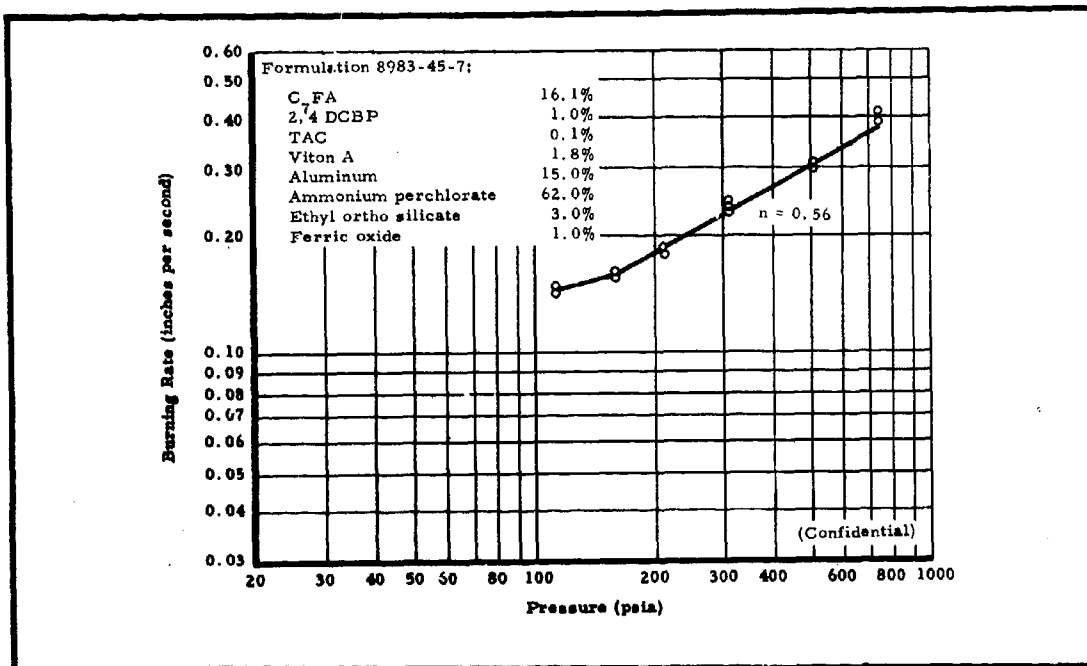


Figure 78 - Strand Burning-Rate Data for Formulation 8983-45-7

**CONFIDENTIAL**

and ammonium oxalate. Initial burning-rate studies indicated that the addition of two percent oxamide in the 78-percent solid loaded, 3-percent aluminum system gave a pressure exponent near unity below 100 psi. However, a more thorough evaluation of this formulation gave an exponent of 0.71 in the pressure region below 100 psi, as shown in Figure 79. Oxamide concentrations of one, two, and five percent in the 15-percent aluminized system with 78 percent solids were also evaluated, but they had very little effect on exponent, as shown in Figures 80, 81, and 82, respectively. Moreover the incorporation of oxamide in the 15-percent aluminized system with 83 percent solids had only a slight effect on pressure exponent, as shown in Figure 83. (Confidential)

Adding both two percent oxamide and two percent copper chromite in the three-percent aluminized system increased the exponent to 0.75 above 150 psi, but below this pressure the exponent was only 0.19 (see Figure 84). (Confidential)

Two other coolants, guanidine carbonate and ammonium oxalate, were evaluated at the five percent and two percent levels, respectively. These additives did not affect exponent significantly, as shown in Figures 85 and 86, respectively. (Confidential)

Other Additives-Various other additives were evaluated in the three-percent aluminum, 78-percent solid loaded C<sub>7</sub>FA system. These additives and the concentrations of each were as follows: cupric oxide (two percent), ammonium dichromate (two percent), nickel oxalate (two percent), iron blue (two percent), and ammonium nitrate (five percent). These additives did not significantly increase the pressure exponent, as shown in Figures 87 through 91, respectively. (Confidential)

#### Effect of Increased Solid Loading

The effect of increasing the solid loading was previously investigated by increasing the loading

# CONFIDENTIAL

AFRPL-TR-209, Vol I

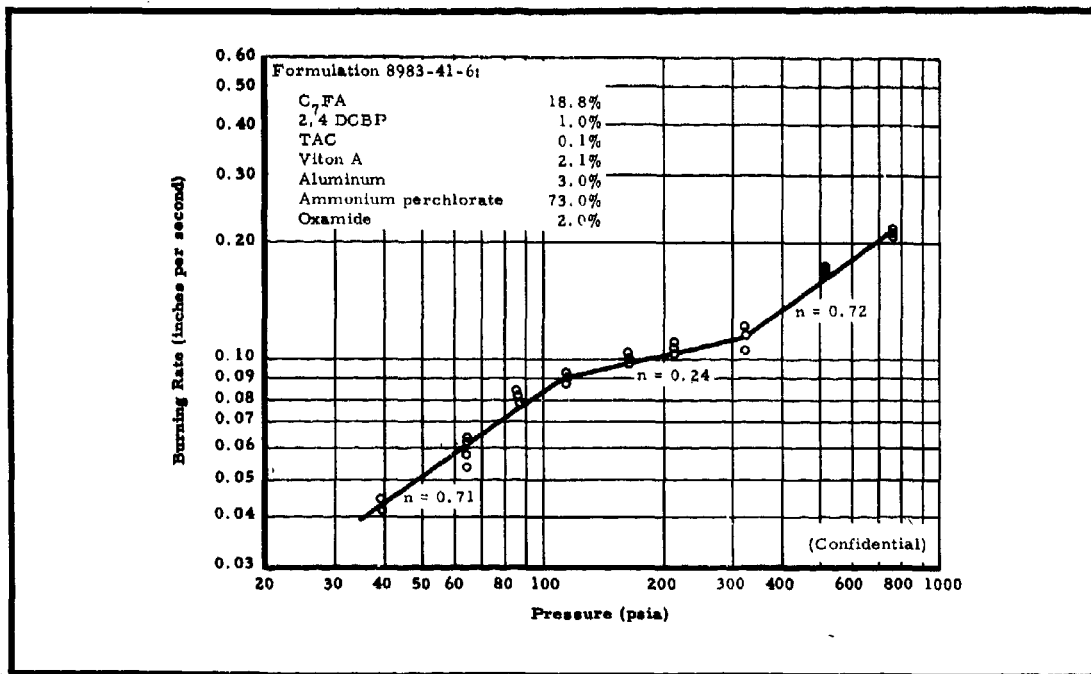


Figure 79 - Strand Burning-Rate Data for Formulation 8983-41-6

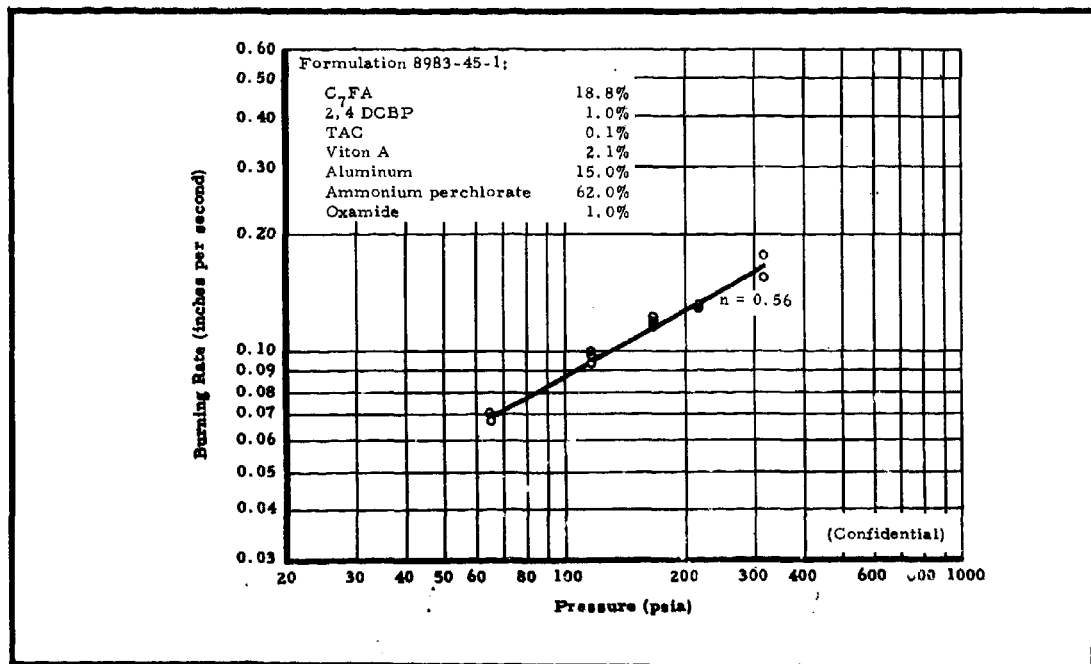


Figure 80 - Strand Burning-Rate Data for Formulation 8983-45-1

**CONFIDENTIAL**

AFRPL-TR-65-209, Vol I

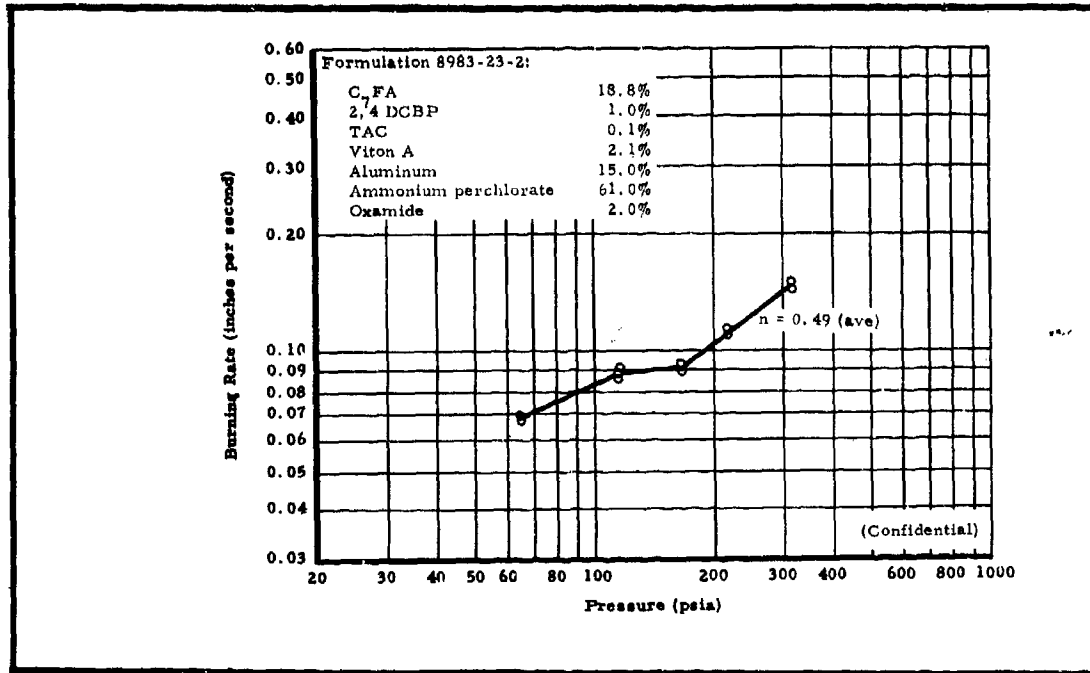


Figure 81 - Strand Burning-Rate Data for Formulation 8983-23-2 With Two Percent Oxamide

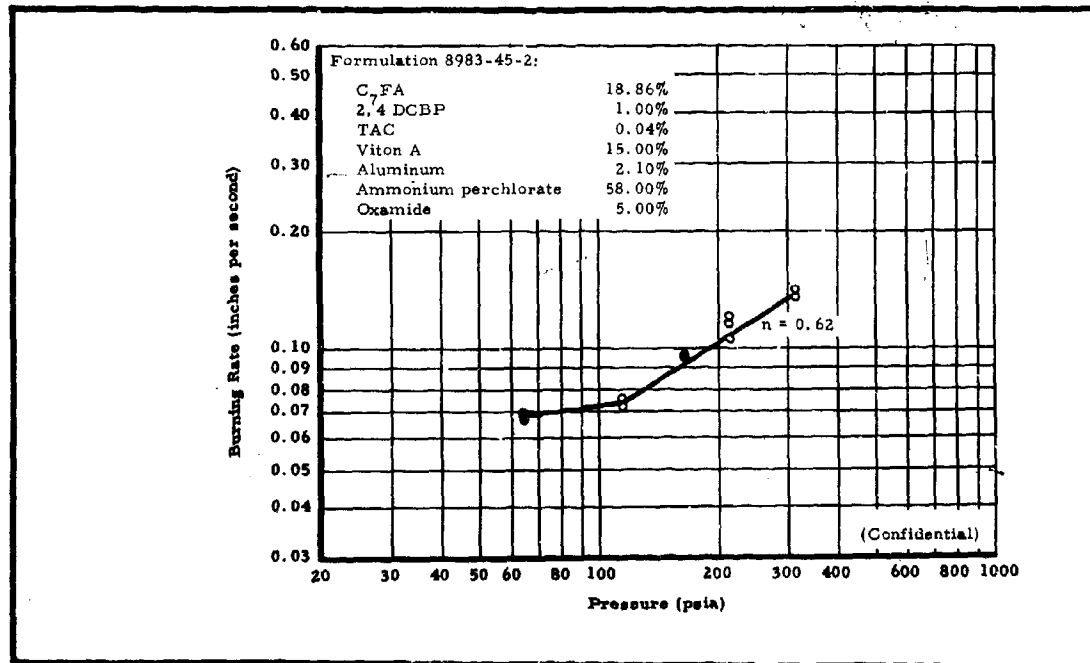


Figure 82 - Strand Burning-Rate Data for Formulation 8983-45-2

**CONFIDENTIAL**

AFRPL-TR-65-209, Vol I

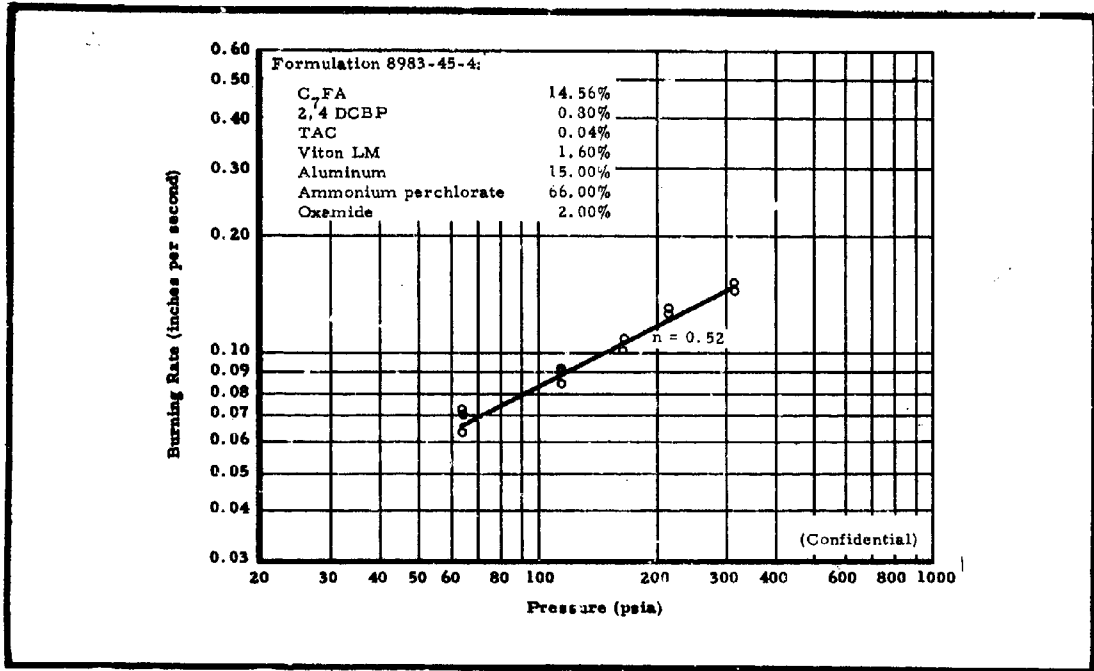


Figure 83 - Strand Burning-Rate Data for Formulation 8983-45-4

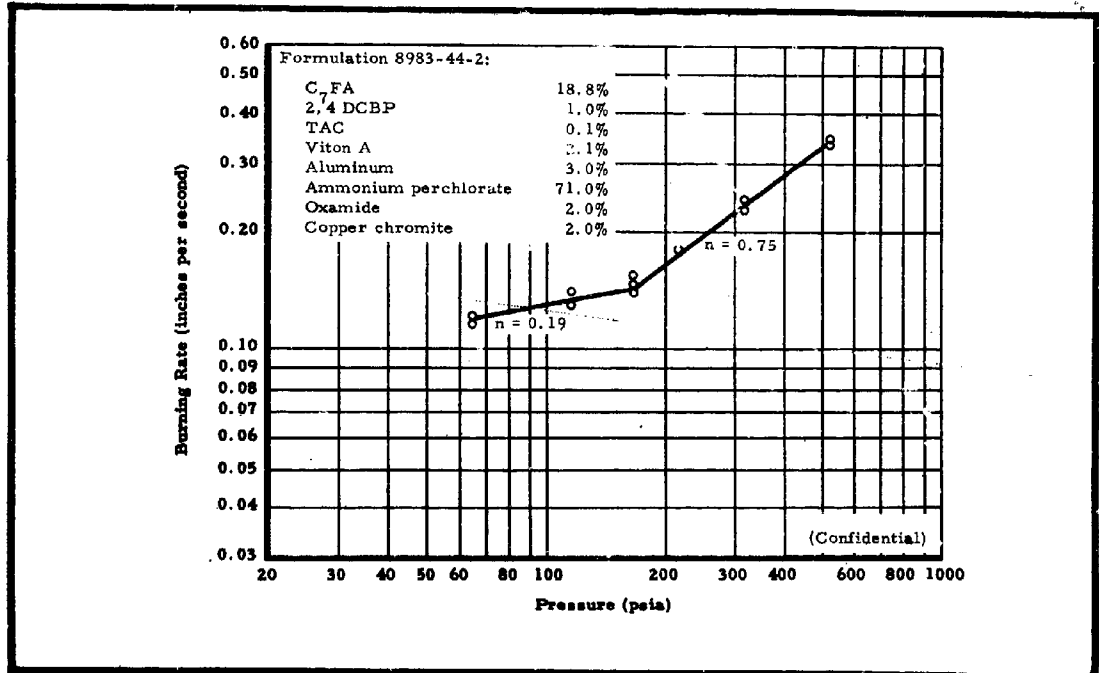


Figure 84 - Strand Burning-Rate Data for Formulation 8983-44-2

**CONFIDENTIAL**

**CONFIDENTIAL**

AFRPL-TR-65-209, Vol I

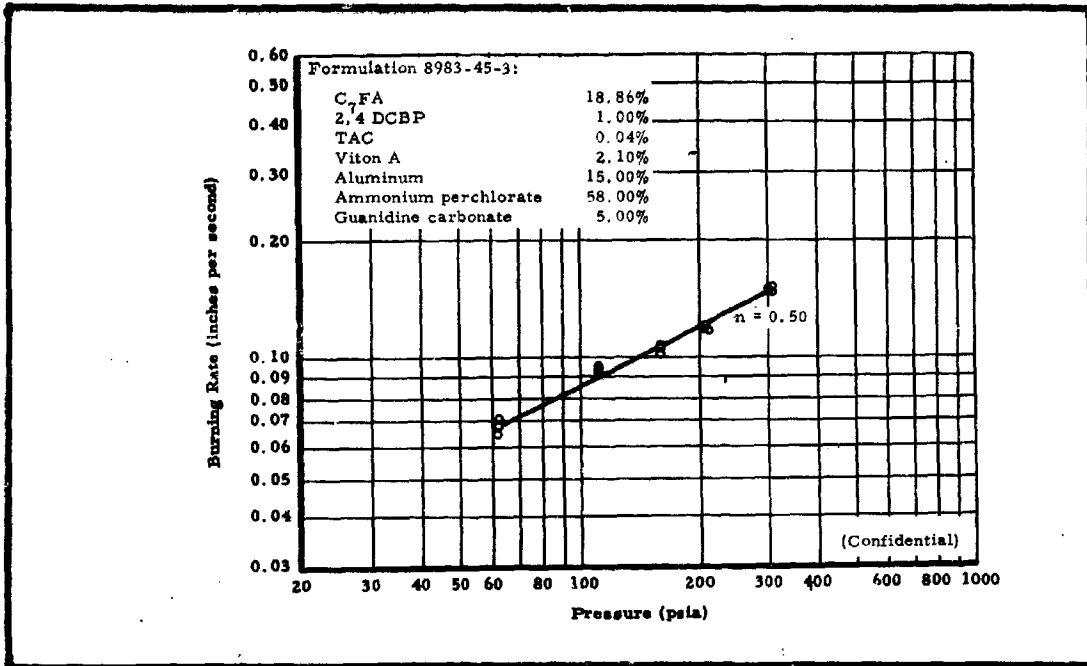


Figure 85 - Strand Burning-Rate Data for Formulation 8983-45-3

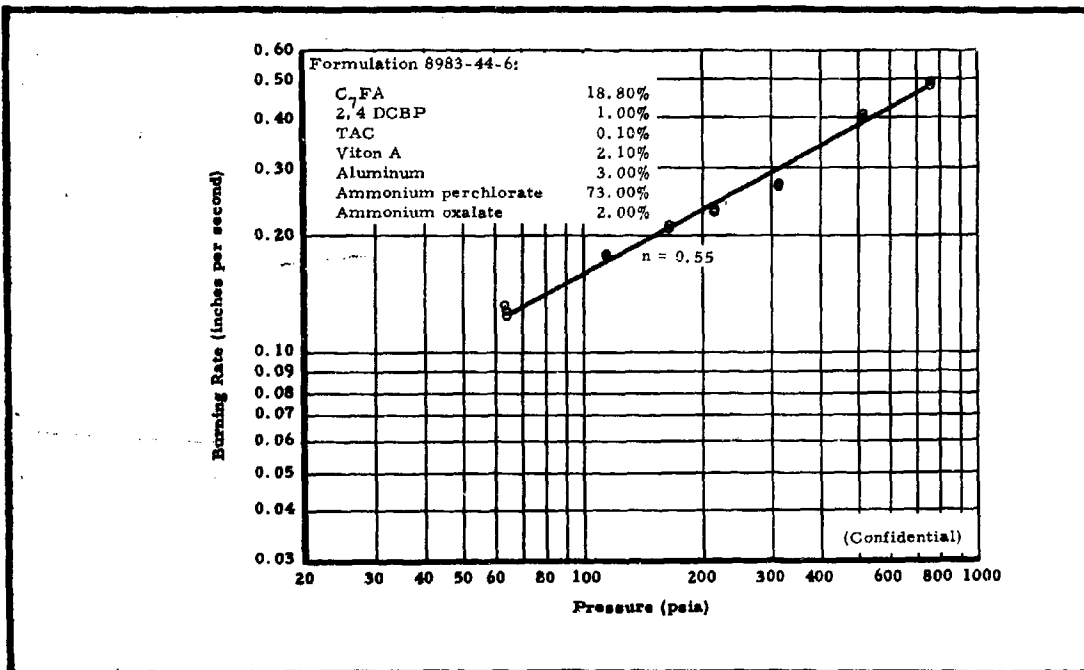


Figure 86 - Strand Burning-Rate Data for Formulation 8983-44-6

**CONFIDENTIAL**

AFRPL-TR-65-209, Vol I

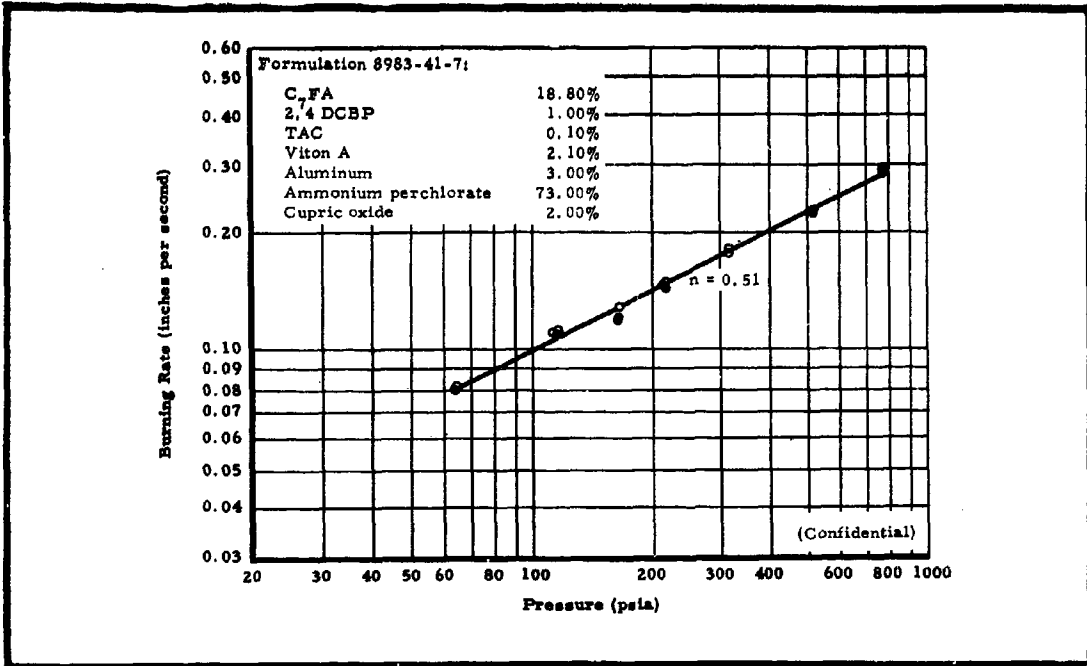


Figure 87 - Strand Burning-Rate Data for Formulation 8983-41-7

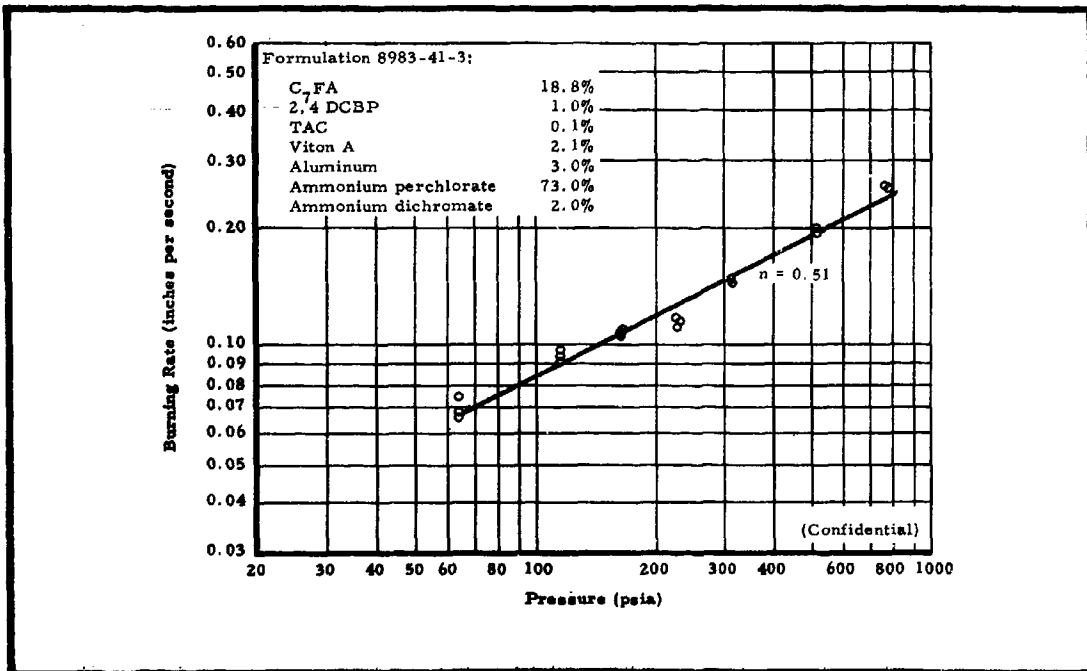


Figure 88 - Strand Burning-Rate Data for Formulation 8983-41-3

**CONFIDENTIAL**

AFRPL-TR-65-209, Vol I

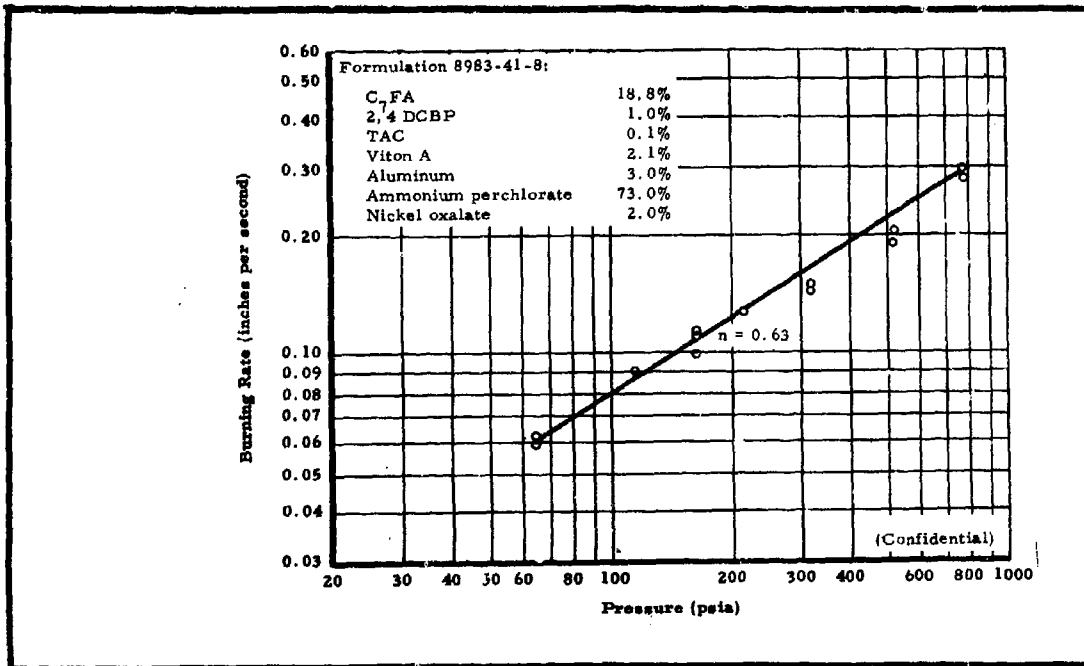


Figure 89 - Strand Burning-Rate Data for Formulation 8983-41-8

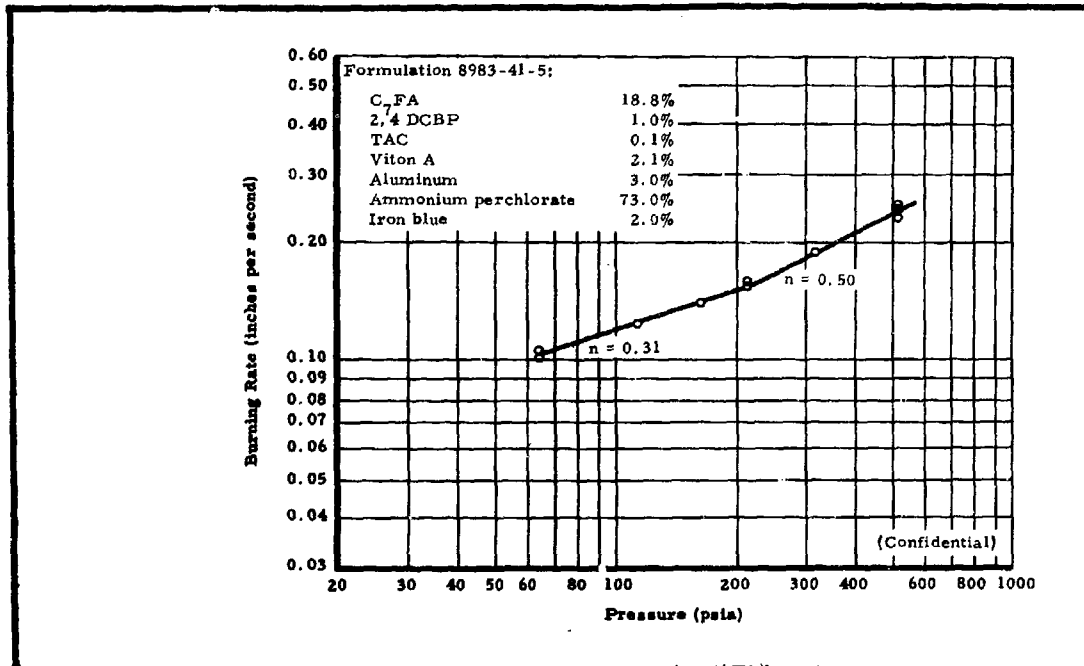


Figure 90 - Strand Burning-Rate Data for Formulation 8983-41-5

**CONFIDENTIAL**

# CONFIDENTIAL

AFRPL-TR-65-209, Vol I

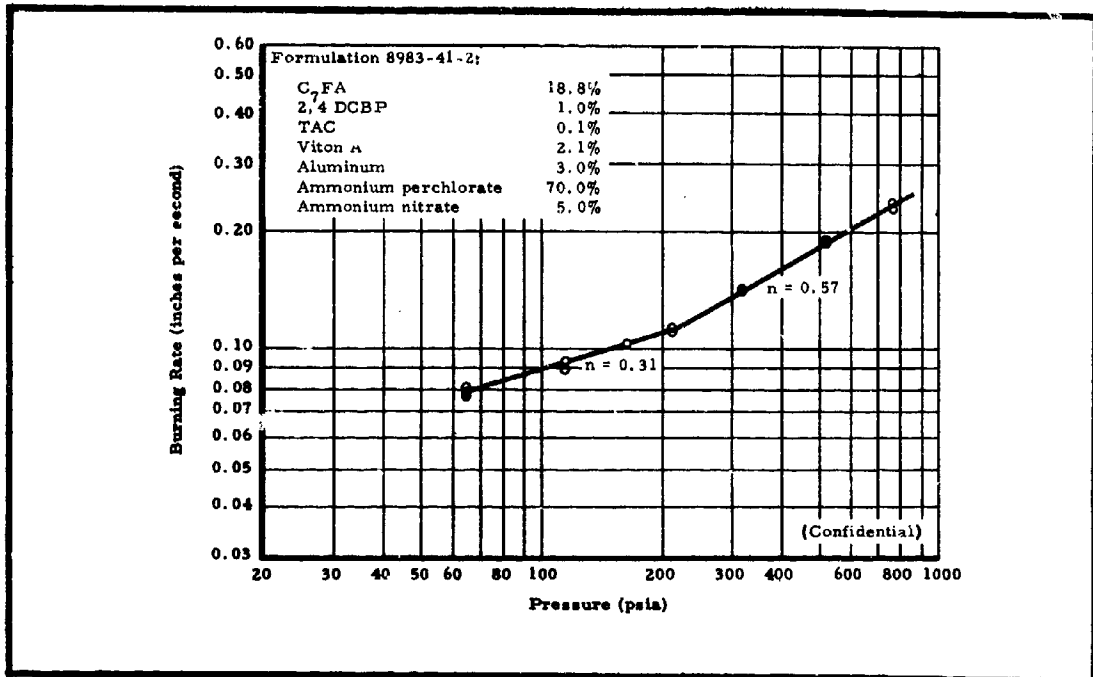


Figure 91 - Strand Burning-Rate Data for Formulation 8983-41-2

from 78 to 80 percent in a three-percent aluminum C<sub>7</sub>FA formulation. As a result, the pressure exponent increased from 0.49 (for formulation 8983-30-2, as presented in Figure 55) to 0.56 for formulation 8983-33-1 as shown in Figure 92. (Confidential)

Additional investigations were conducted in which the solid loading of the C<sub>7</sub>FA system was increased from 78 to 83 percent by substituting 1.6 percent Viton LM for 2.1 percent Viton A plasticizer in both the 3- and 15-percent aluminum formulations. The results of these tests are shown in Figures 93 and 94, respectively. Figure 93 shows that, although the pressure exponent was increased from 0.49 (for the 78-percent loaded formulation) to 0.61 by this decrease in binder concentration, this value was still far from that desired. Again, in Figure 94 for the 15-percent aluminum formulation, the pressure exponent is still low at pressures below 300 psi, the region where high exponents are

**CONFIDENTIAL**

AFRPL-TR-65-209, Vol I

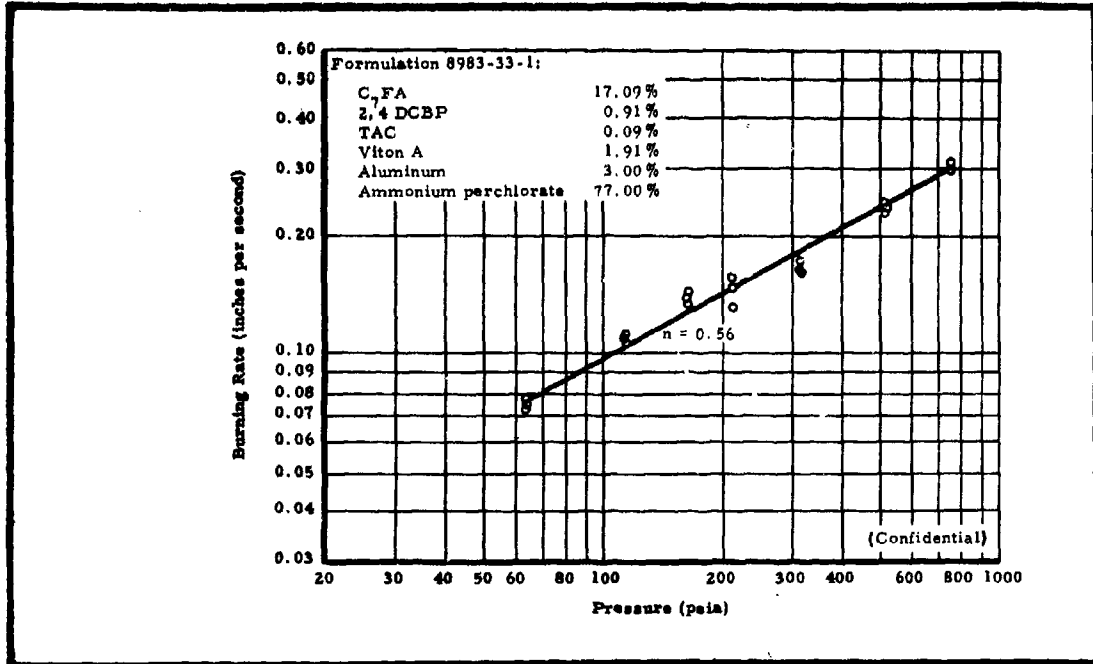


Figure 92 - Strand Burning-Rate Data for Formulation 8983-33-1

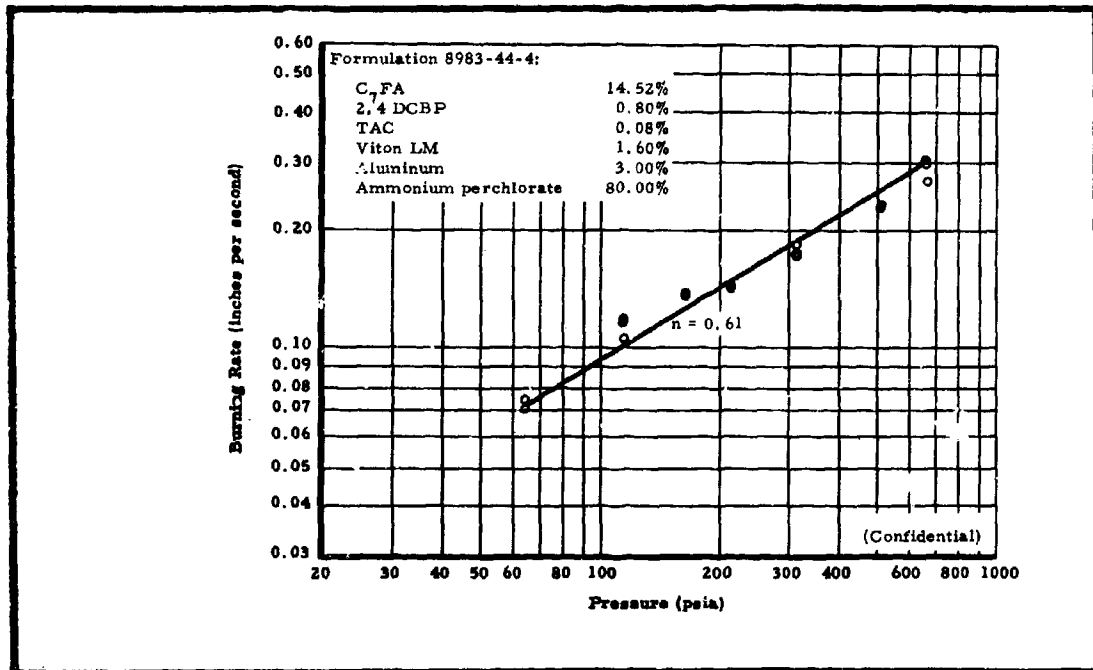


Figure 93 - Strand Burning-Rate Data for Formulation 8983-44-4

**CONFIDENTIAL**

# CONFIDENTIAL

AFRPL-TR-65-209, Vol I

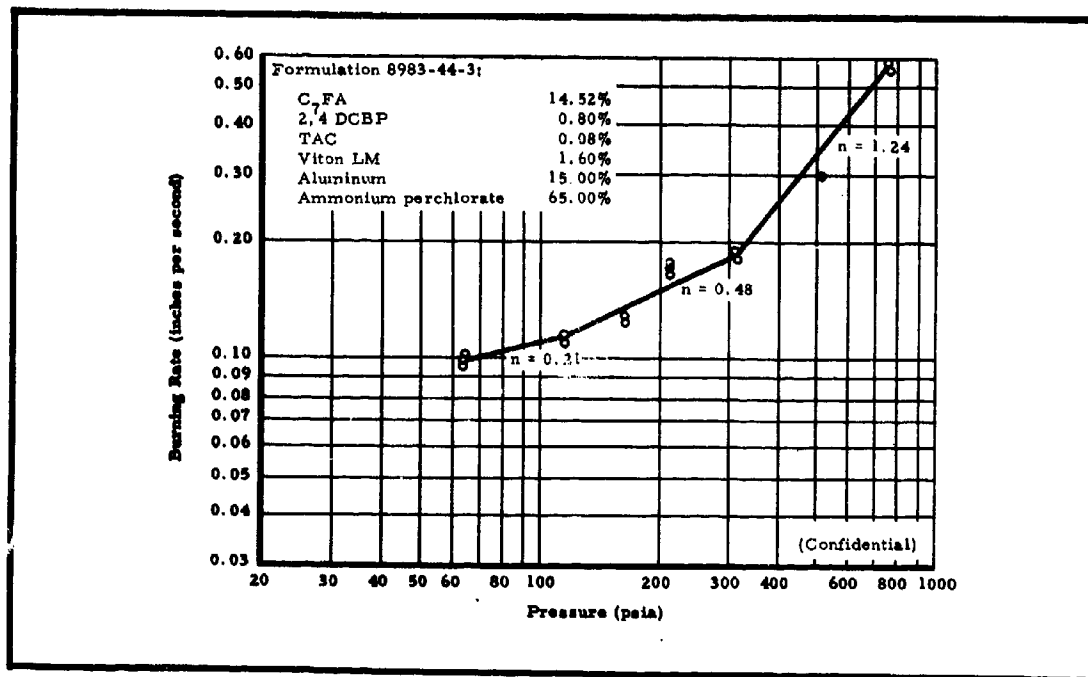


Figure 94 - Strand Burning-Rate Data for Formulation 8983-44-3

desired for proper motor design. (Confidential)

The effect that eliminating aluminum from the propellant had on the pressure exponent was also evaluated. As shown in Figure 95, the presence of aluminum had little effect on exponent, since these results are similar to those for the 3- and 15-percent aluminum formulations (8983-30-2 and 8983-23-2, respectively). (Confidential)

### (3) FX-189 Fluorocarbon Monomer System

#### (a) General

The investigation of a fluorocarbon monomer, designated FX-189 by the manufacturer, Minnesota Mining and Manufacturing Company, was conducted as a parallel effort to the fluoroalkyl acrylate investigation. This monomer is cured with 2, 4 dichlorobenzoyl peroxide. In a preliminary

**CONFIDENTIAL**

AFRPL-TR-65-209, Vol I

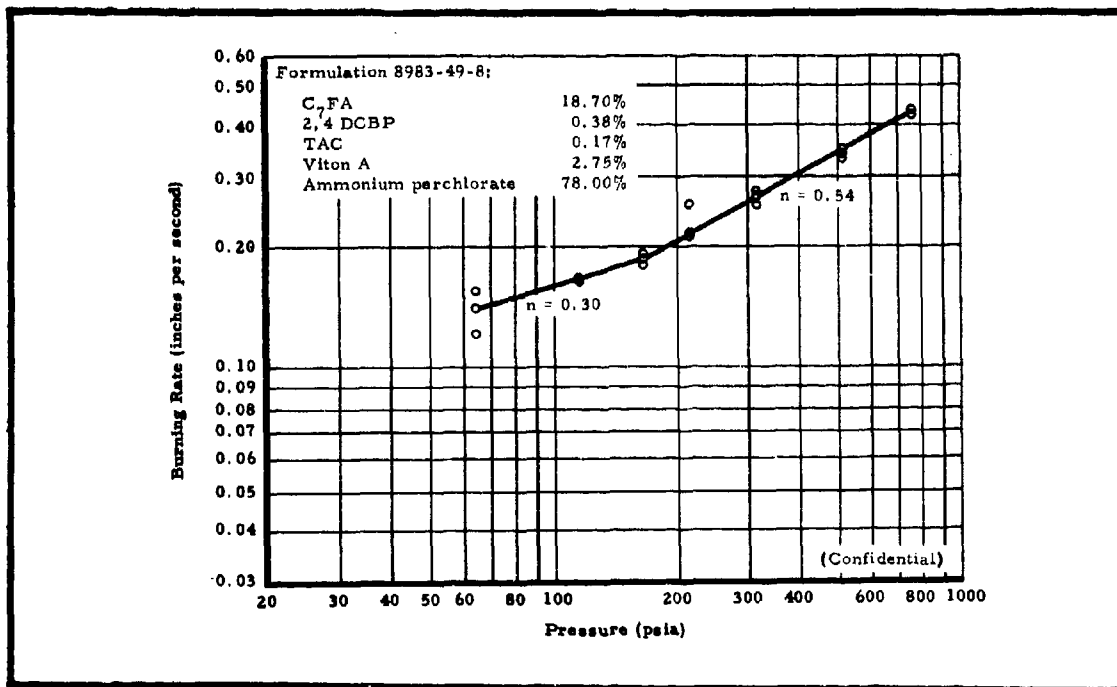


Figure 95 - Strand Burning-Rate Data for Formulation 8983-49-8

investigation, a 77-percent solid loaded formulation with 10-percent aluminum was prepared and allowed to cure for 24 hours at 120°F. This formulation had a tensile strength of 65 psi and a 15-percent elongation. Formulations of this system with 80-percent solids were processable. Combustion could be extinguished easily at ambient pressure with these formulations. (Confidential)

Since the preliminary investigation of FX-189 proved to be promising, additional effort was undertaken to achieve (1) maximum solid loading and improve mechanical properties, and (2) improve the pressure exponent. In general, this binder is easier to process than the C<sub>7</sub>FA binder, and higher solid loadings can thus be achieved. (Confidential)

## (b) Processability and Mechanical Property Improvement

Table XXXII summarizes the first formulations evaluated with FX-189 and gives the measured mechanical properties. The first five formulations (8983-13-2, -16-2, 17-2, -18-1, and -19-4) were made from a laboratory sample of FX-189, whereas the final formulations 8983-28-1 and 8983-34-1, contained material from a second lot, which was quite different in appearance from the former. The first five formulations were evaluated in 100-gram batches, while the latter two were processed in one-gallon and one-quart mixes, respectively. The second lot of FX-189 apparently produced higher tensile strength and elongation, but part of this increase may be attributed to batch size, as in the  $C_7FA$  system. The addition of the cross-linking agent TAC increased the tensile strength and reduced the elongation. The mechanical properties of the formulations incorporating FX-189 were quite superior to those of the  $C_7FA$  formulations with identical solid loadings. (Confidential)

The mix viscosities of these FX-189 formulations were lower than those of the  $C_7FA$  formulations. The viscosity of  $C_7FA$  formulation 8983-23-2, with 15-percent aluminum and 78-percent total solids, was 2.3 to 2.8 kilopoises, compared to a viscosity of 0.8 kilopoises for FX-189 formulation 8983-28-1, which also contained the 15-percent aluminum and 78-percent total solids. Increasing the solid loading to 80 percent in the FX-189 formulation system (8983-33-2) increased the viscosity to 1.9 kilopoises. (Confidential)

The strand burning-rate data for formulation 8983-33-2 are given in Figure 96. This formulation, without additives, had a pressure exponent of 0.58 below 300 psi, compared to an exponent of 0.49 for the comparable  $C_7FA$  formulation (8983-23-2), which also contained 15-percent aluminum. The increased exponent with the FX-189 monomer system may be due to its higher solid loading of 80 percent. (Confidential)

TABLE XXXII - RESULTS OF MECHANICAL PROPERTIES IMPROVEMENT STUDIES OF FLUOROCARBON MONOMER PROPELLANT SYSTEM

Property	Formulation						
	8983-13-2	8983-16-2	8983-17-2	8983-18-1	8983-19-4	8983-28-1	8983-34-1
Composition (percent by weight)							
Fluorocarbon monomer (FX-189)	22.00	20.00	20.75	20.00	20.85	21.00 <sup>†</sup>	20.85 <sup>†</sup>
2,4 DCBP*	1.00	1.00	1.00	1.00	1.00	1.00	1.00
TAC	...	...	0.25	...	0.15	...	0.15
Carbon black	...	1.00	1.00	1.00	1.00	...	...
Iron oxide	1.00	1.00	1.00	1.00	1.00	...	...
Ammonium perchlorate	66.00	67.00	67.00	64.00	66.00	63.00	63.00
Aluminum	10.00	10.00	10.00	15.00	10.00	15.00	15.00
Mechanical properties							
S <sub>m</sub> (psi)	65	55	90	64	70	46	95
ε <sub>m</sub> (in./in.)	0.15	0.16	0.06	0.15	0.10	0.62	0.11

\* A mixture of 50 percent 2,4 dichlorobenzoyl peroxide and 50 percent dibutylphthalate.  
 † The monomer in these formulations was from the second lot of material received from the manufacturer.

(Confidential)

# CONFIDENTIAL

AFRPL-TR-65-209, Vol I

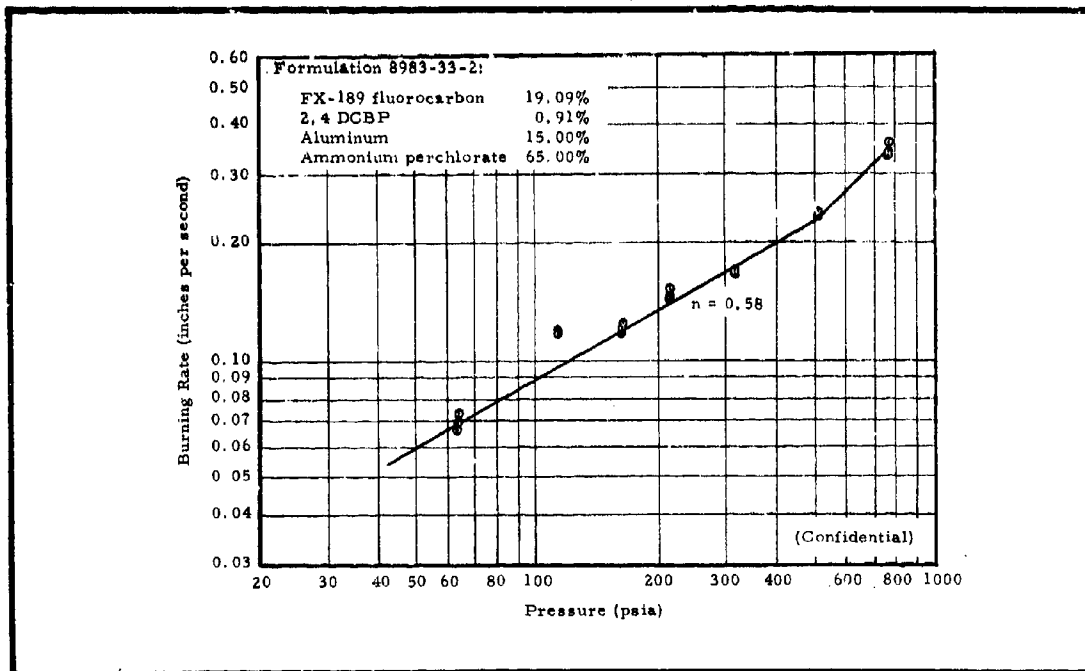


Figure 96 - Strand Burning-Rate Data for Formulation 8983-33-2

The FX-189 used in these initial evaluations was prepared in laboratory batches by the manufacturer, Minnesota Mining and Manufacturing Company. The FX-189 used in the remaining tests was prepared in pilot plant quantities. To ascertain the effect of binder modification and cure time on the mechanical properties of a 78-percent solid loaded FX-189 propellant, the formulations summarized in Table XXXIII were evaluated. It was observed that the propellant made from FX-189 prepared in pilot plant quantities had a lower elongation than that prepared from laboratory batch FX-189. (See page 135). Formulation 8983-40-4, which contained both FX-189 and C<sub>7</sub>FA, offered no improvement over the propellant containing C<sub>7</sub>FA binder only. The effect of varying the concentration of the cross-linking agent, TAC, and cure time is shown for formulations 8983-40-3, 8983-42-4, and 8983-42-3 in Table XXXIII. (Confidential)

# CONFIDENTIAL

AFRPL-TR-65-209, Vol 1

TABLE XXXIII-EFFECT OF BINDER MODIFICATION AND CURE  
TIME ON MECHANICAL PROPERTIES OF FX-189 PROPELLANT

Property	Formulation			
	8983-40-4	8983-40-3	8983-42-4	8983-42-3
Composition (percent by weight)				
C <sub>7</sub> FA	7.20	...	...	...
FX-189	12.90	18.92	18.96	19.00
2, 4 DCBP*	1.00	1.00	1.00	1.00
TAC	0.10	0.08	0.04	...
Viton A	0.80	...	...	...
Aluminum	15.00	15.00	15.00	15.00
Ammonium perchlorate	63.00	65.00	65.00	65.00
Cure data and mechanical properties				
Cured for 24 hr at 120°F				
Stress, S <sub>m</sub> (psi)	40	95	87	63
Strain, ε <sub>m</sub> (in./in.)	0.072	0.092	0.130	0.176
Modulus, E <sub>o</sub> (psi)	830	1310	860	560
Cured for 48 hr at 120°F				
Stress, S <sub>m</sub> (psi)	85	143	112	90
Strain, ε <sub>m</sub> (in./in.)	0.083	0.087	0.120	0.139
Modulus, E <sub>o</sub> (psi)	1550	2090	1300	950

\* A mixture of 50 percent 2, 4 dichlorobenzoyl peroxide and 50 percent dibutylphthalate.

(Confidential)

# CONFIDENTIAL

TABLE XXXIV - EFFECT OF TAC ON MECHANICAL  
PROPERTIES OF FX-189 PROPELLANT

Property	Formulation	
	8983-28-1	8982-1-8
Composition (percent by weight)		
FX-189	21.00	20.98
TAC	. . .	0.02
2, 4 DCBP	1.00	1.00
Aluminum	15.00	15.00
Ammonium perchlorate	63.00	63.00
Mechanical properties		
Stress, $S_m$ (psi)	70.3	89.4
Strain, $\epsilon_m$ (in./in.)	0.159	0.136
Modulus, $E_o$ (psi)	700	970

(Confidential)

An additional evaluation was conducted with a lower concentration of TAC in a similar 78-percent solid loaded formulation. The results, presented in Table XXXIV, show that very small amounts of TAC decrease elongation and increase tensile strength. (Confidential)

Although solid loadings as high as 82 percent have been achieved for the FX-189 system, as described on page 140, the best mechanical properties were achieved with a 78-percent solid loading, using a pilot plant lot of FX-189.

This 15-percent aluminum formulation (8983-28-1) had a tensile strength of 70 psi, with an elongation at maximum stress of 16 percent. Increasing

-139-

**CONFIDENTIAL**

the solid loading to 80 percent, in formulation 8983-40-3, increased the tensile strength to 90 psi, but reduced the elongation to 14 percent. The elongation at which both formulations broke was approximately 50 percent. Neither of these formulations contained a plasticizer. By adding Viton LM to an 82-percent solid loaded formulation, the viscosity was increased from 1.8 to 9.0 kilopoises. (Confidential)

(c) Modification of Burning-Rate Pressure Exponent

Formulation 8983-42-2, an 80-percent solid loaded FX-189 formulation, produced an increase in pressure exponent from 0.56 (for a comparably loaded C<sub>7</sub>FA propellant, shown in Figure 92) to 0.60, as shown in Figure 92. Adding HMX to this FX-189 formulation increased the pressure exponent to 0.72 (see Figure 98), whereas adding Sylon "S" increased the burning rate slightly, but had very little effect on exponent (see Figure 99). (Confidential)

Increasing the solid loading to 82 percent (formulation 8983-43-4) increased the burning-rate exponent to 0.71, as shown in Figure 100, compared to the value of 0.58 obtained for a comparable 80-percent loaded formulation (8983-33-2, page 135). However the exponent below 100 psi for formulation 8983-43-4 was below that of the 80-percent loaded formulation. (Confidential)

Adding two-percent copper chromite to an 80-percent solid loaded, three-percent aluminum FX-189 propellant increased the burning rate, but had little effect on the pressure exponent (see Figure 101). (Confidential)

The effect of large-particle-size ammonium perchlorate on the pressure exponent of the basic FX-189 formulation (8983-28-1, Table XXXII) was investigated. The modified formulation (8982-1-10), which contained 18.9 percent ground ammonium perchlorate and 44.1 percent 500 to 1200 micron ammonium perchlorate, produced a lower pressure exponent than the formulation with the standard trimodal blend, as shown in Figure 102. (Confidential)

**CONFIDENTIAL**

AFRPL-TR-65-209, Vol I

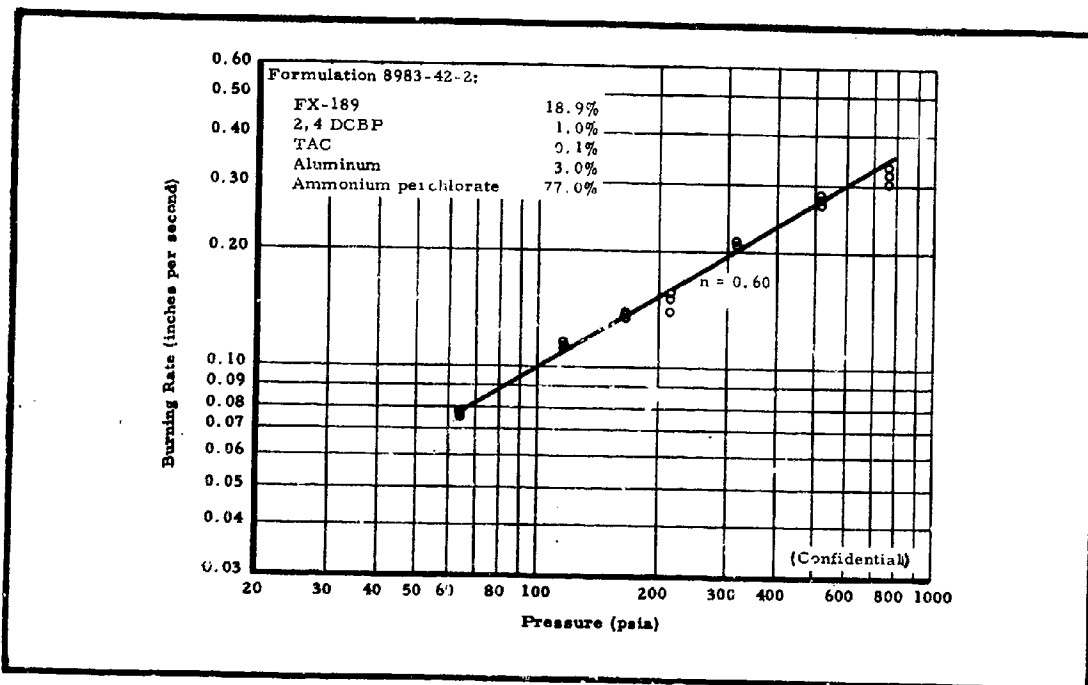


Figure 97 - Strand Burning-Rate Data for Formulation 8983-42-2

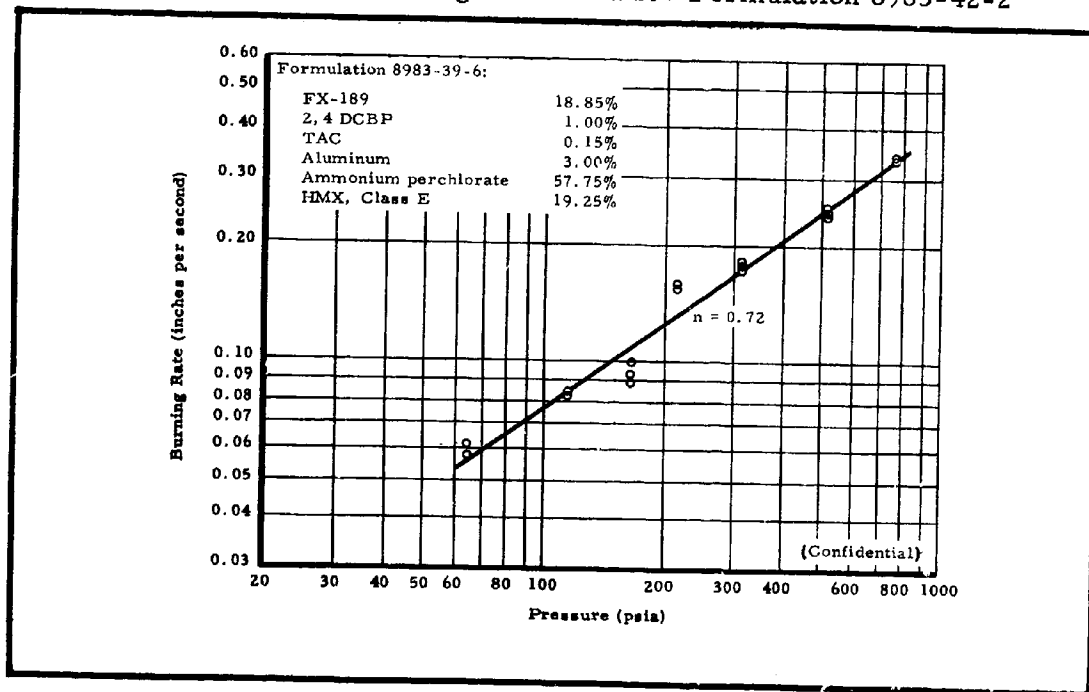


Figure 98 - Strand Burning-Rate Data for Formulation 8983-39-6

**CONFIDENTIAL**

**CONFIDENTIAL**

AFRPL-TR-65-209, Vol I

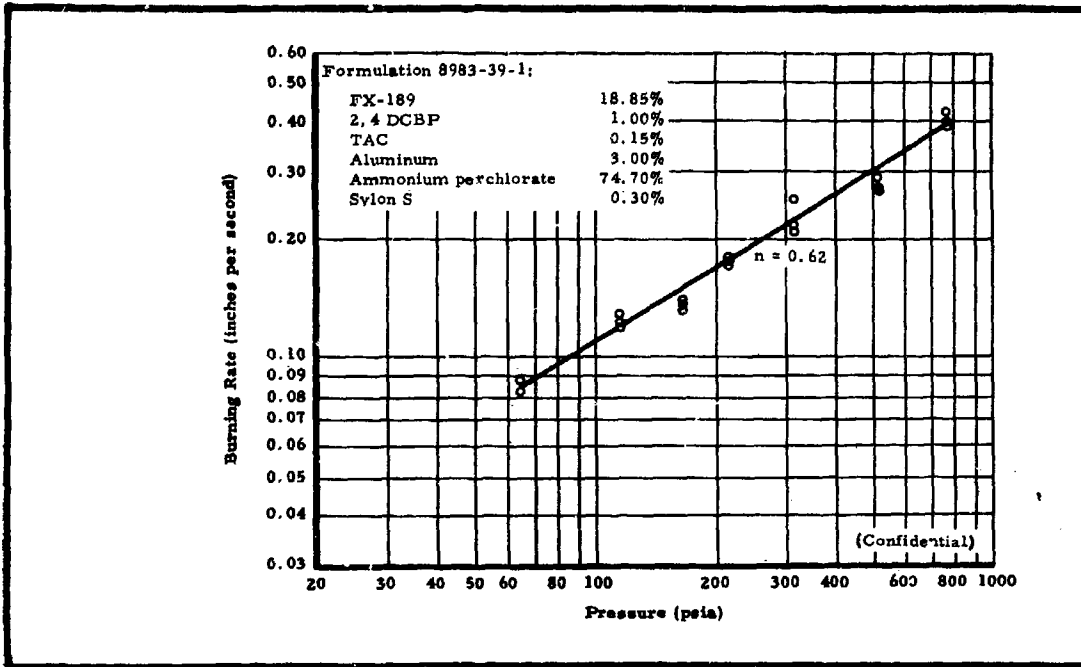


Figure 99 - Strand Burning-Rate Data for Formulation 8983-39-1

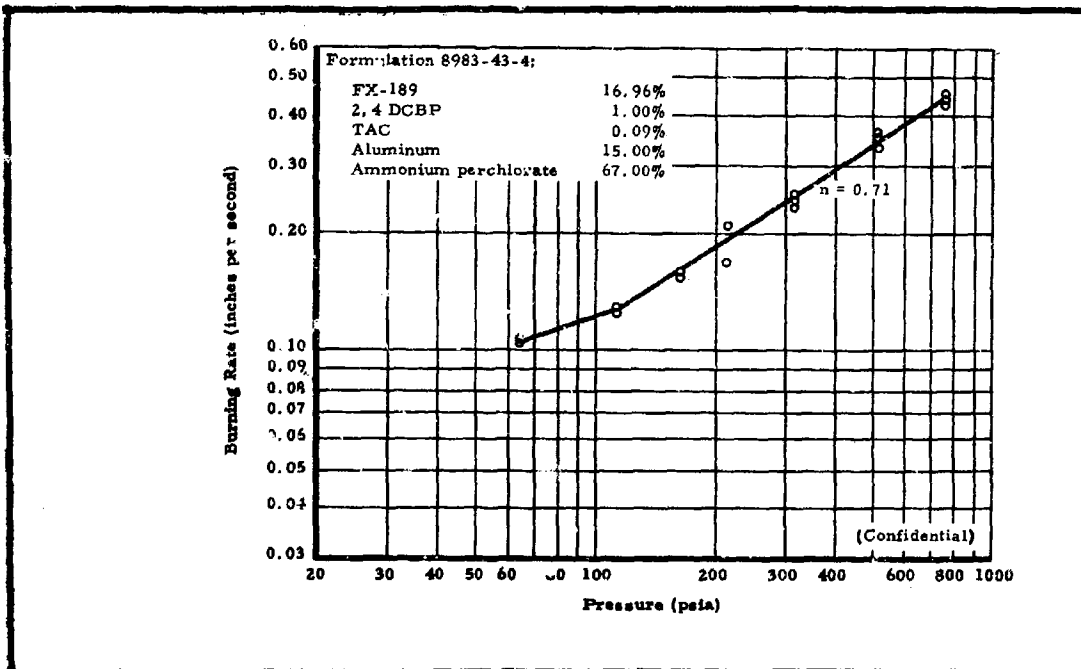


Figure 100 - Strand Burning-Rate Data for Formulation 8983-43-4

**CONFIDENTIAL**

**CONFIDENTIAL**

AFRPL-TR-65-209, Vol I

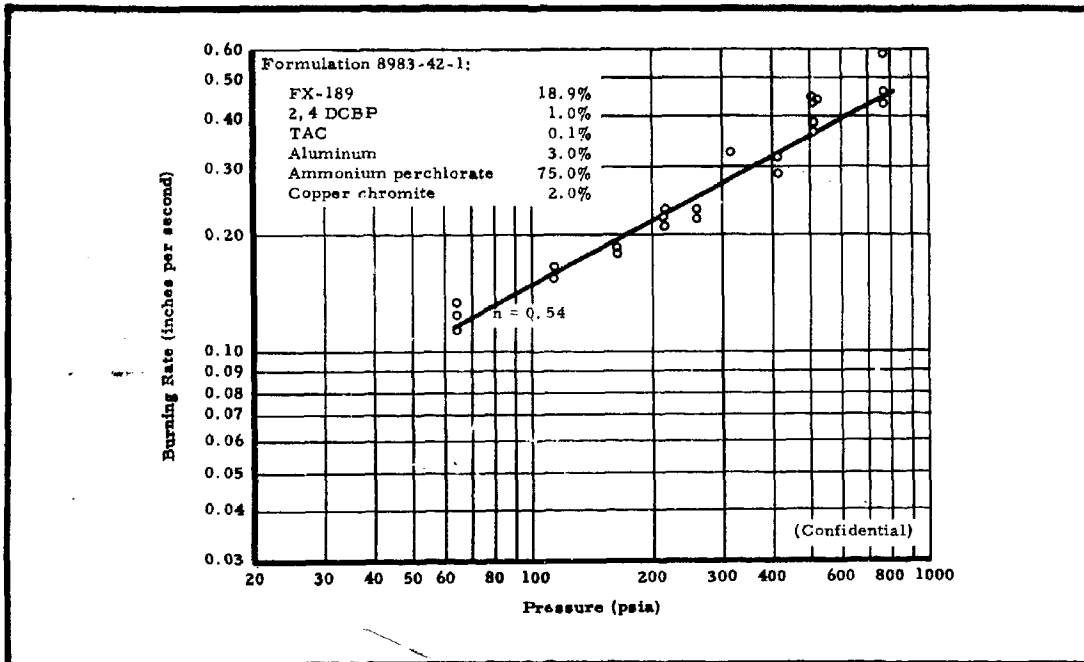


Figure 101 - Strand Burning-Rate Data for Formulation 8983-42-1

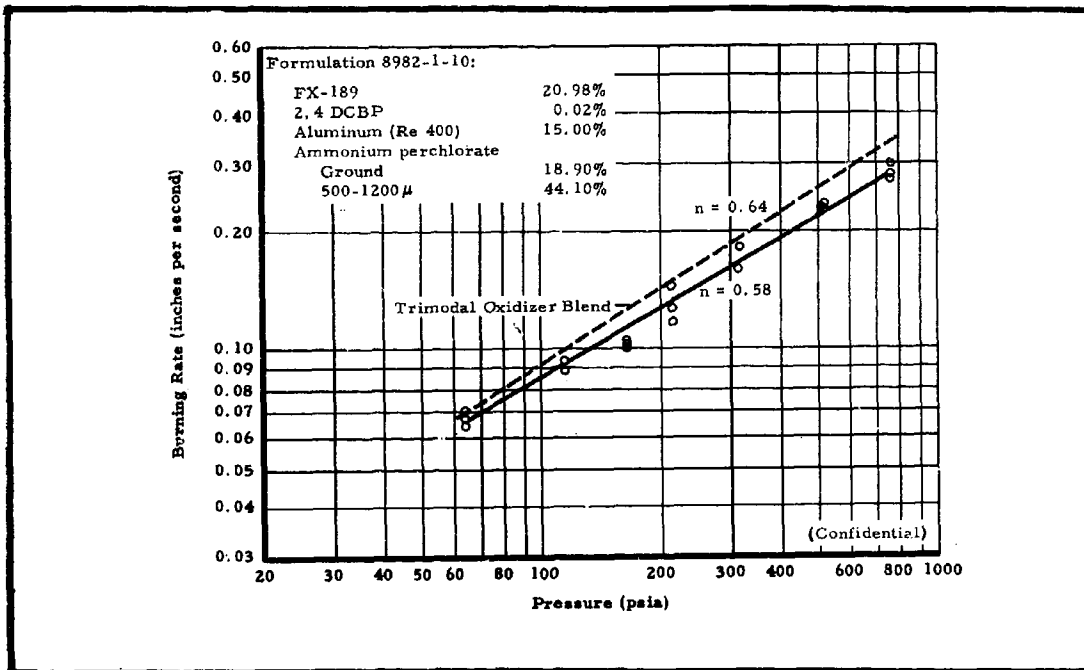


Figure 102 - Strand Burning-Rate Data for Formulation 8982-1-10

**CONFIDENTIAL**

c. Pressed Grain (OX-5) Modifications

Two modified OX-5 formulations were prepared and test fired in an attempt to eliminate the low-frequency instability exhibited by OX-5 at high mixture ratios. This instability was particularly evident in full-scale tests M. 1 and M. 2, in which the propellant reignited after the second pulse cycle (see Section VI, paragraphs 3 and 4). This instability is believed to be caused by a periodic accumulation and combustion of aluminum on the grain surface. (Confidential)

In the first OX-5 modification, designated OX-7, the 25-micron aluminum (Reynolds 120) was replaced with 5-micron aluminum (Reynolds 400). The second modification, OX-8, also contained 5-micron aluminum, but differed from OX-7 in that the particle size of the ammonium perchlorate was fine, rather than "as received." (Confidential)

OX-7 was evaluated in two subscale motor tests, designated H. 15 and H. 16; OX-8, in one test, designated H. 17. For all three tests, an end-burning grain of PPO-13 propellant was used in the forward chamber to provide an aft-to-forward mixture ratio of 3.0. The forward grain was designed to burn out before the aft grain. (Confidential)

Tests H. 15 and H. 16 (in which OX-7 propellant was used) showed evidence of instability during burning. A series of chuffs occurred during and after forward-chamber tail-off in Test H. 15. During Test H. 16, instability occurred in the middle of the trace, as well as during forward chamber tail-off. To prevent the chuffing that occurred after Test H. 15, a nitrogen purge was used after Test H. 16. The motor for Test H. 17, containing OX-8 propellant, burned stably throughout the test. After the forward grain burned out, the aft grain continued to burn stably at a lower pressure. (Confidential)

It was concluded from these tests that fine particle size ammonium perchlorate markedly improved propellant combustion since no instability was evident in Test H. 17, even at an infinite mixture ratio. Changing the aluminum particle size from 25- to 5-micron apparently had little effect, however, since Tests H. 15 and H. 16 displayed pressure oscillations similar to those observed in motors containing OX-5. (Confidential)

The reduced ballistic data for these three tests are presented in Table XXXV. Although the performance values could not be determined for Test H. 15 because of the chuffing, the results for Test H. 16, which also contained OX-7, were low. Performance values for Test H. 17, containing OX-8, were greatly improved. The specific impulse efficiency for Test H. 17, 95.1 percent, compares favorable with that obtained in single-chamber motors with aluminized propellants. Based on this efficiency, a motor specific impulse (at vacuum, with a 20-to-1 expansion and 15-degree half angle) of 271 lb-sec/lb would be expected at the optimum mixture ratio of 2.0. (Confidential)

d. Carboxy-Terminated Polybutadiene Binder

(1) General

Near the end of the program, two aft-grain propellant formulations developed by the Naval Ordnance Test Station (NOTS), China Lake, Calif., were evaluated. These formulations, designated C-445 and C-430, were characterized for processability, mechanical properties, and burning rate in laboratory tests, and for termination capability in sub-scale dual-chamber motor firings. The composition of both formulations is given in Table XXXVI. The superior formulation was to be used for Series N tests (see Section VII).

(2) Laboratory Evaluation

In preparing mixes of both formulations for laboratory evaluation, the ammonium perchlorate particle size distribution was modified by using only 600-micron ammonium perchlorate in order to reduce the mix viscosities. This modification reduced the viscosity by more than 50 percent, but had little effect on the burning-rate characteristics. The physical properties are given in Table XXXVI, and the strand burning rate test results are given in Figures 103 and 104. (Confidential)

Propellant bonding studies were conducted, for which a liner composed of 66.14 percent Butarez CTL II, 3.86 percent MAPO, and 30.00 percent Thermax carbon black was used. The liner was cured for 16 hours at 180°F, with Gen Gard V-44 insulation used as a base. Peel and adhesion tests indicated that failure occurred consistently

**TABLE XXXV-REDUCED BALLISTIC DATA FOR MODIFIED OX-5**  
**PROPELLANT TESTS**

Parameter	Test Number		
	H. 15*	H. 16	H. 17
<b>Forward Chamber</b>			
Weight burned, including igniter (lb)	1.418	1.434	1.424
Web burned (lb)	0.960	0.960	0.950
Burn time (sec)	2.809	2.768	2.776
Burn rate (in./sec)	0.342	0.347	0.342
$\int Pdt$ (psig-sec)	5160	5188	4650
$P_b$ (psia)	1742	1789	1590
Throat area (sq in.)	0.0409	0.0408	0.0406
<b>Aft Chamber</b>			
Propellant type	OX-7†	OX-7	OX-8
Weight burned (lb)	8.255†	5.830	8.040
Web burned (lb)	0.958	0.692	0.224
Burn time (sec)	. . .	2.757	5.180
Burn rate (in./sec)	. . .	0.251	0.043
$\int Pdt$ (psig-sec)	885.2	758.9	992.6
$P_b$ (psia)	299.1	276.7	205.3
<b>Total Motor</b>			
Weight burned (lb)	9.674†	7.264	9.464
Weight <sub>aft</sub> /weight <sub>fwd</sub>	5.83	4.06	5.64
$\int Fdt$ (lb <sub>f</sub> -sec)	(1589)	1373	1855
$F_b$ (lb <sub>f</sub> )	523	477	510
Throat area (sq in.)	1.314	1.327	1.340
Expansion ratio, $A_e/A_t$	2.988	2.964	2.954
Ratio of specific heats, $\gamma$	1.20	1.20	1.20
Characteristic velocity (fps)	(3860)	4460	4522
$I_{sp}$ (lb-sec/lb)	. . .	189.0	196.1
$I_{sp}^{meas}$ (lb-sec/lb)	. . .	218.9	231.5
$I_{sp}^{1000/14.7}$ (lb-sec/lb)	. . .	249.5	263.9
$I_{sp}^{vac, 20/1}$ (%)	. . .	87.3	95.1

\* Motor chuffed after the forward grain burned out.

† Total propellant weight consumed, including chuffs.

(Confidential)

**TABLE XXXVI. COMPOSITION AND PROPERTIES OF C-445 AND C-430  
PROPELLANTS**

Property	Formulation	
	C-445	C-430
<b>Composition (percent by weight)</b>		
Butarez CTL I	7.737	. . .
Butarez CTL II	. . .	9.786
MAPO	0.263	0.214
ZL-496-4M	2.000	2.000
Aluminum, H-5	15.000	15.000
Potassium perchlorate	35.000	40.000
Ammonium perchlorate (600 $\mu$ )	40.000	33.000
Density (lb/cu in.)	0.070	0.069
<b>Mechanical Properties:</b>		
-40 $^{\circ}$ F		
Tensile, maximum (psi)	204	286
Elongation (%)	17	30
Modulus (psi)	2870	3100
+75 $^{\circ}$ F		
Tensile, maximum (psi)	101	105
Elongation (%)	16	36
Modulus (psi)	829	478
+140 $^{\circ}$ F		
Tensile, maximum (psi)	85	86
Elongation (%)	15	28
Modulus (psi)	703	451
<b>Ballistic Properties:</b>		
Extinction pressure (psia)	3.000	3.000
Strand burning rates (in./sec)		
At 39 psia	0.055	0.080
At 150 psia	0.16	0.17
At 1000 psia	0.95	0.89
Strand pressure exponent		
At 39 to 100 psia	0.73	0.74
At 150 to 1000 psia	0.94	0.83

\* Depending on rate of pressure decay.

(Confidential)

**CONFIDENTIAL**

AFRPL-TR-65-209, Vol I

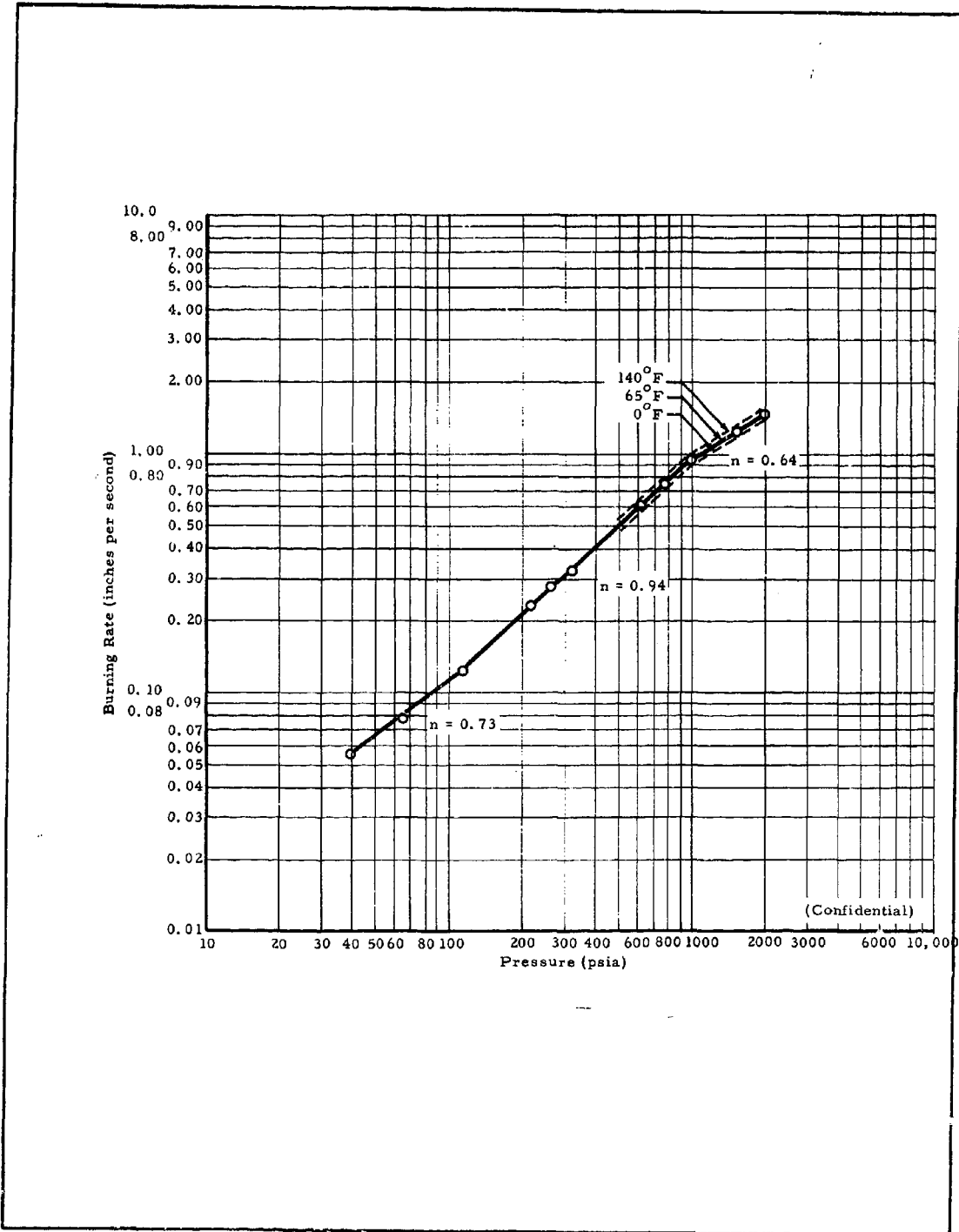


Figure 103 - Strand Burning-Rate Data for C-445 Propellant, Modified by Northrop Carolina

-148-

**CONFIDENTIAL**

**CONFIDENTIAL**

AFRPL-TR-65-209, Vol I

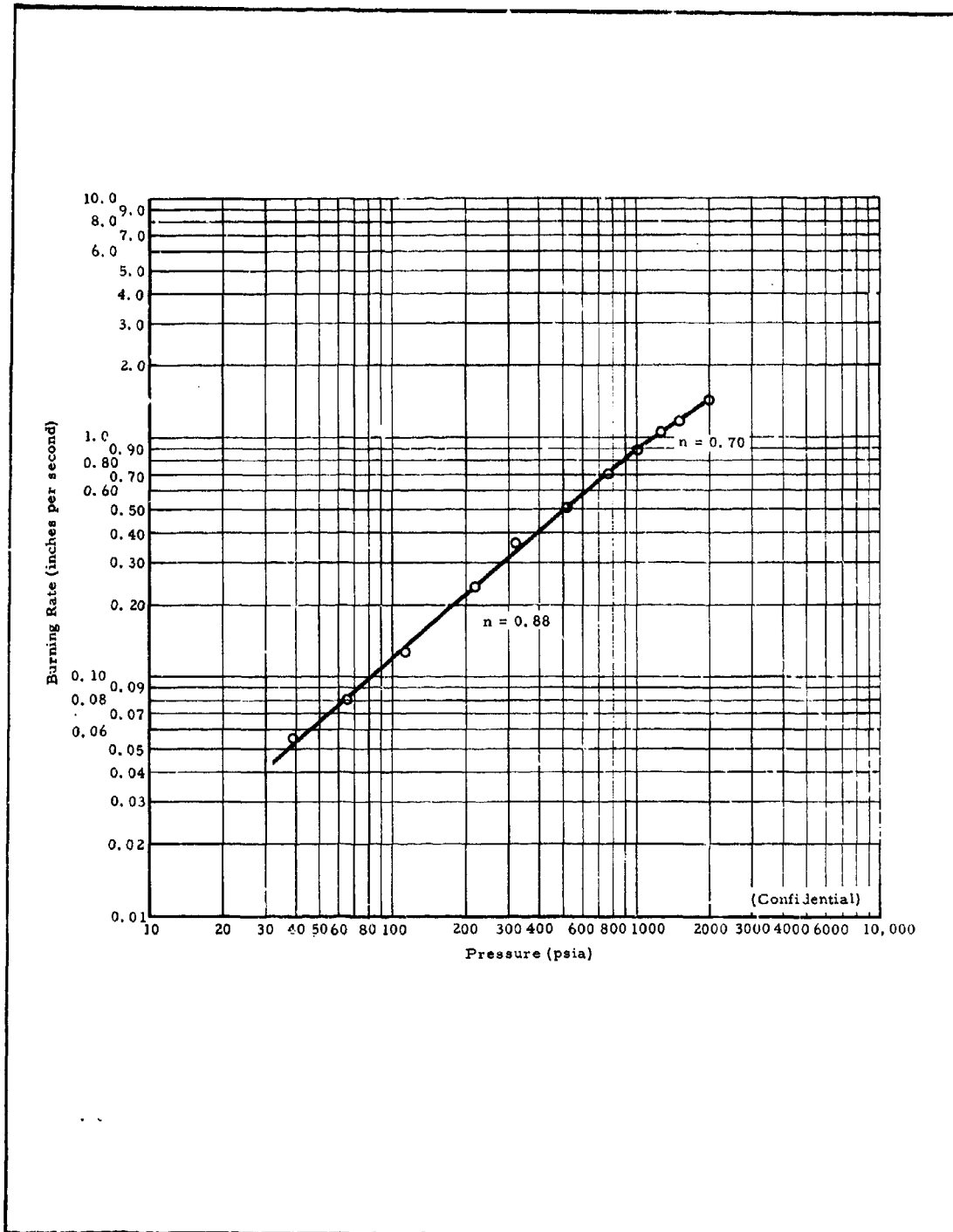


Figure 104 - Strand Burning-Rate Data for C-430 Propellant,  
Modified by Northrop Carolina

**CONFIDENTIAL**

at the propellant-liner interface at 90- to 100-psi stress. This level of bond strength is more than adequate for the low-stress center-perforated grain configuration to be used in Series N. (Confidential)

(3) Subscale Dual-Chamber Motor Tests

(a) Test Motor Description

A total of 11 test motors were fired to evaluate the termination capability of these propellants; C-445 was used in five motors and C-430 in six motors. These subscale test motors consisted of six-inch-diameter cylindrical forward and aft chambers separated by a ball valve. During the tests the ball valve was actuated after 1.0 sec of motor operation, thereby increasing the valve (or forward-chamber throat) area sufficiently to extinguish the forward grain. Normally, after each of these terminations both chambers were purged with nitrogen to expel residual hot gases that otherwise might cause re-ignition. (Confidential)

The forward chamber contained PPO-13 propellant in an internal-burning center-perforated grain configuration. These grains, which were five inches long with a one-inch web, were case bonded on the O. D. and one end to produce a neutral burning surface. The forward grains were ignited by 2D BKNO<sub>3</sub> pellets. (Confidential)

The C-445 and C-430 propellants evaluated in the aft chamber were cast to form internal-burning center-perforated grains 9 to 11 inches long with 1.0-inch webs. The nozzles used on the aft chambers were sized to provide aft-burning-surface-to-throat-area ratios,  $K_n$ , ranging from 27 to 60. (Confidential)

(b) Results of Motor Tests with C-445 Propellant

Five motors were fired with C-445 propellant grains in the aft chamber. The results of these tests, designated O-1.1, O-2.1, O-5.1, O-5.2, and O-7.1, are summarized in Table XXXVII.

# CONFIDENTIAL

AFRPL-TR-65-209, Vol I

TABLE XXXVII - SUMMARY OF TERMINATION TESTS (C-445 AFT PROPELLANT)

Parameter	Test Number:				
	O-1.1	O-2.1	O-5.1	O-5.2	O-7.1
<b>Forward chamber (PPO-13)</b>					
Burning surface area (sq in.)	78.0	78.0	79.1	82.8	80.1
Throat area (sq in.)	0.111	0.110	0.110	0.110	0.110
$K_n (S_b/A_t)$	70.2	70.9	71.9	75.3	72.8
Burn time (sec)	1.029	1.019	1.015	0.910 <sup>†</sup>	1.497
$\bar{P}_b$ (psia)	1,631	1,750	1,979	1,782	1,636
$P_{term}$ (psia)	1,790	1,770	2,034	2,074	1,464
$dp/dt_{term}$ (psi/sec)	85,200	92,000	98,900	90,060	86,800
Termination results	Permanent extinction	Permanent extinction	Permanent extinction*	Reignition*	Permanent extinction
<b>Aft chamber (C-445)</b>					
Burning surface area (sq in.)	172	172	144	143	143
Throat area (sq in.)	2.86	3.80	3.80	3.80	3.39
$K_n (S_b/A_t)$	60.1	45.2	37.8	37.6	42.1
Burn time (sec)					
Pre-termination	0.957	0.920	0.990	0.895	1.483
Post-termination	4.30	13.60	...	...	6.42
$\bar{P}_b$ (psia)					
Pre-termination	252	144	126.5	122.0	144.5
Post-termination	117	29.2	...	...	33.4
Burn rate (in. sec)					
Pre-termination	0.308	0.197 <sup>†</sup>	0.178	0.171	0.197 <sup>†</sup>
Post-termination	0.166 <sup>†</sup>	0.061	...	...	0.062
$P$ , prior to termination (psia)	298	154	134	129	128
$P$ , maximum at termination (psia)	719	505	495	450	404
$dp/dt_{term}$ (psi/sec)	17,000	18,400	15,500	11,800	14,300
Termination results	Continued combustion	Reignition	Permanent extinction	Permanent extinction	Continued combustion

\* For these tests, the forward chamber was not purged.

† Assumed rates, based on Test O-5.1 and O-5.2.

(Confidential)

In Tests O-1.1 and O-7.1, the aft grains did not extinguish when the forward grain was terminated. Instead, the aft-chamber pressure in these tests dropped to a lower level and combustion continued. In Test O-2.1 the aft-chamber pressure dropped to ambient for three seconds after termination, but then rose to approximately 30 psia and remained at this pressure until the aft grain was consumed. However, motion pictures taken during this test show that there was gas flow from the aft nozzle during the period between termination and the pressure rise to 30 psia; this gas flow may signify that the aft grain did not completely extinguish upon termination. The forward grain in this test was extinguished when the valve was actuated and did not reignite, since the amount of the forward web consumed corresponded to the pre-termination pressure-time conditions. In Tests O-5.1 and O-5.2, with  $K_{aft}$  values of 37.8 and 37.6, respectively, the aft grains were permanently extinguished on termination. (Confidential)

The burning-rate data obtained from these tests are plotted in Figure 105. Note that for Tests O-1.1, O-7.1, and O-2.1, in which the aft grain did not permanently extinguish, burning rates were calculated since for these tests the aft chamber operated at two pressure levels. A realistic burning rate was assumed for one pressure level in order to compute the rate at the other. For example, the aft chamber in Test O-1.1 operated at a pressure of 252 psia before the forward grain was terminated and at a pressure of 117 psia after termination. The burning rate of the propellant at 117 psia was approximated with fair accuracy from the rates obtained from Tests O-5.1 and O-5.2, which operated at pressures of 126 and 122 psia, respectively.

Then by using the assumed rate at 117 psia and the burning time at this average pressure, the portion of the web consumed during this period was calculated. The burning rate at 252 psia was then calculated based on the portion of web not consumed at the lower pressure and the burn time at 252 psia. This method

# CONFIDENTIAL

AFRPL-TR-65-209, Vol I

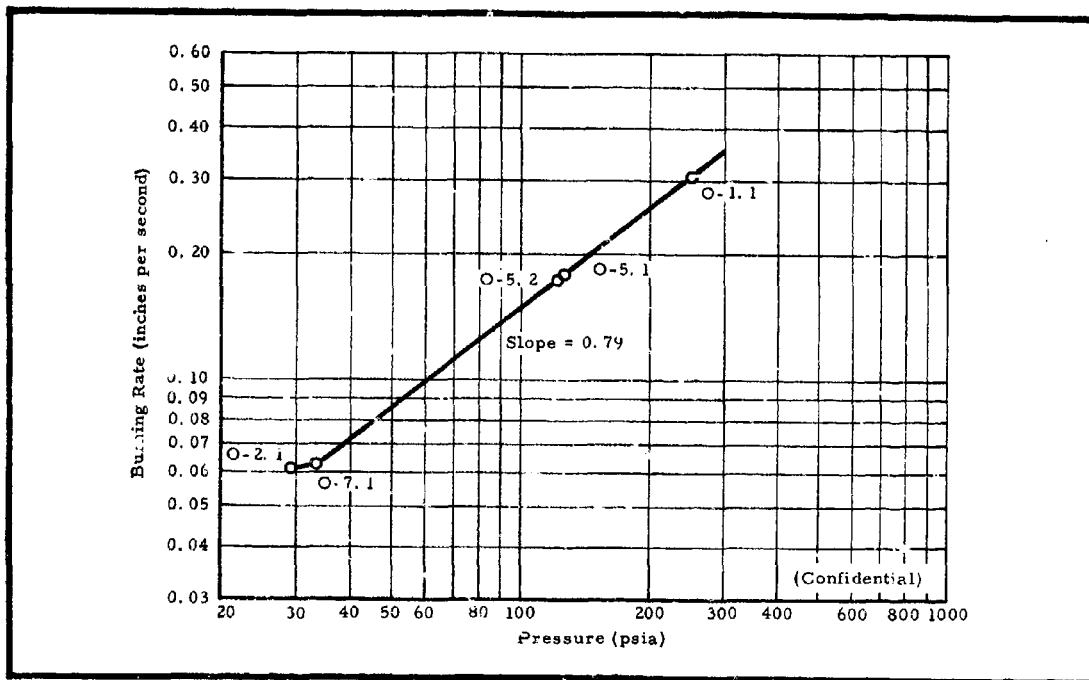


Figure 105 - Burning-Rate Data for C-445 Propellant Obtained from Subscale Motor Tests

of burning-rate analysis for a motor operating at two pressure levels is preferable to using an average burning rate for the over-all test, since for burning-rate exponents other than unity and zero and for exponents that vary with pressure, average burning rate values are erroneous. (Confidential)

The burning-rate data plotted for C-445 propellant in Figure 105 give an exponent of 0.79. Although the exponent may decrease in the low-pressure region, there is insufficient data in this region to determine a value. (Confidential)

These termination tests with C-445 propellant indicate that an aft-chamber  $K_n$  value below 40 is apparently necessary in order to extinguish C-445 propellant. The  $K_n$  value for the aft chamber determines the equilibrium pressure of that chamber when the forward grain is extinguished. For high  $K_n$

values, an aft propellant with an exponent less than unity can attain a stable operating pressure in the absence of mass flow from the forward chamber. As the aft-chamber  $K_n$  is reduced, the corresponding equilibrium pressure becomes less than ambient pressure or the minimum stable operating pressure of the propellant, and combustion is extinguished.

Northrop Carolina believes that the aft grain is extinguished by this foregoing process rather than by the rarefaction wave. It is believed that the rarefaction wave produced in the aft chamber by forward grain termination is too weak to extinguish combustion of the aft grain. This is verified by the lack of correlation between the aft chamber decay rates and extinguishment results (see Table XXXVII). (Confidential)

(c) Results of Motor Tests with C-430 Propellant

Six motors were fired with C-430 propellant grains in the aft chamber. The results of these tests, designated O-3.1, O-3.2, O-4.1, O-6.1, O-8.1, and O-8.2, are summarized in Table XXXVIII.

These tests indicated that C-430 can be permanently extinguished with aft-chamber  $K_n$  values of 41 and below. For Tests O-8.1 and O-8.2, which were conducted with aft-chamber  $K_n$  values of 47, somewhat conflicting results were obtained. In both of these tests, aft-chamber pressure decreased to ambient at termination, but increased to 30 psia when the nitrogen purge was initiated 0.5 sec after termination. In the first test, O-8.1, the 30-psia pressure produced when the nitrogen purge was initiated decreased to ambient after 0.5 sec and the grain was permanently extinguished. However, in Test O-8.2, when the purge was initiated, aft-chamber pressure increased to and remained at 30 psia until the grain burned out. Apparently, at this  $K_n$  value of 47, a marginal extinguishment condition exists. It should be noted that the nitrogen purge mass flow itself is not sufficient to produce a measurable pressure rise in the motor. With an aft-chamber

**CONFIDENTIAL**

AFRPL-TR-65-209, Vol I

TABLE XXCVIII - SUMMARY OF TERMINATION TESTS (C-430 AFT PROPELLANT)

Parameter	Test Number						
	O-3.1	O-3.2	O-4.1	O-6.1	O-8.1	O-8.2	
Forward chamber (PPO-13)							
Burning surface area (sq in.)	74.2	80.4	79.1	83.8	83.5	83.5	
Throat area (sq in.)	0.110	0.110	0.111	0.110	0.110	0.110	
$K_n (S_b/A_t)$	67.4	73.2	71.2	76.2	76.8	76.8	
Burn time (sec)	1.025	1.018	0.994	0.983	1.007	1.005	
$\bar{P}_b$ (psia)	916	1744	1528	1510	1886	2029	
$P_{term}$ (psia)	424	1794	1855	1997	1840	2134	
$dp/dt_{term}$ (psi/sec)	21,500	110,000	73,900	124,000	63,500	65,400	
Termination results	Reignition*	Permanent extinction	Permanent extinction	Permanent extinction	Permanent extinction	Reignition	
Aft chamber (C-430)							
Burning surface area (sq in.)	156	157	156	156	143	143	
Throat area (sq in.)	3.79	3.80	5.75	2.87	3.03	3.03	
$K_n (S_b/A_t)$	41.2	41.3	27.1	54.5	47.1	47.0	
Burn time (sec)	1.010	1.000	0.580	0.760	0.994	0.976	
Pre-termination	...	...	...	...	...	5.07	
Post-termination	...	...	...	...	...	...	
$\bar{P}_b$ (psia)	85.3	117.1	31.9	232.0	175.2	204.4	
Pre-termination	...	...	...	...	...	62.1	
Post-termination	...	...	...	...	...	...	
Burn rate (in./sec)	0.121	0.161	0.066	...	0.246	0.287 <sup>†</sup>	
Pre-termination	...	...	...	...	...	0.096	
Post-termination	...	...	...	...	...	...	
$P_{prior}$ (psia)	52.2	120	30.0	280	196	219	
$P_{max}$ (psia)	159	435	235	710	543	590	
$dp/dt_{term}$ (psia)	6,900	16,200	12,000	20,900	10,000	10,100	
Termination results	Permanent extinction	Permanent extinction	Permanent extinction	Reignition	Permanent extinction	Reignition	

\* For these tests, the forward chamber was not purged.

† Assumed rate, based on extrapolation of data obtained in Tests O-3.1, O-3.2, and O-8.1.

(Confidential)

# CONFIDENTIAL

AFRPL-TR-65-209, Vol I

$K_n$  of 54.5 in Test O-6.1, reignition also appeared to occur when the purge was initiated. (Confidential)

In Figure 106, the burning-rate data for C-430 propellant obtained in these motor tests are plotted as a function of pressure. The burning rate for Test O-8.2 was calculated in a manner similar to that described in (2), above, for the C-445 tests in which burning occurred at two pressure levels. This propellant has a quite high pressure exponent of 0.99 above 85 psi, but decreases to 0.56 below this pressure. A similar decrease in exponent at low pressures for this propellant was observed in the strand burning rates shown in Figure 104. On the basis of the more favorable results obtained with C-430, it was selected for the Series N Tests (see Section VII). (Confidential)

#### (4) Dependence of Motor Design Parameters on Aft-Chamber $K_n$

From the subscale motor test results, the maximum  $K_n$  at which C-430 propellant will be permanently extinguished is between 41 and 47, whereas for C-445 propellant the

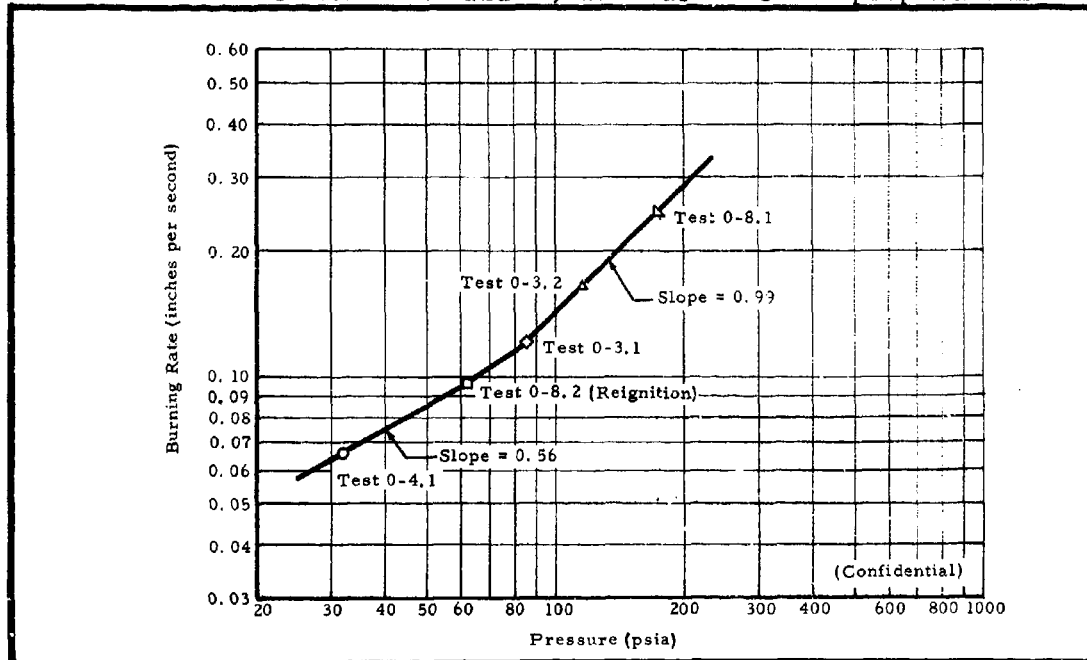


Figure 106 - Burning-Rate Data for C-430 Propellant Obtained from Subscale Motor Tests

-156-

# CONFIDENTIAL

maximum  $K_n$  for extinguishment lies between 37 and 42. The value of  $K_n$  is significant not only from the standpoint of extinguishing the motor, but also for its effect on mixture ratio. That is, a maximum  $K_n$  design value limits the attainable aft-to-forward mixture ratio,  $\theta$ . This can be shown by the following ballistic relationships. (Confidential)

By definition,

$$\theta = \frac{\dot{m}_{\text{aft}}}{\dot{m}_{\text{fwd}}} = \frac{\dot{m}_{\text{aft}}}{\dot{m}_{\text{total}} - \dot{m}_{\text{aft}}} \quad (1)$$

Substituting for the mass flow rates gives

$$\theta = \left( \frac{\rho A_b a P^n}{C_D A_t P - \rho A_b a P^n} \right)_{\text{aft}} \quad (2)$$

where

- $\rho$  = propellant density,
- $A_b$  = burning surface area,
- $a$  = burning rate constant,
- $P$  = chamber pressure,
- $n$  = pressure exponent,
- $C_D$  = discharge coefficient, and
- $A_t$  = throat area.

Equation 2 can be rearranged to give

$$\theta = \left[ \frac{1}{\left( \frac{C_D P^{1-n}}{\rho a} \right) \frac{1}{K_n} - 1} \right]_{\text{aft}} \quad (3)$$

where

$$K_n = \text{aft burning area/aft throat area.}$$

At a given pressure,  $P_1$ , the term in parenthesis in Equation 3 is constant for a given aft propellant ( $C_D$  is influenced slightly by the choice of forward propellant). Therefore,

$$\theta_{P_1} = \frac{K_n}{C_{P_1} - K_n}, \quad (4)$$

where

$$C_{P_1} = \left( \frac{C_D P_1^{1-n}}{\rho_a} \right)$$

From Equation 4 it is obvious that the mixture ratio achievable in any dual-chamber motor is a function of the  $K_n$  design value and the properties of the aft propellant formulation. Also, as the  $K_n$  design value is decreased, the attainable mixture ratio is decreased.  $C_D$  is a function of the mixture ratio,  $\theta$ , increasing somewhat as  $\theta$  is changed from its optimum value. That is, for  $\theta$  values below optimum, a change in  $C_D$  will cause  $\theta$  to decrease at a faster rate as  $K_n$  decreases, whereas for  $\theta$  values above optimum, the decrease in  $\theta$  will be less with decreasing  $K_n$  as  $C_D$  changes. The  $K_n$  limits for C-430 and C-445 propellants correspond to  $\theta$  values below optimum for all forward propellant formulations under consideration. (Confidential)

In Figure 107,  $\theta$  values calculated from Equation 4 are plotted as a function of aft-chamber  $K_n$  at 100 psi for C-430 propellant. Values of  $C_D$  corresponding to the mixture ratio for C-430 with a typical forward propellant were used. The plot of  $\theta$  versus  $K_n$  for C-445 propellant would be similar. (Confidential)

**CONFIDENTIAL****4. CONCLUSIONS**

The following three castable aft propellant systems are feasible for use in the DCCSR motor, with certain limitations:

1. Solid solution binder-lithium perchlorate-ammonium perchlorate
2. Fluoroalkyl acrylate binder-ammonium perchlorate
3. Carboxy-terminated polybutadiene binder-potassium perchlorate-ammonium perchlorate

(Confidential)

System 1 provides higher performance, but is characterized by poor mechanical properties and low-frequency oscillatory burning at low pressures. Low pressure exponents prevent Systems 2 from being operated at high mixture ratios where optimum performance occurs. The same is true to a slightly lesser degree for System 3 due to low pressure exponents below 100 psi. The mechanical properties of System 3 are, however, superior to those of the other two systems. (Confidential)

System 3 was selected for use in the series N motors since less additional development is involved than for the other two systems. Further development is required to improve the mechanical properties and reduce the low pressure oscillatory burning of System 1 and increase the pressure exponents for System 2. (Confidential)

**CONFIDENTIAL**

**CONFIDENTIAL**

AFRPL-TR-65-209, Vol I

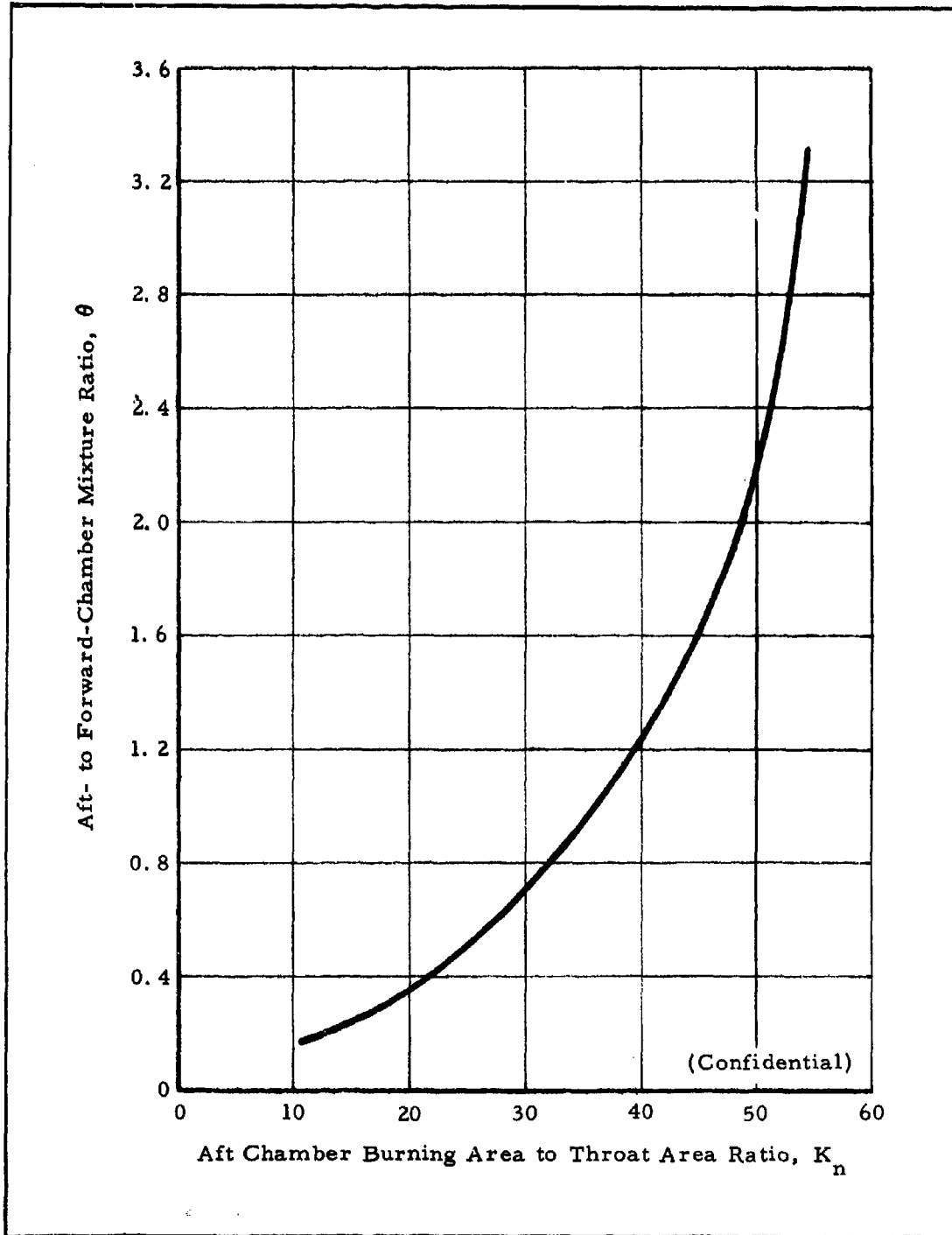


Figure 107 - Aft to Forward - Chamber Mixture Ratio as a Function of  $K_n$  at 100 psia for C-430 Propellant

**CONFIDENTIAL**

SECTION IV - REIGNITION AND INSULATION STUDY

1. GENERAL

A study was conducted during this year's program, as part of Phase III, in preparation for Test Series M, to identify those geometrical and ballistic factors that influence the termination and reignition of motors containing PPO-13 propellant. This information was essential to carrying out the full-scale Series M tests with the highest possible confidence level. This investigation consisted of a study of the compatibility of several insulation materials (insulation study) and an evaluation of the factors that affect reignition (reignition study), as well as the interaction of these two effects on reignition.

2. INSULATION STUDY

a. General

The insulation study consisted of an evaluation to determine the compatibility of several insulation materials with the thermal protection required for the forward chamber of the DCCSR motor. An analysis of the reignition that occurred in Tests E. 1, E. 2, and E. 3, conducted during the previous year's program (Reference 8), indicated that this reignition could be attributed to the hard-char-type insulation used in the forward chamber. The hard-char-layer constitutes a large heat sink, which, at termination, becomes a ready source of heat for radiation, convection, and conduction to the extinguished propellant surface. It is believed that the insulation, acting as a heat source, along with the hot oxygen diffused from the aft chamber, is a prime contributor to the reignitions experienced in these tests. (Confidential)

In selecting the insulation materials for this study, the following criteria were established:

1. The insulation material should pyrolyze completely as heat is supplied to its surface, similar to the conditions that occur at the propellant surface. Thus, when combustion is extinguished, the surface temperature of the insulation is the pyrolysis temperature of the material, and no residual heat sink remains on the surface.

2. The regression (or ablation) rate of the insulation material should be no greater than that of an efficient char-type material, in order to prevent or minimize a mass fraction penalty.
3. The insulation material should be capable of bonding well with both the case walls and the propellant.  
(Confidential)

The insulation materials used in both the Series E and G tests were evaluated to serve as a standard against which the new materials would be compared. The selected materials, listed in Table XXXIX, include phenolic-nylon composites (Reference 16) and other commercially available materials advertised to be purely ablative or to produce little char. Table XXXIX also gives the manufacturers and compositions of these materials.

b. Insulation Tests

(1) General

The following tests were selected to provide data for comparing the various insulations and to provide sufficient information to select the most promising insulation material:

1. "Torch" tests to determine ablation rate and char formation
2. Bond strength tests to determine insulation-to-propellant and insulation-to-metal bond capability
3. "Pancake" motor firings to determine performance under actual motor firing conditions.

(2) Torch Tests

For the torch tests, a methane-oxygen torch was set up to impinge on 2-in. -diameter by 0.40-in. -thick test specimens at an incident angle of 60 degrees. The distance of the flame from the specimen was adjusted so that the temperature at the surface of the test specimen was 2488°F. (A temperature range of 2500 to 2700°F was selected to simulate the flame temperature produced by PPO-13). The specimens were subjected to the flame for cycles of 3, 6, and 30 seconds.

# CONFIDENTIAL

AFRPL-TR-65-209, Vol I

TABLE XXXIX - INSULATION MATERIALS SELECTED FOR STUDY

Insulation Material	Manufacturer	Composition	Remarks
PB-6 (PBAA)	Northrop Carolina formulation	44. 3% PBAA 7. 2% Epon 820 24. 2% Titanium dioxide 24. 3% Carbon black (Thermax)	Vacuum cast; cured 24 hr at 170° F
L-6 Epoxy (unfilled)	Northrop Carolina formulation	25% TF Asbestos 24% Epi-Rez 504 30% Epi-Cure 855	Cured 24 hr at 120° F
L-3	Northrop Carolina formulation	34. 2% Epi-Rez 504 22. 9% Epi-Cure 855 42. 9% TF asbestos	Cured 24 hr at 120° F
BFG 39-322	E. F. Goodrich Co.	Butadiene-acrylonitrile rubber base with silica filler	Used in E series tests
RPD-150	Raybestos-Man- hattan, Inc.	Preimpregnated long spinning-grade chry- sotile asbestos fibers and high-heat-resistant phenolic resin system	Pressure molded
Nylon	.....	Zytel 101	.....
FM 5051	U. S. Polymeric	50% Resin 50% Nylon fibers	Pressure molded
MXN-21	Fiberite Corp.	Phenolic resin per MIL-R-9299, Welling- ton-Sear SN-19 nylon fabric	Pressure molded
4501	Narmco Materials Div., Telecom- puting Corp.	Filled, modified phenolic nitrile resin, non-reinforced	Elastomeric material
4016-C	Narmco Materials Div., Telecom- puting Corp.	Unfilled, non-rein- forced nylon-phenolic material	Pressure molded
4018	Narmco Materials Div., Telecom- puting Corp.	Unfilled, phenolic resin, nylon-fabric-rein - forced material	Pressure molded
PB-5 (PBAA unfilled)	Northrop Carolina formulation	85. 0% PBAA 15. 0% Epon 820	Vacuum cast; cured 24 hr. at 170° F
SE-1 (Epoxy- unfilled)	Shell Oil Co.	23. 3% Epon 820 16. 7% Epon Catalyst Z	.....

Figures 108 and 109 show specimens subjected to 6- and 9-second cycles, respectively. (The 9-second test was the result of an initial 3-second cycle followed by a 6-second cycle.) The specimens shown in Figure 110 were subjected to a 30-second cycle. Table XL lists the results of all the torch tests.

(3) Bond Strength Tests

The ability of the various insulation materials to bond to steel was evaluated by means of case bond jigs. The results of these tests, given in Table XLI, indicate that, with proper surface treatment and adhesive, a good bond to metal can be achieved with the candidate insulation materials.

The ability of the insulation materials to bond to the PPO-13 forward propellant was also studied with bond jigs. The PPO-13 was cast onto the insulation material samples and cured. Peel tests were then conducted to determine the bonding characteristics. The criterion for a good bond was failure in the propellant, not in the bond itself. The results of these tests, presented in Table XLII, show that additional work is needed to ensure a good bond between PPO-13 and both nylon and PB-6. (Confidential)

(4) Pancake Motor Firings

Pancake motor tests, designated Test Series I, were initiated to evaluate insulation materials under actual firing conditions. In the first test, four materials, BFG 39-322, nylon, L-3, and PB-6, were evaluated; both L-3 and PB-6 are Northrop Carolina products.

Figure 111 shows the motor assembly used for Tests I. 1. 1 and I. 1. 2. (The letter I designates the test series, the first numeral represents test number in the series, and the second numeral indicates the first or second firing for the motor). The nozzle was sized to provide a nominal chamber pressure of 1000 psi, so that, with a web of 1.0 in., a burn time of 4.0 sec was anticipated. The insulation specimens were not disturbed between Tests I. 1. 1 and I. 1. 2, but a new loaded propellant cup and nozzle were installed between each firing. The insulation specimens occupied 90-degree segments as shown in Section A. A, Figure 111.

**CONFIDENTIAL**

AFRPL-TR-65-209, Vol I

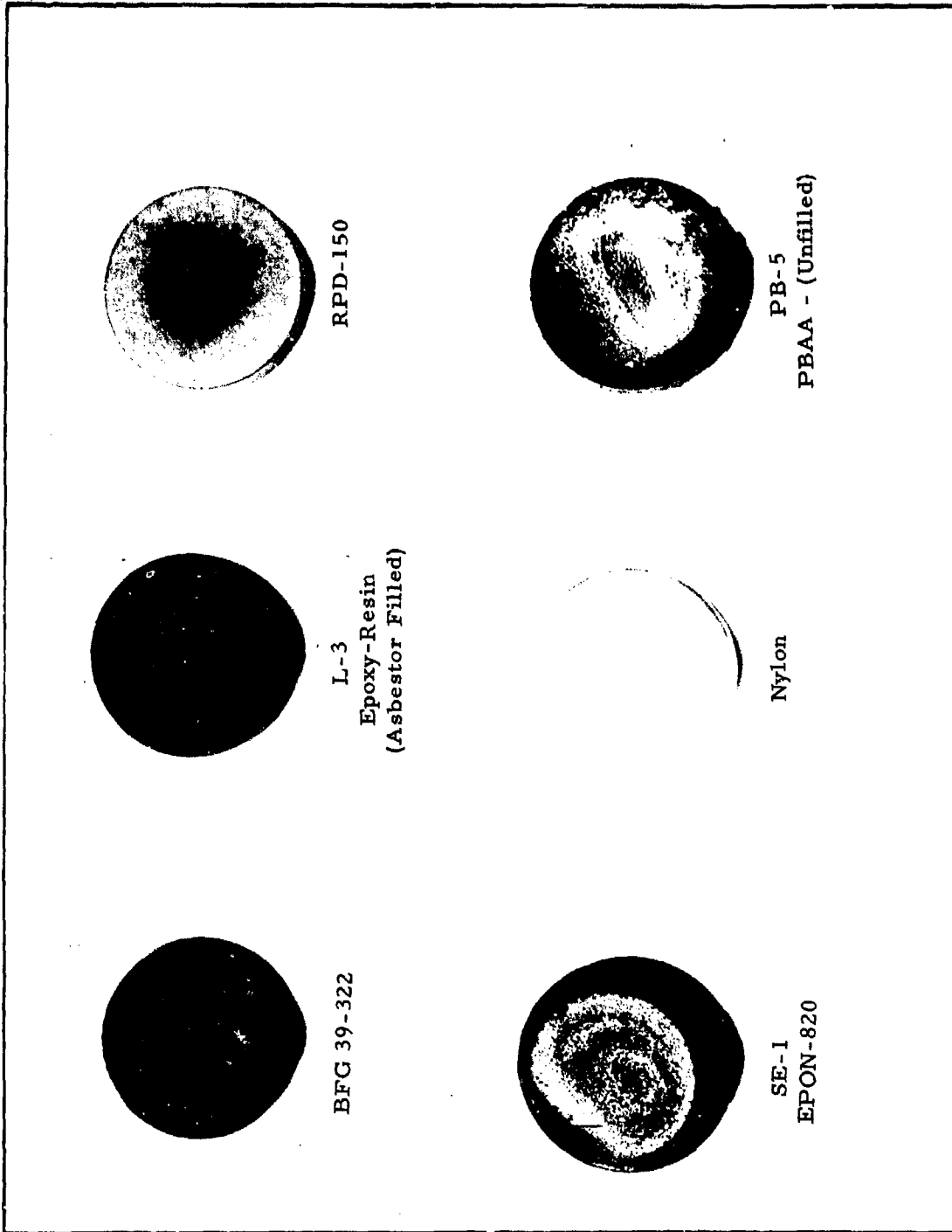


Figure 108 - Insulation Samples After 6-Second Torch Tests

**CONFIDENTIAL**

**CONFIDENTIAL**

AFRPL-TR-65-209, Vol I

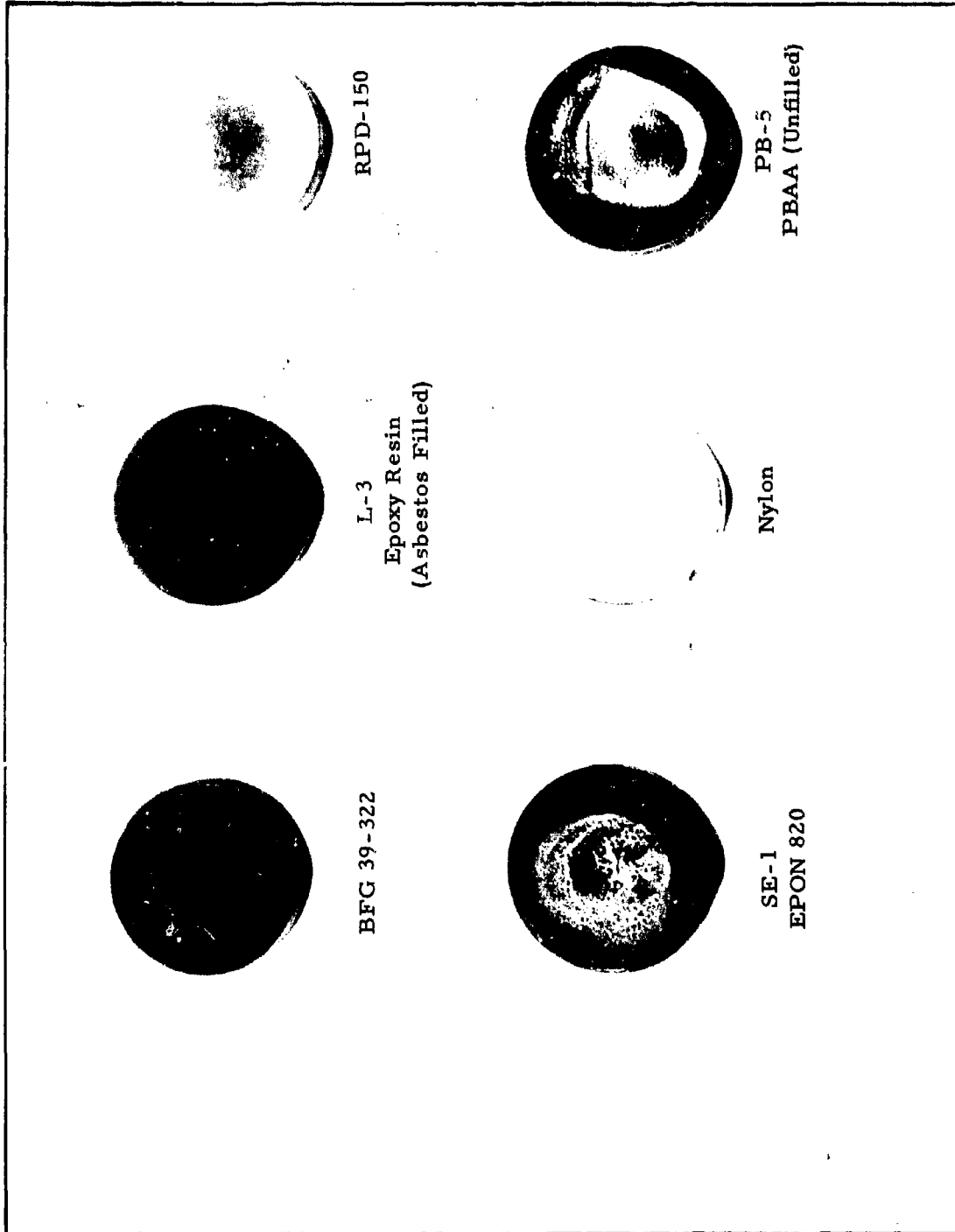


Figure 109 - Insulation Samples After 9-Second Torch Test

**CONFIDENTIAL**

AFRPL-TR-65-209, Vol I

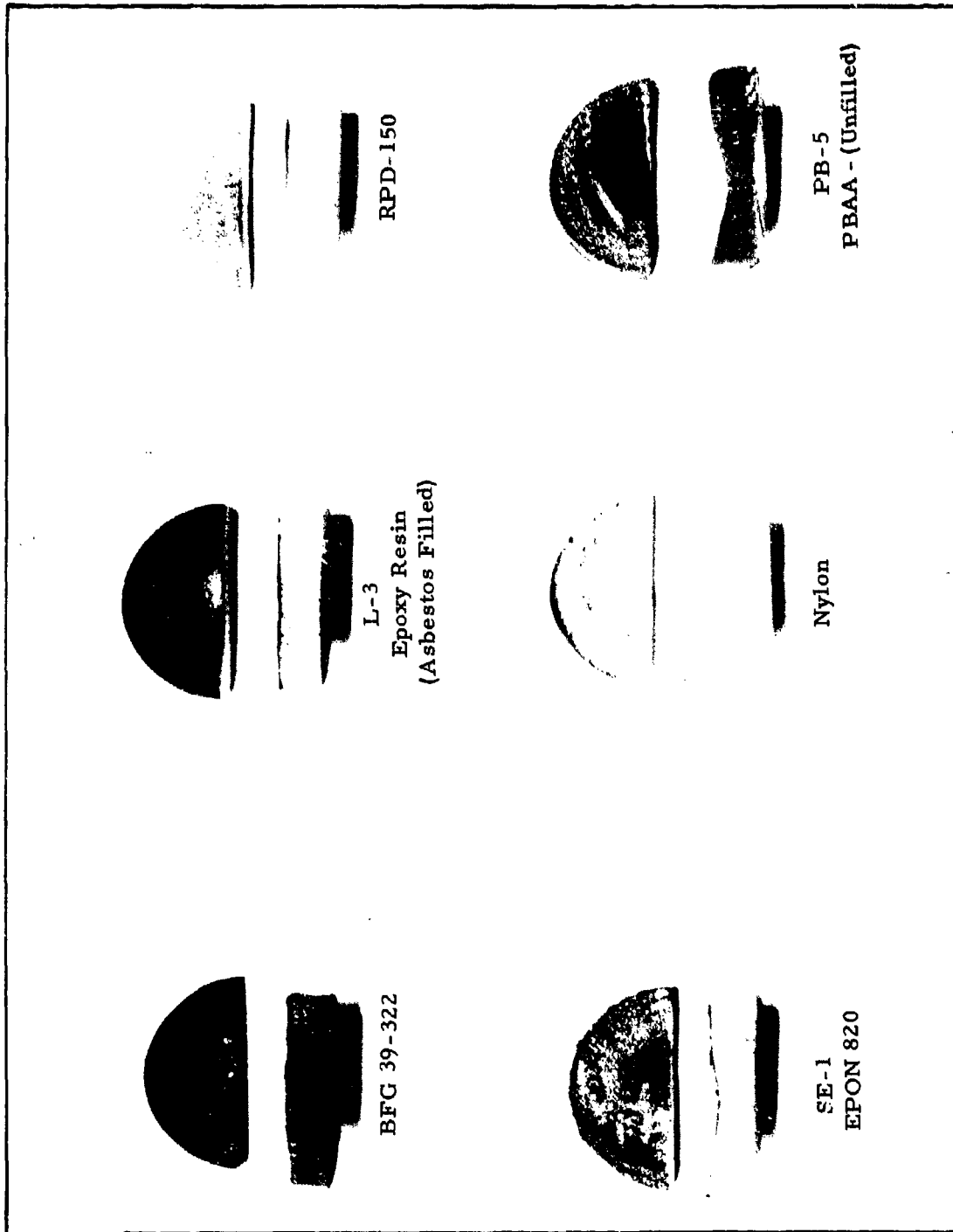


Figure 110 - Insulation Samples after 30 Second Torch Test

**CONFIDENTIAL**

**TABLE XL - TORCH TEST RESULTS**

Material	Specimen No. #	Test Duration (Sec)	Flame Temperature (°F)	Pre-Test		Post-Test		Δt (inches)	ΔW (gm)	Ablative Rates		Char
				Thickness (in.)	Weight (gm)	Thickness (in.)	Weight (gm)			In./Sec X 10 <sup>-4</sup>	Gm./Sec X 10 <sup>-2</sup>	
Nylon	1	3	2488	0.403	22.5344	.....	22.4919	.....	0.0425	.....	1.4	Nylon melted and ablated; no smoke
	1	6	2488	.....	22.4919	.....	22.3955	.....	0.0964	.....	1.6	Nylon melted and ablated; no smoke
	2	6	2488	0.400	.....	.....	.....	.....	.....	.....	.....	Nylon melted and ablated; no smoke
RPD-150	3	30	2488	0.403	22.5165	0.380	21.8870	0.023	0.6295	7.67	2.1	(Tested for visual comparison) Melted material on the outside edge burned slightly after removal of flame; no char
	1	3	2488	0.396	35.7015	.....	35.6668	.....	0.0347	.....	1.16	Smokeless; no residual char
	1	6	2488	.....	35.6668	.....	35.6345	.....	0.0323	.....	0.54	Smokeless; surface blackened. No residual char layer
BFG 39-322	2	6	2488	0.399	.....	.....	.....	.....	.....	.....	.....	Similar to No. 1; tested for visual comparison.
	3	30	2488	0.397	35.6300	0.360	35.0405	0.037	0.5895	12.3	1.96	Char layer formed
	1	3	2488	0.415	23.8235	.....	23.7285	.....	0.0950	.....	3.17	Fine black powder residue formed; easily removed
PB-5 (PBAA Unfilled)	1	6	2488	.....	23.7285	.....	23.5915	.....	0.1370	.....	2.28	Same as above
	2	6	2488	0.394	.....	.....	.....	.....	.....	.....	.....	Same as No. 1
	3	30	2488	0.400	22.9250	0.370	21.7865	0.030	1.1385	10.0	3.8	Fine uniform powder residue (char) formed, similar to No. 1; easily removed
SE-1 (Epoxy Unfilled)	1	3	2488	0.40	20.5155	.....	20.3615	.....	0.1540	.....	5.13	Glassy surface with puddle effect; supported combustion when flame removed.
	1	6	2488	0.40	20.3615	.....	20.1305	.....	0.2310	.....	3.85	
	2	6	2488	0.40	23.7860	0.20	20.1700	0.20	3.6160	66.7	12.05	
L-3 (Epoxy Filled)	1	3	2488	0.402	26.1402	.....	26.0899	.....	0.0503	.....	1.66	Hard crust formed; supported combustion when flame removed
	1	6	2488	0.413	26.0899	.....	25.9240	.....	0.1659	.....	2.77	
	2	6	2488	0.413	.....	.....	.....	.....	.....	.....	.....	Same as No. 1 except that crust layer became irregular
PB-6 (PBAA Filled)	3	30	2488	0.423	26.1250	0.302	23.5775	0.121	2.5475	40.3	8.49	
	1	3	2488	0.403	29.1700	.....	29.1315	.....	0.0385	.....	1.29	Char could be cleaned off.
	1	6	2488	.....	29.1315	.....	29.0590	.....	0.0725	.....	1.21	Supported combustion after removal of torch
PB-6 (PBAA Filled)	2	6	2488	0.396	.....	.....	.....	.....	.....	.....	.....	Same as No. 1 except heavier char
	3	30	2488	0.398	28.9785	0.370	27.4730	0.028	1.5055	9.34	5.02	Same as No. 1 except heavier char similar to RPD-150
	1	30	2330	0.408	27.2670	0.360	25.4220	0.048	1.8450	14.0	6.1	Char, powder like, easily removed

\* Specimen No. 2 used for visual comparison; pretest weights did not have sensitivity required for ablation rates.

**CONFIDENTIAL**

AFRPL-TR-65-209, Vol 1

TABLE XLI - RESULTS OF INSULATION-TO-METAL BOND TESTS

Material	Preparation	Adhesive	Cure	Results
PB-5	Material cast in test jig	None	16 hr at 170° F, 24 hr at 180° F	Failure in insulation at 58 lb <sub>f</sub>
L-3	Material cast in test jig	None	12 hr at 120° F	Failure in insulation at 1787 lb <sub>f</sub>
RPD-150	Surface sandblasted and degreased	SE-1	24 hr at 150° F	Failure in insulation at 4800 lb <sub>f</sub>
Nylon	Nylon surface roughened and degreased with 1% HCl solution in methyl alcohol	SE-1	24 hr at 150° F	Failure in bond at 1500 lb <sub>f</sub> ; nylon cracked during test
Nylon	Same as above	L-6	24 hr at 150° F	No pull test conducted; unable to fail bond in shear manually
BFG 39-322	Surface roughened and degreased	SE-1	24 hr at 150° F	Unable to fail bond manually
PB-6 (Cured)	Specimen cast and cured prior to test	L-6	12 hr at 120° F	Unable to fail bond manually
L-3 (cured)	Specimen cast and cured prior to test	L-6	12 hr at 120° F	Unable to fail bond manually

TABLE XLII-RESULTS OF INSULATION-TO-PROPELLANT BOND TESTS

Material	Preparation	Adhesive/Liner	Cure	Results
RPD-150	Sandblasted and degreased	L-1*	16 hr at 120 <sup>o</sup> F	Good bond, with failure occurring in propellant
Nylon	Nylon degreased	None	16 hr at 120 <sup>o</sup> F	Poor bond
Nylon	Nylon degreased	L-1*	16 hr at 120 <sup>o</sup> F	Poor bond failure between L-1 and nylon
Nylon	Surface roughened and degreased with 1% HCl solution in methyl alcohol	L-1*	16 hr at 120 <sup>o</sup> F	Failure occurred in propellant
Nylon	Same as above	None	16 hr at 120 <sup>o</sup> F	Failure occurred at bond
PB-6	Same as above	None	16 hr at 120 <sup>o</sup> F	Poor bond, with failure occurring between propellant and insulation
PB-6	Same as above	L-1*	16 hr at 120 <sup>o</sup> F	Easily peeled apart, with failure between L-1 and PB-6

\* L-1 is 100% cellulose acetate.



As shown in Figure 111, thermocouples were installed to measure the backside temperature of each test specimen. Figure 112 shows the prefire installation of the test specimens; Figure 113, the test motor on the stand; and Figure 114, a postfire view of the test specimens. A summary of the test results is presented in Table XLIII; the motor data for the tests were as follows:

<u>Test</u>	<u>Average Chamber Pressure (psia)</u>	<u>Burn Time (sec)</u>
I. 1. 1	800	4. 1
I. 1. 2	750	4. 2

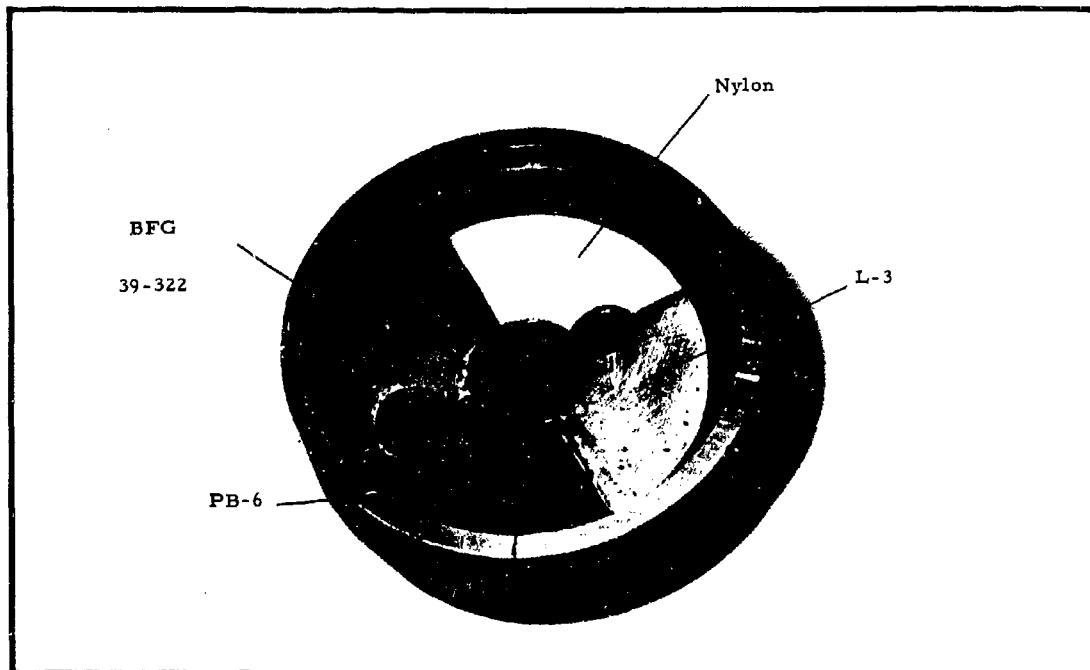


Figure 112 - Interior View of Pancake Motor Aft Closure Before Test I. 1. 1

**CONFIDENTIAL**

AFRPL-TR-65-209, Vol I



Figure 113 - Pancake Motor Mounted on Stand (Test I. 1)

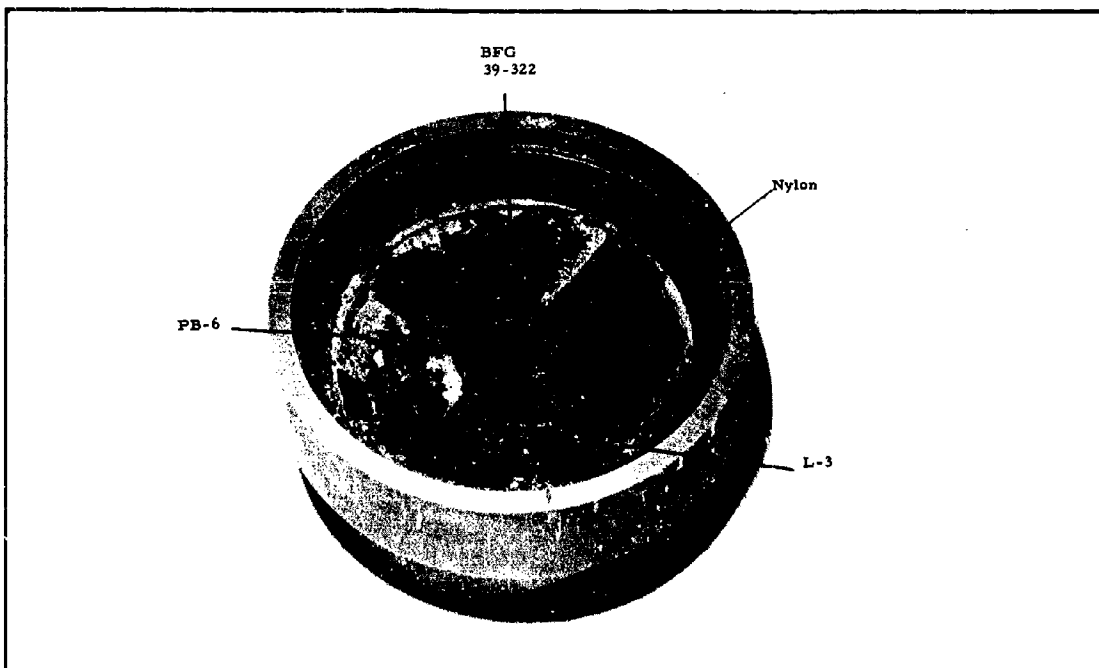


Figure 114 - Interior View of Pancake Motor Aft Closure After Test I. 1

**CONFIDENTIAL**

TABLE XLIII - RESULTS OF PANCAKE MOTOR INSULATION TESTS

Insulation Material	Adhesive	Char	Remarks
Nylon	Surface roughened, wiped with 1% HCL solution in methyl alcohol; L-6 adhesive	Very hard "bubble" surface approximately 0.02-in. deep; char would not scrape off	Gas leakage behind specimen; backside temperature data invalid
L-3	L-6	Scale-like char approximately 0.02-in. thick and tenacious	Same as above
PB-6	L-6	Very soft, loose, scale-like char approximately 0.06-in. thick and easily removed	No gas leakage behind specimen; backside temperature recorded
BFG 39-322	L-6	Soft, loose, scale-like char approximately 0.03-in. thick; similar to PB-6	Same as above

Figure 115 shows the test specimens after removal from the motor. Note that the soft char layer on PB-6 and BFG 39-322, apparent in Figure 114, was lost when the specimens were removed from the motor and prepared for the photograph shown in Figure 115. It is interesting to note that BFG 39-322, PB-6, and L-3 formed char layers as observed in previous torch tests; however, the nylon specimen formed a hard tenacious tissue char layer approximately 0.020 in. thick, which had not been observed during the "torch" tests.

Backside temperatures were obtained for PB-6 and BFG 39-322, but not for nylon and L-3 because of a gas leak between the test specimen and the motor case. Temperature versus time for PB-6 and BFG 39-322 is plotted in Figure 116.

Additional insulation materials were evaluated later in the program; these materials were V-3021 and V-44, both manufactured by General Tire and Rubber Company. V-3021 was installed in the motor for Test I. 15; V-44, was used in Tests I. 16 and I. 17. There was no apparent difference in their effect on motor reignition. For Test I. 18, segments of V-3021, V-44, and 39-322, the latter manufactured by the B. F. Goodrich Co., were installed in the chamber circumference in 120 degree sections to observe the relative ablative and char characteristics of the three materials. The uninstrumented motor used in this test was operated at a low chamber pressure for over two minutes, then disassembled and inspected. There was no significant difference in the char characteristics of the three materials, with each forming a hard, flaky char. However, the ablative properties of V-44 appeared to be slightly superior from this highly qualitative test. On the basis of its performance in Tests I. 15 through I. 18 and its greater availability, V-44 insulation was selected for use in the forward chambers of the Series M motors.

The data obtained in Tests I. 15, I. 16 and I. 17 are presented subsequently in Table XLV, page 187.

### 3. REIGNITION STUDY

**CONFIDENTIAL**

AFRPL-TR-65-209, Vol I

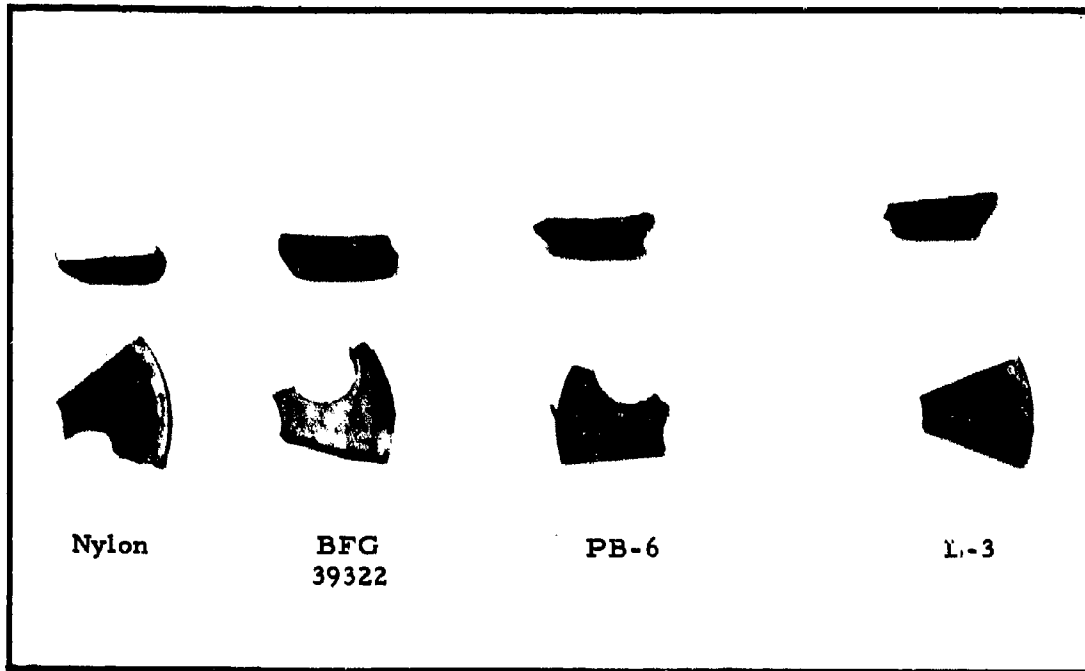


Figure 115 - Insulation Samples After Test I. 1

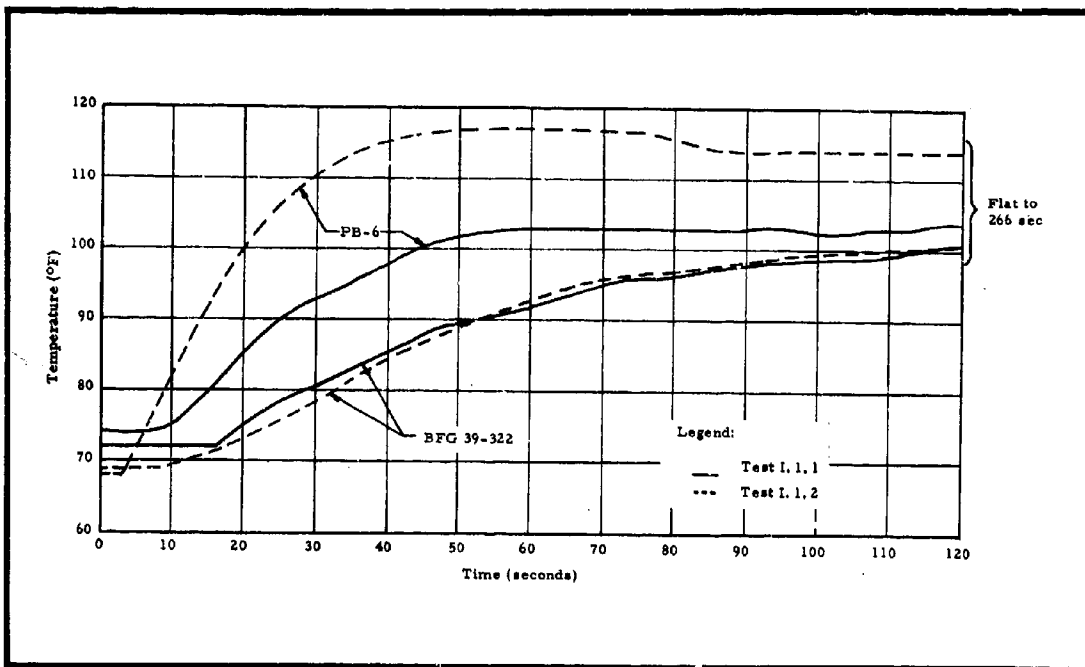


Figure 116 - Temperature Versus Time For Two Insulation Materials (Tests I. 1. 1 and I. 1. 2)

-176-

**CONFIDENTIAL**

**a. General**

In reviewing the results of previous tests (Series C, E, and G; Reference 8), it was apparent that limiting the design considerations to decay rate as the only effective parameter for complete extinction would be inadequate (Series E compared to Series G). The results of work by Anderson and Strand at JPL (Reference 17) and Ciepluch at NASA-Lewis (Reference 18) verify that factors influencing the heat transfer process to the propellant surface after termination must be considered to be predominant factors affecting reignition. Thus, the results obtained by these investigators plus those obtained by Northrop Carolina, strongly indicate that decay rate is the predominant factor in achieving termination, but is relatively insignificant in the reignition process. (Confidential)

A heat balance was made on the propellant surface of an uninsulated pancake motor (see Figure 117) as a function of time, with time equal to zero at termination. This analysis showed that the most important parameter affecting the energy absorbed by the propellant surface is the ratio of chamber free volume to propellant surface area. In this analysis, the chamber residual gas temperature was assumed to be that resulting from an isentropic expansion from termination to sea-level pressures and the propellant flash temperature. Thus, the heat transfer process becomes one of equilibrating the chamber residual gas and propellant surface temperatures. It follows then, that this equilibrium temperature is a function of the ratio of the internal energy of the chamber residual gases to the propellant surface area that receives heat flux from these residual gases. The internal energy of the chamber residual gases is a function of the total moles of residual gas present (chamber free volume) and the residual gas temperature (termination pressure). Therefore, if either (1) the ratio of chamber free volume to propellant surface area or (2) the residual gas temperature increases, the equilibrium temperature of the system increases. But, once the equilibrium temperature exceeds the propellant autoignition temperature, reignition occurs. (Confidential)

**b. Series I Tests**

To verify the analysis described in a, above, additional Series I tests using pancake termination motors, was conducted. In these tests, the ratio of chamber free volume to propellant surface area ( $V_f/S_b$ ) was varied over a range similar to that

**CONFIDENTIAL**

AFRPL-TR-65-209, Vol I

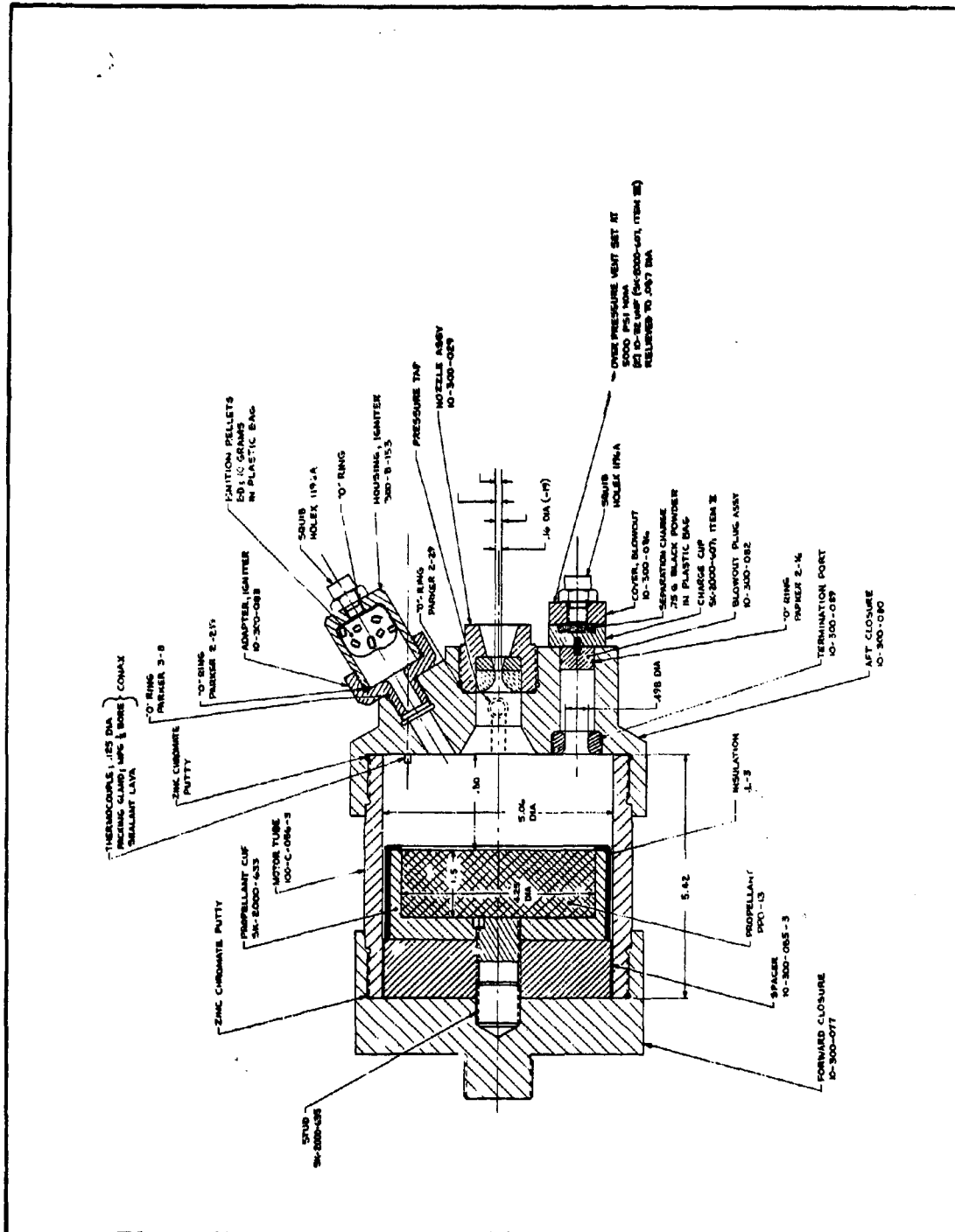


Figure 117 - Paucake Test Motor Assembly Used in Tests 1. 2 Through 1. 14

-178-

**CONFIDENTIAL**

encountered in the Series C, E, and G tests. The results of Series I Tests I. 2 through I. 14 are summarized in Table XLIV. Pressure and temperature versus time, for a typical Series I test, are plotted in Figure 118, and  $V_f/S_b$  is plotted as a function of chamber pressure at termination in Figure 119, for Series I Tests I. 2 through I. 14.

Figure 119 shows that the critical value of  $V_f/S_b$  above which complete extinction could not be achieved is a function of the termination chamber pressure. Two factors exist that are functions of termination chamber pressure. First, the residual gas temperature is higher at low chamber pressures (from assumed isentropic expansion). Therefore, for an equal  $V_f$  (with  $S_b$  constant in all tests), the internal energy of the residual gases is greater at low pressures. Second, the expression for the propellant preheat,  $q$  (from Reference 19),

$$q = \frac{k}{r_b} (T_s - T_u),$$

where

- $k$  = propellant thermal conductivity,
- $r_b$  = propellant burning rate,
- $T_s$  = propellant flash temperature, and
- $T_u$  = propellant initial temperature,

shows that the preheat is inversely proportional to  $P^n$ . Therefore, as pressure decreases, the preheat increases.<sup>c</sup> As a result of these factors, less heat transfer from the residual chamber gases is required to raise the propellant surface to autoignition temperature at the lower chamber pressures than at higher pressures. (Confidential)

The preceding results indicate that grain geometry and/or motor size are also factors that must be considered in evaluating the reignition characteristics of a particular motor. This is borne out by the fact that complete extinction was repeatedly demonstrated in the Series C and G motor tests at values of  $V_f/S_b$  that lie in a region of probable reignition based on the Series I results. (Confidential)

# CONFIDENTIAL

AFRPL-TR-65-209, Vol I

TABLE XLIV - SUMMARY OF DATA FOR SERIES I TESTS

Test No.	$V_f/S_b$	$L^*$ $(V_f/A_t)$	$A_m/S_b$	$V_f/A_m$	$P_{c\text{ term}}$ (psi)	$(dp/dt)_{75\%}$	Time from Termination to Reignition, $\tau$ (sec)
I. 2	3. 81	134	6. 23	0. 606	1610	213, 070	27
I. 3. 1	1. 65	108	3. 88	0. 425	1550	182, 990	...
I. 3. 2	1. 90	125	4. 11	0. 462	1520	157, 216	...
I. 3. 3	2. 12	139	4. 32	0. 491	1480	157, 754	...
I. 3. 4	2. 33	153	4. 50	0. 517	1500	134, 369	...
I. 3. 5	2. 67	176	4. 83	0. 554	1460	133, 800	9
I. 4. 1	2. 42	159	4. 52	0. 535	1760	159, 700	...
I. 4. 2	2. 70	178	4. 76	0. 567	2155	173, 200	19
I. 5. †	2. 30	147	4. 39	0. 525	328	30, 600	20
I. 6. †	...	...	...	...	...	...	...
I. 7. 1	1. 82	123	4. 04	0. 450	3710	...	...
I. 7. 2	2. 12	143	4. 40	0. 485	3903	386, 000	...
I. 7. 3	2. 59	175	4. 76	0. 545	3548	294, 000	...
I. 8	1. 59	104	3. 82	0. 417	293	35, 450	19
I. 9. 1	3. 15	204	5. 09	0. 621	2215	201, 000	...
I. 9. 2	3. 46	234	5. 38	0. 644	2760	240, 000	23
I. 10. 1	0. 94	60	3. 19	0. 295	215	19, 550	...
I. 10. 2 <sup>‡</sup>	...	...	...	...	...	...	...
I. 11. 1	0. 94	60	3. 18	0. 295	238	52, 700	...
I. 11. 2	1. 04	66	3. 30	0. 316	297	42, 500	...
I. 11. 3	1. 15	73	3. 39	0. 339	341	42, 700	16
I. 12. 1	0. 95	33	3. 21	0. 296	283	91, 000	...
I. 12. 2 <sup>‡</sup>	...	...	...	...	...	...	...
I. 13. 1	0. 94	33	3. 19	0. 296	337	86, 500	...
I. 13. 2	1. 03	35	3. 29	0. 315	370	99, 000	18
I. 14	3. 20	207	5. 13	0. 624	3140	285, 000	22

**\* Legend**

- $V_f$  = Chamber free volume
- $S_b$  = Propellant burning surface
- $A_t$  = Nozzle throat area
- $A_m$  = Exposed metal surface area
- $t$  = Time from termination to reignition

<sup>†</sup> Thermocouple plug ejected at ignition, and propellant burned out at very low pressure.

<sup>‡</sup> Leak occurred in termination pyrotechnic charge; termination plug did not eject; propellant burned out at design pressure.

(Confidential)

# CONFIDENTIAL

AFRPL-TR-65-209, Vol I

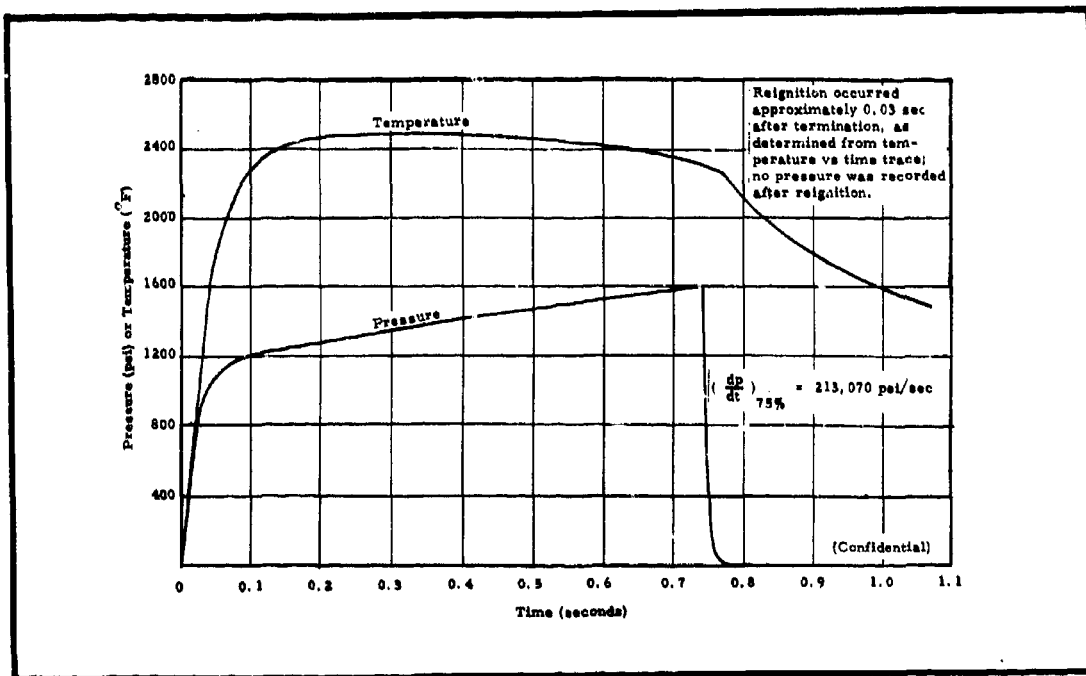


Figure 118 - Pressure and Temperature Versus Time for Test I. 2.

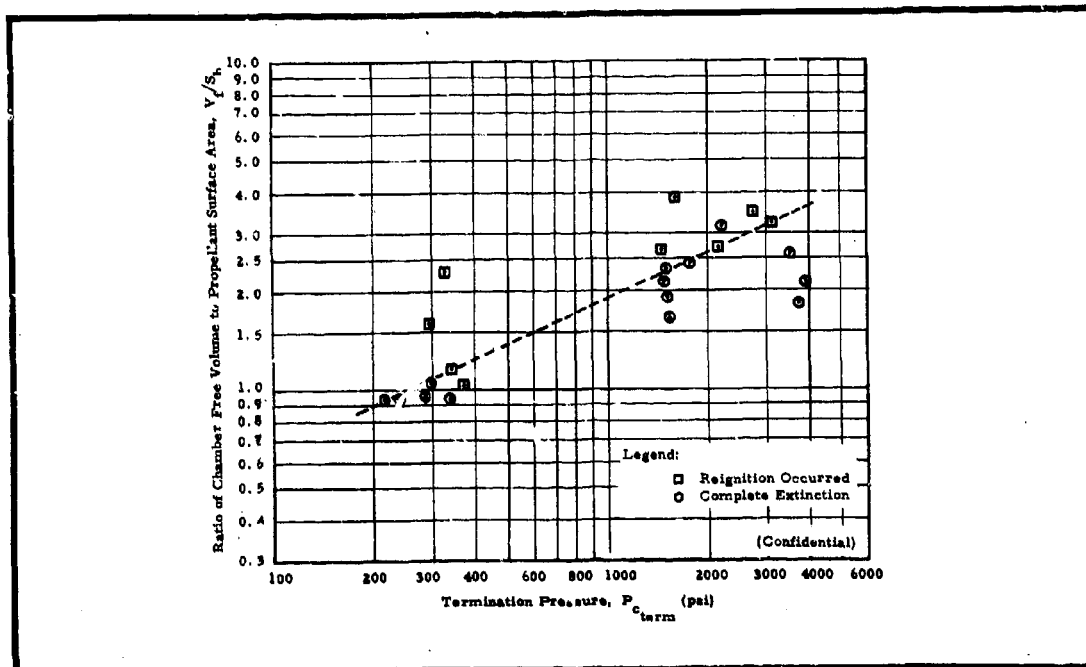


Figure 119 -  $V_f/S_p$  versus Termination Pressure for Series I Tests I. 2 through I. 14

The necessary external cooling to prevent reignition under the most severe  $V_f/S_b$  condition is analyzed in c, below.

c. Chamber Purge Technique

(1) Analysis

The results of the Series I Tests I. 2 through I. 14, described in b, above, demonstrated that the quantity and temperature of residual chamber gases, following termination, strongly influence the probability of reignition at sea-level conditions. (Confidential)

One of the primary objectives of the Series M full-scale tests is to generate a performance map. To meet this objective, the motors must be operated over the full range of chamber free volumes in these tests. From the results of the Series E and I tests and the known range of chamber free volume to propellant surface ratios to be covered, it is highly probable that reignition will occur in certain of these sea-level tests. Therefore, to achieve the highest possible confidence that reignition will not occur, it was decided to purge the chamber with an inert cool gas just after termination. This post-termination purge would allow the full objectives of the Series M full-scale tests to be met without incurring additional cost or scheduling difficulties associated with conducting the tests in an altitude chamber.

After termination there are three sources of residual heat: heat stored in the chamber gasses, in the propellant, and in the chamber case (or insulation) wall. An analysis of reignition in Series E and I tests, as well as the results reported by Ciepluch (Reference 18), has shown that the propellant surface may be reignited either by heat supplied to the propellant surface from the residual gases or the wall surface, or by a combination of both. The selected purge system will provide cooling for all three heat sources existing in the chamber. (Confidential)

Since the heat stored in a gas is equal to the internal energy of that gas, the heat that must be removed,  $Q$ , is equal to the change in internal energy, or

$$Q = U_2 - U_1 = W_g C_v \Delta T_g, \quad (6)$$

where

$$C_v = \frac{\bar{R}}{J(\gamma - 1)M},$$

$\bar{R}$  = universal gas constant,

J = mechanical equivalent of heat,

$\gamma$  = specific heat ratio of gas,

M = gas molecular weight,

$\Delta T_g$  = temperature drop of the gases, and

$W_g$  = gas weight.

Using the pancake motor, for example, and assuming a gas volume of 100 cu in. and a required temperature drop from 1800 to 300°F, the amount of heat that must be removed is 0.56 Btu. Since nitrogen was to be used as the coolant, the above equation was used to predict the theoretical amount of nitrogen required, which amounts to about 0.0145 lb, or 2.6 cu in. if it is stored at 2000 psi. This procedure was used to prepare a plot of (1) nitrogen coolant weight as a function of hot-gas volume and (2) coolant volume as a function of coolant weight, for various storage pressures (see Figure 120).

Since this analysis is theoretical and does not consider the heat stored in the propellant or motor insulation, a larger volume of coolant may be required in an actual motor. Additional Series I tests were used to develop a procedure for predicting the exact amount of coolant required in the full-scale Series M tests; these tests are described in paragraph (2), below.

The nitrogen purge system is shown in Figure 121. Nitrogen gas is supplied by a standard cylinder through a regulator to a purge accumulator, in which gas at a pressure up to 2000 psi can be stored. When the termination valve is opened, a microswitch located on the valve activates a time-delay relay, which then supplies 12 v to a Holec squib in the

**CONFIDENTIAL**

AFRPL-TR-65-209, Vol I

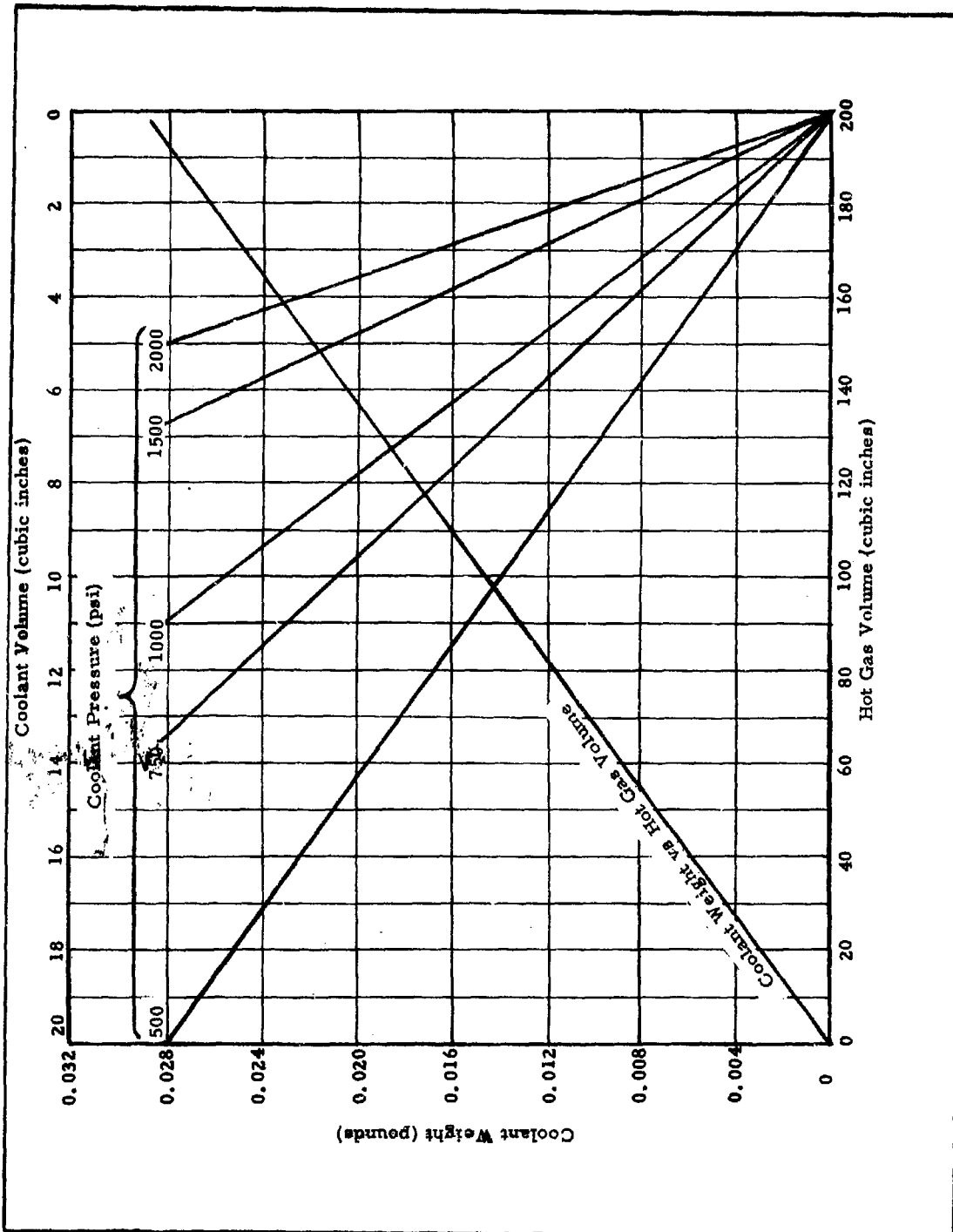


Figure 120 - Nitrogen Coolant Characteristics at Various Storage Pressures

**CONFIDENTIAL**

**CONFIDENTIAL**

AFRPL-TR-65-209, Vol I

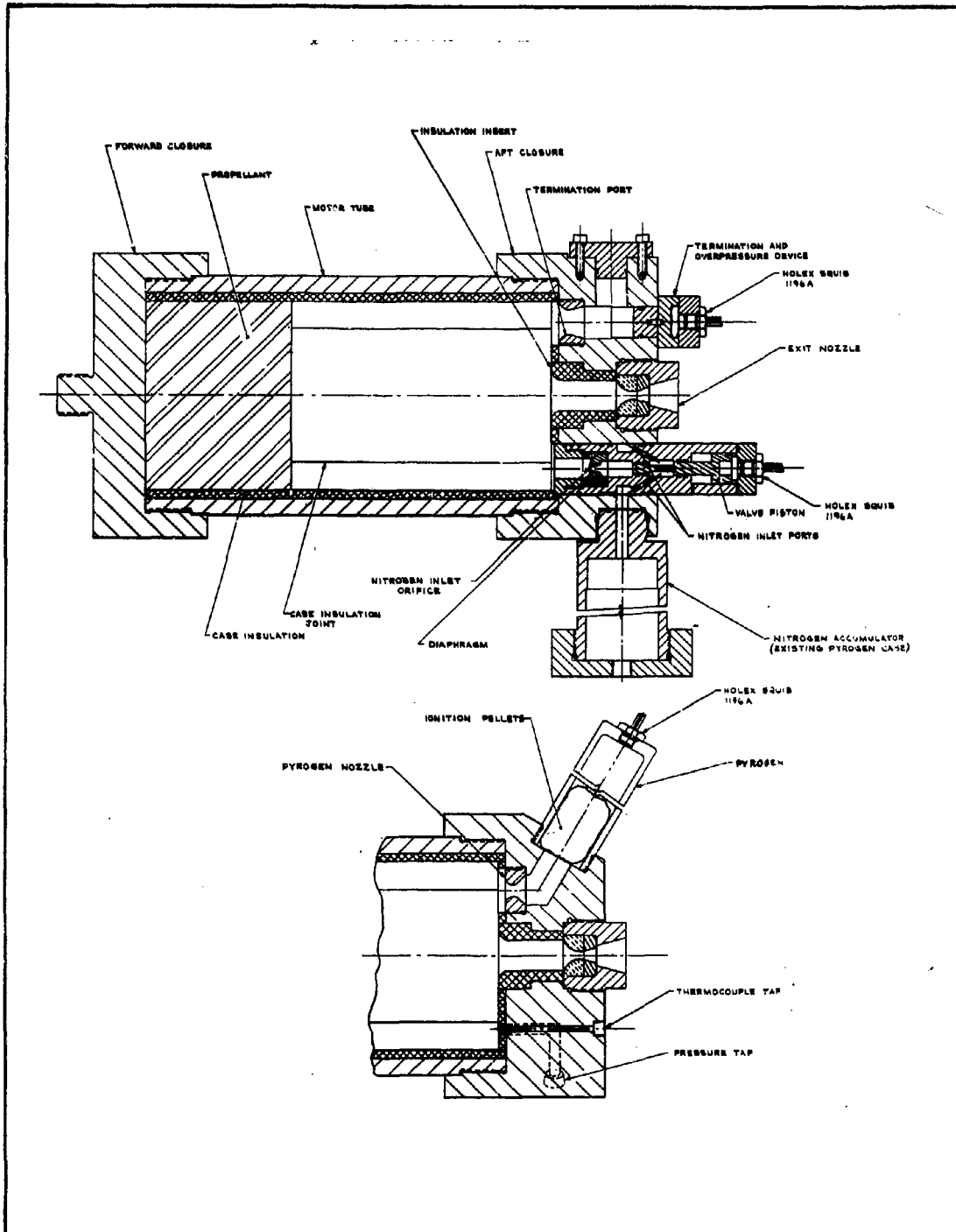


Figure 121 - Diagram of Nitrogen Purge System

**CONFIDENTIAL**

accumulator. The gas pressure developed by the squib opens a vent in the nitrogen line to the chamber, allowing nitrogen gas to fill the combustion chamber. Since some of the hot gas is thus displaced from the chamber, absorbing heat in the process, the chamber will be cooled below the autoignition temperature of the propellant. The amounts of nitrogen used in this test series was varied, by changing the free volume in the accumulator, to develop a general procedure for predicting the amount of coolant that will be required in the large test motors.

(2) Purge Tests

Four Series I tests (I. 15 through I. 18) were conducted, using dual-chamber motors (with the pancake motor of Figure 121 as the forward chamber), to evaluate the purge technique. As a secondary objective, various insulation materials were used in the pancake motors to evaluate their effect on paragraph 2, b, (4), above. Data for Tests I. 15 through I. 18 are summarized in Table XLV. The gaseous nitrogen purge system described above was used in Tests I. 15 through I. 17, except for certain duty cycles, as noted in Table XLV.

The major objective of Test I. 15 was to check out the operation of the purge system and evaluate its effectiveness in preventing reignition in a forward-only configuration containing PPO-13 propellant, under conditions as severe as the worst conditions to be encountered in Test Series M. As shown in Figure 119, there exists a critical ratio of chamber free volume to propellant surface area ( $V_f/S_b$ ), as a function of chamber pressure, above which there is a high probability of reignition. In Tests I. 15 through I. 17, a minimum  $V_f/S_b$ , equivalent to the maximum that exists in the spherical full-scale forward chamber was used. This maximum value ( $V_f/S_b = 9.78$ ), used in Test I. 15.1, was greater by a factor of approximately three than the maximum critical value of  $V_f/S_b$  shown in Figure 119. The earlier tests of Series I (Figure 119) had shown that the probability of reignition increased as forward-chamber pressure decreased. Therefore, a forward-chamber pressure below 500 psia was used for all duty cycles of Tests I. 15 through I. 17. (Confidential)

# CONFIDENTIAL

AFRPL-TR-65-209, Vol I

TABLE XLV - SUMMARY OF DATA FOR TESTS I. 15 THROUGH I. 18

Test No.	Date Fired	Propellant	Type of Insulation	$V_f/S_b$	$L^*$ ( $V_f/A_t$ )	Time from Termination to Purge, $\Delta t_{term-purge}$ (sec)	Aft-Chamber Pressure, $P_{aft}$		Forward-Chamber Termination Pressure, $P_{fwdterm}$ (psia)	Pressure Decay Rate, (dp/dt) (psi/sec)		Reignition Occurred
							Termination (psig)	Spike (psia)		Forward	Aft	
I. 15. 1	8/5/64	PPO-13	V-3021 <sup>†</sup>	9.78	380	0.822	...	...	422	20,877	...	No
I. 15. 2	8/5/64	PPO-13	V-3021 <sup>†</sup>	10.39	403	...	...	...	469	17,949	...	Yes
I. 16. 1	8/10/64	PPO-13/OX-1	V-44 <sup>†</sup>	10.03	376	0.820	67.4	240	291	10,857	3,693	No
I. 16. 2	8/11/64	PPO-13/OX-1	V-44 <sup>†</sup>	10.44 <sup>‡</sup>	391	0.463	60.0	210	261	8,925	3,098	No
I. 16. 3	8/11/64	PPO-13/OX-1	V-44 <sup>†</sup>	10.82	405	0.554	69.5	238	296	10,901	3,451	No
I. 16. 4	8/12/64	PPO-13/OX-1	V-44 <sup>†</sup>	11.20	418	0.351	76.8	215	355	11,297	3,080	No
I. 16. 5	8/12/64	PPO-13/OX-1	V-44 <sup>†</sup>	11.60	433	0.371	76.8	229	297	9,485	3,093	No
I. 16. 6	8/14/64	PPO-13	V-44 <sup>†</sup>	...	...	...	...	...	...	...	...	...
I. 17. 1	8/17/64	PPO-13/OX-1	V-44 <sup>†</sup>	13.66	473	0.661	64.7	216	297	8,550	3,652	No
I. 17. 2	8/19/64	PPO-13/OX-1	V-44 <sup>†</sup>	14.16	491	0.550	58.7	235	283	7,517	2,647	No
I. 17. 3	8/19/64	PPO-13/OX-1	V-44 <sup>†</sup>	...	...	...	...	...	...	...	...	...
I. 18	8/19/64	PPO-13	Combination <sup>§</sup>	...	...	...	...	...	...	...	...	...

Symbols are defined as follows:  $V_f$  = chamber free volume;  $S_b$  = propellant surface area; and  $A_t$  = throat area.

<sup>†</sup> Manufactured by General Tire and Rubber Company.

<sup>‡</sup> Termination achieved, but no  $N_2$  purge; reignition occurred.

<sup>§</sup> No termination signal given, but  $N_2$  purge introduced; combustion was not interrupted, but continued to web burnout.

<sup>¶</sup> No termination signal given.

<sup>§</sup> Forward chamber insulated with General Tire V-44 and V-3021 and B. F. Goodrich 39322, each covering 120° of the chamber circumference.

(Confidential)

In the second cycle of Test I. 15, the N<sub>2</sub> purge system was not actuated following the termination signal. As expected, the forward chamber reignited approximately 30 seconds after termination. (Confidential)

For the first five cycles of Test I. 16 and all cycles of Test I. 17, an aft chamber containing OX-1 propellant was installed. The aft chamber had no apparent effect on reignition in these tests. (Confidential)

In Test I. 16.6, the termination port was not actuated; however, the N<sub>2</sub> purge was introduced into the operating forward chamber. The forward-chamber pressure increased slightly while the nitrogen was exhausting into the chamber, but no interruption of combustion occurred.

The nitrogen purge volume was reduced by 50 percent in the second cycle of Test I. 17, but no reignition occurred. However, the minimum quantity of nitrogen required to prevent reignition has not been established for PPO-13 propellant. The purge system for the Series M tests was scaled up, based on (1) nitrogen volume found to be effective in Series I, and (2) the free forward chamber volumes of the two motor sizes for Series I and M.

SECTION V - PARAMETRIC STUDY

1. GENERAL

A separate parametric study was conducted as part of this year's effort under Contract AF 04(611)-9067. The effects of scaling on internal ballistics, physical properties, and general operating and control characteristics of the DCCSR motor were determined. The scope of this study is presented briefly in paragraph 2, below, and the conclusions in paragraph 3, below. An interim report of this study was prepared (Reference 20), while Volume II presents the detailed results of the entire study, including tables, charts, and graphs.

2. SCOPE OF STUDY

This study was conducted to establish trends and optimum conditions of mass fraction, boost velocity, and motor envelope with variations in motor performance parameters and propellant characteristics for the DCCSR concept. Off-optimum as well as optimum conditions were examined.

Five independent variables (motor performance parameters and propellant characteristics) were selected for this study: (1) total impulse, (2) minimum thrust, (3) thrust throttling range, (4) number of on-off cycles available, and (5) motor specific impulse. The first four variables define the capability of a throttleable stop-restart motor, and each directly affects mass fraction, boost velocity, and motor envelope. The fifth variable, which is a function of propellant composition, directly affects motor size and boost velocity.

The ranges of total impulse, minimum thrust, and thrust throttling range values included in this study are presented in Table XLVI. Minimum thrust was varied from  $1/500$  to  $1/20$  of total impulse, that is, for maximum burn times of 20 to 500 sec. The thrust throttling ranges considered were 1 to 1, 5 to 1, and 20 to 1; the number of on-off cycles used was 1, 10, 20, and 40. Vacuum specific impulse, at an expansion ratio of 20 to 1, was varied from 265 to 280 to 300 lb-sec/lb. These ranges of independent variables encompass those required in most applications of a DCCSR. (Confidential)

The entire range of variables investigated is summarized as follows:

**CONFIDENTIAL**

AFRPL-TR-65-209, Vol I

TABLE XLVI-TOTAL IMPULSE AND THRUST RANGE  
FOR PARAMETRIC ANALYSIS

Total Impulse (lb-sec)	Minimum Thrust (lb <sub>f</sub> )	Maximum Thrust (lb <sub>f</sub> )		
		Case 1	Case 2	Case 3
10,000	20	20	100	400
10,000	50	50	250	1,000
10,000	100	100	500	2,000
10,000	500	500	2,500	10,000
100,000	200	200	1,000	4,000
100,000	500	500	2,500	10,000
100,000	1,000	1,000	5,000	20,000
100,000	5,000	5,000	25,000	100,000
500,000	1,000	1,000	5,000	20,000
500,000	2,500	2,000	10,000	40,000
500,000	5,000	5,000	25,000	100,000
500,000	25,000	25,000	125,000	500,000
1,000,000	2,000	2,000	10,000	40,000
1,000,000	4,000	4,000	20,000	80,000
1,000,000	10,000	10,000	50,000	200,000
1,000,000	50,000	50,000	250,000	1,000,000

(Confidential)

1. Total impulse (see Table XLVI)
2. Minimum thrust (see Table XLVI)
3. Maximum thrust or throttling range (see Table XLVI)
4. Specific impulse ( $I_{vac} = 265, 280^*$ , and 300 lb-sec/lb)
5. Number of on-off cycles available (1, 10, 20, and 40)
6. Case material (steel\*, fiberglass, and titanium)
7. Propellant mixture ratio (2, 3\*, and 4)
8. Propellant burning-rate constants (forward chamber: 0.0002, 0.0008\*, and 0.0032; aft chamber: 0.0002, 0.0004\*, and 0.0010)
9. Propellant pressure exponents (forward chamber: 0.6, 0.8\*, and 0.9; aft chamber: 0.8, 1.0\*, and 1.1)  
(Confidential)

The analysis was divided into two phases. In Phase I, the independent variables were investigated independently, with propellant properties and case materials fixed (starred values listed above). In Phase II, case material, propellant mixture ratio, burning-rate constants, and burning-rate pressure exponents were varied.

This study was carried out by means of Northrop Carolina's IBM 1620 Data Processing System. Data was processed through four separate computer subroutines. A detailed description of the subroutines and the over-all computer program is presented in Volume II.

### 3. SUMMARY

It was found that, by increasing specific impulse, mass fraction was reduced but delta velocity and total motor weight increased. For 10,000-lb-sec motors, an increase in specific impulse from 265 to 300 lb-sec/lb increased delta velocity by 7 percent, whereas for 1,000,000-lb-sec motors, the increase was 12 percent. (Confidential)

The mass fraction penalty imposed by a 20-to-1 thrust modulation was 2.5 percent for low-impulse (10,000 lb-sec), low-thrust (100 lb<sub>f</sub>) motors. This penalty increased to above 4 percent as impulse increased to 1,000,000 lb-sec and thrust to 4,000 lb<sub>f</sub>. These values were based on the characteristics of available propellants. Improved propellant pressure exponents would reduce the penalties. (Confidential)

For motors with stop-restart capability, the number of restarts available had little effect on mass fraction and delta velocity. The mass fraction penalty for additional igniters was less than 0.1 percent per restart. (Confidential)

At each impulse level, there was an optimum thrust range for throttleable motors which was close to the optimum thrust level for nonthrottling motors. If the thrust was increased or decreased beyond this range, both mass fraction and delta velocity decreased. (Confidential)

SECTION VI - CONCEPT DEMONSTRATION TESTS (SERIES M)

1. GENERAL

Eight full-scale tests were conducted in Phase III. These tests, designated Series M, were to demonstrate present technology and to establish a performance envelope of the DCCSR. The knowledge and technology derived from the reignition and insulation study (Section IV) were incorporated in the Series M designs. In addition, new hot-gas control valve, new control system, and new nozzle designs were developed and used in Series M motors. However, since these new motor components were introduced at various points in the Test Series, and since the propellants, duty cycles, and other items varied during Series M, Table XLVII was prepared to summarize the designs and facilitate identifying the configurations for each test.

Tests M.1 through M.6, conducted at Northrop Carolina's facilities, were sea-level tests. Tests M.7 and M.8 were altitude tests conducted at the Navy's Ordnance Aerophysics Laboratory, Daingerfield, Texas. Prior to conducting M.7 and M.8, a brief series of tests was conducted to ascertain what effect, if any, the vacuum conditions under which these tests were to be conducted would have on the operation of the pyrogen igniters. The results of these tests (Series K) are presented in paragraph 9, below.

The hardware used in the test motors, as well as the components, are described in detail in paragraph 2, below. Each individual test is described in separate paragraphs (3 through 11) below, including the programmed duty cycle, test results, and problems encountered. The data reduction parameters used in Series M and N are defined in paragraph 12, below.

2. MOTOR HARDWARE AND COMPONENTS

a. General Description

All series M motors were full-scale dual-chamber motors containing approximately 300 lb of propellant. Spherical forward chambers (17.5-in. I.D.) were used for tests M.1 and M.2; cylindrical forward chambers (13-in. I.D.) were used for the remaining tests. PPO-13 propellant was used in the forward chambers of all motors. OX-5 propellant, which contains 10

# CONFIDENTIAL

AFRPL-TR-65-209, Vol I

TABLE XLVII - SUMMARY OF SERIES M MOTOR CONFIGURATIONS

Test Number	Date of Test	Sea Level or Altitude	Number and Type of Cycles	Forward Chamber Design	Aft Chamber Design	Propellant Forward	Alt.	Valve Design	Nozzle Design	Control System	Nitrogen Purge	Figure
M.1	10/14/65	Sea Level	Two, pulse	Spherical	Cylindrical	PPO-13	OX-5	Northrop Carolina design	Sea level (2 to 1)	Northrop Carolina design	Yes	122
M.2	10/23/65	Sea level	Two, pulse	Spherical	Cylindrical	PPO-13	OX-5	Northrop Carolina design	Sea level (2 to 1)	Northrop Carolina design	Yes	123
M.3	12/8/65	Sea level	Four, pulse	Cylindrical	Cylindrical	PPO-13	OX-1	Northrop Carolina design	Sea level (2 to 1)	Northrop Carolina design	Yes	124
M.4	12/22/65	Sea level	Five: Four pulse, one throttling	Cylindrical	Cylindrical	PPO-13	OX-1	TRW design	Sea level (2 to 1) modified	TRW design	Yes	125
M.5	1/12/65	Sea level	Five: Four pulse, one throttling	Cylindrical	Cylindrical	PPO-13	OX-1	TRW design	Sea level (2 to 1) modified	TRW design	Yes	125
M.6	1/26/65	Sea level	Five: Four pulse, one throttling	Cylindrical	Cylindrical	PPO-13	OX-1	TRW design	TRW sea level (2 to 1) *	TRW design	Yes	125
M.7	7/15/65	Altitude	Five: Four pulse, one throttling	Cylindrical	Cylindrical	PPO-13	OX-1	TRW design	Vacuum (20 to 1)	TRW design	No	125†
M.8	7/21/65	Altitude	Five: Four pulse, one throttling	Cylindrical	Cylindrical	PPO-13	OX-1	TRW design	Vacuum (20 to 1)	TRW design	No	125 †

\* The Northrop Carolina-designed nozzle was used for the first two cycles; a TRW nozzle for the remainder. Both had a 2/1 expansion ratio.

† Figure 125 shows the basic motor design for Tests M. 7 and M. 8 except for the altitude nozzle.

percent aluminum, was used in the aft-chamber for Tests M. 1 and M. 2, while OX-1 grains (non-aluminized) were used in the remaining tests. All motors employed hot-gas valves, described in b, below, and a nitrogen gas purge system, as shown in Table XLXII. The over-all motor configurations used for each test are shown in the following figures:

<u>Test</u>	<u>Figure</u>
M. 1	122
M. 2	123
M. 3	124
M. 4, M. 5, M. 6	125
M. 7, M. 8	125(except for altitude nozzle)

The motor hardware for tests M. 1 and M. 2 was identical to that used previously in Test Series E (Reference 8).

The propellant formulations are given in the following tables:

PPO-13	Table II
OX-5	Table X (Reference 8)
OX-1	Table X (Reference 8)

The individual motor components are described in the following paragraphs.

Throughout this Test series, the motors were disassembled and weighed between duty cycles.

b. Hot-Gas Valves

(1) General

As shown in Table XLVII, a Northrop Carolina-designed hot-gas valve was used for Tests M. 1, M. 2, and M. 3. A proportional valve, designed, developed, and fabricated by Thompson Ramo Wooldridge, Inc. (TRW), was used for the remaining tests.

(2) - Northrop Carolina-Designed Valve

In the preparation for the initial Series M tests, it

**CONFIDENTIAL**

AFRPL-TR-65-209, Vol I

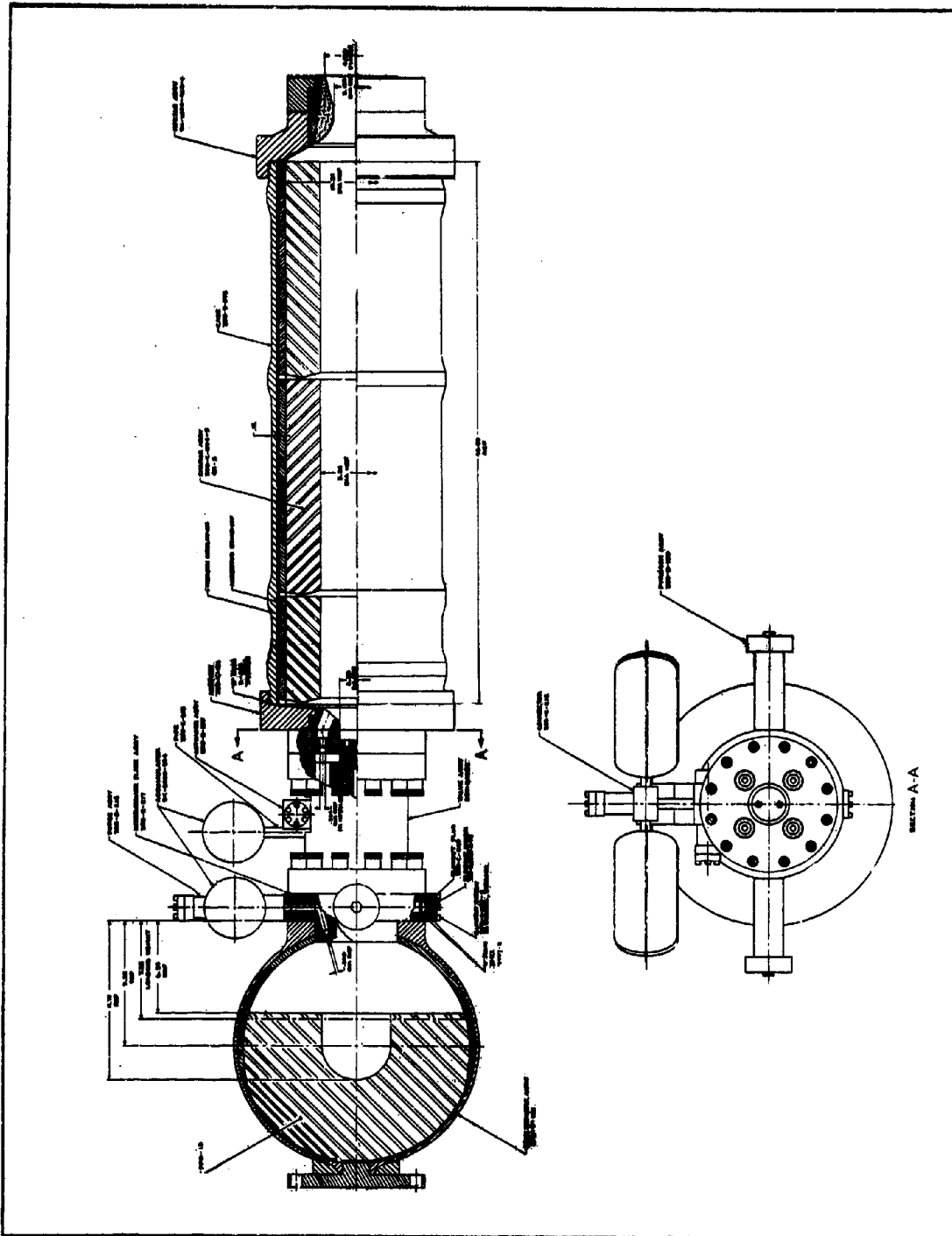


Figure 122 - Motor Assembly Used in Test M. 1

**CONFIDENTIAL**

**CONFIDENTIAL**

AFRPL-TR-65-209, Vol I

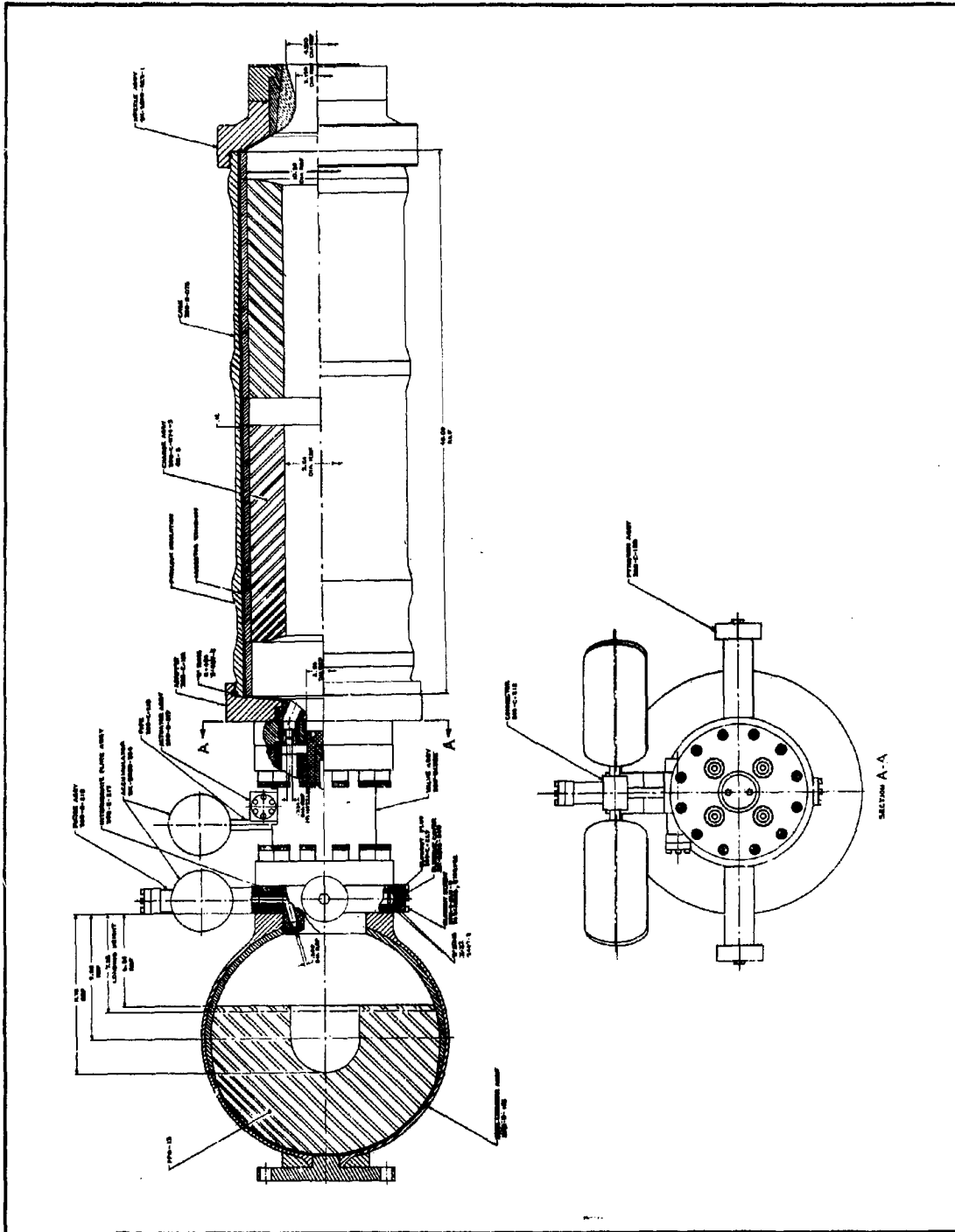
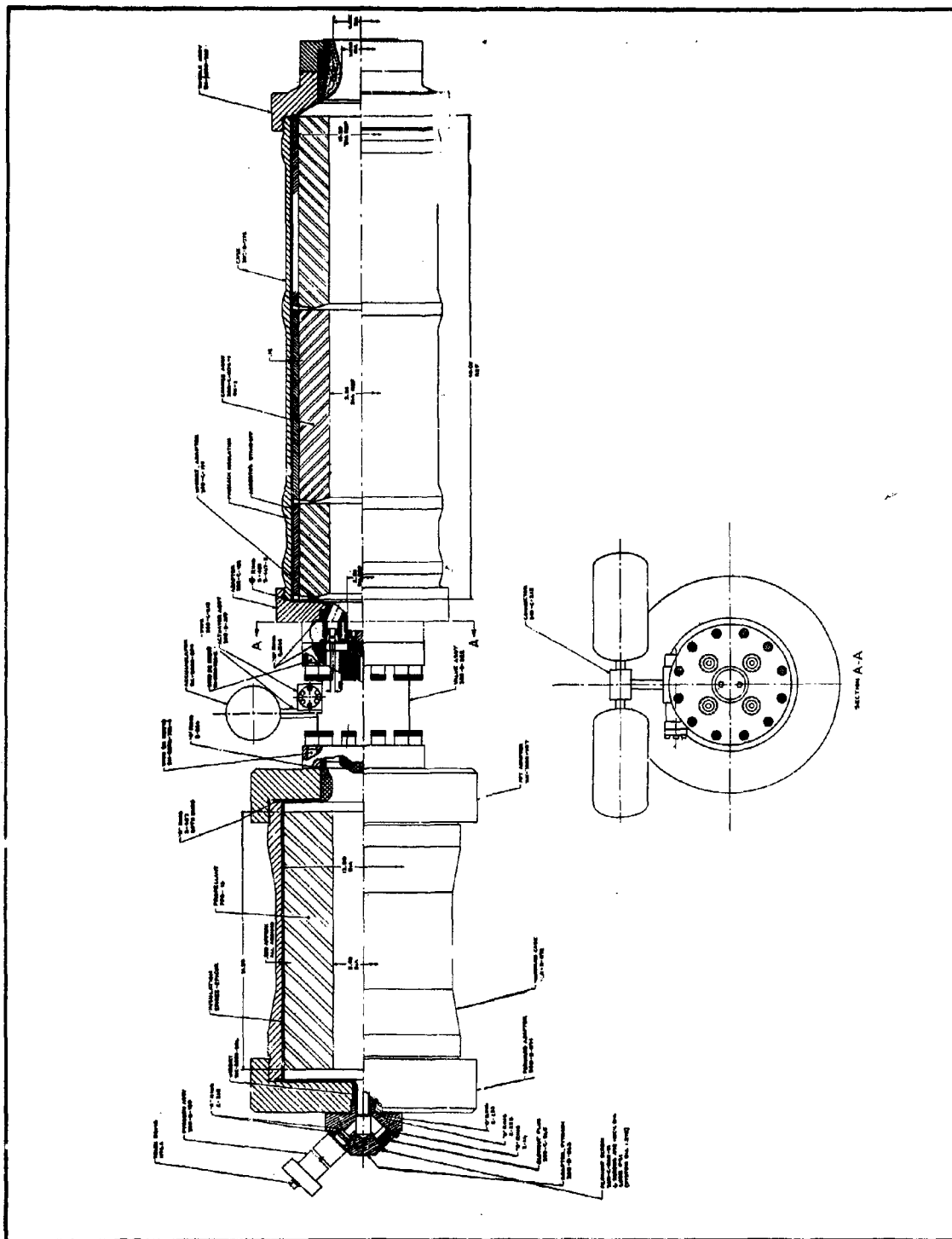


Figure 123 - Motor Assembly Used in Test M. 2

**CONFIDENTIAL**

**CONFIDENTIAL**

AFRPL-TR-65-209, Vol I



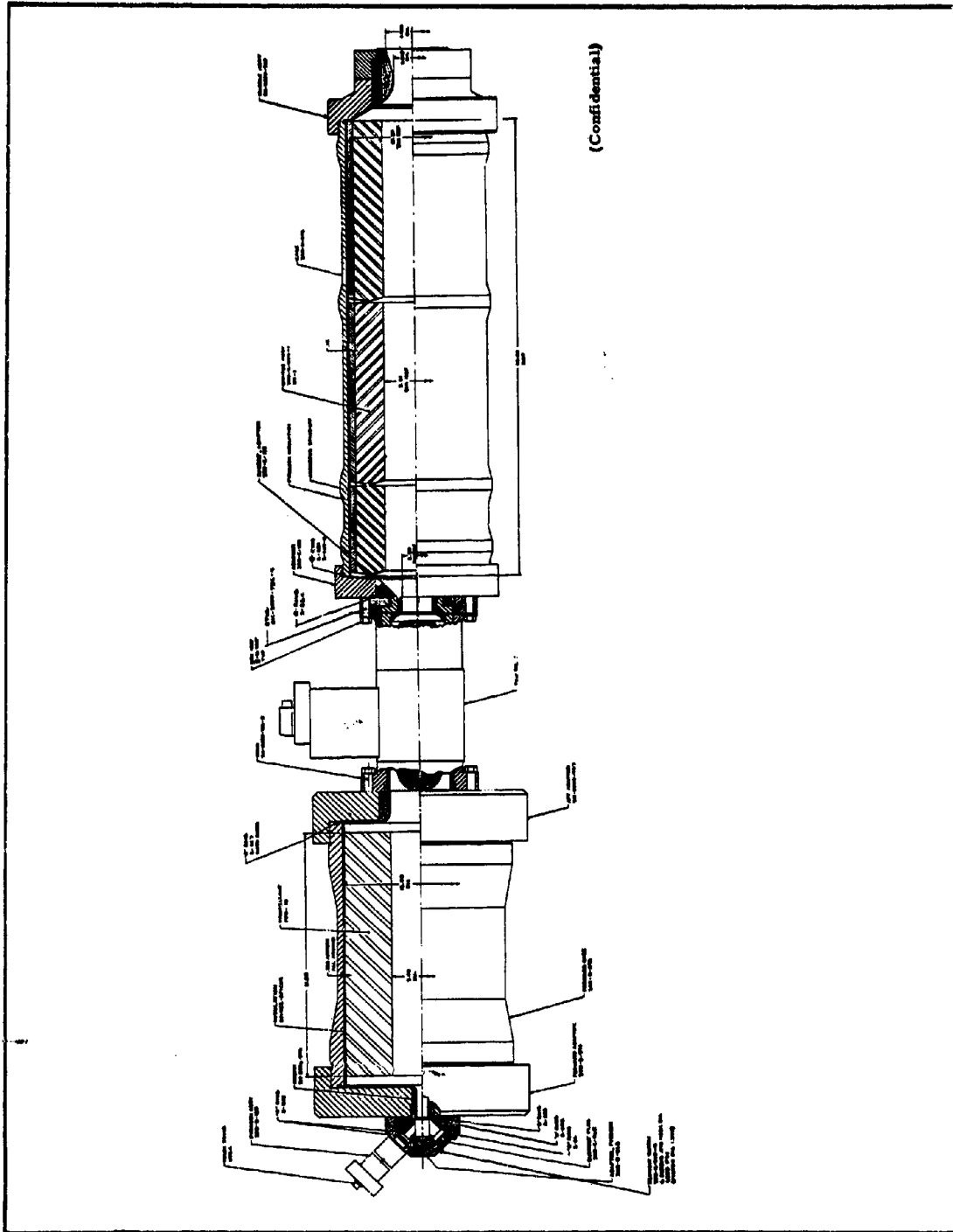
-198-

Figure 124 - Motor Assembly Used for Test M.3

**CONFIDENTIAL**

**CONFIDENTIAL**

AFRPL-TR-65-209, Vol I



(Confidential)

Figure 125 - Motor Assembly Used for Tests M. 4, M. 5, and M. 6 -199-

**CONFIDENTIAL**

was planned to use a standard off-the-shelf Jamesbury ball valve, with a 2.5-in. port, between chambers. This valve was selected on the basis of the successful use of a 1.25-in. Jamesbury valve in the Series H subscale dual-chamber tests, and for the economy resulting from the use of existing valves. However, it was learned that the manufacturer could not meet the required delivery schedule for the Series M tests, nor could possible alternate suppliers. It was therefore decided to design and fabricate an on-off hot-gas valve at Northrop Carolina in order to minimize the delay of the Series M tests.

In Northrop Carolina's on-off valve, shown in Figure 126, nitrogen bottle gas at 2000 psi is used to actuate the termination port. The forward chamber control flow area is provided by four fixed orifices located at the downstream end of the valve on a 5-in. -diameter circle. A 2.5-in. -diameter termination port is exposed by moving a piston upstream along the valve centerline. Initially, all interior valve cavities are pressurized to 2000 psi with nitrogen gas and remain at this pressure throughout motor operation. When the termination signal is received, a rupture diaphragm vents the pressure on the upstream side of the actuating piston, while the downstream side remains at 2000 psi. The force generated by this unbalanced pressure across the actuating piston moves the piston very rapidly upstream, thus exposing the termination port. During motor operation, while both sides of the actuating piston are at 2000 psi, the effective upstream piston area is larger than the effective downstream area, thereby producing a net closing force that counteracts the opening force resulting from the aft-chamber pressure acting on the downstream end of the pintle.

The valve housing was fabricated from a 10-in. -diameter bar of 4340 steel. Six equally spaced holes, drilled axially on a 5-in. diameter through the 11-in. -long bar, provide gas passage from the forward chamber to the orifice plate. A 2.5-in. -diameter port based on the bar centerline provides the actuating piston bore. All interior surfaces exposed to forward-chamber gases were insulated with either RPD-150 or Epi-rez/Epi-cure (cast) material. The flanges mate with the existing spherical forward and cylindrical aft chambers.



# CONFIDENTIAL

AFRPL-TR-65-209, Vol I

To prove the operating characteristics of this design, the valve was checked out and tested before it was used in Test M. 1. Tests with 2000-psi nitrogen were made to check for leaks with the valve pressurized first from the hot-gas side to the actuating cavities, and then in reverse. The actual piston response times were checked by conducting an actual valve duty cycle with (1) both ends of the valve sealed, (2) the hot gas cavities pressurized with 2000-psi nitrogen, and (3) both sides of the actuating piston charged at 2000 psi.

To further check out the valve, a hot firing was conducted (Test I-19B) with two six-inch forward motors, containing PPO-13 propellant, arranged in tandem. The two motors had a combined burning-surface area equivalent to that of the forward grain in the motor for Test M. 1. The motor was operated for 0.96 sec and then terminated. The valve operated very satisfactorily, and the motor extinguished permanently. The pressure-time trace for this valve checkout test is given in Figure 127.

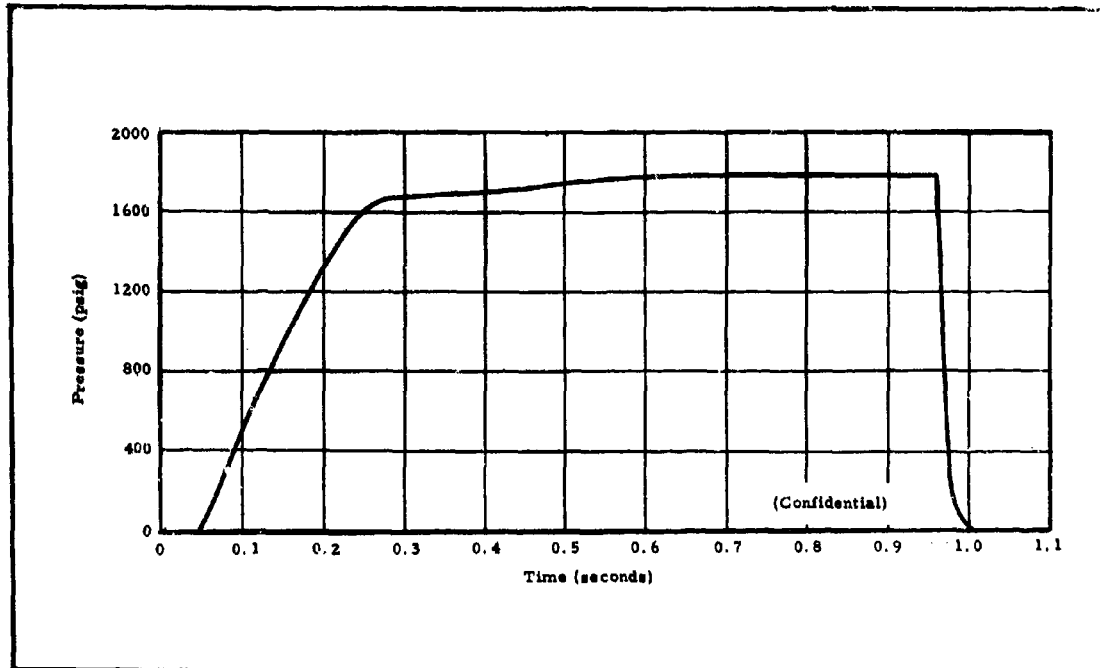


Figure 127 - Pressure Time Trace for Valve Checkout Test I-19B

## (3) TRW-Designed Hot-Gas Valve

The proportional hot-gas valve used in Tests M. 4 through M. 8 was designed and fabricated by the Structures Division of TRW, Cleveland, Ohio, under Northrop Carolina subcontract, in accordance with specification AMS-10018 (Reference 21). A cross-section of the valve assembly is shown in Figure 128. RPD-150 insulation was used in the low-velocity regions, while RPD-41 was used in parts 5 and 30 (see Figure 128) because of its higher erosion resistance. Unalloyed molybdenum, a high-temperature material, was used for parts 28 and 34 to ensure dimensional stability for precise flow control.

c. Control System

For Tests M. 1 through M. 3, the control system for operation of the hot-gas control valve was identical to that used in Test Series E. This Northrop-Carolina-designed system employed closed-loop control of the forward-chamber pressure. A complete analysis and description of the control system, along with system block diagrams and schematics, are presented in Reference 8.

A new control system was used in Tests M. 4 through M. 8. This closed-loop (around forward-chamber pressure) proportional plus integral control system was designed and analyzed by TRW, under Northrop Carolina subcontract. A detailed report on the analysis and design of this control system, prepared by TRW is presented in Appendix B.

d. Nozzle Designs

Sea level nozzles (2-to-1 expansion ratio) designed by Northrop Carolina were employed for Tests M. 1 through the first two cycles of M. 6. The last three cycles of M. 6 used nozzles designed, developed, and fabricated by TRW, under Northrop Carolina subcontract, in accordance with Work Statement AWS-2, (Reference 22), fulfilling the requirements of Phase IV of the program (see Section II). A design report for this sea-level nozzle is given in Appendix C.

The nozzle used in Tests M. 1 through M. 3 (see Figure 124) employed CGW graphite backed up by RPD-41 in a steel housing.

**CONFIDENTIAL**

AFRPL-TR-65-209, Vol I

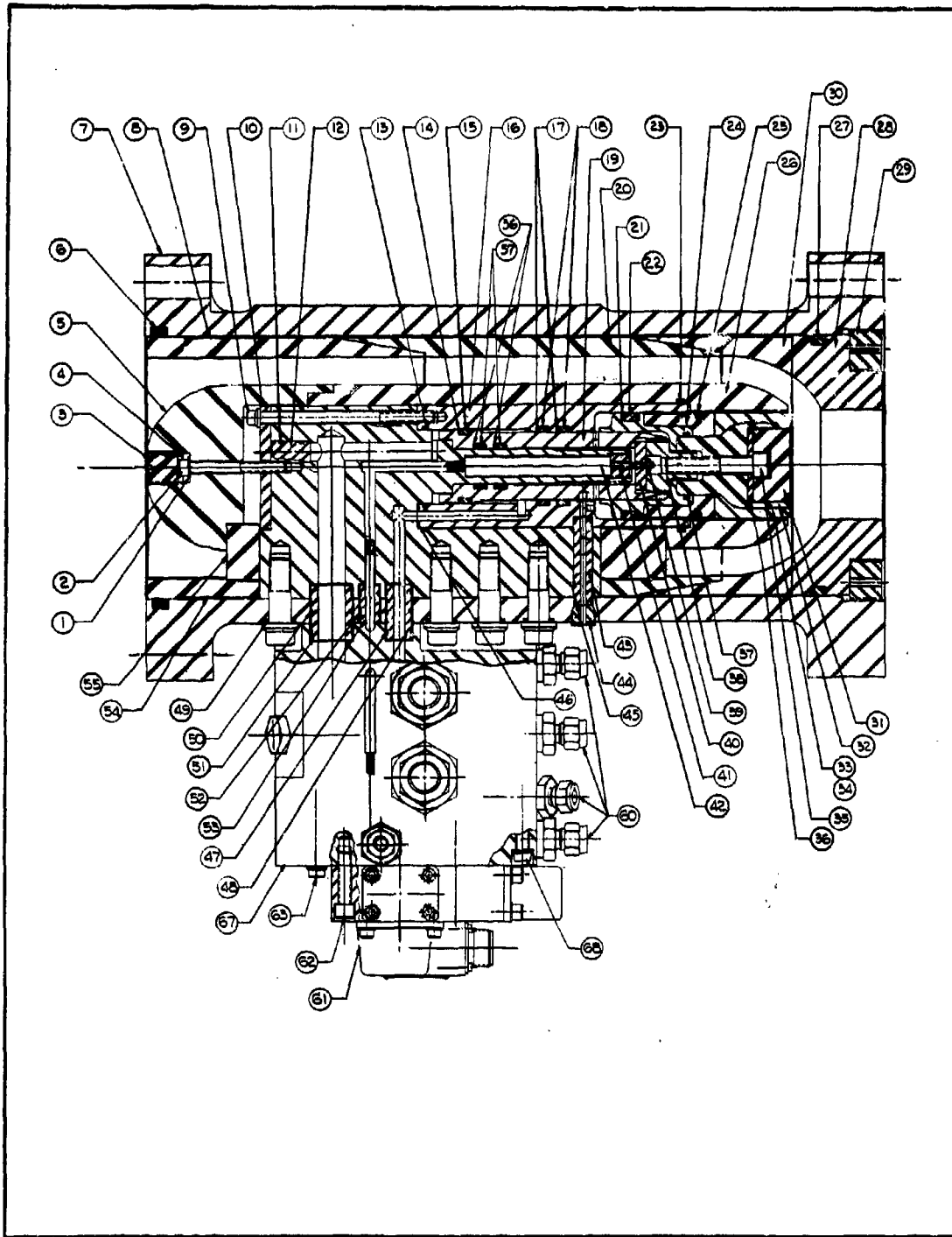


Figure 128 - Cross-Section of Proportional Hot-Gas Valve

-204-

**CONFIDENTIAL**

The Fastax movies of Test M. 3 revealed that afterburning, originating at the nozzle, occurred. Since reignition occurred after the first and fourth cycles of Test M. 3, it was decided to eliminate the RPD-41 back-up in the nozzle for Tests M. 4 through M. 6 (as shown in Figure 125) to remove the afterburning of the plastic as a possible source of reignition.

A vacuum nozzle with a 20-to-1 expansion ratio, also designed and fabricated by TRW, was used for Tests M. 7 and M. 8, which were conducted at altitude conditions. A design report for this nozzle is presented in Appendix D.

An evaluation of the nozzle designs, based on post-test results, is presented in Section VIII.

e. Purge System

A nitrogen gas purge system, designed on the basis of the results of the reignition study reported in Section IV, was used on several sea-level Series M tests (Tests M. 1 through M. 6). The purge was not required for altitude tests M. 7 and M. 8 since reignition caused by residual gases in the motor following termination should not occur at low pressures. The purge system was attached to the forward chamber as shown in Figures 122 through 125. The purge system was manually actuated following each termination, as desired, to prevent reignition. In Test M. 1, the nitrogen was vented through a port into the forward chamber only. In subsequent tests, a purge port was placed in the aft chamber, as well, to improve the effectiveness of the nitrogen in expelling residual gases in the chambers. The volume of nitrogen purge was increased during subsequent tests to prevent reignitions that occurred in the early tests.

3. TEST M. 1

a. Motor Configuration

The motor used in Test M. 1 was as shown in Figure 122 and Table XLVII. The aft chamber contained three OX-5 segments, two of which were 16-in. long; the other, 8 in. These segments were fitted tightly into the aft case, with little space between them. All other components were as described in paragraph 2, above.

**CONFIDENTIAL****b. Test Program and Test Conditions**

Test M. 1 was programmed for two pulse cycles. For the first cycle, a forward pressure of 900 psi, an aft pressure of 205 psi, and a thrust of 2200 lb<sub>f</sub> were desired. The second cycle was programmed for a forward pressure of 2000 psi, and aft pressure of 320 psi, and a thrust of 3700 lb<sub>f</sub>. The actual values closely approached the desired values, as described in c, below.

**c. Test Results**

The actual pressure- and thrust-time curves for the first cycle of Test M. 1 (see Figure 129) show that the motor approached the design values very closely after the ignition transient. It is evident from the aft pressure and thrust curves that the OX-5 aft grain burned unstably. This instability, also observed in previous tests, became more severe at low chamber pressures and at high aft-to-forward mixture ratios. It is believed that the periodic accumulation and combustion of aluminum on the grain surface caused this unstable burning. The motor extinguished permanently when terminated. (Confidential)

Forward pressure was not measured during the second cycle because of an error in the electronic circuits. However, a calculated forward-chamber pressure-time trace is given in Figure 129, based on the unsteady-state ballistic program. Since no heat loss was assumed in this program, the rise time was more rapid than would actually occur. The aft pressure and thrust approached the expected levels very closely. Instability was again evident in the aft chamber, although the amplitude of the oscillations decreased as pressure increased during this cycle. Upon termination, the motor extinguished, but reignited 106 sec later; the remaining propellant was then consumed at low pressure. (Confidential)

It was thought that this reignition could have resulted from insufficient nitrogen to purge all the hot residual gases from the motor. In each cycle of Test M. 1, 0.56 lb of nitrogen was used.

The reduced ballistic data for Test M. 1 are given in Table XLVIII. Performance data for the second cycle of this test are incomplete since the propellant weight burned before reignition is unknown. The measured weight of the propellant burned in the forward chamber in Test M. 1. 1 is believed to be in error.

**CONFIDENTIAL**

**CONFIDENTIAL**

AFRPL-TR-65-209, Vol I

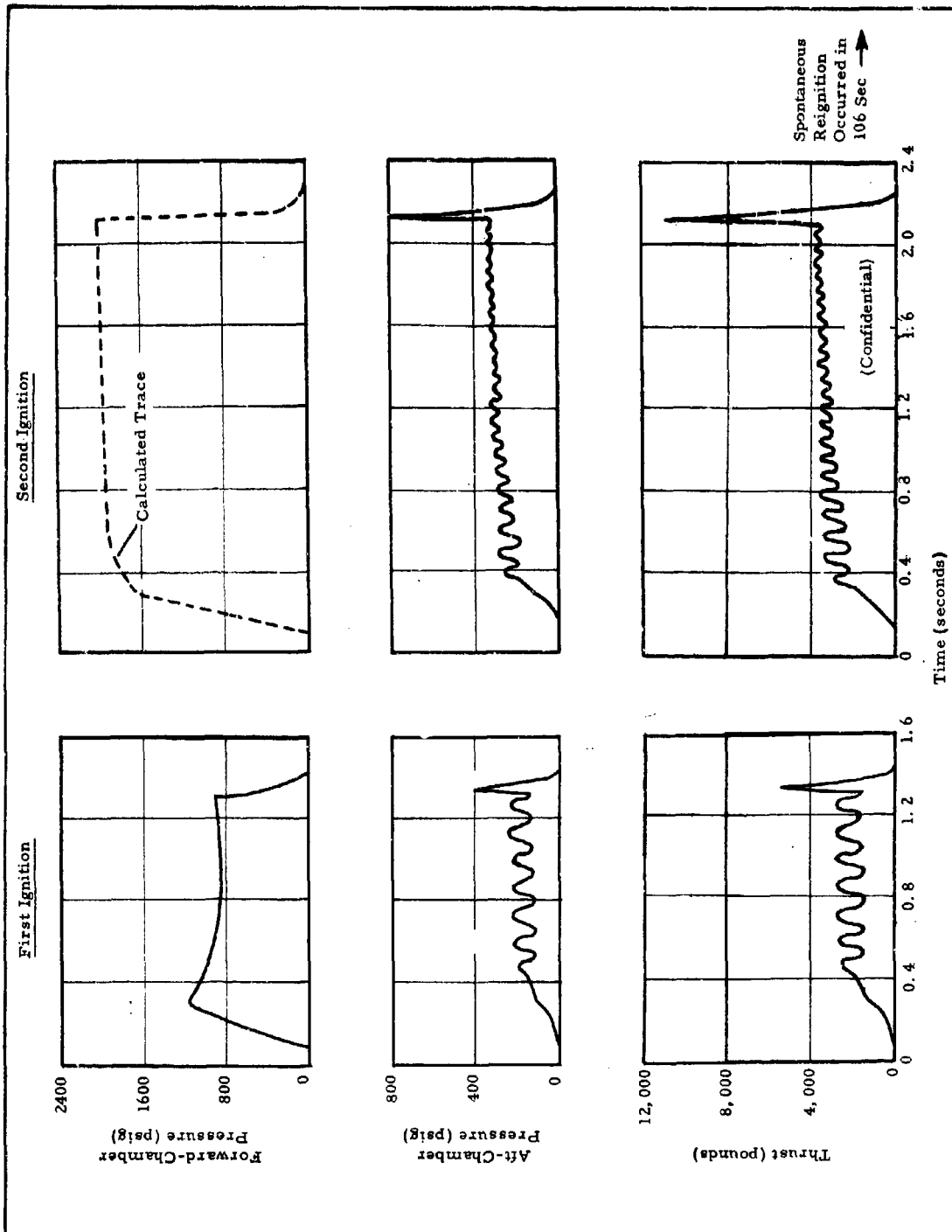


Figure 129 - Pressure- and Thrust-Time Traces for Test M. 1

**CONFIDENTIAL**

# CONFIDENTIAL

AFRPL-TR-65-209, Vol I

TABLE XLVIII - SUMMARY OF DATA FOR TESTS M. 1 AND M. 2

Parameter	Test Number			
	M. 1. 1	M. 1. 2	M. 2. 1	M. 2. 2
<b>Forward chamber (PPO-13)</b>				
Weight burned (lb)	6.40*	. . .	6.491	. . .
Burn time (sec)	1.202	†	2.059	2.052
Total time (sec)	1.340	†	2.257	2.225
$\int Pdt_b$ (psig-sec)	994.6	†	1710.6	2314.9
$\int Pdt_p$ (psig-sec)	1083.7	†	1736.0	2348.4
$\bar{P}_b$ (psia)	841.1	†	844.5	1141.9
Throat area (sq in.)	0.4606	0.380	0.4603	0.4603
$P_{term}$ (psia)	913	†	1104	1220
$dp/dt_{term}$ (psi/sec)	45,700	†	64,900	52,000
Characteristic velocity (fps)	2509*	†	3961	. . .
<b>Aft chamber (OX-5)</b>				
Weight burned (lb)	8.73	. . .	11.000	. . .
Burn time (sec)	1.105	1.899	1.860	1.943
Total time (sec)	1.338	2.160	2.240	2.250
$\int Pdt_b$ (psig-sec)	158.6	513.4	279.3	358.3
$\int Pdt_p$ (psig-sec)	184.9	548.6	298.8	381.5
$\bar{P}_b$ (psia)	157.3	284.1	163.8	198.1
$P_{prior to term}$ (psia)	151	340	206	248
$P_{maximum at term}$ (psia)	430	839	425	486
$dp/dt_{term}$ (psi/sec)	11,900	18,900	10,500	11,300
<b>Total motor</b>				
Weight burned (lb)	15.13*	. . .	17.491	. . .
Weight <sub>aft</sub> /weight <sub> fwd</sub>	1.36*	. . .	1.695	. . .
$\int Fdt_f$ (lb <sub>f</sub> -sec)	2121.0	6291.7	3109.8	3985.2
$\bar{F}_b$ (lb <sub>f</sub> )	1629.7	3121.3	1584.9	1929.5
Throat area (sq in.)	8.002	8.002	7.505	7.505
Expansion ratio	1.996	1.996	2.131	2.131
Ratio of specific heats, $\gamma$	1.20	. . .	1.19	. . .
Characteristic velocity (fps)	3146*	. . .	4125	. . .
$I_{sp_{meas}}$ (lb-sec/lb)	140.2	. . .	177.8	. . .
$I_{sp_{corr}}$ (lb-sec/lb)	173.6*	. . .	222.2	. . .
$I_{sp_{corr - 1000/14.7}}$ (lb-sec/lb)	197.9*	. . .	253.7	. . .
$I_{sp_{corr-vac, 20/1}}$ (lb-sec/lb)	197.9*	. . .	253.7	. . .
$I_{sp_{eff}}$ (%)	69.1*	. . .	87.7	. . .

\* These values are believed to be low due to error in measured weight burned in forward chamber.

† Pressure-time data for the forward chamber were not obtained.

(Confidential)

This weight was calculated to be 4.09 lb, based on a burning rate of 841 psi, the burn time, and average burning surface area and grain density. This calculated weight gives a forward chamber characteristic velocity of 3930 fps, which is comparable to that obtained in Test M. 2. 1 as shown in Table XLVIII. Likewise, the specific impulse and aft chamber characteristic velocity values would be increased considerably. (Confidential)

4. TEST M. 2

a. Motor Configuration

The motor configuration for Test M. 2, shown in Figure 123 and Table XLVII, was essentially the same as that for Test M. 1. The chief modification was that the eight-inch aft-grain segment used in Test M. 1 was omitted for this test, allowing the remaining two segments to be separated from one another and from the end closures with salt spacers, as shown in Figure 123. Also, the nitrogen purge volume was increased, and, in addition to the normal purge port in the forward chamber, a purge port was placed in the aft chamber.

b. Test Program and Test Conditions

Test M. 2 was also programmed for two pulse cycles at a forward-chamber pressure of 1000 psi, an aft-chamber pressure of 200 psi, and a thrust of 2000 lbf.

c. Test Results

The pressure- and thrust-time traces for Test M. 2 are given in Figure 130. One pyrogen was used for the first ignition and two pyrogens for the second, which explains the difference in ignition characteristics of the two cycles. As was observed in Test M. 1, low-frequency instability occurred in the aft grain. Permanent extinction was achieved upon termination of the first cycle, but the motor reignited 126 sec after termination of the second cycle; the grains were completely consumed as in Test M. 1. (Confidential)

Obviously, the increased nitrogen purge used in this test had very little effect on preventing reignition. For this reason, the cause of reignition was believed to be unrelated to the residual hot gases in the motor, since most of these gases should have

**CONFIDENTIAL**

AFRPL-TR-65-209, Vol I

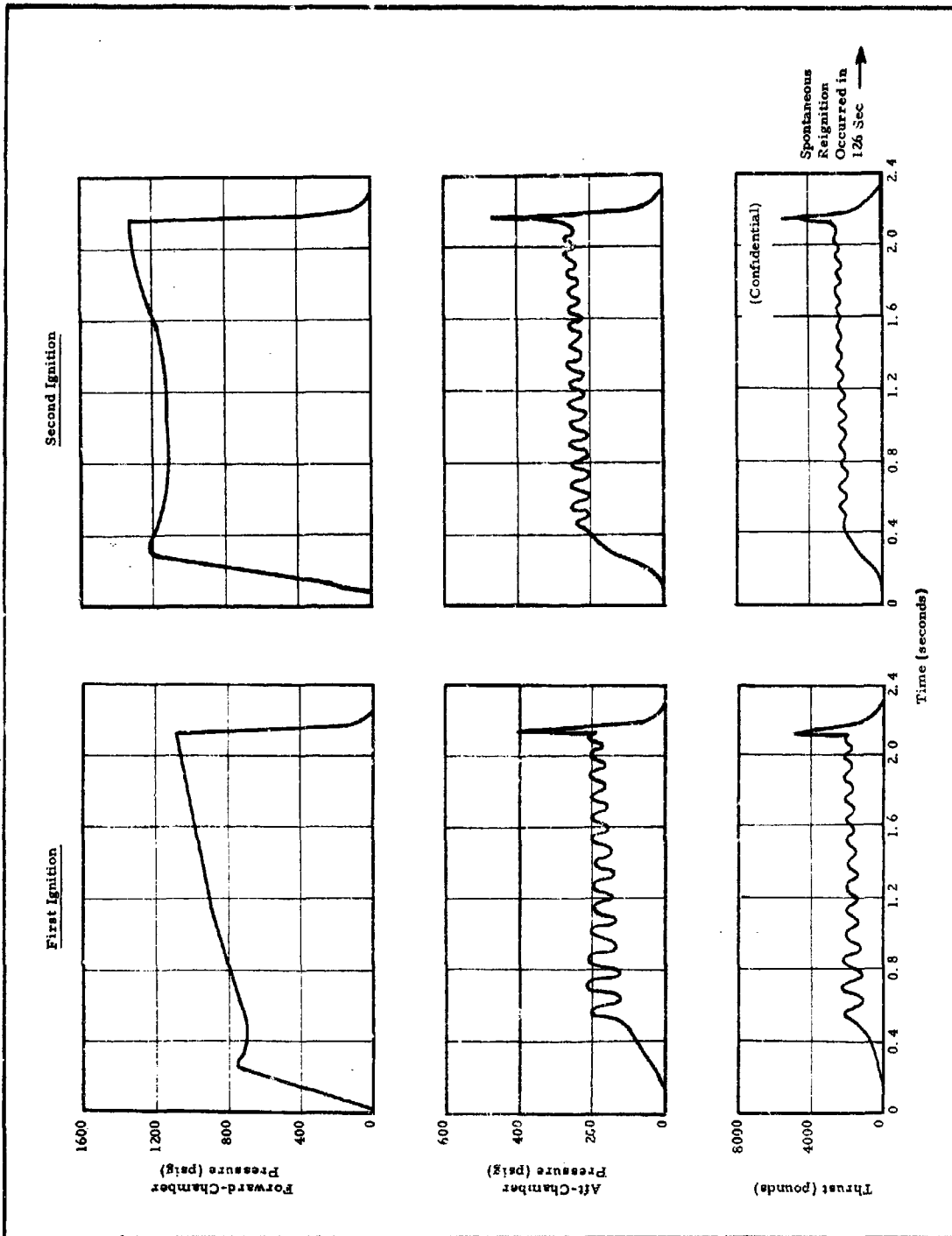


Figure 130 - Pressure- and Thrust-Time Traces for Test M. 2

**CONFIDENTIAL**

been expelled by the purge. It is considered more likely that reignition resulted from the hot aluminum or aluminum oxide that remained on the surface of the aft grain after termination. A thin layer of aluminum was observed on the aft grain following the first cycles of Tests M. 1 and M. 2. (Confidential)

The reduced ballistic data for Test M. 2 are also given in Table XLVIII. Again, the performance data for the second cycle of this test are incomplete since the propellant weight burned before reignition was unknown.

## 5. TEST M. 3

### a. Motor Configuration

The motor configuration used for Test M. 3 is shown in Figure 124 and described in Table XLVII. The chief differences in this configuration and that used in Tests M. 1 and M. 2 was the use of a 13-in. -diameter cylindrical forward chamber (rather than spherical) and the use of non-aluminized OX-1 propellant in the aft chamber instead of the aluminized OX-5 used previously. Otherwise, the configuration was the same as that used for Tests M. 1 and M. 2; it was also the same as that used for Test Series G, as described in Reference 8, except for the hot-gas valve.

### b. Test Program and Test Conditions

Four two-second pulse cycles were programmed for this test. Throughout this test, the effective valve orifice area was constant at 0.957 sq in., and the thrust nozzle throat area was 10.0 sq in. Since the forward-grain surface area increases from an initial value of 550 sq in. to 617 sq in. at the web midpoint, forward-chamber pressure, and hence aft-chamber pressure and thrust, increased slightly from cycle to cycle. The predicted forward and aft chamber pressures, and thrust values are 1500, 200 psi and 3000 lb<sub>f</sub>, respectively. (Confidential)

### c. Test Results

The pressure- and thrust-time traces for the four cycles of this test are shown in Figure 131. Note that spontaneous reignition occurred 40 to 50 sec after termination of the first cycle, M. 3. 1, and also after the fourth cycle, M. 3. 4. The nitrogen purge was not used following the first termination, but was used for the last three.

**CONFIDENTIAL**

AFRPL-TR-65-209, Vol I

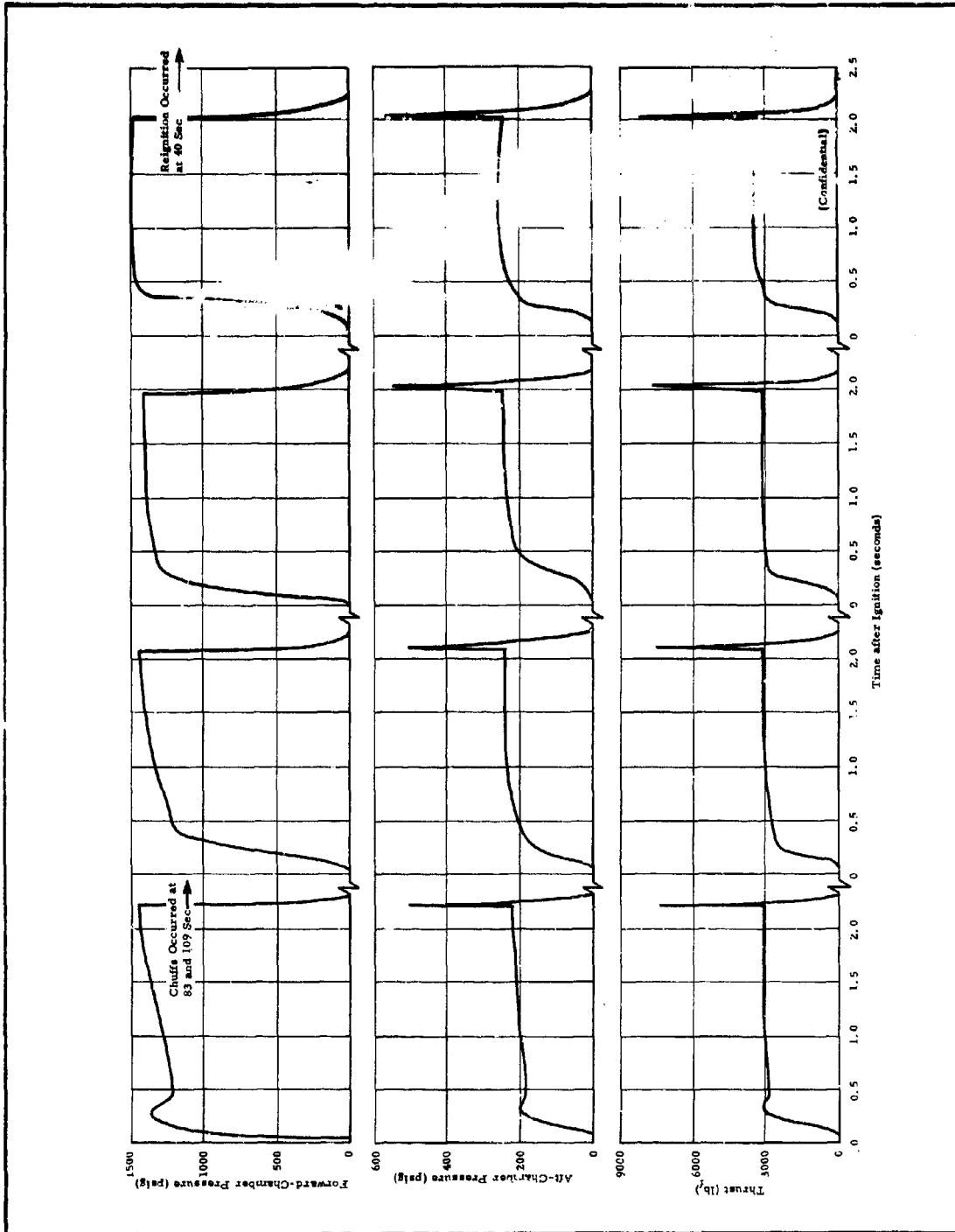


Figure 131 - Pressure- and Thrust-Time Traces for Test M. 3

The second and third cycles, M. 3. 2 and M. 3. 3, terminated successfully, with no reignition. (Confidential)

After termination of the first cycle, reignition was observed visually at 40 to 50 sec and chuffs were observed in the pressure and thrust traces at 83 and 109 sec on the oscillograph record; however, the grains extinguished permanently following these chuffs. Most of the burning following termination occurred at atmospheric pressure since no pressure and thrust, other than the two brief chuffs, could be detected on the trace. Approximately 12 lb of forward grain and 18 lb of aft grain were consumed during reignition. An examination of the motor following cycle M. 3. 1 revealed that both grains reignited on the ends nearest the valve since the amount of web consumed on these ends was significantly greater than that burned at the other ends. The amount of web burned at the center of the forward grain was near the average of the amount burned at the two ends, indicating that the forward grain reignited at the valve end and burned progressively and slowly back along the grain toward the head end, since both grains normally burn very uniformly along their length. However, it was impossible to determine which grain reignited first. (Confidential)

After the fourth cycle, M. 3. 4, the motor reignited approximately 40 sec after termination, burning at approximately atmospheric pressure until the forward grain burned out. A thin shell (approximately 0.2 in.) of aft propellant remained in the motor.

The reduced ballistic data for Test M. 3 are summarized in Table XLIX. Since the weight of propellant burned prior to termination could not be measured for cycles M. 3. 1 and M. 3. 4 because of reignition, performance data for these two cycles were not obtainable.

6. TEST M. 4

a. Motor Configuration

The motor configuration for Test M. 4 is shown in Figure 125 and described in Table XLVII. This motor was identical to that used for Test M. 3, except for the hot-gas valve and aft nozzle. The proportional hot-gas valve and control system, designed and built by TRW, was used on this and subsequent

# CONFIDENTIAL

AFRPL-TR-65-209, Vol I

TABLE XLIX - REDUCED BALLISTIC DATA FOR TEST M. 3

Parameter	Test Number			
	M. 3. 1	M. 3. 2	M. 3. 3	M. 3. 4
<b>Forward chamber</b>				
Delay time, 0 to 10% (sec)	0.074	0.086	0.095	0.150
Rise time, 10 to 90% (sec)	0.150	0.194	0.187	0.176
Burn time (sec)	2.131	2.017	1.790	1.863
Decay time, 100 to 0% (sec)	0.095	0.130	0.165	0.220
$\int Pdt_p$ (psig-sec)	2,703	2,604	2,395	2,671
$\bar{P}_b$ (psia)	1,269	1,283	1,314	1,399
$\bar{P}_k$ (psia)	1,308	1,390	1,404	1,473
$P_{term}$ (psia)	1,404	1,459	1,422	1,463
$dp/dt_{term}$ (psig/sec)	66,500	49,300	42,200	38,400
Weight burned (lb)				
Grain	...	19.697	18.443	...
Pyrogens	0.370	0.370	0.556	0.740
Throat area (sq in.)	0.9566	0.9566	0.9566	0.9566
Characteristic velocity (fps)	...	3,994	3,880	...
<b>Aft chamber</b>				
Delay time, 0 to 10% (sec)	0.118	0.156	0.175	0.218
Rise time, 10 to 90% (sec)	0.122	0.142	0.120	0.108
Burn time (sec)	2.081	1.948	1.710	1.780
$\int Pdt_p$ (psig-sec)	420	438	412	443
$\bar{P}_b$ (psia)	207	225	234	237
$\bar{P}_k$ (psia)	213	239	244	250
$P$ , prior to termination (psia)	251	250	252	250
$P$ , maximum at termination (psia)	521	563	546	586
$dp/dt$ (psig/sec)	17,600	12,200	10,700	9,570
Weight burned (lb)	...	13,519	13,133	...
<b>Total motor</b>				
Weight burned (lb)	...	33.586	32.132	...
Weight <sub>aft</sub> /weight <sub>fwd</sub>	...	0.674	0.691	...
$\int Fdt_f$ (lb <sub>f</sub> -sec)	5,988	6,012	5,654	6,082
$\bar{F}_b$ (lb <sub>f</sub> )	2,763	2,895	3,000	3,150
$\bar{F}_k$ (lb <sub>f</sub> )	2,826	3,090	3,164	3,299
$\int Fdt_{term}$ (lb <sub>f</sub> -sec)	220	346	453	511
Characteristic velocity (fps)	...	4,198	4,127	...
$C_f$ measured	1.426	1.373	1.372	1.373
$I_{sp_{meas}}$ (lb-sec/lb)*	...	179.1	176.0	...
$I_{sp_{P1000/14.7}}$ (lb-sec/lb)*	...	216.9	213.1	...
$I_{sp_{vac, 15^\circ, \epsilon = 20/1}}$ (lb-sec/lb)*	...	246.8	242.4	...
$I_{sp_{eff}}$ (%)	...	92.6	90.9	...

\*Based on weights burned over total time.

(Confidential)

tests. The sea-level aft nozzle used previously for Tests M. 1 through M. 3 was modified as described in 2, d, above. Because of the reignitions experienced in Test M. 3, the volume of nitrogen purge was increased from that used in Test M. 3, and increased successively for each pulse cycle.

b. Test Program and Test Conditions

Since the proportional hot-gas valve used in this test provides pressure feedback control, Test M. 4 was programmed to utilize this capability. Four 1.0-sec pulse cycles, with forward-chamber pressure maintained at 3000 psi, followed by a throttling cycle over three pressure levels (1000, 3000, and 100 psi) were planned. The throttling cycle was programmed as follows: (1) ignition at 1000-psi forward-chamber pressure, (2) operation at this pressure for 1.0 sec, (3) throttle to 3000 psi over 1.5 sec, (4) operation at 3000 psi for 0.5 sec, (5) throttle to 100 psi over 1.5 sec, and (6) operation at 100 psi until the forward web burned out, after approximately 1.5 sec. The three pressure levels for the throttling cycle are subsequently referred to as levels 1, 2, and 3, respectively. The predicted aft-chamber pressure and thrust values for the pulse cycles are 350 psi and 5000 lb<sub>f</sub>, respectively. (Confidential)

c. Test Results

The pressure- and thrust-time traces for the five cycles of Test M. 4 are shown in Figure 132. Each of the pulse cycles terminated permanently with no reignition; nitrogen purge was used after each termination, and an off-time of at least two hours between cycles was observed. After the fourth cycle, M. 4. 4, the motor was disassembled and both chambers weighed so that performance data for the four pulse cycles could be calculated independently from that of the throttling cycle. Four pyrogens were used in each of the pulse cycles and three pyrogens in the fifth (throttling) cycle. Each pyrogen delivers 0.91 lb/sec of PPO-13 propellant exhaust products for 0.20 sec.

The reduced ballistic data for the four pulse cycles of M. 4 are given in Table L. Since rise time increased on each successive cycle because of increased free-chamber volume, the forward-chamber pressure-time integral decreased from M. 4. 1 to M. 4. 4. However, since the forward-grain surface area increased during these four cycles, the increased forward-chamber mass flow caused successive aft-chamber pressure and

**CONFIDENTIAL**

AFRPL-TR-65-209, Vol I

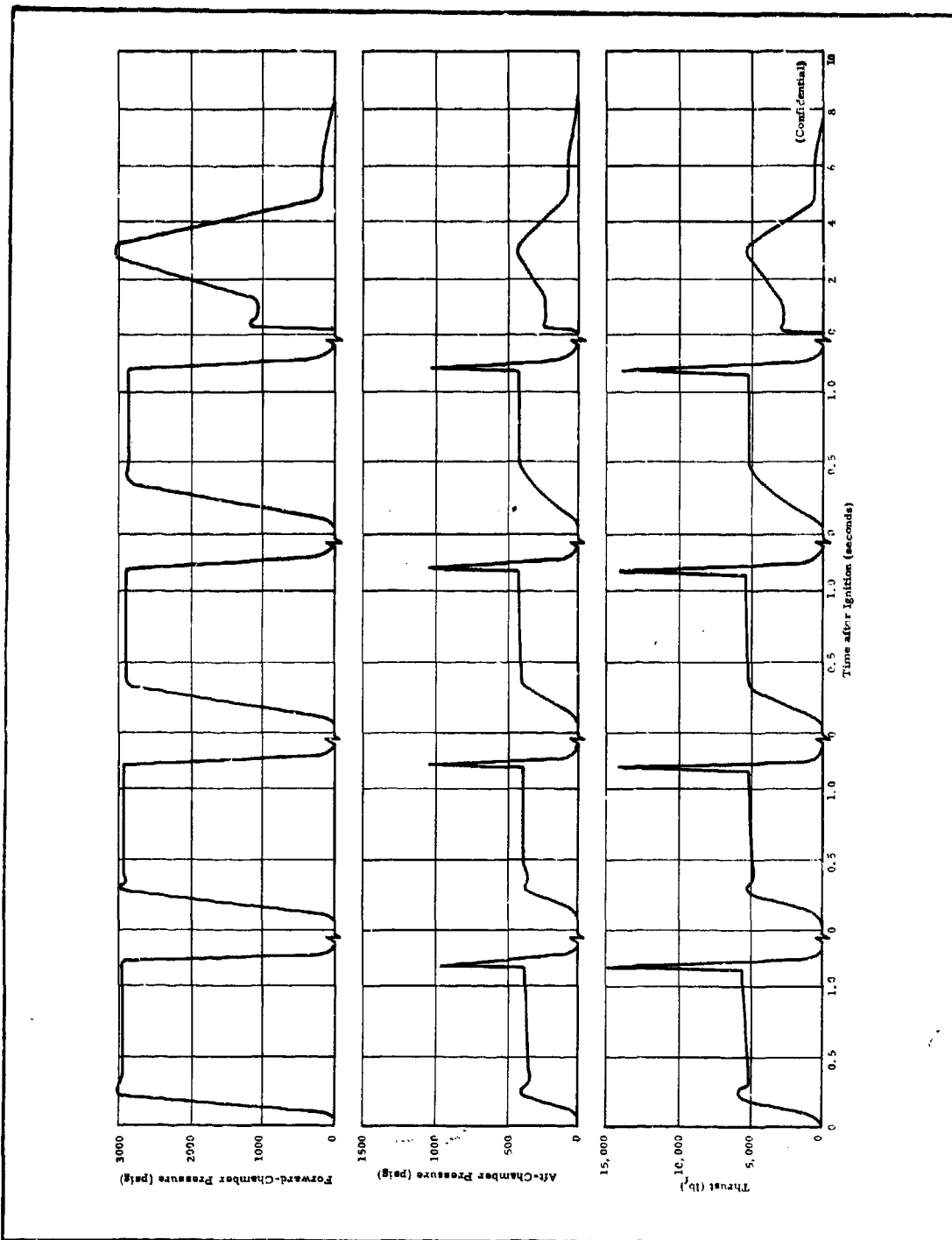


Figure 132 - Pressure- and Thrust-Time Traces for Test M. 4

-216-

**CONFIDENTIAL**

# CONFIDENTIAL

AFRPL-TR-65-209, Vol I

TABLE L - REDUCED BALLISTIC DATA FOR PULSE CYCLES OF TEST M. 4

Parameter	Test Number				Total
	M. 4. 1	M. 4. 2	M. 4. 3	M. 4. 4	
<b>Forward chamber</b>					
Delay time, 0 to 10% (sec)	0.068	0.076	0.075	0.088	...
Rise time, 10 to 90% (sec)	0.122	0.163	0.194	0.254	...
Burn time (sec)	1.062	1.065	1.061	1.054	4.242
Decay time, 100 to 0% (sec)	0.133	0.165	0.186	0.217	...
$\int Pdt_p$ (psig-sec)	3,065	3,009	2,869	2,778	11,721
$\bar{P}_b$ (psia)	2,822	2,745	2,624	2,609	2,701
$\bar{P}_k$ (psia)	2,980	2,976	2,884	2,930	2,944
$P_{term}$ (psia)	2,977	2,950	2,900	3,000	...
$dp/dt_{term}$ (psig/sec)	146,000	115,000	97,600	80,100	...
Weight burned (lb)					
Grain	...	...	...	...	65.423
Pyrogens	0.723	0.754	0.750	0.749	2.976
<b>Aft chamber</b>					
Delay time, 0 to 10% (sec)	0.108	0.126	0.125	0.146	...
Rise time, 10 to 90% (sec)	0.121	0.146	0.168	0.251	...
Burn time (sec)	1.022	1.019	0.010	0.099	4.047
$\int Pdt_p$ (psig-sec)	375	394	406	405	1,594
$\bar{P}_b$ (psia)	344	356	362	361	356
$\bar{P}_k$ (psia)	359	381	396	406	384
$P_{prior}$ (psia)	379	383	416	406	...
$P_{max}$ (psia)	955	1,031	1,053	1,032	...
$dp/dt$ (psig/sec)	30,100	23,600	20,400	16,500	...
Weight burned (lb)	...	...	...	...	47.63
<b>Total motor</b>					
Weight burned (lb)					116.033
$Weight_{aft}/Weight_{fwd}$					0.70
$\int Fdt_f$ (lb-sec)	5,251	5,443	5,513	5,568	21,775
$\bar{F}_b$ (lb <sub>f</sub> )	4,632	4,764	4,768	4,736	4,725
$\bar{F}_k$ (lb <sub>f</sub> )	4,834	5,069	5,194	5,338	5,096
$\int Fdt_{term}$ (lb-sec)	475.4	598.2	706.5	828.0	...
Characteristic velocity (fps)	...	...	...	...	3,392
$C_f$ , measured	1.400	1.381	1.358	1.361	1,375
Expansion ratio, $A_e/A_t$	1.494	1.494	1.474	1.494	1.494
Ratio of specific heats, $\gamma$	...	...	...	...	1.22
Throat area (sq in.)	10.00	10.00	10.00	10.00	10.00
$I_{sp_{meas}}$ (lb-sec/lb) <sup>*</sup>	...	...	...	...	187.7
$I_{sp_{1000/14.7}}$ (lb-sec/lb) <sup>*</sup>	...	...	...	...	223.8
$I_{sp_{vac, 15^\circ, \epsilon = 20/1}}$ (lb-sec/lb) <sup>*</sup>	...	...	...	...	254.9
$I_{sp_{eff}}$ (%)	...	...	...	...	95.4

<sup>\*</sup> Based on weights burned over total time.

thrust integrals to increase slightly.

Table LI presents the reduced ballistic data for the throttling cycle, M. 4.5. Pressure and thrust integrals were obtained during steady-state operation at each of the three constant pressure levels. The level 1 integrals were obtained after the ignition transient was completed, but before the ramp to 3000 psi. From these integrals, steady-state pressures and thrust were obtained as a basis for comparison at the same levels. The measured thrust levels were corrected to vacuum values. The measured thrust modulation from level 2 to level 3 was 8.0 to 1, which corresponds to a 6.4-to-1 range in vacuum with a constant thrust coefficient. (Confidential)

In Figure 133, the steady-state aft-chamber pressure and vacuum thrust levels are plotted as a function of forward-chamber pressure level for Tests M. 4 and M. 5. Between levels 1 and 3, the curves have the same slope as the pressure exponent, 0.67, of the PPO-13 forward-grain propellant, which indicates that the pressure exponent of the OX-1 aft-grain propellant is 1.0 in this aft-chamber pressure region (64 to 226 psi). Between levels 2 and 1, however, the slope of the curves is 0.53 to 0.54, which indicates that the pressure exponent of OX-1 changed to a lower value in this region, from 226 to 400 psi. A mean exponent in this pressure range of 0.69 was calculated from these data. The specific impulse efficiency for this cycle was 89 percent, well below the 95 percent measured for the four pulse cycles. This is probably due to reduced efficiency at low chamber pressures, particularly since a long tail-off occurred on Test M. 4. (Confidential)

The hot-gas valve and control system performed exceptionally well during this test. However, when the motor was disassembled for weighing after the fourth cycle, the valve was inspected visually and dimensionally at the throat, and several hairline cracks were observed in the throat section (part 28, made of unalloyed molybdenum, as shown in Figure 128). It was decided that these cracks would not affect motor performance during the fifth cycle; this was verified by satisfactory performance of the valve during that cycle. When the motor was disassembled and inspected after the fifth cycle, it was observed that the cracks in the throat had propagated and widened during the final cycle. Post-test photographs of the forward and aft ends of the valve are shown in Figures 134 and 135, respectively; two of the cracks are visible

# CONFIDENTIAL

AFRPL-TR-65-209, Vol I

TABLE LI - REDUCED BALLISTIC DATA FOR  
THROTTLING CYCLE OF TEST M. 4

Parameter	Value
<b>Level 1</b>	
Steady-state time (sec)	0.600
Forward-chamber pressure (psia)	1053
Aft-chamber pressure (psia)	226
Thrust, measured (lb <sub>f</sub> )	2868
C <sub>f</sub> , theoretical (measured conditions)	1.300
C <sub>f</sub> , theoretical (vacuum, $\epsilon = 20/1$ )	1.808
C <sub>f</sub> , measured	1.269
Thrust (vacuum, $\epsilon = 20/1$ ) (lb <sub>f</sub> )	3990
<b>Level 2</b>	
Steady-state time (sec)	0.270
Forward-chamber pressure (psia)	2996
Aft-chamber pressure (psia)	397
Thrust, measured (lb <sub>f</sub> )	5155
C <sub>f</sub> , theoretical (measured conditions)	1.338
C <sub>f</sub> , measured	1.298
Thrust (vacuum, $\epsilon = 20/1$ ) (lb <sub>f</sub> )	6966
<b>Level 3</b>	
Steady-state time (sec)	0.500
Forward-chamber pressure (psia)	157.5
Aft-chamber pressure (psia)	63.6
Thrust, measured (lb <sub>f</sub> )	644.4
C <sub>f</sub> , theoretical (measured conditions)	1.068
C <sub>f</sub> , measured	1.013
Thrust (vacuum, $\epsilon = 20/1$ ) (lb <sub>f</sub> )	1090.6
<b>Total firing</b>	
<b>Forward chamber</b>	
$\int P dt_p$ (psig-sec)	8291
Total time (sec)	8.420
Weight burned (lb)	
Grain	56.631
Pyrogens	0.556
<b>Aft chamber</b>	
$\int P dt_a$ (psig-sec)	1385.3
Total time (sec)	8.360
Weight burned (lb)	51.687
$\int F dt_f$ (lb <sub>f</sub> -sec)	18533
<b>Overall motor</b>	
Weight burned (lb)	108.373
Characteristic velocity (fps)	4074
I <sub>sp</sub> (lb-sec/lb)	170.2
meas	
Weight <sub>aft</sub> /weight <sub> fwd</sub>	0.904
I <sub>sp</sub> 1300/14.7, 15° (lb-sec/lb)	211.9
I <sub>sp</sub> vac, $\epsilon = 20/1$ , 15° (lb-sec/lb)	241.2
I <sub>sp</sub> eff (%)	99.0

(Confidential)

# CONFIDENTIAL

AFRPL-TR-65-209, Vol I

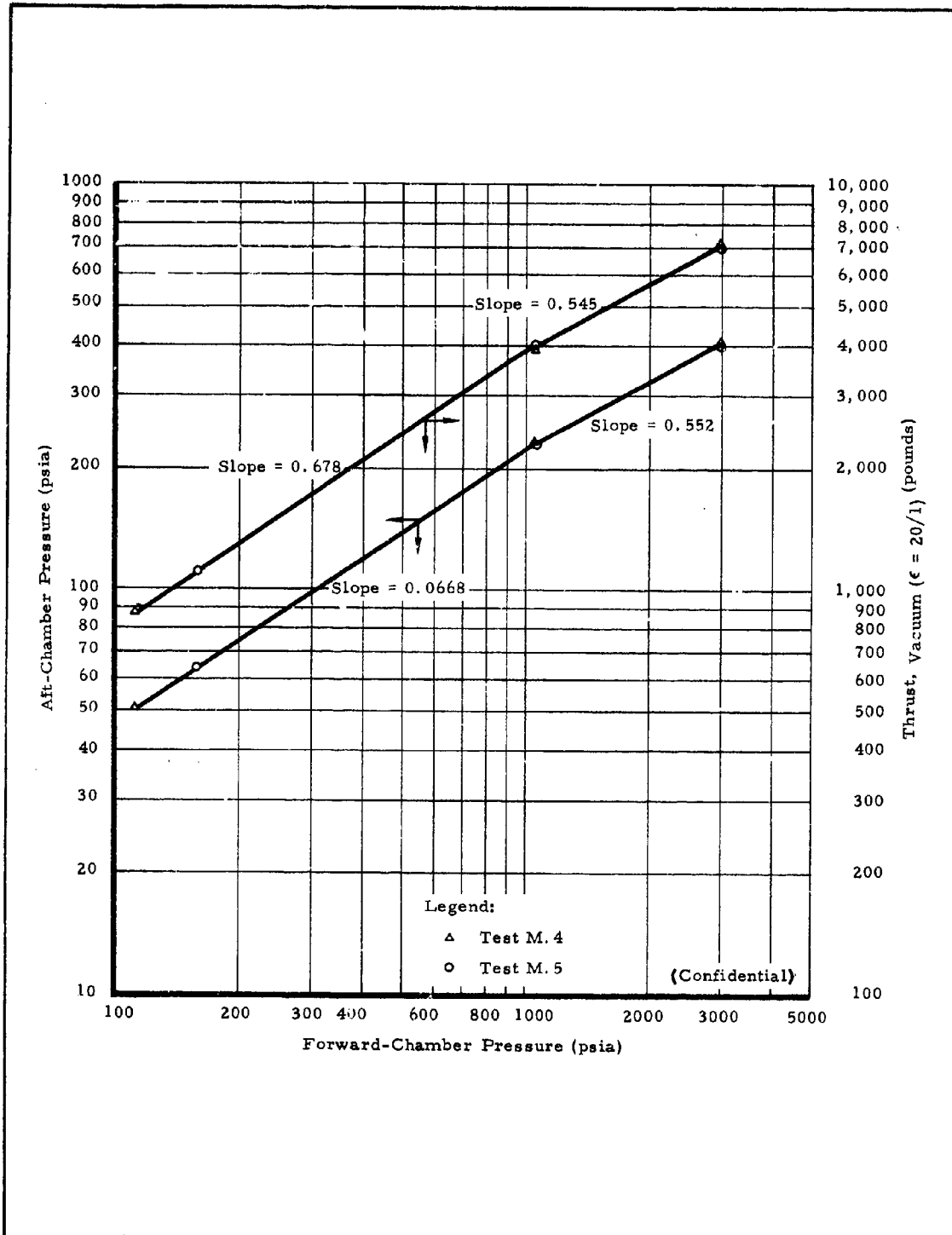


Figure 133-Steady-State Aft-Chamber Pressure and Vacuum Thrust Values as a Function of Steady-State Forward Chamber Pressure for Tests M. 4 and M.5

# CONFIDENTIAL

**CONFIDENTIAL**

AFRPL-TR-65-209, Vol I

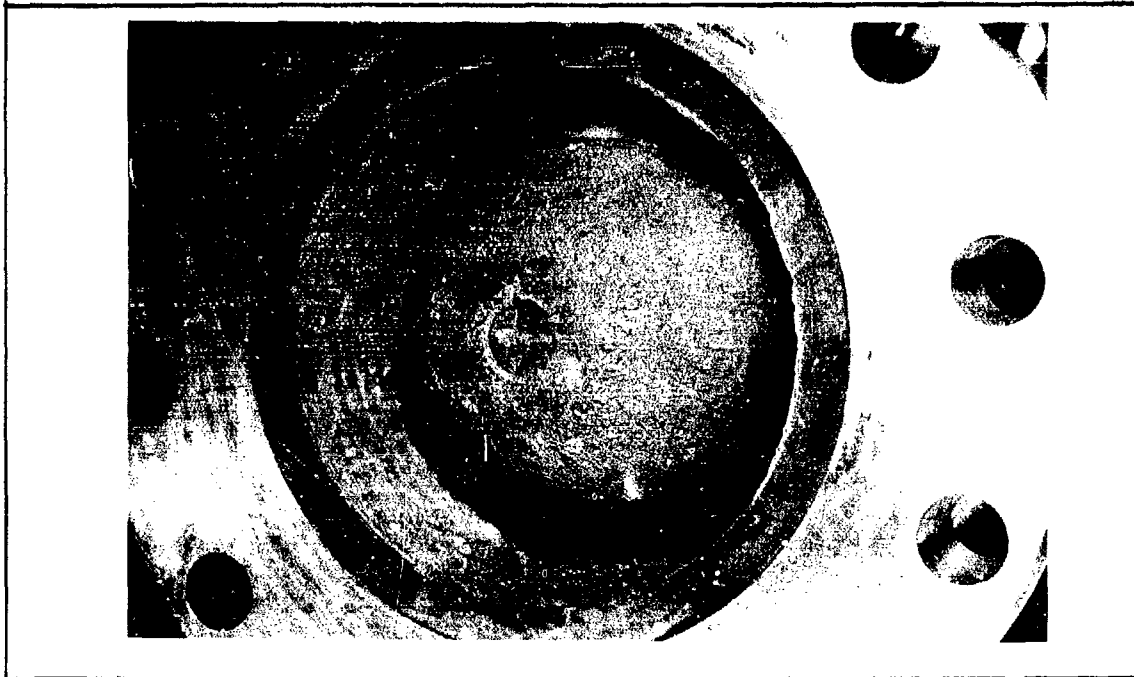


Figure 134 - Post-Test View of Forward End of Hot-Gas Valve Used in Test M. 4



Figure 135 - Post-Test View of Aft End of Hot-Gas Valve Used in Showing Cracks 180° Apart

**CONFIDENTIAL**

in Figure 134. It was concluded that these cracks occurred during the cool-down following a firing cycle.

7. TEST M. 5

a. Motor Configuration

The motor used for Test M. 5 was identical to that used for Test M. 4, and incorporated a second hot-gas valve supplied by TRW (see Figure 125 and Table XLVII).

b. Test Program and Test Conditions

The test program consisted of four duty cycles identical to those for Test M. 4, followed by a fifth (throttling) cycle. A higher thrust range was programmed for the fifth cycle of this test by throttling to a lower pressure at the end of the cycle. The predicted aft chamber pressure and thrust values for the pulse cycles are 350 psi and 5000 lb<sub>f</sub>, respectively.

c. Test Results

The pressure- and thrust-time traces for the five cycles of Test M. 5 are shown in Figure 136. Each of the pulse cycles terminated permanently without reignition; the nitrogen purge was used after each termination. The fifth cycle continued until the forward web burned out. As in Test M. 4, the motor was disassembled and weighed after the fourth cycle. The third and fourth pulse cycles were slightly shorter than the first two because of an error in the timer setting. Again, four pyrogens were used for each pulse cycle and three on the throttling cycle.

The reduced ballistic data for the four pulse cycles of Test M. 5, given in Table LII compare very favorably with the four pulse cycles of Test M. 4 (see Table L). The termination impulse values for Test M. 5 were within 0.9 percent of those for M. 4, and the average steady-state thrust levels for the two tests were within 1.0 percent. The average thrust values over burn time agreed within 1.7 percent; this difference is larger because the operating times for the third and fourth cycles of Test M. 5 were shorter than the others. The specific impulse for Test M. 5 was slightly less than that of Test M. 4, but was still 94.2 percent of theoretical. These specific impulse values were calculated for the total weight consumed in the firings, including igniter and insulation weights. (Confidential)

**CONFIDENTIAL**

AFRPL-TR-65-209, Vol I

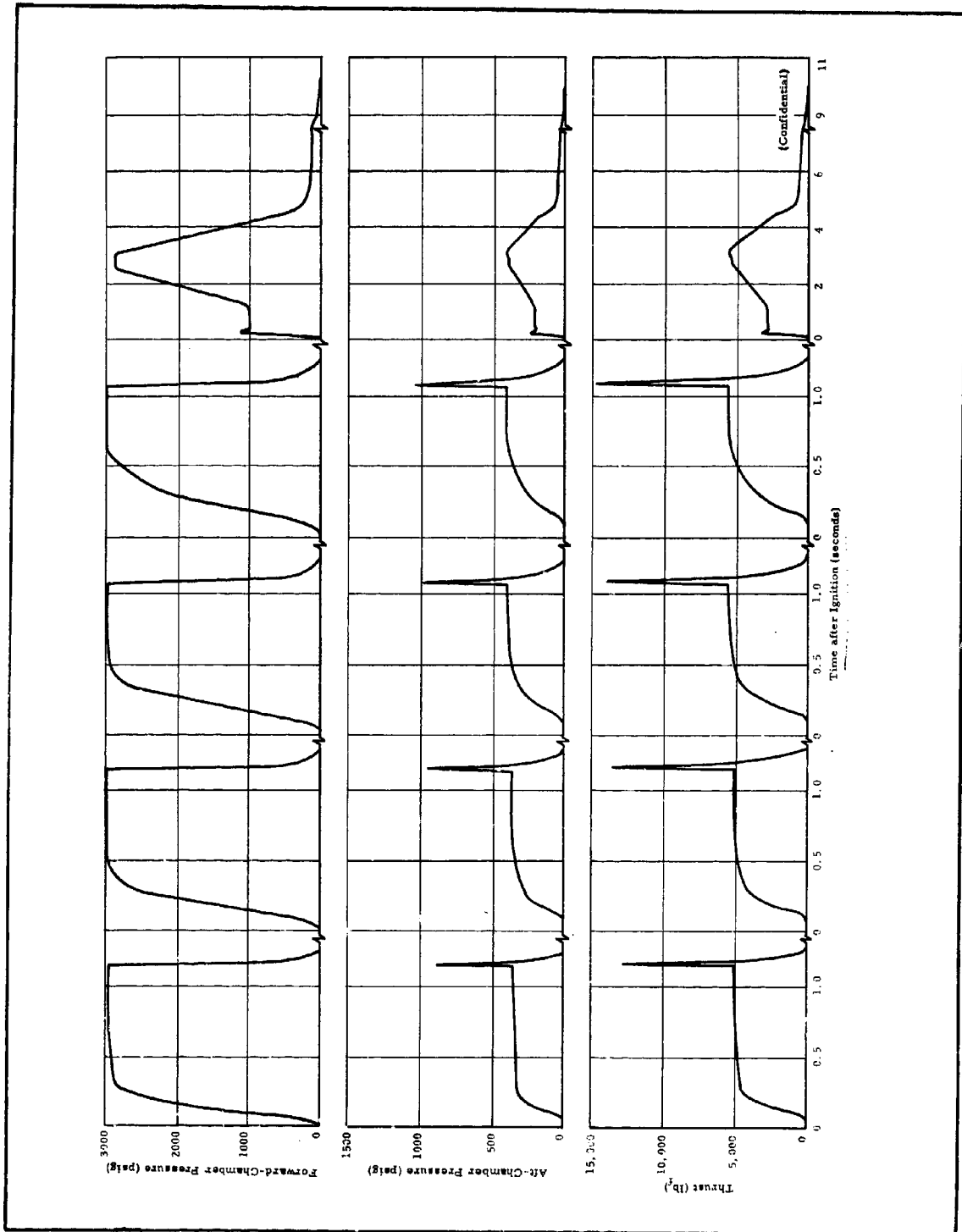


Figure 136 - Pressure- and Thrust-Time Traces for Test M. 5

**CONFIDENTIAL**

# CONFIDENTIAL

AFRPL-TR-65-209, Vol I

TABLE LII - REDUCED BALLISTIC DATA FOR PULSE CYCLES OF TFRT M. 5

Parameter	Test Number				Total
	M. 5. 1	M. 5. 2	M. 5. 3	M. 5. 4	
<b>Forward chamber</b>					
Delay time, 0 to 10% (sec)	0.070	0.080	0.093	0.096	...
Rise time, 10 to 90% (sec)	0.135	0.260	0.226	0.365	...
Burn time (sec)	1.083	1.065	0.976	0.968	4.092
Decay time, 100 to 0% (sec)	0.120	0.150	0.190	0.205	...
$\int P dt_p$ (psig-sec)	3,050	2,982	2,670	2,595	11,297
$\bar{P}_b$ (psia)	2,769	2,734	2,573	2,580	2,687
$\bar{P}_k$ (psia)	2,981	3,058	3,025	3,058	3,024
$P_{term}$ (psia)	3,009	3,007	3,045	3,017	...
$dp/dt_{term}$ (psig/sec)	143,000	117,000	97,500	91,500	...
Weight burned (lb)					
Grain	...	...	...	...	62.428
Pyrogens	0.734	0.750	0.754	0.745	2.983
<b>Aft chamber</b>					
Delay time, 0 to 10% (sec)	0.113	0.136	0.148	0.166	...
Rise time, 10% to 90% (sec)	0.096	0.274	0.256	0.402	...
Burn time (sec)	1.037	0.010	0.923	0.896	3.866
$\int P dt_p$ (psig-sec)	369	380	357	362	1,468
$\bar{P}_b$ (psia)	335	344	345	349	343
$\bar{P}_k$ (psia)	352	380	394	410	379
$P_{prior}$ (psia)	366	380	412	418	...
$P_{max}$ (psia)	907	994	1,012	1,063	...
$dp/dt$ (psig/sec)	28,800	22,700	19,700	18,100	...
Weight burned (lb)	...	...	...	...	45.854
<b>Total motor</b>					
Weight burned (lb)	...	...	...	...	111.305
$Weight_{aft}/Weight_{fwd}$	...	...	...	...	0.70
$\int F dt_f$ (lb <sub>f</sub> -sec)	5,226	5,330	5,141	5,058	20,756
$\bar{F}_b$ (lb <sub>f</sub> )	4,487	4,658	4,779	4,677	4,644
$\bar{F}_k$ (lb <sub>f</sub> )	4,799	5,132	5,417	5,512	5,148
$\int F dt_{term}$ (lb <sub>f</sub> -sec)	465.3	599.8	711.7	823.0	...
Throat area (sq in.)	10.02	10.02	10.02	10.02	10.02
Characteristic velocity (fps)	...	...	...	...	4,252
$C_f$ , measured	1.413	1.400	1.43	1.394	1.411
Expansion ratio, $A_e/A_t$	1.589	1.589	1.589	1.589	1.589
Ratio of specific heats, $\gamma$	...	...	...	...	1.221
$I_{sp_{meas}}$ (lb-sec/lb)*	...	...	...	...	186.5
$I_{sp_{1000/14.7, 15^\circ}}$ (lb-sec/lb)*	...	...	...	...	221.0
$I_{sp_{vac, 15^\circ, \epsilon = 20/1}}$ (lb-sec/lb)*	...	...	...	...	251.7
$I_{sp_{eff}}$ (%)	...	...	...	...	94.2

\* Based on weights burned over total time.

(Confidential)

Table LIII presents the reduced ballistic data for the throttling cycle, M. 5.5. Steady-state pressures and thrust values are given for the three pressure (throttling) levels. The measured thrust values were corrected to vacuum conditions. The measured sea-level thrust modulation from levels 2 to 3 was 11.2 to 1, which corresponds to an 8.1-to-1 thrust range in vacuum. (Confidential)

The steady-state aft-chamber pressure and vacuum thrust levels, plotted as a function of the forward-chamber pressure levels for the throttling cycles of Tests M. 4 and M. 5, were shown in Figure 132. As shown, the agreement between the two tests is excellent. Again, below an aft-chamber pressure of 226 psi, the slope of the curves equals the pressure exponent, 0.67, of the forward grain propellant, indicating that the pressure exponent of the aft-grain propellant is 1.0 in the pressure region of 50 to 226 psi. Above a 226-psi aft-chamber pressure, the slope of the curves is 0.55, which corresponds to an aft-grain pressure exponent of 0.74 in the pressure region of 226 to 405 psi. (Confidential)

This cycle had a specific impulse efficiency of 86 percent, which was well below the 94 percent obtained for the four pulse cycles. A very long tail-off occurred at burnout of the forward grain, because of the low operating pressure. After tail-off of the forward chamber, the aft grain continued to burn at atmospheric pressure for a few seconds. It is believed that this continued burning contributed to the lower impulse for the test and the higher aft-to-forward mixture ratio than could be explained from the internal ballistic data for the test. (Confidential)

#### 8. TEST M. 6

##### a. Motor Configuration

The motor used in Test M. 6 was identical to that used in Tests M. 4 and M. 5, as shown in Figure 125 and Table XLVII, except that the Northrop Carolina-designed nozzle was replaced with a TRW sea-level nozzle between the second and third pulses.

##### b. Test Program and Test Conditions

This test was similar to Tests M. 4 and M. 5 in that four 1.0-sec pulse cycles and one throttling cycle were programmed.

# CONFIDENTIAL

AFRPL-TR-65-209, Vol I

TABLE LMI - REDUCED BALLISTIC DATA FOR  
THROTTLING CYCLE OF TEST M, 5

Parameter	Value
<b>Level 1</b>	
Steady-state time (sec)	0.660
Forward-chamber pressure (psia)	1049
Aft-chamber pressure (psia)	229
Thrust, measured (lb <sub>f</sub> )	2848
C <sub>f</sub> , theoretical (measured conditions)	1.311
C <sub>f</sub> , theoretical (vacuum, $\epsilon = 20/1$ )	1.810
C <sub>f</sub> , measured	1.241
Thrust (vacuum, $\epsilon = 20/1$ ) (lb <sub>f</sub> )	3904
<b>Level 2</b>	
Steady-state time (sec)	0.260
Forward-chamber pressure (psia)	2962
Aft-chamber pressure (psia)	408
Thrust, measured (lb <sub>f</sub> )	5298
C <sub>f</sub> , theoretical (measured conditions)	1.353
C <sub>f</sub> , measured	1.296
Thrust (vacuum, $\epsilon = 20/1$ ) (lb <sub>f</sub> )	7087
<b>Level 3</b>	
Steady-state time (sec)	0.500
Forward-chamber pressure (psia)	112.1
Aft-chamber pressure (psia)	50.8
Thrust, measured (lb <sub>f</sub> )	471.6
C <sub>f</sub> , theoretical (measured conditions)	0.977
C <sub>f</sub> , measured	0.927
Thrust (vacuum, $\epsilon = 20/1$ ) (lb <sub>f</sub> )	873.7
<b>Total firing</b>	
Forward chamber	
$\int P dt$ (psig-sec)	8354
Total time (sec)	10.66
Weight burned (lb)	
Grain	58.318
Pyrogens	0.571
Aft chamber	
$\int P dt$ (psig-sec)	1466
Total time (sec)	10.57
Weight burned (lb)	60.526
Overall motor	
Weight burned (lb)	119.415
Weight <sub>aft</sub> /weight <sub> fwd</sub>	1.028
Characteristic velocity (fps)	3953
$\int F dt$ (lb <sub>f</sub> -sec)	19514
I <sub>sp meas, 15°</sub> (lb-sec/lb)	163.4
I <sub>sp 1000/14.7, 15°</sub> (lb-sec/lb)	205.5
I <sub>sp vac, <math>\epsilon = 20/1, 15°</math></sub> (lb-sec/lb)	233.9
i <sub>sp off</sub> (%)	85.7

(Confidential)

# CONFIDENTIAL

**CONFIDENTIAL**

However, the nitrogen purge was not to be used automatically following each termination in order to ascertain at which pulse cycle spontaneous reignition of the motor would occur. That is, since free chamber volume increases during burning, the possibility of spontaneous reignition from residual chamber gases becomes more favorable from pulse to pulse at sea level. When reignition occurred, it was planned to throttle the motor to achieve a high pressure, reterminate the motor, and then use the nitrogen purge in order to save the remaining propellant for the remaining duty cycles. The predicted chamber pressure and thrust values for the pulse cycles are 350 psi and 5000 lb<sub>f</sub>, respectively.

(Confidential)

c. Test Results

The pressure- and thrust-time traces for the first two pulses of this test, M. 6. 1 and M. 6. 2, are shown in Figure 137. As shown, the motor was permanently extinguished after the first cycle, whereas reignition occurred approximately 30 sec after termination of the second cycle. When the motor reignited, the valve was reset to the full-closed position, which corresponds to 4500-psi forward-chamber pressure. As motor pressure increased, the valve "terminate" signal was manually actuated. However, due to operator error, the "terminate" signal was interrupted before the motor was extinguished. The signal sequence was repeated, as shown in Figure 137, with the second manual termination being successful. The nitrogen purge was used, and the grain was permanently extinguished. This test confirmed that hot residual gases must be removed from a motor terminated at sea level to obtain reproducible, permanent extinguishment. At altitude, however, the problem of reignition is reduced considerably as ambient pressure, and hence the pressure of the residual chamber gases, decreases. (Confidential)

After the second pulse, the Northrop Carolina nozzle was replaced by a TRW sea-level nozzle (described in 2, d, above, and two additional pulses (M. 6. 3 and M. 6. 4) similar to the first two were fired, except that the nitrogen purge was used for both. Aft-chamber pressure for M. 6. 3 and M. 6. 4 and the subsequent throttling cycle was measured in the head end of the aft chamber since transducer ports could not be located in the aft end of the chamber with the TRW nozzle and end closure installed. Pressures measured in the head end of the aft chamber generally are not reliable due to the aspirating effect of the high-velocity forward-chamber exhaust gases in this region.

**CONFIDENTIAL**

**CONFIDENTIAL**

AFRPL-TR-65-209, Vol I

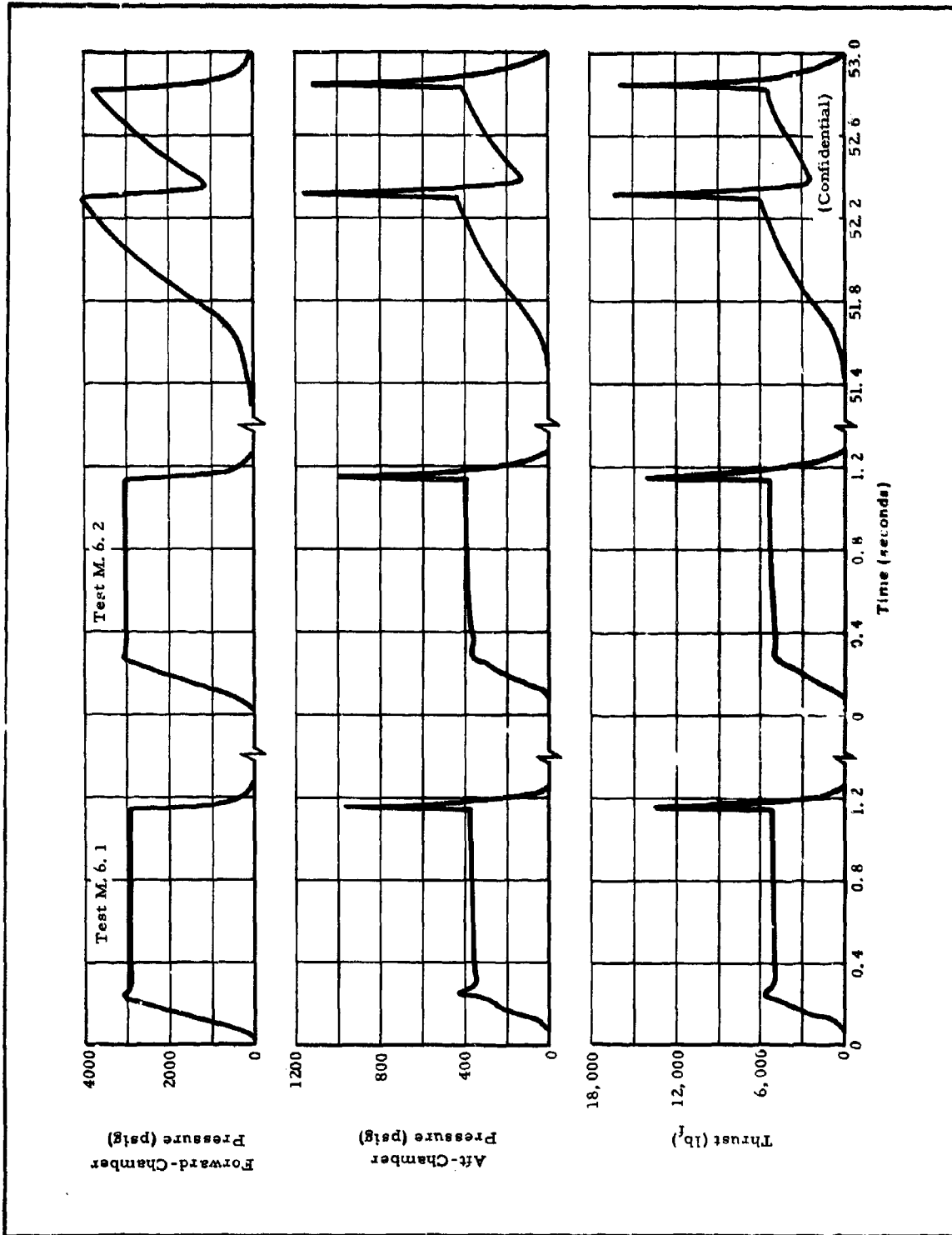


Figure 137 - Pressure- and Thrust-Time Traces for Tests M. 6. 1, M. 6. 2, and Reignition Following M. 6. 2

**CONFIDENTIAL**

The measured pressure- and thrust-time traces for M. 6. 3 and M. 6. 4 are shown in Figure 138. The motor permanently extinguished after both terminations. Four pyrogen igniters were used for each of the four pulse cycles (total of 16). (Confidential)

The fifth ignition of this test, M. 6. 5, was a throttling cycle. This cycle was programmed for (1) ignition at a 500-psia forward-chamber pressure, (2) operation at this pressure for 0. 5 sec, (3) throttling to 90 psia over a 0. 5-sec interval, (4) operation at 90 psia for 3. 0 sec, (5) throttling to 4500 psia as rapidly as the system is capable (approximately 1. 25 sec at a consumed web fraction of 0. 85), and (6) operation at 4500 psia until the forward web burned out, which was expected to occur 0. 5 sec later. (Confidential)

The actual pressure- and thrust-time traces for M. 6. 5 are shown in Figure 139. The motor operated as planned until a forward-chamber pressure of 4264 psia was attained, near the end of the test. At this point, the overpressure switch actuated, sending a termination signal to the valve. The valve terminated the motor. Since this termination was not planned, the nitrogen purge system was not actuated and the motor reignited, burning out the small amount of propellant remaining. A post-test analysis of the components revealed that the overpressure switch, set to actuate at 5000 psia as a safety device, was actuated by vibrations in the test bay. (Confidential)

The reduced ballistic data for the four pulse cycles are given in Table LIV. Weight measurements were made after M. 6. 2 and M. 6. 5, but since the motor reignited after these cycles, performance results could not be determined. Note that the steady-state thrust values are higher for M. 6. 3 and M. 6. 4. This apparent discrepancy resulted from the fact that pressure for M. 6. 3 and M. 6. 4 was measured at the head end of the aft chamber, as explained earlier; the true steady-state aft pressure was probably near 400 psia for these two pulses, rather than the measured 351 to 355 psia. (Confidential)

In Figure 140, the shut-down impulse (the impulse delivered during termination) is plotted as a function of the forward grain web fraction consumed at the time of termination for all pulse cycles of Tests M. 4, M. 5, and M. 6. The delivered impulse at termination is obviously predictable and dependent on the motor free volume. (Confidential)

**CONFIDENTIAL**

AFRPL-TR-65-209, Vol I

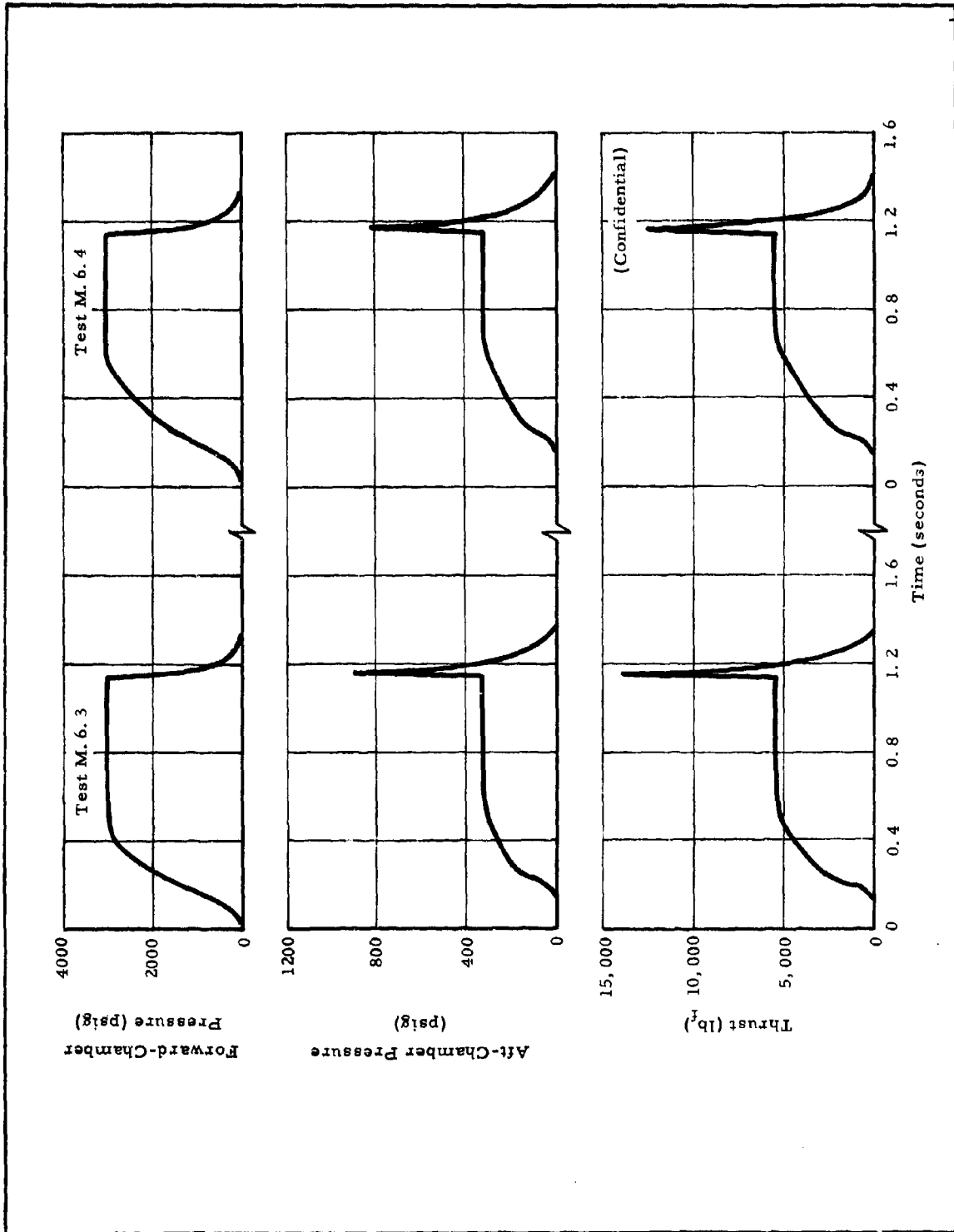


Figure 138 - Pressure- and Thrust-Time Traces for Tests M. 6. 3 and M. 6. 4

**CONFIDENTIAL**

AFRPL-TR-65-209, Vol I

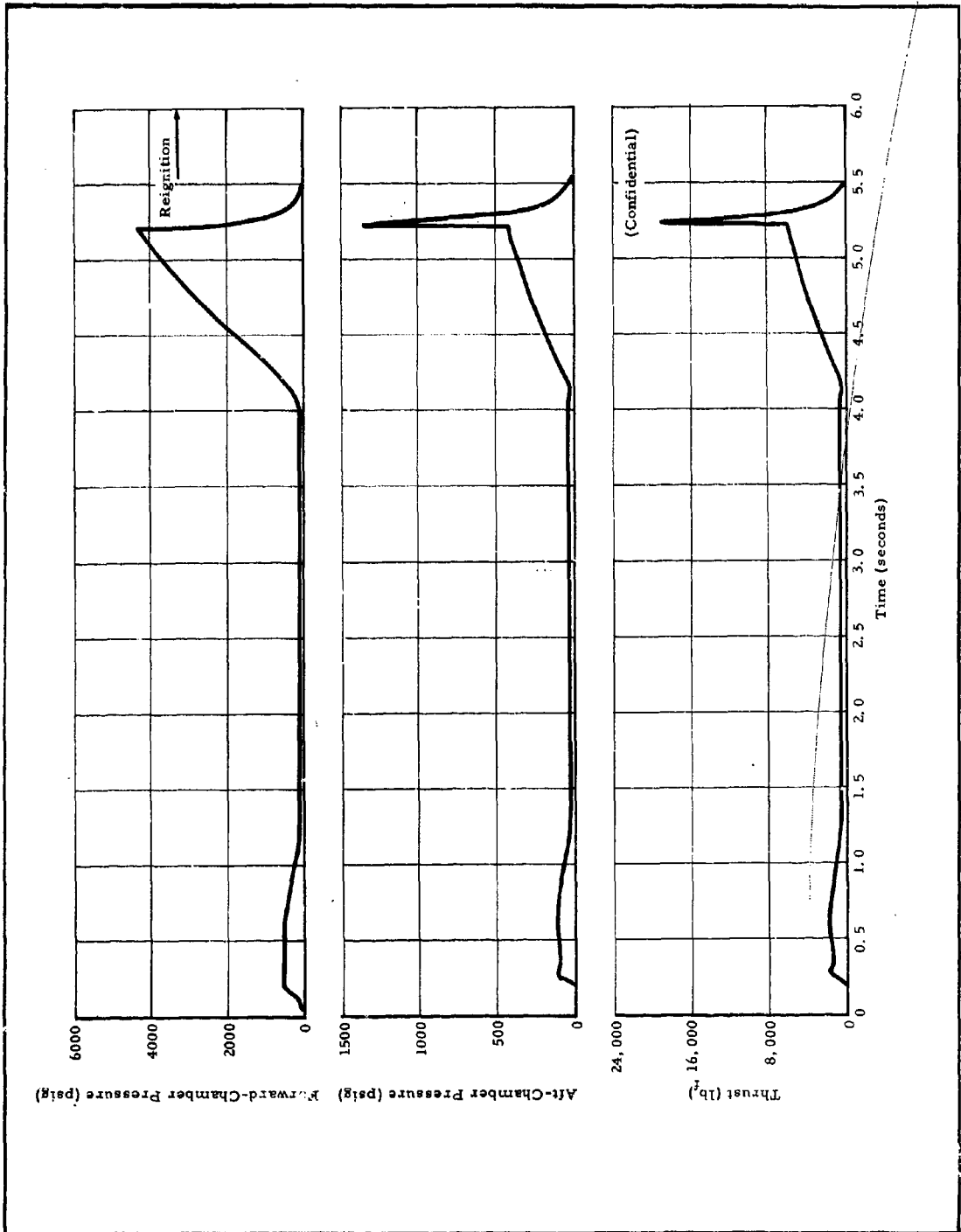


Figure 139 - Pressure- and Thrust-Time Traces for Test M. 6. 5

**CONFIDENTIAL**

# CONFIDENTIAL

AFRPL-TR-65-209, Vol I

TABLE LIV - REDUCED BALLISTIC DATA FOR PULSE CYCLES OF TEST M. 6

Parameter	Test Number			
	M. 6. 1	M. 6. 2	M. 6. 3	M. 6. 4
<b>Forward Chamber</b>				
Delay time, 0 to 10% (sec)	0. 073	0. 085	0. 109	0. 120
Rise time, 10 to 90% (sec)	0. 139	0. 170	0. 281	0. 378
Burn time (sec)	1. 070	1. 061	1. 038	1. 025
Decay time, 100 to 0% (sec)	0. 113	0. 140	0. 200	0. 245
$\int Pdt_p$ (psig-sec)	3, 098	3, 033	2, 857	2, 757
$F_b$ (psia)	2, 849	2, 794	2, 658	2, 578
$F_k$ (psia)	3, 035	3, 029	3, 016	3, 071
$P_{term}$ (psia)	2, 984	3, 044	3, 004	3, 034
$dp/dt_{term}$ (psig/sec)	159, 000	123, 000	89, 000	80, 900
Weight burned (pyrogens) (lb)	0. 750	0. 750	0. 750	0. 750
<b>Aft Chamber</b>				
Delay time, 0 to 10% (sec)	0. 117	0. 135	0. 187	0. 210
Rise time, 10 to 90% (sec)	0. 120	0. 140	0. 258	0. 390
Burn time (sec)	1. 026	1. 012	0. 959	0. 934
$\int Pdt_p$ (psig-sec)	386	396	339*	336*
$F_b$ (psia)	355	362	306*	298*
$F_k$ (psia)	371	388	351*	355*
$P_{prior}$ (psia)	392	410	340*	324*
$P_{max}$ (psia)	980	1014	919*	838*
$dp/dt$ (psig/sec)	29, 200	24, 900	15, 000	11, 500
<b>Total Motor</b>				
$\int Fdt_f$ (lb <sub>f</sub> -sec)	5, 434	5, 541	5, 480	5, 235
$F_b$ (lb <sub>f</sub> )	4, 780	4, 918	4, 765	4, 558
$F_k$ (lb <sub>f</sub> )	5, 030	5, 213	5, 416	5, 391
$\int Fdt_{term}$ (lb <sub>f</sub> -sec)	467. 8	589. 0	863. 5	983. 0
Throat area (sq in.)	10. 0	10. 0	10. 0	10. 0

\* Pressure measurements in error due to location of transducer port in head end of chamber, hence measured  $C_f$  and Characteristic Velocity not obtainable.

(Confidential)

**CONFIDENTIAL**

AFRPL-TR-65-209, Vol I

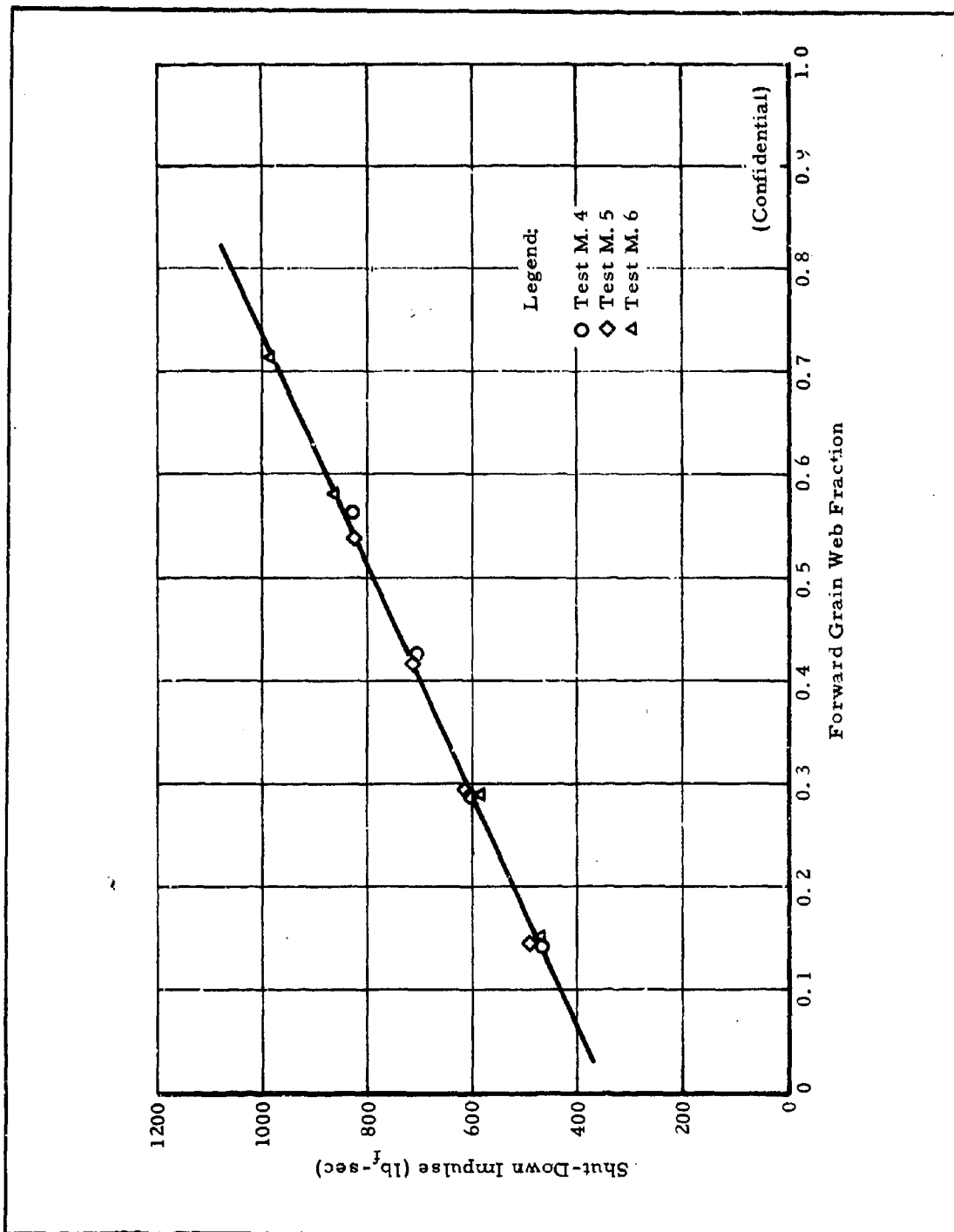


Figure 140 - Shut-Down Impulse as a Function of Web Fraction Consumed for Tests M. 4, M. 5, and M. 6

**CONFIDENTIAL**

The reduced data for M. 6. 5 are given in Table LV. Levels 1 and 2 represent steady-state periods of motor operation, whereas level 3 gives point values of thrust and pressures just prior to motor termination. A sea-level thrust range of 14.2 to 1 was measured, which corresponds to a vacuum thrust range of approximately 8.8 to 1. This latter range is questionable, however, since the corrections to vacuum involve aft-chamber pressure, which was erroneous. (Confidential)

#### 9. PYROGEN VACUUM IGNITION TESTS (TEST SERIES K)

In preparation for Tests M. 7 and M. 8, which were conducted under altitude condition, pyrogen vacuum ignition tests were conducted in order to ascertain the effect of vacuum conditioning and ignition on pyrogen operation. Pyrogens containing PPO-13 propellant were conditioned at 0.5 mm Hg pressure for various times and then ignited in vacuo. Nozzle closures were not used.

The pressure-time traces for the six pyrogens conditioned in a vacuum for 0, 2.25, 3.25, 4.25, 5.25, and 6.25 hours are shown in Figure 141. The traces show no effect of vacuum conditioning. The rate of pressurization was slightly less for the pyrogen that was not vacuum conditioned, but there was no trend for the pressurization rate of the others. All traces exhibited long tail-offs, which is probably attributable to grain slivers.

From these tests, it is concluded that the PPO-13 nitroplastic propellant used in the pyrogens and forward chambers of the Series M motors will not be appreciably affected by vacuum conditioning up to six hours, the maximum anticipated exposure time for Tests M. 7 and M. 8. (Confidential)

#### 10. TEST M. 7

##### a. Motor Configuration

Tests M. 7 and M. 8 were conducted in an altitude chamber at the Navy's Ordnance Aerophysics Laboratory (OAL), Daingerfield, Texas. The motors for these tests were identical to those used in Tests M. 4 through M. 6, except for the nozzle; a vacuum nozzle with a 20-to-1 expansion ratio, designed and fabricated by TRW, was used for Tests M. 7 and M. 8 instead of a sea-level nozzle. See Figure 125 and Table XLVII.

TABLE LV- REDUCED BALLISTIC DATA FOR THROTTLING  
CYCLE OF TEST M. 6

Parameter	Value
Level 1	
Steady-state time (sec)	0.300
Forward-chamber pressure (psia)	505.7*
Aft-chamber pressure (psia)	119.4*
Thrust, measured (lb <sub>f</sub> )	1529
C <sub>f</sub> , theoretical (measured conditions)	1.237
C <sub>f</sub> , theoretical (vacuum, $\epsilon = 20/1$ )	1.810
Thrust (vacuum, $\epsilon = 20/1$ ) (lb <sub>f</sub> )	2235
Level 2	
Steady-state time (sec)	1.000
Forward-chamber pressure (psia)	91.7*
Aft-chamber pressure (psia)	45.7*
Thrust, measured (lb <sub>f</sub> )	429
C <sub>f</sub> , theoretical (measured conditions)	0.866
Thrust (vacuum, $\epsilon = 20/1$ ) (lb <sub>f</sub> )	896
Level 3	
Forward-chamber pressure (psia)	4264*
Aft-chamber pressure (psia)	421*
Thrust, measured (lb <sub>f</sub> )	6088
C <sub>f</sub> , theoretical (measured conditions)	1.401
Thrust (vacuum, $\epsilon = 20/1$ ) (lb <sub>f</sub> )	7860

\* Pressure measurements in error due to location of transducer port in head end of aft chamber, hence measured C<sub>f</sub> and Characteristic Velocity not obtainable.

(Confidential)

# CONFIDENTIAL

AFRPL-TR-65-209, Vol I

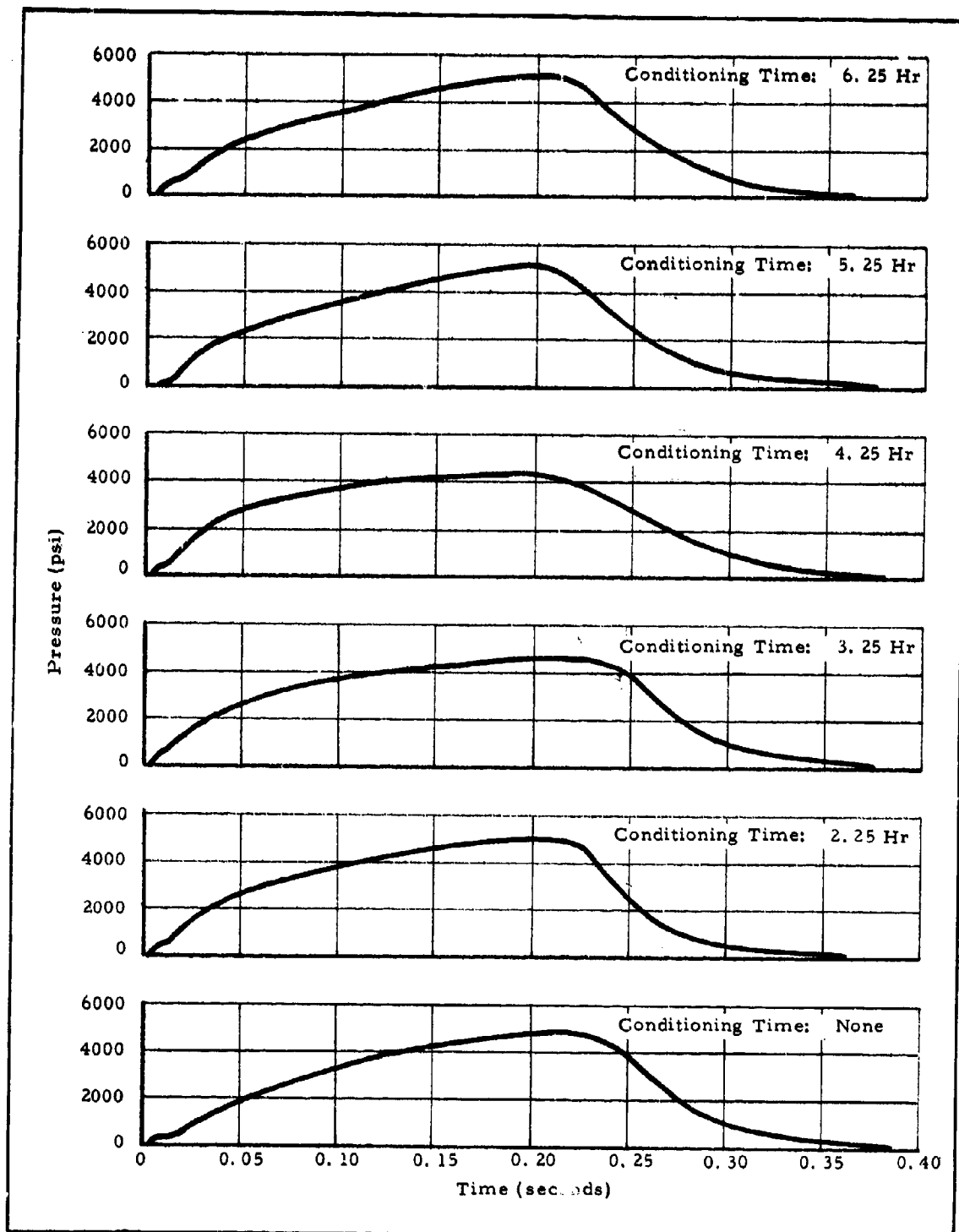


Figure 141 - Pressure-Time Traces for Pyrogen Vacuum Ignition Tests

-236-

# CONFIDENTIAL

# CONFIDENTIAL

AFRPL-TR-65-209, Vol I

b. Test Program and Test Conditions

Test M.7 was programmed over the same duty cycles (four pulse cycles and one throttling cycle) as Test M.6 (see paragraph 8, above). The nitrogen purge was not used in these two altitude chamber tests since reignition caused by residual gases in the motor following termination should not occur due to the low pressure at the chamber altitude of 60,000 ft.

The motor for Test M.7 is shown mounted in the altitude test chamber in Figure 142. Before the motor was fired, the test cell was inadvertently flooded with water, partially filling the motor. The motor was drained and dried before firing and appeared to be in normal condition; however, this flooding did adversely affect performance as discussed in c, below.

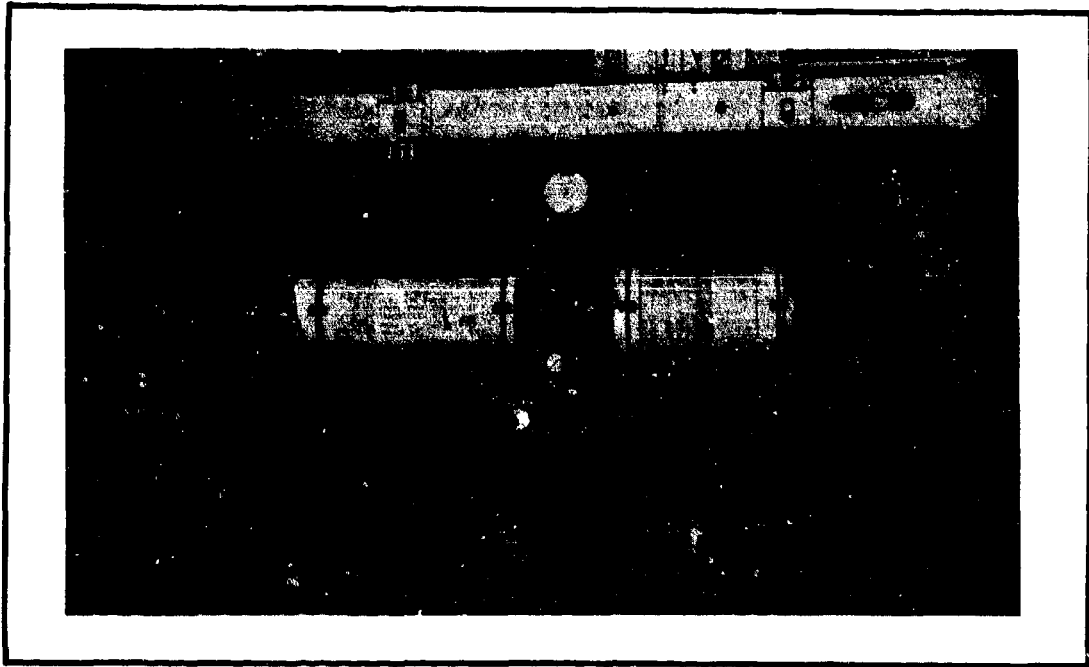


Figure 142 - Motor for Test M.7 Mounted in Altitude Chamber at OAL

-237-

# CONFIDENTIAL

**c. Test Results**

This test was conducted on 15 July 1965. The motor terminated permanently without the nitrogen purge after each pulse cycle. The pressure-and thrust-time traces are shown in Figure 143.

A comparison of the traces for this test (Figure 143) and those for Test M. 6 (Figures 137, 138 and 139) reveal two apparent differences. First, the forward-chamber pressure for M. 7 did not stabilize as quickly at the desired 3000-psi value for the four pulse cycles as it did in Test M. 6. This was particularly true for the first pulse cycle, M. 7. 1, where forward-chamber pressure showed a rapid ramp decrease following the ignition pressure rise. The second difference was the erratic behavior of aft-chamber pressure, particularly during the third and fourth pulse cycles and the throttling cycle. Also, aft-chamber pressure was slightly higher than normal during M. 7. (Confidential)

The second peculiarity, the erratic behavior of aft-chamber pressure (Figure 143), is believed to have been caused by the moisture that entered the motor when the chamber was flooded. The moisture apparently saturated the Kel-F/sodium chloride inhibitor on the aft grain O. D. It was obvious after the test that a large amount of the inhibitor was lost during firing (see Figures 144 and 145), thus permitting the aft grain outside diameter to burn in areas between the grain and inhibitor. This effect increased the aft-grain surface area, which accounts for the higher-than normal aft-chamber pressure. Erratic aft pressure spikes resulting from inhibitor failure have been observed previously in subscale motor tests (Reference 4).

The reduced ballistic data for the four pulse cycles of Test M. 7 are given in Table LVI. These data compare favorably with those obtained in Tests M. 4 and M. 5, which were identical tests conducted under sea-level conditions, except that the aft propellant weight burned in Test M. 7 was 14 percent higher than in Test M. 4 and 18 percent higher than in Test M. 5. This increase cannot be attributed to the slightly higher aft-chamber pressures in Test M. 7 since the aft pressure integral of Test M. 4 actually exceeded that of M. 7 due to the slightly longer operating times for M. 4 (note that the integrals of Tests M. 4 and M. 5 are given in psig-sec, whereas those for M. 7 and M. 8 are in psia-sec, which correspond to the integrals that the motor actually produced in both cases). (Confidential)

**CONFIDENTIAL**

AFRPL-TR-65-209, Vol I

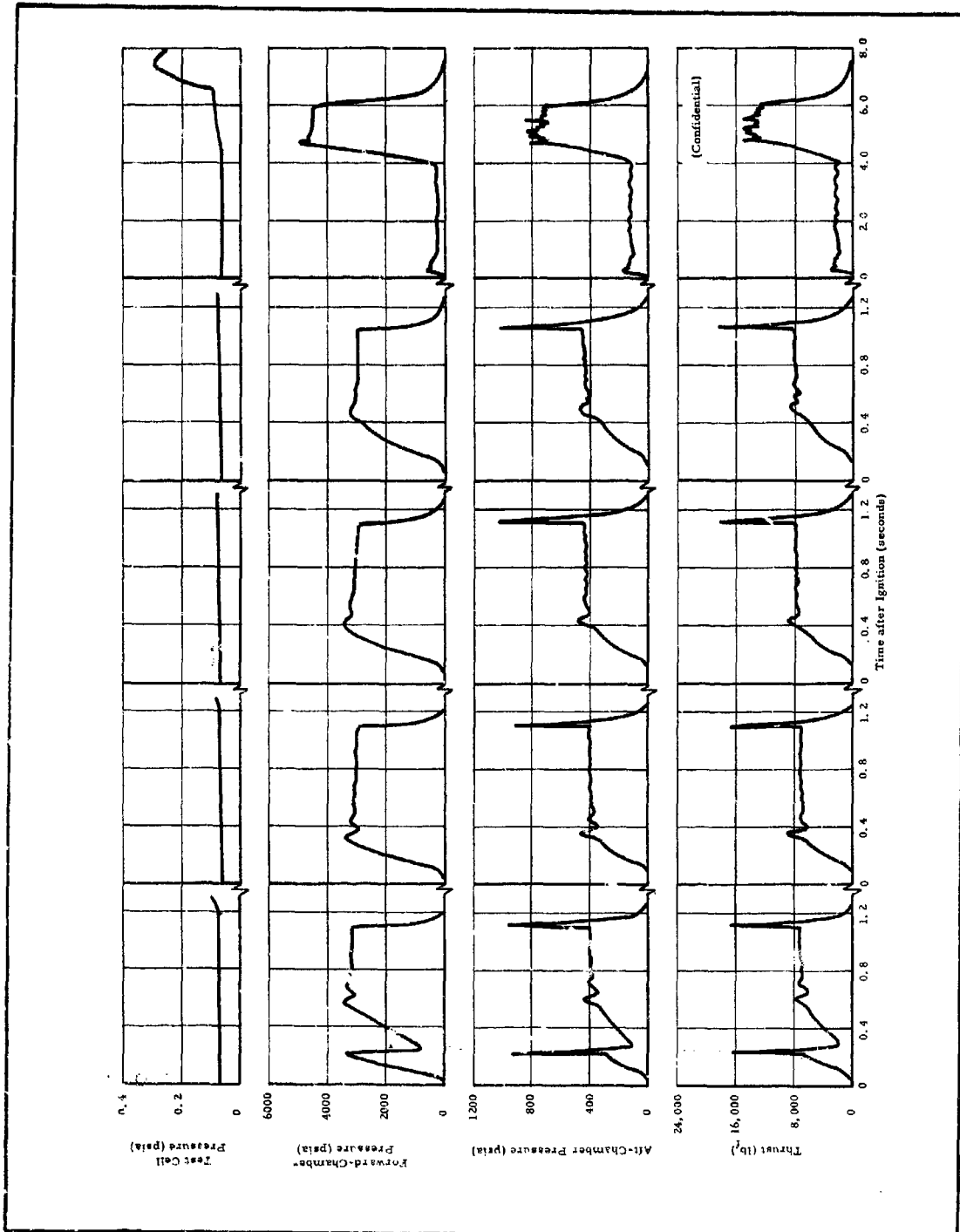


Figure 143 - Pressure and Thrust-Time Traces for Test M. 7

**CONFIDENTIAL**

**CONFIDENTIAL**

AFRPL-TR-65-209, Vol I

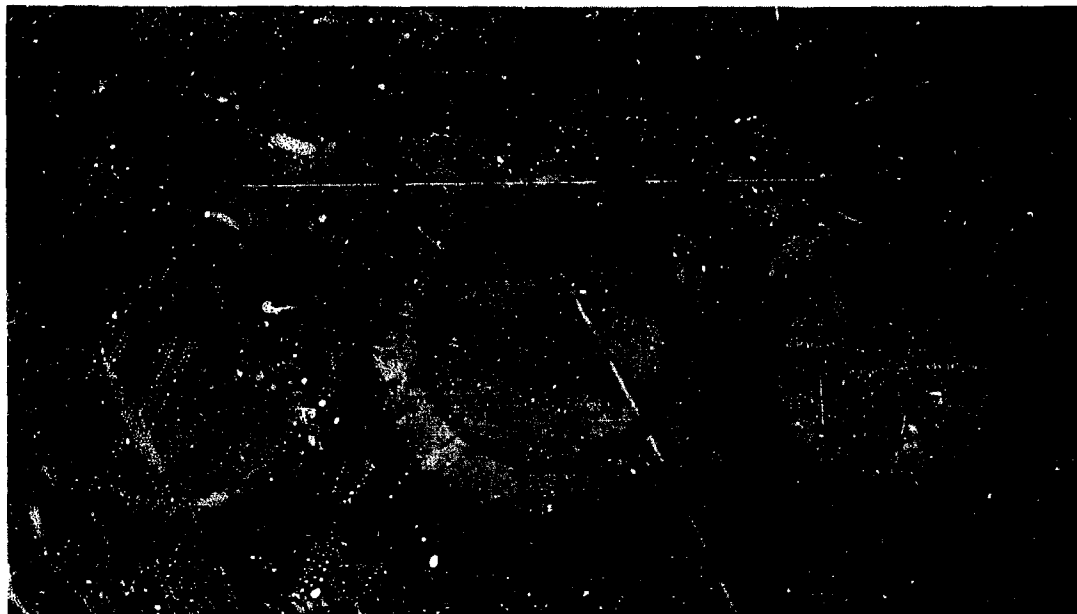


Figure 144 - End View of Aft Grains after Test M. 7

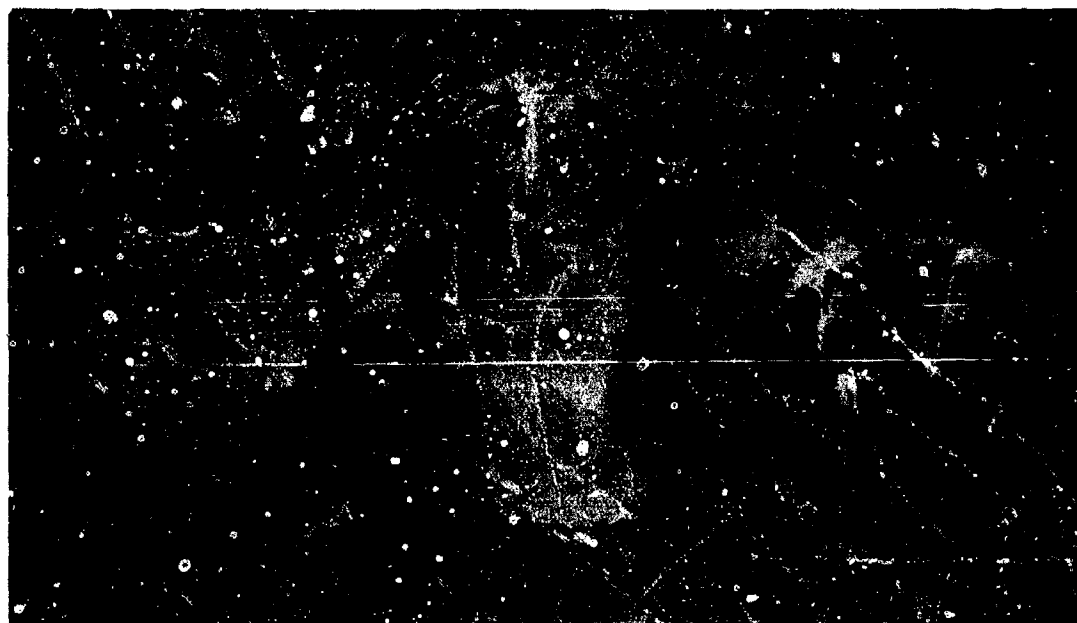


Figure 145 - Three-Quarter Side View of Aft Grains after Test M. 7

-240-

**CONFIDENTIAL**

# CONFIDENTIAL

AFRPL-TR-65-209, Vol I

TABLE LVI - REDUCED BALLISTIC DATA FOR PULSE CYCLES OF TEST M.7

Parameter	Test Number				Total
	M. 7. 1	M. 7. 2	M. 7. 3	M. 7. 4	
<b>Forward Chamber</b>					
Delay time, 0 to 10% (sec)	0.0720	0.1080	0.1332	0.1440	...
Rise time, 10 to 90% (sec)	0.1224	0.1692	0.2088	0.2520	...
Burn time (sec)	1.0332	0.9792	0.9684	0.8964	3.8772
Decay time, 100 to 10% (sec)	0.0668	0.0792	0.0974	0.1056	...
$\int P dt_p$ (psia-sec)	2,840	2,934	2,877	2,563	11,214
$\bar{P}_b$ (psia)	2,655	2,869	2,835	2,708	2,778
$\bar{P}_k$ (psia)	3,202	3,093	3,099	3,024	...
$P_{term}$ (psia)	3,150	3,031	3,007	2,983	...
$dp/dt_{term}$ (psia/sec)	115,000	103,000	82,000	75,000	...
Weight burned (lb)					
Grain	10.44	15.50	18.32	16.68	60.94
Pyrogens	0.77	0.77	0.76	0.77	3.07
<b>Aft Chamber</b>					
Delay time, 0 to 10% (sec)	0.0936	0.1512	0.1836	0.1980	...
Rise time, 10 to 90% (sec)	0.1152	0.1872	0.2268	0.2700	...
Burn time (sec)	1.0872	1.0404	1.0404	0.9792	4.1472
$\int P dt_p$ (psia-sec)	367	396	423	390	1576
$\bar{P}_b$ (psia)	324	368	393	378	365
$\bar{P}_k$ (psia)	384	395	433	436	...
$P_{prior}$ to termination (psia)	395	395	435	455	...
$P_{maximum}$ at termination (psia)	1,010	972	1,030	1,053	...
$dp/dt$ (psia/sec)	22,000	16,000	19,000	18,000	...
Weight burned (lb)	9.31	15.06	16.10	13.87	54.34
<b>Total Motor</b>					
Weight burned (lb)*	20.52	31.33	35.18	31.32	118.35
Weight <sub>aft</sub> /weight <sub>fwd</sub>	0.83	0.93	0.84	0.80	0.85
$\int F dt_f$ (lb <sub>f</sub> -sec)	6,460	7,125	7,551	7,053	28,189
$\bar{F}_b$ (lb <sub>f</sub> )	5,775	6,617	7,015	5,851	6,315
$\bar{F}_k$ (lb <sub>f</sub> )	6,878	7,114	7,735	6,084	...
$\int F at_{term}$ (lb <sub>f</sub> -sec)	55	55	86	125	...
Throat area (sq in.)	10.00	9.99	10.00	10.00	10.00
Expansion Ratio, $A_e/A_t$	19.9	19.9	19.9	19.9	19.9
$I_{sp_{meas}}$ (lb <sub>f</sub> -sec/lb <sub>m</sub> )	315.0	227.5	214.6	225.2	237.8
$C_{f_{meas}}$	1.759	1.801	1.786	1.809	1.789
Characteristic velocity (fps)	5,740	4,059	3,865	4,004	4,270

\* Includes weight of insulation and inhibitor expelled during test.

(Confidential)

The higher value for aft weight burned during M. 7 can, however, be explained on the basis of the amount of salt inhibitor expelled during the test. A quantitative value for the weight of expelled salt could not be obtained. However, more than 50 lb of inhibitor was used on these grains, and from Figures 144 and 145, it is evident that a considerable portion of this amount was lost. Hence, it is reasonable to assume that this accounts for the excessive weight consumed and the corresponding low measured specific impulse and characteristic velocity values. The measured thrust coefficient, 1.789, is 99 percent of the theoretical value of 1.805. (Confidential)

The reduced ballistic data for the throttling cycle, M. 7. 5, are given in Table LVII. In this cycle the forward motor was ignited at 500 psi, with a ramp decrease after 0.5 sec to 280 psi. At 4.0 sec, forward-chamber pressure was ramp increased to 4500 psi and remained at this pressure until the forward web burned out. Again, low specific impulse and characteristic velocity values were observed, which are also attributed to the salt inhibitor being expelled during the test. A thrust ratio of 6.1 to 1 was obtained in M. 7. 5, with a 16 to-1 forward-chamber pressure ratio attained between steady-state levels 2 and 3. (Confidential)

11. TEST M. 8

a. Motor Configuration

The motor for Test M. 8 was identical to that used for Test M. 7 (see Figure 125 and Table XLVII).

b. Test Program and Test Conditions

Test M. 8 was similar to Test M. 7 (four pulse and one throttling cycle), except that nonlinear compensation was not used until the throttling cycle, M. 8. 5. For this cycle, the nonlinear element was modified to prevent a recurrence of the control instability experienced in Test M. 7. 1.

c. Test Results

The pressure- and thrust-time traces for M. 8 are presented in Figure 146. Again, the motor was terminated after the four

# CONFIDENTIAL

AFRPL-TR-65-209, Vol I

TABLE LVII- REDUCED BALLISTIC DATA FOR  
THROTTLING CYCLE OF TEST M. 7

Parameter	Value
<b>Level 1</b>	
Steady-state time (sec)	0.1116
Forward-chamber pressure (psia)	531.7
Aft-chamber pressure (psia)	136.8
Thrust (lb <sub>f</sub> )	2,439
<b>Level 2</b>	
Steady-state time (sec)	3.0277
Forward-chamber pressure (psia)	278.9
Aft-chamber pressure (psia)	121.9
Thrust (lb <sub>f</sub> )	2170
<b>Level 3</b>	
Steady-state time (sec)	0.9072
Forward-chamber pressure (psia)	4,488.6
Aft-chamber pressure (psia)	739.0
Thrust (lb <sub>f</sub> )	13,180
<b>Total Firing</b>	
<b>Forward Chamber</b>	
$\int Pdt_p$ (psia-sec)	10,200
Total time (sec)	8.1720
Weight burned (lb)	
Grain	56.74
Pyrogens	0.38
<b>Aft Chamber</b>	
$\int Pdt_p$ (psia-sec)	1,833
Total time (sec)	8.1720
Weight burned (lb)	87.63
<b>Total Motor</b>	
Weight burned (lb)*	144.75
Weight <sub>aft</sub> /weight <sub>fwd</sub>	1.53
Characteristic velocity (fps)	4078
$\int Fdt_f$ (lb <sub>f</sub> -sec)	32,671
Throat area (sq in.)	10.01
Expansion ratio, $A_e/A_t$	19.8
$C_{f_{meas}}$	1.781
$I_{sp_{meas}}$ (lb <sub>f</sub> -sec/lb <sub>m</sub> )	225.7

\* Includes weight of insulation and inhibitor expelled.

(Confidential)

# CONFIDENTIAL

pulse cycles without reignition. Control stability was greatly improved in this test.

The instability evident in the throttling cycle of this test (Figure 146) during the ramp from 500 to 1000 psi and at 4500 psi is believed to be due to faulty operation of the position loop portion of the control system since these oscillations are of very low frequency. The position loop includes the servovalves, the hydraulic supply, and the position potentiometer. (Confidential)

The aft-chamber pressure in this test was not erratic, as it was in Test M. 7, which substantiates the belief that the erratic behavior for M. 7 was due to the water that saturated the motor before firing. It was evident, after this test, that the grain O. D. was successfully inhibited throughout the test, with no burning on the grain O. D., although some salt inhibitor was expelled, as shown in Figures 147 and 148.

The reduced ballistic data for Test M. 8 are summarized in Tables LVIII and LIX. The aft propellant weights burned during this test are much more reasonable than those of Test M. 7. The aft-to-forward weight ratio,<sup>9</sup> for the four pulse cycles of M. 8 was 0.72, which was only slightly higher than the 0.70 measured for similar cycles in Tests M. 4 and M. 5. The specific impulse measured during these four pulse cycles varied appreciably from pulse to pulse, ranging from 230 to 256 lb-sec/lb, and averaged less than that for Tests M. 4 and M. 5. Again, these differences may be due to the salt inhibitor lost in this test. The measured thrust coefficient for the pulse cycles was 1.789, which is 99 percent of theoretical. (Confidential)

A 9-to-1 throttling ratio was obtained in the fifth cycle, between the second and third steady-state levels. (Confidential)

**CONFIDENTIAL**

AFRPL-TR-65-209, Vol I

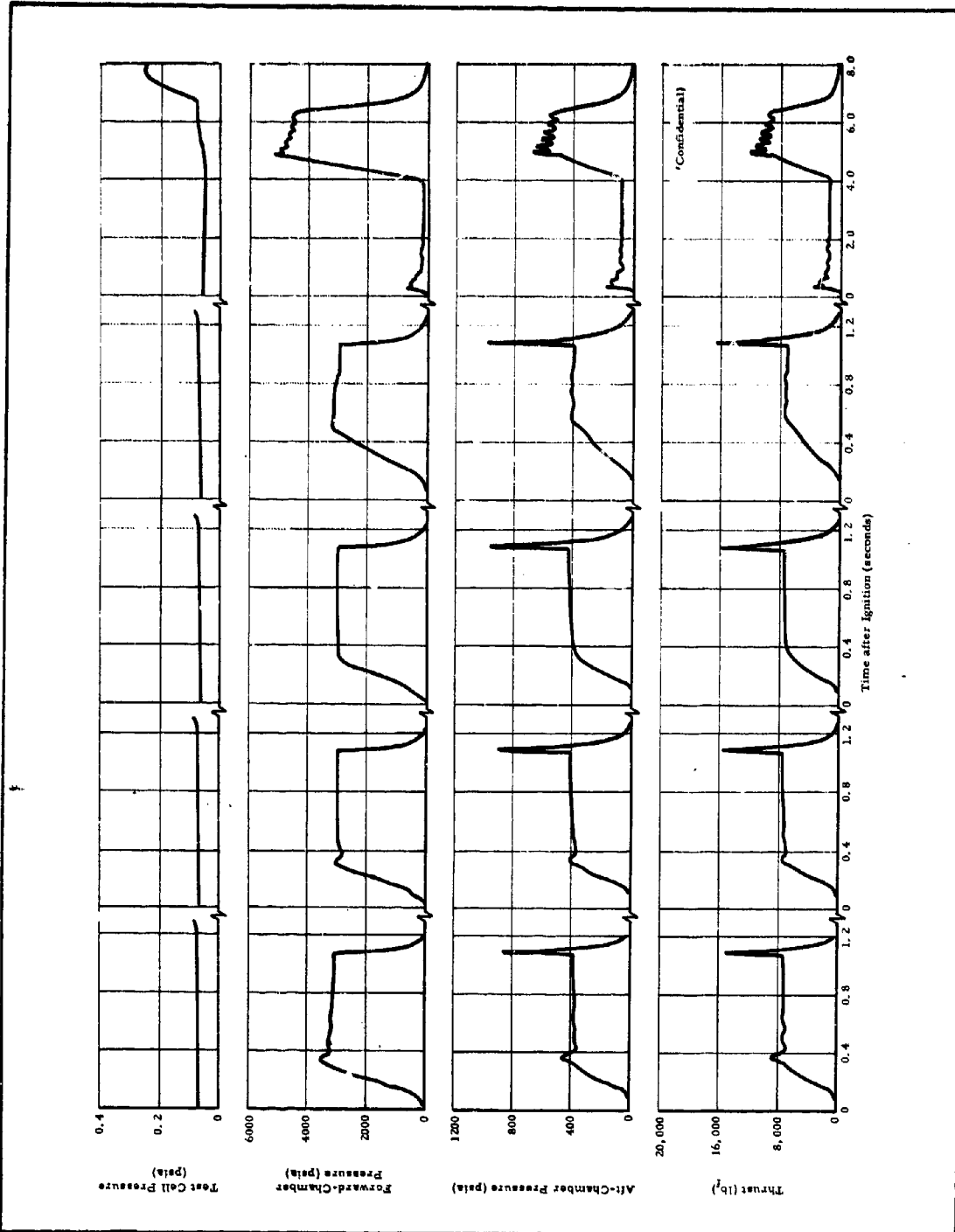


Figure 146 - Pressure and Thrust-Time Traces for Test M. 8

**CONFIDENTIAL**

**CONFIDENTIAL**

AFRPL-TR-65-209, Vol I



Figure 147 - End View of Aft Grains after Test M. 8

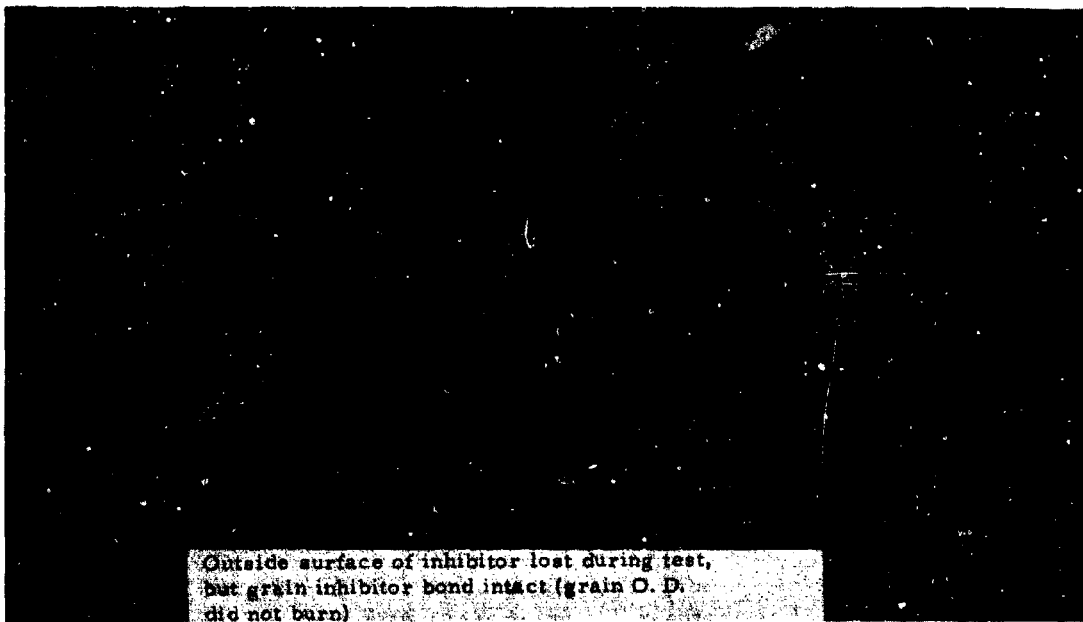


Figure 148 - Three-Quarter Side View of Aft Grains after Test M. 8

-246-

**CONFIDENTIAL**

# CONFIDENTIAL

AFRPL-TR-65-209, Vol I

TABLE LVIII- REDUCED BALLISTIC DATA FOR PULSE CYCLES OF TEST M. 8

Parameter	Test Number				Total
	M. 8. 1	M. 8. 2	M. 8. 3	M. 8. 4	
<b>Forward Chamber</b>					
Delay time, 0 to 10% (sec)	0. 1152	0. 1044	0. 0936	0. 1656	. . .
Rise time, 10 to 90% (sec)	0. 1800	0. 1476	0. 1764	0. 2808	. . .
Burn time (sec)	0. 9648	0. 9648	0. 9684	0. 8928	3. 7908
Decay time, 100 to 10% (sec)	0. 0700	0. 0756	0. 0916	0. 1044	. . .
$\int Pdt_p$ (psia-sec)	2, 882	2, 786	2, 784	2, 494	10, 946
$\bar{P}_b$ (psia)	2, 892	2, 776	2, 748	2, 641	2, 766
$\bar{P}_k$ (psia)	3, 110	3, 030	3, 048	3, 093	. . .
$P_{term}$ (psia)	3, 082	3, 053	3, 063	2, 951	. . .
$dp/dt$ (psia/sec)	113, 000	88, 000	65, 000	65, 000	. . .
Weight burned (lb)					
Grain	15. 97	14. 40	16. 39	13. 86	60. 62
Pyrogens	0. 77	0. 77	0. 76	0. 77	3. 07
<b>Aft Chamber</b>					
Delay time, 0 to 10% (sec)	0. 1548	0. 1440	0. 1440	0. 2232	. . .
Rise time, 10 to 90% (sec)	0. 1836	0. 1476	0. 1728	0. 2880	. . .
Burn time (sec)	1. 0080	1. 0296	1. 0404	0. 9684	4. 0464
$\int Pdt_p$ (psia-sec)	361	378	396	351	1486
$\bar{P}_b$ (psia)	348	356	367	343	354
$\bar{P}_k$ (psia)	371	387	405	405	. . .
$P_{prior}$ to termination (psia)	385	404	419	400	. . .
$P_{max}$ at termination (psia)	1, 010	972	1, 030	1, 053	. . .
$dp/dt$ (psia/sec)	23, 000	28, 000	23, 000	15, 000	. . .
Weight burned (lb)	11. 53	11. 29	12. 29	10. 53	45. 64
<b>Total Motor</b>					
Weight burned (lb)	28. 27	26. 46	29. 44	25. 16	109. 33
Weight <sub>aft</sub> /weight <sub> fwd</sub>	0. 69	0. 74	0. 72	0. 72	0. 72
$\int Fdt_f$ (lb <sub>f</sub> -sec)	6, 495	6, 777	7, 052	6, 214	26, 538
$\bar{F}_b$ (lb <sub>f</sub> )	6, 252	6, 323	6, 507	6, 039	6, 285
$\bar{F}_k$ (lb <sub>f</sub> )	6, 671	6, 896	7, 195	7, 150	. . .
$\int Fdt_{term}$ (lb <sub>f</sub> -sec)	49	110	111	112	. . .
Throat area (sq in.)	9. 90	9. 94	9. 98	9. 99	9. 95
Expansion ratio, $A_e/A_t$	20. 0	19. 8	19. 7	19. 8	19. 8
$I_{sp_{meas}}$ (lb <sub>f</sub> -sec/lb <sub>m</sub> )	229. 7	256. 1	239. 4	247. 0	242. 7
$C_{f_{meas}}$	1. 817	1. 802	1. 785	1. 771	1. 789
Characteristic velocity (fps)	4, 069	4, 574	4, 316	4, 486	4, 351

Confidential)

# CONFIDENTIAL

AFRPL-TR-65-209, Vol I

TABLE LIX - REDUCED BALLISTIC DATA FOR  
THROTTLING CYCLE OF TEST M. 8

Parameter	Value
Level 1	
Steady-state time (sec)	0.3312 to 0.4392
Forward-chamber pressure (psia)	576.1
Aft-chamber pressure (psia)	146.2
Thrust (lb <sub>f</sub> )	2,565
Level 2	
Steady-state time (sec)	3.7368 to 3.9168
Forward-chamber pressure (psia)	106.5
Aft-chamber pressure (psia)	67.0
Thrust (lb <sub>f</sub> )	1,176
Level 3	
Steady-state time (sec)	0.2016
Forward-chamber pressure (psia)	4,861
Aft-chamber pressure (psia)	604
Thrust (lb <sub>f</sub> )	10,600
Total Firing	
Forward Chamber	
$\int Pdt_p$ (psia-sec)	11,300
Total time (sec)	8.1792
Weight burned (lb)	
Grain	59.96
Pyrogens	0.38
Aft Chamber	
$\int Pdt_p$ (psia-sec)	1,564
Total time (sec)	8.1792
Weight burned (lb)	57.81
Total Motor	
Weight burned (lb)	118.15
Weight <sub>aft</sub> /weight <sub>fwd</sub>	0.96
Characteristic velocity (fps)	4,271
$\int Fdt_f$ (lb <sub>f</sub> -sec)	27,542
Throat area (sq in.)	10.03
Expansion ratio, $A_e/A_t$	19.7
$C_f$ <sub>meas</sub>	1.756
$I_{sp}$ <sub>meas</sub> (lb <sub>f</sub> -sec/lb <sub>m</sub> )	233.1

(Confidential)

# CONFIDENTIAL

## 12. DATA REDUCTION PARAMETERS \*

a. General

Data reduction parameters for the DCCSR are presented in the subsequent paragraphs. They are arranged in sequence, beginning with the forward-chamber parameters, aft-chamber parameters, thrust, and finally over-all motor performance parameters. Each parameter is defined, and the units in which it is expressed and its symbol are given. The representative pressure-time and thrust-time traces given in Figure 149 show the parameters graphically. The methods by which the measured parameters are corrected for vacuum, standard, and theoretical conditions are presented in f, below.

b. Forward-Chamber Parameters

The forward-chamber ballistic parameters are listed below, and shown graphically in Figure 149.

<u>Parameter</u>	<u>Units</u>	<u>Symbol</u>	<u>Definition</u>
Zero time	sec	$t_o$	Time at initial departure of ignition signal from its base line
Ignition delay time	sec	$t_{dp}$	Time interval from zero time to 10% $P_i$
Ignition rise time	sec	$t_{rp}$	Time interval from 10% $P_i$ to 90% $P_i$
Burn time	sec	$t_{bp}$	Time interval from 10% $P_i$ to start of termination transient on the pressure-time trace
Steady-state time	sec	$t_{Kp}$	Time interval from end of ignition transient (selected from trace) to end of burn time
Total time	sec	$t_p$	Time interval from zero to zero on the pressure-time trace

\* Additional symbols are listed on page xxxi.

# CONFIDENTIAL

AFRPL-TR-65-209, Vol I

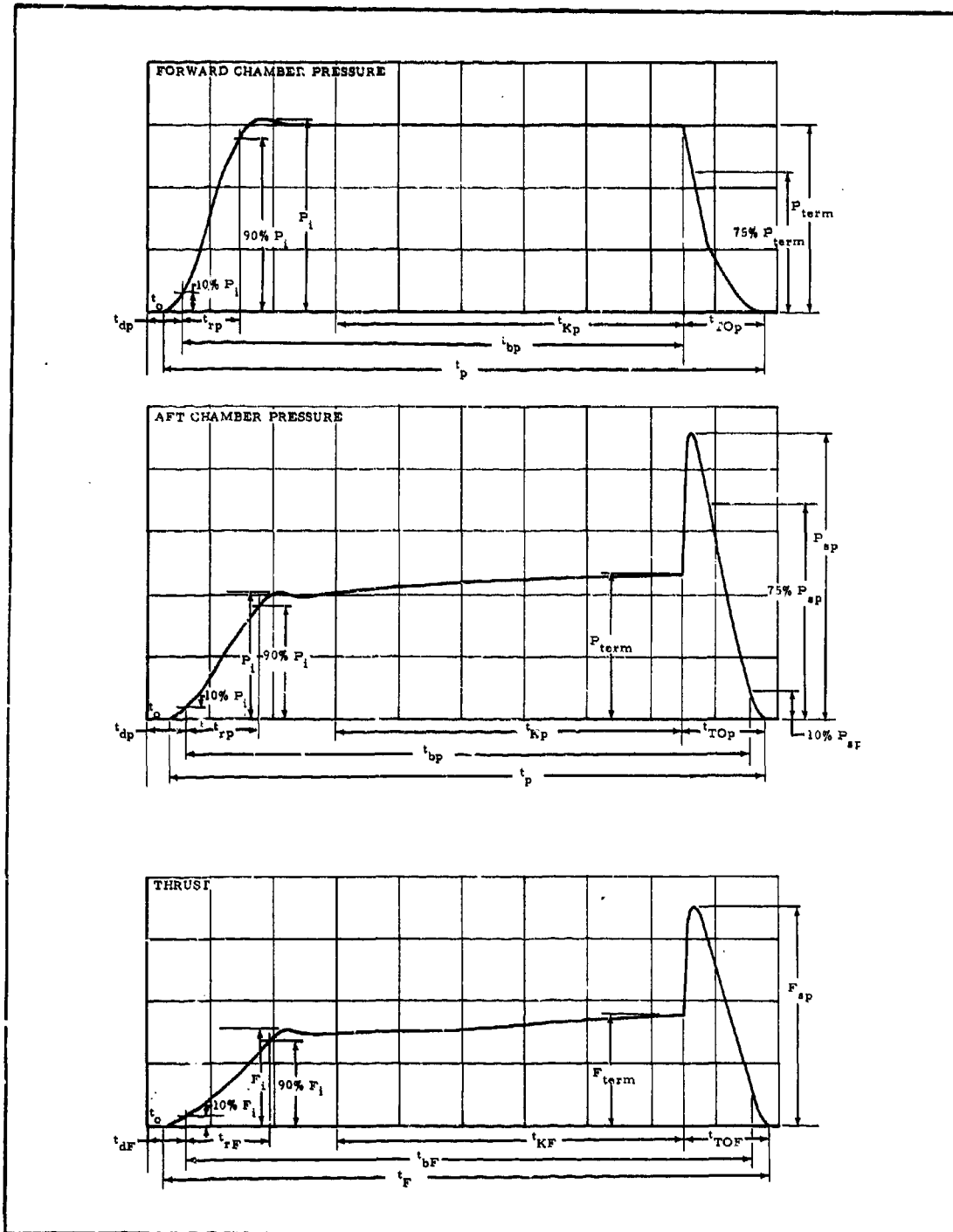


Figure 149 - Representative DCCSR Pressure and Thrust-Time Traces

<u>Parameter</u>	<u>Units</u>	<u>Symbol</u>	<u>Definition</u>
Tail-off time	sec	$t_{TOp}$	Time interval from start of termination transient to 10% $P_{term}$ on the pressure-time trace
Ignition pressure	psia	$P_i$	Maximum pressure that occurs during the ignition transient
Maximum pressure	psia	$P_{max}$	Maximum pressure that occurs over steady-state time
Termination pressure	psia	$P_{term}$	Value of pressure at the end of burn time
Decay rate	psi/sec	$\dot{P}$	Slope (dp/dt) of a line tangent to the pressure-time trace at 75% $P_{term}$
Web burned	in.	$Web_b$	(Final port diameter - initial port diameter)/2
Average burn rate	in./sec	$\bar{r}_b$	$\frac{Web_b}{t_{bp}}$
Burn integral	psig-sec	...	$\int P dt_{bp}$
Steady-state integral	psig-sec	...	$\int P dt_{Kp}$
Total integral	psig-sec	...	$\int P dt_p$
Tail-off integral	psig-sec	...	$\int P dt_{TOp}$
Average burn pressure	psia	$\bar{P}_b$	$\frac{1}{t_{bp}} \int P dt_{bp}$
Average steady-state pressure	psia	$\bar{P}_K$	$\frac{1}{t_{Kp}} \int P dt_{Kp}$
Average pressure (total time)	psia	$\bar{P}_p$	$\frac{1}{t_p} \int P dt_p$
Propellant weight burned	lb <sub>m</sub>	$W_{bpf}$	Initial weight-final weight

<u>Parameter</u>	<u>Units</u>	<u>Symbol</u>	<u>Definition</u>
Ignition weight loaded	lb <sub>m</sub>	W <sub>bi</sub>	Ignition weight loaded
Total weight consumed	lb <sub>m</sub>	W <sub>bf</sub>	W <sub>bpf</sub> + W <sub>bi</sub>
Forward mass flow rate	lb <sub>m</sub> /sec	m <sub>f</sub>	$\frac{W_{bf}}{t_{bp}} \int \frac{P dt_{bp}}{P dt_p}$
Average throat area	in. <sup>2</sup>	A <sub>tf</sub>	$\frac{1}{t_{Kp}} \int A dt_{Kp}$ (from valve position trace)
Discharge coefficient	lb <sub>m</sub> /lb <sub>f</sub> -sec	C <sub>D</sub>	$\frac{W_{bf}}{A_{tf}} \int P dt_p$
Characteristic velocity	ft/sec	C*	$\frac{g_c}{C_D}$
C* Efficiency	%	η <sub>C*</sub>	$\left[ \frac{C^*(\text{measured})}{C^*(\text{theoretical})} \right] (100)$

c. Aft-Chamber Parameters

The aft-chamber ballistic parameters are listed below, and shown graphically in Figure 149.

<u>Parameter</u>	<u>Units</u>	<u>Symbol</u>	<u>Definition</u>
Zero time	sec	t <sub>o</sub>	Time at initial departure of ignition signal from its base line
Ignition delay time	sec	t <sub>dp</sub>	Time interval from zero time to 10% P <sub>i</sub>
Ignition rise time	sec	t <sub>rp</sub>	Time interval from 10% P <sub>i</sub> to 90% P <sub>i</sub>
Burn time	sec	t <sub>bp</sub>	Time interval from 10% P <sub>i</sub> to 10% P <sub>sp</sub>

<u>Parameter</u>	<u>Units</u>	<u>Symbol</u>	<u>Definition</u>
Steady-state time	sec	$t_{Kp}$	Time interval from end of ignition transient (selected from trace) to end of burn time
Total time	sec	$t_p$	Time interval from zero to zero on the pressure-time trace
Tail-off time	sec	$t_{TOp}$	Time interval from start of termination transient to 10% $P_{sp}$ on the pressure-time trace
Ignition pressure	psia	$P_i$	Maximum pressure that occurs during the ignition transient
Maximum pressure	psia	$P_{max}$	Maximum pressure that occurs over steady-state time
Termination pressure	psia	$P_{term}$	Value of pressure at the end of burn time
Pressure spike	psia	$P_{sp}$	Maximum pressure that occurs during tail-off time
Decay rate	psi/sec	$\dot{P}$	Slope (dp/dt) of a line tangent to the pressure-time trace at 75% $P_{sp}$
Web burned	in.	$Web_b$	(Final port diameter - initial port diameter)/2
Average burn rate	in./sec	$\bar{r}_b$	$\frac{Web_b}{t_{bp}}$
Burn integral	psig-sec	...	$\int P dt_{bp}$
Steady-state integral	psig-sec	...	$\int P dt_{Kp}$
Total integral	psig-sec	...	$\int P dt_p$
Tail integral	psig-sec	...	$\int P dt_{TOp}$
Average burn pressure	psia	$\bar{P}_b$	$\frac{1}{t_{bp}} \int P dt_{bp}$

<u>Parameter</u>	<u>Units</u>	<u>Symbol</u>	<u>Definition</u>
Average steady state pressure	psia	$\bar{P}_K$	$\frac{1}{t_{Kp}} \int P dt_{Kp}$
Average pressure (total time)	psia	$\bar{P}_p$	$\int P dt_p$
Propellant weight burned	lb <sub>m</sub>	$W_{bpa}$	Initial weight - final weight
Aft mass flow rate	lb <sub>m</sub> /sec	$\dot{m}_a$	$\frac{W_{bpa}}{t_{bp}} \int \frac{P dt_{bp}}{P dt_p}$

d. Thrust Parameters

Thrust parameters are shown graphically in Figure 149. and defined below.

<u>Parameter</u>	<u>Units</u>	<u>Symbol</u>	<u>Definition</u>
Zero time	sec	$t_o$	Time at initial departure of ignition signal from its base line
Ignition delay time	sec	$t_{dF}$	Time interval from zero time to 10% $F_i$
Ignition rise time	sec	$t_{rF}$	Time interval from 10% $F_i$ to 90% $F_i$
Burn time	sec	$t_{bF}$	Time interval from 10% $F_i$ to 10% $F_{sp}$ on the thrust-time trace
Steady-state time	sec	$t_{KF}$	Time interval from end of ignition transient (selected from trace) to end of burn time on the thrust-time trace
Total time	sec	$t_F$	Time interval from zero to zero on the thrust-time trace
Tail-off time	sec	$t_{TOF}$	Time interval from start of termination transient to final zero on the thrust-time trace
Ignition thrust	lb <sub>f</sub>	$F_i$	Maximum thrust that occurs during the ignition transient

<u>Parameter</u>	<u>Units</u>	<u>Symbol</u>	<u>Definition</u>
Maximum thrust	lb <sub>f</sub>	F <sub>max</sub>	Maximum thrust that occurs over steady-state time
Termination thrust	lb <sub>f</sub>	F <sub>term</sub>	Value of thrust at the end of burn time
Thrust spike	lb <sub>f</sub>	F <sub>sp</sub>	Maximum thrust that occurs during tail-off time
Burn integral	lb <sub>f</sub> -sec	...	$\int F dt_{bF}$
Steady-state integral	lb <sub>f</sub> -sec	...	$\int F dt_{KF}$
Total integral	lb <sub>f</sub> -sec	...	$\int F dt_F$
Average burn thrust	lb <sub>f</sub>	...	$\frac{1}{t_{bF}} \int F dt_{bF}$
Average steady-state thrust	lb <sub>f</sub>	$\bar{F}_K$	$\frac{1}{t_{KF}} \int F dt_{KF}$
Average total thrust	lb <sub>f</sub>	$\bar{F}_F$	$\frac{1}{t_F} \int F dt_F$
Shut-down impulse	lb <sub>f</sub> -sec	...	$\int F dt_{TOF}$

e. Parameters for Over-all Motor

The ballistic parameters for the over-all motor are listed below.

<u>Parameter</u>	<u>Units</u>	<u>Symbol</u>	<u>Definition</u>
Average throat area	in. <sup>2</sup>	$\bar{A}_{ta}$	$\frac{\pi}{4} \left( \frac{D_{ti} + D_{tf}}{2} \right)^2$
Average exit area	in. <sup>2</sup>	$\bar{A}_e$	$\frac{\pi}{4} \left( \frac{D_{ei} + D_{ef}}{2} \right)^2$
Expansion ratio	...	$\epsilon$	$\frac{\bar{A}_e}{\bar{A}_{ta}}$
Mixture ratio (weight burned basis)	...	$\theta_w$	$\frac{W_{bpa}}{W_{bf}}$

<u>Parameter</u>	<u>Units</u>	<u>Symbol</u>	<u>Definition</u>
Mixture ratio (mass flow basis)	...	$\theta_m$	$\frac{m_a}{m_f}$
Total weight consumed	lb <sub>m</sub>	$W_{pt}$	$W_{bf} + W_{bpa}$
Discharge coefficient	$\frac{lb_m}{lb_f \cdot sec}$	$C_D$	$\frac{W_{pt}}{A_{ta}} \int P dt_p$
Characteristic velocity	ft/sec	$C^*$	$\frac{g_c}{C_D}$
Specific impulse	$\frac{lb_f \cdot sec}{lb_m}$	$I_{sp}$	$\frac{1}{W_{pt}} \int F dt_F$
Thrust coefficient	...	$C_F$	$C_D I_{sp}$
Theoretical thrust coefficient	...	$C_{F, theo}$	From thrust coefficient tables at the expansion ratio, $\bar{P}_{p, aft}$ , and ambient pressure from test.
Nozzle efficiency	%	$\eta_{C_F}$	$\frac{C_F}{C_{F, theo}} \quad (100)$

f. Correction Methods

In order to correct the preceding measured parameters for vacuum, standard, and theoretical conditions, the following methods are used.

First the following theoretical curves are required:

1. Curve 1 - Ratio of specific heats ( $\gamma$ ) versus mixture ratio ( $\theta$ )
2. Curve 2 - Characteristic velocity ( $C^*$ ) versus mixture ratio ( $\theta$ )
3. Curve 3 - Specific impulse ( $I_{sp}$ , 1000/14.7) versus mixture ratio ( $\theta$ )

Next, theoretical thrust coefficients are obtained, for standard and vacuum conditions ( $C_{F, 1000/14.7, \text{theo}}$  and  $C_{F, \text{vac}, 20/1, \text{theo}}$ , respectively), using  $\gamma_F$  from the Curve 1, above, and the value of  $\theta_w$  from the particular test.

The actual corrections are listed below:

<u>Parameter</u>	<u>Units</u>	<u>Symbol</u>	<u>Procedure</u>
Vacuum thrust	lb <sub>f</sub>	$\bar{F}_{K, \text{vac}}$	$\bar{F}_K \left( \frac{C_{F, \text{vac}, 20/1, \text{theo}}}{C_{F, \text{theo}}} \right)$
Vacuum total impulse	lb <sub>f</sub> -sec	$I_{T, \text{vac}}$	$\int F dt_F \left( \frac{C_{F, \text{vac}, 20/1, \text{theo}}}{C_{F, \text{theo}}} \right)$
Standard specific impulse	$\frac{\text{lb}_f\text{-sec}}{\text{lb}_m}$	$I_{sp, 1000/14.7}$	$I_{sp} \left( \frac{C_{F, 1000/14.7, \text{theo}}}{C_{F, \text{theo}}} \right)$
Vacuum specific impulse	$\frac{\text{lb}_f\text{-sec}}{\text{lb}_m}$	$I_{\text{vac}, 20/1}$	$I_{sp} \left( \frac{C_{F, \text{vac}, 20/1, \text{theo}}}{C_{F, \text{theo}}} \right)$
$I_{sp}$ Efficiency	%	$\eta_{I_{sp}}$	$\frac{I_{sp, 1000/14.7}}{I_{sp, 1000/14.7, \text{theo}}}$ (theoretical value from curve 3 above, at $\theta_w$ from test)
$C^*$ Efficiency	%	$\eta_{C^*}$	$\frac{C^*}{C^*_{\text{theo}}}$ (theoretical $C^*$ from curve 2, above, at $\theta_w$ from test)

SECTION VII - DEMONSTRATION OF NEW TECHNOLOGY

(TEST SERIES N)

1. GENERAL

The objective of Phase V, demonstration of new technology, was to demonstrate the operation and performance capability of the DCCSR which incorporated all the design refinements and advancements developed during Phases II through IV (Sections III and VI, along with Appendixes C and D). This phase consisted largely of the design of the full-scale motor for Test Series N, based on the technology derived from all previous work, and then conducting the Series N tests. Three of these were sea-level tests conducted at Northrop Carolina's facilities; the remaining were altitude tests conducted at Arnold Engineering Development Center, Tullahoma, Tenn. The Series N motor design is described in paragraph 2, below; the tests in paragraph 3, below.

2. SERIES N MOTOR DESIGN

The motor design for the Series N tests is shown in Figure 150. The hardware used for the cylindrical forward chamber was the same as that used in Series M for Tests M.3 through M.8 (see Section VI, paragraph 2). The TRW-supplied valve was the same basic design as that used for Series M, except the stroke-area relationship and controller settings were modified for the ballistic characteristics of a different forward propellant. The cylindrical aft case was a completely new design. The aft nozzle, supplied by TRW, was the same basic design as that for Series M, with minor changes at the aft case/nozzle interface and the throat area.

The forward chamber contained PPO-90 propellant in a center-perforated grain configuration. The characteristics of this formulation are given in Table III. The forward grain was ignited with pyrogens identical to those used in Series M tests.

C-430 propellant was selected for the aft grain on the basis of the tests described in Section III, Subsection II, paragraph 3, d. This propellant has been extinguished successfully at slightly higher  $K_n$  values than C-445, and has a higher pressure exponent above 100 psia, thereby providing a greater throttling capability. (Confidential)

REMOVED PAGE WAS BLANK THEREFORE WAS NOT REPRODUCED

**CONFIDENTIAL**

AFRPL-TR-65-209, Vol I

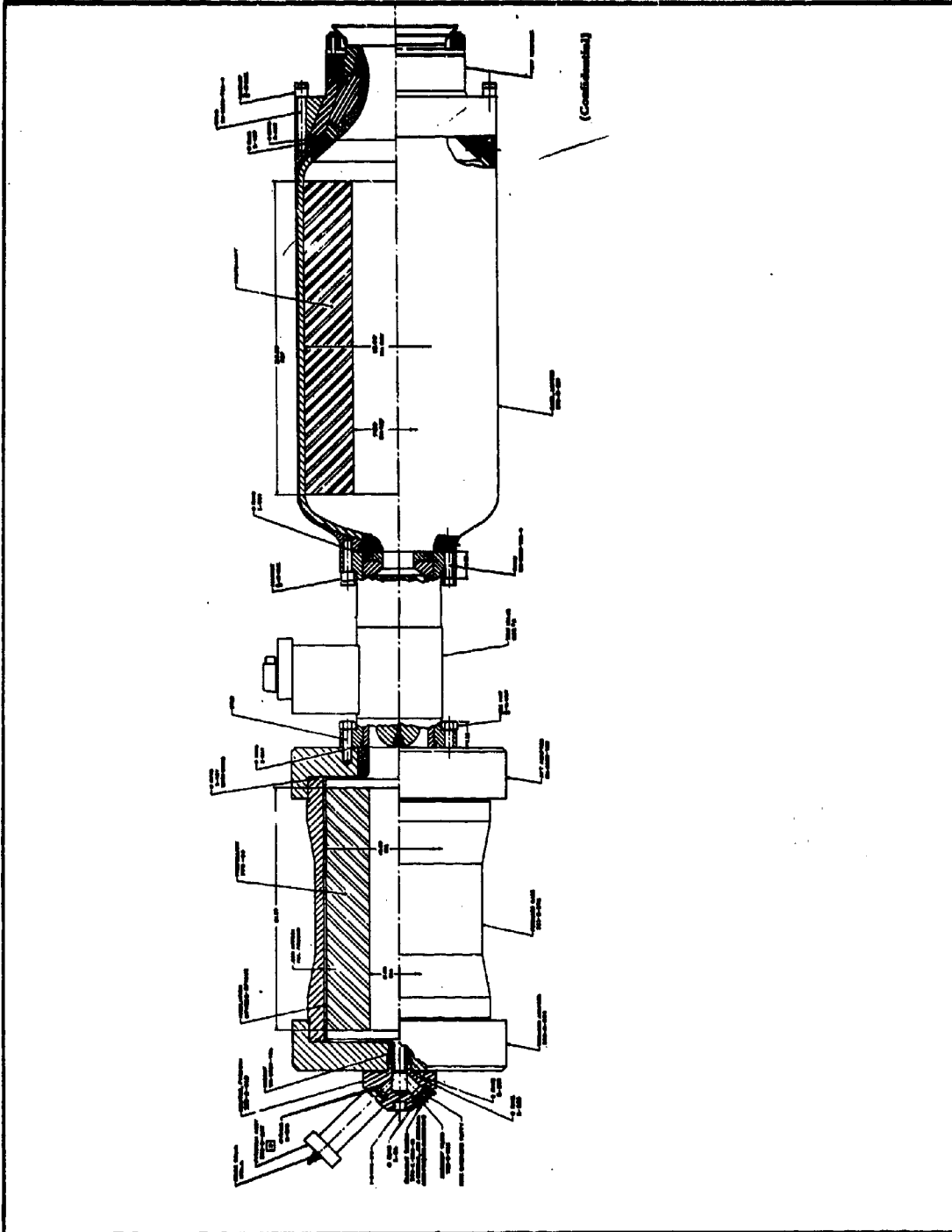


Figure 150 - Motor Assembly for Test Series N

**CONFIDENTIAL**

It was desired to operate the Series N motors at an aft-to-forward mixture ratio of 3 to 1. However, this was not feasible because of the limiting aft-chamber  $K_n$  required for termination. This limit corresponded to an aft-to-forward mixture ratio of about 1.3 to 1 above 100 psia (see Figure 106).

Originally, the aft grain was designed with a center-perforated grain 16.0-in. in diameter and 27.5-in. long, with a 4.2-in. web. With this design, the loaded aft chamber would contain 300 lb of propellant, and the average burning surface area would be 1,020 sq in. This design was not suitable for the chosen propellant, however, since this motor would have had an average  $K_n$  of 47 based on a 21.6-sq-in. aft throat area, which is the maximum area attainable without radically changing the nozzle design. The grain was therefore redesigned to reduce the burning surface area to correspond to a maximum  $K_n$  of 41 with the same 21.6-sq-in. throat area. To maintain the aft propellant weight at 300 lb with this lower surface area would have necessitated increasing the grain web to more than 5-in. and inhibiting a portion of one end face to achieve a reasonable surface area neutrality. The increased web would also have resulted in an initial port-to-throat ratio below 1.2, which is undesirable. Since it would be possible to consume only 150 lb of aft propellant with the limiting mixture ratio of 1.3, it was decided to decrease the aft propellant weight to achieve a more reasonable aft grain design. (Confidential)

Table LX summarizes the Series N design parameters. A plot of burning surface area as a function of web burned for the final aft grain design is given in Figure 151, and Figure 152 shows aft-chamber pressure as a function of forward-chamber pressure.

The aft case and insulation designs are shown in Figure 153. The aft case was fabricated from three sections of 4130 steel, heat-treated to 160,000 to 180,000 psi. The fore and aft sections were rough machined from forgings, while the center section was rolled and seam welded. The three sections were girth welded together, heat treated, and machined to final dimensions.

Gen Gard V-44, a silica-filled buna N rubber insulation, one inch thick, was bag-molded into the finished case. V-44 was selected on the basis of its immediate availability, excellent liner-to-insulation bond characteristics, and good ablative and insulative properties.

To optimize the control system gain and time constants for the

TABLE LX - BALLISTIC DESIGN FOR SERIES N MOTOR

Parameter	Value
<b>Forward chamber</b>	
Propellant	PPO-90
Grain O. D. (in.)	12.60
Grain I. D. (in.)	5.00
Grain length (in.)	21.50
Burning surface area (sq in.)	
Average	595
Maximum	617
Grain web (in.)	3.80
Propellant weight (lb <sub>m</sub> )	120
<b>Aft chamber</b>	
Propellant	C-430
Grain O. D. (in.)	15.00
Grain I. D. (in.)	7.50
Grain length (in.)	24.00
Grain web (in.)	3.75
Burning surface area (sq in.)	
Average	848
Maximum	873
Throat area (sq in.)	21.6
Port area (sq in.)	44.2
Surface-to-throat area ratio, K	
Average	39.3
Maximum	40.4
Propellant weight (lb <sub>m</sub> )	224
Exit area (sq in.), sea level/vacuum	34.7/200
Expansion ratio, sea level/vacuum	1.6/9.3

(Confidential)

**CONFIDENTIAL**

AFRPL-TR-65-209, Vol I

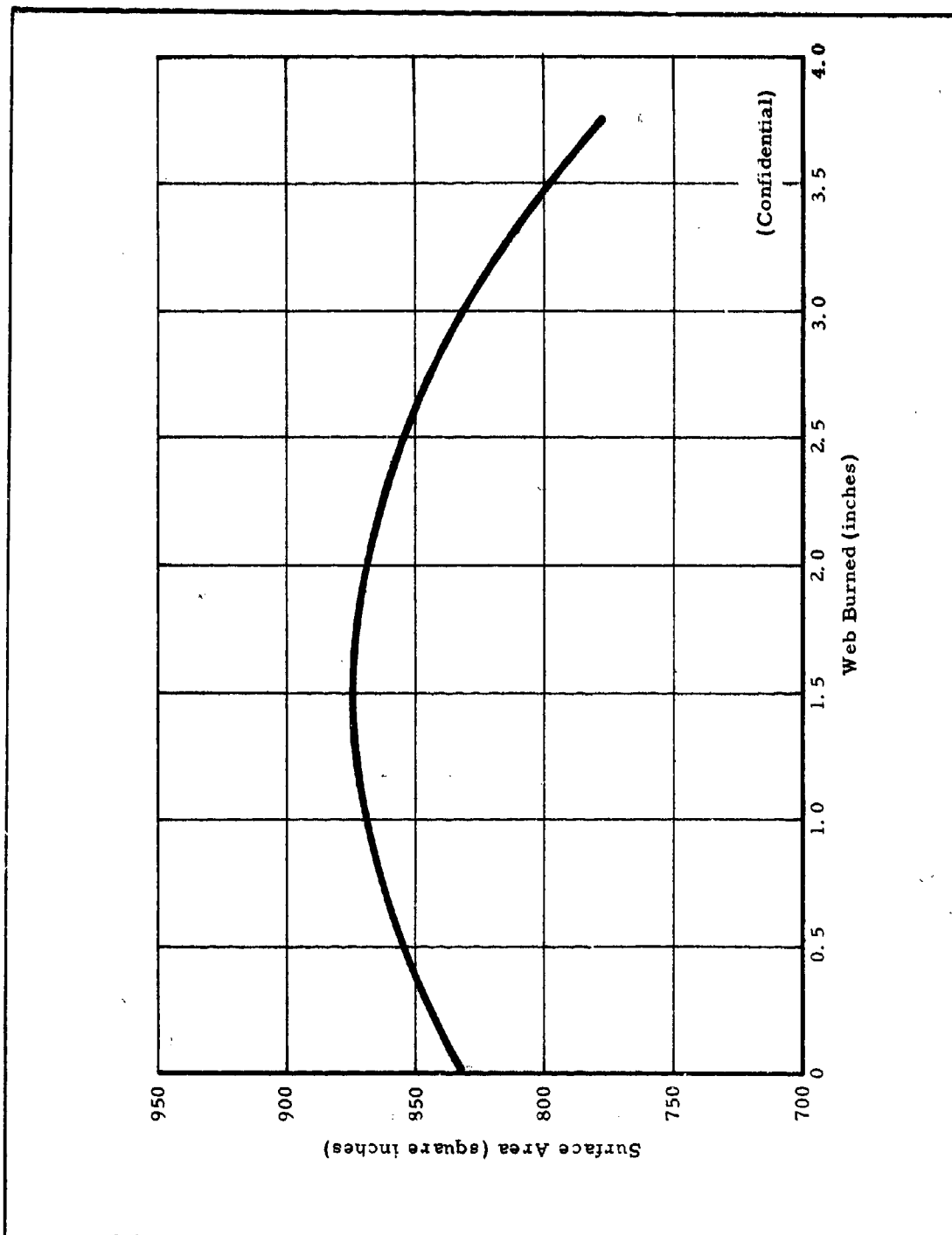


Figure 151 - Calculated Burning Surface Area as a Function of Web Burned for Series N Aft Grain

-263-

**CONFIDENTIAL**

**CONFIDENTIAL**

AFRPL-TR-65-209, Vol I

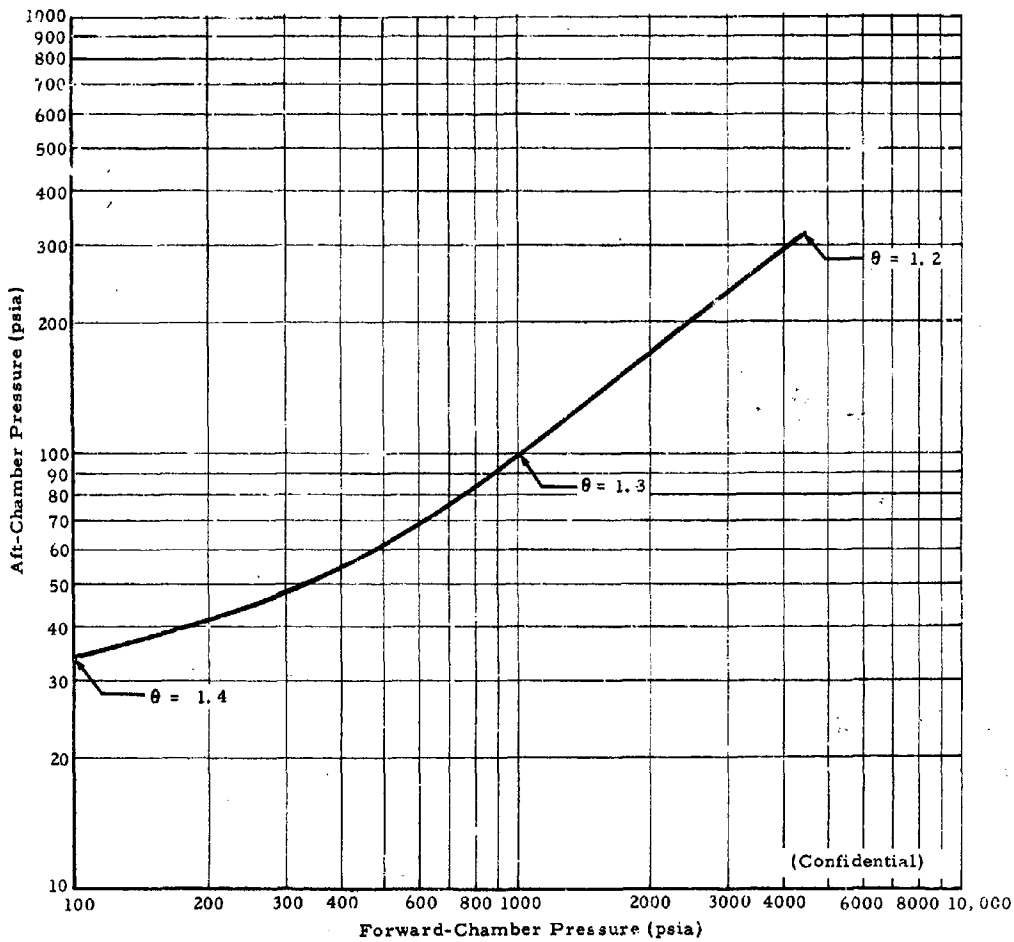


Figure 152 - Aft-Chamber Pressure versus Forward-Chamber Pressure for Series N Aft Grain

**CONFIDENTIAL**

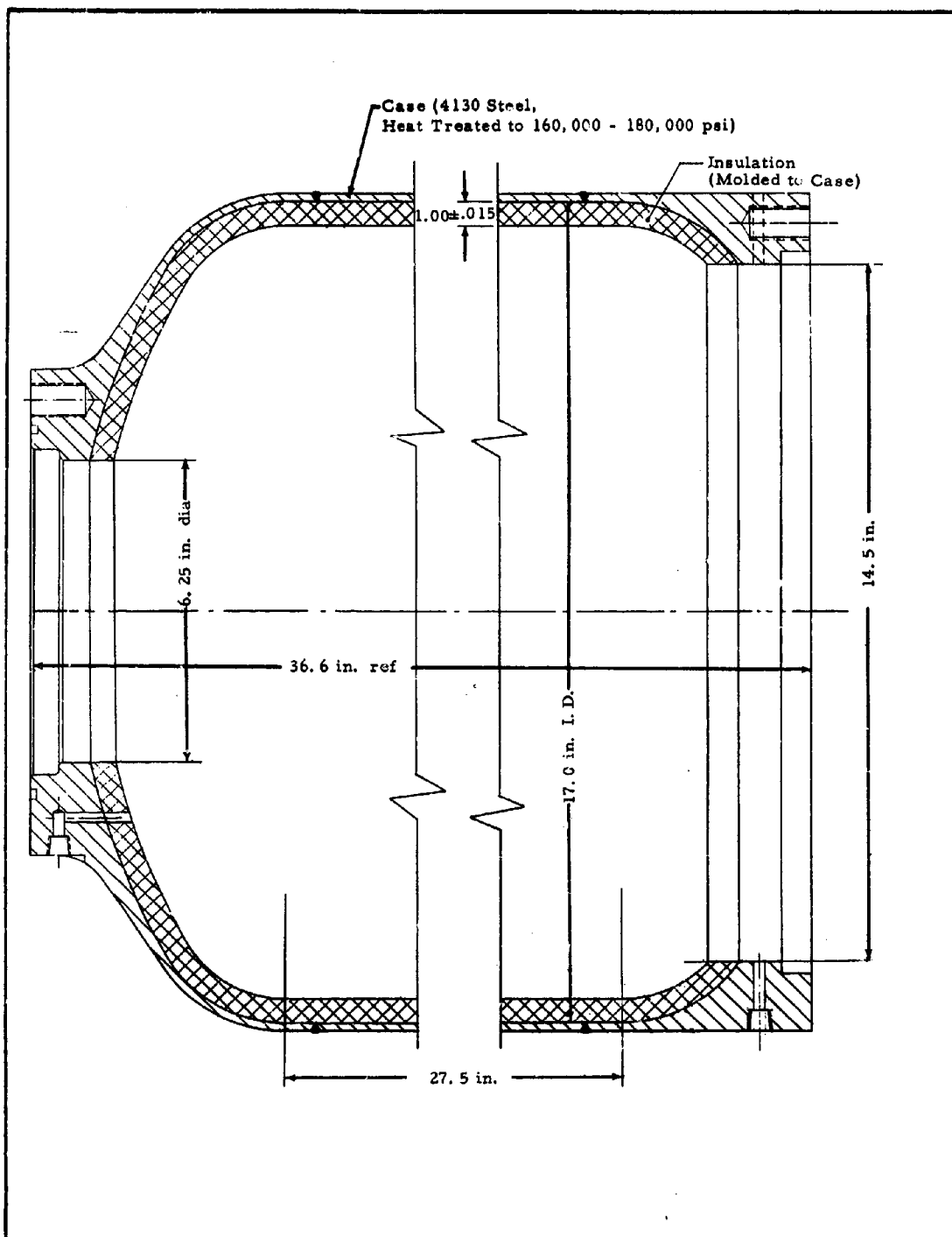


Figure 153 - Aft Case and Insulation Design for Series N Motor

Series N motor, it was necessary to conduct a process simulation based on differential equations for the forward- and aft-chamber process pressures. These differential equations, in turn, contain terms that define the burning rate and the physical, thermodynamic, and geometrical characteristics of both the forward and aft propellant formulations and grain configurations (see Appendix B). Therefore, since Series N motors contain PPO-90 and C-430 in the forward and aft chambers, respectively, instead of the PPO-13 and OX-1 used in Series M, it was necessary to rerun the computer analog of the control system to redefine the optimum controller gain and time constants.

Moreover, since the burning-rate levels versus pressure and the pressure index,  $n$ , for PPO-90 differ from those for PPO-13, the required valve stroke-area relationship was also different. This difference is shown graphically in Figure 154. Condition 1 is for PPO-13 in a spherical forward chamber (which was not used), Condition 2 is for PPO-13 in the cylindrical forward chamber used in Series M, and Condition 3 is for PPO-90 in the cylindrical forward chamber used in Series N. The valve used for Tests M. 7 and M. 8 (serial No. 1b) had the relationship shown in Condition 2. However, the values for Series N (serial No. 2a and 3) had the relationship shown for Condition 3.

### 3. SERIES N TEST RESULTS

#### a. Sea-Level Tests

##### (1) Test N. 1

The initial Series N tests were to evaluate the operation of the Series N motor at sea level before the altitude chamber tests, conducted at Arnold Engineering Development Center.

For Test N. 1, the motor was to be operated for a series of 1.0-sec duration pulse cycles at a forward pressure of 1500 psia, aft pressure of 125 psia and thrust of 3200 lb<sub>f</sub>. Following each termination, the two chambers were to be purged with nitrogen to expel the hot residual gas from the chambers. The motor configuration was as shown in Figure 150.

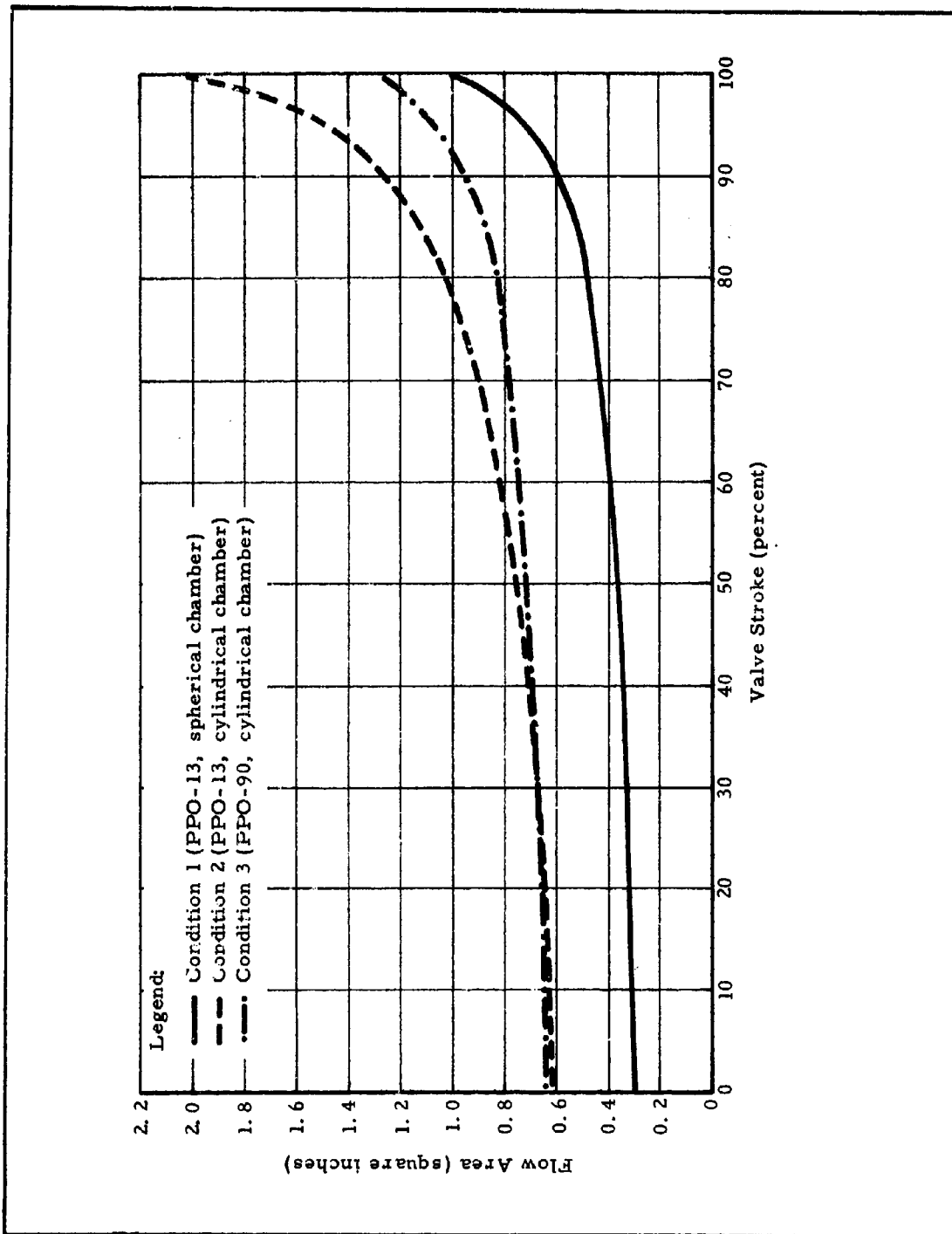


Figure 154 - Valve Stroke-Area Relationships for Various Motor Configurations

The pressure-and thrust-time traces for Test N. 1 are shown in Figure 155. Following the first pulse cycle, the aft grain reignited and burned at the very low pressure of 7 to 8 psig. The forward grain did not reignite and was, in fact, re-used in Test N. 2. By purging the forward chamber with nitrogen, aft-grain gases were probably prevented from entering the forward chamber and igniting the PPO-90 grain. Valve control stability resembled somewhat the last cycle of M. 8, in which low-frequency oscillations occurred (see Section VI, paragraph 11).

Test N. 1 verified that the full-scale Series N motor operated in a fashion familiar to the subscale six-inch motors. The long ignition delay of the aft grain was also evidenced in the subscale motors in which C-430 and C-445 propellants were used (see Section III, Subsection 2, paragraph 3, d). The aft grain was temporarily extinguished when the forward grain was terminated. The reignition of the full-scale grain, in contrast to permanent extinguishment of the subscale motor, may be due to the quantity of nitrogen employed in the purge system. The purge flow rate was not scaled up with motor size, but was actually increased only slightly for Series N due to the limited capacity of the purge equipment. (Confidential)

(2) Test N. 2

For Test N. 2, a throttling cycle somewhat similar to those programmed for the Series M tests was planned. The objectives of this test were to (1) check valve control stability over a wide pressure range of 80 to 4500 psia, (2) obtain additional ballistic data for the aft-grain propellant, and (3) demonstrate a 10-to-1 throttling range. The nonlinear compensation element was incorporated in the control system for this test to increase control sensitivity in the low-pressure range. (Confidential)

Low-frequency valve oscillations of three cycles per second occurred in Test N. 2 (see Figure 156). The forward-chamber pressure oscillated about the desired initial value of 1000 psi for 1.0 sec, followed by a ramp decrease to 80 psi. The predicted aft chamber pressure and thrust values are 210 and 40 psia, respectively. However, the oscillations occurring on the down ramp extinguished the

**CONFIDENTIAL**

AFRPL-TR-65-209, Vol I

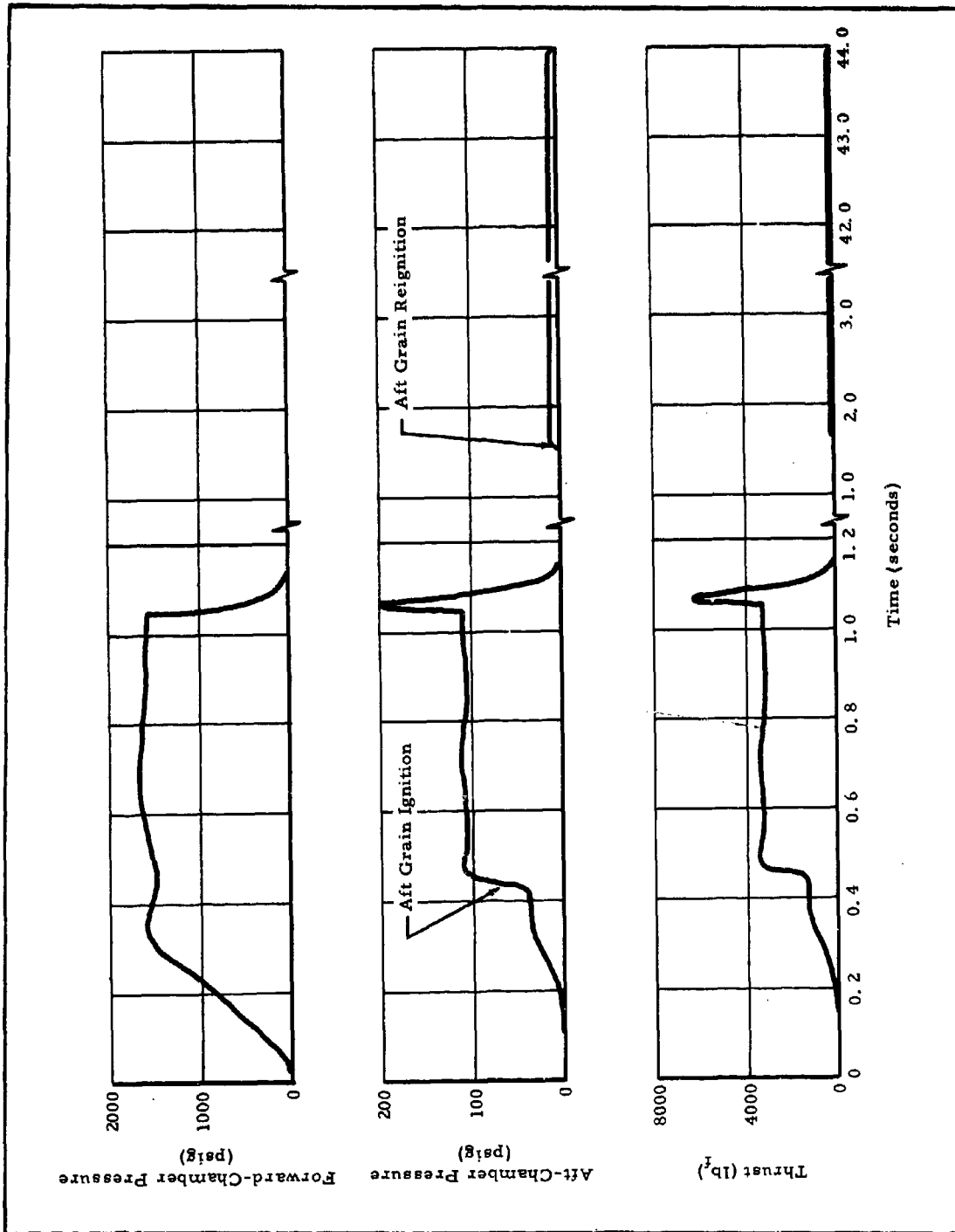


Figure 155 - Pressure and Thrust Time Traces for Test N. 1

**CONFIDENTIAL**

**CONFIDENTIAL**

AFRPL-TR-65-209, Vol I

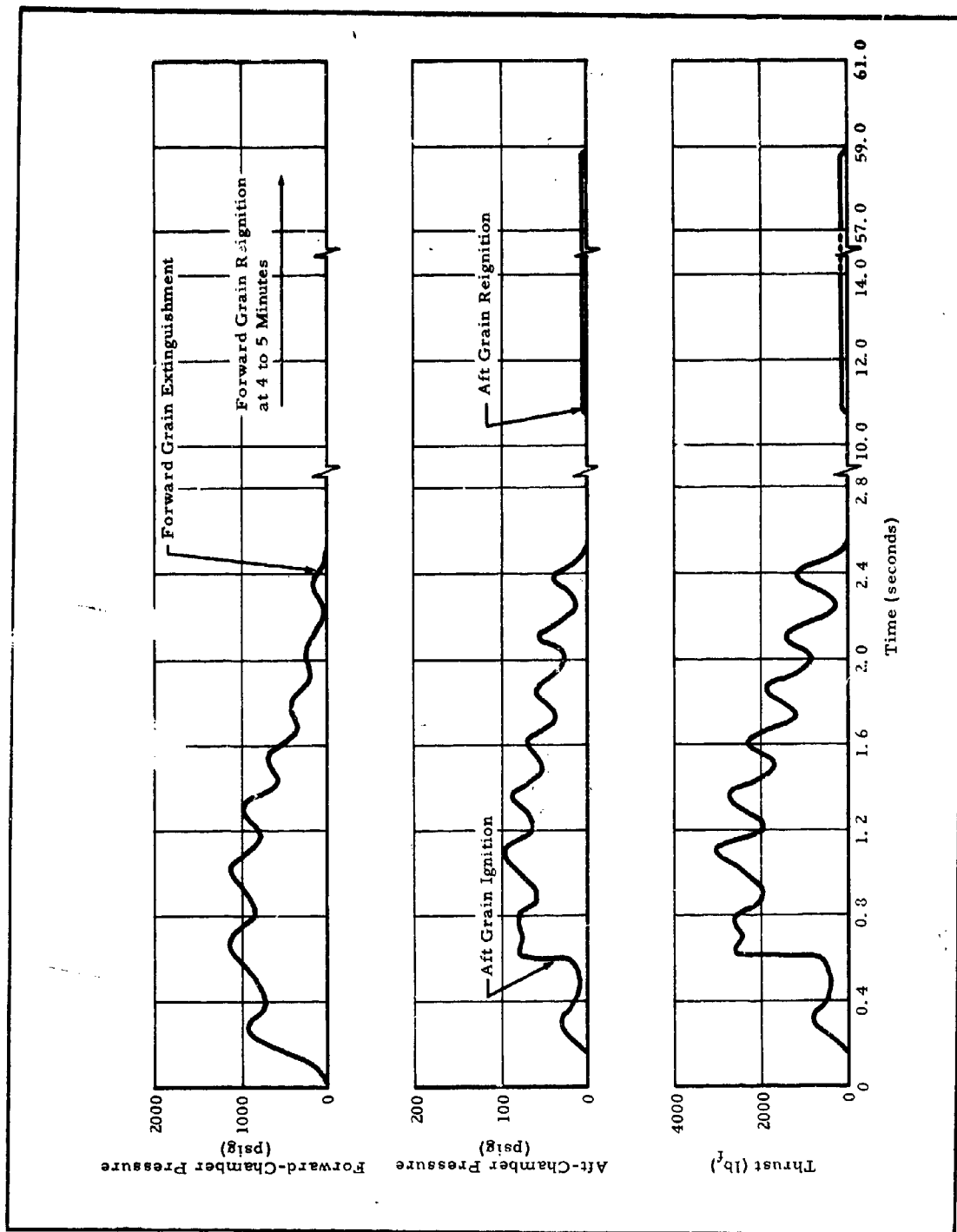


Figure 156 - Pressure and Thrust Time Traces for Test N. 2

**CONFIDENTIAL**

forward grain; the aft grain was also extinguished. The oscillatory behavior of forward-chamber pressure corresponded to valve movement. The aft grain reignited after about eight seconds and was consumed at a low pressure. After approximately four minutes, the forward grain reignited and burned out.

The instability evidenced in this test was concluded to be caused, as in Test M. 8, by a faulty element in the position loop portion of the control system. The position loop includes only the servovalves, the hydraulic supply, and the position potentiometer. It was decided to replace the servovalves and drain and refill, under vacuum, the hydraulic lines. The position potentiometer was checked and found to operate satisfactorily.

(3) Test N. 3

For Test N. 3 only the forward chamber and control valve were used since it was desired to check the control system, with the new servovalves, in short pulse cycles and incorporate any necessary modifications between pulses. Also, it was desired to evaluate both throttle valves (Serial No. 2a and 3) which were subsequently to be used in the altitude chamber tests.

The pressure-time traces obtained in Test N. 3 are shown in Figure 157. The first two pulse cycles of this Test, N. 3. 1 and N. 3. 2, employed TRW valve Serial No. 2a, which had been used in Test N. 2. In the first pulse cycle, pressure stabilized at the programmed value of 1000 psi shortly after the pyrogen burned out. The second cycle was programmed for 4000 psi pressure. However, the minimum area of the valve was too great to provide this pressure; instead, the minimum valve area corresponded to about 2500 psi. The progressive rise in pressure in this cycle is due to an increasing burning surface area of the grain.

In the final two cycles, N. 3. 3 and N. 3. 4, TRW valve Serial No. 3 was used. Cycle N. 3. 3 was programmed for 4000 psi. The throat dimensions of the valve physically changed during this test, as can be observed from the trace. Following ignition, pressure appeared to be stabilizing at

**CONFIDENTIAL**

AFRPL-TR-65-209, Vol I

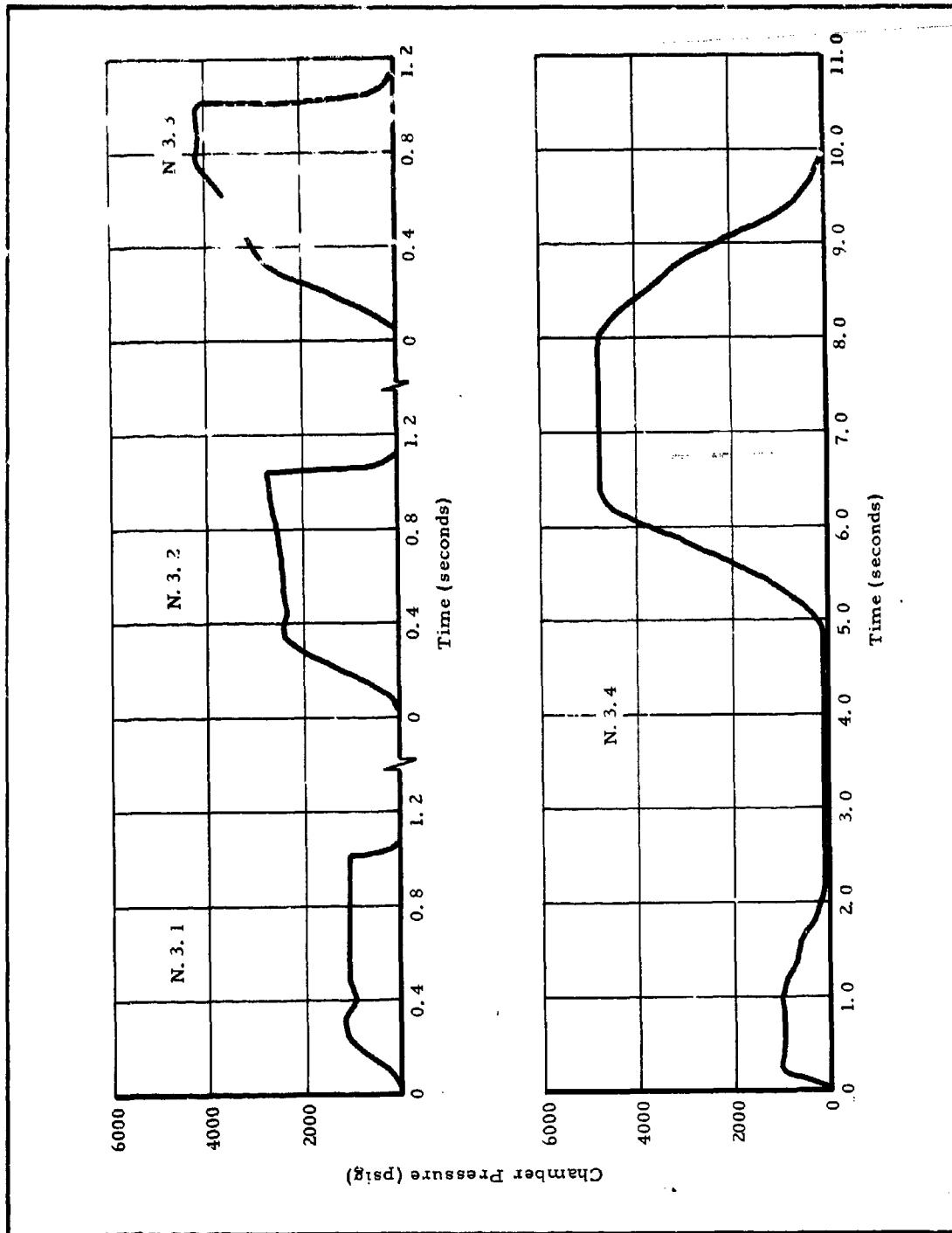


Figure 157 - Pressure-Time Traces for Test N. 3

**CONFIDENTIAL**

## CONFIDENTIAL

AFRPL-TR-65-209, Vol I

300 psi. However, the slope increased again, with the pressure increasing to the programmed value of 4000 psi, where it stabilized. The valve remained at the stroke corresponding to its minimum area throughout the rise portion of the pulse. When the design pressure level was attained the control system caused the valve to open and control pressure around 4000 psi. Measurements of the valve seat and pintle taken before and after this pulse confirmed that the minimum area did decrease during the test.

A throttling cycle, similar to that planned for Test N. 2, was programmed for the fourth cycle. Control stability was excellent throughout this cycle. Three steady-state levels of 1000, 75, and 4800 psia were obtained. The maximum to minimum pressure levels corresponded to a mass flow ratio of 29 to 1. The motor was allowed to burn out in this cycle. (Confidential)

The encouraging results of Test N. 3 confirm that the valve control stability problems encountered in N. 1, and particularly in N. 2, were in the position loop and that the problem was corrected.

### b. Altitude Tests

#### (1) General

The final two series N motors, N. 4 and N. 5, were tested in a simulated altitude environment at Arnold Engineering Development Center, Arnold Air Force Station, Tennessee. These motors were identical to the previous dual-chamber series N motors, except that the nozzle expansion cone was extended to a 9-to-1 area ratio for the altitude chamber tests. The purpose of these tests was to demonstrate stop-restart and thrust modulation capability of the dual-chamber motor containing a castable aft propellant at simulated altitude conditions.

The installation of the motors in Test Cell T-3 at AEDC is shown in Figures 158 and 159. The motors were mounted on a thrust cradle which was supported from the cradle support stand by three vertical and two horizontal double flexure columns. Axial thrust was transmitted

CONFIDENTIAL

**CONFIDENTIAL**

AFRPL-TR-65-209, Vol I

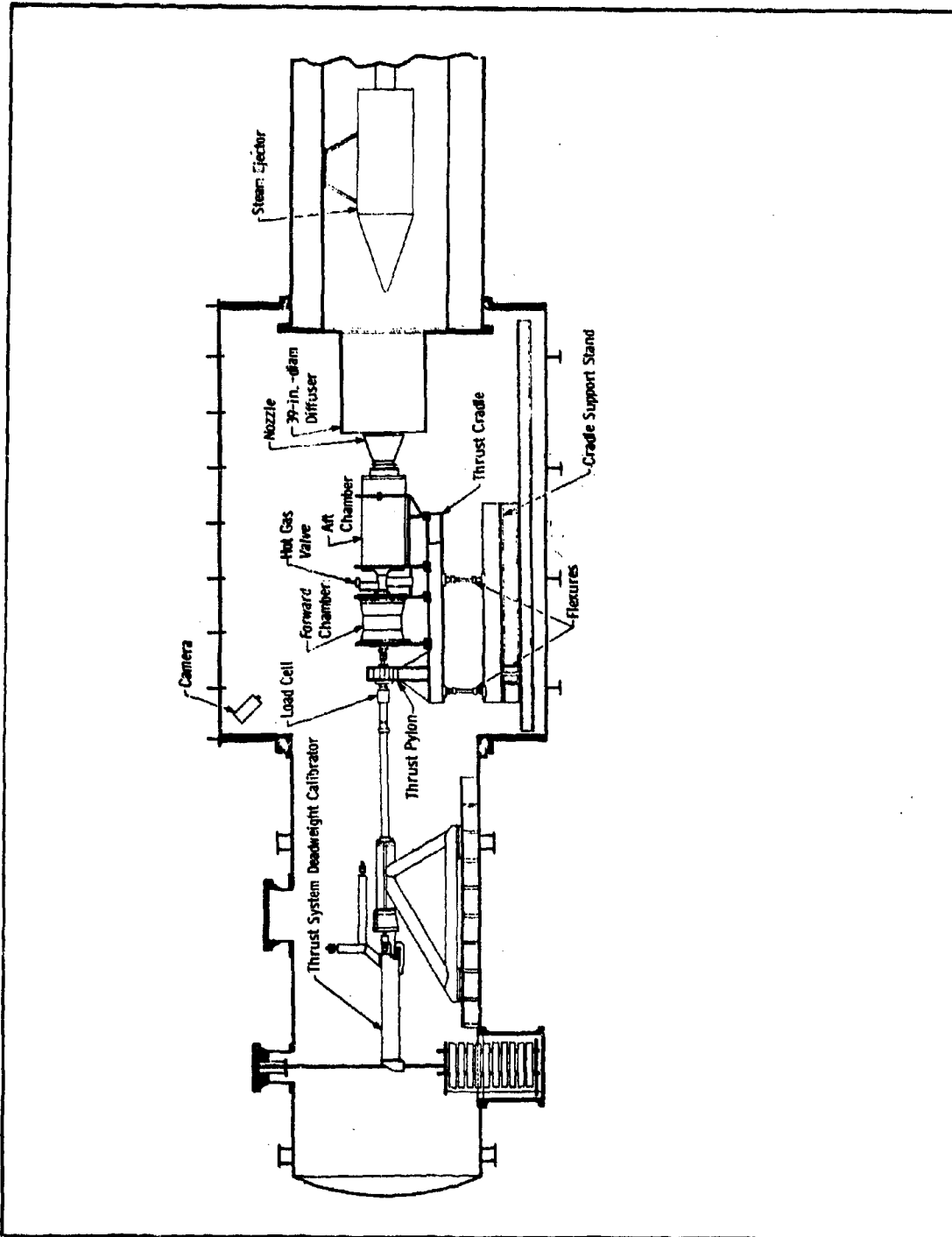


Figure 158 - Diagram Showing Installation of Motor in Test Cell T-3

**CONFIDENTIAL**

**CONFIDENTIAL**

AFRPL-TR-65-209, Vol I

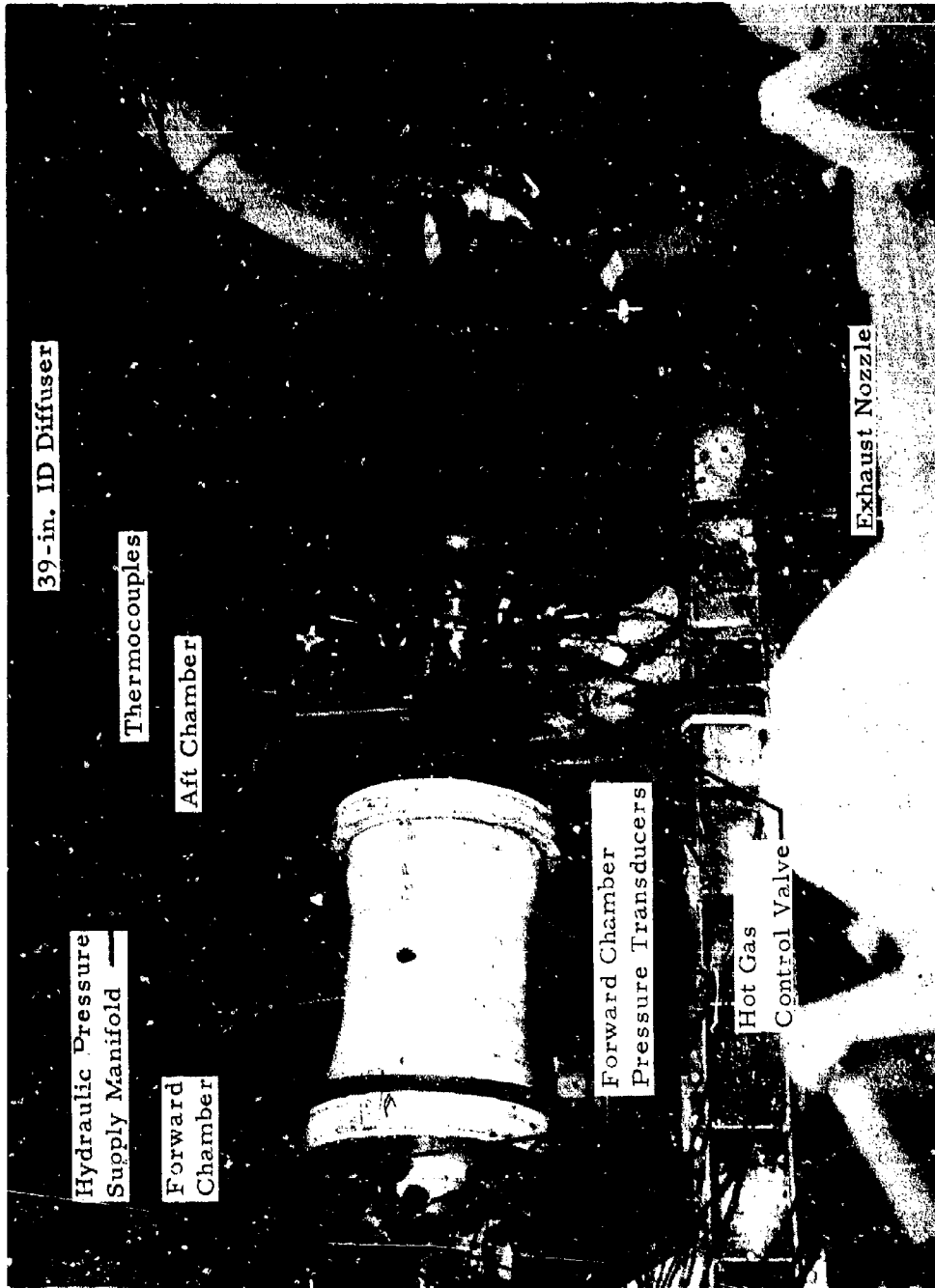


Figure 159 - Photograph of Motor Installed in Test Cell

-275-

**CONFIDENTIAL**

through the thrust pylon to one load cell mounted in a double-flexure column on the motor axial centerline. A remotely operated thrust stand calibrator was used to obtain pre- and post-firing axial thrust system calibrations.

The hydraulic pump assembly used to actuate the hot gas valve was located outside of and adjacent to the test cell. The high-pressure hydraulic lines were connected to the valve and positioned perpendicular to the motor axial centerline (to eliminate thrust measurement interaction effects) and coupled to sealed junctions at the test cell wall.

Preignition pressure altitude conditions were maintained in the test cell by a steam ejector operating in series with RTF exhaust gas compressors. During a test, the motor exhaust gases were used as the driving gas for the 39-in. -diameter ejector-diffuser system to maintain test cell pressure at an acceptable level.

The test plan called for each of the two motors to be fired over ten cycles (ignition and termination), with each cycle of nominal one-second duration, followed by a final three-second cycle, during which the throttling capabilities of the motor would be demonstrated.

(2) N. 4 Test Results

Motor N. 4 was successfully cycled (ignited and terminated) five times, with each cycle nominally of one-second duration. On the sixth cycle, the motor failed to terminate. A post-fire inspection revealed that the insulation around the valve pintle had failed and moved forward into the throat area of the valve, thereby preventing the throat area from attaining termination conditions.

The pressure- and thrust-time traces for the six cycles of N. 4 are shown in Figures 160 through 166. Motor ballistic and performance data are given in Tables LXI, LXII and LXIII.

**CONFIDENTIAL**

AFRPL-TR-65-209, Vol I

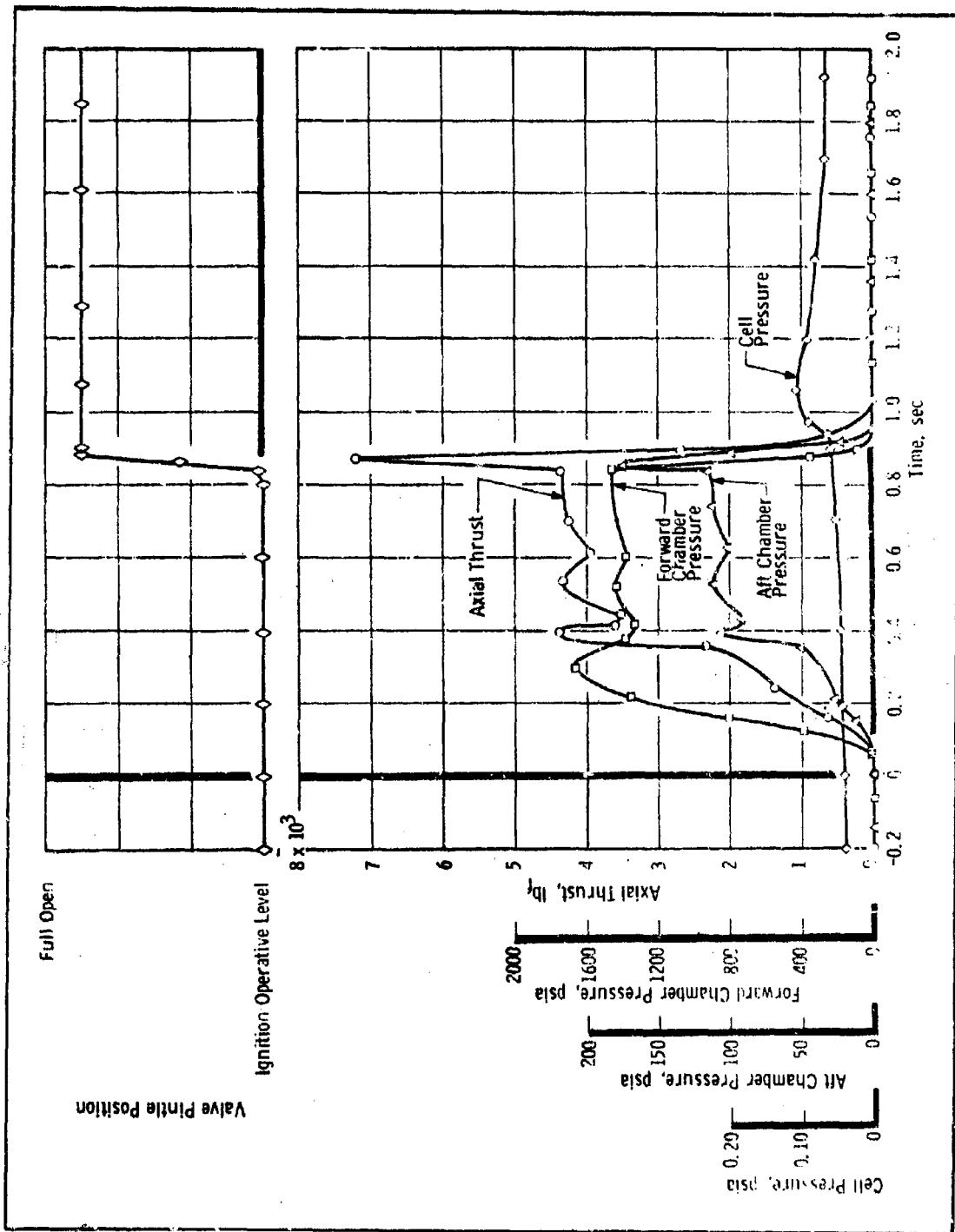


Figure 16C - Traces for Test N. 4. 1

**CONFIDENTIAL**

**CONFIDENTIAL**

AFRPL-TR-65-209, Vol I

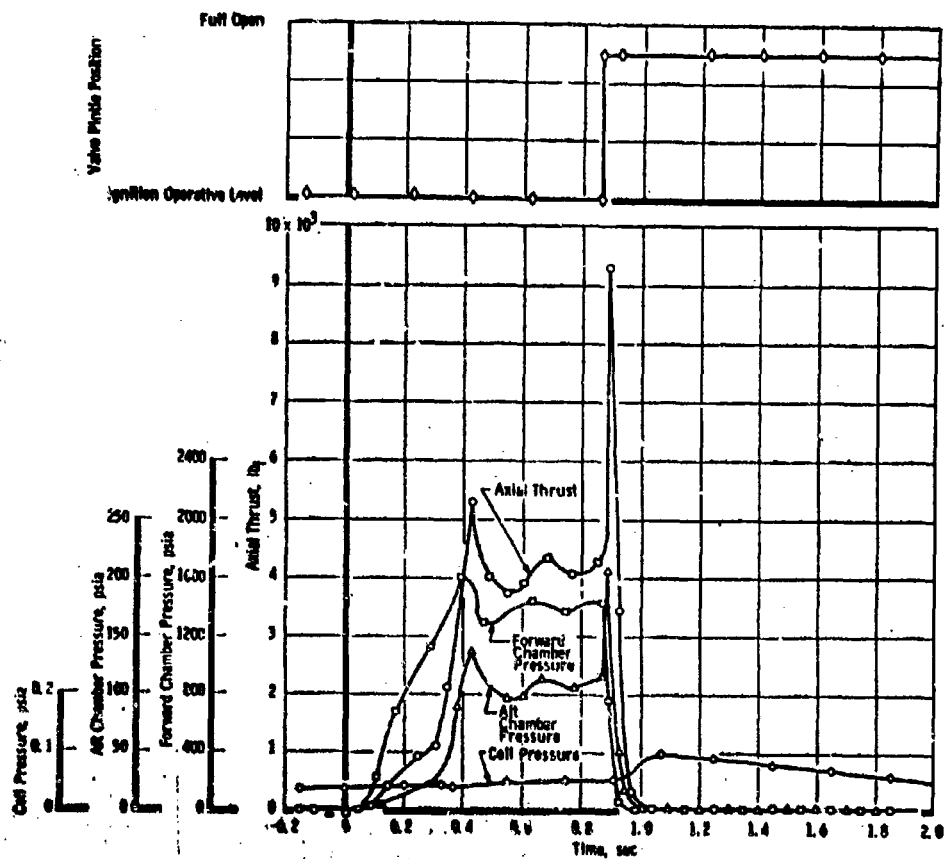


Figure 161 - Traces for Test N. 4.2

**CONFIDENTIAL**

**CONFIDENTIAL**

AFRPL-TR-65-209, Vol I

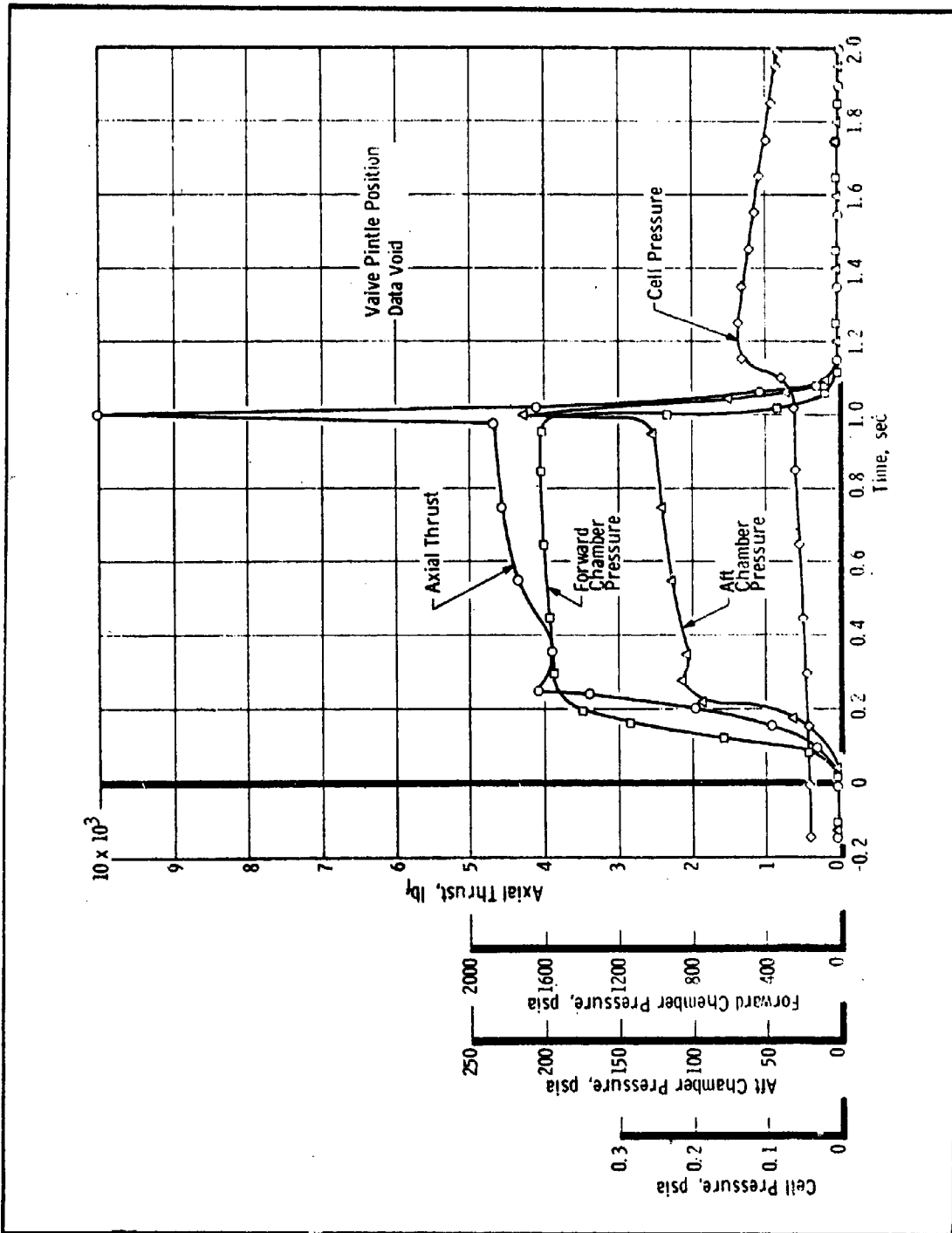


Figure 162 - Traces for Test N. 4.3

**CONFIDENTIAL**

**CONFIDENTIAL**

AFRPL-TR-65-209, Vol I

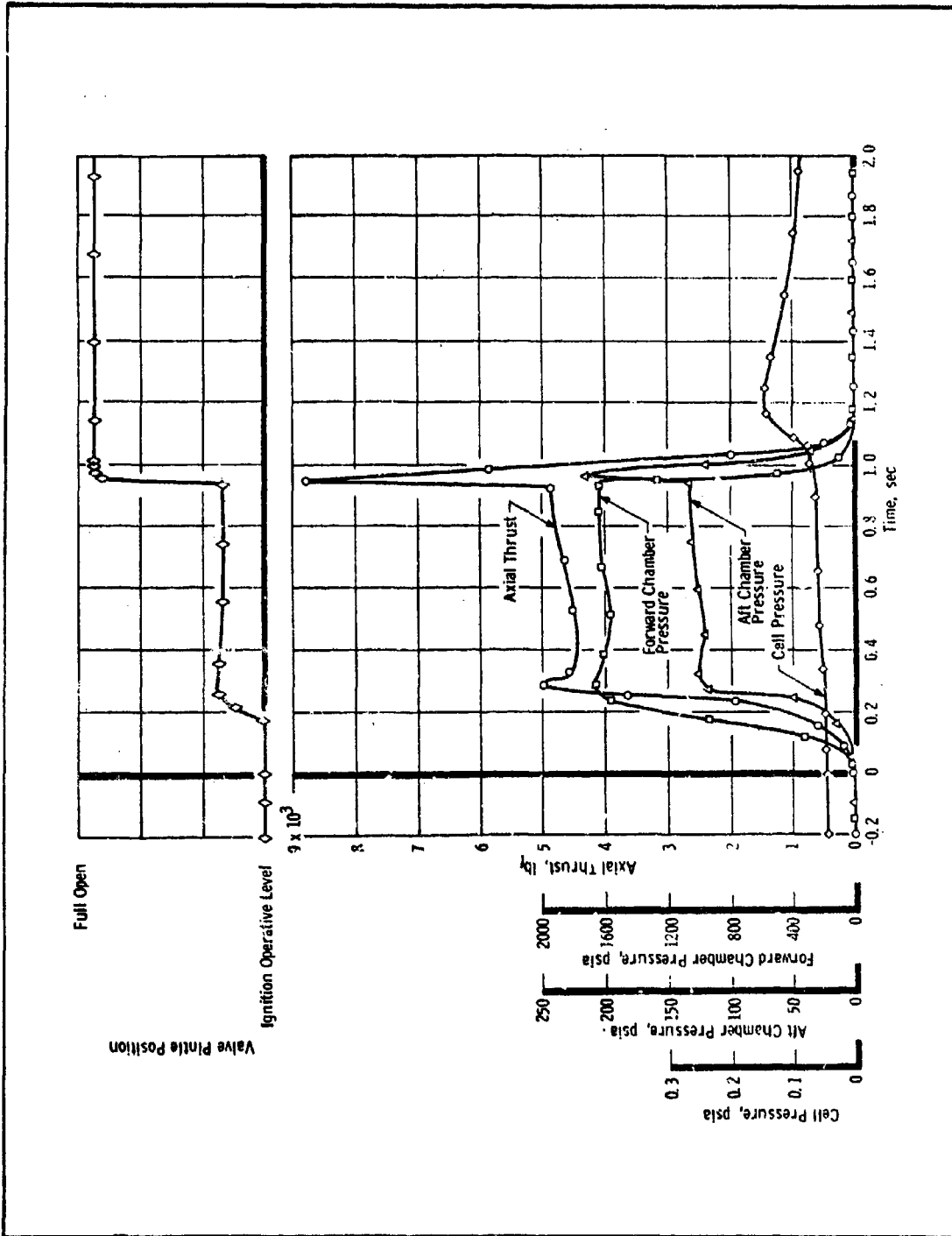


Figure 163 - Traces for Test N. 4. 4

**CONFIDENTIAL**



**CONFIDENTIAL**

AFRPL-TR-65-209, Vol I

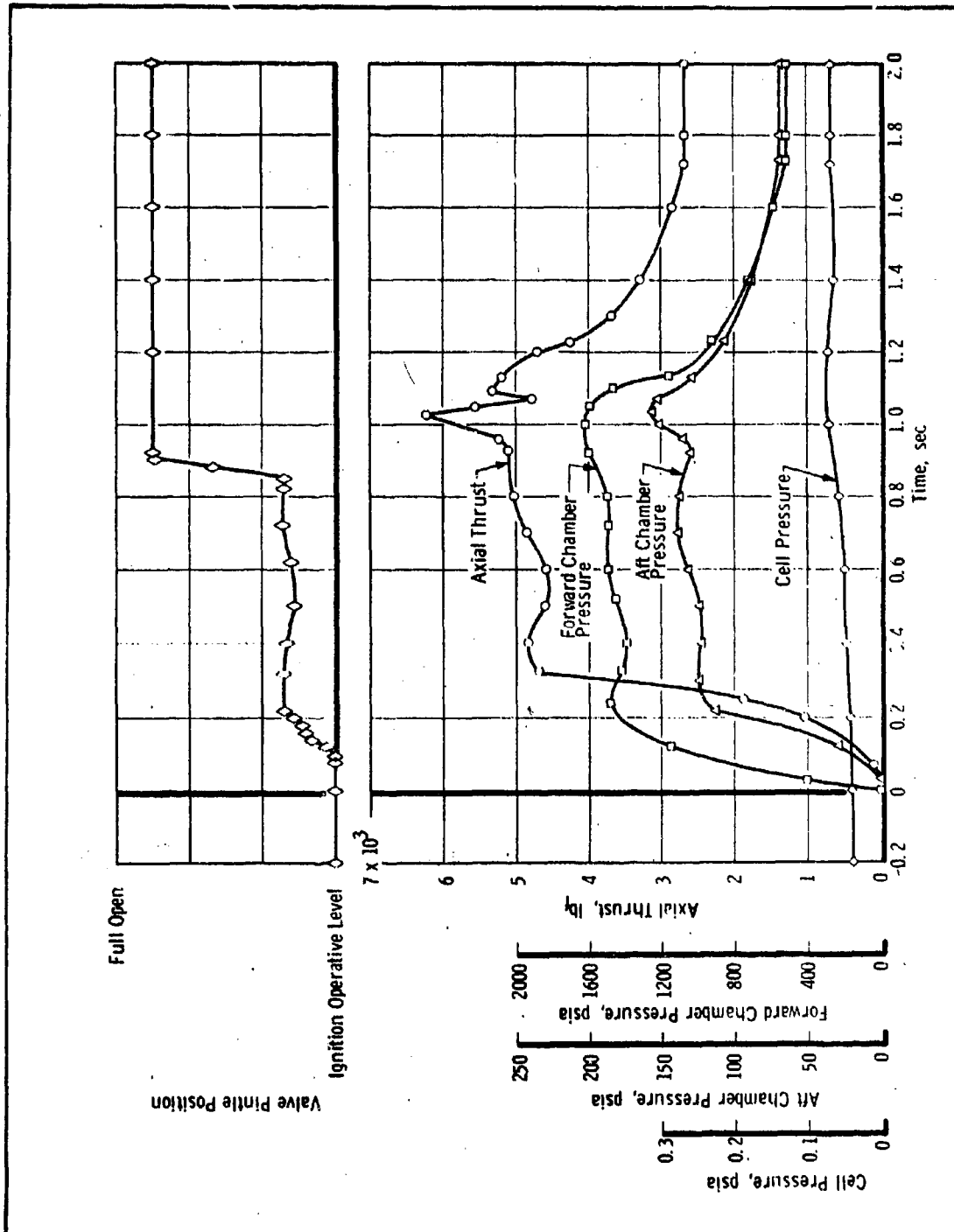


Figure 165 - Traces for Test N. 4. 6 (First 2-sec of Operation)

**CONFIDENTIAL**

**CONFIDENTIAL**

AFRPL-TR-65-209, Vol I

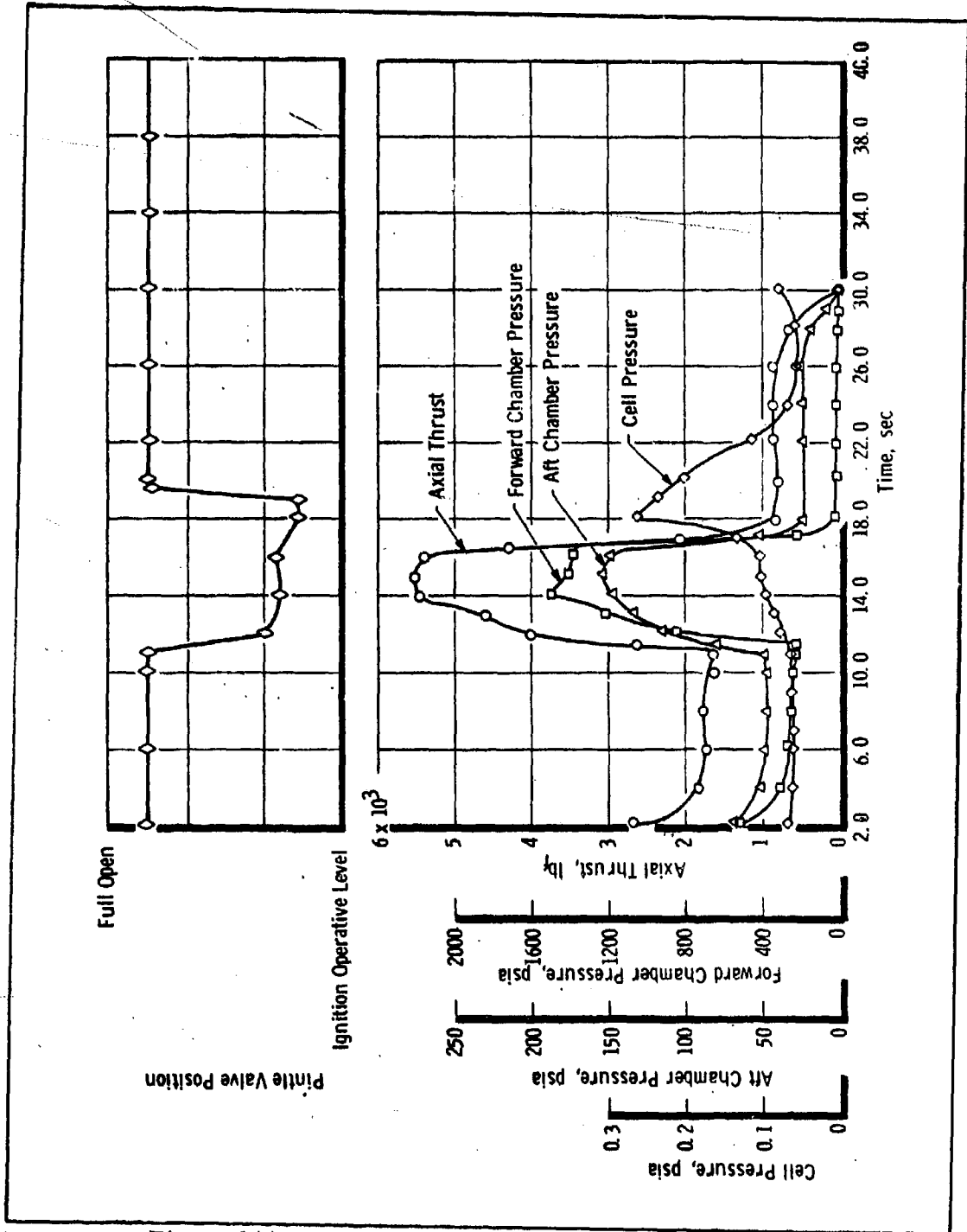


Figure 166 - Traces for Test N. 4. 6 (t + 2-sec to Burnout)

**CONFIDENTIAL**

TABLE LXI-MOTOR SUMMARY FOR TEST N. 4

Parameter	Ignition Cycle					
	1	2	3	4	5	6
Test Date	11/22/65	11/24/65	11/30/65	12/1/65	12/1/65	12/2/65
Ignition Altitude (ft)	126,500	129,500	132,000	132,500	132,500	133,000
Average Altitude During Firing (ft)	122,500	124,500	124,000	122,500	121,000	112,000
Number of Pyrogens	2	2	3	4	3	4
Valve Serial Number	1	1	3	3	3	2
Nozzle Serial Number	3A	3A	3A	3A	3A	3A
Nozzle Throat Area (sq in.)						
Pre-Fire	21.623	21.631	21.623	21.625	21.623	21.629
Post-Fire	21.631	21.623	21.625	21.623	21.629	20.169
Average	21.627	21.627	21.624	21.624	21.626	20.899
Nozzle Exit Area (sq in.)						
Pre-Fire	200.485	200.409	200.409	200.450	200.465	200.480
Post-Fire	200.409	200.409	200.450	200.465	200.480	199.933
Average	200.447	200.409	200.430	200.458	200.472	200.206
Nozzle Area Ratio						
Pre-Fire	9.272	9.265	9.268	9.269	9.271	9.269
Post-Fire	9.265	9.268	9.269	9.271	9.269	9.913
Average	9.268	9.266	9.268	9.270	9.270	9.591

# CONFIDENTIAL

AFRPL-TR-65-209, Vol I

**TABLE LXII - SUMMARY OF REDUCED BALLISTIC DATA FOR TEST N.4**

Parameter	Ignition Cycle						Total (Cycles 1-5)
	1	2	3	4	5	6	
<b>Forward Chamber</b>							
Delay Time, 0 to 10% (sec)	0.242	0.242	0.076	0.142	0.179	0.14	...
Rise Time, 10 to 90% (sec)	0.163	0.273	0.165	0.167	0.211	0.22	...
Burn Time, 10% to Termination (sec)	0.773	0.780	0.940	0.875	0.858	15.96	4.226
Decay Time, Termination to 10% (sec)	0.037	0.043	0.049	0.051	0.058	...	...
$\int P dt_p$ (psia-sec)	1,063	998.1	1,403	1,293	1,273	11,435	6,030
$\bar{P}_b$ (psia)	1,346	1,239	1,462	1,448	1,439	675	1,392
Web Burned (in.)	0.212	0.215	0.273	0.253	0.255	2.450	1.208
Burn Rate (in./sec)	0.274	0.276	0.290	0.289	0.297	...	0.286
<b>Weight Burned (lb)</b>							
Grain	6.362	6.250	8.629	8.063	8.021	82.130	37.325
Pyrogen	0.376	0.376	0.563	0.751	0.563	0.751	2.629
Total	6.738	6.626	9.192	8.814	8.584	82.881	39.954
<b>Aft Chamber</b>							
Delay Time, 0 to ignition (sec)	0.515	0.462	0.225	0.313	0.350	0.363	...
Rise Time, Ignition to 90% (sec)	0.035	0.028	0.028	0.041	0.046	0.046	...
Burn Time, Ignition to 10% (sec)	0.580	0.600	0.875	0.794	0.787	27.68	3.636
Decay Time, Termination to 10% (sec)	0.076	0.082	0.104	0.114	0.132	...	...
$\int P dt_p$ (psia-sec)	69.29	71.02	102.64	101.56	103.45	1,680.0	448.0
$\bar{P}_b$ (psia)	106.5	108.4	113.0	122.3	125.1	60.3	115.9
Web Burned (in.)	0.096	0.087	0.135	0.131	0.141	2.962	0.590
Burn Rate (in./sec)	0.166	0.145	0.154	0.165	0.179	...	0.162
Weight Burned (lb)	5.044	5.449	8.005	7.984	8.281	180.205	34.763
<b>Total Motor</b>							
Weight Burned (lb)	11.782	12.075	17.197	16.798	16.865	263.086	74.717
Weight Aft/Weight Forward	0.749	0.822	0.871	0.906	0.965	...	0.870
$\int F dt_{i \text{ meas}}$ (lb <sub>f</sub> -sec)	2,689	2,724	3,861	3,824	3,887	60,567	16,985
$\int F dt_{i \text{ vac}}$ (lb <sub>f</sub> -sec)	2,698	2,733	3,871	3,834	3,897	61,137	17,033
$\bar{F}_b$ (lb <sub>f</sub> )	4,046	4,112	4,232	4,592	4,680	2,175	4,358
$\int F dt_{i \text{ term}}$ (lb <sub>f</sub> -sec)	351	328	397	507	622	...	...
Throat Area (sq in.)	21.627	21.627	21.624	21.624	21.626	20.899	21.626
Expansion Ratio	9.268	9.266	9.268	9.270	9.270	9.591	9.269
Cell Pressure Integral (psia-sec)	0.04603	0.04317	0.05086	0.04995	0.05085	2.848	0.24086
Characteristic Velocity (fps)	4,092	4,093	4,152	4,206	4,268	4,294	4,172
<b>Specific Impulse (lb-sec/lb)</b>							
Measured, 17.5°	228.2	225.6	224.5	227.6	230.5	230.2	227.3
Corrected to Vacuum, 17.5°	229.0	226.3	225.1	228.2	231.1	232.4	228.0
Corrected to Vacuum, 20/1, 17.5°	239.7	237.1	235.9	239.1	242.2	...	238.9
Theoretical, Vac, 20/1, 17.5°	258.0	259.7	260.6	261.2	262.1	...	260.5
Efficiency (%)	92.9	91.3	90.6	91.6	92.4	...	91.7
Ratio of Specific Heats, $\gamma$	1.23	1.22	1.22	1.22	1.22	...	1.22
Measured Thrust Coefficient	1.794	1.773	1.738	1.740	1.738	1.725	1.753

(Confidential)

**TABLE LXIII - MOTOR TERMINATION SUMMARY FOR TEST N. 4**

Parameter	Ignition Cycle					
	1	2	3	4	5	6
<b>Forward Chamber</b>						
Termination Pressure (psia)	1, 472	1, 448	1, 615	1, 604	1, 622	1, 476
Decay Rate, $dp/dt$ (psi/sec)	63, 100	60, 700	51, 300	54, 600	49, 200	2, 840
Decay Rate/ $P_{term}$ ( $sec^{-1}$ )	42.9	41.9	31.8	34.0	30.3	1.9
Valve Actuation Time (sec)	0.010	0.013	0.020	0.026	...	...
<b>Aft Chamber</b>						
Termination Pressure (psia)	116.9	117.4	120.4	132.4	135.1	128.1
Maximum Pressure at Termination (psia)	251.0	266.1	247.2	273.3	279.7	158.3
Decay Rate, $dp/dt$ (psi/sec)	6, 180	5, 910	4, 410	4, 940	3, 870	163
Decay Rate/ $P_{term}$ ( $sec^{-1}$ )	24.6	22.2	17.8	18.1	13.8	1.0
Free Volume at Termination (cu. in.)	2, 392	2, 476	2, 568	2, 692	2, 847	2, 980
Free Volume/Throat Area, $L^*$ (in)	110.6	114.5	118.9	124.5	131.6	137.8
Surface Area/Throat Area, $K_n$	32.7	32.9	33.6	33.8	35.0	...

(Confidential)

Valve stability was very poor during the first two cycles of N. 4. Forward pressure and, hence aft pressure and thrust, oscillated following ignition. This instability was attributed to a faulty valve pintle position potentiometer. Another valve, S/N 3, was employed for the next three pulse cycles, and stability improved considerably. Forward-chamber pressure was closely controlled around the preset value of 1600 psia. (Confidential)

A third valve, S/N 2, was substituted before the sixth cycle for S/N 3, which was inoperable following the fifth cycle. The stability of this third valve during the sixth cycle was poorer than that of S/N 3, but much superior to S/N 1 used in the first two cycles. During termination of the sixth cycle very little throat area change was evidenced, based on the decay rates in the forward and aft chambers (Table LXIII). Neither grain extinguished at termination, and flow through the valve remained choked at lower pressure levels. After 10 sec, the valve was recycled to the higher pressure. The forward grain burned out 5 sec after the valve was recycled; the aft-chamber pressure then dropped to a low level and the aft grain burned for an additional 12 sec to burnout. A post-fire inspection of the valve revealed the partial blockage of the valve annulus by the insulation from the pintle. This cycle demonstrated a throttling ratio of approximately 3 to 1 from the steady-state thrust levels before and after actuation of the valve. (Confidential)

A specific impulse efficiency of 91.7 percent was measured for the first five cycles of N. 4. This low efficiency is probably due to the low aft-chamber pressure of 116 psia during these cycles. The performance results of the sixth cycle were not included in these averages because a portion of this cycle consisted of the aft grain burning alone. (Confidential)

(3) N. 5 Test Results

Motor N. 5 was successfully cycled nine times, with each cycle nominally of one-second duration. On the tenth cycle, the aft grain failed to extinguish when the valve was actuated and, the C-461 aft propellant burned at a low pressure of 20 to 22 psia until the entire grain was consumed.

The forward propellant, PPO-90, extinguished when the valve actuated without reigniting during the low-pressure aft-grain combustion. (Confidential)

Due to the failure of the pintle insulation in valve S/N 2 during the sixth cycle of N. 4, it was necessary to use valve S/N 1 for the entire N. 5 test. This valve continued to display instability during N. 5, as was evident in the first two cycles of N. 4; this instability is shown in the pressure- and thrust-time traces for Test N. 5 presented in Figures 167 through 177. In the third, eighth, ninth, and tenth cycles of N. 5, the preset pressure around which the valve feedback loop controls was set very high so that the pintle would move to the closed position (corresponding to about 2500 to 2600 psia). The pintle is thus prevented from oscillating since it rests on a stop in the pintle housing. During these cycles the motor operated stably. (Confidential)

The reduced ballistic and performance data for Test N. 5 are tabulated in Tables LXIV and LXV. Performance values for this test are very similar to those obtained in Test N. 4. Table LXVI summarizes the termination parameters, with each succeeding cycle, the decay rate at a given pressure became less,  $L^*$  of the aft chamber increased, and the aft chamber  $K_n$  increased. As shown previously in subscale testing, C-461 will not extinguish at a  $K_n$  value above 40 to 42. The failure of the propellant to extinguish in the tenth cycle was perhaps due to a combination of the low decay rate and high  $K_n$ . (Confidential)

**CONFIDENTIAL**

AFRPL-TR-65-209, Vol I

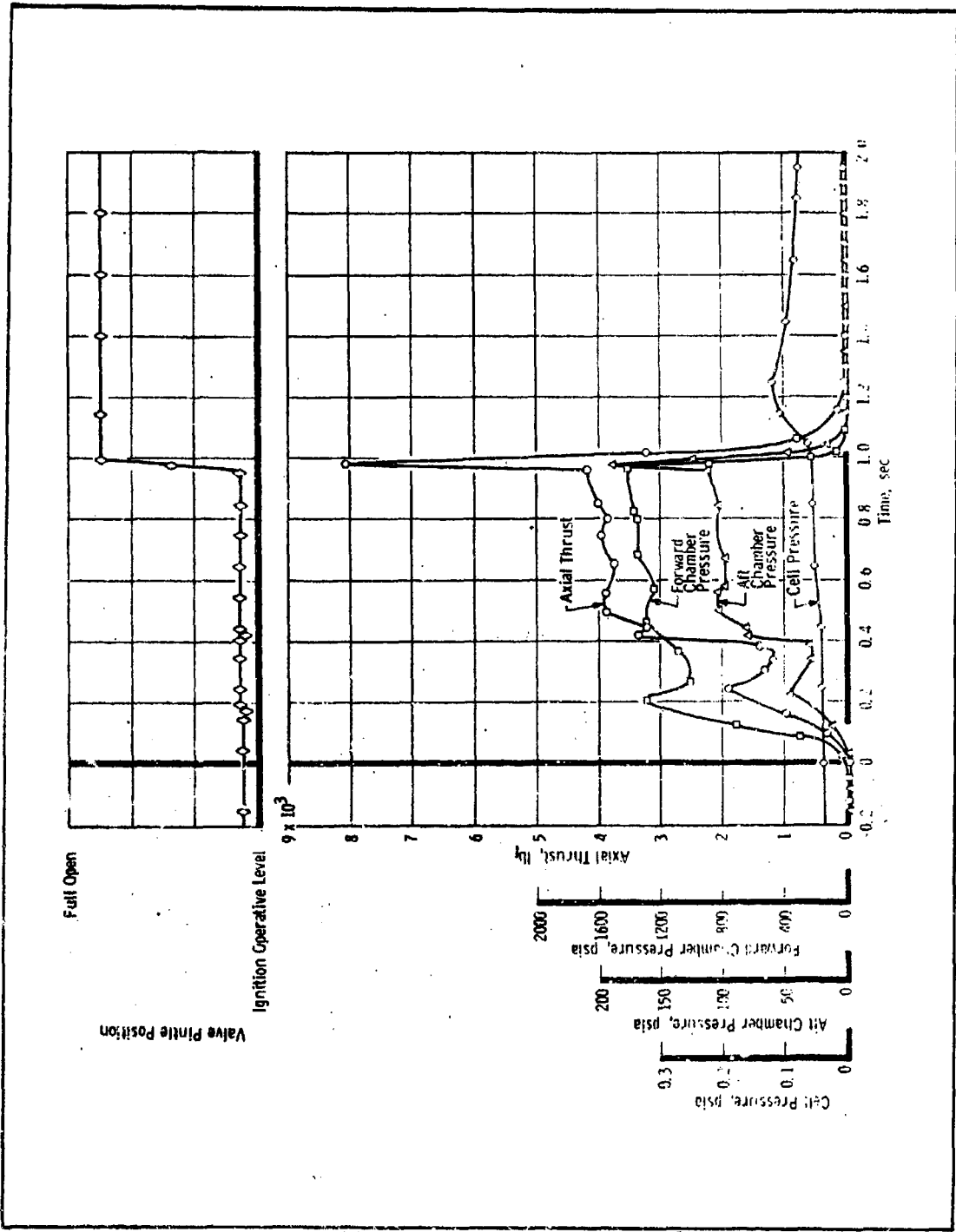


Figure 167 - Traces for Test N. 5. 1

**CONFIDENTIAL**

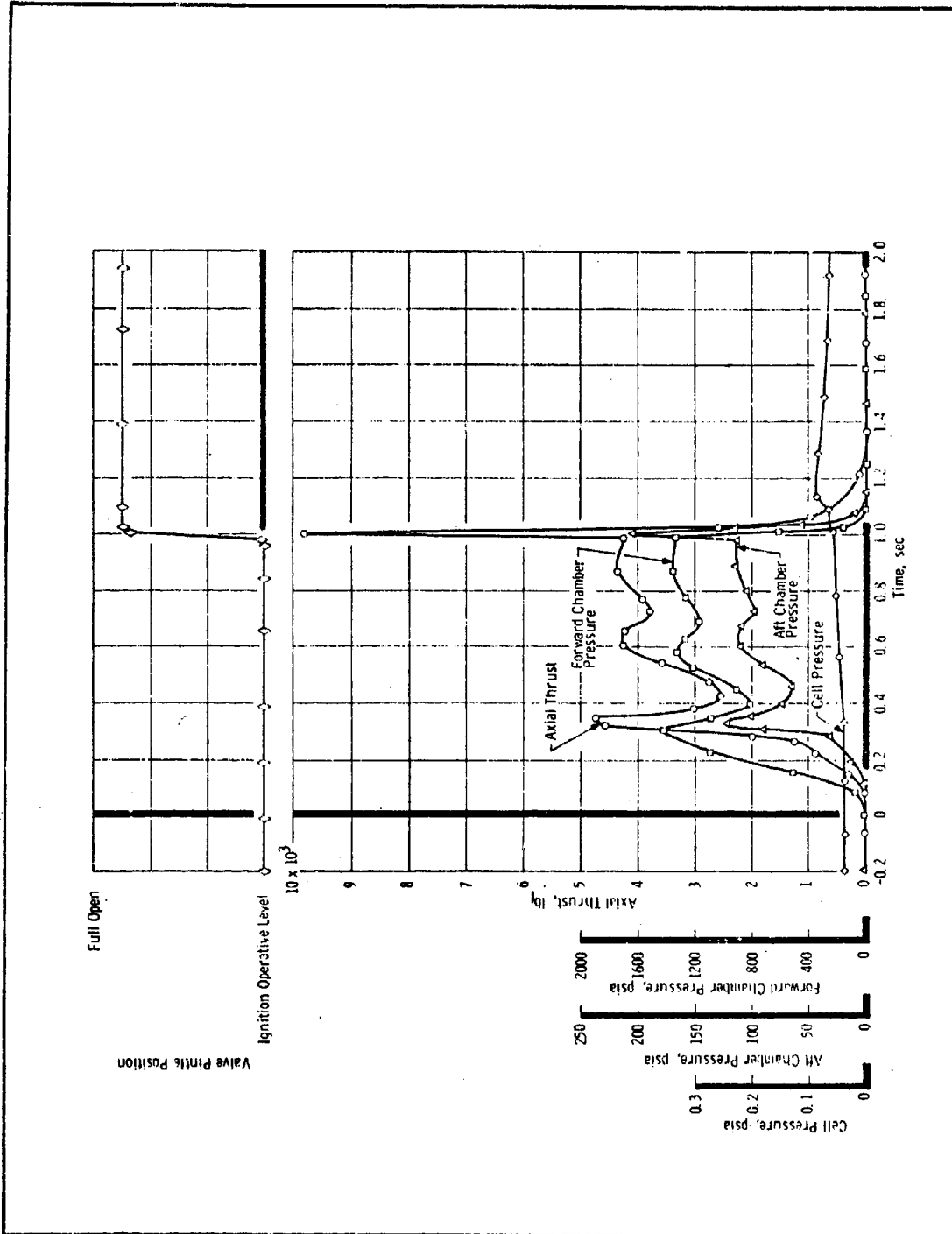


Figure 168 - Traces for Test N. 5.2

# CONFIDENTIAL

AFRPL-TR-65-209, Vol I

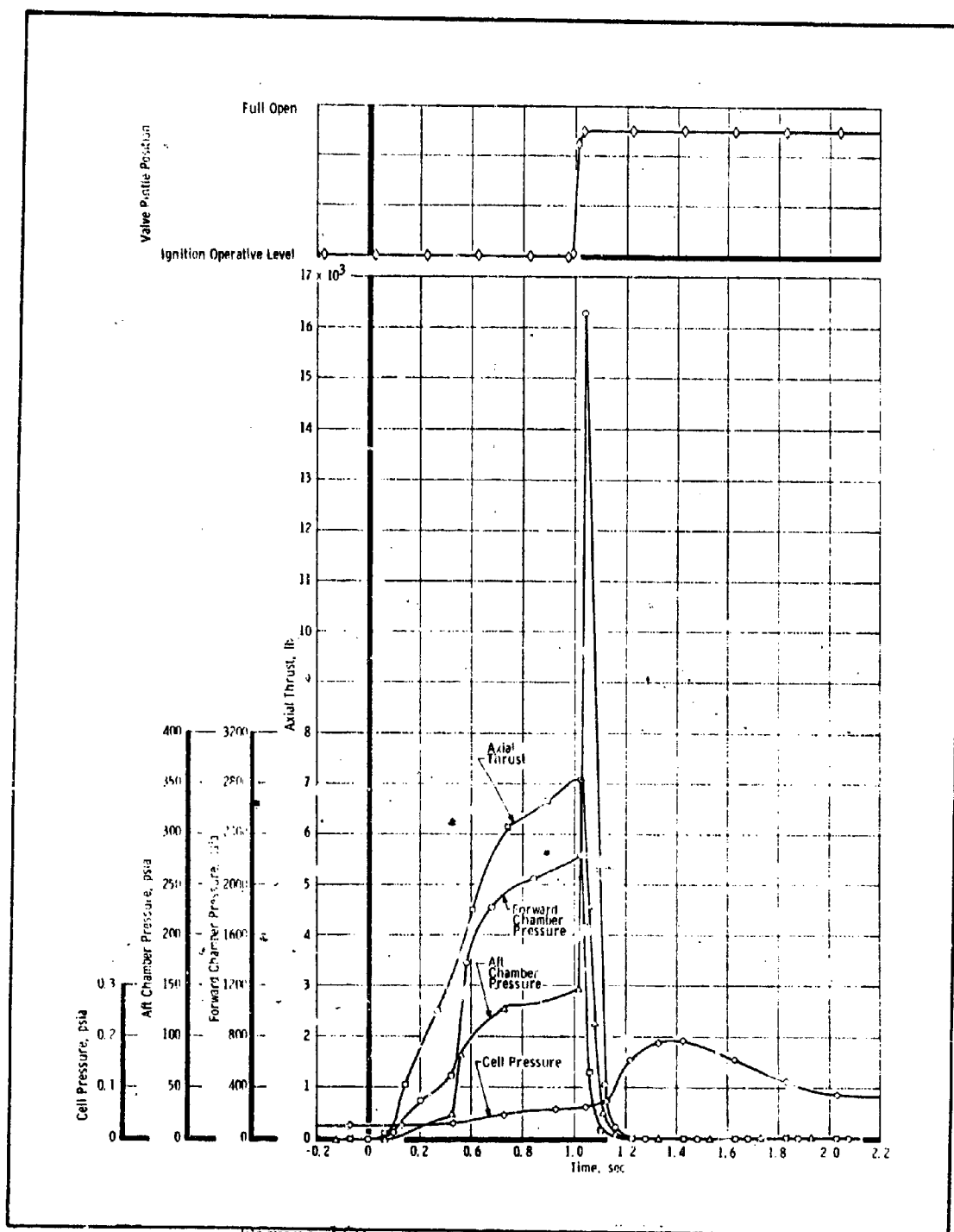
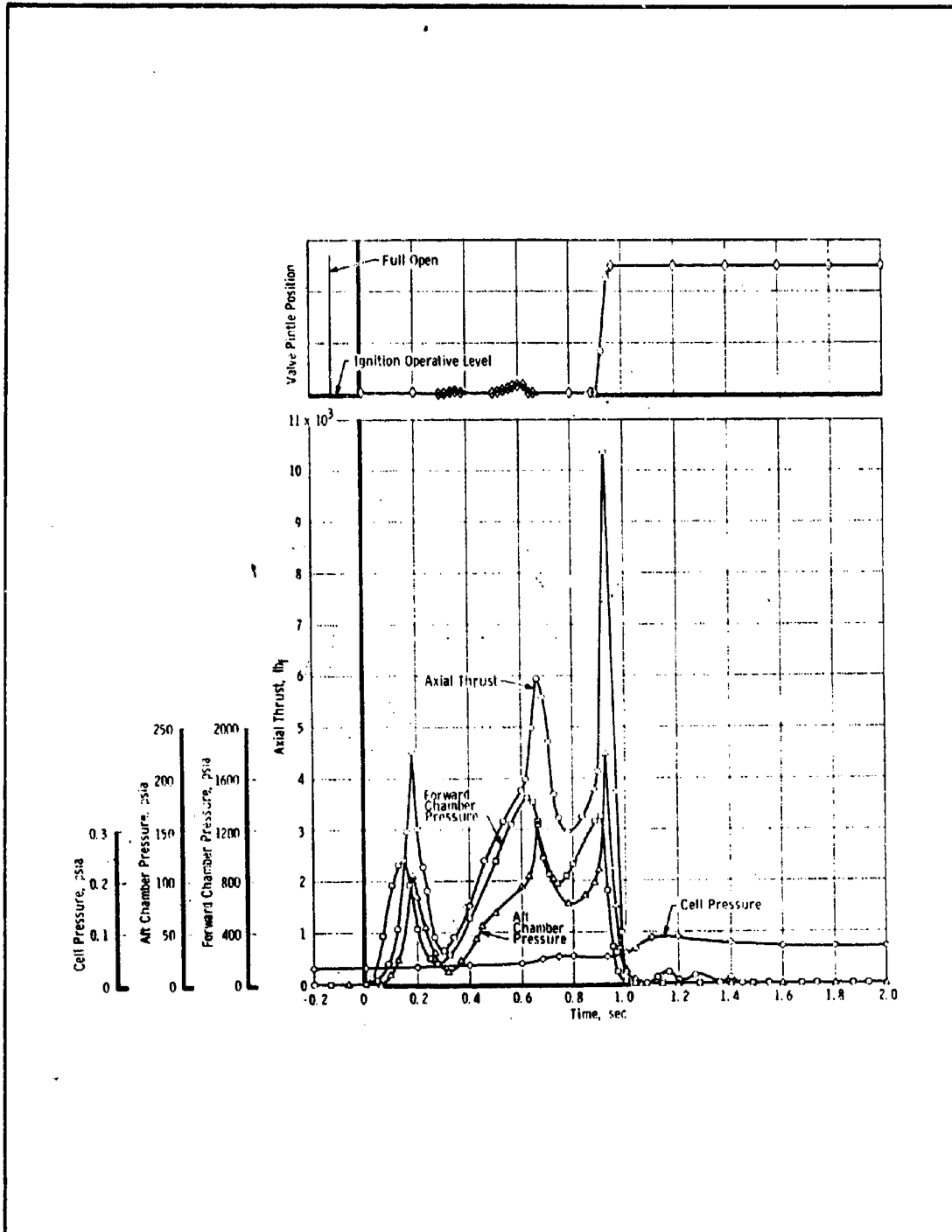


Figure 169 - Traces for Test N. 5.3

# CONFIDENTIAL

**CONFIDENTIAL**

AFRPL-TR-65-209, Vol I



**CONFIDENTIAL**

**CONFIDENTIAL**

AFRPL-TR-65-209, Vol I

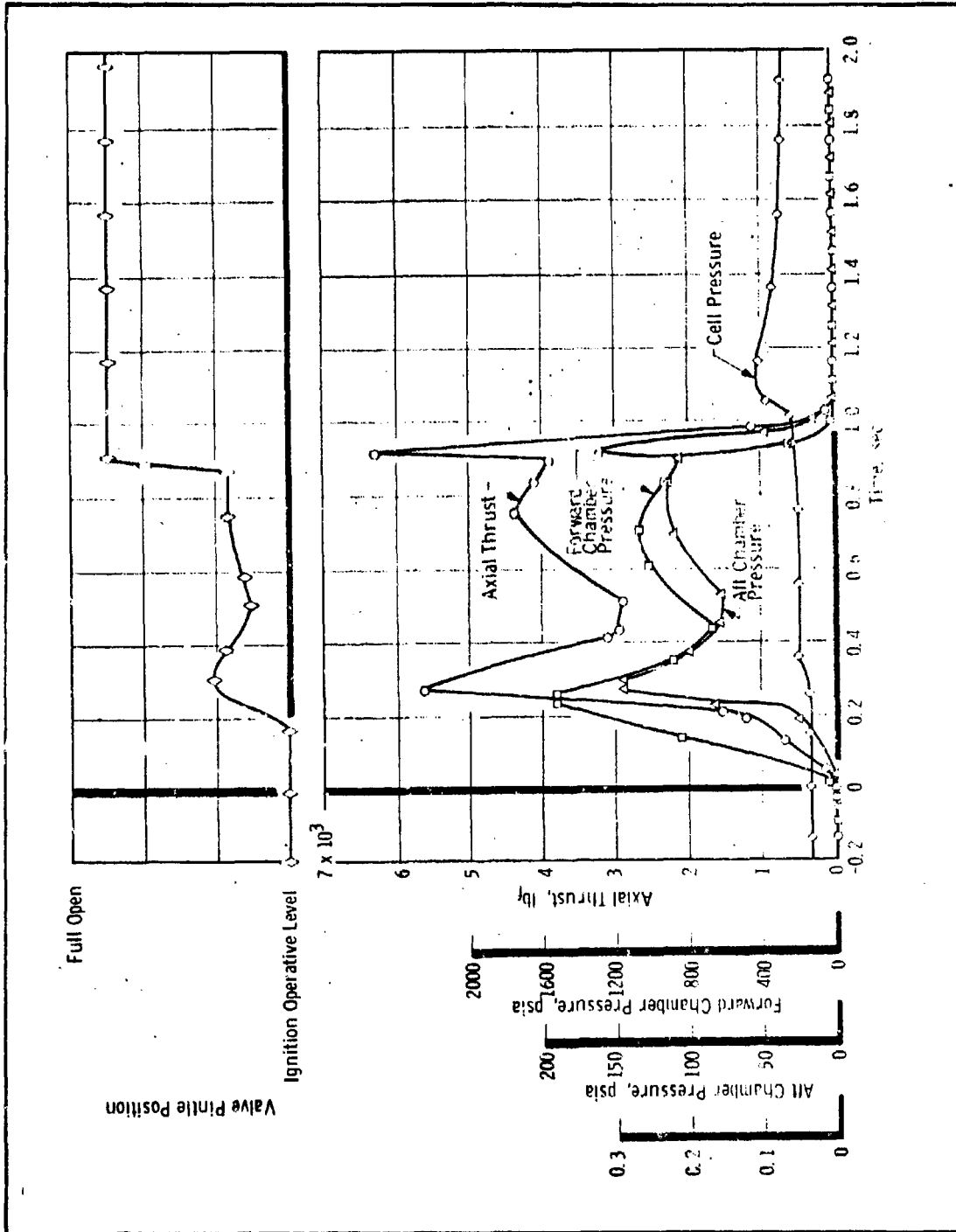


Figure 171 - Traces for Test N. 5. 5

**CONFIDENTIAL**

**CONFIDENTIAL**

AFRPL-TR-65-209, Vol I

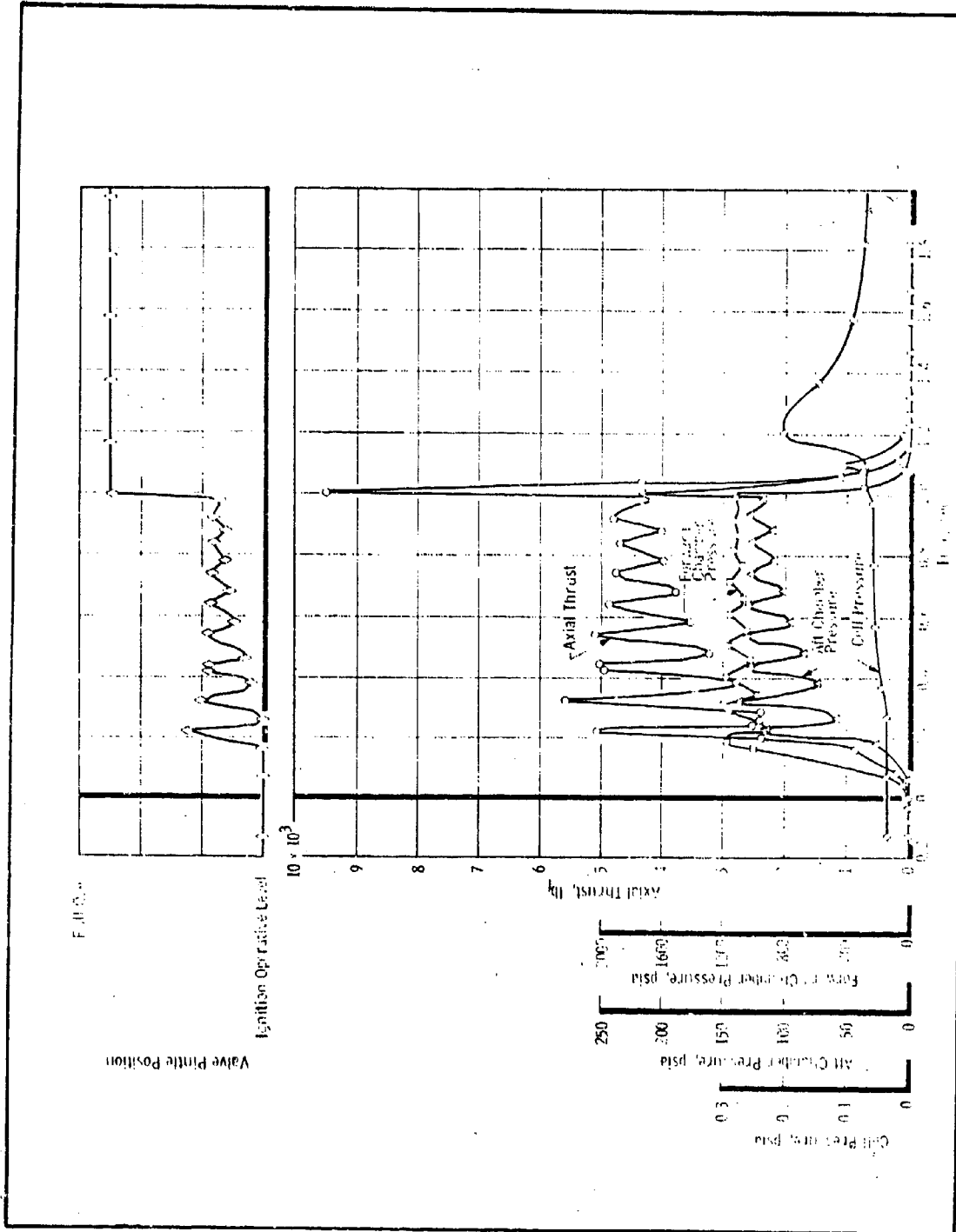


Figure 172 - Traces for Test N. 5.6

**CONFIDENTIAL**

# CONFIDENTIAL

AFRPL-TR-65-209, Vol I

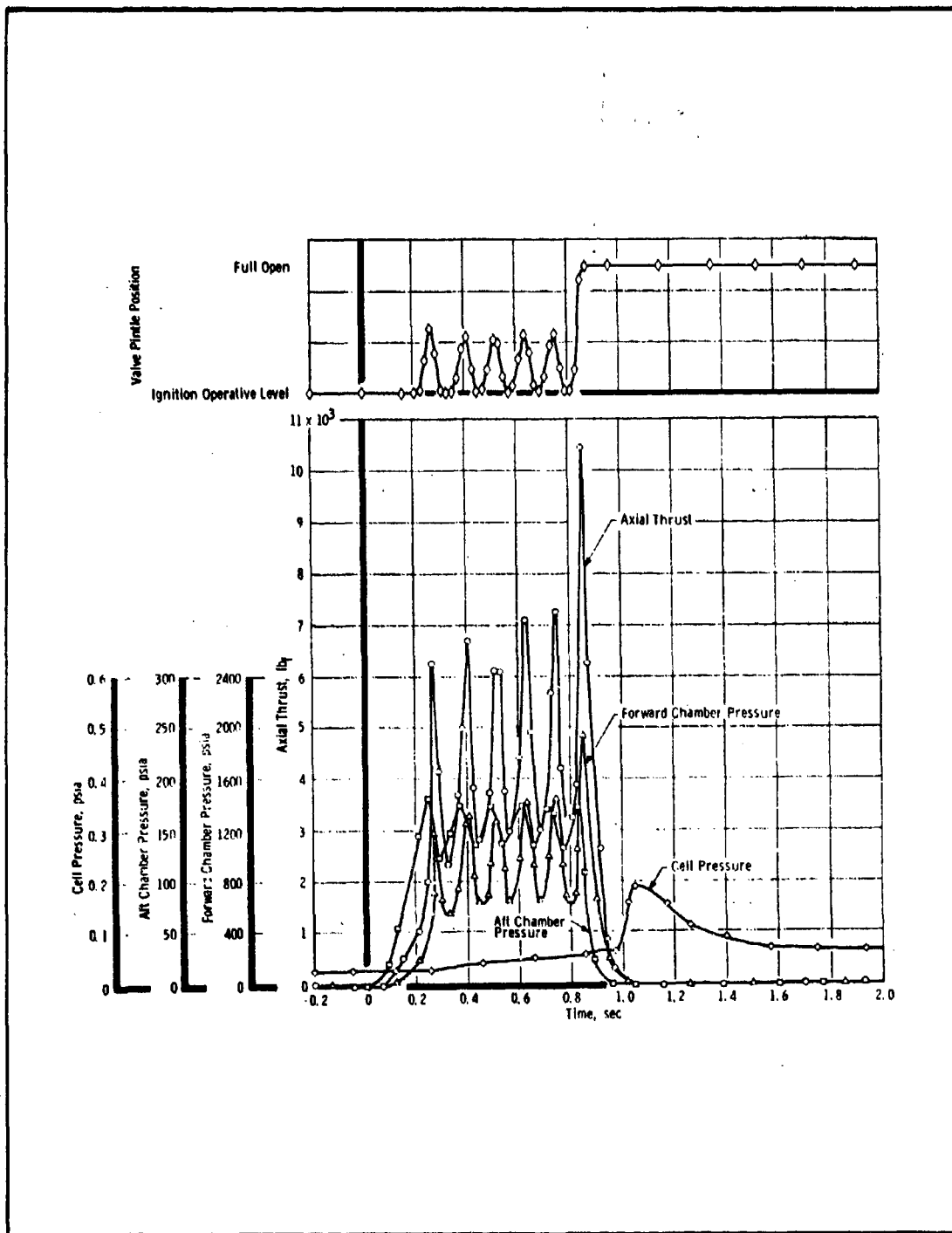


Figure 173 - Traces for Test N. 5.7

# CONFIDENTIAL

**CONFIDENTIAL**

AFRPL-TR-65-209, Vol I

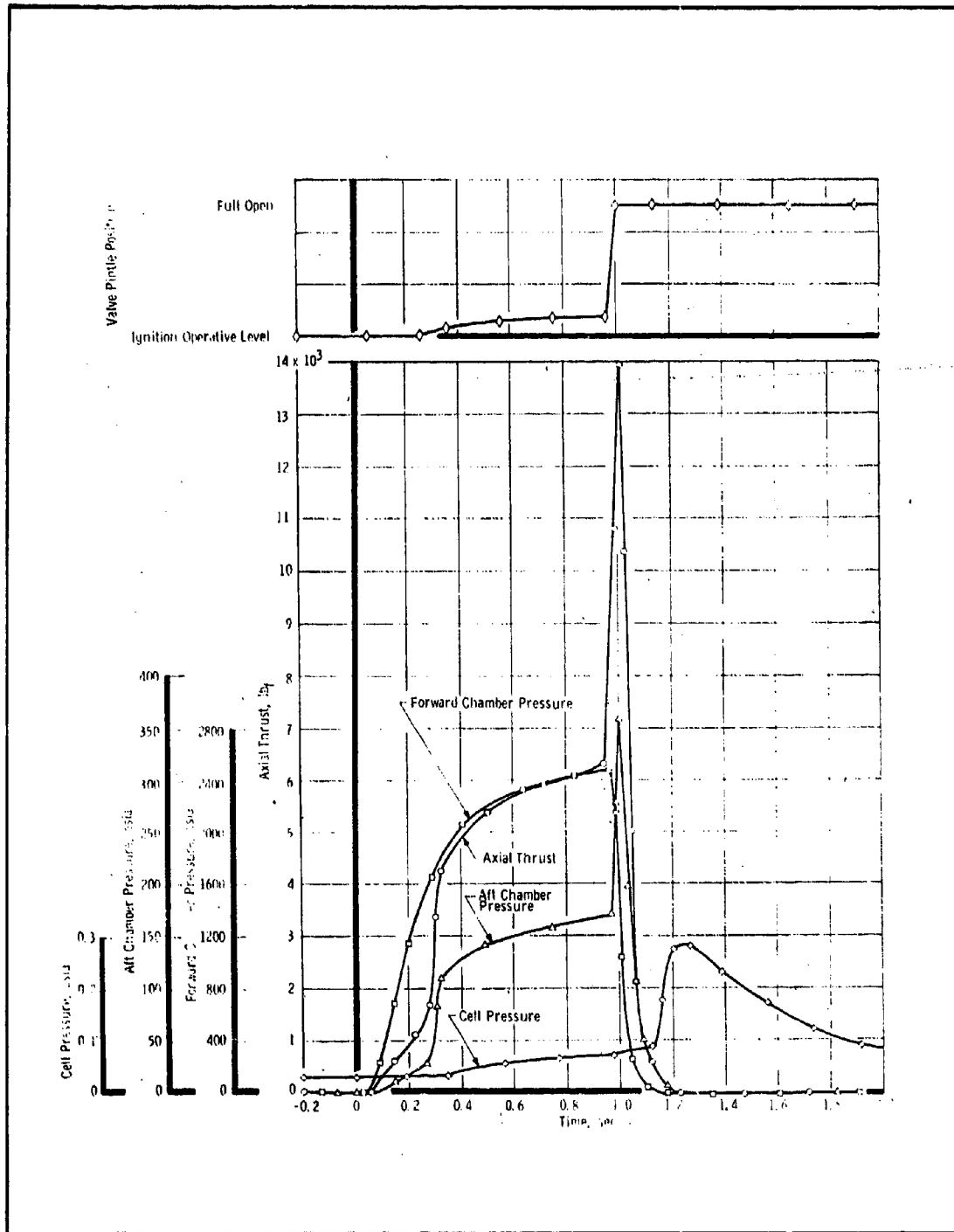


Figure 174 - Traces for Test N. 5.8

**CONFIDENTIAL**

# CONFIDENTIAL

AFRPL-TR-65-209, Vol I

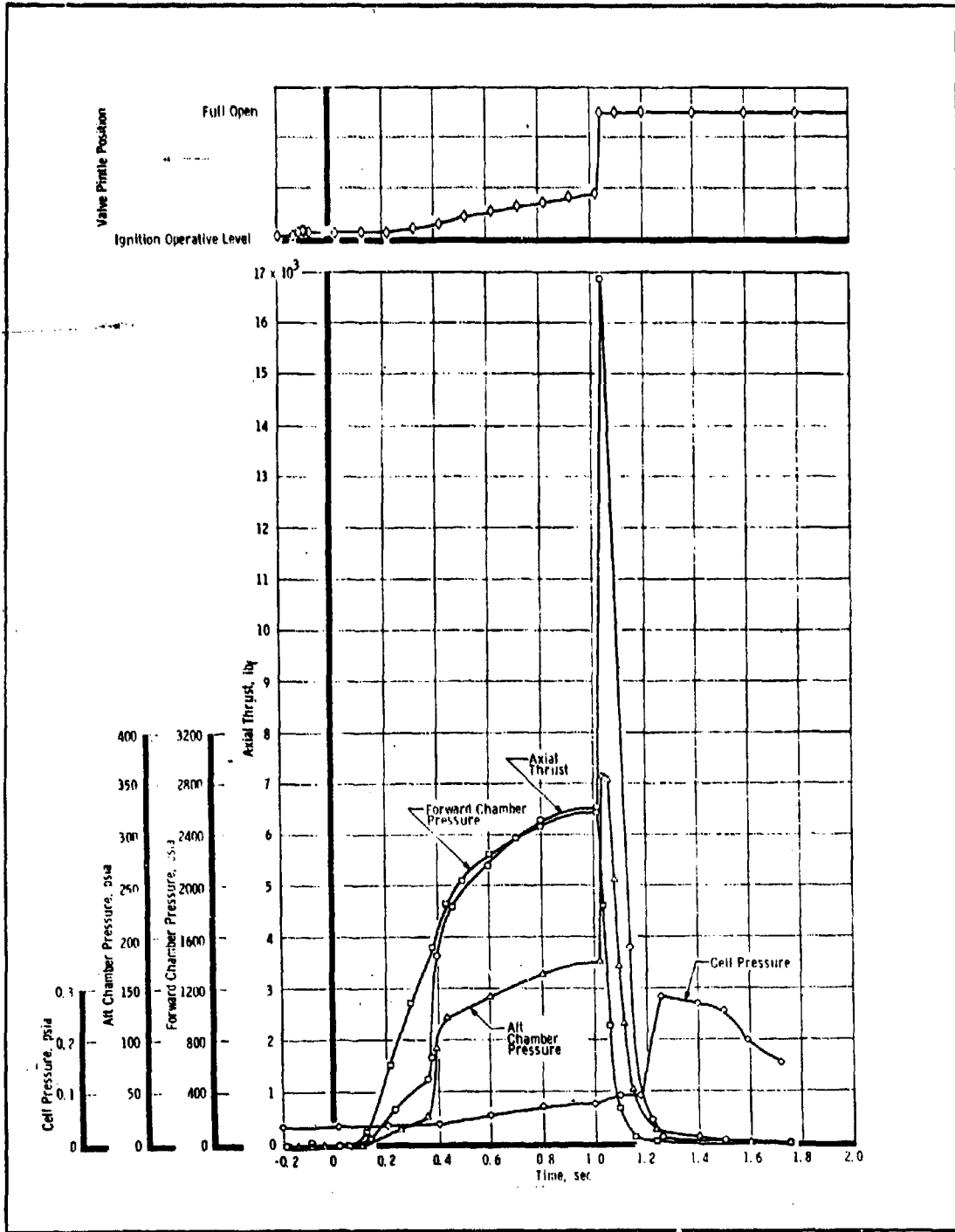


Figure 175 - Traces for Test N. 5. 9

# CONFIDENTIAL

# CONFIDENTIAL

AFRPL-TR-65-209, Vol I

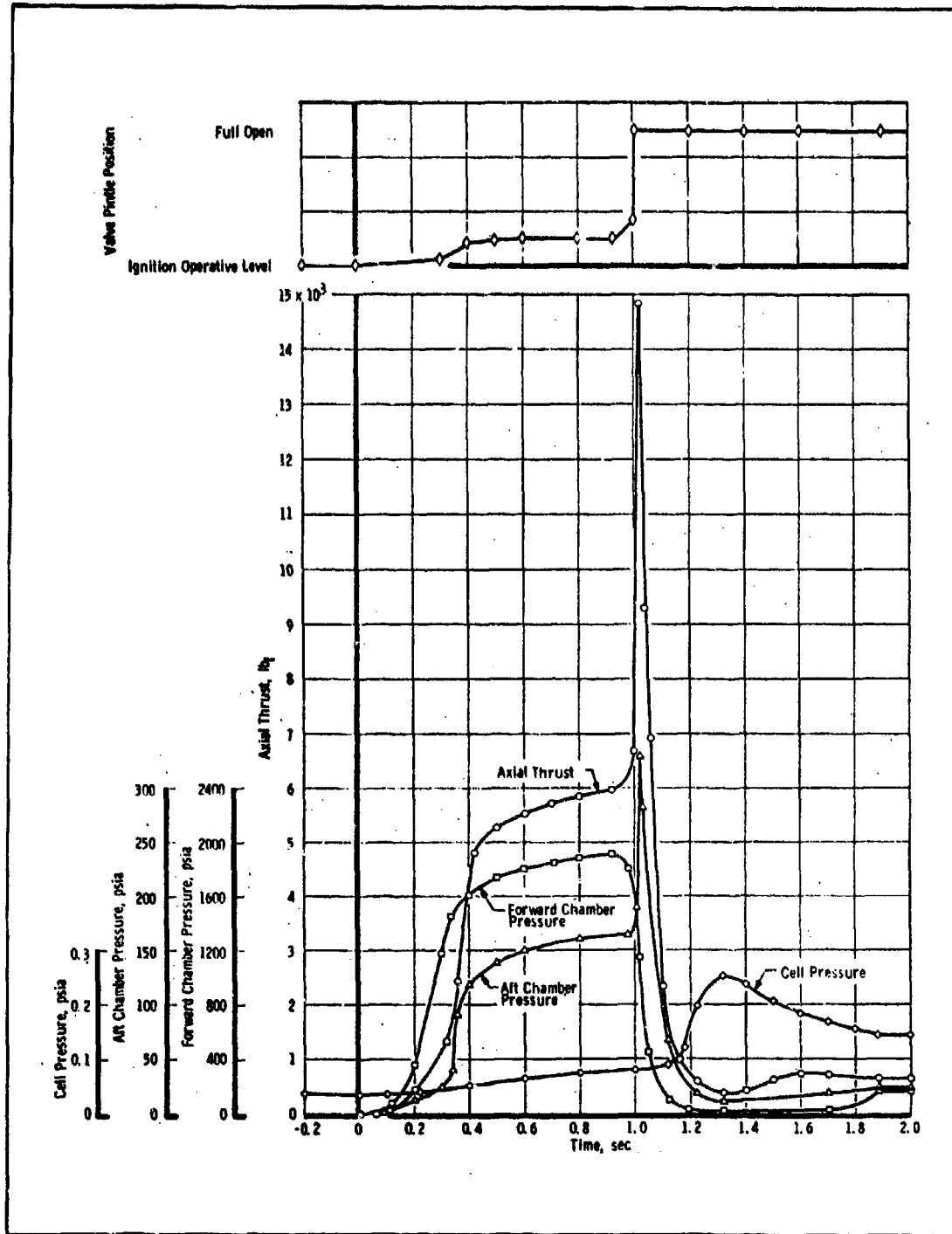


Figure 176 - Traces for Test N. 5.10 (First 2-sec of Operation)

# CONFIDENTIAL

**CONFIDENTIAL**

AFRPL-TR-65-209, Vol I

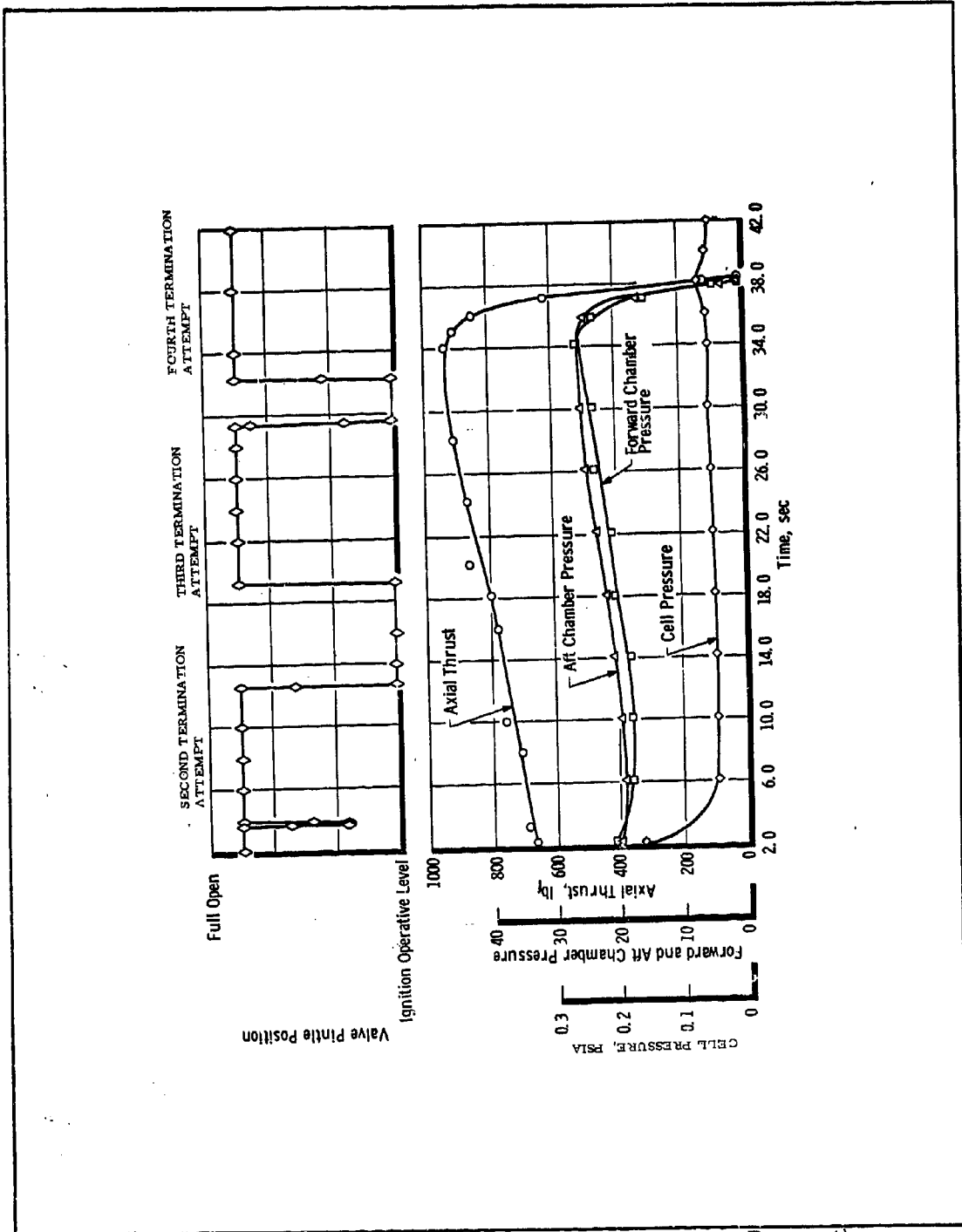


Figure 177 - Traces for Test N. 5.10 (t + 2-sec to Burnout)

**CONFIDENTIAL**

**CONFIDENTIAL**

AFRPL-TR-65-209, Vol I

TABLE LXIV - MOTOR SUMMARY FOR TEST N. 5

Parameter	Ignition Cycle									
	1	2	3	4	5	6	7	8	9	10
Test Date	12/3/65	12/10/65	12/13/65	12/14/65	12/14/65	12/16/65	12/16/65	12/17/65	12/17/65	12/20/65
Ignition Altitude (ft)	130,000	128,500	137,000	131,000	133,000	131,000	135,000	133,000	132,000	132,000
Average Altitude During Firing (ft)	124,000	123,000	120,000	120,500	122,500	119,000	118,000	110,000	108,000	127,000
Number of Pyrogens	2	2	2	3	3	3	3	3	3	4
Valve Serial Number	1	1	1	1	1	1	1	1	1	1
Nozzle Serial Number	3A	3A	3A	3A	3A	3A	3A	3A	3A	3A
Nozzle Throat Area (sq in.)										
Pre-Fire	21.615	21.615	21.615	21.606	21.598	21.598	21.586	21.573	21.590	21.610
Post-Fire	21.615	21.615	21.606	21.598	21.598	21.586	21.573	21.590	21.610	19.652
Average	21.615	21.615	21.610	21.602	21.598	21.592	21.580	21.582	21.600	20.631
Nozzle Exit Area (sq in.)										
Pre-Fire	199.933	199.933	199.995	200.008	199.880	199.956	200.006	199.956	199.956	200.119
Post-Fire	199.933	199.995	200.008	199.880	199.956	200.006	199.956	199.956	200.119	200.006
Average	199.933	199.964	200.002	199.944	199.918	199.981	199.981	199.956	200.038	200.063
Nozzle Area Ratio										
Pre-Fire	9.250	9.250	9.253	9.257	9.255	9.258	9.266	9.269	9.262	9.260
Post-Fire	9.250	9.253	9.257	9.255	9.258	9.266	9.269	9.262	9.260	10.173
Average	9.250	9.252	9.255	9.256	9.256	9.262	9.268	9.266	9.261	9.697

**CONFIDENTIAL**

# CONFIDENTIAL

AFRPL-TR-65-209, Vol I

TABLE LXXV - SUMMARY OF REDUCED BALLISTIC DATA FOR TEST N.5

Parameter	Ignition Cycle										Total 1-9
	1	2	3	4	5	6	7	8	9	10	
<b>Forward Chamber</b>											
Delay Time, 0 to 10% (sec)	0.120	0.126	0.295	0.148	0.155	0.096	0.286	0.110	0.066	0.183	...
Rise Time, 10 to 90% (sec)	0.117	0.172	0.218	0.091	0.171	0.117	0.139	0.160	0.276	0.180	...
Burn Time, 10% to Termination(sec)	0.920	0.896	0.735	0.882	0.872	0.936	0.754	0.912	0.903	0.880	7.810
Decay Time, Termination to 10% (sec)	0.038	0.042	0.041	0.050	0.058	0.061	0.064	0.069	0.076	0.110	...
$\int \text{Pd}_t$ (psia-sec)	1,130	1,056	1,440	746.8	858.7	1,025	915.7	1,868	1,805	1,422	10,845.
$\bar{P}_b$ (psia)	1,196	1,153	1,866	815.5	952.8	1,062	1,159	1,948	1,907	1,519	1334.
Web Burned (in.)	0.246	0.231	0.247	0.167	0.200	0.220	0.200	0.323	0.366	0.273	2.200
Burn Rate (in./sec)	0.267	0.258	0.336	0.189	0.229	0.235	0.265	0.354	0.405	0.310	0.282
Weight Burned (lb.)											
Grain	7.150	6.953	7.680	5.405	6.273	7.317	6.625	10.546	10.280	9.127	68.229
Pyrogen	0.390	0.383	0.390	0.581	0.589	0.585	0.577	0.574	0.582	0.766	4.651
Total	7.540	7.336	8.070	5.986	6.862	7.902	7.202	11.120	10.862	9.893	72.880
<b>Aft Chamber</b>											
Delay Time, 0 to ignition (sec)	0.464	0.321	0.535	0.250	0.341	0.225	0.434	0.322	0.380	0.383	...
Rise Time, Ignition to 90% (sec)	0.076	0.036	0.046	0.043	0.045	0.031	0.035	0.036	0.039	0.060	...
Burn Time, Ignition to 10% (sec)	0.653	0.796	0.597	0.882	0.798	0.921	0.739	0.879	0.848	0.820/ 36.94	7.113
Decay Time, Termination to 10% (sec)	0.076	0.092	0.104	0.102	0.109	0.125	0.141	0.179	0.199	0.220	...
$\int \text{Pd}_t$ (psia-sec)	76.71	84.80	82.74	73.41	85.60	103.1	87.21	134.9	135.2	916.4	863.7
$\bar{P}_b$ (psia)	100.9	100.6	129.0	81.9	102.6	108.2	112.3	146.8	151.8	148.4/ 21.9	114.9
Web Burned (in.)	0.101	0.114	0.101	0.109	0.132	0.145	0.120	0.184	0.192	2.143	1.198
Burn Rate (in./sec)	0.155	0.143	0.169	0.124	0.165	0.157	0.162	0.209	0.226	...	0.168
Weight Burned (lb)	5.406	6.696	6.029	6.337	7.254	8.771	7.264	11.040	11.450	138.126	70.247
<b>Total Motor</b>											
Weight Burned (lb)	12.946	14.032	14.099	12.323	14.116	16.673	14.466	22.160	22.312	148.019	143.127
Weight Aft/Weight Forward	0.117	0.913	0.747	1.059	1.057	1.110	1.009	0.993	1.054	...	0.964
$\int \text{Pd}_t$ meas. (lb <sub>f</sub> -sec)	2,921.6	3,202.7	3,168.4	2,745.7	3,187.6	3,823.0	3,245.3	5,042.8	5,077.3	33,248	32,414
$\int \text{Pd}_t$ vac. (lb <sub>f</sub> -sec)	2,930.5	3,213.5	3,176.5	2,755.7	3,197.4	3,834.9	3,260.0	5,056.8	5,092.2	33,631	32,518
$\bar{P}_b$ (lb <sub>f</sub> )	3,854	3,884	4,893	3,031	3,775	3,955	4,110	5,458	5,572	5,116/ 789	4,276
$\int \text{Pd}_t$ term (lb <sub>f</sub> -sec)	302	327	638	486	366	468	586	1,057	1,196	1,328	...
Throat Area (sq in.)	21.613	21.615	21.610	21.602	21.598	21.592	21.580	21.582	21.600	20.631	21.599
Expansion Ratio	9.250	9.252	9.255	9.256	9.256	9.262	9.268	9.266	9.261	9.697	9.258
Cell Pressure Integral (psia-sec)	0.04470	0.05398	0.04027	0.05014	0.04926	0.05960	0.07367	0.07019	0.07428	1.915	0.5161
Characteristic Velocity (fps)	4,121	4,203	4,080	4,140	4,214	4,296	4,186	4,227	4,211	4,110	4,194
<b>Specific Impulse (lb-sec/lb)</b>											
Measured, $\alpha = 17.5^\circ$	225.7	228.2	224.7	222.8	225.8	229.3	224.3	227.6	227.6	224.6	226.5
Corrected to Vacuum, $\alpha = 17.5^\circ$	226.4	229.0	225.3	223.6	226.5	230.0	225.4	228.2	228.2	227.2	227.2
Corrected to Vacuum, 20/1, $\alpha = 17.5^\circ$	237.1	240.0	236.1	234.3	237.4	241.0	236.2	239.2	239.2	238.1	238.1
Theoretical, Vacuum, 20/1, $\alpha = 17.5^\circ$	257.1	261.2	258.0	263.4	263.4	264.0	262.8	262.6	263.3	...	262.1
Efficiency (%)	92.2	91.9	91.5	89.0	90.1	91.3	89.9	91.1	90.8	...	90.8
Ratio of Specific Heats	1.23	1.22	1.23	1.22	1.22	1.22	1.22	1.22	1.22	1.22/ 1.18	1.22
Measured Thrust Coefficient	1.762	1.747	1.772	1.732	1.724	1.717	1.724	1.732	1.739	1.758	1.738

(Confidential)

# CONFIDENTIAL

# CONFIDENTIAL

AFRPL-TR-65-209, Vol I

TABLE LXVI - TERMINATION SUMMARY FOR TEST N.5

Parameter	Ignition Cycle									
	1	2	3	4	5	6	7	8	9	10
<b>Forward Chamber</b>										
Termination Pressure (psia)	1,401	1,383	2,836	1,350	855	1,132	1,401	2,501	2,595	1,928
Decay Rate, dp/dt (psi/sec)	59,400	54,300	114,300	48,900	26,900	32,000	40,400	63,100	66,000	36,800
Decay Rate/P <sub>term</sub> (sec <sup>-1</sup> )	42.4	39.3	40.3	36.3	31.5	28.3	28.8	25.2	25.4	19.1
Valve Actuation Time(sec)	0.031	0.034	0.032	0.038	0.033	0.026	0.029	0.029	0.011	...
<b>Air Chamber</b>										
Termination Pressure (psia)	112.9	109.3	153.8	115.9	102.2	123.8	121.1	170.6	186.2	163.4
Maximum Pressure at Termination (psia)	239.3	233.5	406.6	247.1	207.2	247.8	286.7	403.1	406.7	329.2
Decay Rate, dp/dt (psi/sec)	6,520	5,300	8,770	4,080	3,910	3,650	4,490	4,930	4,380	3,120
Decay Rate/P <sub>term</sub> (sec <sup>-1</sup> )	27.2	22.7	21.6	16.5	18.9	14.7	15.7	12.2	10.8	9.5
Free Volume at Termination (cu in.)	2,416	2,514	2,592	2,676	2,783	2,902	3,000	3,150	3,260	3,380
Free Volume/Throat Area, L* (in.)	111.8	116.3	120.0	123.9	128.9	134.4	139.1	145.9	150.9	156.4
Surface Area/Throat Area, K <sub>n</sub>	32.6	33.0	33.4	33.8	34.2	34.7	35.1	35.7	36.2	...

(Confidential)

# CONFIDENTIAL

SECTION VIII - EVALUATION OF NOZZLE DESIGNS

1. GENERAL

Three TRW-designed nozzles were fabricated for this program. Nozzle No. 1 used for the latter cycles of Test M. 6 (see Section VI, item 2, d), had a 2-to-1 expansion ratio, and is described in Appendix C. Nozzles 2 and 3, with 20-to-1 expansion ratios, were used in tests M. 7 and M. 8 (nozzle No. 2) and N. 4 and N. 5 (nozzle No. 3). These two nozzles are described in detail in Appendix D. A post-firing analysis and evaluation of these nozzles was conducted to ascertain their performance under cycling operating conditions. The results of this evaluation are reported in the following paragraphs.

2. EVALUATION OF NOZZLES 1 AND 2

An examination of post-fired M. 6 nozzle No. 1 showed little evidence of exposure to the environment. The post-fired throat diameter was measured to be 3.567-in., which compared exactly to the pre-fired dimension, indicating negligible erosion had occurred in the throat.

Char depths were minimal (0.06) on the silica motor insulation ring, and no complete char formation had occurred on the insulators behind the CGW and RVD graphite sections. A slight discoloration existed, however, indicating a minimal degree of polymerization had occurred. The carbon cloth-phenolic entrance ring was not delaminated and char had progressed to only about 3/16-in. Erosion on this part was negligible, also. All joints appeared tight with no evidence of flow in split lines. No indication of axial expansion of the aft section against the Belleville springs was evident. All O-rings were flexible and not discolored, indicating no heat penetration to these surfaces.

Examination of post-fired nozzle No. 2 showed traces of exposure to the environment. The motor insulation ring (molded silica-phenolic) showed traces of alumina deposit along its forward face. Material char depth was minimal (1/8 inch) and no measurable erosion was evident. No gas flow paths were evident down any interface.

The carbon phenolic material in the inlet showed the greatest degradation. Erosion loss of approximately 0.350 in. ( $\Delta R$ ) of carbon-phenolic material was evident at the interface between the graphite throat insert and the throat approach. The material shows evidence of eroding uniformly without spalling or delamination loss. No evidence of thermal pulse cracking along ply lines was evident and aside from the rather pronounced erosion at the throat interface, the carbon-phenolic approach section appeared to be sound, with uniform (circumferential) erosion along its entire length. A plot of the erosion profile is shown in Figure No. 178. The area of maximum erosion corresponded fairly well with expected positions of maximum particle impingement (area ratio of 1-1/2 to 2).

The expansion gap between the graphite throat insert and carbon-phenolic throat approach increased from the nominal 0.048 to approximately 0.120 in. this is believed to be a result of shrinkage of the carbon-phenolic due to resin pyrolysis during the thermal pulsing, as no axial shift in position was noted nor was there any ply loss down the throat insert-throat approach section interface. This shrinkage amounted to 3 percent of the throat approach section length perpendicular to the ply orientation (90 deg with respect to  $\phi$ ) and matched closely data generated in laboratory tests on shrinkage of reinforced phenolic materials after pyrolysis. Nominal values show shrinkage rates ranging from 0.030 to 0.045 in. per inch in a direction perpendicular to the plies. Without knowing the extent of the char depth in the approach section and examining the cross section of the interface joint, further hypotheses on the reason for the expansion gap growth is difficult. It stands to reason, however, that for optimized nozzle design configurations for pulsed applications, additional consideration should be given to the shrinkage problem either through incorporation of processing methods or resin systems with less gross shrinkage, or through use of more stabilized materials. The PTB material used in the throat extension of the nozzle section is one such candidate material.

Examination of the graphite throat insert showed no trace of cyclic failure (cracking) from thermal pulsing. The forward (upstream) portion of the insert was roughened, but minor erosion had occurred. One small chip was apparent in the inlet portion of the insert which was attributed to striking of the insert wall by ejection of a plastic segment from the valve body during the test.

Measurement of the nozzle throat diameter after test showed a value of 3.582 in., compared to 3.568 in. measured just prior to delivery by TRW. The resulting erosion rate, based on a 30-sec total

**CONFIDENTIAL**

AFRPL-TR-65-209, Vol I

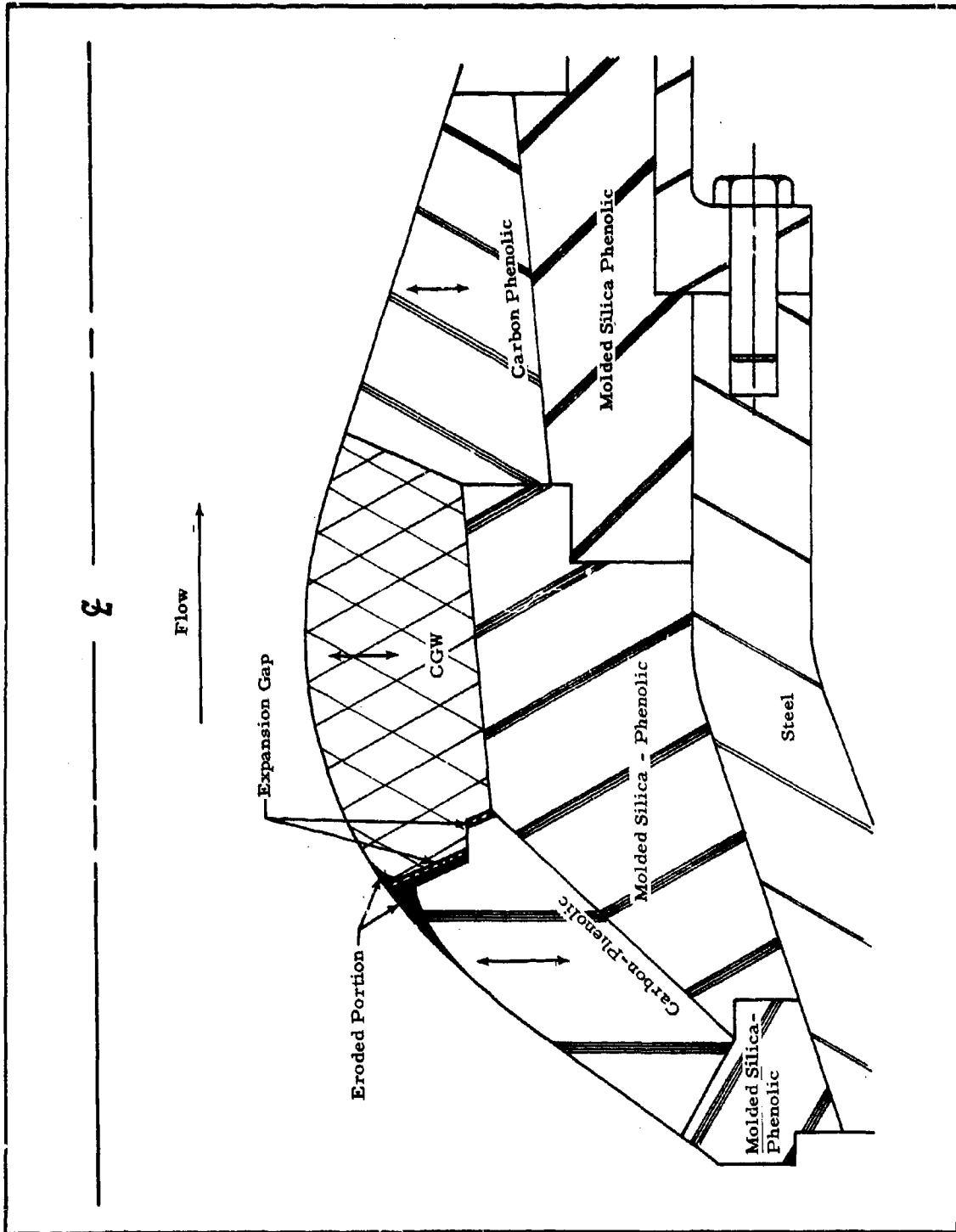


Figure 178 - Sketch of Nozzle No. 2 after Series M Tests, Showing Erosion Profile

**CONFIDENTIAL**

burn time, was approximately 0.2 mils per second. Erosion was uniform circumferentially everywhere along the throat insert length. Aft of the throat centerline, the insert showed almost no trace of environment exposure. The graphite surface was smooth and unroughened. The slight contour deviation (hollow) in the aft portion of the insert was closely examined and reviewed on the basis of an unexplainable appearance. A subsequent review of the machining records indicated a deviation from the true profile had occurred as a result of movement of the profile cam during machining. The ensuing minor difference was well within allowable limits for performance or reliability purposes, however, and hence was not cause for rejection of the insert.

The throat extension (carbon-phenolic) showed no measurable erosion. Likewise, the exit cone (silica-phenolic in Convolvey form) was free from measurable dimensional loss. Visible areas of sporadic local resin loss without melting of the silica reinforcement was indicated in the exit cone. This is indicative of a maximum surface temperature below 3000°F (melting temperature of silica). The visible char depth in the exit cone (at the aft extremity) was approximately 0.030 in.

Thermocouple data from the tests of nozzle No. 2 were examined relative to correlation of data and theory. It was noted for the pulse tests (1.5 sec for M 7.1 through M 7.4 and 8.1 through 8.4), no rise was evident in any of the thermocouples even after heat soakback. This is indicative of the surface material possessing sufficient heat storage capacity to absorb and then re-convect the minor heat pulse imposed. The longer duration runs (M 7.5 and M 8.5) show traces of heat penetration at the end of the heat pulse, followed by a heat soakback influence. The maximum temperature measured in the carbon-cloth reinforced phenolic throat approach section in the M 7.5 test was 120°F, and this peak was reached after approximately 10 min of heat soakback. The insulator beneath the graphite throat insert reached 750°F at 30 sec and declined thereafter. Data obtained during nozzle development showed that the temperature at the carbon-silica interface after a three-second burst is ambient (70°F) and at the CGW graphite-silica interface is 250°F.

The average temperature reached by the plastic components is related to the heat stored within the section from the inner surface to the position in question and the heat convected and radiated from the inner surface. Again, data from development tests indicate the average temperature in the carbon-phenolic is approximately 150°F, which reasonably well matches the 120°F measured in M.7.5. For low temperatures, resin decomposition, radiation, and convection are minor

influences so that stored heat energy  $C(\Delta T)$  is closely preserved. For the insulator behind the throat insert, the average temperature of the graphite is approximately 1700°F, and radiation, convection, and resin pyrolysis become significant factors. The peak temperature was reached much quicker than in the carbon-phenolic part as would be expected both due to the higher thermal diffusivity value for polycrystalline graphite (CGW) and the greater driving potential ( $\Delta T$ ). The temperature dies out quickly, however, because of the energy absorbed in resin pyrolysis and the ease in temperature dispersion throughout the CGW graphite throat insert. The temperature measurements made confirm the conservative nature of the design for the actual duty cycle imposed, but also correlate substantially the predicted cyclic heat pulse predictions.

### 3. EVALUATION OF NOZZLE 3

#### a. General

Upon completion of Series N tests, nozzle No. 3 was disassembled and the components were examined. The plastic sections were removed from the steel shell and each section was separated for close visual and dimensional checks.

#### b. Visual Examination

The three component sections (throat, throat extension, and exit cone, shown in Figure D-1) were closely examined for visual appearance. Each section appeared to be in excellent condition with little evidence of heat penetration into the insulator materials. The inner diameter appeared uniformly circular, and all mating edges were sharp. Measurements indicated that diametral changes in the throat extension and exit cone sections were negligible. The aft end of the exit cone was slightly out of round (0.020 in. on the diameter) from warpage. No delaminations were apparent in any of the plastic sections and shrinkage was not evident in the carbon-phenolic entrance ring. A shrinkage of approximately three percent was observed on this section of nozzle No. 2. This difference is attributed to more closely controlled processing of the material for Nozzle No. 3, arising from the performance knowledge gained on No. 2.

Resin loss in the Convolve exit cone appeared to be minimal, but was more uniform than in Nozzle No. 2. Some deposit was visible at the upstream limit of the exit cone for a distance of

approximately 2 in., but none thereafter. Char depth was a maximum of 0.100 in. at the interfaces of the various plastic sections.

A very close examination of the throat extension revealed a hairline circumferential crack in the PTB liner material about midway down its axial length. No incipient failure mode was evident nor was there any evidence of "washing." It was concluded that the crack was formed by thermal fatigue (repeated expansion contraction during 16 pulses), and that with the extension adequately supported, as it was, it would perform as if the crack were a planned joint line, which pulse caused the piece to crack could not be ascertained.

c. Dimensional Examination

Before and after the various duty cycles imposed on the nozzle, measurements were taken of the throat diameter and exit plane diameter. A plot of the average diametral values, as they deviated from the initial values, is given in Figure 179 as a function of accumulated pulse (burning) time. The average aft-chamber pressure during the pulse is also shown.

Appreciable build-up occurred during the extended pulses (cycles 6 and 16\*). After the first long pulse (cycle number 6), the build-up had reduced the throat diameter to 5.067 in., which was a radial decrease of approximately 0.090 in. During the second long pulse (cycle number 16), the build-up reached a radial thickness of approximately 0.125 in. In both cases, the adherent material was scale-like and easily flaked off so that the original throat diameter was restored.

The build-up is believed to result from condensable species in the propellant gases that coagulate as a deposit on the relatively cool nozzle walls. Where pulse durations are short (1.5 sec), insufficient material is created to provide gross build-up. For the longer pulses, however, the deposition accumulates and reaches measurable proportions. This build-up is directly affected by the pressure conditions imposed. For higher aft-chamber pressures (maximum value for this test series 180 psi), gas shear values as well as heat transfer coefficients were higher, providing conditions less conducive to build up.

---

\* Since this nozzle was used for both Series N tests, the cycles referred to are cumulative; cycles 1 through 6 were for Test N. 4, and cycles 6 through 16 were on N. 5.

**CONFIDENTIAL**

AFRPL-TR-65-209, Vol I

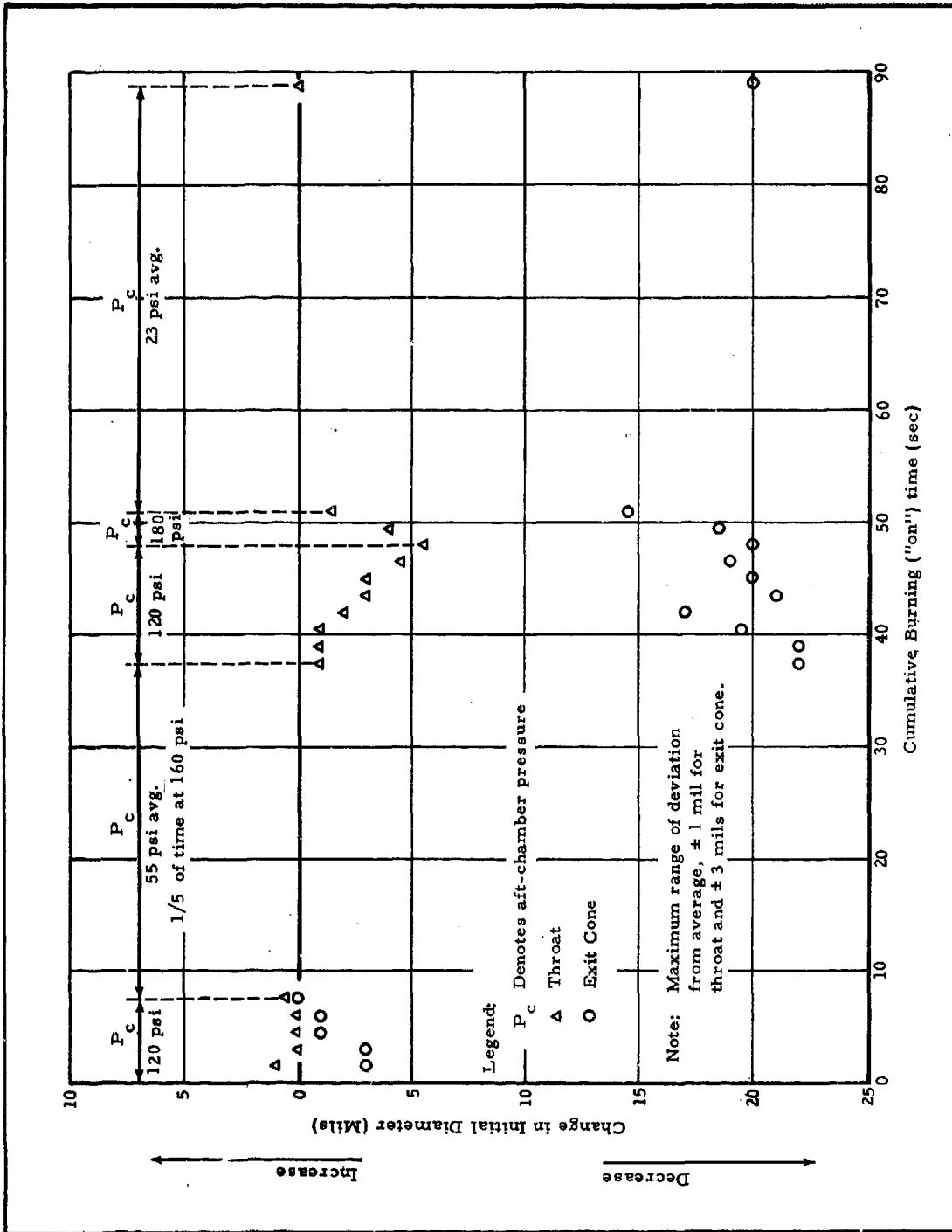


Figure 179 - Dimensional Variations at Nozzle Throat and Exit Cone (Series N)

-309-

**CONFIDENTIAL**

It is interesting to note that no erosion was evident in the throat region of these Series N AEDC tests, whereas for the Series M tests (nozzle No. 2) an 0.2 mil/second throat erosion was measured, based on 10 off-on cycles with a total pulse duration of 30 sec. In both nozzles, the throat material was CGW graphite. The throat contour used for the Series N tests was more gradual, causing some speculation that the erosive and shear forces would be somewhat reduced. Also, the deposited material may have helped to reduce the erosive effects somewhat. A third possible contributor to the reduced rate may have been the different aft propellant.

d. Data Analysis and Comparison

The data obtained from thermocouples inserted in the nozzle at the locations shown in Figure 180 were examined to provide material evaluation and design verification. The temperature rise versus time, for certain duty cycles is shown in Figure 181 for thermocouple No. 5; the cycles shown are 1 and 2 (to show heating of virgin material), 6 and 7 (to show effects of the first long pulse), 14 (to show the highest average chamber pressure), and 16 (to show the second sustained pulse). As is evident in the plot, the effects of the short cycles (1.5 sec) is minimal with respect to degradation of the plastic materials. For each cycle, the nozzle was allowed to cool completely to ambient, thereby limiting the total heat rise to that incurred from each heat pulse. For the sustained pulses (cycles 6 and 16, of 30 and 38 sec duration, respectively), the plastic materials began to degrade as the resin pyrolysis temperature was approached.

The PTB material, although essentially graphite, became an appreciably better conductor with time as shown in Figure 181 for thermocouple No. 6, located in the PTB. This phenomenon is related to the degree of resin pyrolysis of the resin volume contained in the final reimpregnation process.

Thermocouples 1 and 2 (located in the carbon phenolic throat approach) and 9 and 10 (located in the silica phenolic exit cone) did not reach pyrolysis temperature even during the long pulses. The surface temperature of the throat (CGW) and throat extension (PTB), in the plane of the thermocouples, is shown in Figure 182, for each of the long pulses.

The predicted throat temperature gradient for 1.5-sec

**CONFIDENTIAL**

AFRPL-TR-65-209, Vol I

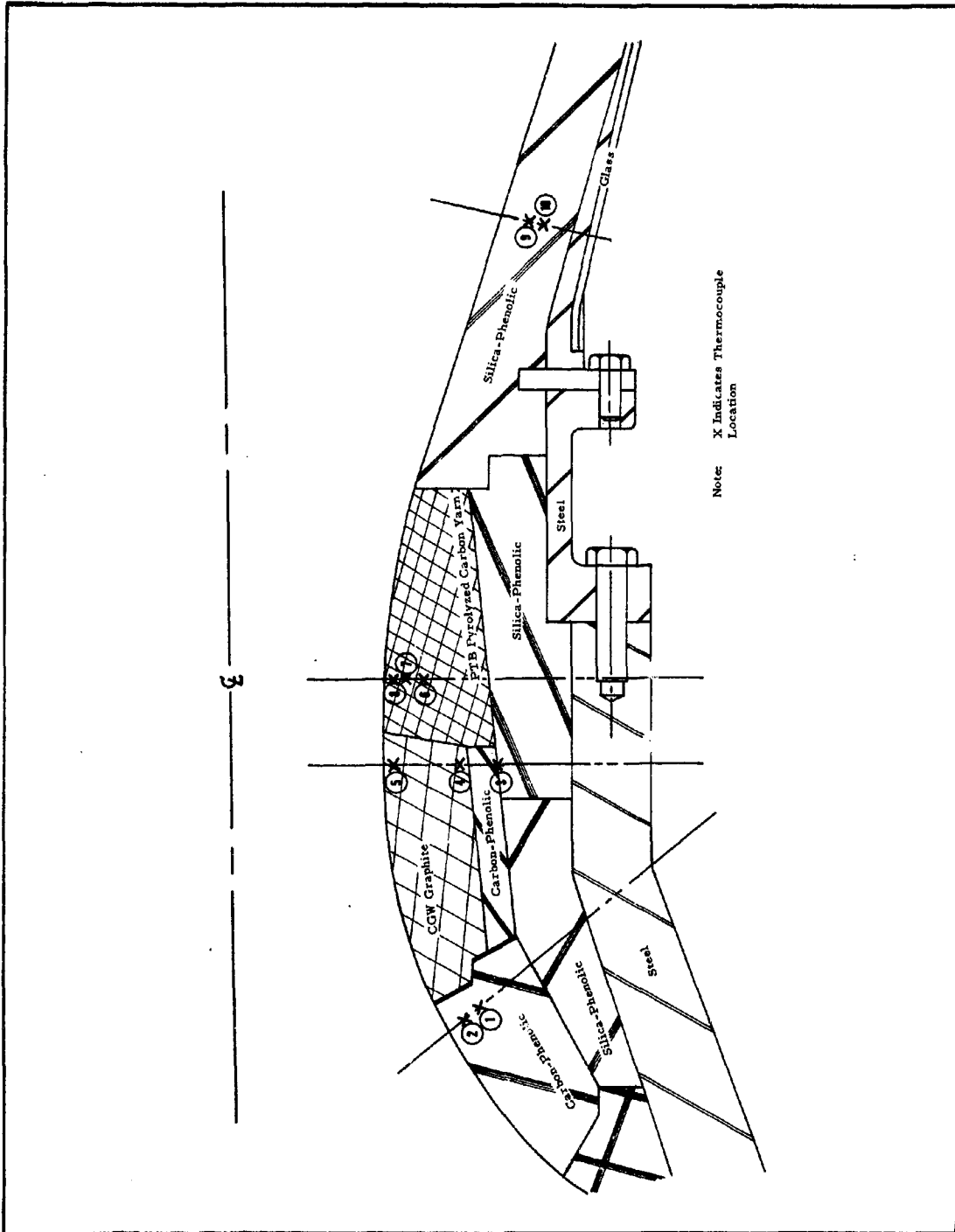


Figure 180 - Sketch of Nozzle Cross Section, Showing Thermocouple Locations

**CONFIDENTIAL**

**CONFIDENTIAL**

AFRPL-TR-65-209, Vol I

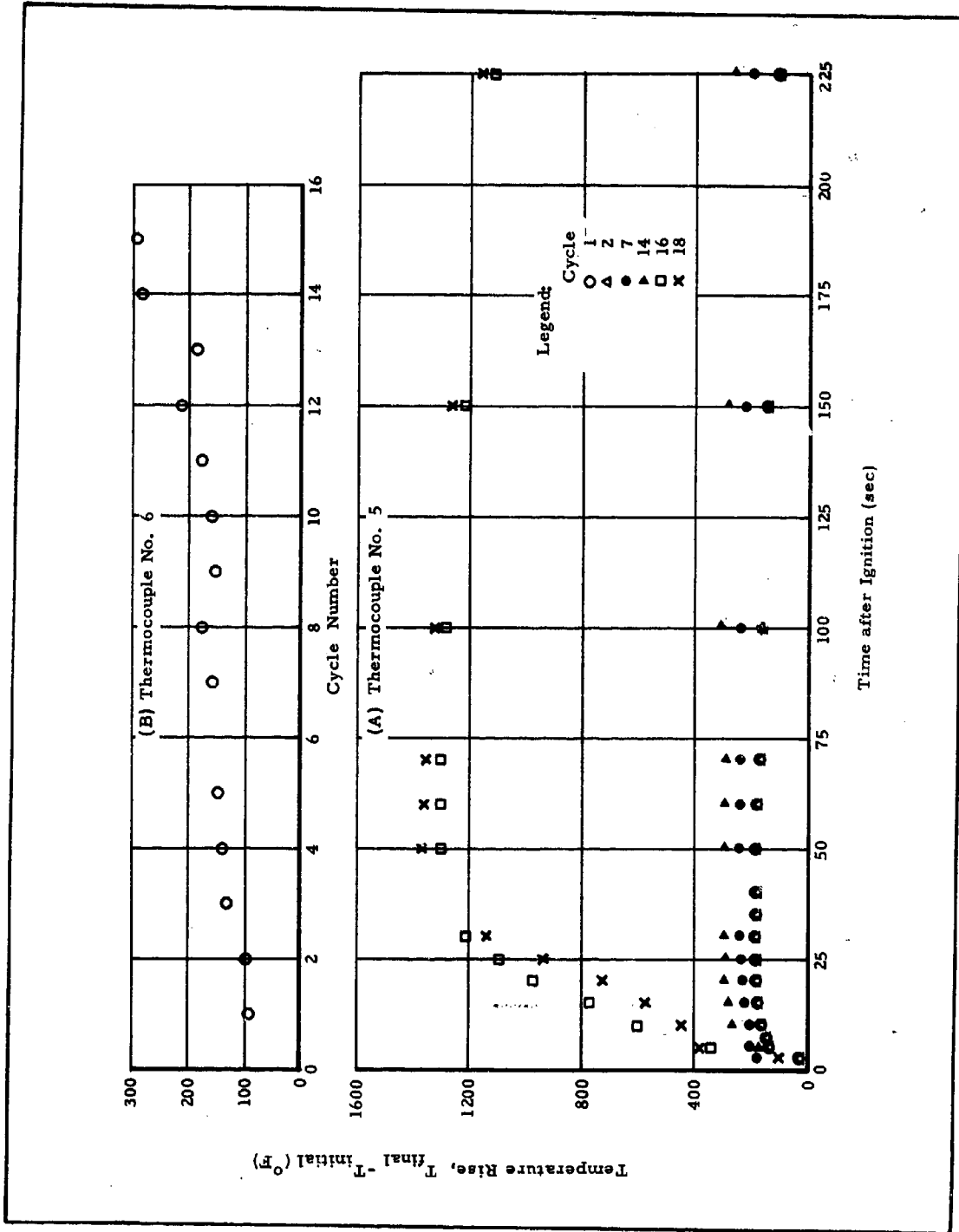


Figure 181 - Temperature Rise Data for Series N Tests

**CONFIDENTIAL**

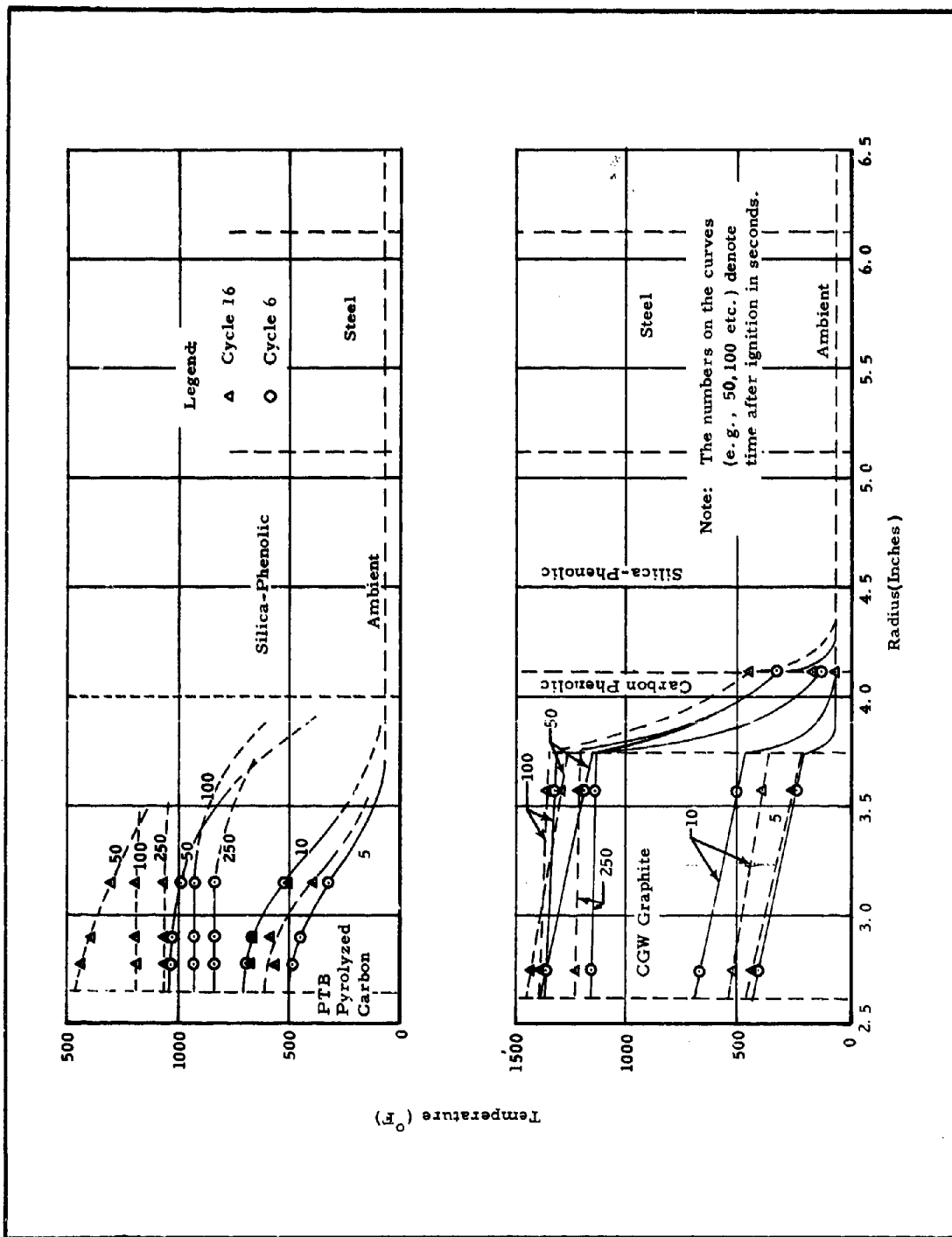


Figure 182 - Temperature Gradients Occurring at Throat and Throat Extension

pulse is shown in Figure 183, with the actual throat temperature data for cycle 14 superimposed. The calculations were based upon an aft-chamber pressure of approximately 300 psi, whereas the actual peak values were 170 psi and varied somewhat. Nevertheless, a fair degree of correlation exists. Figure 184 shows the correlation achieved for the throat surface temperature for the sustained pulses of both the high pressure (160 psi, cycle 6) and low pressure (20 psi, cycle 16) pulses. In this case, very good correlation was achieved since the actual pressure more closely approximated that assumed for the calculations.

**CONFIDENTIAL**

AFRPL-TR-65-209, Vol I

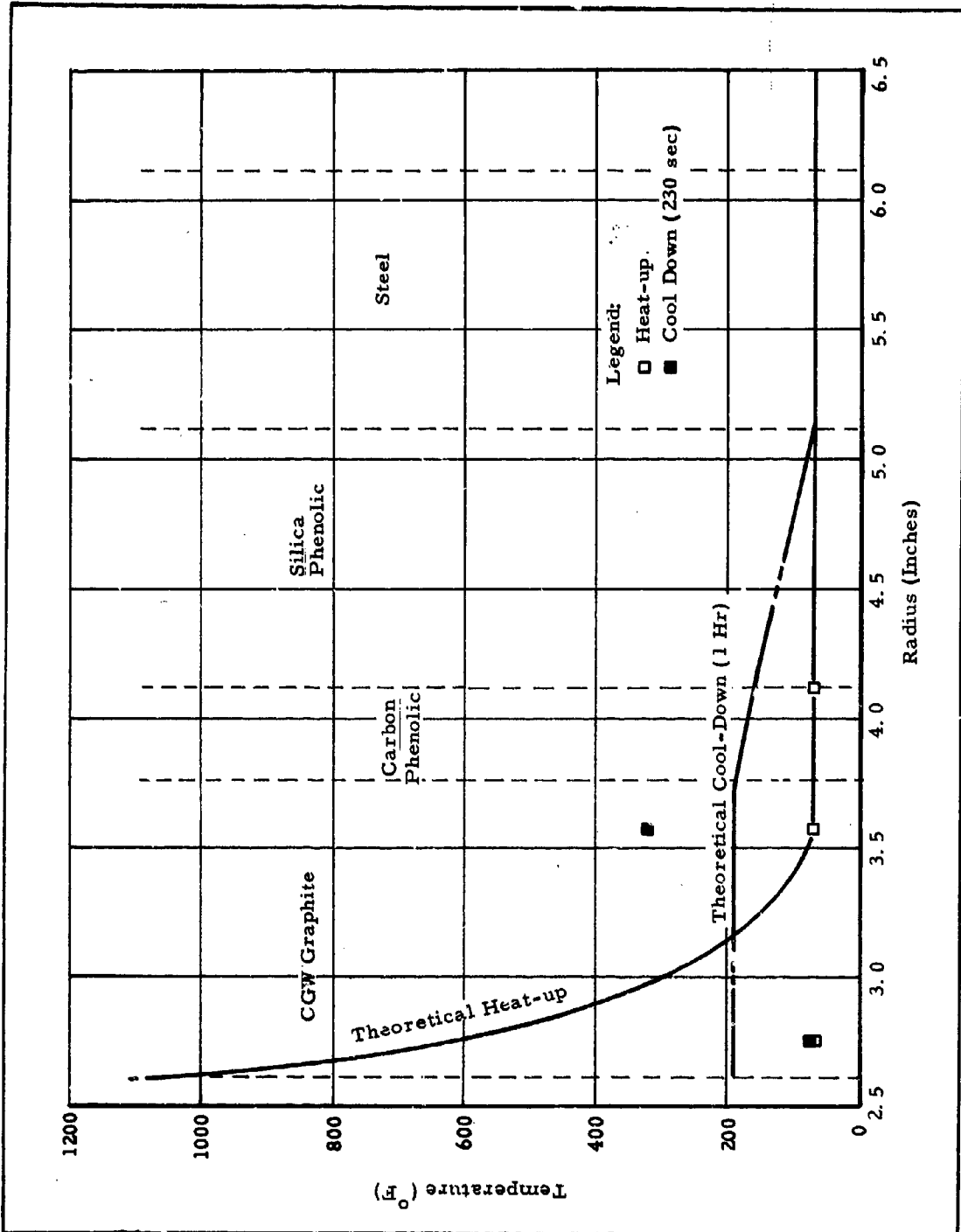


Figure 183 - Comparison of Predicted and Measured Temperature Gradient for a 1.5-Sec Pulse

**CONFIDENTIAL**

**CONFIDENTIAL**

AFRPL-TR-65-209, Vol I

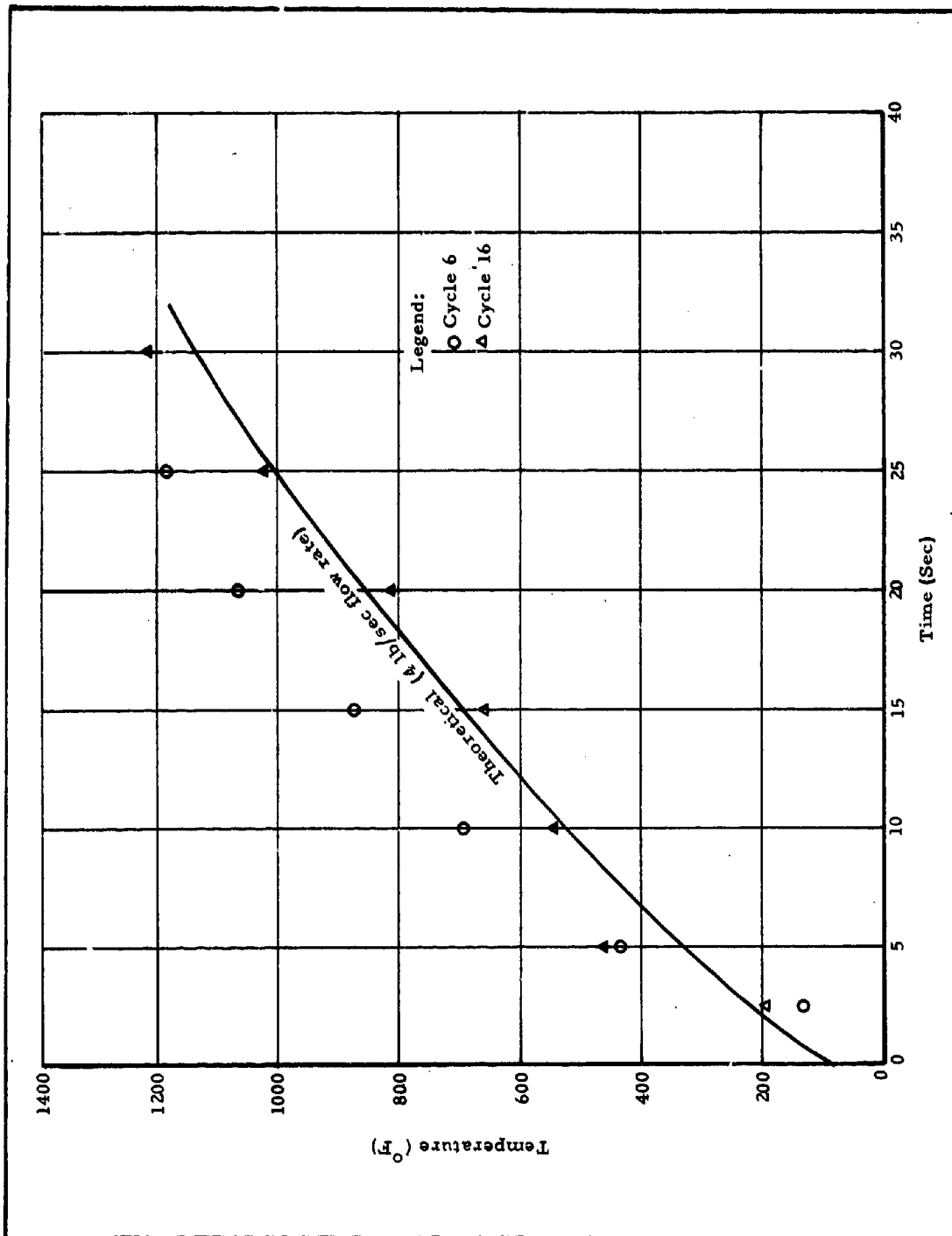


Figure 184 - Comparison of Predicted and Measured Surface Temperature for Long-Duration Pulses

**CONFIDENTIAL**

SECTION IX - POST BOOST PROPULSION SYSTEM  
DEMONSTRATION TESTS

1. GENERAL

Considerable effort is currently being expended to increase the capabilities (that is, improve the accuracy and versatility) of existing weapon systems such as Minuteman, Titan, Polaris (Poseidon), and Pershing. One of the most feasible techniques to evolve from these advanced studies is post-boost propulsion, in which a separate propulsion system is added to an existing system to provide the capability for making velocity and orientation corrections following burnout of the final boost stage. To meet these requirements, the Post-Boost Propulsion System (PBPS) must include an attitude (pitch and yaw) and roll control system, along with axial thrust for  $\Delta V$  addition. (Confidential)

Although the total available time for post-boost corrections is relatively short (100 to 400 sec) due to the mission requirements, this short propulsion system operating time is well within the current state of the art of solid propellant motors. Moreover, during this mission time, the axial thrust and attitude control forces may be required either simultaneously or independently. Therefore, an on-command controllable propulsion system is necessary to meet the post-boost propulsion requirements. (Confidential)

It is obviously desirable to use an all-solid-propellant propulsion system for these weapon systems, where instant readiness, long-term field storage, and minimum field maintenance are of paramount importance. The proven low development and production costs of solid propellant systems is a significant factor in the overall consideration. (Confidential)

Northrop Carolina's DCCSR concept provides an ideal solution to the PBPS requirements. It offers, on command, variable-impulse axial thrust pulses and a continuously operating attitude control system. It is an all-solid-propellant system, whose feasibility for stop-restart, thrust magnitude control, and post-boost propulsion had been demonstrated in motors containing 300 lb of propellant. (Confidential)

**CONFIDENTIAL**

In view of the urgent requirements for a PBPS and the obvious applicability of the DCCSR to post-boost control missions, the Air Force Rocket Propulsion Laboratory (AFRPL), Edwards AFB, California, sponsor of the basic DCCSR development programs, and Northrop Carolina agreed jointly to demonstrate the feasibility of adapting the DCCSR to a PBPS. AFRPL permitted Northrop Carolina to use residual hardware from the DCCSR program for a PBPS demonstration test. (Confidential)

## 2. DCCSR OPERATION FOR A PBPS APPLICATION

The forward chamber (or gas generator) of the basic DCCSR contains a relatively low flame temperature (2200 to 2900° F) propellant formulations, thus making it an ideal source of gases for attitude and roll control thrust. The axial thrust is generated by injecting the gas generator gases into the aft, or axial, chamber where further reaction takes place, yielding high-temperature (5300° F) products. Yet, this axial thrust is delivered at the respectable specific impulse of  $260 \text{ lb}_f\text{-sec}/\text{lb}_m$  (vacuum conditions, 20-to-1 expansion). (Confidential)

Pulse operation of the axial thrust system is achieved by a simple on-off flow-control valve located between the gas generator and the axial thrust chamber. The familiar thrust spike that occurs at termination in the basic DCCSR (see Figure 138) is eliminated in the PBPS configuration because axial thrust termination is achieved by shutting off the flow of gases from the gas generator to the axial thrust chamber; axial thrust then decays to zero since the axial motor propellant will not sustain combustion alone. (Confidential)

The gas generator can be ignited as soon as either attitude control or axial thrust is initially required and will operate continuously until the post-boost propulsion requirement ends. The gas generator gases are supplied continuously to the attitude control nozzles and supplied intermittently, on command, to the axial chamber. The gases are supplied to the attitude control system at a constant mass flow. It is therefore necessary to operate the gas generator at two different pressure levels to meet the mass flow requirements of (1) the attitude control system (constant mass flow), and (2) the axial thrust chamber (in pulses).

The attitude control system uses dual outlet valves with counter-acting nozzles so that when attitude control forces are not required, the valves maintain a null position where the mass flow is spilt equally

**CONFIDENTIAL**

between the counteracting nozzles and zero net force is applied to the system. When axial thrust is not required, the gas generator operates at a low pressure level and all gases are vented through the attitude control system nozzles; when no control forces are required, the gases are expelled through the counteracting nozzles. When axial thrust is required, the axial flow control valve opens and at the same time the flow area to the attitude control system is restricted so that the net flow area sensed by the gas generator is less than that for attitude control only. Thus, the gas generator pressure increases and, in turn, gas generator mass flow increases, which meets the additional requirement for axial thrust. By properly sizing the flow areas to the axial motor and the attitude control supply line restriction (venturi), the attitude control mass flow is held constant for both conditions.

To assist in visualizing the operation of the DCCSR in a post-boost propulsion mode, a simplified diagram of the system is presented in Figure 185. With the axial thrust control valve in the position shown, the gas generator gases are supplied to both the axial thrust chamber and to the attitude control valve. The controlling flow area for the gas generator is thus formed by the sum of the areas of the orifice to the axial thrust chamber (denoted as Orifice B in Figure 185) and the annular orifice (forward end of the axial thrust control valve, denoted as Orifice A in Figure 185) in the attitude control supply line. When axial thrust is not required, the axial thrust control valve is moved aft, sealing off the axial thrust chamber and terminating axial thrust. In this position, the venturi at the attitude control valve inlet now controls gas generator pressure. Although Figure 185 is not to scale, the sum of the flow areas of the two orifices (when axial thrust is "on") is smaller than the flow area of the valve inlet venturi, thus resulting in a higher gas generator pressure when axial thrust is "on" than when axial thrust is "off." This schematic (Figure 185) is an actual representation of the motor and valve configuration used in the demonstration test described below.

### 3. DEMONSTRATION TEST

#### a. General

A sea-level test to demonstrate the feasibility of adapting the DCCSR concept to a PBPS was conducted at Northrop Carolina on 29 July 1965. The motor used in this successful test is shown schematically in Figure 185. Figures 186 and 187 show the demonstration motor mounted on the test stand before the test. The motor design, propellants, duty cycles, etc., are described in detail in the following paragraphs.

**CONFIDENTIAL**

AFRPL-TR-65-209, Vol I

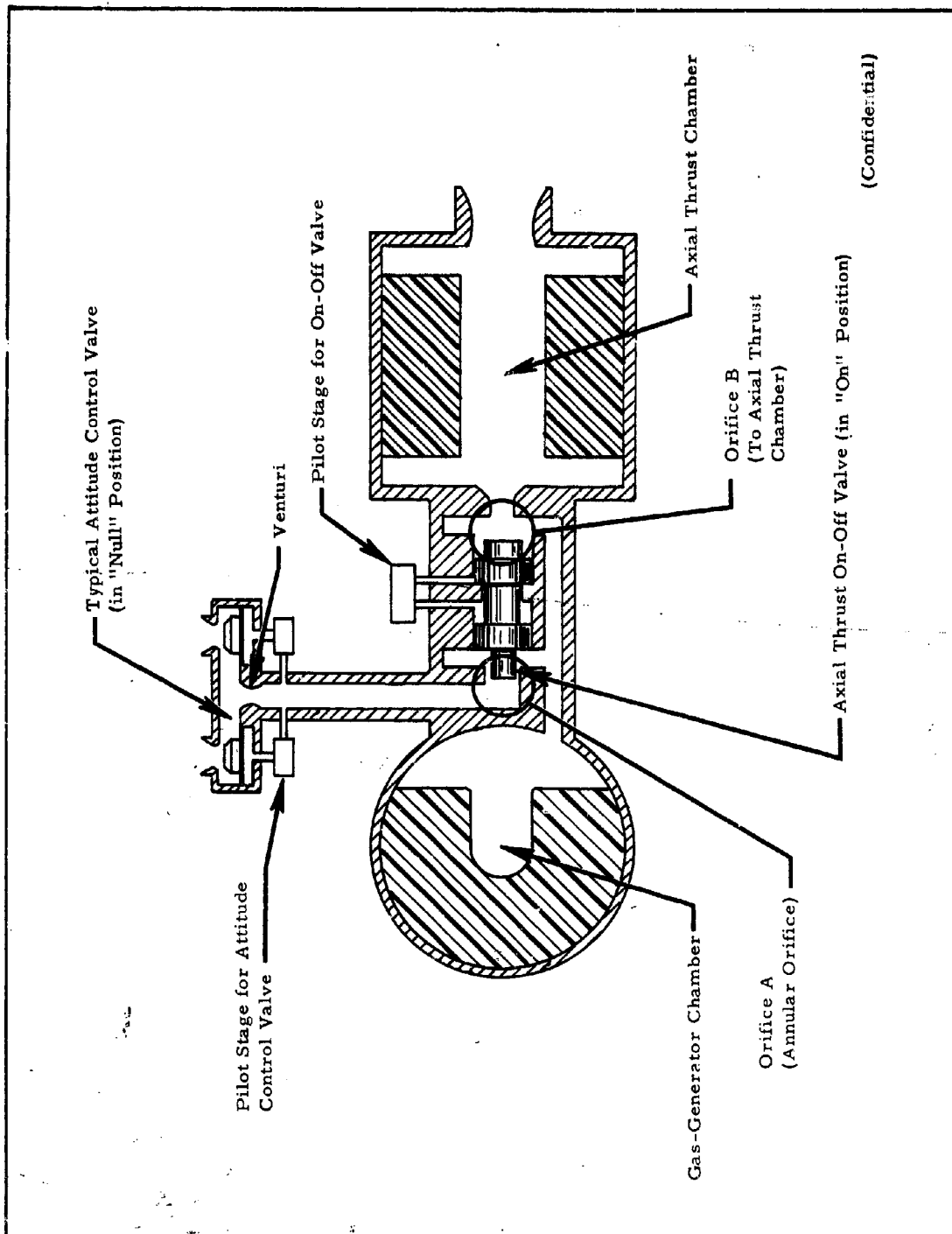


Figure 185 - Schematic Diagram of DCSR Motor for PBPS Application

-320-

**CONFIDENTIAL**

**CONFIDENTIAL**

AFRPL-TR-65-209, Vol I

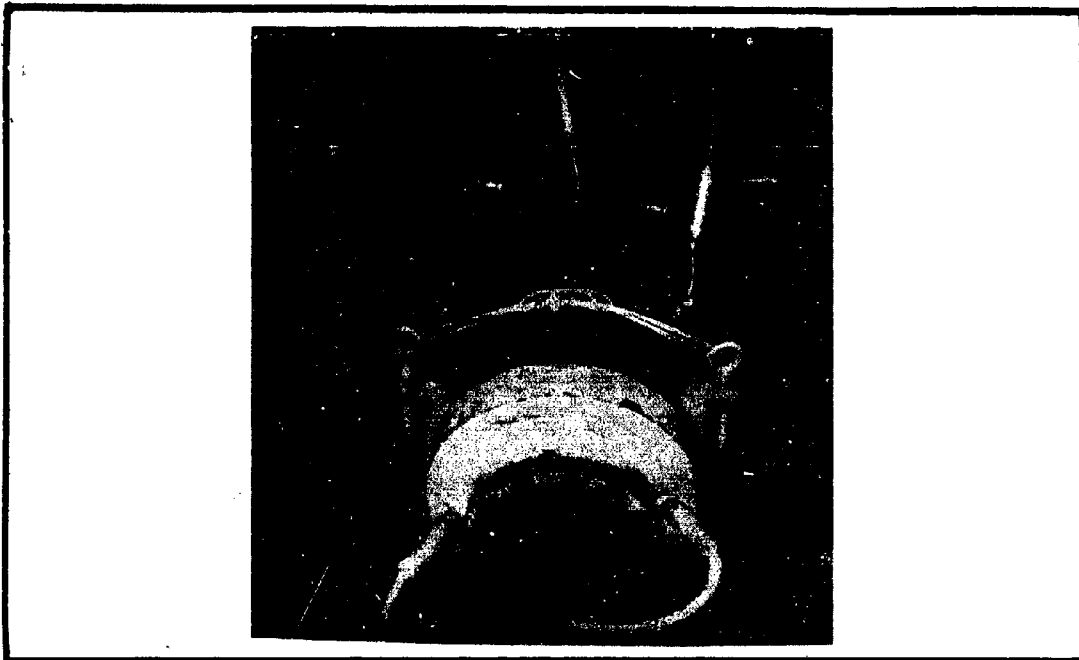


Figure 186 - PBPS Demonstration Motor Mounted on Test Stand



Figure 187 - Close-up of PBPS Demonstration Motor, Showing Attitude Control System Valving

-321-

**CONFIDENTIAL**

b. Motor Components

The gas generator used in this test was a 17.5-in. I. D. spherical case insulated with 0.250 in. of Gen Gard V-44. The axial thrust on-off valve was one previously used for on-off operation of the basic DCCSR, but was modified for this test to provide for bleeding gases to the attitude control system. These two components constituted the residual hardware from the DCCSR program. The cylindrical axial thrust chamber was 11.0 in. I. D. by 16.0 in. long, and insulated with 0.100-in. of "Pyrolock." A heat-sink-type nozzle with a CGW graphite insert, a 2.05-in. -diameter throat, and a 2.82-to-1 expansion ratio was used.

c. Propellants

The formulation and characteristics of the gas generator and axial motor propellants are given in Tables LXVII and LXVIII respectively. Both propellants were developed during the AFRPL-sponsored DCCSR program.

d. Attitude Control System

A valve used on the Minuteman roll control system, supplied by Aeronutronic, Div. of Philco, Newport Beach, California, was used for the attitude control system. The characteristics of this valve are given in Table LXIX. Since the venturi flow area of this off-the-shelf valve was not large enough to meet the desired minimum gas generator pressure, two fixed-area bleed nozzles were added to the attitude control system.

e. Test Program and Test Conditions

Four axial thrust pulses of four seconds duration each were planned for this test. The total gas generator web burning time at the planned pressure levels was 40 sec. Since the gas generator grain surface area increases from an initial value of 250 sq in. to 294 sq in. at the web midpoint and then decreases to 265 sq in. at burnout, the gas generator, and hence the attitude control and axial motor, pressures are initially progressive and then regressive during the gas generator burn time. The complete duty cycle planned for this test, including the attitude control system operation, is shown schematically in Figure 188, (Confidential)

**TABLE LXVII - FORMULATION OF GAS GENERATOR PROPELLANT  
USED IN PBPS DEMONSTRATION TEST**

Property	Value
Composition (percent by weight)	
Triethyleneglycoldinitrate (TEGDN)	29.0
Nitrocellulose powder	60.0
Resorcinol	1.0
Triacetin	10.0
Burning rate data	
Burning rate at 1000 psia (in./sec)	0.197
Pressure index, 100 psi to 4500 psi	0.74
Temperature coefficient of rate (%/°F)	0.12
Density (lb <sub>m</sub> /cu in.)	0.053
Shore "A" hardness	64
Five-second autoignition temperature (°F)	397
Drop sensitivity with 2-kg weight, 50% fire (cm)	105
Flame temperature, measured (°F)	2320
Solids in chamber combustion products (% by weight)	None
$I_{vac} (A_e/A_t = 40, 15^\circ)$	224
Mechanical properties	
140°F	
Maximum stress (psi)	136
Strain at maximum stress (in./in.)	1.35
Modulus (psi)	243
77°F	
Maximum stress, psi	422
Strain at maximum stress (in./in.)	1.11
Modulus (psi)	480
-40°F	
Maximum stress (psi)	4810
Strain at maximum stress (in./in.)	0.07
Modulus (psi)	77,200

(Confidential)

**TABLE LXIII - FORMULATION OF AFT PROPELLANT  
USED IN PBPS DEMONSTRATION TEST**

Property	Value
<b>Composition (percent by weight)</b>	
Ammonium perchlorate	90
KEL-F	10
<b>Burning rate data</b>	
Burning rate at 100 psia (in./sec)	0.053
Pressure index, < 225 psia	1.0
Pressure index, > 225 psia	0.74
Temperature coefficient of rate (%/°F)	0.200
Density (lb <sub>m</sub> /cu in.)	0.069
Five-second autoignition temperature (°F)	730
Drop sensitivity with 2-kg weight, 50% fire (cm)	74
Theoretical flame temperature, with gas generator propellant (°F)	5300
$I_{vac} (A_e/A_t = 20, 15^\circ)$	264
<b>Mechanical properties</b>	
<b>165° F</b>	
Tensile strength (psi)	210
Compressive strength (psi)	700
Modulus (psi)	$0.14 \times 10^6$
<b>70° F</b>	
Tensile strength (psi)	340
Compressive strength (psi)	1260
Modulus (psi)	$0.3 \times 10^6$
<b>-65° F</b>	
Tensile strength (psi)	990
Compressive strength (psi)	8000
Modulus (psi)	$1.4 \times 10^6$

(Confidential)

**TABLE LXIX - ATTITUDE CONTROL SYSTEM VALVE \* CHARACTERISTICS**

Parameter	Value
<b>Solenoid circuit characteristics</b> (per side, A or B)	
Voltage	22 to 30 v dc
Current	1 amp (maximum at 22 v dc)
Resistance	22 ohms (minimum)
Inductance	300 to 350 mh (nominal)
<b>Position transducer primary excitation characteristics</b>	
Frequency	5 kc $\pm$ 250 cps
Wave shape	Square
Rise time	0.5 $\mu$ sec
Voltage	26 v $\pm$ 0.25 (rms)
<b>Operating pressure range</b> (at valve inlet)	
Maximum	1500 psig
Minimum	400 psig
<b>Response times (electrical command to 90% thrust), nominal maximum</b> (22 v dc, back emf 30 v dc)	
Null to hardover	25 msec
Hardover to null	15 msec
Hardover to hardover	25 msec
<b>Pressure recoveries</b>	
Venturi	0.835
Poppet	0.900
Nozzle/inlet	0.750
<b>Prefire static leakages (cfm, standard conditions), maximum</b>	
External, valve body	0.1 at 200 psig
Internal, past main valve seat	5.0 at 130 psig

\* RC 180 sp warm gas control valve, S/N P003X, manufactured by Aeronutronic Division, Philco Corporation, Newport Beach, California.

**CONFIDENTIAL**

AFRPL-TR-65-209, Vol 1

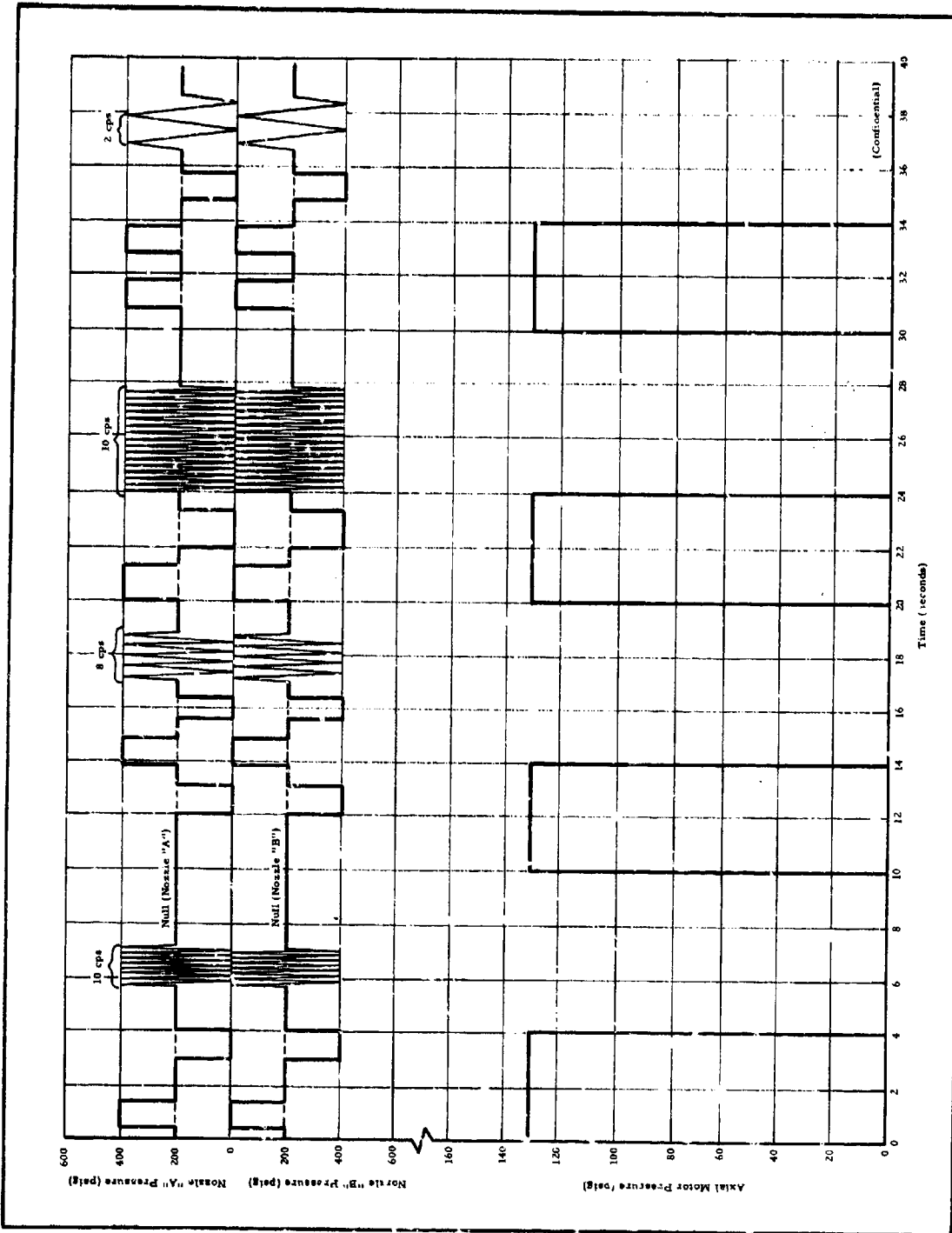


Figure 188 - Programed Duty Cycle for PB-S Demonstration Test

-326-

**CONFIDENTIAL**

f. Test Results

This test was completely successful from the standpoint of demonstrating the feasibility of adapting the DCCSR to post-boost propulsion operation. Both the axial thrust and attitude control forces responded to commands as planned. The only deviation from the planned duty cycle arose from lower orifice coefficients and higher pressure losses than had been anticipated in the motor design. These higher pressure losses and lower orifice coefficients resulted in higher-than-anticipated gas generator pressure levels, which in turn reduced the total gas generator operating time from 40 to 30 sec. (Confidential)

One of the axial motor pressure-time pulses is plotted in Figure 189. Figures 190 and 191 are plots of the attitude control nozzle inlet pressures versus time for two different attitude control system duty cycles. In Figure 190 the duty cycle was null-to-hardover "A"-to-null-to-hardover-"B"-to-null, while in Figure 191 the attitude control valve was being operated in a 10-cps (hardover-to-hardover) mode. The difference in null and maximum pressures between Figures 190 and 191 is discussed subsequently. Note that the response times for the attitude control valve vary between 20 and 28 msec. The attitude control response is limited by the valve action since the valve is a flow-diversion device and not dependent on filling and emptying significant free volumes.

A plot of the gas generator chamber, valve inlet, and axial thrust chamber pressures versus time is shown in Figure 192. As mentioned previously, the orifice coefficients were lower and the pressure losses in the axial thrust control valve were higher than anticipated. The relatively high burning-rate pressure exponent for the gas generator propellant, 0.74, actually magnifies any pressure loss occurring in the attitude control ducts and valves, as shown by the following analysis. (Confidential)

For steady-state conditions, the gas generator mass flow rate,  $\dot{m}_g$ , is equal to the mass flow rate through a choked nozzle,  $\dot{m}_o$ , or

$$\dot{m}_g = \dot{m}_o \quad (7)$$

Now,  $\dot{m}_g$  and  $\dot{m}_o$  can be expressed in terms of gas generator

**CONFIDENTIAL**

AFRPL-TR-65-209, Vol I

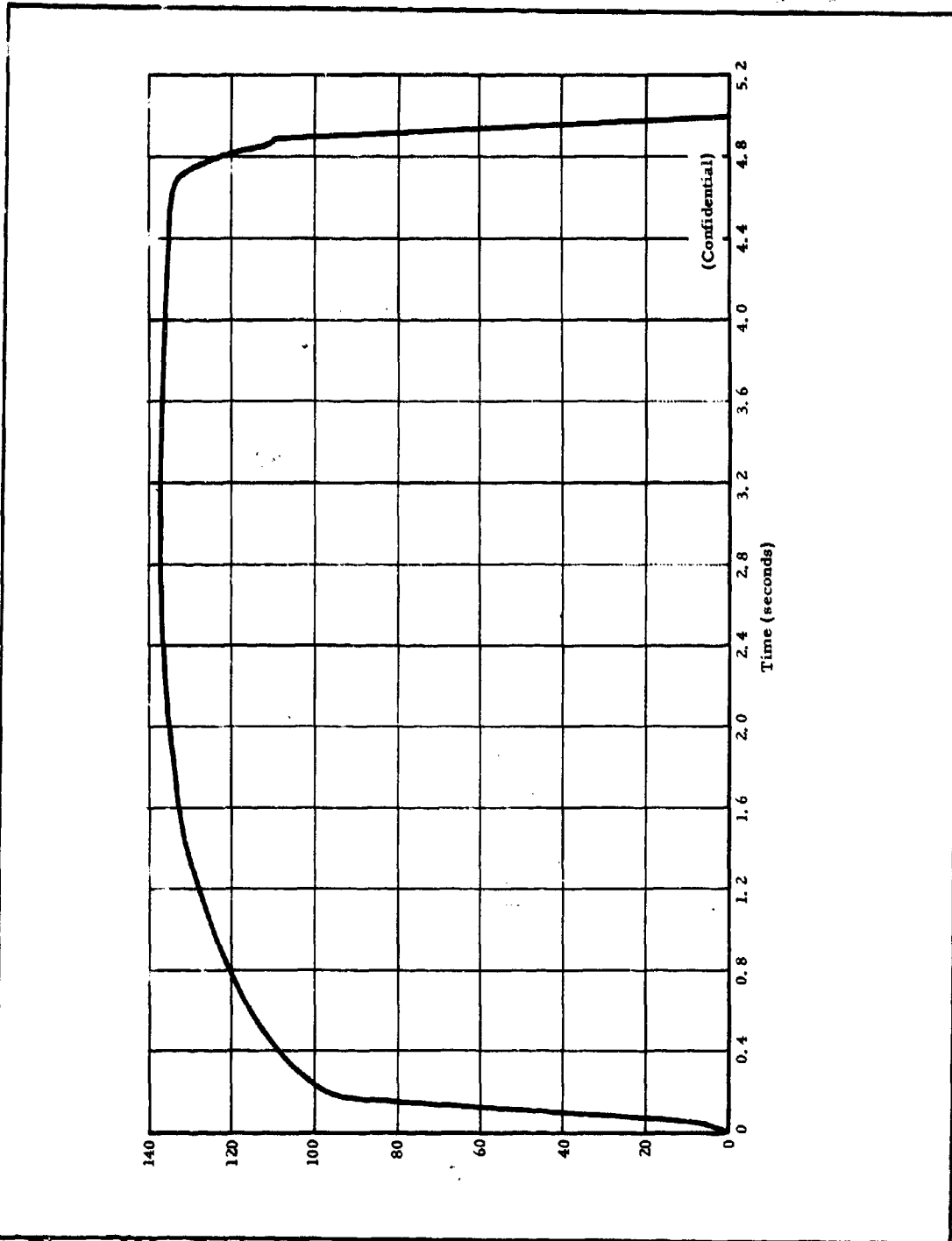


Figure 189 - Typical Pressure-Time Trace for Axial Pulse Cycle (PBPS Demonstration Test)

**CONFIDENTIAL**

**CONFIDENTIAL**

AFRPL-TR-65-209, Vol I

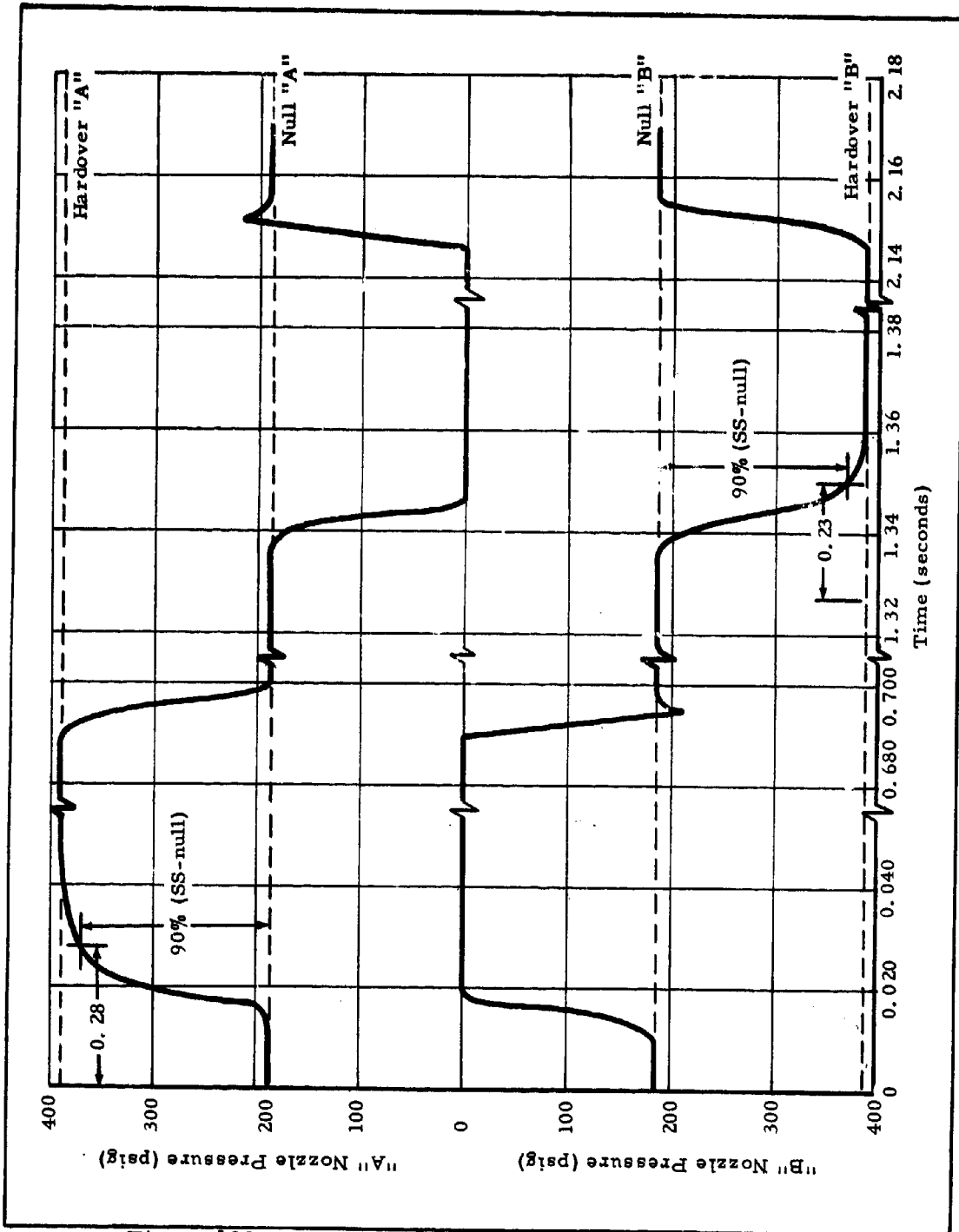


Figure 190 - Typical Pressure-Time Trace for Attitude Control System Cycle (PBPS Demonstration Test)

**CONFIDENTIAL**

**CONFIDENTIAL**

AFRPL-TR-65-209, Vol I

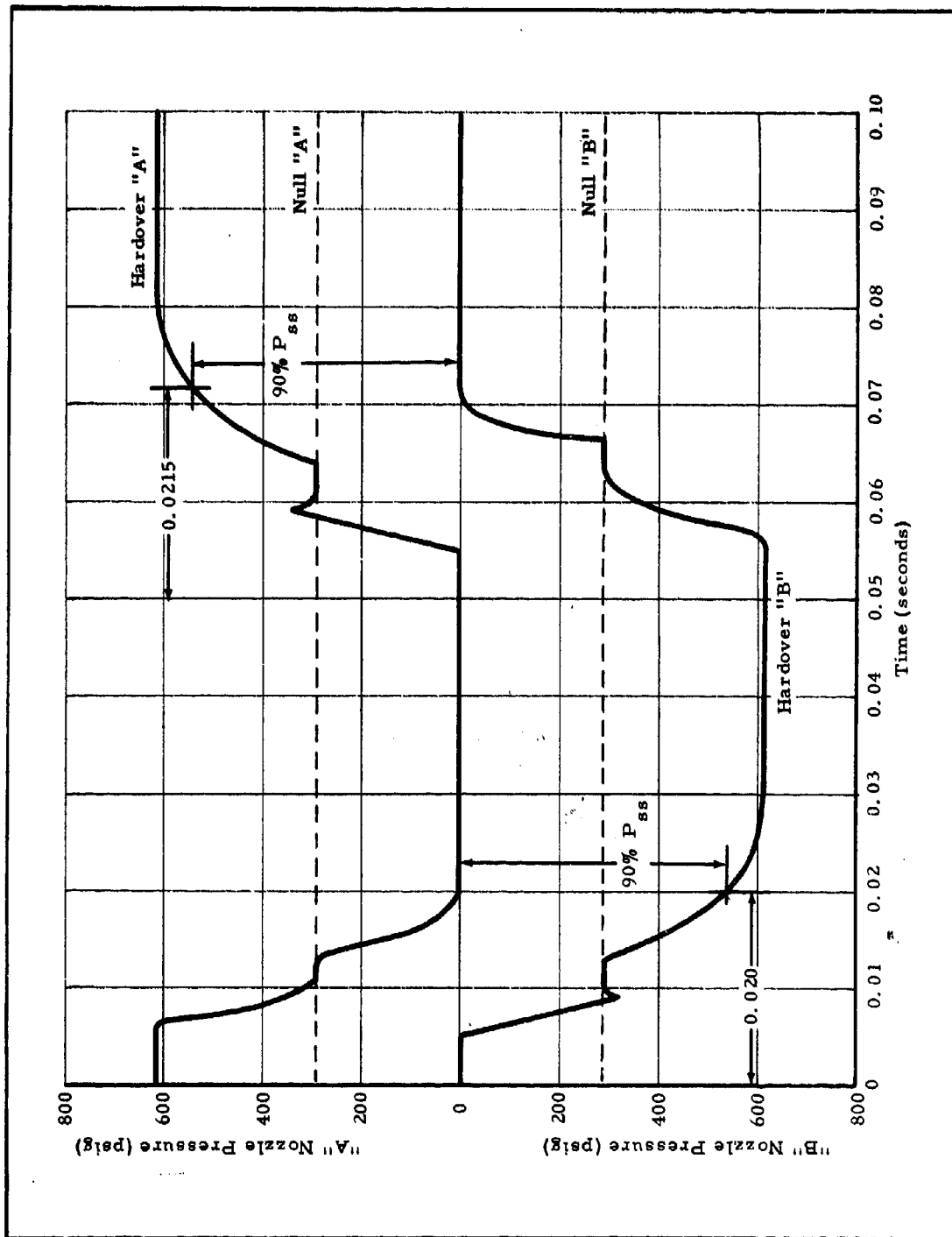


Figure 191 - Typical Pressure-Time Trace for 10-CPS Cycle of Attitude Control System (PBPS Demonstration Test)

**CONFIDENTIAL**

**CONFIDENTIAL**

AFRPL-TR-65-209, Vol I

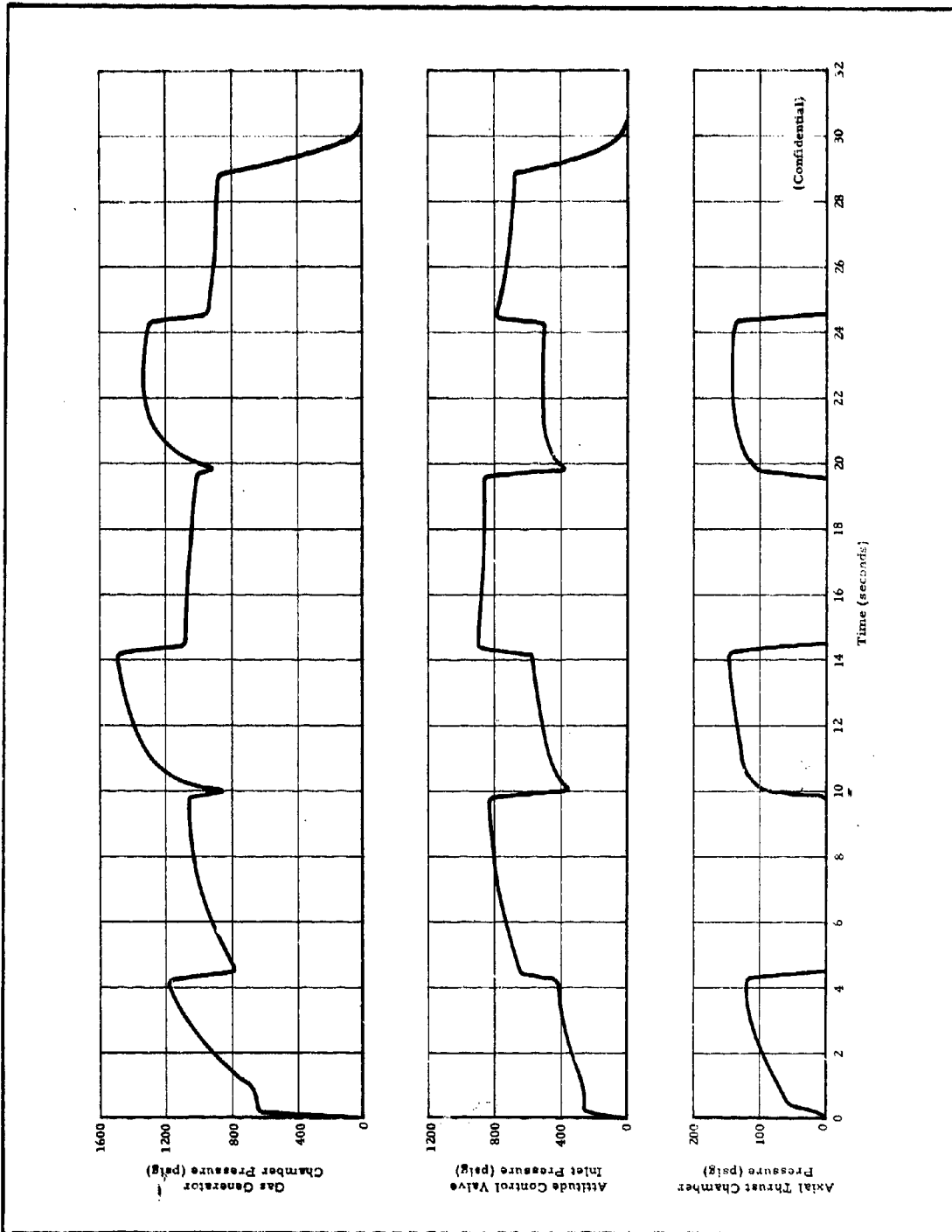


Figure 192 - Pressure-Time Trace for Entire PBPS Demonstration Test

**CONFIDENTIAL**

chamber pressure (P), as follows:

$$\dot{m}_g = \rho A_b a P^n \quad (8)$$

and

$$\dot{m}_o = C_D P A_t \quad (9)$$

Substituting Equations 8 and 9 into Equation 7, and solving for P, yields

$$P = \left( \frac{\rho A_b a}{C_D A_t} \right)^{\frac{1}{1-n}} \quad (10)$$

In the demonstration test, a pressure drop occurred between the gas generator chamber and its restricting nozzles. However, insofar as the gas generator chamber pressure is concerned, any pressure loss occurring downstream of the chamber has the same effect on the chamber pressure as decreasing the effective  $A_t$  in Equation 10. Therefore, any pressure loss in the axial thrust control valve or the attitude control supply ducts, regardless of the cause (such as sudden contraction or expansion, friction, turns, etc.), is sensed by the gas generator chamber as an effective reduction in flow area. If, for example,  $A_t$  is reduced by 10 percent, chamber pressure is increased by 48 percent. The significant point is that pressure losses increase the mass flow rate in a solid propellant gas generator, whereas in a conventional flow system a pressure loss reduces the mass flow rate.

In Figure 192, when the axial thrust is "off," the attitude control inlet pressure is approximately 78 percent of gas generator chamber pressure. This corresponds to a 6 percent reduction in effective flow area, from Equation 10.

However, when the axial thrust is "on," the mass flow to the attitude control system is reduced, as evidenced by the lower valve inlet pressure. Under this condition, the gas generator pressure is determined by the sum of the two orifice areas of the axial thrust control valve (see Figure 185). The orifices were sized so that the attitude control mass flow (through annular orifice A) would be the same with axial thrust "on" or "off." However, the annular orifice is only

a part of the total effective gas generator flow area since the axial motor orifice (B) is also open. The effect of a lower annular orifice coefficient, then, is to decrease the ratio of attitude control/axial motor gas generator mass flow below what it was designed for. Again, the pressure losses resulted in a higher-than-anticipated gas generator chamber pressure (and mass flow).

In summary, this test demonstrated the feasibility of utilizing the DCCSR concept for post-boost propulsion applications. The axial thrust was pulsed on command at the same time the high-response attitude control system was operating.

**CONFIDENTIAL**SECTION X - CONCLUSIONS

## 1. GENERAL

The conclusions for Phases II, III, and V of this third year of effort on the DCCSR program are summarized in this section. The conclusions derived from Phase IV were presented in Section VIII.

## 2. PHASE II - PROPELLANT DEVELOPMENT PROGRAM

The objectives of the forward-grain development program were met with the PPO-90 formulation. Although this formulation may not be storable in space for long periods of time, it performed well following exposure to vacuum, conditions for one to two hours preceding each ignition in the altitude test chamber (see Section III). A large number of additional forward-grain formulations were characterized, which will allow considerable flexibility in future dual-chamber motor designs. (Confidential)

Although the specific impulse objectives were not achieved in the aft-grain development program, three castable aft-grain systems were characterized, on which further development can be based to obtain propellant formulations with desirable properties. The termination capability of each of these systems was demonstrated in subscale dual-chamber tests. Improved specific impulse and higher pressure exponents and/or threshold pressures are desirable areas for improvement in each of these systems. (Confidential)

## 3. PHASE III - DEMONSTRATION OF PRESENT TECHNOLOGY

On the basis of an analysis of forward-chamber conditions following termination and subscale motor terminations, chamber free volume is concluded to be the predominant factor affecting propellant reignition after termination at sea level. Above a critical chamber volume for a given motor design, the heat content of the residual chamber gas is sufficient to heat the grain to its autoignition temperature. This critical chamber volume increases with increasing chamber pressure prior to termination since, at higher chamber pressures, the residual chamber gas following termination is at a lower temperature due to the increased expansion. (Confidential)

**THIS PAGE WAS BLANK THROUGHOUT THE TEST PROGRAM****CONFIDENTIAL**

## CONFIDENTIAL

AFRPL-TR-65-209, Vol I

For most practical motor designs, critical chamber volume is attained at some point during propellant consumption. A practical method to prevent sea-level reignition involves expelling the hot gas remaining in the chamber after termination with an inert gas purge. For motor termination under altitude conditions, a purge is unnecessary since very little residual gas remains in the chamber; this gives a very high critical chamber volume (infinite at vacuum conditions).

These conclusions concerning reignition were verified in the six sea level and two altitude tests with full-scale motors during Phase III. The only apparent contradictory results were obtained in the first two motors, which contained an aluminized aft propellant, OX-5. These two motors reignited even with nitrogen purge. The reignition source with OX-5 propellant is believed to be hot aluminum and/or aluminum oxide remaining on the grain surface following termination, rather than the hot residual chamber gas. Low-frequency oscillations occur with this propellant due to aluminum buildup on the surface followed by its periodic combustion. (Confidential)

The five full-scale motor tests in this phase, with very similar duty cycles, demonstrated that the shutdown impulse on termination is predictable and repeatable from motor to motor. Also, a proportional valve with feedback control gives very stable and predictable performance. (Confidential)

#### 4. PHASE V - DEMONSTRATION OF NEW TECHNOLOGY

A castable aft-grain propellant is feasible for use in the dual-chamber controllable motor, based on full-scale tests in Phase V. The burning-rate characteristics of the aft propellant can place limitations on the motor designs with which termination can be achieved successfully. (Confidential)

## CONFIDENTIAL

LIST OF REFERENCES

1. APR-7-1: Development of an Intermittent Operating Variable Thrust Solid Propellant Rocket Motor (U). (First Quarterly Report). Amcel Propulsion Company, Asheville, North Carolina, July 1962. (Confidential Report)
2. APR-7-2: Development of an Intermittent Operating Variable Thrust Solid Propellant Rocket Motor (U). (Second Quarterly Report). Amcel Propulsion Company, Asheville, North Carolina, October 1962. (Confidential Report).
3. APR-7-3: Development of an Intermittent Operating Variable Thrust Solid Propellant Rocket Motor (U). (Third Quarterly Report). Amcel Propulsion Company, Asheville, North Carolina, January 1963. (Confidential Report).
4. APR-7-4: Development of an Intermittent Operating Variable Thrust Solid Propellant Rocket Motor (U). RPL-TDR-63-1061 (First Annual Report - Fiscal Year 1962) Amcel Propulsion Company, Asheville, North Carolina, December 1963. (Confidential Report).
5. APR-21-1: Controllable Solid Propellant Rocket Motor (U). (First Quarterly Report). Amcel Propulsion Company, Asheville, North Carolina, June 1963. (Confidential Report).
6. APR-21-2: Controllable Solid Propellant Rocket Motor (U). (Second Quarterly Report). Amcel Propulsion Company, Asheville, North Carolina, September 1963. (Confidential Report).
7. APR-21-3: Controllable Solid Propellant Rocket Motor (U). (Third Quarterly Report). Amcel Propulsion Company, Asheville, North Carolina, December 1963. (Confidential Report).
8. APR-21-4: Controllable Solid Propellant Rocket Motor (U). RPL-TDR-64-52. (Second Annual Report - Fiscal Year 1963). Amcel Propulsion Company, Asheville, North Carolina, September 1964. (Confidential Report).

LIST OF REFERENCES (CONT'D)

9. APR-21-5: Dual-Chamber Controllable Solid Propellant Rocket Motor (U). (Fourth Quarterly Report). Amcel Propulsion Company, Asheville, North Carolina, May 1964. (Confidential Report).
10. APR-21-6: Dual-Chamber Controllable Solid Propellant Rocket Motor (U). (Fifth Quarterly Report). Amcel Propulsion Company, Asheville, North Carolina, August 1964. (Confidential Report).
11. APR-21-7: Dual-Chamber Controllable Solid Propellant Rocket Motor (U). (Sixth Quarterly Report). Amcel Propulsion Company, Asheville, North Carolina, November 1964. (Confidential Report).
12. APR-21-8: Dual-Chamber Controllable Solid Propellant Rocket Motor (U). (Seventh Quarterly Report). Amcel Propulsion Company, Asheville, North Carolina, February 1965. (Confidential Report).
13. APR-21-9: Dual-Chamber Controllable Solid Propellant Rocket Motor (U). (Eighth Quarterly Report). Amcel Propulsion Company, Asheville, North Carolina, September 1965. (Confidential Report)
14. ATP-102: Program Plan for the Second Year Development under Contract AF 04(611)9067 (U), Revision A, Amcel Propulsion Company, Asheville, North Carolina, 21 August 1964. (Confidential Report)
15. Heaston, Robert J.: "Solid Propellant Combustion Research," Bulletin of the Interagency Solid Propulsion Meeting. Vol. IV, July 1963.(Confidential Report)
16. Peters, R.; and Wodlin, K.: The Effect of Resin Composition and Filler on the Performance of a Molded Charring Ablator. NASA, TD-2024.
17. Anderson, Floyd A.; and Strand, Leon D.: "An Experimental Investigation of the Low Pressure Combustion Limits of Some Solid Propellants," Bulletin of the Interagency Solid Propellant Meeting, July 1963; p. 157. (Confidential Report)
18. Ciepluch, C. C., Spontaneous Re-ignition of Previously Extinguished Solid Propellants. NASA TN D-2167, March 1964.

LIST OF REFERENCES (CONT'D)

19. Von Elbe, Guenther, "Theory of Solid Propellant Ignition and Response to Pressure Transients," Bulletin of the Interagency Solid Propellant Meeting, July 1963; p. 95. (Confidential Report)
20. ATR-54: Interim Report on an Analytical Study of the Effect of Various Parameters on Performance of the Dual-Chamber Controllable Solid Propellant Rocket Motor (U). Amcel Propulsion Company, Asheville, North Carolina, June 1965. (Confidential Report)
21. AMS-10018: Hot Gas Control Valve. Amcel Propulsion Company, Asheville, North Carolina, 1 June 1964.
22. AWS-2: Controllable Solid Rocket Nozzle Development (U). Amcel Propulsion Company, Asheville, North Carolina, 8 June 1964. (Confidential Report)

# CONFIDENTIAL

AFRPL-TR-65-209, Vol I

## APPENDIX A - DETAILED DESCRIPTION OF SERIES H TESTS

### H. 1 THROUGH H. 6

#### 1. GENERAL

This appendix presents a detailed description of Series H tests H. 1 through H. 6, along with a plot of the pressure- and thrust-time traces obtained for each. A description of the motor hardware used and an analysis of the data obtained were presented in Section III, paragraph, 3, a. Data for these Series tests were summarized in Table XVIII.

#### 2. TEST H. 1 (2 February 1964)

The aft chamber of the motor was loaded with formulation 8133-19-4, which contains ten percent aluminum (see Table III). As shown in Figure A-1, the forward chamber operated for 1.1 sec before the ball valve was actuated and the motor terminated. The forward-chamber decay rate at 2090 psi was 110,000 psi per second, and the decay rate for the aft chamber was 13,400 psi per second at the 25 percent decay pressure of 300 psi. (Confidential)

After termination, hot particles, presumably aluminum or aluminum oxide, were observed as they were discharged from the nozzle. Approximately 25 sec after termination, pressure built up in the motor to a low level, and burning continued until the aft grain was consumed. A portion of the forward grain remained unburned in the motor after the test. Apparently very little of the PPO-13 grain burned after the motor reignited, for the portion of the web burned corresponded closely with that calculated from burning time and average pressure before termination. (Confidential)

It was concluded that the aft grain reignited, rather than the forward grain, since the latter did not sustain combustion even after the aft grain burned out.

#### 3. TEST H. 2 (19 March 1964)

To determine whether aluminum in the aft-grain propellant contributed to the reignition that occurred in Test H. 1, a formulation with no aluminum, 8133-35-6, was cast into the aft chamber of the motor for this test. As shown in Figure A-2, the valve was not actuated in this test due to a faulty connection in the electrical circuit. However,

A-1

CONFIDENTIAL

**CONFIDENTIAL**

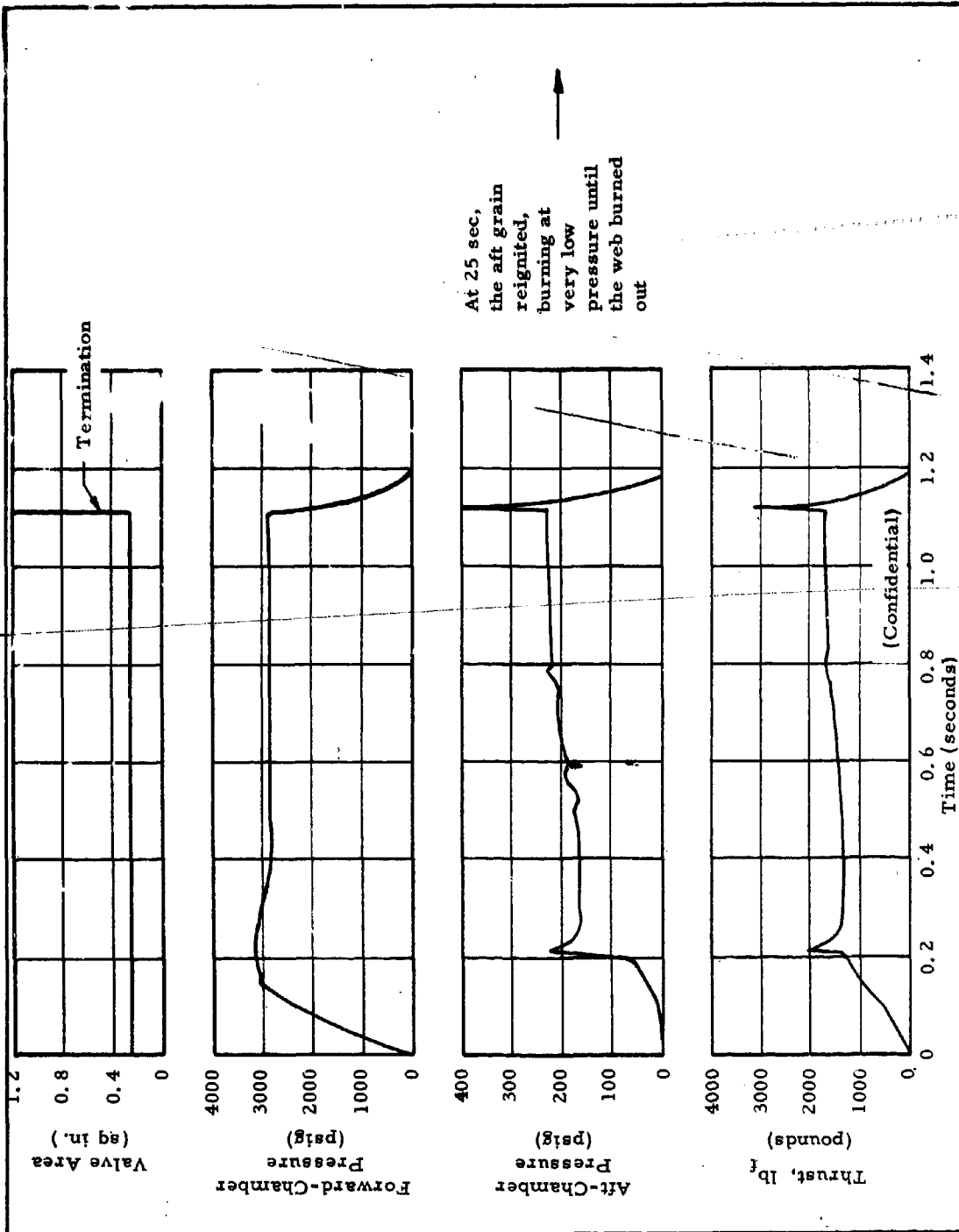


Figure A-1 - Traces for Test H.1

A-2

**CONFIDENTIAL**

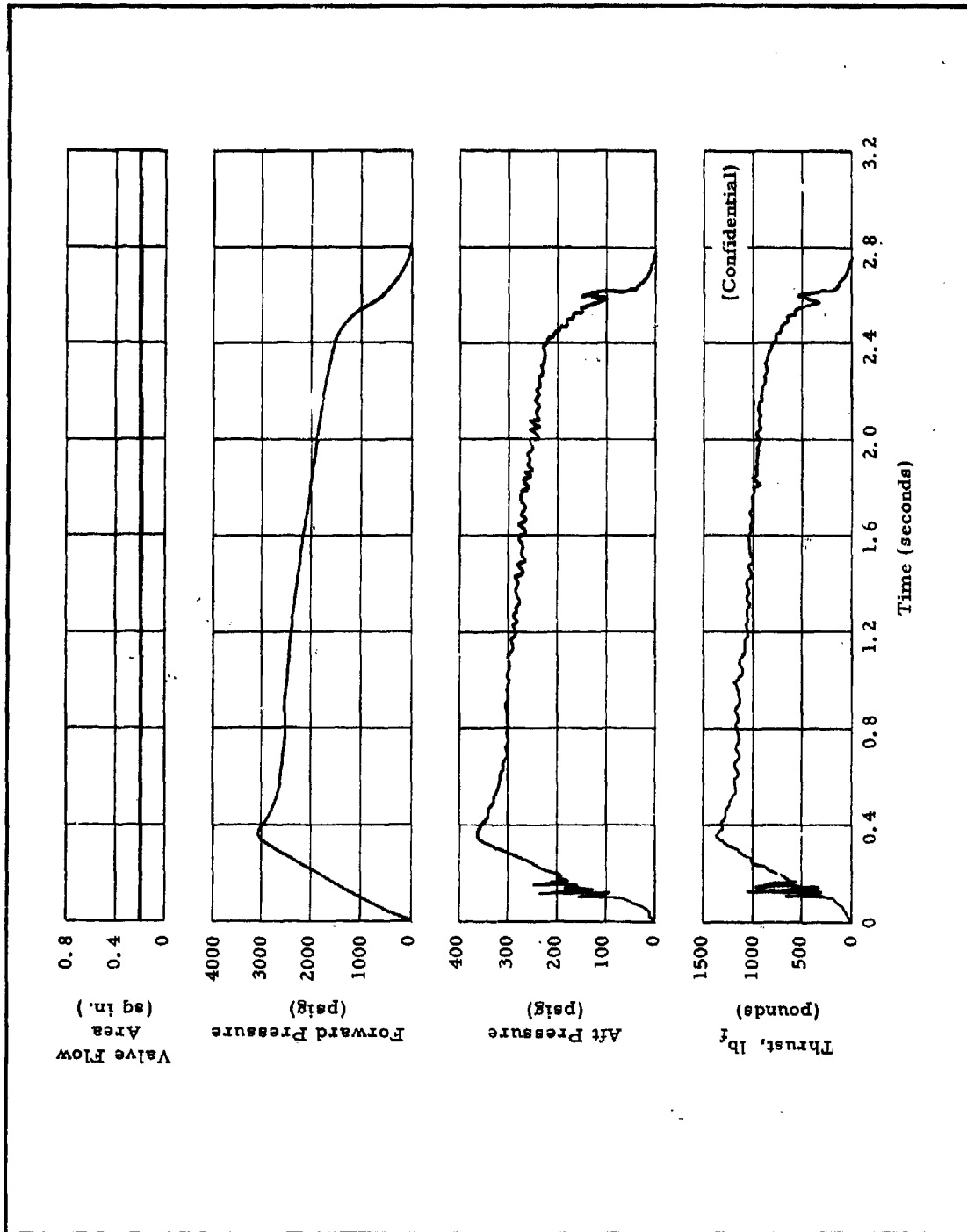


Figure A-2 - Traces for Test H. 2

## CONFIDENTIAL

AFRPL-TR-65-209, Vol I

the aft grain extinguished at the same time the forward web burned out. These results were more encouraging than if the valve had been actuated to achieve termination.

There was some evidence of irregular burning from the aft grain on this test, particularly during the ignition rise and tail-off portions of the trace. The pressure peaks during the ignition rise portion are believed to be caused by a surface effect on the initial inside diameter of the grain; this surface appeared to have a thin layer of only partially cured propellant. This layer may have been swept off the surface, causing a temporary increase in the burning surface. The aft pressure peak during the tail-off portion was similar to those observed for forward pressure tail-off in the Series B tests with OX-5 propellant. These peaks did not occur with OX-5 propellant when termination was accomplished with the valve; that is, when forward pressure decayed very rapidly. (Confidential)

#### 4. TEST H. 3 (1 April 1964)

The aft chamber of the motor for this test was cast with formulation 8133-35-5 (89 percent solids loading, 12 percent lithium perchlorate). The grain was 10.6 in. long and had a 0.92-in. web. The aft throat area was 3.125 sq in., and the expansion ratio of the nozzle was 2.90. The pressure, thrust, and valve area traces are shown in Figure A-3.

The motor reignited spontaneously 24 sec after termination, operating at a very low pressure for 120 sec. The aft grain was completely consumed during the test. On the basis of the average pressure of 258 psia existing in the aft chamber prior to termination, only 0.2 in. of aft web should have burned. Hence, the remaining web burned following reignition. (Confidential)

A forward web of 0.60 in. remained in the motor. Very little, if any, forward grain burned following reignition, based on the burning rate and characteristic velocity calculated during the test prior to reignition, as shown in Table XVIII. On the basis of these results, it is concluded that the aft grain reignited, rather than the forward grain. (Confidential)

#### 5. TEST H. 4 (9, 10 April 1964)

In view of the reignition that occurred in Test H. 3 with formulation 8133-35-5, it was decided to use formulation 8133-35-6 (90

## CONFIDENTIAL

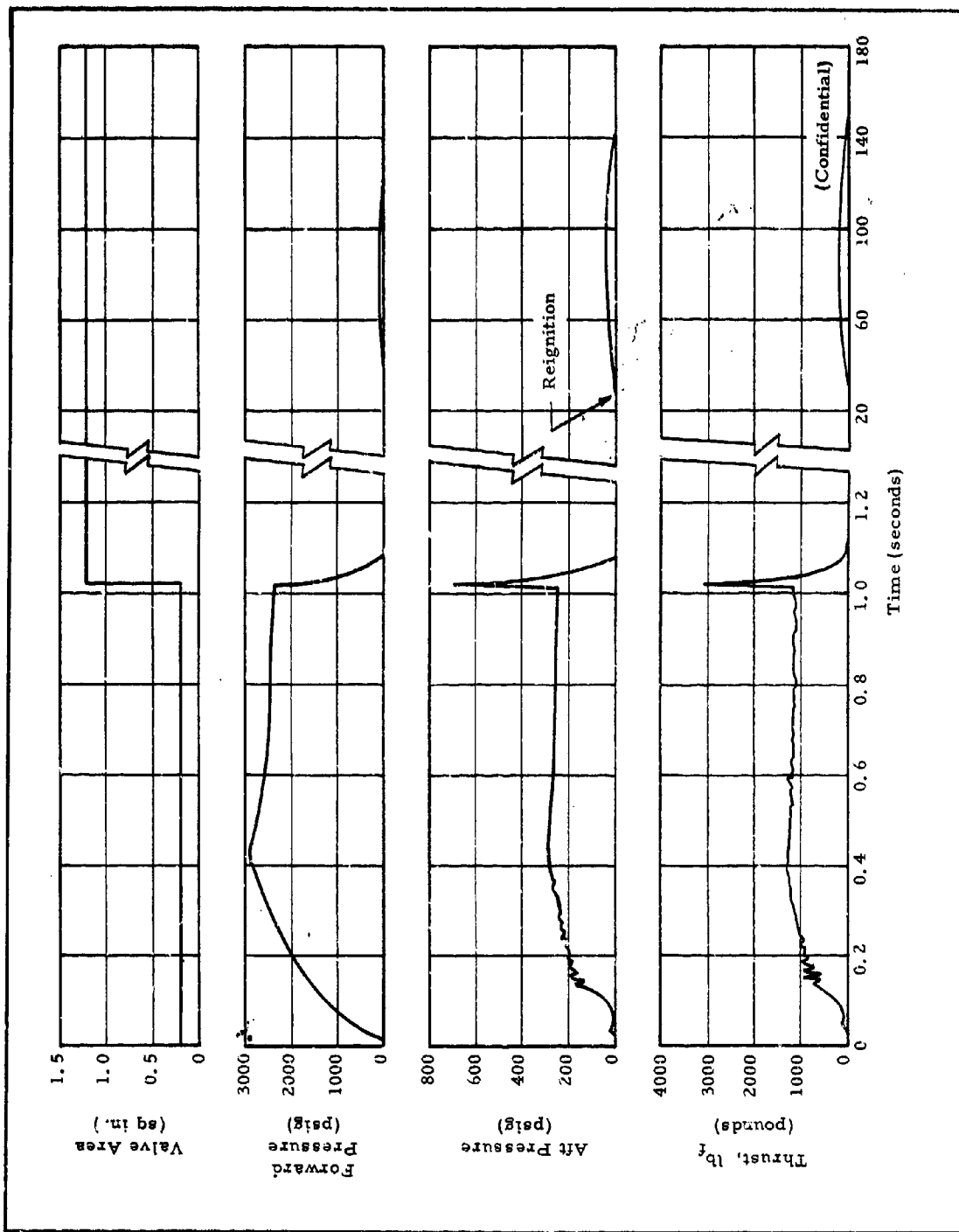


Figure A-3 - Traces for Test H. 3

## CONFIDENTIAL

AFRPL-TR-65-209, Vol I

percent solids loaded, 14 percent lithium perchlorate) to verify the results of Test H. 2, in which permanent extinction was obtained with this latter formulation. The pressure, thrust, and valve flow area traces for this test are given in Figure A-4.

The motor was operated through two cycles on successive days; permanent terminations were obtained on both cycles. The aft pressure and thrust traces show that some instability in aft-grain combustion occurred. The instability became more severe at pressures less than 250 psi. Some evidence of this behavior had been observed in previous tests, particularly during rise-times. In the second cycle of this test, H. 4. 2, the aft chamber was operated at 216 psi, a lower average pressure than for previous tests, and the irregular behavior was correspondingly more pronounced. (Confidential)

The reduced ballistic data for this test are given in Table XVIII. The performance values for the first cycle are unrealistically high, whereas the specific impulse calculated for the second cycle is close to that expected for the propellant combination at the low O/F ratio.

### 6. TEST H. 5 (17 April 1964)

Test H. 5 was designed to verify the results obtained in Test H. 3, in which formulation 8133-35-5 reignited spontaneously after termination. The physical integrity of the aft grain used in Test H. 5 was very poor, however; the grain broke up shortly after ignition, causing the motor to overpressure and fail.

As shown in Figure A-5, the aft pressure and thrust values increased sharply at 0.0475 sec. This increase in aft pressure and thrust was so rapid that the lines were lost on the oscillograph trace. At 0.0525 sec aft pressure apparently equaled forward pressure, since the forward pressure increased sharply at this point. The aft chamber became disconnected from the valve shortly thereafter and was blown off the stand. An inspection of the aft case and unburned aft propellant after the test indicated that case bond failure as well as grain break-up occurred. (Confidential)

### 7. TEST H. 6 (23, 24 April 1964)

Test H. 6 was designed to investigate the effect of aluminum powder in the aft formulation on the low-pressure unstable combustion observed in Test H. 4. Two percent aluminum powder (five micron)

A-6

## CONFIDENTIAL

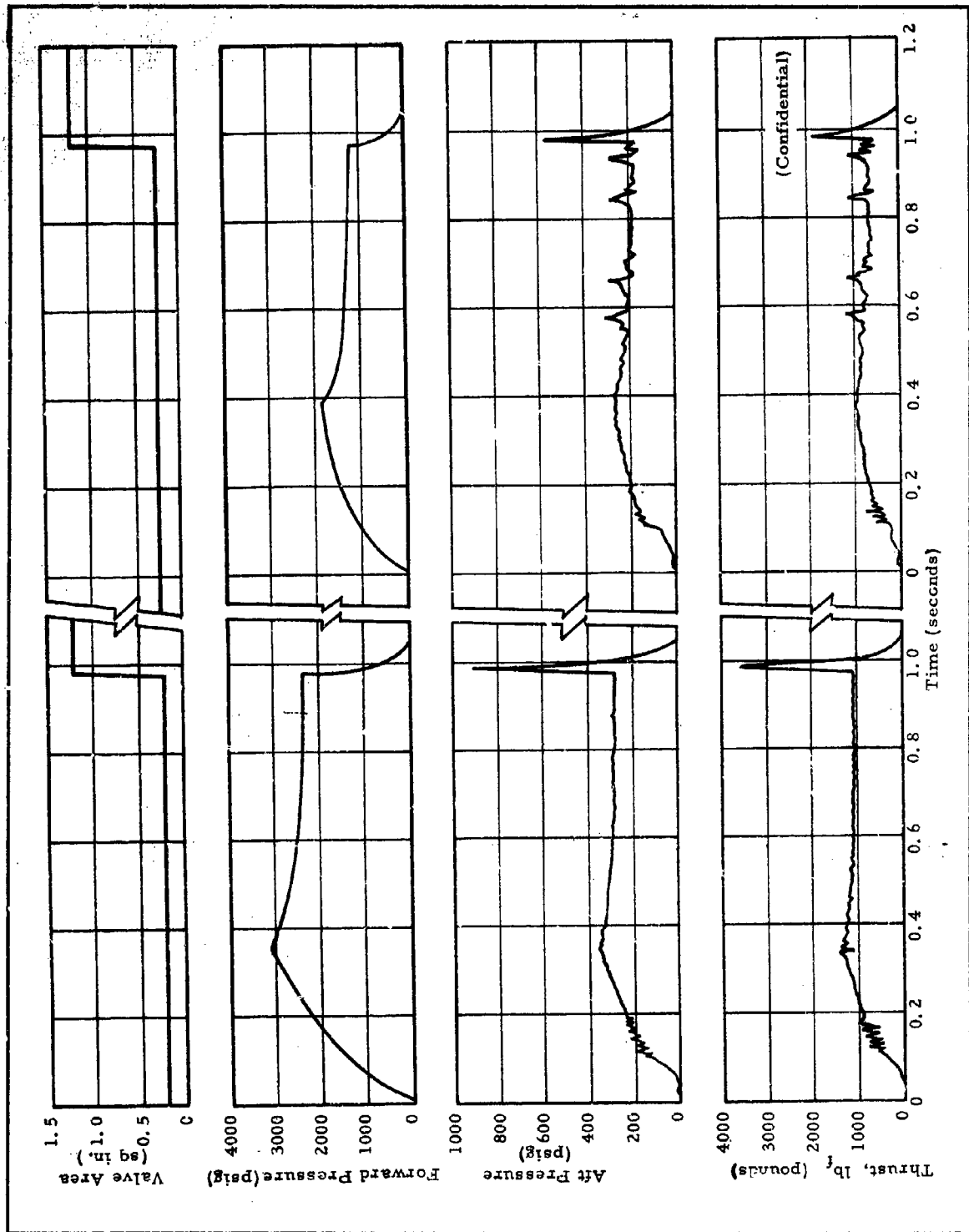


Figure A-4 - Traces for Tests H. 4. 1 and H. 4. 2

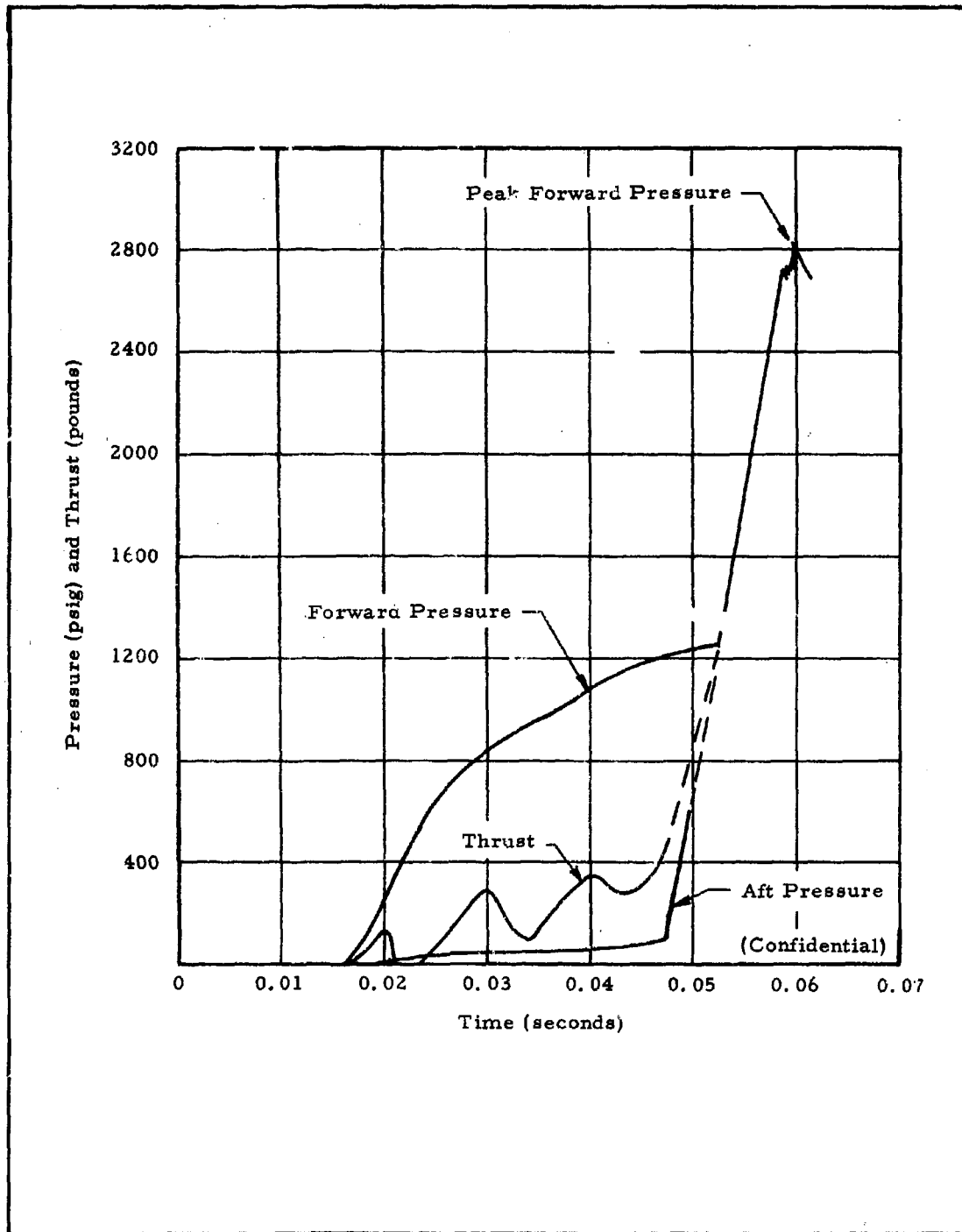


Figure A-5 - Traces for Test H. 5

**CONFIDENTIAL**

AFRPL-TR-65-209, Vol I

was incorporated in formulation 8133-35-6 for this test, replacing the two percent ammonium perchlorate. The aluminized formulation was designated 8133-36-1. The motor was operated through two termination cycles. The forward pressure was decreased for the second cycle, which correspondingly decreased aft pressure. The pressure, thrust, and valve flow area traces are shown in Figure A-6. (Confidential)

The incorporation of aluminum in the propellant for this test did not prevent combustion instability, which was quite severe during the second ignition cycle. A frequency of 40 to 50 oscillations per second was observed in both cycles. At times the thrust measurements for these tests did not correspond to the pressure measurements. This inconsistency is believed to have been caused by oscillations in the thrust stand, resulting from the rapid pressure changes occurring in the motor.

Permanent termination was achieved after the first cycle of this test. However, about 30 sec after termination of the second cycle, four chuffs occurred. An aft web of 0.30 in. remained after the second cycle, whereas the forward propellant was completely consumed. Since a forward web of 0.3 in. should have remained following the second cycle, it is concluded that the forward grain reignited and chuffed after the second cycle. Reduced ballistic data for the first cycle of this test are given in Table XVIII. (Confidential)

**CONFIDENTIAL**

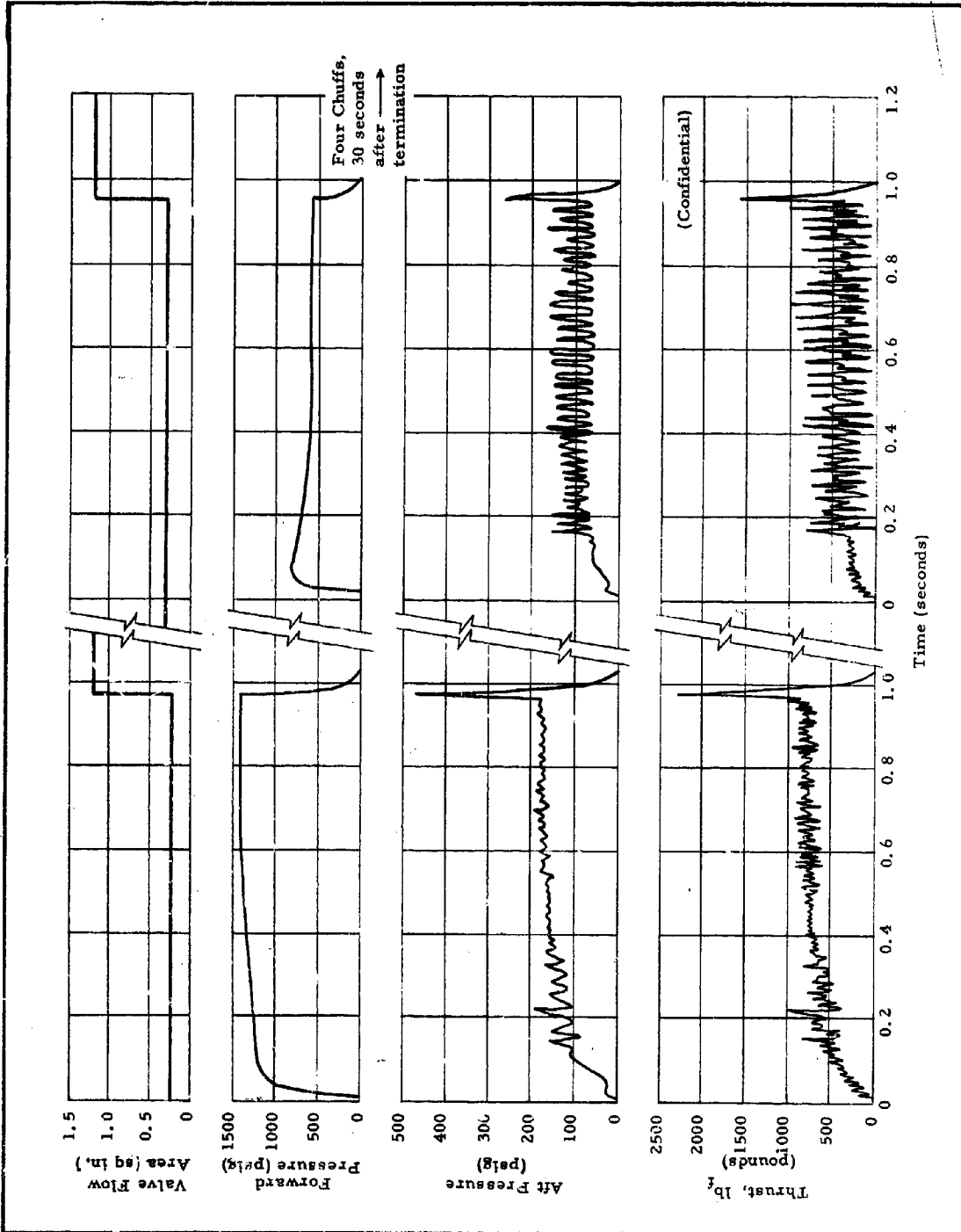


Figure A-6 - Traces for Tests H. 6. 1 and H. 6. 2

APPENDIX B - SYSTEM ANALYSIS AND CONTROL DESIGN  
FOR PROPORTIONAL HOT-GAS VALVE

1. INTRODUCTION

A system analysis and control design for the proportional hot-gas valve has been conducted. This effort has included simulation of the process to be controlled on an analog computer and the design of a control system for the process. The results of this effort are summarized in this appendix.

The system involved includes a chemical process and a valve used to control the process. The control equipment includes elements to place the valve and its servo-controlled actuator in a position loop plus elements to control an output pressure of the process in response to a desired pressure program. All elements of the system were simulated on an analog computer and their characteristics established. From this work a control configuration was selected. This was added to the simulation and the controlled system studies to obtain optimum performance. The results of this effort will be used to design the control equipment to be used in actual tests of the controlled process.

2. SUMMARY OF RESULTS

From the results of the system simulation, a control configuration was selected along with optimum values for the gain and time constant. The form of control selected for the process control is proportional plus integral. The control transfer function is as follows:

$$\frac{V_X}{V_E}(s) = K_C \left( 1 + \frac{1}{\tau_C s} \right)$$

$V_E$  = Pressure error signal (volts)

$V_X$  = Valve position command signal (volts)

$K_C$  = Control gain (volts per volt)

$T_C$  = Integral time constant (seconds)

$s$  = Laplace transform operator

Over the extreme conditions of the process, the best results were obtained with a control gain of 6.67 and an integral time constant of 0.5 seconds. This value of gain for the process control is based on the use of specific gains in the position loop and pressure sensor. A more detailed discussion of all gains is presented in paragraph 5, below. Under the initial conditions of the process, a higher value of gain and a smaller time constant provided improved performance. A small lead network was also effective in improving performance. For the final conditions of the process, a low gain and a larger integral time constant proved more optimum, but the lead network had little effect on performance. The values selected represent the best compromise to provide acceptable performance and good stability over the complete range of operation. Under the initial conditions of the process the response is relatively fast. Considerably slower operation results at the final condition. Under any condition the process is much more rapid for decreasing pressures than for increasing pressures.

The results for the process control were obtained with a relatively conservative design of the position loop. Under all conditions, the position loop response is significantly faster than the process. No attempt was made, however, to push the response of the position loop to extremes. The loop gain was selected for fast but well-damped response. More detailed information on the position loop is presented in paragraph 4, a, below.

Along with the selection of the control form and constants, the pressure program utilized with the system can have an important bearing on performance. The pressure program should be designed to command the fastest ramps in pressure that the controlled system can follow without greatly exceeding the capability of the system. For decreasing pressure ramps, the rate of decrease must also consider a limitation of the process. If extremely rapid pressure decreases are programmed, the chemical process may extinguish. Consideration of all these factors indicates that a pressure change of 50% should be programmed for approximately a one-second time duration. The controlled system can follow more rapid changes under the initial conditions of the process or for pressure decreases. The one-second limitation

does give satisfactory results with small overshoot and stable operation for the complete range of the process.

Another important factor in the control design is the proper establishment of limits in the control system. The integrator must be limited to prevent output voltages in excess of those corresponding to the physical limits of the valve and actuator. The overall control system output must be limited to prevent saturation of the computer elements to be used in the control configuration. The amplifiers used in the valve position loop should present no unusual problems. The bias levels which set the range of valve operation must, however, be properly established to work in conjunction with the output signals from the control. More detailed information on the overall control system setup for actual tests is presented in paragraph 5, below.

In addition to the results related specifically to the control system design, considerable data has been taken on the dynamic behavior on all parts of the system. Both step and frequency response data were taken on the simulated position loop and process. This was done for these elements individually and in combination. The frequency response data, in particular, was used as the basis for selecting the control configuration and constants. This data also provides a theoretical basis for evaluation of the system during actual operation. Preliminary checkout of the positioning loop, for example, can be compared to the computer results to test the validity of these results prior to actual control operation. Should unstable operation be encountered, the frequency response data provides a basis for checking the behavior of the oscillating system. With this type of information, the faulty component or the deviation from theoretical performance can be rapidly and effectively localized. This type of data is presented in paragraph 4, c, below.

### 3. GENERAL SYSTEM DESCRIPTION

All of the elements involved in the controlled system are presented in block diagram form in Figure B-1. The desired variation of pressure with time is established as the pressure program. This program provides a signal ( $V_P$ ) indicating the desired level of pressure as a function of time. This signal is compared to a signal indicating the level of pressure in the process. The pressure signal ( $V_S$ ) represents the amplified output of a pressure sensor. The difference between the desired and actual pressure signals forms the pressure error signal ( $V_E$ ). This error

**CONFIDENTIAL**

AFRPL-TR-65-209, Vol I

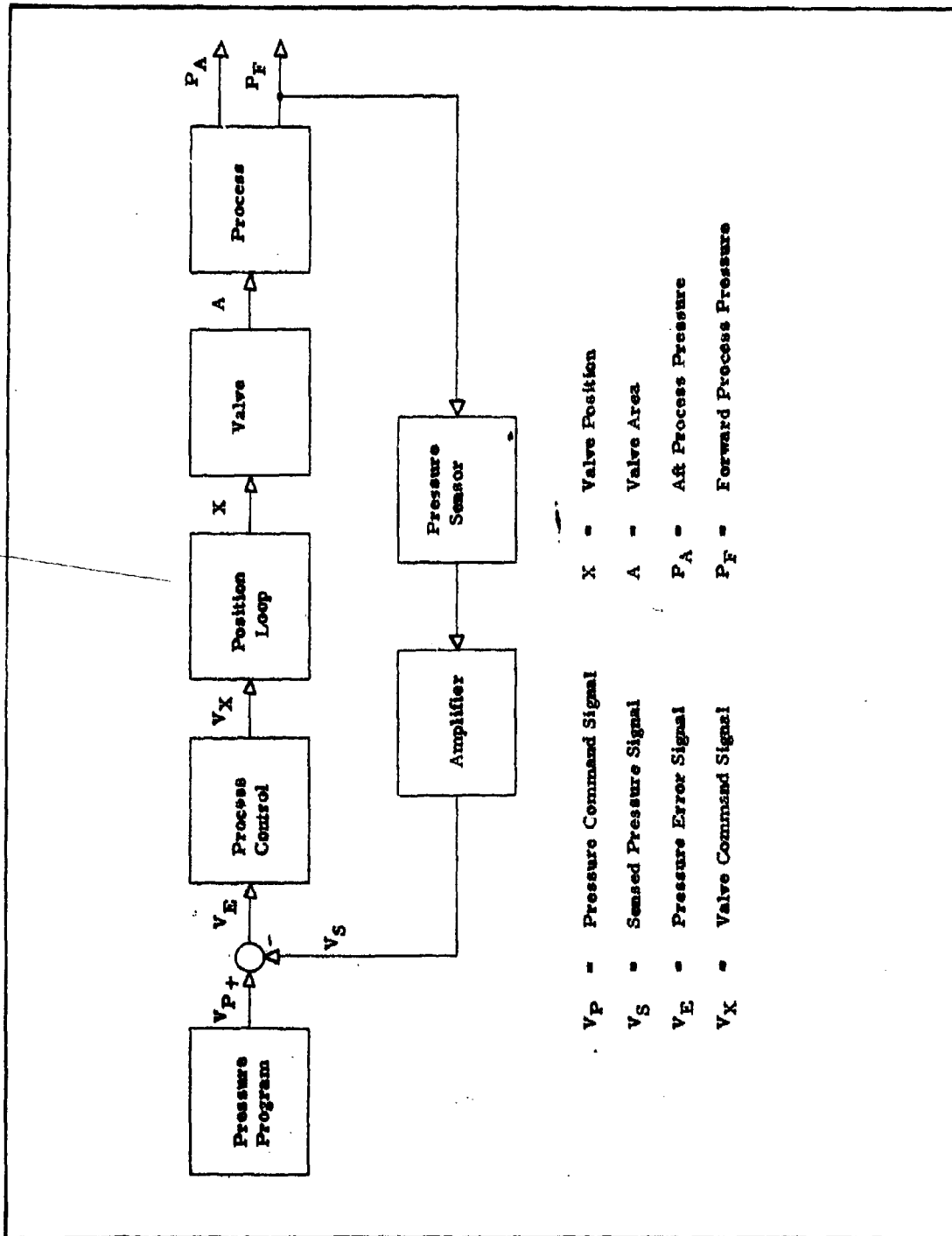


Figure B-1 - Basic Block Diagram of Controlled System

B-4

**CONFIDENTIAL**

signal is acted upon by the process control to obtain a valve command signal ( $V_X$ ). The position loop is designed to produce a valve position ( $X$ ) proportional to the level of the valve command signal. The valve proper is designed to provide the desired variation of valve area ( $A$ ) as a function of valve position. The process responds to valve area to produce two pressure outputs. One of these, the forward process pressure ( $P_F$ ), is sensed for the control operation. The aft position pressure ( $P_A$ ) is related to the forward pressure by the characteristics of the process. By controlling forward pressure, aft pressure is also automatically set.

The elements which comprise the position loop are presented in block diagram form in Figure B-2. The input signal to the position loop is the valve command signal ( $V_X$ ) from the process control. This is compared to a position feedback signal ( $V_F$ ). The difference between these signals is amplified to produce a current to the servovalve. The level of current ( $I$ ) in the servovalve coil produces a flow of hydraulic fluid ( $Q$ ) to the actuator. This flow causes the position of the actuator and valve ( $X$ ) to vary. When a position corresponding to the command position is attained, the position error is reduced to zero and the position loop maintains the desired position.

In simulating the system on the computer, a mathematical description was derived for each element of the system. The general approach and a more detailed discussion of each element is presented in the paragraphs that follow.

#### 4. SYSTEM SIMULATION

The basic approach to an analog computer simulation problem consists of three steps: the derivation of the mathematical model describing the system; the scaling of the problem parameters to be compatible with the computer capabilities; and the formation of a detailed computer diagram which expresses the scaled model in terms of the computer components. From the computer diagram, the simulation can readily be effected.

The derivation of the mathematical model of this problem is straightforward, requiring only the application of mechanical, hydraulic, and electronic fundamentals. Both time and amplitude scaling are required for the simulation. Amplitude scaling is applied to establish a compatible correlation between the physical parameters of the system (pressures, flows, etc.) and the voltage

**CONFIDENTIAL**

AFRPL-TR-65-209, Vol I

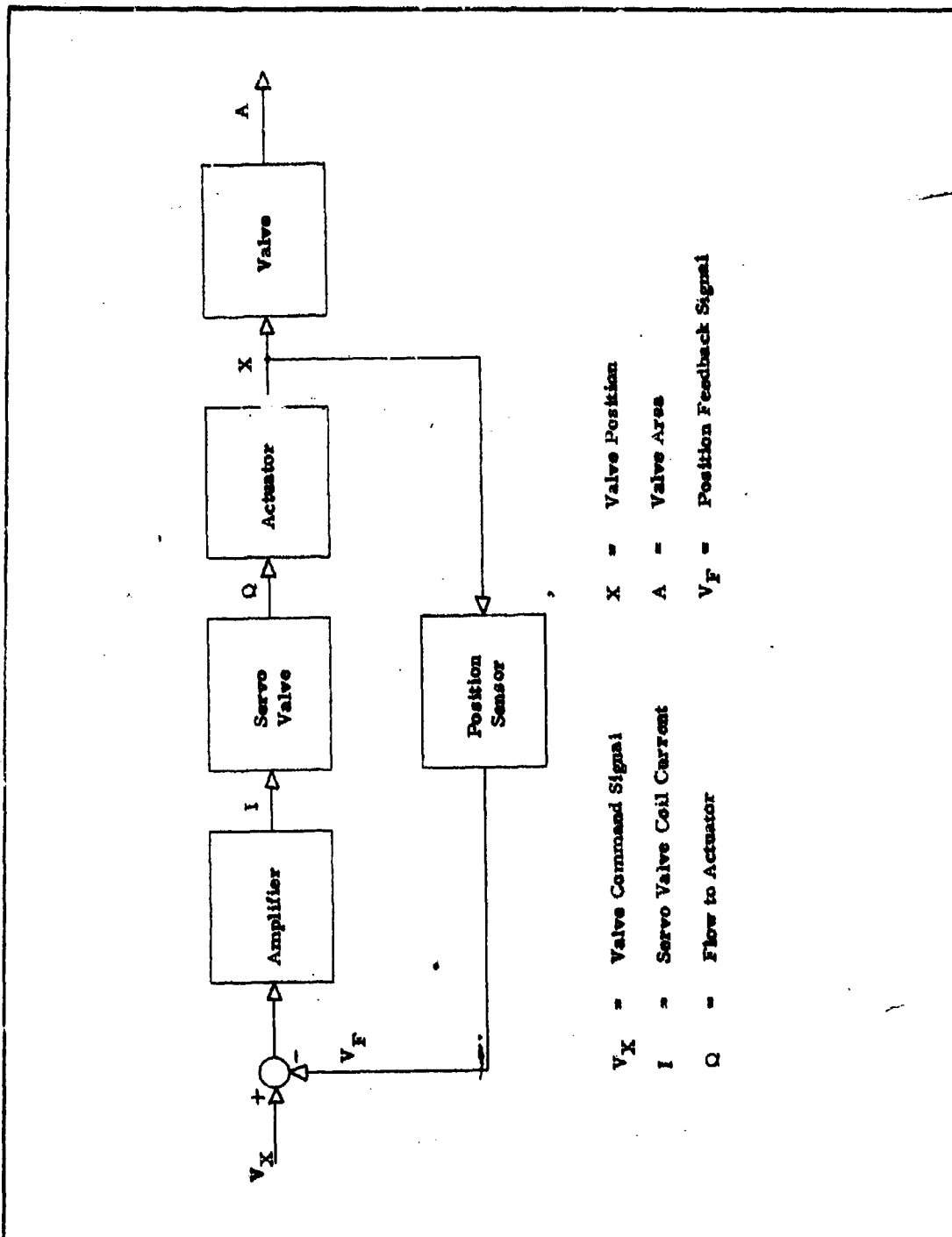


Figure B-2 - Basic Block Diagram of Position Loop

B-6

**CONFIDENTIAL**

levels which represent these parameters in the computer. These scale factors are selected to maintain high voltage levels for accuracy while avoiding saturation limits.

The necessity for time scaling arises out of the fast response times of portions of the position loop compared to the remainder of the problem and the ease and accuracy of simulation. Time scaling must be considered first and on the basis of the complete system. Amplitude scaling will be affected by time scaling because of the resultant change in the magnitudes of the various derivatives and integrals of the problem.

The most important dynamic limitations of the computer are the multipliers and the strip chart recorder. The faster time constants of the system are on the order of one millisecond, and the longest time constant is around one second. An increase in time scale by a factor of ten will allow accurate computer operation and recordings of transients without causing unreasonably long system response times. Based on this selection,

$$T = 10 t$$

$$dT = 10 dt$$

$$dT^2 = 100 dt^2$$

where,

$$t = \text{Real time (seconds)}$$

$$T = \text{Computer time (seconds)}$$

The implication of this scale factor is simply that the simulated system will respond ten times more slowly than the physical system it represents. Computer results are then interpreted on this basis. Recordings of the results, for example, are corrected to real time by decreasing the time scale of the computer recording by a factor of ten.

No attempt will be made to explain the fundamentals of analog computation. In the paragraphs which follow, the simulation approach will be derived in detail for each portion of the system. The symbols used for each of the major elements of the computer are presented in Figure B-3.

# CONFIDENTIAL

AFRPL-TR-65-209, Vol I

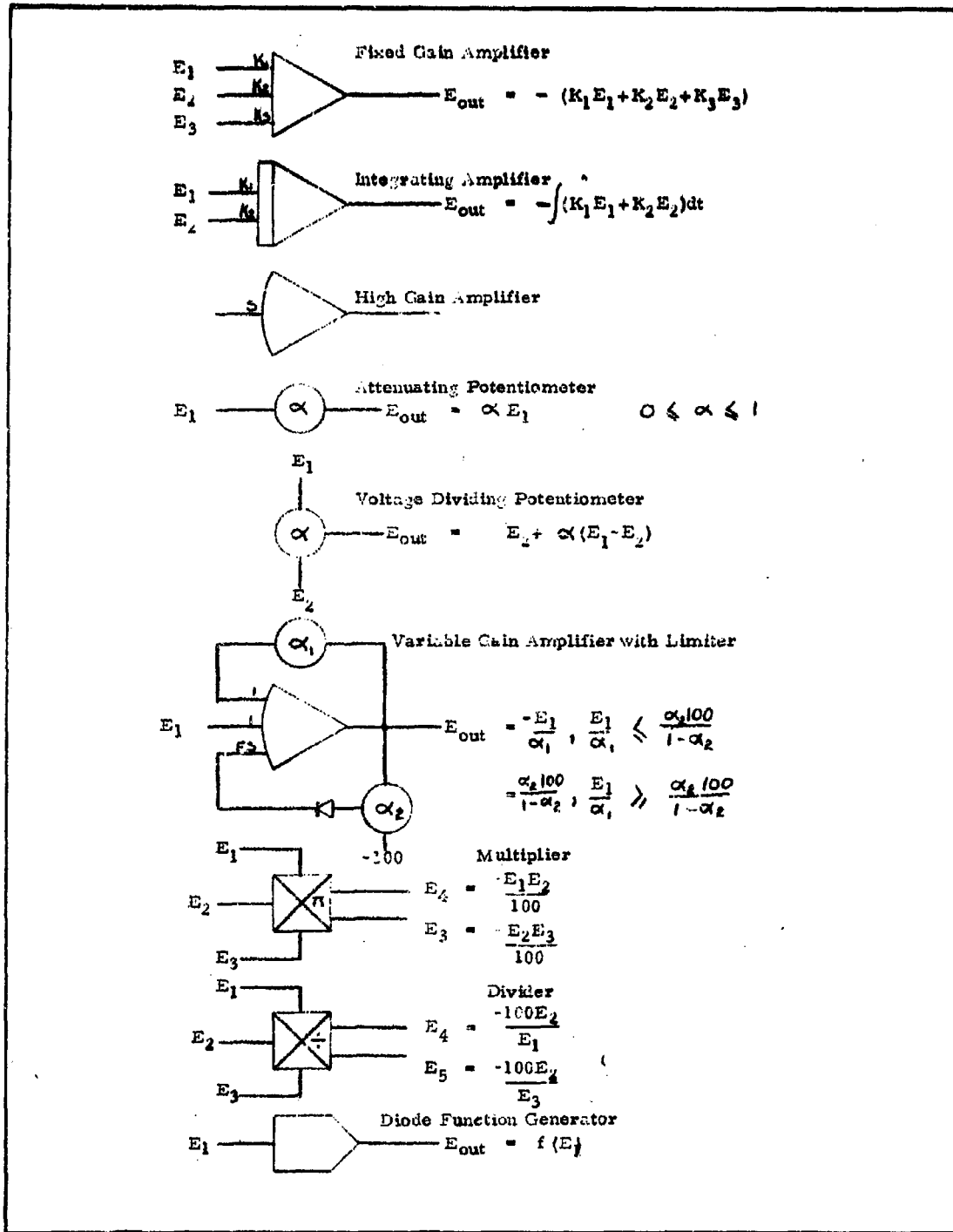


Figure B-3 - Major Analog Computer Elements

a. Position Loop Simulation

The position loop was the first of the major system elements to be simulated. Its simulation was based on the design parameters of the control actuator and the specified characteristics of the servovalve, the electronic equipment, and the hydraulic fluid and supply system. A pictorial representative of the position loop is shown in Figure B-4 along with the definition of the symbols. The specifications and design parameters are listed in Table B-1.

(1) Actuator

The equation describing the actuator position is

$$m\ddot{X} + D\dot{X} = \Sigma F$$

Simply stated, this equation relates the acceleration and velocity of the actuator to the summation of all forces acting upon it and the mass and viscous damping present. For the actuator to remain stationary, the forces must sum to zero. Any unbalanced force will produce motion as described by this equation.

The forces which act upon the actuator are shown in Figure B-4. These include the forces developed by the hydraulic fluid acting on the actuator piston, the force developed by the aft process pressure on the pintle of the process control valve, and the friction forces which oppose motion of the actuator. Those forces due to the hydraulic and aft process pressures sum directly. No motion results until these forces exceed the friction force. Once these forces exceed the friction force, the friction force will be constant and in a direction to oppose motion. Physically, this acts as a deadband in the system. Mathematically, this can be expressed as:

$$F = 0, \text{ for } A_A P_A + A_O P_O - A_C P_C < F_F$$

$$F = A_A P_A + A_O P_O - A_C P_C - F_D,$$

$$\text{for } (A_A P_A + A_O P_O - A_C P_C) > F_F$$

# CONFIDENTIAL

AFRPL-TR-65-209, Vol I

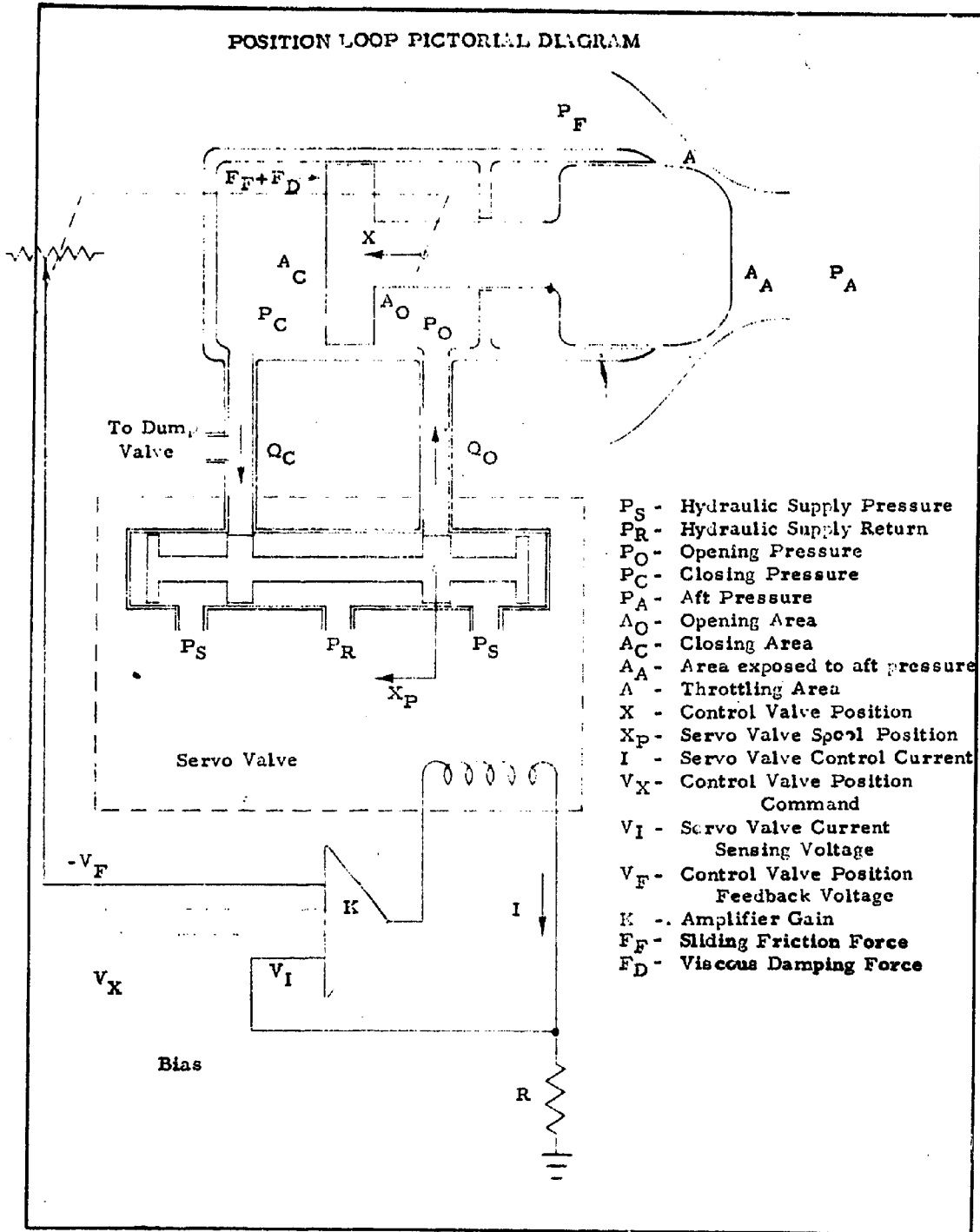


Figure B-4 - Position Loop Pictorial Diagram

# CONFIDENTIAL

AFRPL-TR-65-209, Vol I

TABLE B-1 - POSITION LOOP COMPONENT SPECIFICATIONS

<u>Control Valve and Actuator</u>		
$\hat{A}_A$	=	5.2 in. <sup>2</sup>
A	=	As shown in Figure A-14
$A_D$	=	0.390 in. <sup>2</sup>
$A_C$	=	1.86 in. <sup>2</sup>
Actuator Mass, m	=	0.0089 lb/in./sec <sup>2</sup>
Actuator Damping, D	=	3.0 lb/in./sec
Actuator Friction, $F_P$	=	547 lb, opening
	=	392 lb, closing
<u>Hydraulic Line Losses</u>		
Opening $P_{LL}$	=	210 psi at 10 gpm
Closing $P_{LL}$	=	57 psi at 40 gpm
<u>Hydraulic Volumes, X=O</u>		
$V_{O(O)}$	=	1.00 in. <sup>3</sup>
$V_{C(O)}$	=	4.91 in. <sup>3</sup>
Upstream Free Volume	=	130 in. <sup>3</sup>
<u>Hydraulic System</u>		
$P_S$	=	5000 psi
$P_R$	=	0 psi
Compressibility Factor, C	=	$\frac{1}{75,000}$ for worst case

Servovalve

Moog 73-182

Single orifice pressure drop at 10 gpm,  $P_C$

500 psi, with  $X_P = \pm 1$  (maximum spool displacement)

Torque motor coil

R = 200 ohms each

L = 1 henry each

Control characteristics (series connected coils)

$$X_P(s) = \frac{133/\text{amp } I(s)}{\frac{s^2}{(879)^2} + \frac{2X_9s}{879} + 1} - \frac{1}{s}$$

where  $X_P = \pm 1$  represents maximum spool displacement from null.

Dump Valve

Moog 72-164

Parallel orifice pressure drop P = 500 psi at 50 gpm,  $X'_P = \pm 1$

Torque motor coil

R = 200 ohms each

L = 1 henry each

Control characteristics (series connected coils)

$$X'_P = \frac{133/\text{amp } I'(s)}{\frac{s^2}{(377)^2} + \frac{2X_9s}{377} + 1} - \frac{1}{s}$$

Amplifier

Philbrick

K2KA driving SK2B

Nominal Gain = 120,000

Voltage Range =  $\pm 100$  volts

Potentiometer

Carter plastic film, 2K rectilinear

$$V_P = (a + bX) \frac{10 \text{ volts}}{a + b + c}, \quad a + b + c = 1.25 \text{ in.}, \quad b = 1.0 \text{ in.}$$

# CONFIDENTIAL

$$F = A_A P_A + A_O P_O - A_C P_C + F_D,$$

$$\text{for } (A_A P_A + A_O P_O - A_C P_C) < - F_F$$

Applying the time scale factors,

$$\ddot{X} = m \frac{d^2 X}{dt^2} = 100m \frac{d^2 X}{dT^2}$$

$$\dot{X} = D \frac{dX}{dt} = 10D \frac{dX}{dT}$$

The equation becomes

$$100m \frac{d^2 X}{dT^2} + 10D \frac{dX}{dT} = \Sigma F.$$

All of the relations for the actuator are shown in block diagram form in Figure B-5(a). The equation is solved by summing the hydraulic and aft pressure forces and applying the deadband representing the friction force to obtain  $\Sigma F$ . The viscous damping force  $10K \frac{dX}{dT}$  is subtracted to obtain

$$100m \frac{d^2 X}{dT^2} = \Sigma F - 10D \frac{dX}{dT}.$$

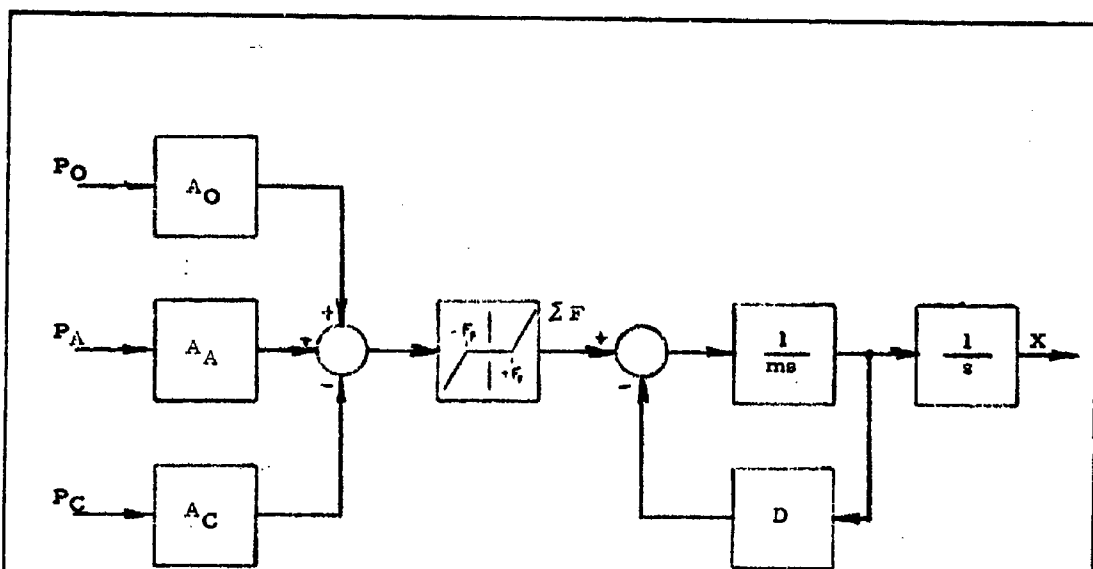
This is divided by 100m and integrated with respect to time to solve for  $\frac{dX}{dT}$ . The velocity is then integrated to obtain the actuator position X.

Actual computer implementation of this portion of the position loop is shown in Figure B-5(b). The amplitude scaling factors for this part of the simulation are included in Figure B-5 (b).

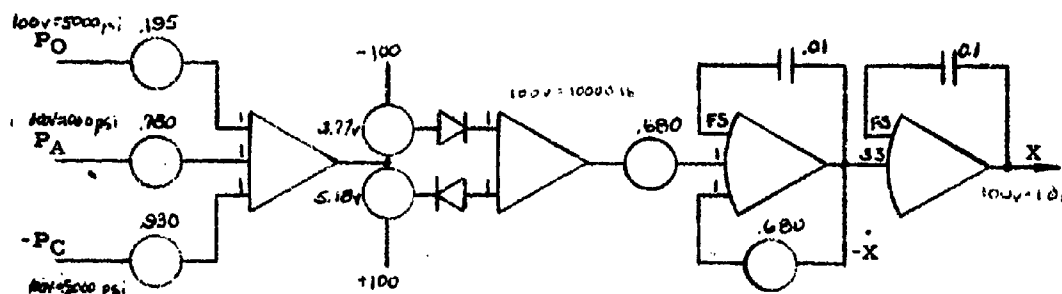
The actuator simulation is based on the initial design specifications of the control valve. Subsequent finalization of the valve caused the actuator mass to be reduced to  $0.00383 \frac{\text{lb} \times \text{sec}^2}{\text{in.}}$ . This change in mass can only improve the dynamics of the valve by reducing the

# CONFIDENTIAL

AFRPL-TR-65-209, Vol I



(a) Actuator Block Diagram



(b) Actuator Computer Diagram

Figure B-5 - Actuator Block Diagram and Computer Diagram

# CONFIDENTIAL

time constant of the actuator. The time constant of the actuator is the ratio of the mass to the fluid damping, including both the damping of the actuator and the damping due to the metering orifices of the servovalve. This time constant is small compared to the dynamics of the rest of the position loop and the effect on the position loop due to this mass change should not be measurable. Data will be taken on the position loop to verify its correlation to the computer results.

(2) Pressure Relationships

The derivation of the three pressures,  $P_A$ ,  $P_O$  and  $P_C$ , are required in order to determine the force summation on the actuator and, therefore, to determine the actuator position. The aft process pressure will be determined as part of the process simulation. The two hydraulic pressures  $P_O$  and  $P_C$  have similar derivations, a general derivation being shown below.

Assuming linear compressibility, the hydraulic pressure in a cavity can be expressed as an initial pressure plus the change in the pressure generated by a change in the density of the fluid. This density change could be caused by an addition (or subtraction) of fluid to that of the fixed volume or by decreasing (or increasing) the volume of a fixed amount of fluid. For either type of change the pressure change can be expressed as

$$\Delta P = \frac{\Delta M}{KV} ,$$

where  $\Delta P$  is the pressure change,  $\Delta M$  is the mass change,  $V$  is the volume, and  $K$  is the compressibility constant. Since the compressibility is small, the addition of mass can be represented by the addition of a volume of fluid

$$\Delta M = \Delta VD ,$$

where  $D$  is the density. The pressure can now be expressed as

$$\Delta P = \frac{\Delta V}{CV} ,$$

where the new compressibility factor  $C = \frac{K}{D}$ .

Referring to Figure B-4, the change in fluid density depends on the amount of fluid flowing through the servovalve orifice and on the movement of the actuator, and the pressure can be expressed as

$$P = P_i + \frac{\Delta V_Q - \Delta V_X}{VC}$$

where  $\Delta V_Q$  is the fluid volume supplied through the servovalve orifice and  $\Delta V_X$  is the fluid volume displaced by the actuator. Since the fluid from the servovalve is the accumulation of fluid flow,  $Q$ , the expression becomes

$$P = P_i + \frac{\int Qdt - A\Delta X}{VC}$$

where  $A$  is the piston area of the actuator and  $\Delta X$  the actuator displacement.

If the initial condition is taken to be  $P = 0$  when  $X = 0$ , the pressure is

$$P = \frac{\int Qdt - AX}{[V(0) + AX]C}$$

The opening and closing pressures,  $P_O$  and  $P_C$ , expressed in terms of the polarities of Figure B-4 and of the new time variables, are

$$P_O = \frac{\frac{1}{10} \int Q_O dT - A_O X}{[V_C(0) - A_C X]C}$$

$$P_C = \frac{A_C X - \frac{1}{10} \int Q_C dT}{(V_C(0) - A_C X)C}$$

The position of the actuator,  $X$ , has already been determined.

The fluid flow  $Q$  must now be established. Turbulent flow through the metering orifices and around the hydraulic strut obstructions is assumed such that the pressure drops take the form

$$\Delta P = \frac{Q^2}{K}$$

The flow constant of the servovalve is proportional to the spool position  $X_P$ , and the total pressure drop across one strut and orifice is

$$\Delta P = \frac{Q^2}{X_P^2 K_M^2} + \frac{Q^2}{K_S^2}$$

where  $K_M$  and  $K_S$  are the metering orifice and strut flow constants. Since the pressure losses across the struts are small, and because the simplest, yet valid, simulation is desired, the above expression is approximated by

$$\Delta P = \frac{Q^2}{X_P^2} \left( \frac{1}{K_M^2} + \frac{1}{K_S^2} \right)$$

Solving for Q,

$$Q = X_P K \sqrt{\Delta P}$$

where

$$K = \frac{K_M K_L}{\sqrt{K_M^2 + K_S^2}}$$

Referring to Figure B-4, the movement of the servovalve spool connects either the pressure supply or the pressure return to each strut, depending on the direction of the movement. The equations expressing the summation of the pressure drops is either

$$P + \Delta P = P_S$$

for the spool movement in one direction, or

$$P - \Delta P = P_R = 0$$

for the opposite displacement. Incorporating this fact along with the flow conventions of Figure B-4,

$$Q_O = X_P K_O \sqrt{P_O(X_P)}$$

$$Q_O = X_P K_C \sqrt{P_C(-X_P)}$$

where

$$\left. \begin{aligned} P(X_P) &= P_S - P \\ P(-X_P) &= P \end{aligned} \right\} \text{for } X_P > 0$$

$$\left. \begin{aligned} P(X_P) &= P \\ P(-X_P) &= P_S - P \end{aligned} \right\} \text{for } X_P < 0$$

A block diagram describing the derivation of  $P_O$  and  $P_C$  is presented in Figure B-6(a). Computer mechanization of this portion of the simulation is shown in Figure B-6(b).

### (3) Servovalve and Position Loop Control Elements

The function of the position loop is to fix the position of the actuator as dictated by the position command signal. Since the position of the actuator is dependent on the integration of the fluid flowing through the servovalve, the steady-state position of the actuator can be made exactly proportional to the command signal such that  $K_1 X = V_X$ . The intended operation of the position loop is to compare the position signal with the command signal in an amplifier and to cause any error or difference to control the servovalve. If the signals are equal, the servovalve spool position will be zero, and no fluid will flow. A positive error (position command signal greater than position signal) will cause displacement of the servovalve and fluid flow in a direction to increase actuator position. A negative error causes operation in the opposite direction.

A normal servovalve characteristic produces steady-state spool position proportional to the control current. To satisfy the control valve requirement

# CONFIDENTIAL

AFRPL-TR-65-209, Vol I

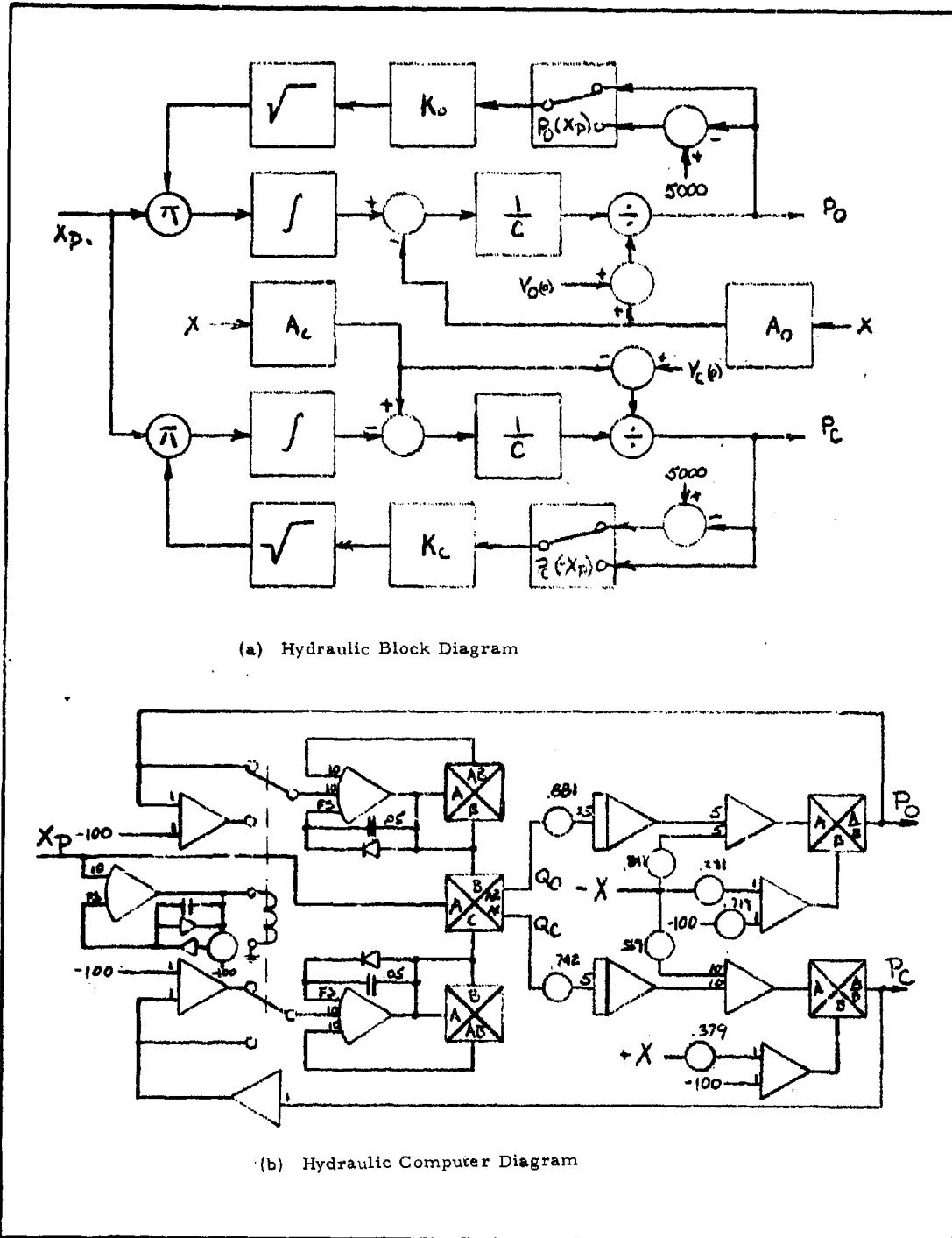


Figure B-6 - Hydraulic Block Diagram and Computer Diagram

that the motor extinguishes upon loss of power, the spool position with no control current is full open in the direction which opens the actuator. This is accomplished by a mechanical bias and requires a compensating electrical bias for zero spool position. The dynamic characteristic for the valve, including the mechanical bias, is specified in Table B-I as

$$X_P(s) = \frac{K_1 I_c(s)}{\frac{s^2}{W_n^2} + \frac{2\zeta s}{W_n} + 1} - \frac{X_P(o)}{s}$$

Here  $X_P(o)$  represents the open spool position with no control current. This expression can be derived from the differential equation

$$\begin{aligned} \frac{1}{W_n^2} \frac{d^2}{dt^2} [X_P + X_P(o)] \\ + \frac{1}{W_n} \frac{d}{dt} [X_P + X_P(o)] \\ + X_P + X_P(o) = K_1 I_c \end{aligned}$$

By simplifying and applying the time scaling, this expression becomes

$$\begin{aligned} \frac{100}{W_n^2} \frac{d^2 X_P}{dT^2} = K_1 \left[ I - \frac{X_P(o)}{K_1} \right] \\ - \frac{10}{W_n} \frac{dX_P}{dT} - X_P \end{aligned}$$

The steady-state servovalve spool position must be  $X_P = 0$ , requiring that  $I - \frac{X_P(o)}{K_1} = 0$ . If the

error voltage  $E$  is the difference between the position command voltage  $V_X$  and the actuator position feedback voltage  $V_F$ . The above steady-state condition indicates that the relationship between  $I - \frac{X_{P(0)}}{K_1}$  and  $E$  must be proportional in the steady state. If  $E$  is set to zero, it is necessary that  $I_{(s)} = I'_{(s)} + \frac{I_0}{s}$ , where  $I_0 = \frac{X_{P(0)}}{K_1}$ .  $I_0$  is a bias current which sets the spool to its null position. A small lag is caused by the servovalve coil inductance. The relationship between  $I'_{(s)}$  and  $E$  will therefore be

$$I'_{(s)} = \frac{K_3 E_{(s)}}{\tau_s + 1},$$

where  $\tau$  is the time constant due to the coil inductance. An amplifier configuration with current feedback is selected to minimize  $\tau$  as shown in Figure B-4. The gain of the amplifier  $K$  is chosen as large as possible, yet not allowing the amplifier to saturate; and the current sensing resistor is sized such that a maximum servovalve spool displacement will result from a maximum error voltage.

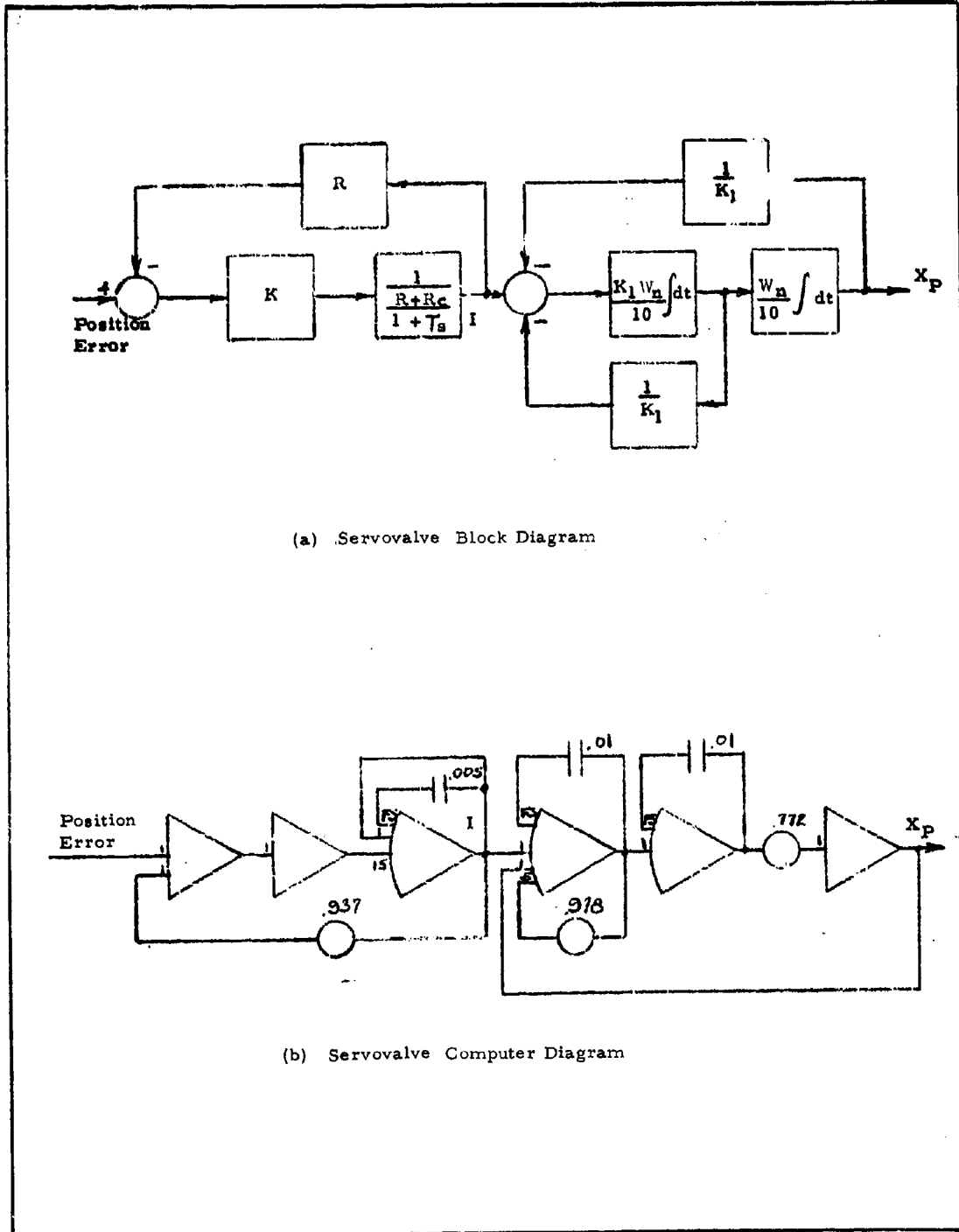
The effect of this current feedback on the response of the servovalve coil current is to improve the time constant from  $\tau = \frac{L}{R + R_C}$  to  $\tau = \frac{L}{KR}$ ,  $R_C$  being the coil resistance and  $R$  being the current sensing resistance. The block diagram representing the mathematical description of the amplifier and servovalve is shown in Figure B-7(a), and the corresponding computer diagram in B-7 (b).

#### (4) Steady-State and Transient Performance

The desired steady-state performance of the position loop is that the actuator position be proportional to the position command signal. Since the dominant characteristic of the position loop is integration with proportional feedback, the steady-state condition must be zero error signal, thus satisfying the requirement.

**CONFIDENTIAL**

AFRPL-TR-65-209, Vol I



(a) Servovalve Block Diagram

(b) Servovalve Computer Diagram

Figure B-7 - Servovalve Block Diagram and Computer Diagram

B-21

**CONFIDENTIAL**

Steady-state measurements of the position loop simulation verified this desired proportional operation within the accuracy of the digital voltmeter.

Position loop transient response recordings were made for input step magnitudes of 0.1 and 1.0 inches with constant aft process pressures of 0 and 1500 psi and also with the process simulated. The responses to position command signal steps from 0 to 0.1 to 0 inches and from 0 to 1.0 to 0 inches with  $P_A = 0$  are shown in Figure B-8 and B-9. The responses to the same input steps but with  $P_A = 1500$  psi are shown in Figures B-10 and B-11.

As can be predicted from the actuator geometry, the opening transient is much slower than the closing transient when  $P_A = 0$ . This phenomenon is the result of the difference between  $A_O$  and  $A_C$ . When the actuator is opening, the pressure drop across the actuator is greater than when closing, providing a lower pressure drop across the servovalve and resulting in a lower flow rate.

When  $P_A = 1500$  psi, the opposite effect is observed. In this case  $P_A$  aids the opening direction. The system acts as if the pressure supply is increased to the opening cavity and is decreased to the closing chamber, the result being that the system is speeded up when opening and is slowed when closing. The actuator was designed so that a medium aft pressure,  $P_A = 750$  psi, would result in equal opening and closing response times.

b. Process and Control Valve Simulation

The position loop simulation described in a, above, produces a determination of the valve displacement (X). From this result, the valve area must be obtained to provide the controlling parameter for the process. Finally, the process must be simulated to determine the variation of the forward and aft process pressures in response to the control valve area.

**CONFIDENTIAL**

AFRPL-TR-65-209, Vol I

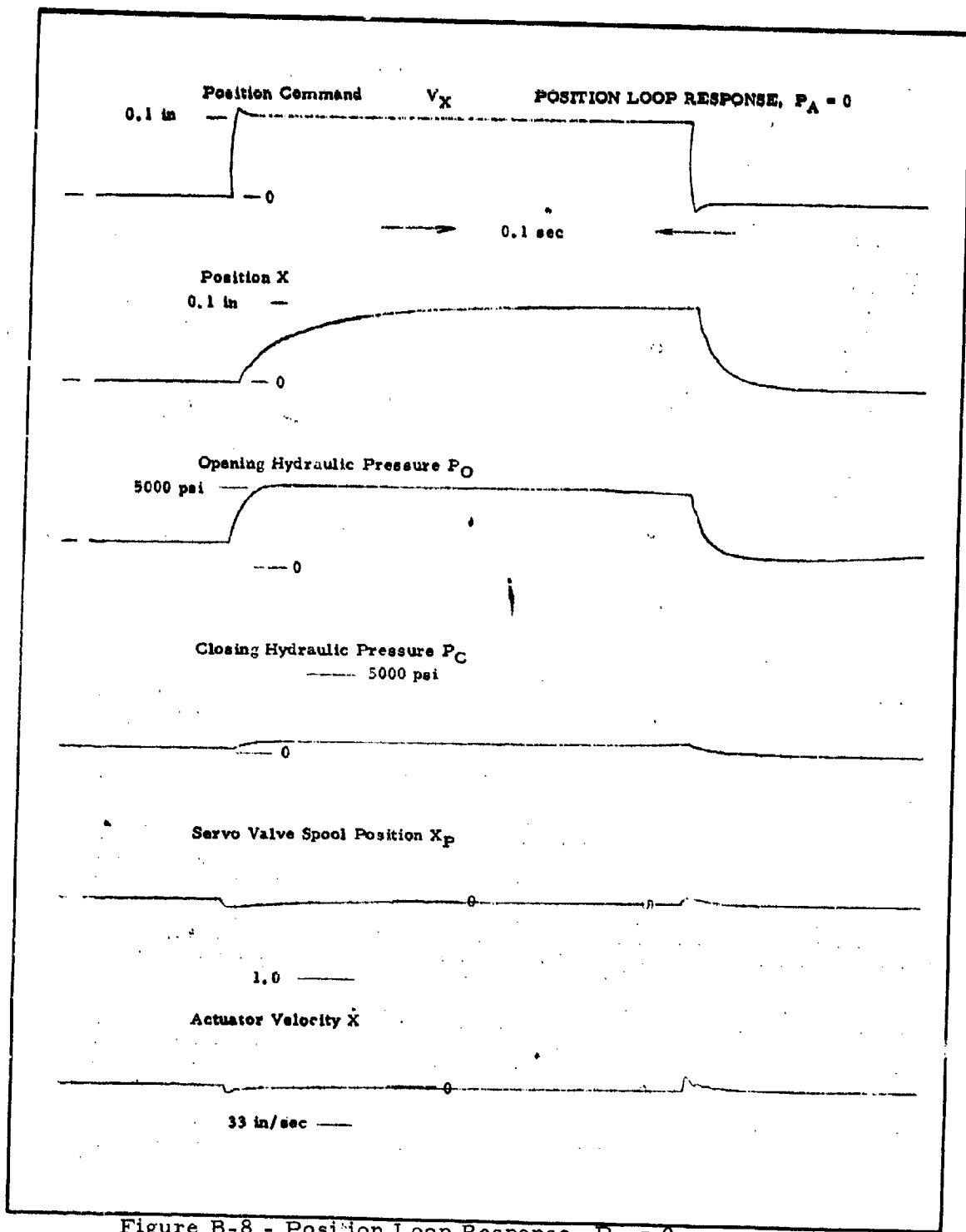


Figure B-8 - Position Loop Response,  $P_A = 0$

**CONFIDENTIAL**

**CONFIDENTIAL**

AFRPL-TR-65-209, Vol I

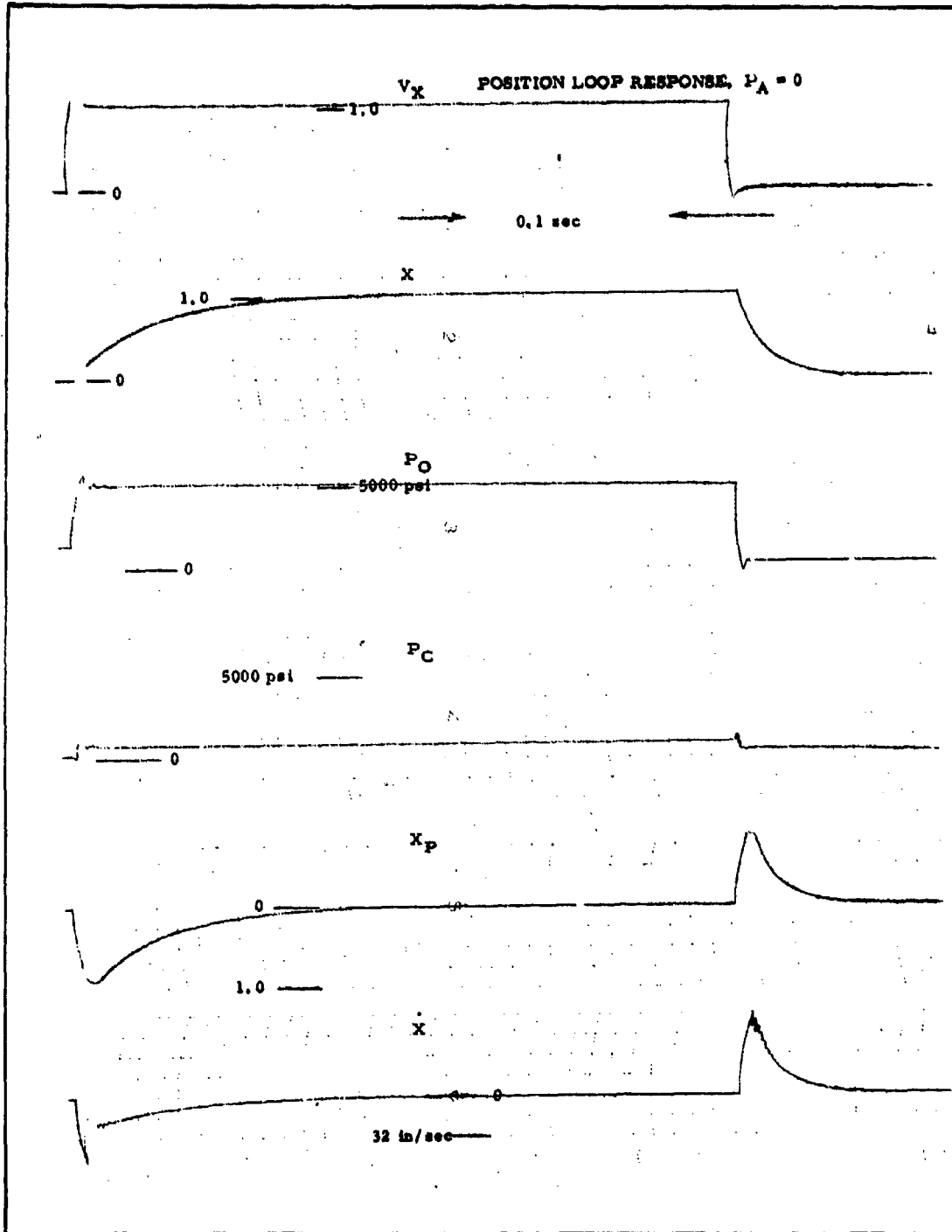


Figure B-9 - Position Loop Response,  $P_A = 0$

**CONFIDENTIAL**

AFRPL-TR-65-209, Vol I

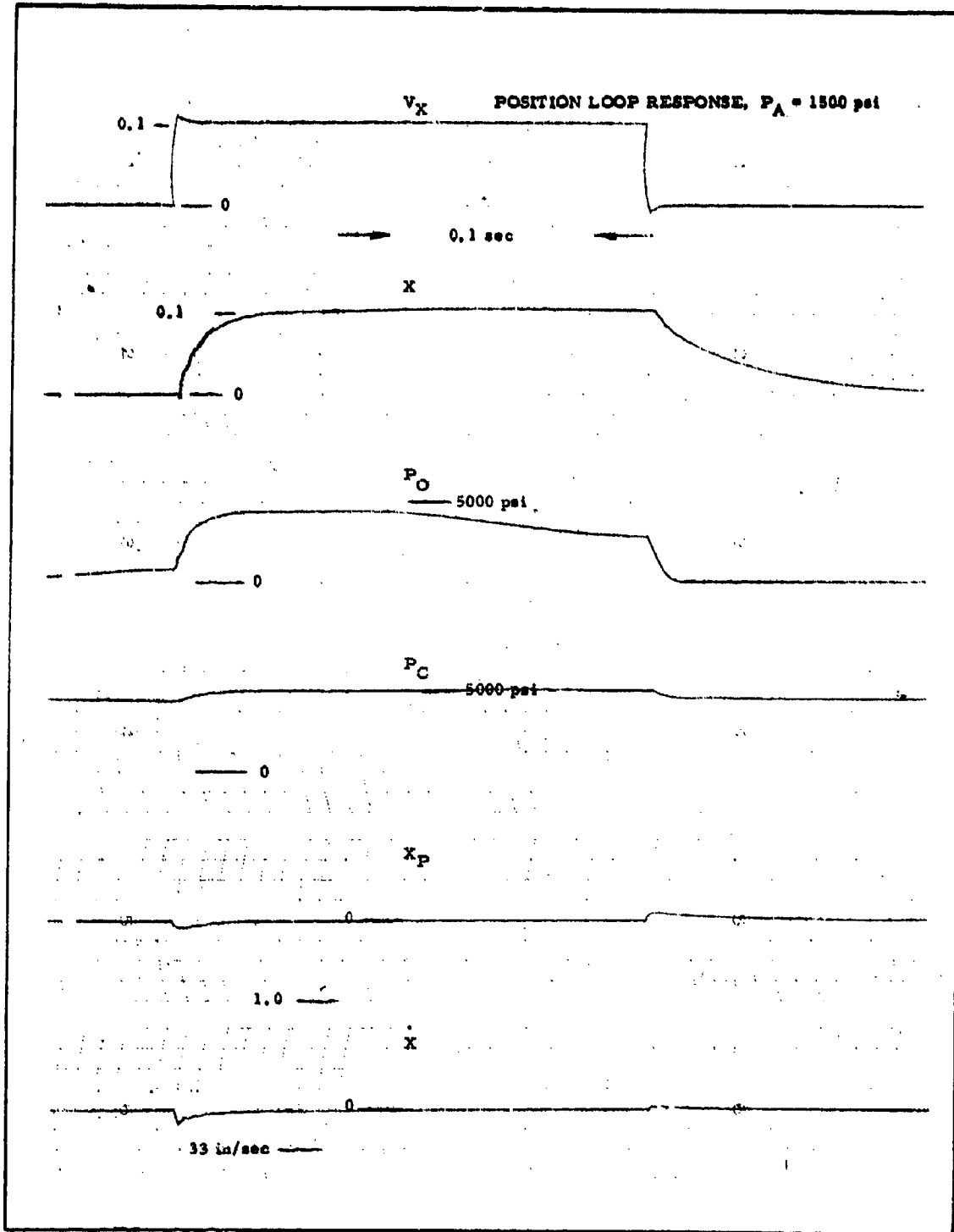


Figure B-10 - Position Loop Response,  $P_A = 1500$  psi

**CONFIDENTIAL**

**CONFIDENTIAL**

AFRPL-TR-65-209, Vol I

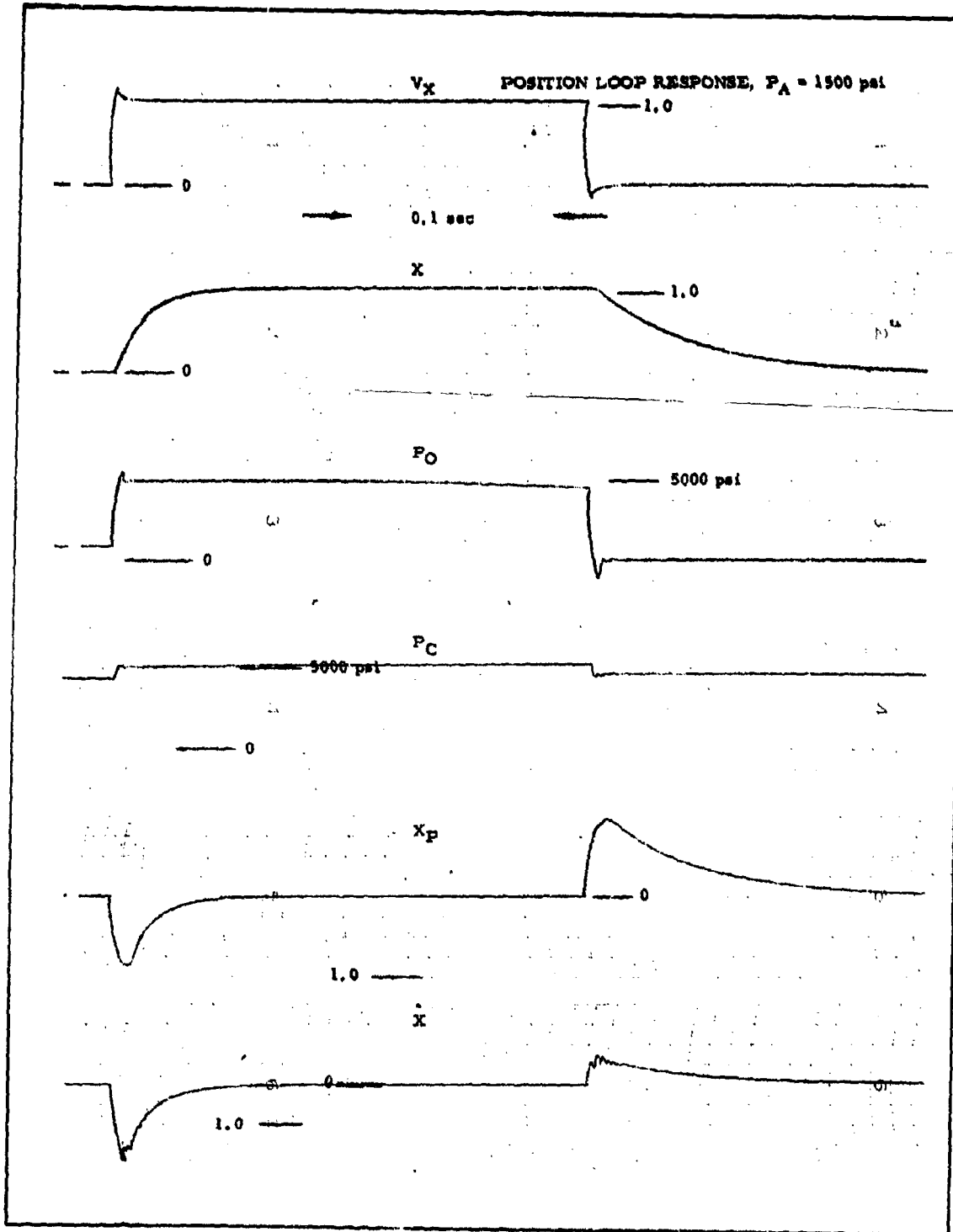


Figure B-11 - Position Loop Response,  $P_A = 1500$  psi

B-26

**CONFIDENTIAL**

It is required that the valve be capable of varying the area in a controlled manner to produce a specified range of pressures. Translated to valve requirements, this demands that a minimum valve area of 0.29 in.<sup>2</sup> and a maximum controlled area of 1.01 in.<sup>2</sup> be available. These limits and the corresponding values of displacement represent the control range of the valve. The valve is designed to produce the minimum area at the closed position of the actuator. This is defined as zero displacement (X = 0). The open end of the control range is determined by specified area and the displacement which produces this area.

The valve must also be capable of providing areas greater than that required for the control range. This is used only for rapid opening to extinguish the process and requires a maximum area of 5.2 in.<sup>2</sup> with the full open displacement of the valve.

(1) Process Simulation

Simulation of the process was based on differential equations for the forward and aft process pressures and a definition of all parameters involved in these equations. The equations are as follows:

$$\frac{dP_F}{dt} = \left( \frac{RT}{MV} \right)_F \left[ (\rho Sa)_F P_F^n - (C_{D,F})_F A P_F \right]$$

$$\frac{dP_A}{dt} = \left( \frac{RT}{MV} \right)_A \left[ (\rho Sa)_A P_A^{n'} + (C_{D,F})_F A P_F - (C_{D,A})_A P_A \right]$$

The first equation establishes the rate of change of the forward process pressure in response to the control valve area (A), the resulting level of forward pressure (P<sub>F</sub>) and the constants for this part of the process. The second equation describes the rate of change of the aft process pressure as a function of the level of this pressure (P<sub>A</sub>), the level of the forward process pressure (P<sub>F</sub>), the control valve area (A) and constants involving both portions of the process.

For the simulation, all parameters except the variables ( $P_F$ ,  $P_A$  and  $A$ ) and the free volume ( $V$ ) of both parts of the process were assumed to be constant. The variation in the free volume is quite large in both portions of the process. This variation has a very significant effect on the dynamic behavior of the process. Values for all of the constants are presented in Table B-II. Using these values, the equations were reduced to the following form:

$$\frac{dP_F}{dt} = K_1 (K_2 P_F^{0.672} - K_3 A P_F)$$

$$\frac{dP_A}{dt} = K_4 (K_5 P_A + K_3 A P_F - K_6 P_A)$$

The calculated values for  $K_1$  through  $K_6$  are presented in Table B-II. Values for  $K_1$  and  $K_4$  were calculated for both the initial and final conditions of the process as effected by the free volume. It should be noted that the equations permit the calculation of the steady-state relation between the control valve area and both process pressures. This is accomplished by setting the rate of change of pressure to zero so that:

$$K_2 P_F^{0.672} = K_3 A P_F$$

$$P_F^{0.328} = \frac{K_2}{K_3 A}$$

$$P_F = \left( \frac{K_2}{K_3} \right)^{3.05} A^{-3.05}$$

and

$$(K_6 - K_5) P_A = K_3 A P_F$$

$$P_A = \frac{K_3}{K_6 - K_5} \frac{K_2^{3.05} A^{-2.05}}{K_3} = \frac{K_2^{0.672}}{K_6 - K_5} P_F$$

# CONFIDENTIAL

AFRPL-TR-65-209, Vol I

TABLE B-II - PROCESS EQUATION CONSTANTS

Forward Process:

R	=	18,510 in/or-mole
T	=	3440°R
$\bar{M}$	=	21/mole
V	=	849 in. <sup>3</sup> , initially
	=	2626 in. <sup>3</sup> , finally
P	=	0.053 lb/in. <sup>3</sup>
S	=	270 in. <sup>2</sup>
a	=	0.0025 in./sec
n	=	0.672
C <sub>D</sub>	=	0.00756
A	=	Valve area - in. <sup>3</sup>

Aft Process:

R	=	18,510 in/or-mole
T	=	5520°R
$\bar{M}$	=	27.7/mole
V	=	865 in. <sup>3</sup> , initially
	=	2305 in. <sup>3</sup> , finally
P	=	0.069 lb/in. <sup>3</sup>
S	=	1000 in. <sup>2</sup>
a	=	0.0004 in./sec
n	=	1.0
C <sub>D</sub>	=	0.0067
A <sub>t</sub>	=	7.0 in. <sup>2</sup>

Constants for Equations:

K <sub>1</sub>	=	3571, initially
	=	1155, finally
K <sub>2</sub>	=	0.0358
K <sub>3</sub>	=	0.00756
K <sub>4</sub>	=	4268, initially
	=	1601, finally
K <sub>5</sub>	=	0.0276
K <sub>6</sub>	=	0.0469

Derivative - K<sub>7</sub>, K<sub>8</sub> and K<sub>9</sub>:

P <sub>max</sub>	=	4500 psi
P <sub>min</sub>	=	100 psi
A	=	$\frac{K_2}{K_3 P} \cdot 328$
A <sub>min</sub>	=	0.29 in. <sup>2</sup>
A <sub>max</sub>	=	1.01 in. <sup>2</sup>

Establishing X as follows:

X	=	0 gives A <sub>min</sub>
X	=	1 gives A <sub>max</sub>
A <sup>-3.05</sup>	=	K <sub>7</sub> - K <sub>8</sub> X
A <sub>min</sub> <sup>-3.05</sup>	=	K <sub>7</sub>
K <sub>7</sub> <sup>-3.05</sup>	=	45
A <sub>max</sub> <sup>-3.05</sup>	=	45 - K <sub>8</sub>
K <sub>8</sub>	=	44
A	=	$\left(\frac{1}{45-44X}\right)^{0.328}$

If K<sub>9</sub> = 0.1

$$A = \left(\frac{0.1}{4.5-1.4X}\right)^{0.328} = \left(\frac{0.475}{4.5-4.4X}\right)^{0.328}$$

as given in the valve specification.

Since  $K_1$  and  $K_4$  are not involved in the steady-state relations, there is no effect on these relations between the initial and final conditions of the simulated process. Only the dynamic behavior is affected by the change in the free volumes.

Proper time scaling of the equations for the computer is obtained as follows:

$$\frac{dP_F}{dT} = \frac{K_1}{10} (K_2 P_F^{0.672} - K_3 A P_F)$$

$$\frac{dP_A}{dT} = \frac{K_4}{10} [(K_5 - K_6) P_A + K_3 A P_F]$$

A block diagram for the process equations is presented in Figure B-12(a). The computer circuit for this portion of the simulation is shown in Figure B-12(b). The function  $P_F^{0.67}$  was simulated with a diode function generator. An X-Y recording of the simulated function is shown in Figure B-13.

(2) Control Valve Simulation

The ideal requirement for the control valve is that its area variation as a function of displacement be such that the steady-state variation of forward process pressure with displacement be linear over the control range. As shown previously,

$$P_F = \left( \frac{K_2}{K_3} \right)^{3.05} A^{-3.05}$$

To produce the desired result,

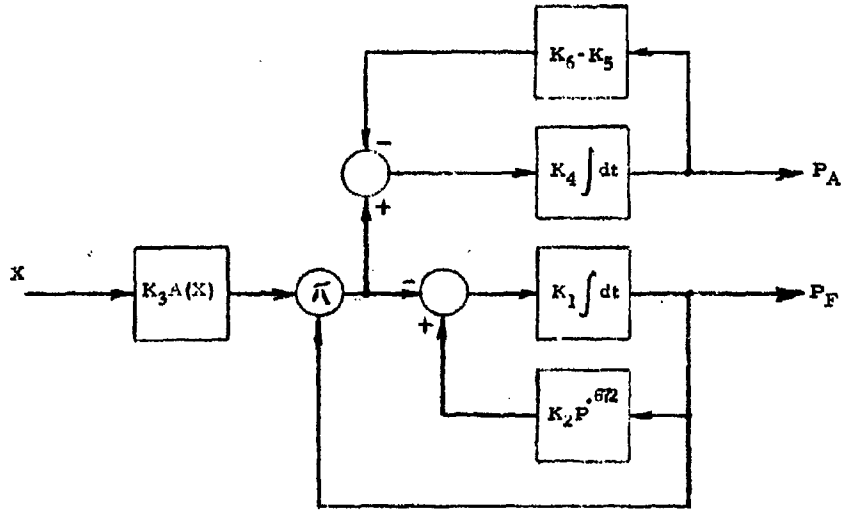
$$A^{-3.05} = K_7 - K_8 X$$

This requires that the valve characteristic be

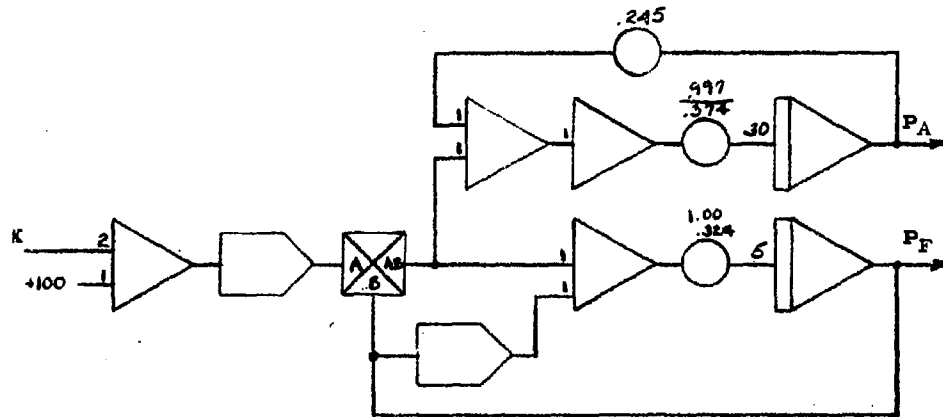
$$A = (K_7 - K_8 X)^{-0.328} = \frac{1}{(K_7 - K_8 X)^{0.328}}$$

# CONFIDENTIAL

AFRPL-TR-65-209, Vol I



(a) Process Block Diagram



(b) Process Computer Diagram

Figure B-12 - Process Block Diagram and Computer Diagram

B-31

# CONFIDENTIAL

**CONFIDENTIAL**

AFRPL-TR-65-209, Vol I

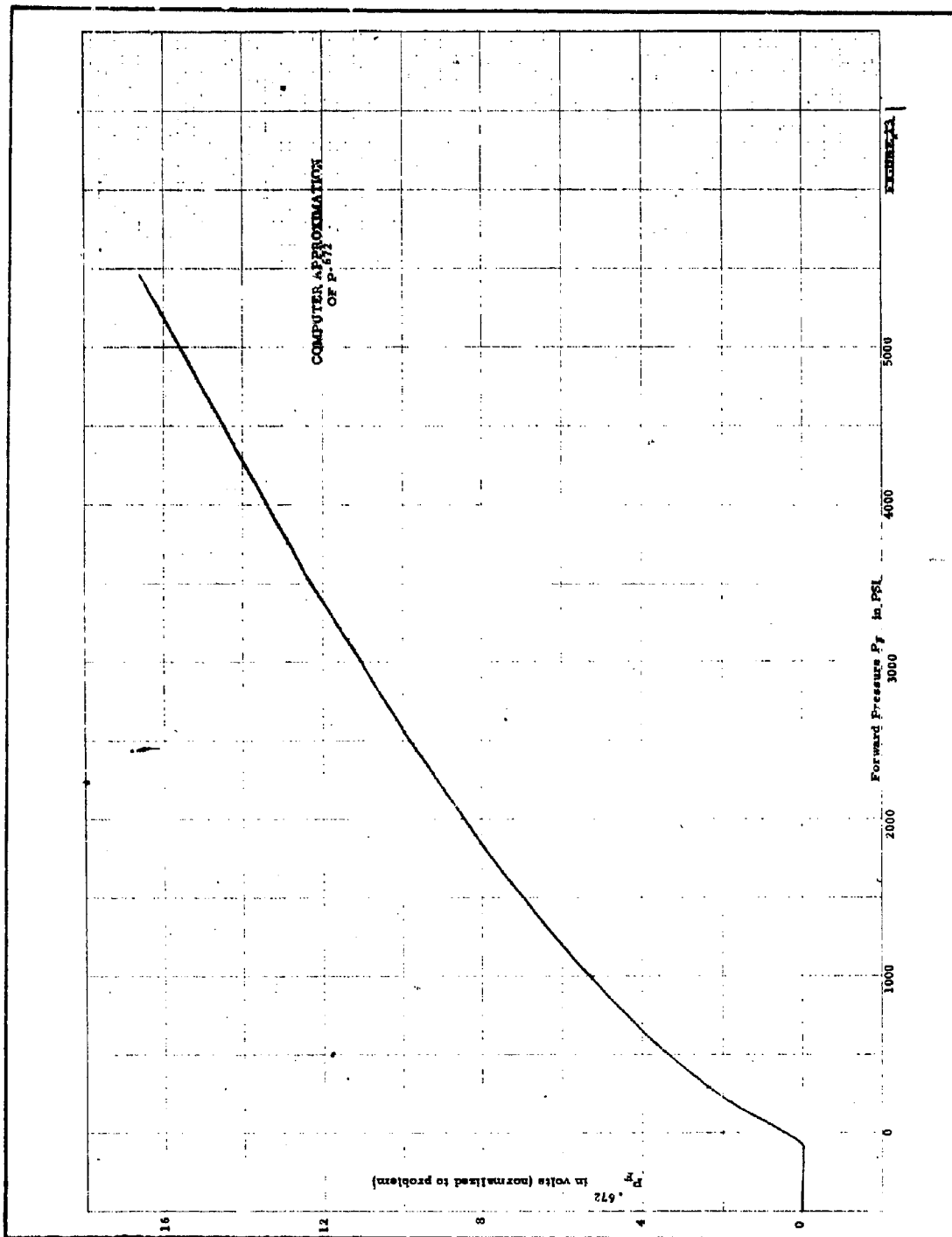


Figure B-13 - Computer Approximation of  $P^{672}$

B-32

**CONFIDENTIAL**

Derivation of the constants  $K_7$  and  $K_8$  is included in Table B-II. As shown there, the ideal relation between A and X can also be expressed in the form:

$$A = \frac{K_9^{0.328}}{(K_7 K_9 - K_8 K_9 X)^{0.328}}$$

The need for a linear relationship between forward process pressure and valve displacement arises from the control requirements. If this relationship can be realized, valve and process will have a constant gain for any level of pressure within the desired control range. This greatly simplifies the control design.

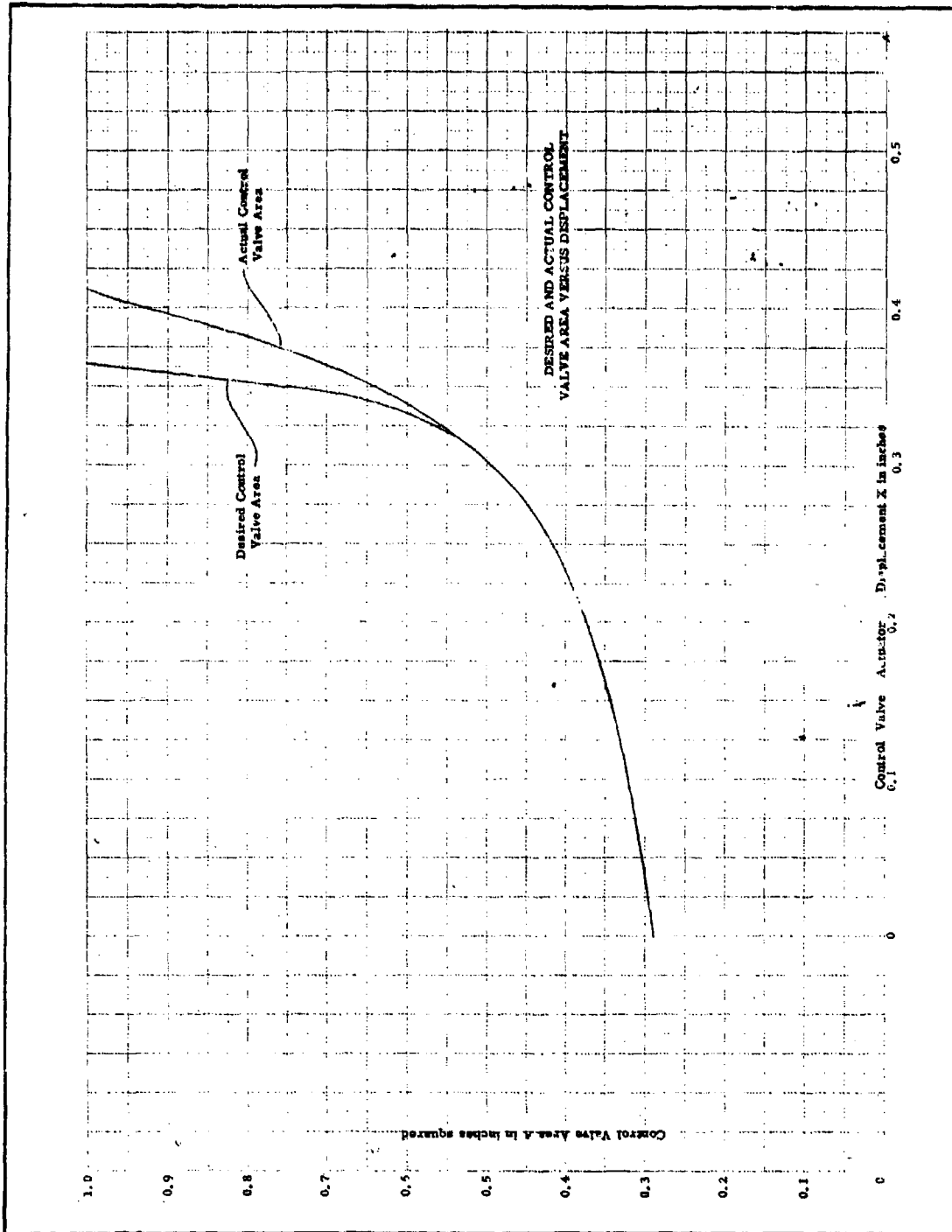
In the actual design of the valve, it was found necessary to deviate from the ideal relationship. From the desired relationship between valve displacement and area, a rate of change of area with respect to displacement can be established. The required physical dimensions of the valve preclude realization of the required rate of change. This aspect is covered in greater detail in paragraph 6, below.

The actual variation of control valve area with displacement, predicted from the valve design, is presented in Figure B-14. A curve corresponding to the ideal relation is included for comparison. The actual relationship was simulated on the computer using a diode function generator, as shown in Figure B-12(b). Data was obtained on the simulated valve by slowly varying X and recording area versus displacement on an X-Y recorder. The resultant curve is shown in Figure B-15.

From the characteristic for the valve, the control range can be determined. A displacement of 0.412 in. produces the maximum required control area of 1.01 in.<sup>2</sup> The simulation of the valve was extended beyond this point to cover any overshoot of the valve beyond the normal control range.

**CONFIDENTIAL**

AFRPL-TR-65-209, Vol I



B-34

Figure B-14 - Desired and Actual Control Valve Area Versus Displacement

**CONFIDENTIAL**

**CONFIDENTIAL**

AFRPL-TR-65-209, Vol I

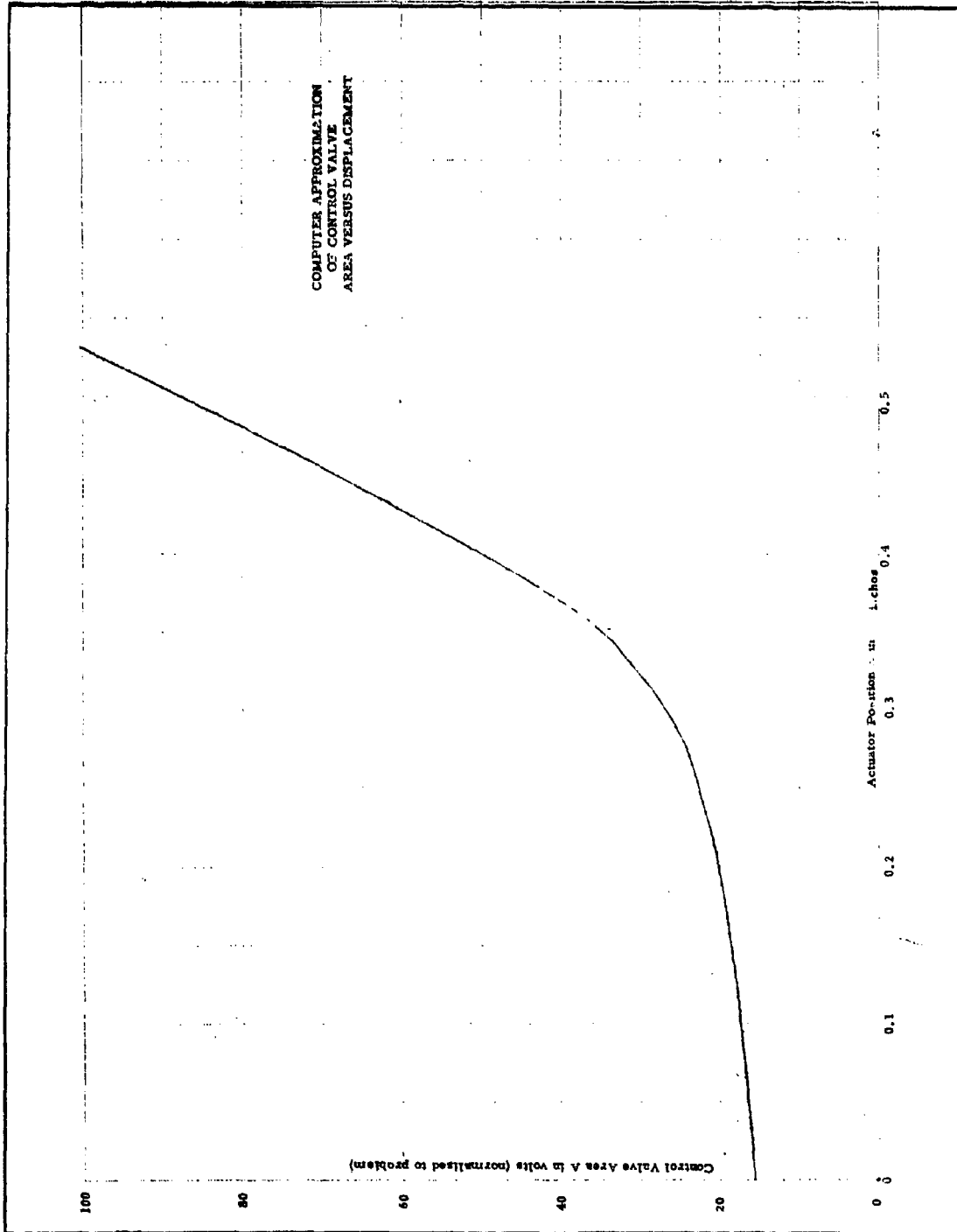


Figure B-15 - Computer Approximation of Control Valve Area Versus Displacement

**CONFIDENTIAL**

**(3) Steady-State and Transient Behavior of Valve and Process**

Steady state and transient responses were obtained for the combined valve and process simulation. Figure B-16 presents the steady-state variation of forward process pressure with displacement. This data was obtained by slowly varying displacement and recording the parameters on an X-Y recorder. Examination of this data indicates that this relationship is very nearly linear over the control range despite the deviation in the valve characteristics from an ideal relation. Some small bumps are also evident in this characteristic. These arise from deviations in the simulated valve characteristic at the break points of the diode function generator. The process is extremely sensitive to these deviations and considerable effort was expended in minimizing this effect.

Note that the maximum steady-state pressure occurring when  $X = 0$  in Figure B-16 is slightly above 5000 psi. This chart appears to conflict with the desired maximum pressure of 4500 psi. This discrepancy can be explained as follows. The process equation coefficient  $S$  was assumed constant for this analysis. However,  $S$  actually can vary over some small range. This variation does not affect the dynamic characteristic of the process but does change the steady-state solution. The minimum area  $0.29 \text{ in.}^2$  was selected to allow 4500 psi when  $S$  is minimum. The average value of  $S$  was used in this simulation, and the corresponding maximum pressure is 4975 psi. In addition, the actual minimum area of the control valve is  $0.289 \text{ in.}^2$ . The maximum steady-state pressure, therefore, is slightly above 5000 psi for the simulation.

Transient response data was taken by inserting various size step changes in displacement and recording the parameters of the process for both the initial and final free volumes. Response data with the initial free volume is shown in Figure B-17. Here the displacement steps correspond to pressure changes from 100 to 5000 to 100 psi. Response data with the final free volume are shown in Figures B-18 through B-21 for displacement steps which correspond to steady-state forward pressure changes from 100 to 5000

**CONFIDENTIAL**

AFRPL-TR-65-209, Vol I

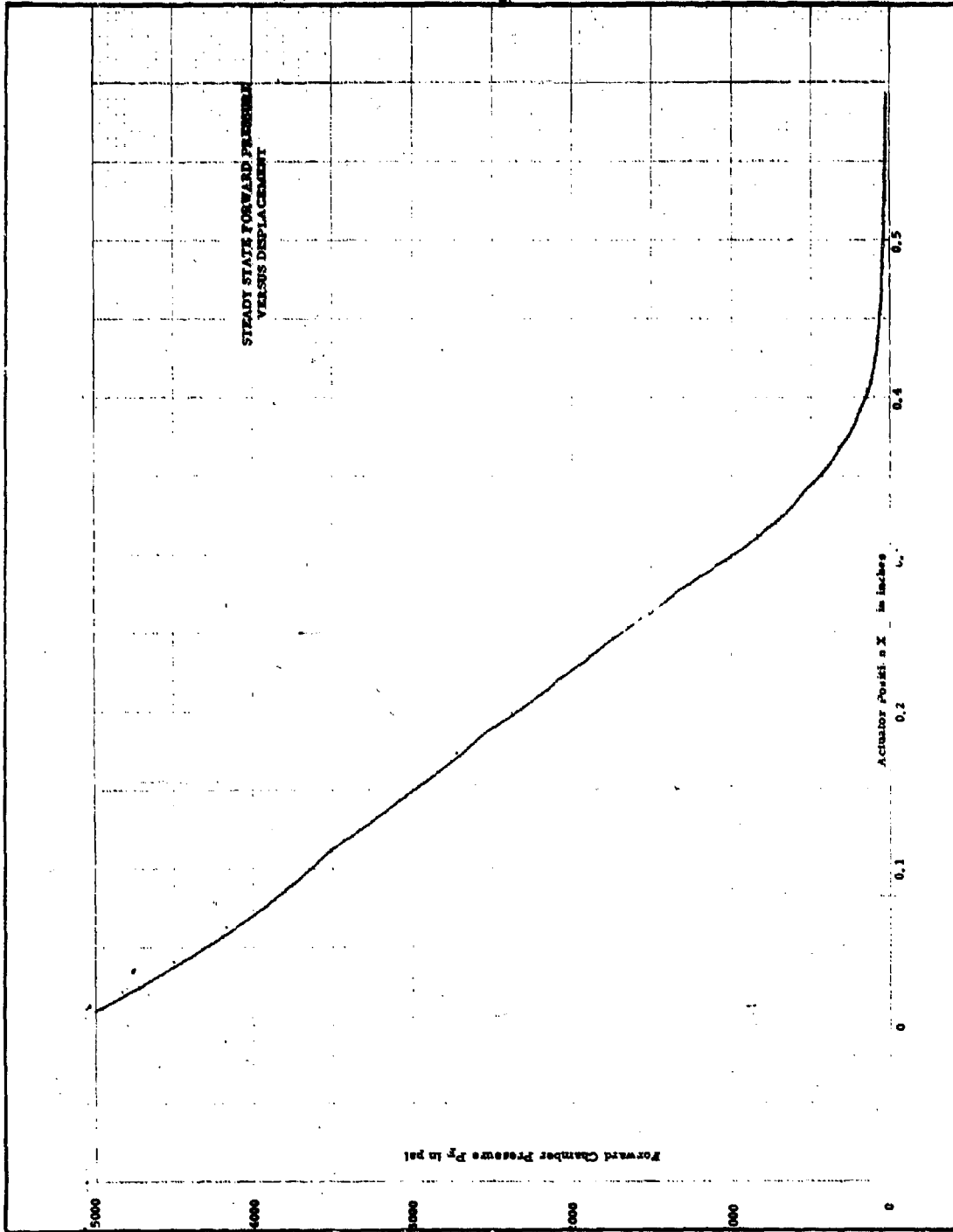


Figure B-16 - Steady-State Forward Pressure Displacement

**CONFIDENTIAL**

B-37

# CONFIDENTIAL

AFRPL-TR-65-209, Vol I

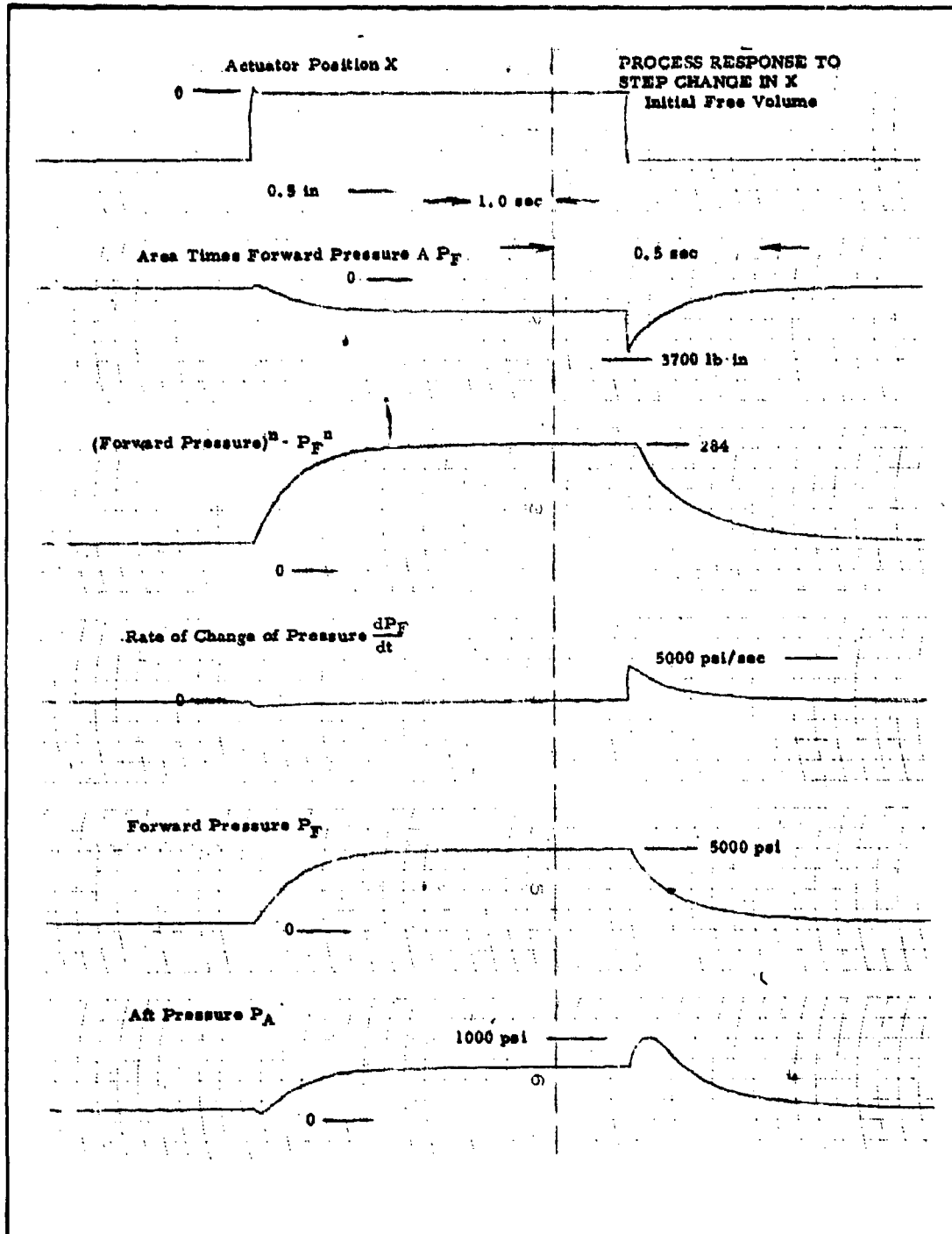


Figure B-17 - Process Response to Step Change in Displacement Initial Free Volume

**CONFIDENTIAL**

AFRPL-TR-65-209, Vol I

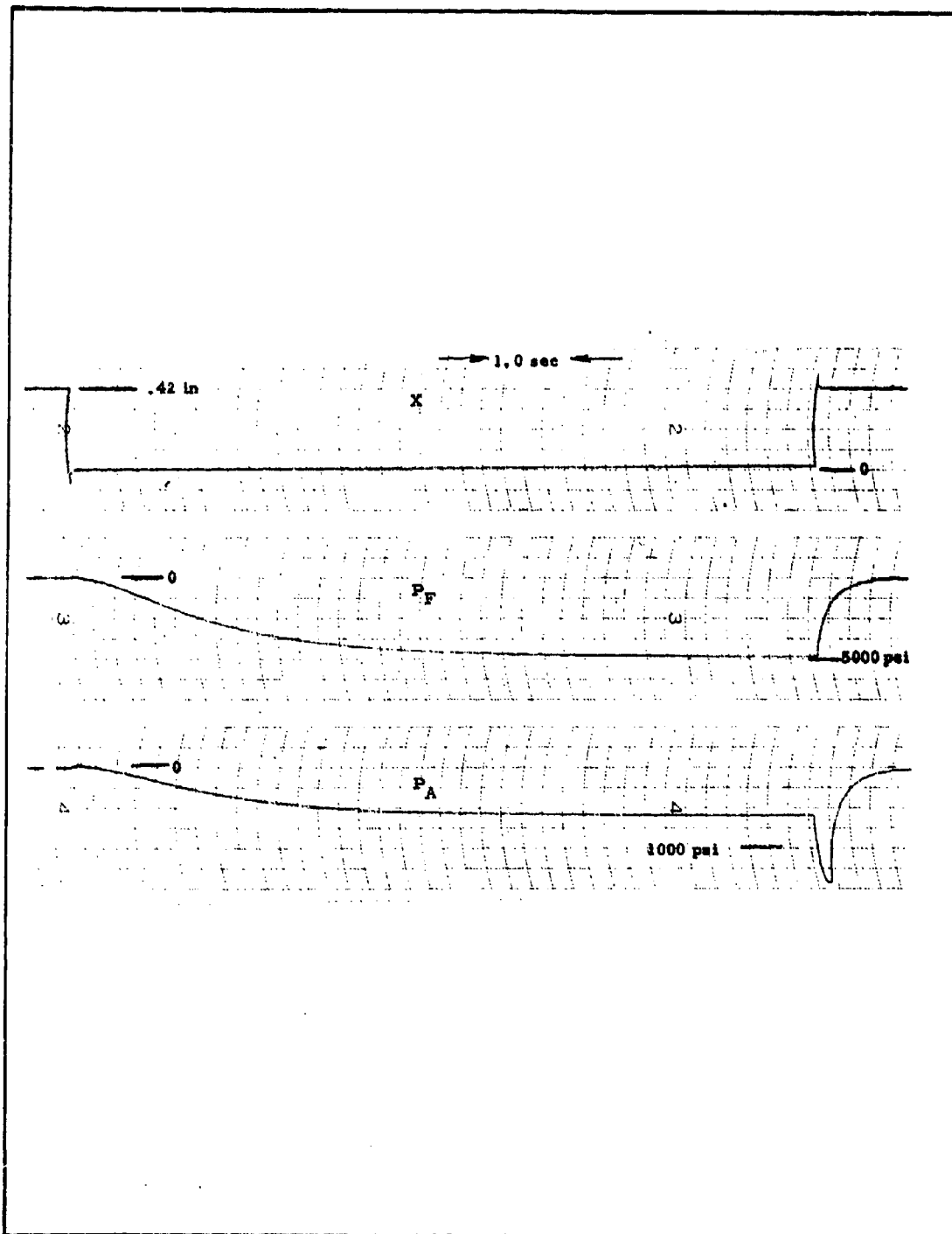


Figure B-18 - Process Response to Step Change in Displacement  
Final Free Volume

B-39

**CONFIDENTIAL**

**CONFIDENTIAL**

AFRPL-TR-65-209, Vol I

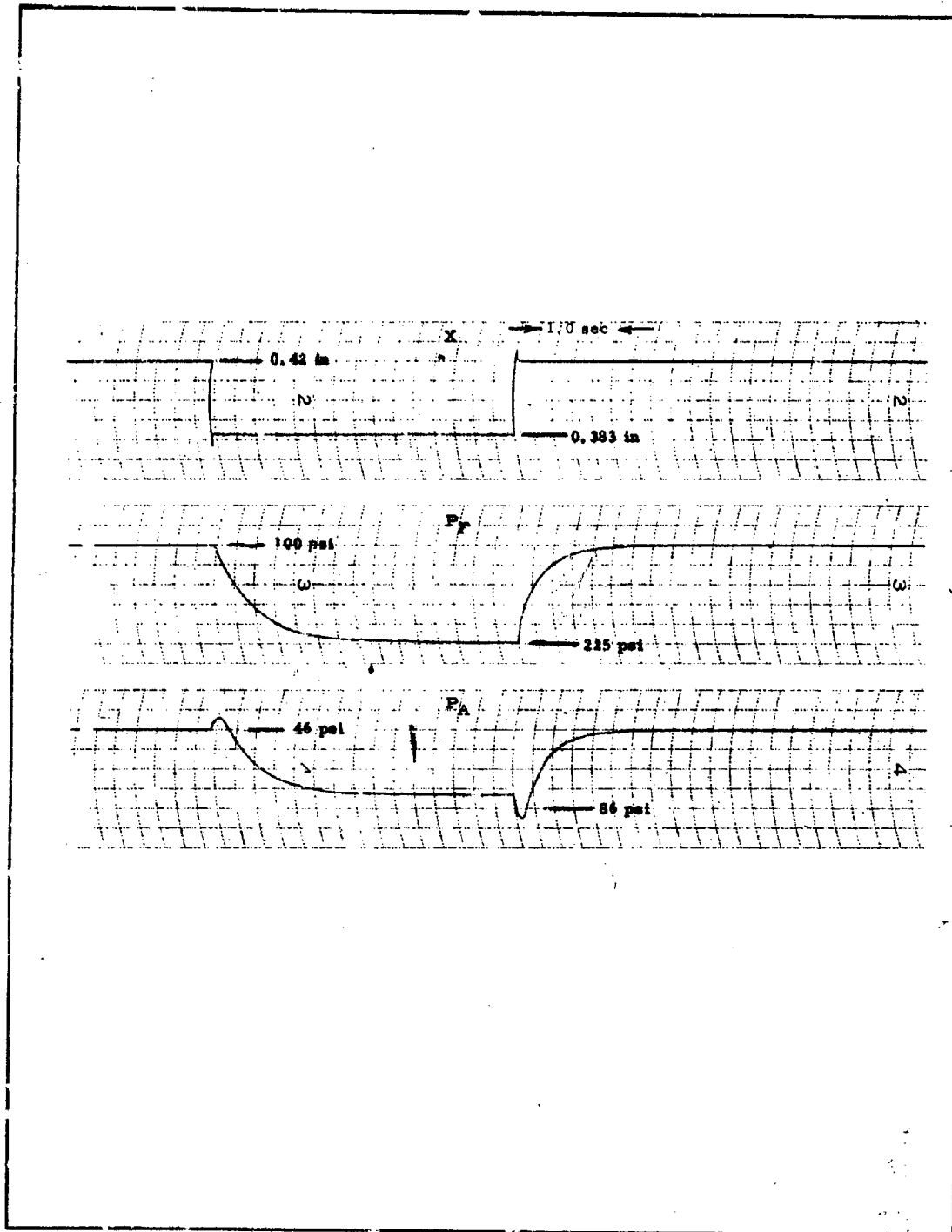


Figure B-19 - Process Response to Step Change in Displacement,  
Final Free Volume

B-40

**CONFIDENTIAL**

**CONFIDENTIAL**

AFRPL-TR-65-209, Vol I

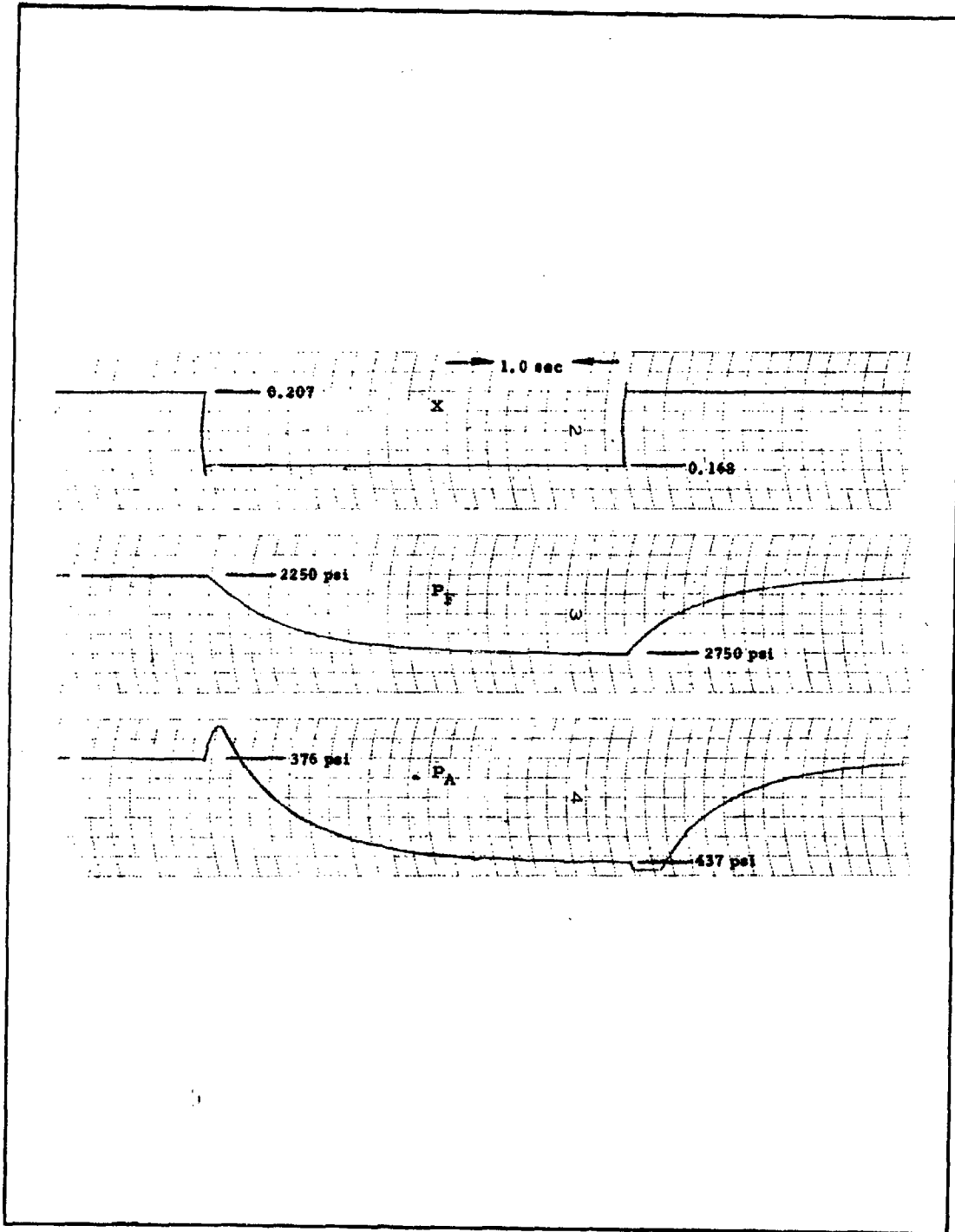


Figure B-20 - Process Response to Step Change in Displacement,  
Final Free Volume

B-41

**CONFIDENTIAL**

**CONFIDENTIAL**

AFRPL-TR-65-209, Vol I

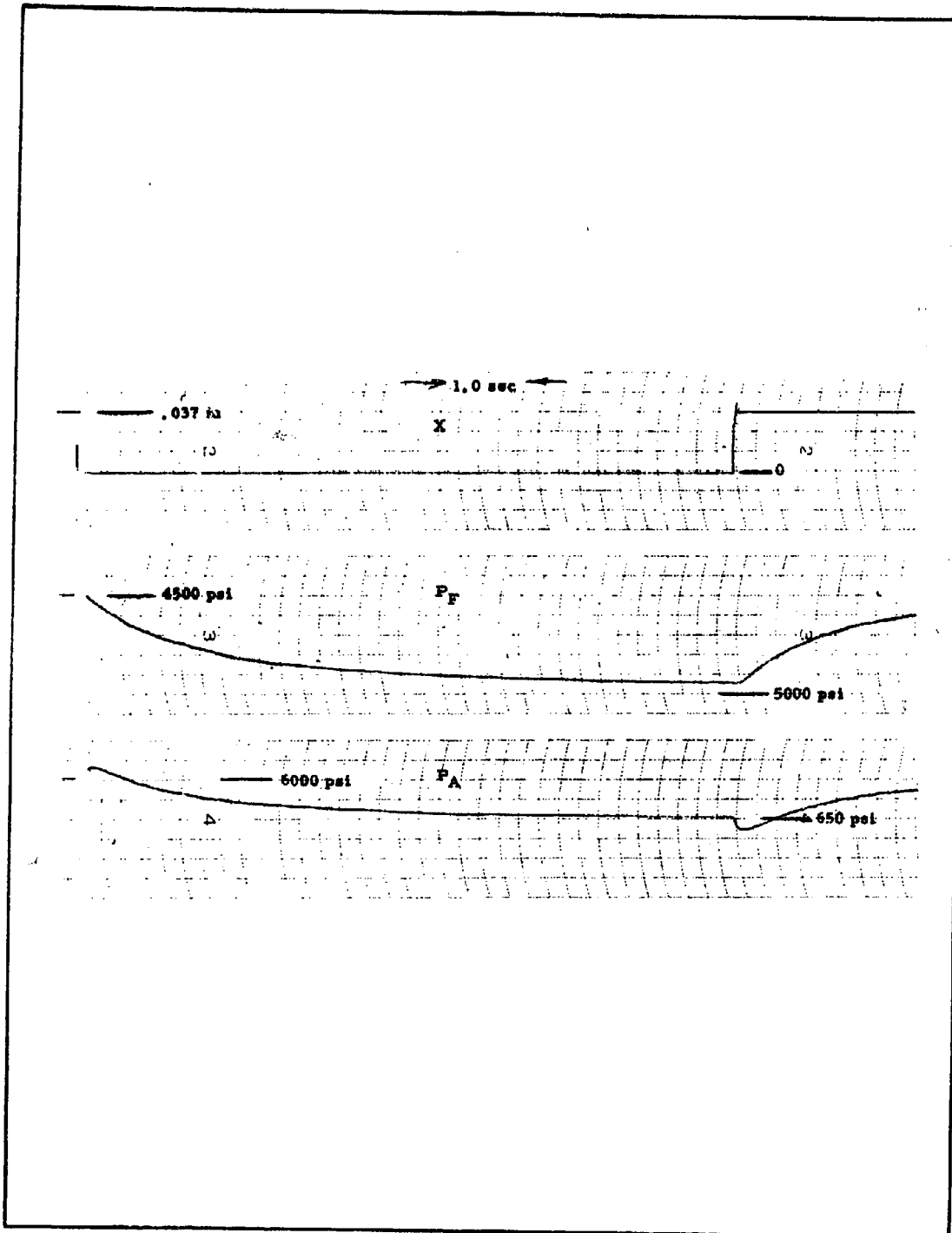


Figure B-21 - Process Response to Step Change in Displacement,  
Final Free Volume

to 100 psi, from 100 to 225 to 100 psi, from 2250 to 2750 to 2250 psi, and from 4500 to 5000 to 4500 psi. The data of Figures B-17 and B-18 indicate that the process responds fastest when both the pressure and area are high and are the slowest when both are low. Also, comparison of Figures B-19 and B-21 shows that the large area and low pressure condition is faster than that of the small area and high pressure. The most important observation from this data is that the process with the final free volume is approximately three times slower than with the initial free volume. Several other size step changes have been recorded to insure that this observation is general, though the data is not included herein.

The aft process pressure displays an interesting response to a displacement step, as seen in Figures B-17 through B-21. The steady-state flow of material through the control valve increases with decreasing area. However, if the area is changed quickly, the forward process pressure does not respond immediately, as shown above. The result is that the initial material flow through the control valve increases with increasing area, thus causing the aft process pressure to change initially in the opposite direction from that expected from the steady-state operation. The maximum aft process pressure occurs during such a transient. Figure B-17 shows a maximum aft pressure of slightly over 1000 psi. With the final free volume as in Figure B-18, this maximum pressure approaches 1500 psi. The steady state maximum aft pressure theoretically is 572 psi.

c. Frequency Response of Simulated System

The preceding sections have presented the simulation of the position loop and the process plus some results on the response of these portions of the simulated system. When these elements are operated together, some change in characteristics can be expected. The aft process pressure produces a force which acts on the actuator and affects the position loop. Both transient and frequency response data were obtained for the position loop and for the process.

The transient responses have been presented for these portions of the simulated system. Additional frequency response data was obtained on the overall system. This can be compared to results for the individual elements.

Frequency response information was obtained by injecting a sinusoidal disturbance of a small amplitude into the simulated system and recording all parameters of interest. Data was obtained for a wide range of disturbance frequencies. The data was reduced by measuring the gain and phase shift between the input and output signals at each frequency. These results were plotted as a function of frequency. In the proper form, this result identifies the dynamic behavior of the system. A typical recording is presented in paragraph 7, below, along with the reduction of the data to a useful form. As noted previously, the basic computer data must be adjusted to relate it to the physical system. This conversion is also covered in paragraph 7.

The frequency response plot for the position loop is presented in Figure B-22. Analysis of this plot indicates that the position loop behaves in the region of interest as a highly damped second-order system with a natural frequency around 15 cps. The deviation from the ideal second-order response at higher frequencies is the result of non-sinusoidal waveforms occurring in the displacement for sine wave position command signals. In this case, gain and phase shift measurements become inaccurate.

The valve and the forward process pressure frequency response data is shown in Figure B-23 with the initial free volume and in Figure B-24 with the final free volume. The valve and the forward process respond like a single-order system with a nearly constant gain and a variable time constant. This type of performance is as predicted in b, above. The gain varies as the slope of the curve in Figure B-16. The time constant is a function of the operating pressure and of the free volume. The variation of the free volume has the greater effect on the time constant.

The frequency response plot of the combined position loop and process is displayed in Figure B-25. In this case only one operating pressure was used. If neither the position loop nor the process changes when the two are put together, the combined frequency response curves should be the sum

**CONFIDENTIAL**

AFRPL-TR-65-209, Vol I

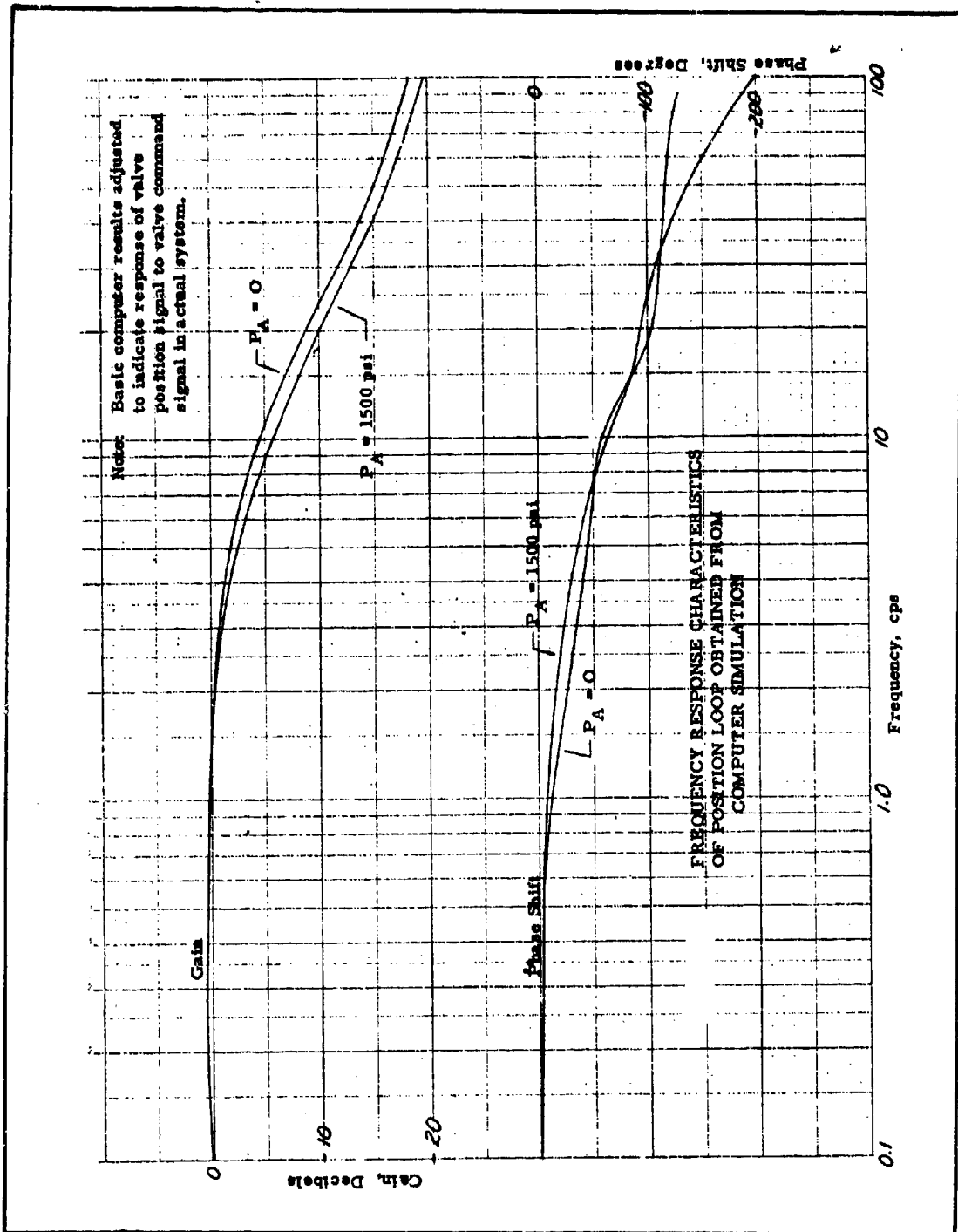


Figure B-22 - Frequency Response Characteristics of Position Loop Obtained from Computer Simulation

**CONFIDENTIAL**

# CONFIDENTIAL

AFRPL-TR-65-209, Vol I

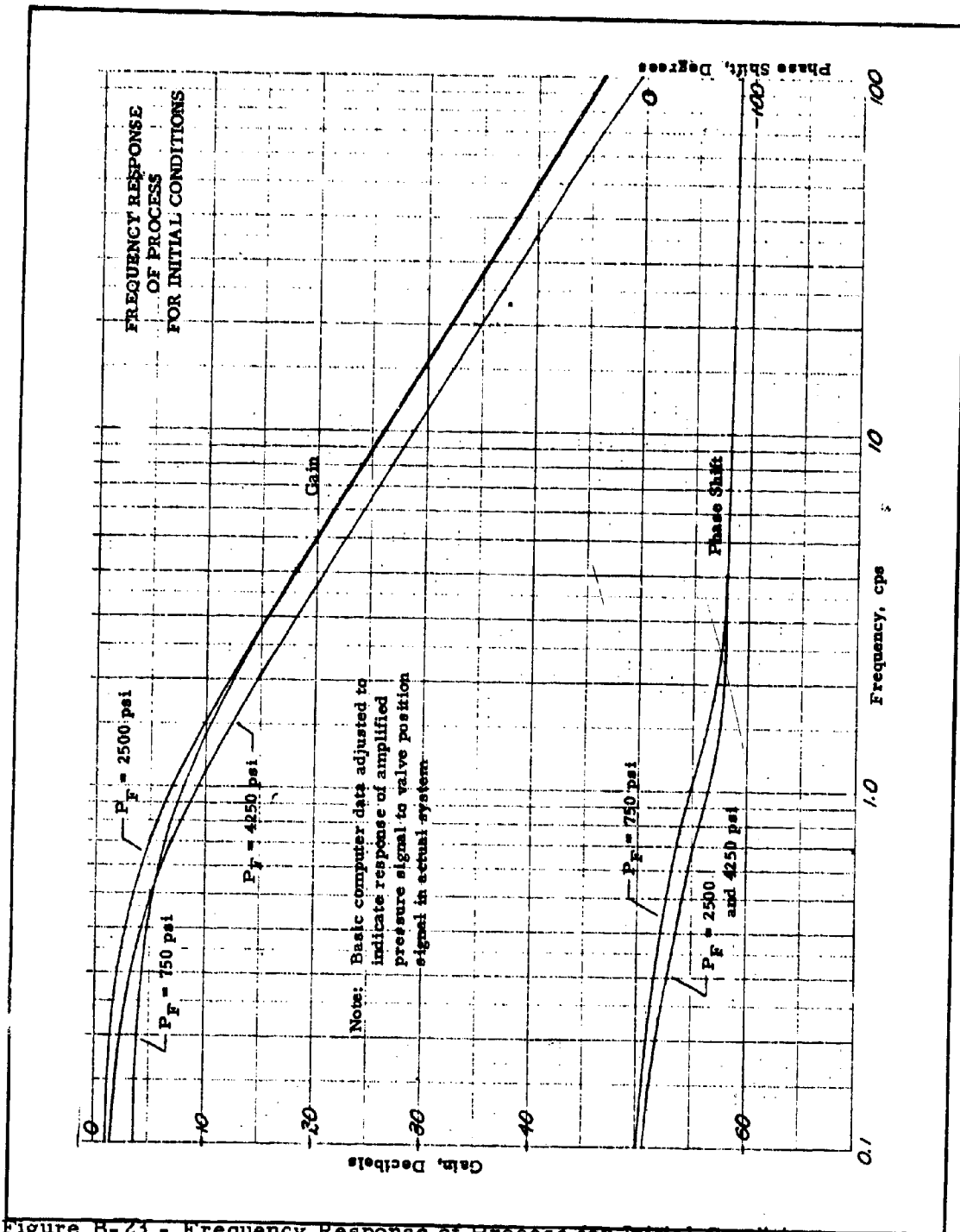


Figure B-23 - Frequency Response of Process for Initial Conditions

B-46

# CONFIDENTIAL

**CONFIDENTIAL**

AFRPL-TR-65-209, Vol I

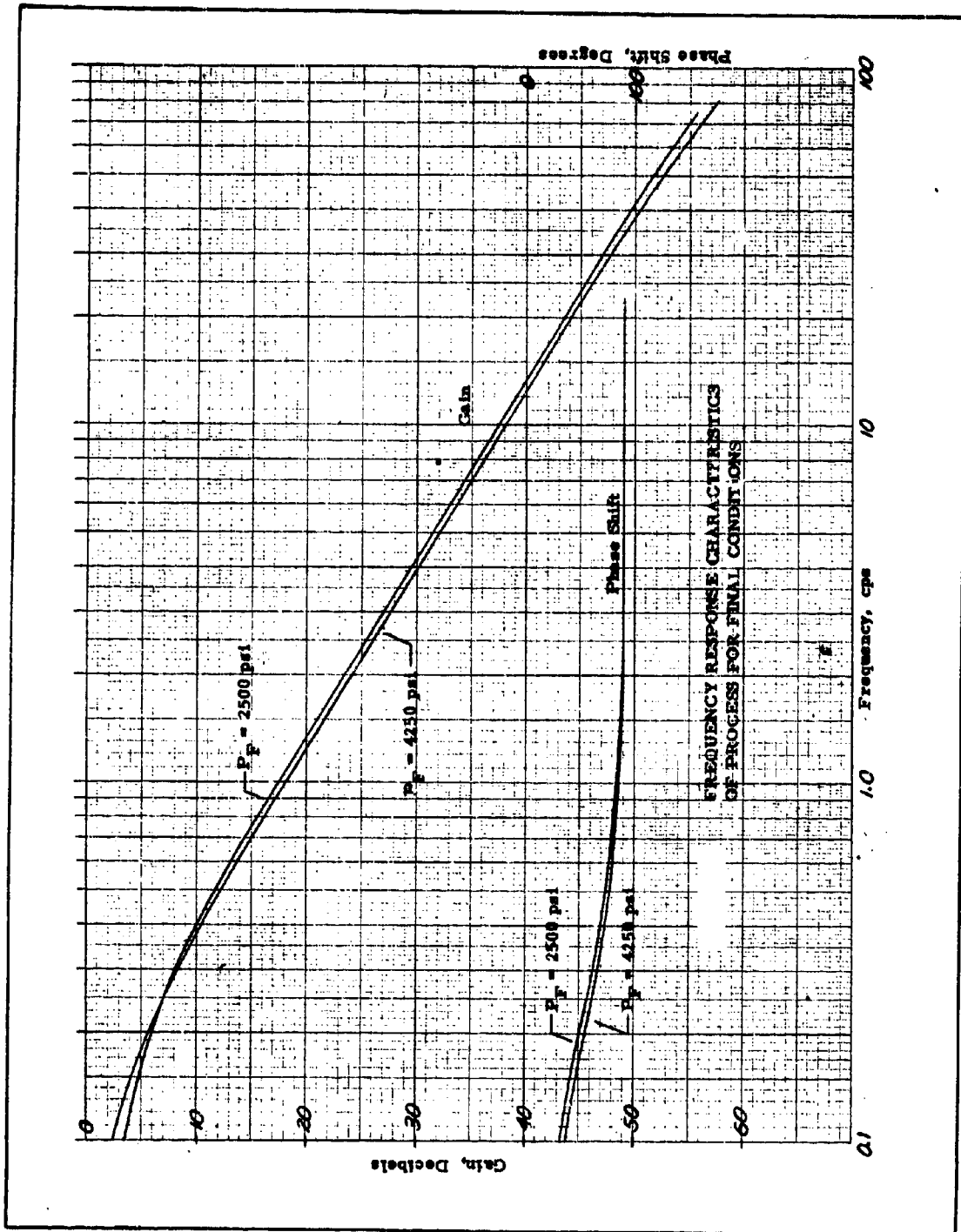


Figure B-24 - Frequency Response Characteristics of Process for Final Conditions

B-47

**CONFIDENTIAL**

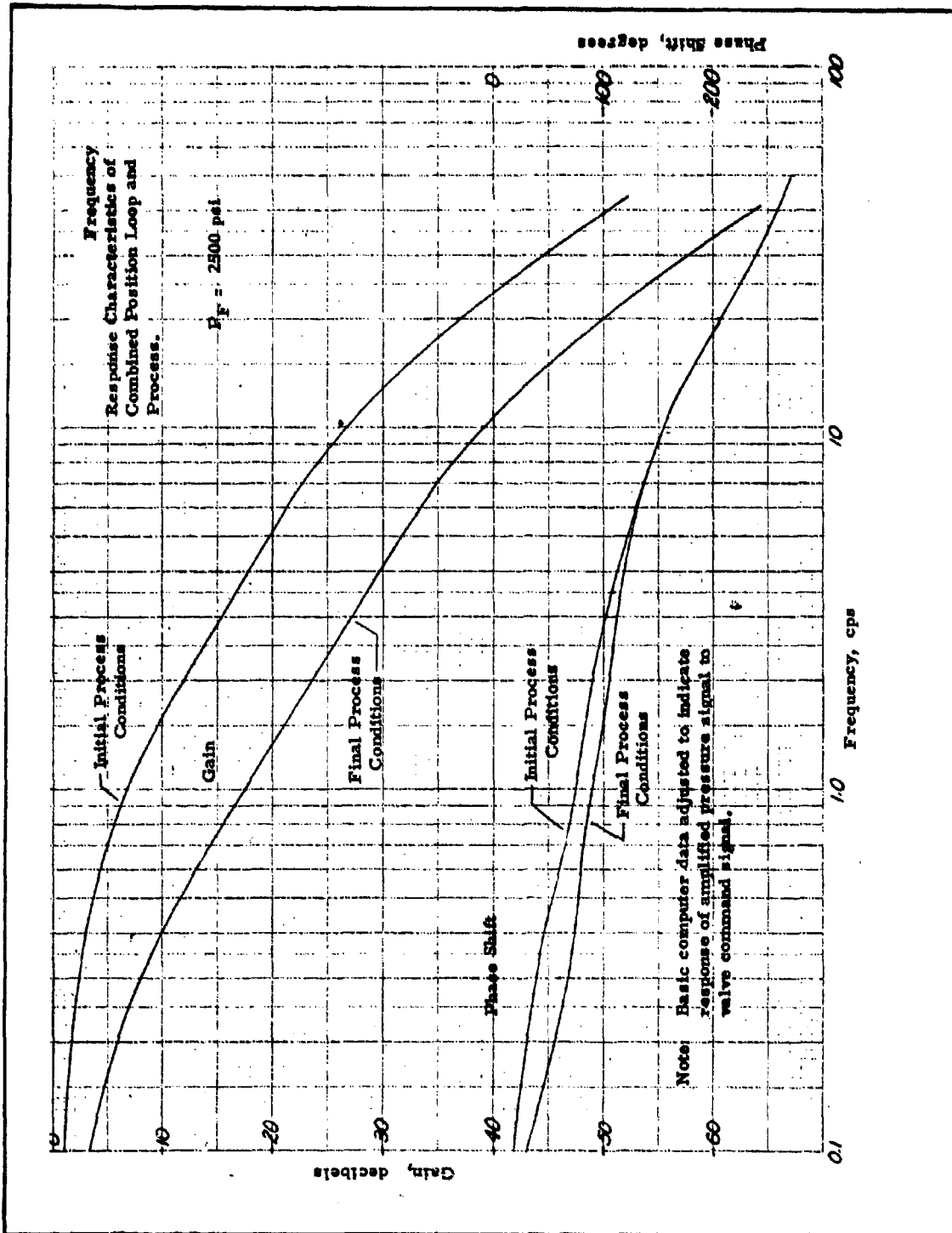


Figure B-25 - Frequency Response Characteristics of Combined Position Loop and Process

of the individual curves. By noting that the position loop is quite flat up to 5 cps, the combined gain plot should conform to the process plot up to 5 cps. General agreement is seen in Figure B-25, except at the higher frequencies. The aft process pressure acting on the end of the actuator does change the position loop frequency response slightly. Figure B-26 shows the position loop frequency response when coupled to the process. This set of curves is the difference between the corresponding plots of the position loop and process and the process alone. In this case the position loop acts as a second-order system with a natural frequency of 14 cps and with a lower damping ratio than when the position loop operates alone.

d. Control Design

The selection of a control configuration for the system composed of the position loop, the control valve, and the chemical process demands that some criteria be selected for the control performance. In general, the performance requirements are that the controlled system be capable of producing large and rapid ramp changes in forward system pressure. Most desirably, this should be accomplished with little overshoot in the pressure at the end of the programmed changes. Of primary importance, the controlled system must be stable throughout its complete range of operation.

Much of the work on control system synthesis has been based on the minimization of the integral of the error squared. The use of the theory developed for this criterion can form a worthwhile starting point in control system design. Modifications to the selected control for the specific requirements of a system are then accomplished by optimization studies of the system. With a computer simulation available for the controlled system, this is readily accomplished.

For the type of process involved, studies and tests<sup>1</sup> have shown that an optimum control configuration includes a

---

<sup>1</sup> Boksenbom, Aaron S.; Novik, David; and Heppler, Herbert: Optimum Controllers for Linear Closed-Loop Systems. NACA TN 2039, 1953.

**CONFIDENTIAL**

AFRPL-TR-65-209, Vol I

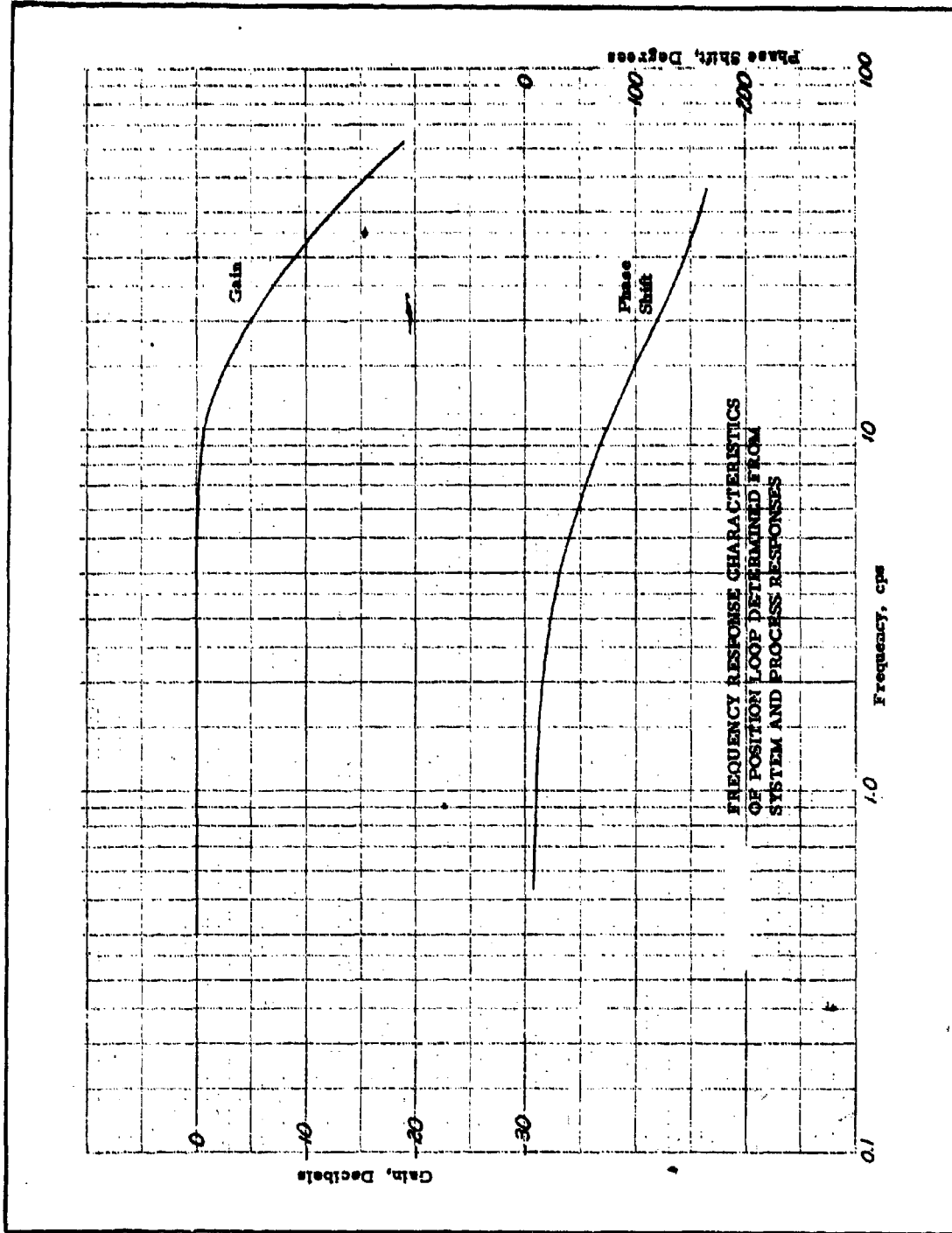


Figure B-26 - Frequency Response Characteristics of Position Loop Determined from System and Process Response

B-50

**CONFIDENTIAL**

proportional plus integral transfer function as the primary control element. For optimum performance, the integral time constant should be selected equal to the principal time constant in the process to be controlled. Where additional dynamics are present beyond the main time constant, a lead network can compensate for these effects and will generally provide improved performance. With the primary transfer function and the lead network selected in this fashion, the gain is established to provide the fastest response consistent with stability and a reasonable amount of overshoot.

A brief explanation of the factors involved in the selection of the process control may aid in understanding the principles involved. As noted previously, the process acts as a simple first-order lag and is the dominant factor in the dynamic behavior of the system. The process can be described by the following transfer function:

$$\frac{V_P}{V_F}(s) = \frac{K_P}{1 + \tau_P s}$$

The transfer function of a proportional plus integral control is as follows:

$$\frac{V_X}{V_E}(s) = K_C \left( 1 + \frac{1}{\tau_C s} \right) = K_C \left( \frac{1 + \tau_C s}{\tau_C s} \right)$$

Neglecting the dynamics of the position loop for the moment, the combination of the process control and the process is expressed as

$$\frac{K_C K_P}{\tau_C s} \times \left( \frac{1 + \tau_C s}{1 + \tau_P s} \right)$$

If the process and integral time constants are set equal ( $\tau_C = \tau_P$ ), the expression simplifies to

$$\frac{K_C K_P}{\tau_C s}$$

The result is a simple integration term. If this type of behavior can be established and maintained for the complete open loop of the controlled system, the dynamic behavior of the closed-loop system is most readily optimized.

Frequency response information for a proportional plus integral control is presented in normalized form in Figure B-27. Examination of this figure reveals that below the break frequency ( $W = \frac{1}{\tau_C}$ ) the control approaches the behavior of an integrator with a gain slope of -20 decibels per decade and a phase shift of  $-90^\circ$ . Above the break frequency, the control acts as pure gain.

The position loop acts as a well-damped second-order system as noted in c, above. Inclusion of this term yields a complete open-loop transfer function of the form

$$\frac{V_P}{V_E} = K_C \left( 1 + \frac{1}{\tau_C s} \right) \frac{K_P}{1 + \tau_P s} \frac{K_L}{\frac{s^2}{W_n^2} + \frac{2\zeta}{W_n} s + 1}$$

With the ideal condition of  $\tau_C = \tau_P$  this reduces to

$$\frac{V_P}{V_E}(s) = \frac{K_C K_P}{\tau_C s} \frac{K_L}{\frac{s^2}{W_n^2} + \frac{2\zeta}{W_n} s + 1}$$

The dynamics of the position loop occur at a high frequency relative to the process and control. Their effect will, however, have some effect on the controlled system's performance. This effect can be reduced by including lead networks. Ideally, these lead networks should be of the form to cancel out the effect of the position loop completely. Practically, a simple lead network is worth trying in the optimization of the system design.

The frequency response data for the position loop and process presented in Figure B-25 forms the basis for selection of the control constants. As indicated in this data, there is a significant change in the process between the initial and final conditions. For the initial conditions, the time constant of the

**CONFIDENTIAL**

AFRPL-TR-65-209, Vol I

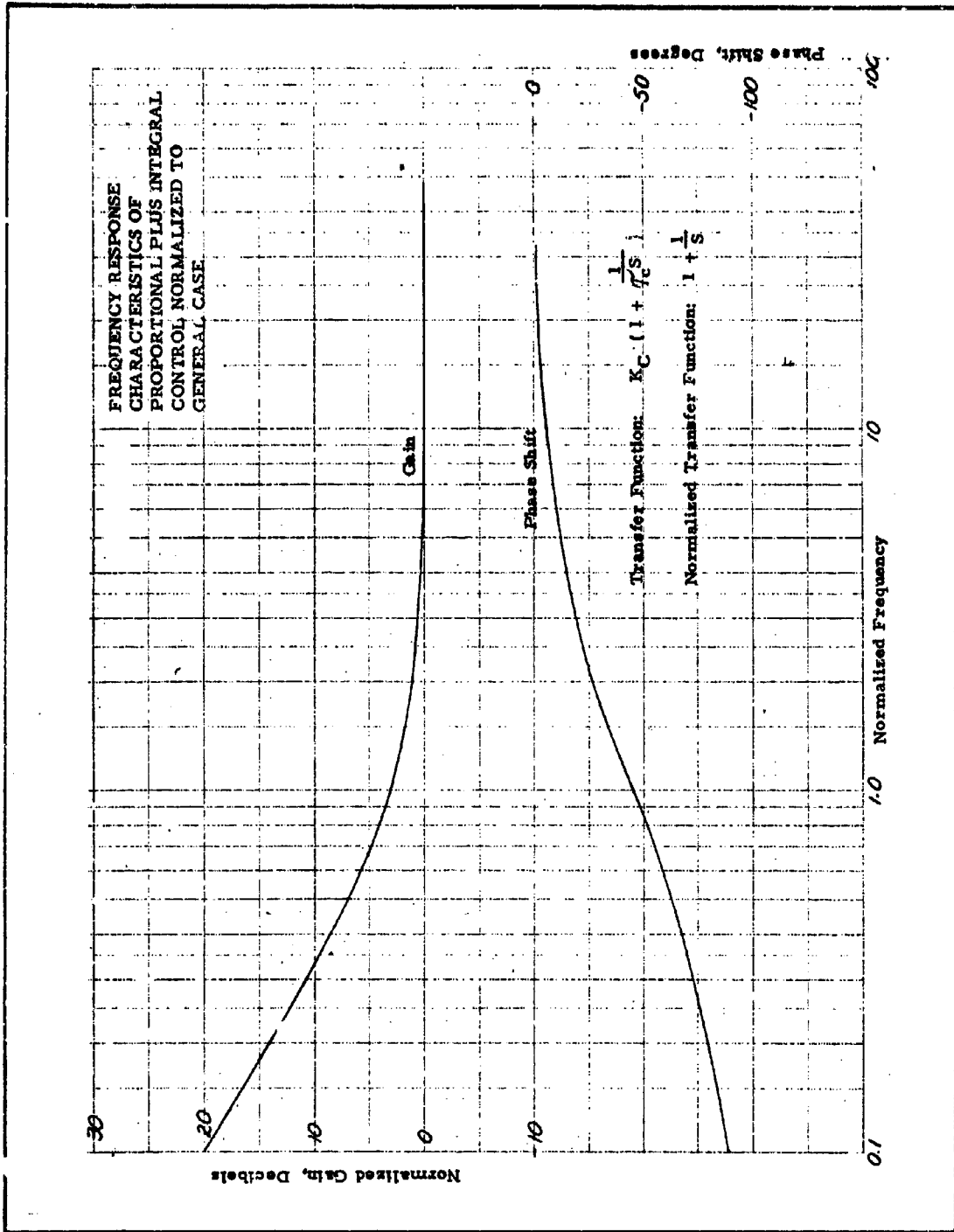


Figure B-27 - Normalized Frequency Response of Proportional Plus Integral Controller

B-53

**CONFIDENTIAL**

process produces a break frequency of 0.4 cps. This indicates that the integral time constant for the initial conditions should ideally be approximately 0.4 seconds. Additional dynamics are introduced by the position loop at a frequency of approximately 10 cps. This would indicate that a lead network having a lead time constant of approximately 0.0167 seconds should improve performance. For a tentative selection of gain, a final gain margin of approximately 12 decibels was selected. This corresponds to a control gain of 20 decibels or 10 volts per volt. For the final condition of the chemical process, the main process lag produces a break frequency of approximately 0.15 cps. This indicates that the optimum integral time constant for the final condition should be in the order of one second. Since the position loop does not significantly change, the same rate network should be effective. Since a greater margin of stability is available, higher gains should be possible for the final condition of the process.

In addition to the selection of the basic control configuration and constants, the establishment of proper limits in the control must be considered. Most important of these limits are those imposed on the integrator. These should be set to correspond with the physical limits of the valve. Beyond this, limits on the overall control signal must be imposed to prevent saturation of the control elements.

Computer mechanization of the control system is presented in Figure B-28. Figure B-28 (a) presents the basic proportional plus integral control. Figure B-28 (b) illustrates the method of adding a lead network to the control.

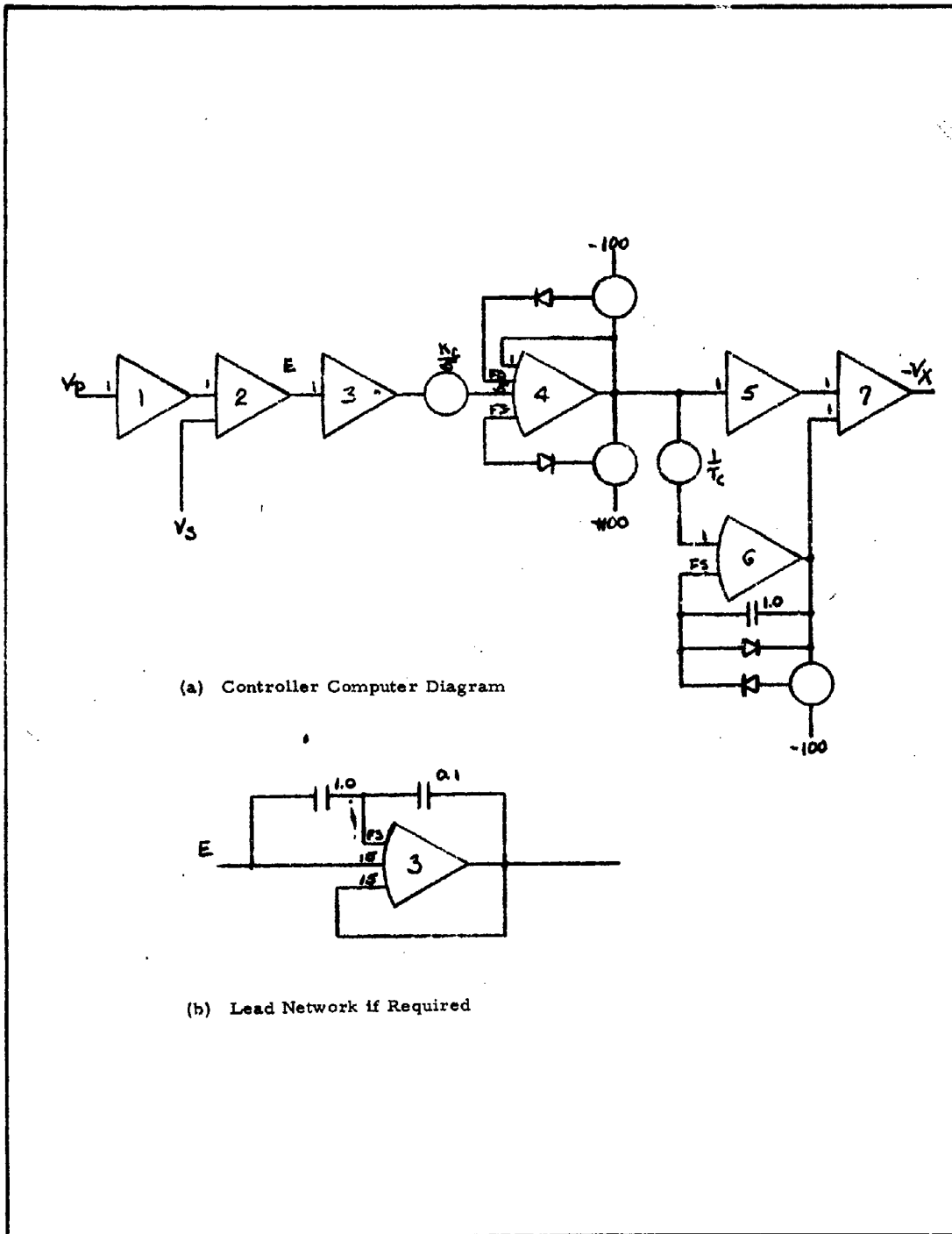
e. Control Optimization Studies

Following the selection of the control configuration and constants, the control performance was studied. This study included the response to large and small step changes in the pressure command signal and small and large ramp changes in the pressure command signal. This work was continued until an optimum control configuration for the complete range of operation was determined.

The intended purpose of the controller is to allow controlled pressure operation for pressure programs which include large ramp changes between levels of constant pressure.

**CONFIDENTIAL**

AFRPL-TR-65-209, Vol I



(a) Controller Computer Diagram

(b) Lead Network if Required

Figure B-28 - Controller Block Diagram and Computer Diagram

Since there is no set specification for the required time and magnitude of the ramps, a step command signal was selected for the controller optimization. The objective was to find a controller which would provide fast operation yet would allow only minimal overshoot and would be stable under all conditions. Realization of this type of performance for step changes will provide the desired performance for any type of input. Once optimization was obtained for step changes, performance in the intended mode was verified by using large ramp input commands.

Initial attempts to optimize the controller revealed that if any input change caused any system parameter to saturate, then the response to this input change was an invalid indication of the acceptability of the controller. Some parameter saturation was most likely to occur when the process is slowest, as with the final free volume. With this condition, it was determined that a maximum input step of 250 psi could be used without causing saturation. The pressure command signal used for controller analysis was a step change in either direction between 2250 psi and 2500 psi.

Operation of the system under the above described conditions led to the following general observations. The proportional plus integral controller provides satisfactory closed-loop operation. Both the proportional and integral gains must be optimized to each other to achieve the desired response shape with slightly less than critical damping. Both can be increased or decreased together within limits to get a faster or slower system with the desired response shape. If only the proportional gain is increased or the integral gain is decreased, the system tends to become overdamped. Likewise, if the proportional gain is decreased or the integral gain is increased, the system becomes underdamped and oscillations begin to occur. There is a maximum value of both proportional and integral gains after which greater values will cause underdamping regardless of any attempts to optimize the two with respect to each other. This condition of maximum usable gains is considered the optimum controller configuration for any one free volume condition.

The controller analysis was performed for both the initial and final free volume condition of the process. With the final free volume, the optimum proportional gain was

higher and the integral gain was lower than with the initial free volume. This characteristic can be predicted from the process Bode diagrams. The final controller configuration was a compromise providing a relatively fast response with the final free volume, yet not causing excessive overdamping with the initial free volume.

As indicated in paragraph d, above, the addition of a lead network to the controller might permit better system performance. If the lead network were set to compensate for the dynamics of the position loop, a higher gain could be used in the controller to provide faster system response.

The lead network was included in the controller for observation. The result was that the lead produced a noticeable improvement only in the optimum controller for the initial free volume condition. When the lead network was used with the final controller configuration, there was no discernible improvement in the system performance.

The final values of proportional and integral gain were 6.67 volts per volt and 2.0 volts per volt-second, respectively. Figures B-29 and B-30 show the system response for the two process conditions when these gains were used. A higher set of gains, 10 volts per volt and 3 volts per volt-second, were used in Figures B-31 and B-32. These higher gains were considered optimum with the initial free volume. Figures B-33 and B-34 show the system response to ramp changes in the pressure command. For these ramp command responses, the final controller configuration was used. Response to pressure command changes of 2500 psi are shown in Figures B-35 and B-36. Note that the control valve actuator hits a limit in both directions of the transients. The resulting pressure response appears to have less overshoot because of this limiting.

The complete computer diagram for the simulated system is shown in Figure B-37.

f. Termination Simulation

The control valve specification requires that the valve change area from minimum to maximum in 15 milliseconds under the termination condition. The resulting control valve

# CONFIDENTIAL

AFRPL-TR-65-209, Vol I

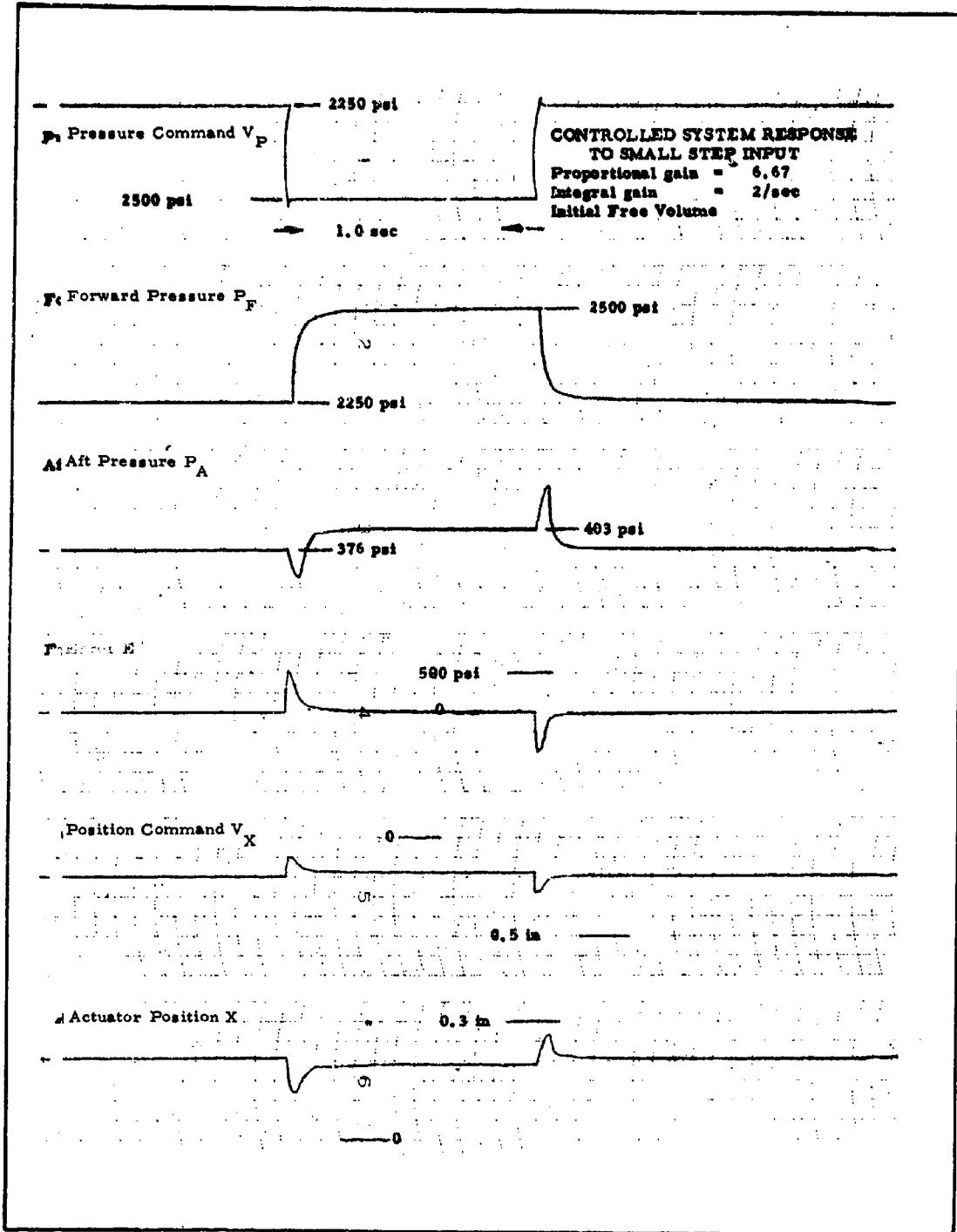


Figure B-29 - Controlled System Response to Small Step Input

B-58

# CONFIDENTIAL

**CONFIDENTIAL**

AFRPL-TR-65-209, Vol I

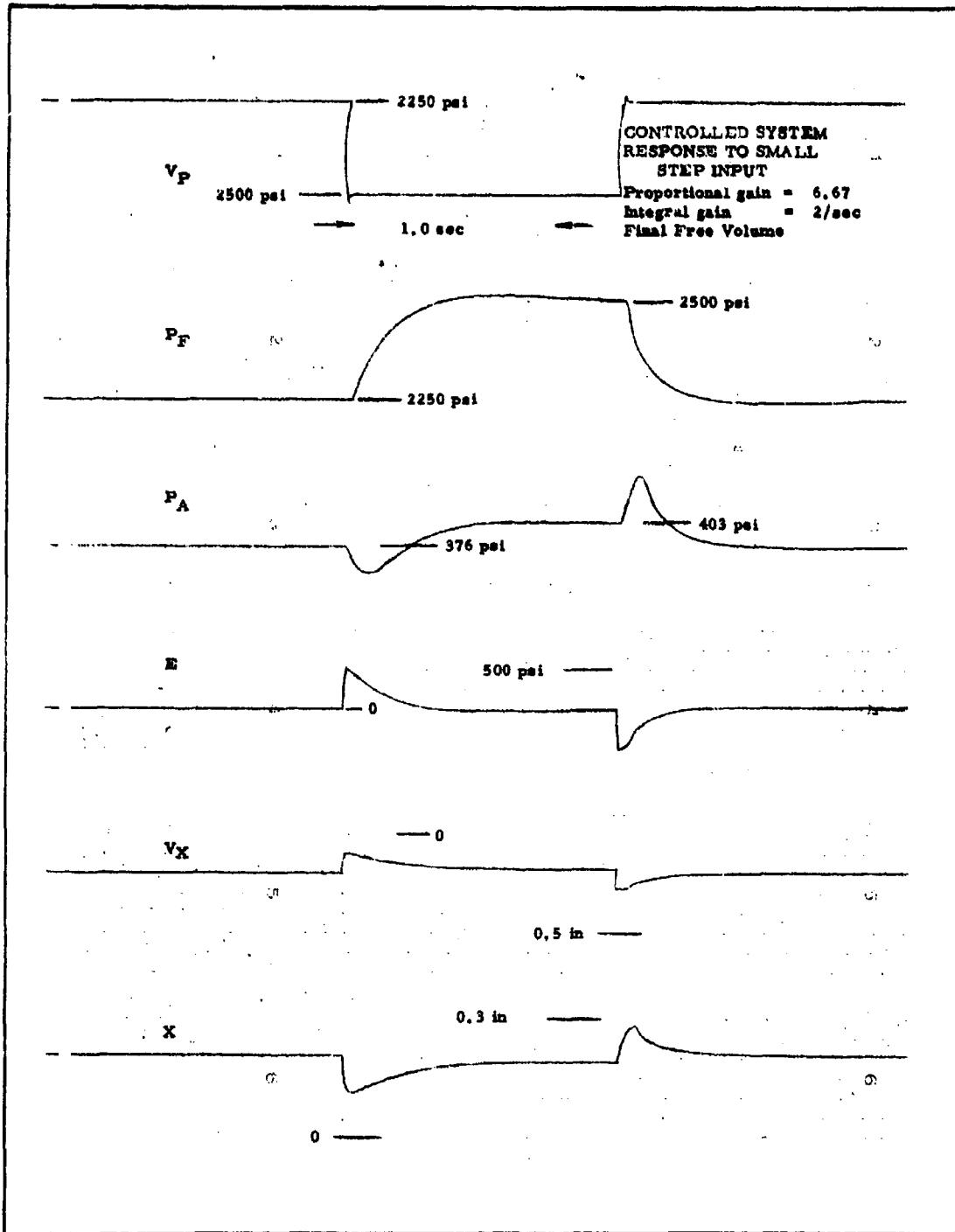


Figure B-30 - Controlled System Response to Small Step Input

**CONFIDENTIAL**

# CONFIDENTIAL

AFRPL-TR-65-209, Vol I

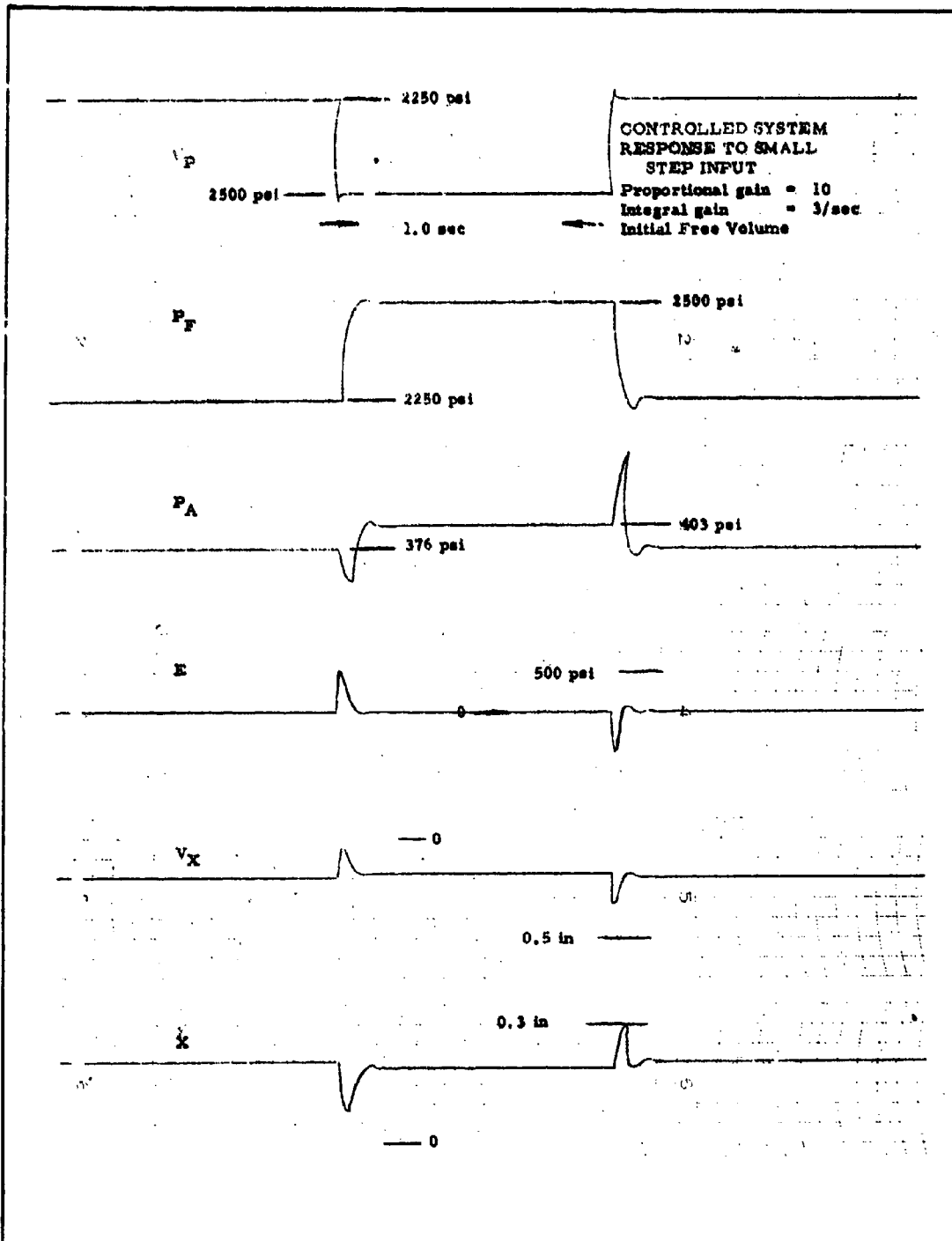


Figure B-31 - Controlled System Response to Small Step Input

B-60

# CONFIDENTIAL

**CONFIDENTIAL**

AFRPL-TR-65-209, Vol I

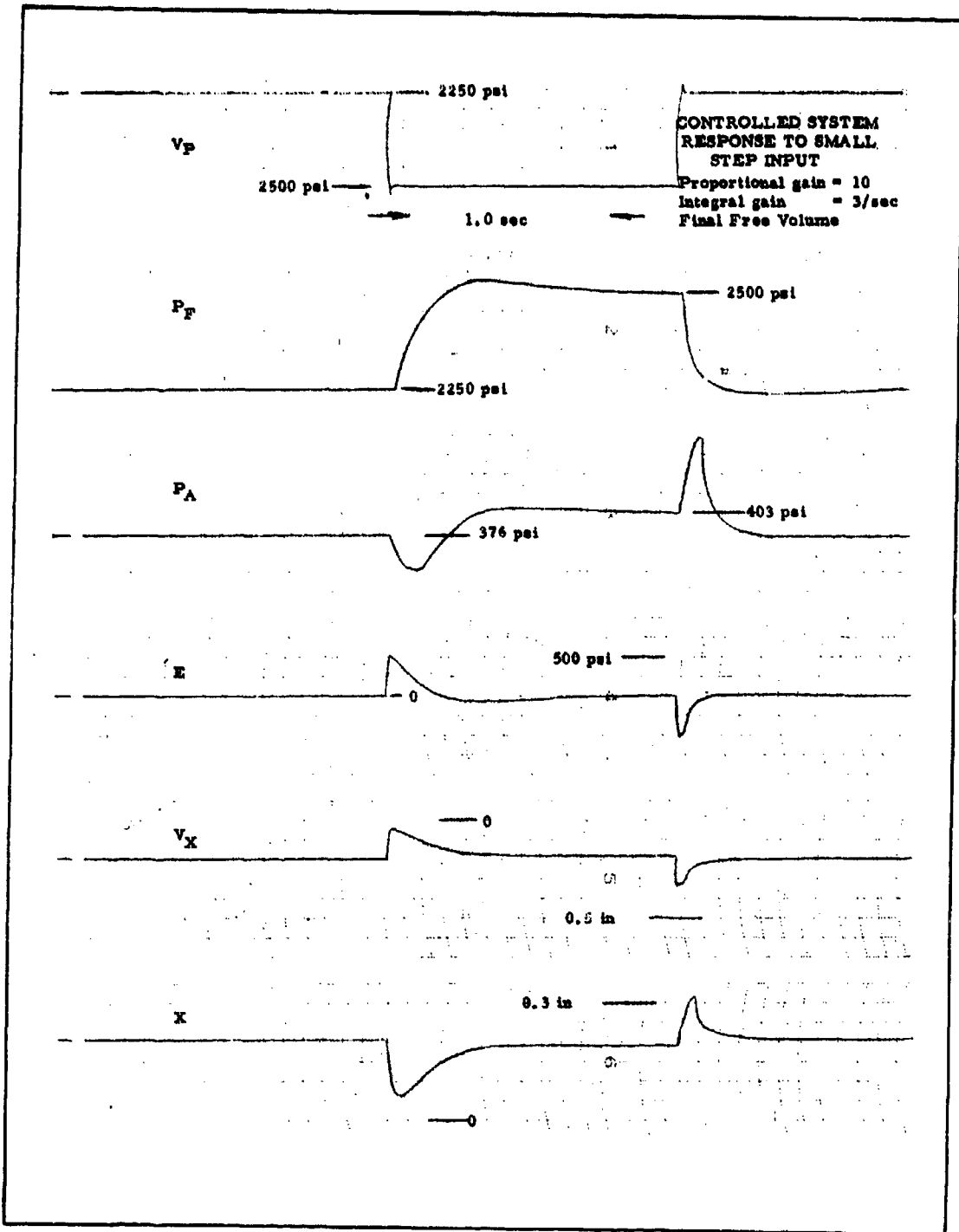


Figure B-32 - Controlled System Response to Small Step Input

**CONFIDENTIAL**

**CONFIDENTIAL**

AFRPL-TR-65-209, Vol I

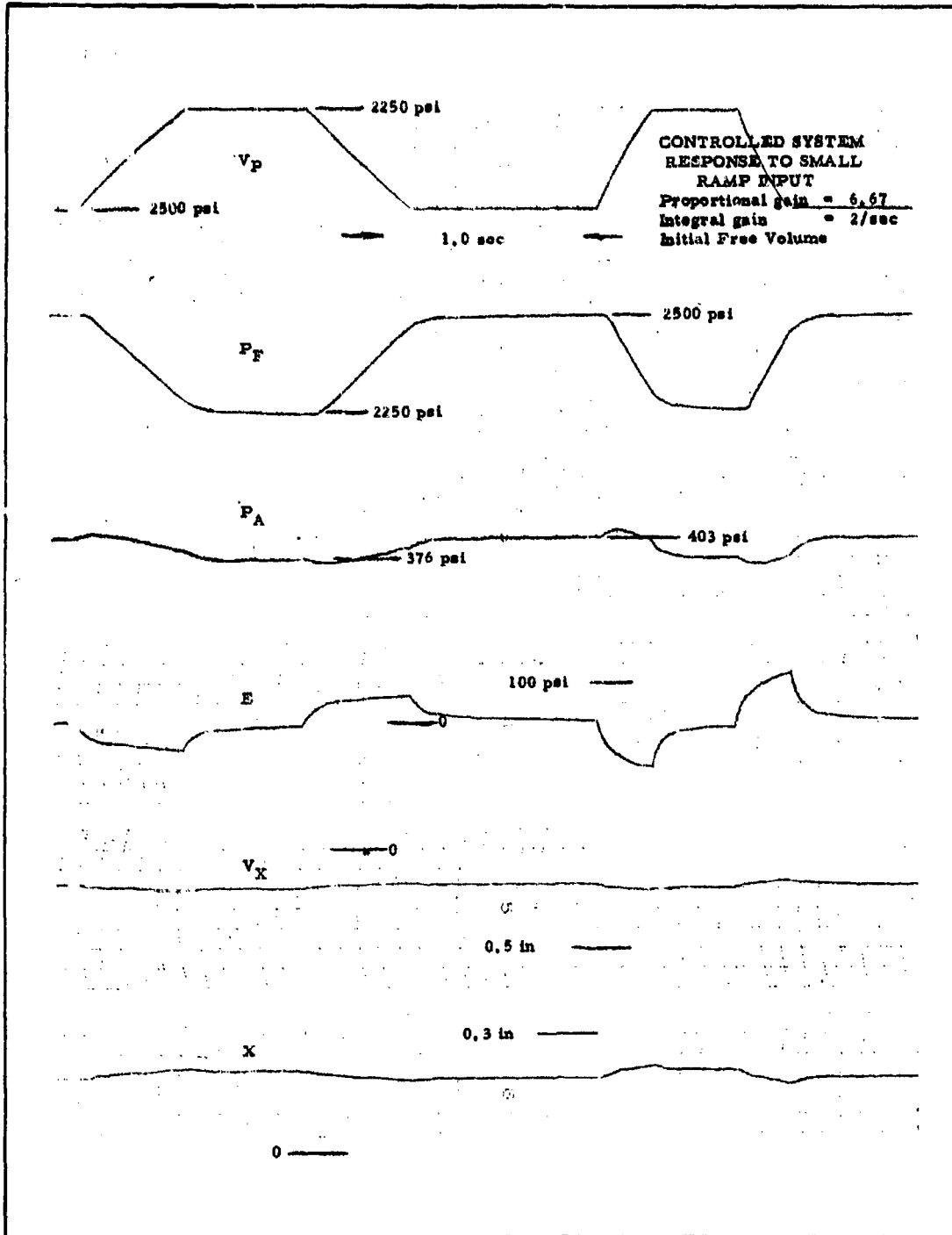


Figure B-33 - Controlled System Response to Small Ramp Input

B-62

**CONFIDENTIAL**

**CONFIDENTIAL**

AFRPL-TR-65-209, Vol I

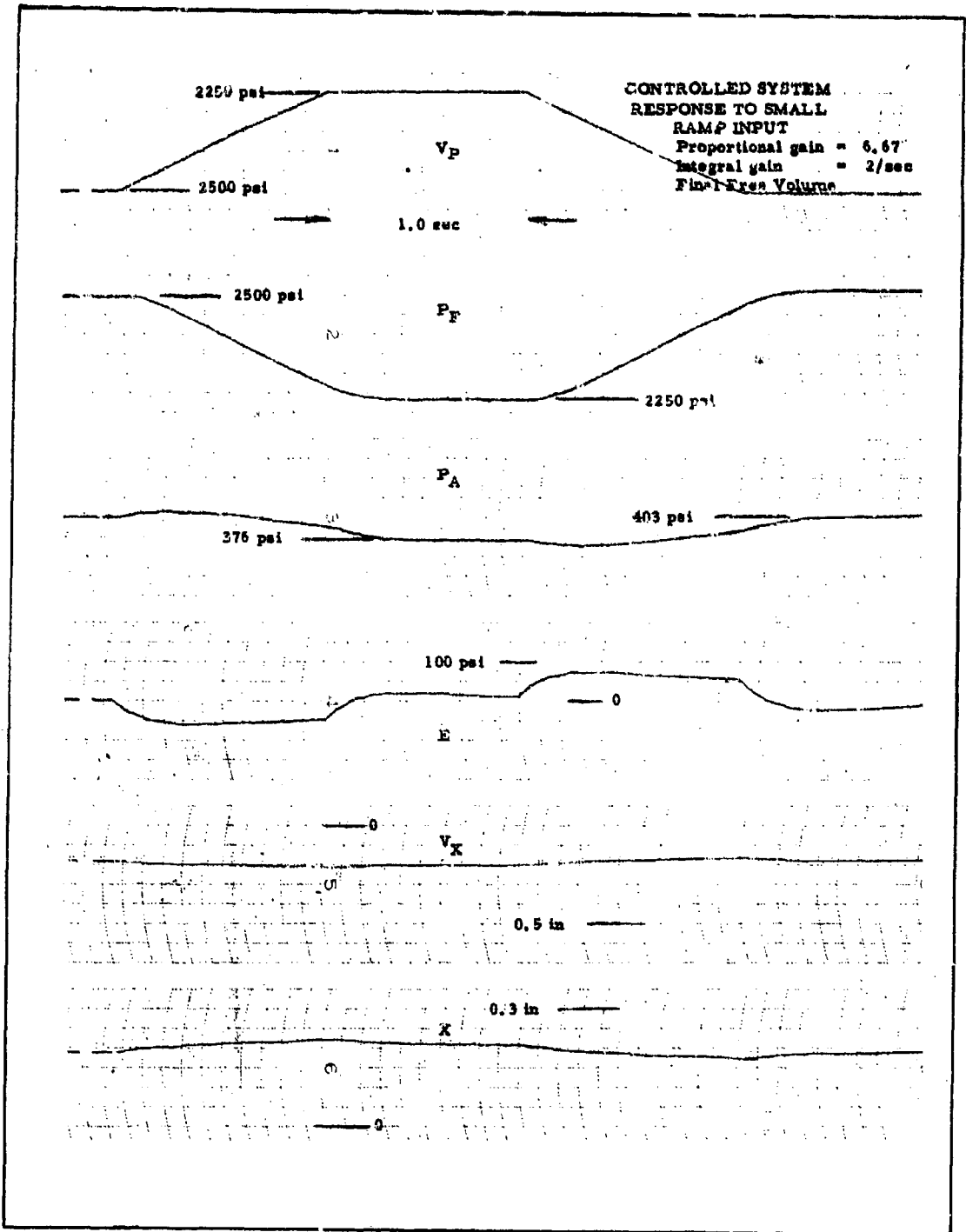


Figure B-34 - Controlled System Response to Small Ramp Input

**CONFIDENTIAL**

**CONFIDENTIAL**

AFRPL-TR-65-209, Vol I

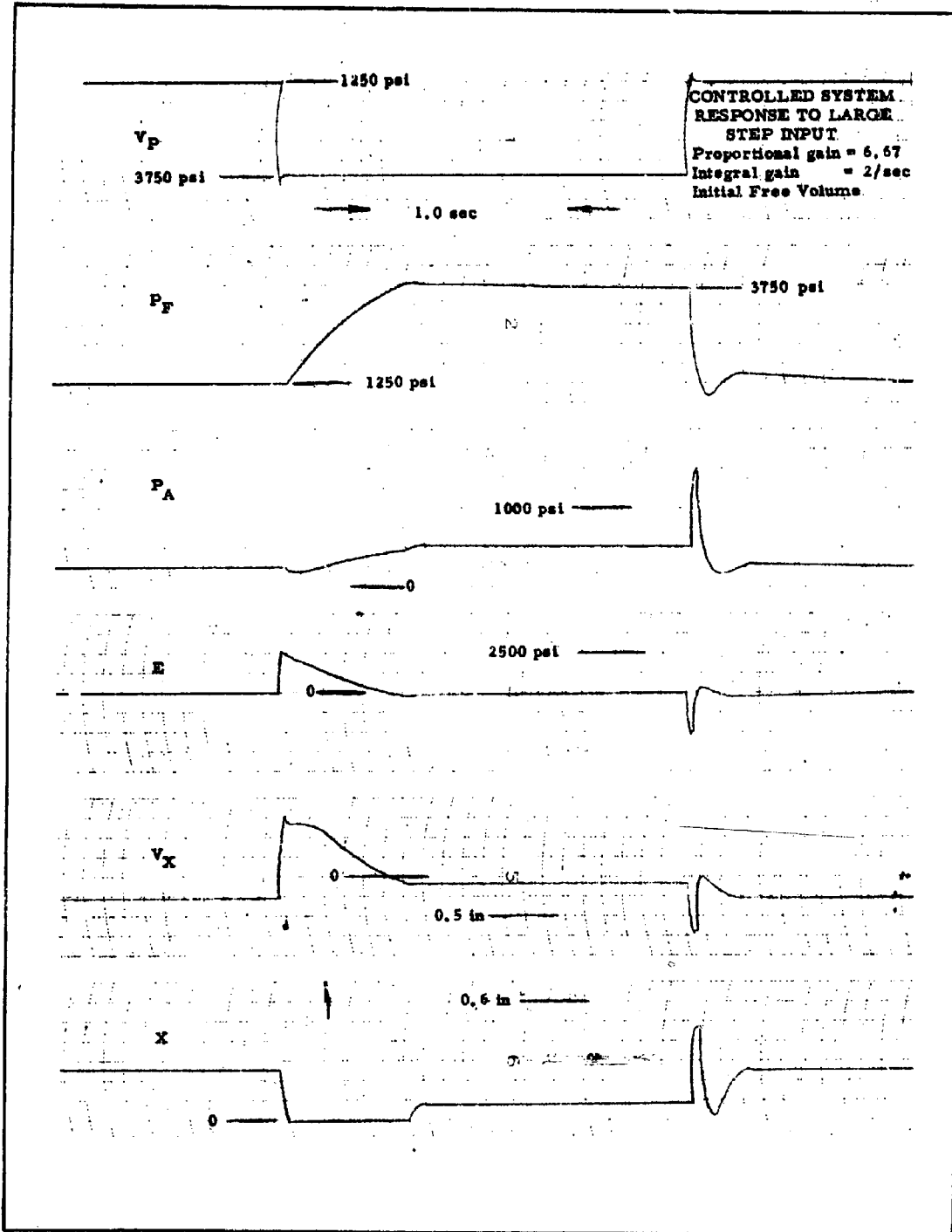


Figure B-35 - Controlled System Response to Large Step Input

B-64

**CONFIDENTIAL**

# CONFIDENTIAL

AFRPL-TR-65-209, Vol I

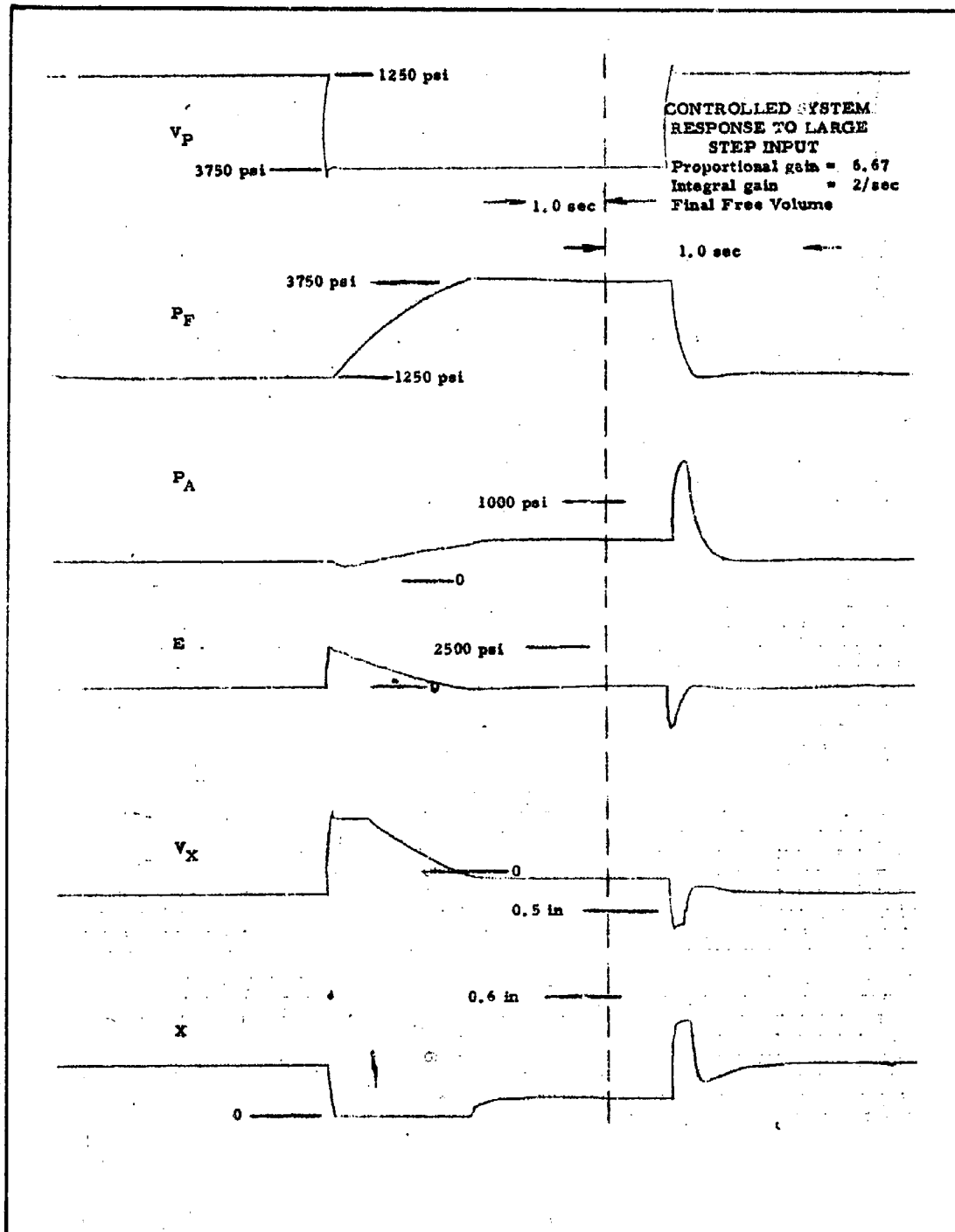


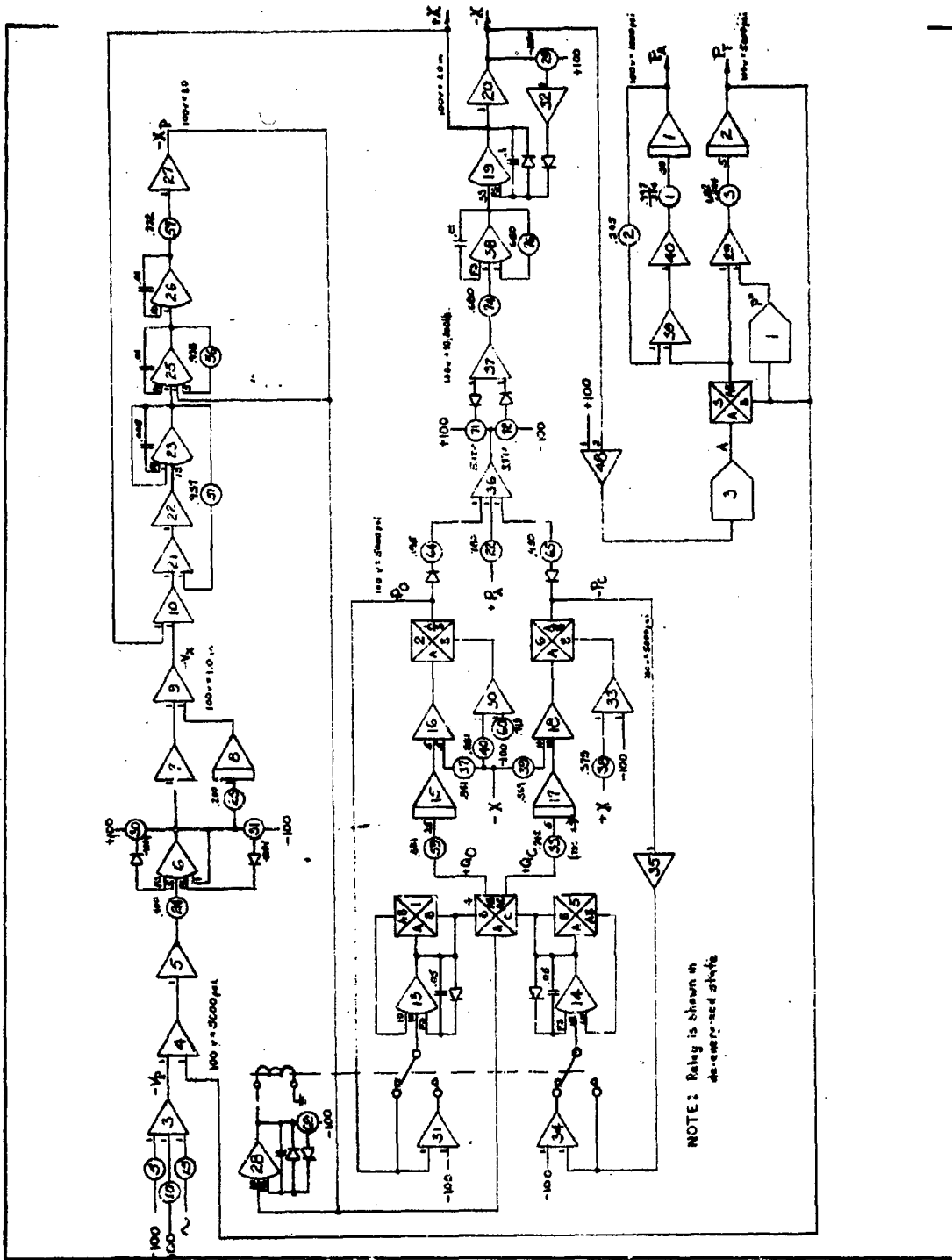
Figure B-36 - Controlled System Response to Large Step Input

# CONFIDENTIAL

B-65

**CONFIDENTIAL**

AFRPL-TR-65-209, Vol I



B-66

Figure B-37 - Complete Computer Diagram for Controlled System

**CONFIDENTIAL**

design utilized two servovalves in the hydraulic system. Only one servovalve was used for normal position loop operation. The other, used only during termination, was called the dump valve. Both ports of the dump valve were connected in parallel to vent the closing hydraulic side of the actuator to the hydraulic return during termination. This connection allows the fluid contained behind the larger closing area of the actuator to be expelled with a minimal combined orifice pressure drop. This connection is shown pictorially in Figure B-4.

As an approximation of the dump condition, the following assumptions were made. The combined operation of the servo and dump valves acted as a servovalve with an enlarged orifice to the closing side of the actuator, where the effective opening orifice area was held constant. Upon termination, the torque motor current of the servovalve went immediately to zero, as explained in paragraph 5, below.

The above changes were incorporated into the computer simulation and the termination was recorded. As shown in Figure B-38, the actuator traveled the required one inch in 12 milliseconds. In this termination simulation the control valve was not operated with the process.

## 5. RECOMMENDED CONTROL OPERATION

The preceding paragraphs described the utilization of the analog computer amplifiers to effect the system simulation. The use of these amplifiers was not necessarily most efficient or most practical. This section describes the recommended usage of amplifiers to effect the CSR control system, along with other important considerations, such as the use of limits.

### a. Control Configuration

Paragraph 4, e, above, identified the desirable controller characteristics for use with the CSR system. The amplifier configuration of Figure B-39 (a) will display these desired characteristics. The effective gains of this controller are 6.67 volts per volt for  $A_1$  and 2 volts per volt-second for integrator  $A_3$ . The parameter scaling is +3 volts = 5000 psi for  $V_P$  and  $V_S$  and +10V = 1 inch for  $V_X$ . If  $V_X$  is not available as a negative signal, then  $A_5$  will be required for inversion.

# CONFIDENTIAL

AFRPL-TR-65-209, Vol I

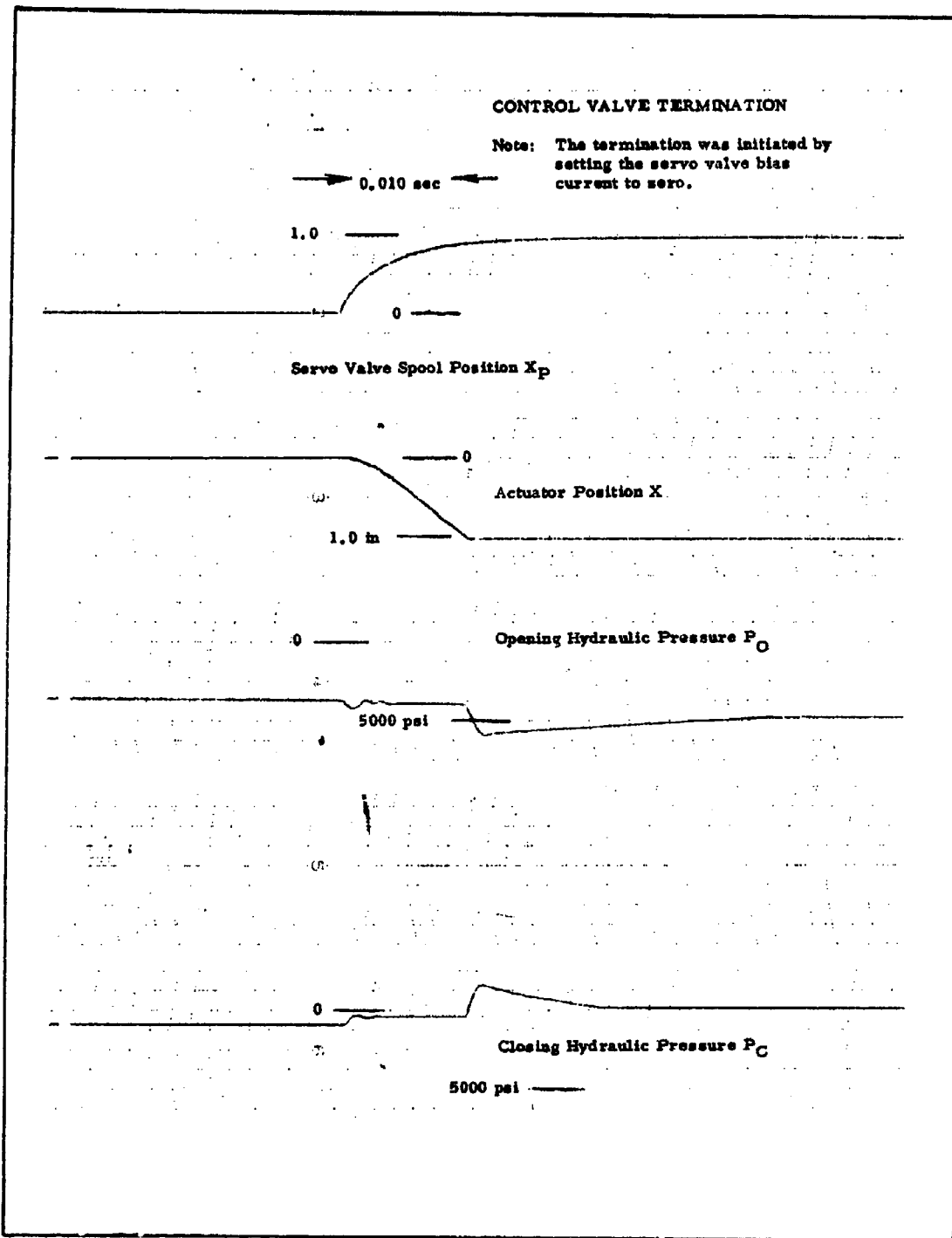


Figure B-38 - Control Valve Termination.

B-68

# CONFIDENTIAL

**CONFIDENTIAL**

AFRPL-TR-65-209, Vol I

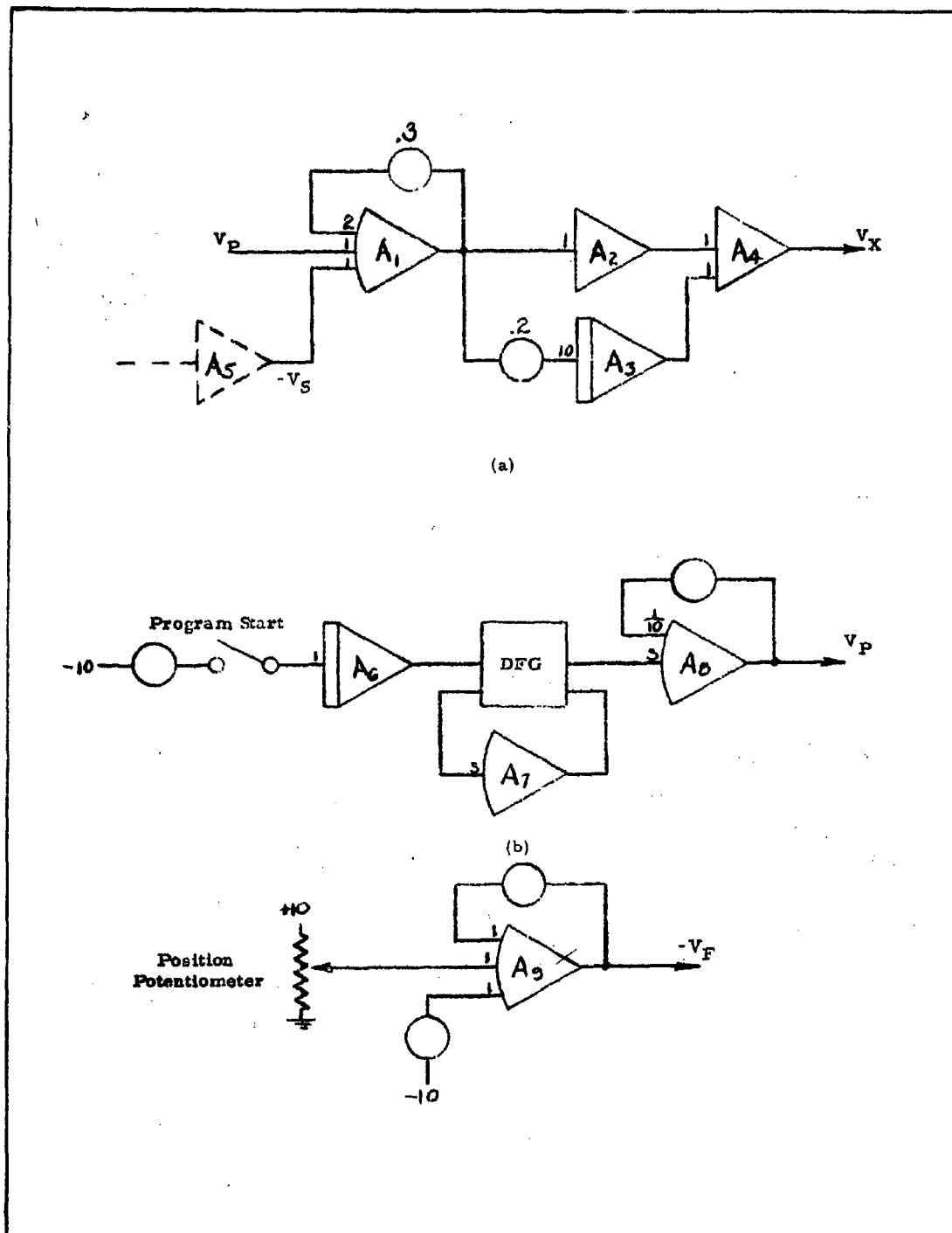


Figure B-39 - TR-10 Computer Diagram for Actual System

B-69

**CONFIDENTIAL**

The pressure program  $V_P$  should be generated by a DFG rather than an X-Y plotter. The DFG should be more stable and definitely more reliable. In the specific case of the use of the TR-10, the pressure program may have to be tailored to the limited capabilities of the DFG, though this should not be a serious restriction. Figure B-39 (b) shows the TR-10 DFG configuration. Integrator  $A_6$  generates the time base after the program is started.  $A_7$  and  $A_8$  are required to complete the DFG.

The position loop feedback voltage  $-V_F$  must have the negative of the amplitude scale of  $V_X$ . If the position potentiometer is supplied by zero to 10 volts, the potentiometer output will probably have less than zero to 10 volts output. An amplifier connection should therefore be used to get the proper scaling of  $V_F$  as shown in Figure B-39 (c).

The position loop configuration can be effected with only one amplifier. A bias is required to return the spool position to null from its normally open condition. Figure B-40 shows the amplifier connections. Shown also is the bias for the dump valve, which nulls this spool the same as for the servo-valve. The method of termination is shown with relay contacts for both the servo and dump valves. In both cases, the torque motor current is made zero and the spools return to their normally open positions, and the actuator opens rapidly. As can be seen, the control valve will terminate upon loss of power because of the choice of normally closed contacts from the terminated signal. Either loss of power or opening these contacts will cause the terminate relay to open.

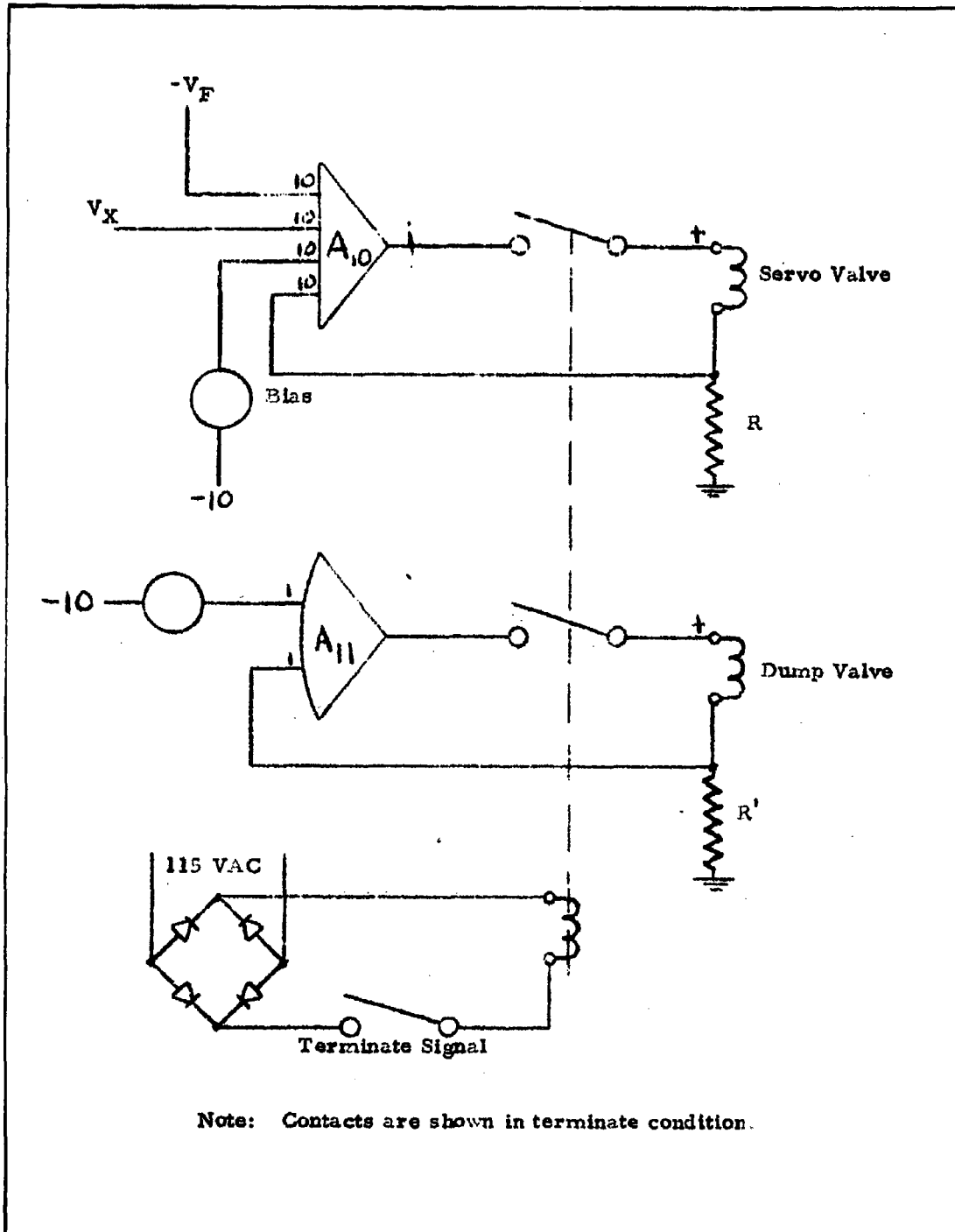
b. Limits

The selection of the controller gains discussed in paragraph 4, e, above, was based on the system performance where all parameters remained within the normal operating limits. Normal operation is not consistent with this condition because the valve obviously must close completely to make the pressure maximum. When parameter saturation does occur, the system performance is affected. Care must be taken to prevent this saturation from adversely changing the system performance.

Consider a programmed increase in pressure. In the steady state, the integrator voltage is  $V_X$  because the error is

**CONFIDENTIAL**

AFRPL-TR-65-209, Vol I



Note: Contacts are shown in terminate condition.

Figure B-40 - Servovalve Drive and Termination Circuitry

B-71

**CONFIDENTIAL**

zero. The integrator gain was chosen so that the new steady-state voltage is reached just as the pressure reaches its programmed level. In this case the overshoot is at a minimum. If, however, the valve completely closes during the transient, the process will respond more slowly than if the problem was linear and the area could get smaller as commanded by the controller output. In this case the integrator will change more than that which corresponds to the new steady-state value and considerable overshoot can occur.

Though this problem cannot be eliminated, it can be reduced sufficiently by limiting the output of the integrator such that its operating range corresponds to the steady-state operating range of the control valve.

The output of an amplifier or integrator can be limited by the use of semiconductor diodes as shown in Figure B-41 (a) and (b). In Figure B-41 (a) the amplifier output voltage cannot be higher than that which satisfies the equation

$$\alpha (E_{out} + 10) = 10 + v_f,$$

where  $v_f$  is the forward voltage drop of the diode. Figure B-41(b) shows an amplifier limited for both positive and negative voltages where  $\alpha = 1/2$ .

Another need for limiting is introduced by an undesirable characteristic of a good operational amplifier. If a TR-10 amplifier is saturated, an internal compensating network causes the amplifier to recover slowly, a typical recovery time being several seconds. Therefore, all TR-10 amplifiers which could saturate under normal startup and operating conditions should be limited by a circuit as shown in Figure B-41(b). In Figures B-38 and B-39 amplifiers  $A_1$ ,  $A_4$ ,  $A_6$  and  $A_{11}$  should have limiters.

c. System Performance

The controller configuration determined through this analysis will provide the desired system performance only if the simulation of the system has been accurate. Duplication of the characteristics of the differential equations given in paragraph 4, above, is assured because of the accuracy of analog computer. The differential equations, however, were assumed to be correct. If the system position loop deviates

**CONFIDENTIAL**

AFRPL-TR-65-209, Vol I

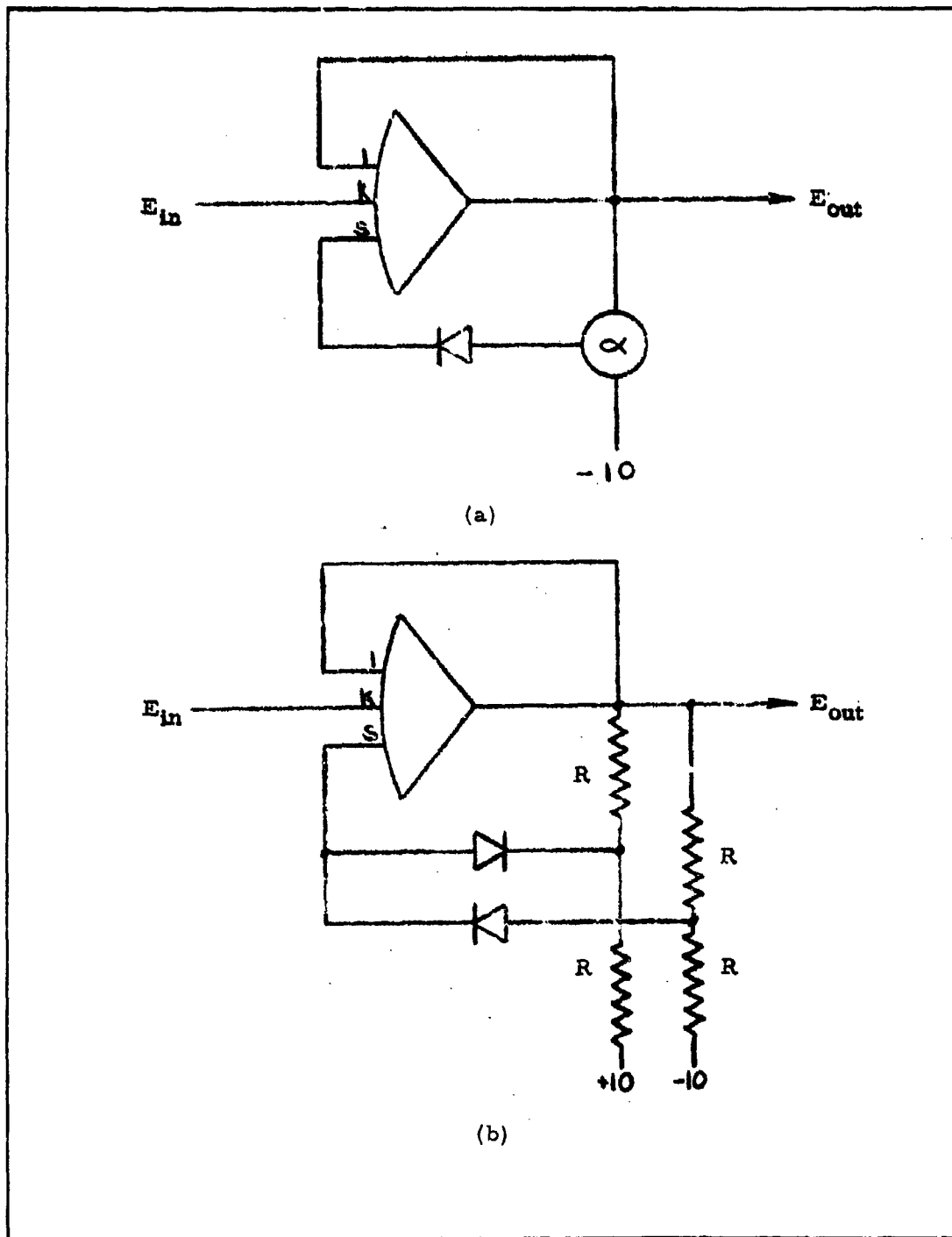


Figure B-41 - Computer Amplifier Limiting Circuitry

B-73

**CONFIDENTIAL**

from that described by these equations, the closed-loop system performance must be different from that predicted.

Acknowledging the possibility of a somewhat inaccurate system simulation, consider the effect of using the above controller in the actual system. Refer to Figure B-25, recalling that a Nyquist type instability, where oscillations are sustained, can occur only when the open loop gain is greater than unity when the phase shift is 180 degrees. Add the characteristics of the controller to this Bodie diagram to obtain the open loop characteristic of the system. Analysis of this diagram shows that a Nyquist type instability can occur only under one of the following conditions: the proportional gain was increased by a factor of 4.7 or either the process time constant was decreased or the position loop time constant was increased by a factor of 4. The conclusion is obvious that the stability criterion used in this analysis was very conservative. The safety factor on each of the system parameters should be sufficient to absorb a deviation in the actual system open loop performance from that predicted in this analysis.

6. CONTROL VALVE LIMITATIONS

As stated in paragraph 4, b, the control valve area versus stroke relationship does not conform to the ideal control valve characteristic. This deviation was forced by the geometric limitations of the valve as shown below.

The limitation is the maximum rate of change of area versus stroke for a particular sized valve pintle. First, the required rate of change of area can be calculated from

$$A = \frac{0.475}{(4.5 - 4.4X)} \quad 0.328 \quad ,$$

where X = 1 represents the maximum valve area. Then

$$\begin{aligned} \frac{dA}{dX} &= \frac{0.475}{(4.5 - 4.4X)} \quad 1.328 \times (-0.328) \times (-4.4) \\ &= \frac{0.686}{(4.5 - 4.4X)} \quad 1.328 \end{aligned}$$

and

$$\frac{dA}{dX}_{\max} = \frac{dA}{dX}_{X=1} = \frac{0.686}{(0.1)} 1.328 = 14.6 \text{ in.}^2 / 100\% \text{ useful}$$

stroke.

Now consider the maximum rate of change of area for a valve where the pintle diameter is D. The increase in area caused by a movement of the pintle will be at best the area swept by the pintle circumference. In this case,

$$\frac{dA}{dX} \leq \pi D \text{ in.}^2 / \text{in.}$$

The specified control valve envelope restricts the maximum pintle diameter to 2.57 in. To meet the area versus stroke relationship shown above, the useful stroke must be

$$\text{Useful Stroke} \geq \frac{14.6}{D} = 1.81 \text{ in.}$$

requiring the total stroke to be over 2 in. However, a total stroke of over 2 in. is unrealistic when considering that the control valve must terminate in 15 milliseconds. If a valve with a 0.5 in. stroke was to be made to conform to the specification, then

$$D = \frac{14.6}{\pi \times 0.5} = 9.3 \text{ in.}$$

which is also unreasonable for several reasons. The actual valve is made with D = 2.57 in. and the useful stroke = 0.5 in. Here

$$\frac{dA}{dX}_{\max} = 2.57 \times \pi \times 0.5 = 4.04 \text{ in.}^2 / 100\% \text{ useful stroke.}$$

The valve area does conform to the specification for approximately 85% of the stroke; the maximum conforming stroke with ideal pintle and seat configuration occurs when

$$\frac{0.686}{(4.5 - 4.4X)} 1.328 = 4.04$$

or

$$X = \frac{4.5 - (.170)^{.753}}{4.4}$$

$$= 96\%$$

## 7. FREQUENCY RESPONSE DATA

All the performance data from the simulated control system was recorded on six-channel curvilinear strip charts, as in Figure B-42. All transient response and frequency response data was obtained from these recordings. In the particular case of reducing the frequency response data to a usable form, the Bodie diagram, the recordings must be taken with a known computer parameter scale; amplitude and phase shift information must be measured for each frequency, and the resulting data must be rescaled to the actual problem parameters and plotted.

An example is included to show the frequency response data reduction for the combined position loop and process open loop operation. Figure B-42 shows the computer response of the initial process to the sinusoidal variation of the position command signal at 0.1 cycle per second. Recall that this frequency corresponds to an actual system variation at 1.0 cps because of the time scaling. Shown also is the recording calibration and the amplitude, period, and phase shift of the two signals of interest,  $V_X$  and  $V_S$  ( $V_S = P_F$  in the computer simulation).

The desired final form for this is  $\left. \frac{V_S(s)}{V_X(s)} \right|_{1 \text{ cps}} = K$  decibels at an angle  $\theta$  degrees, where  $V_S$  and  $V_X$  are actual system parameters. As a definition,

$$K = 20 \log_{10} \left| \frac{V_S}{V_X} \right| \text{ decibels}$$

and

$$\theta = \frac{\text{phase shift}}{\text{period}} \times 360^\circ$$

In order to properly scale the measured parameters, the following scale factors must be used:

**CONFIDENTIAL**

AFRPL-TR-65-209, Vol I

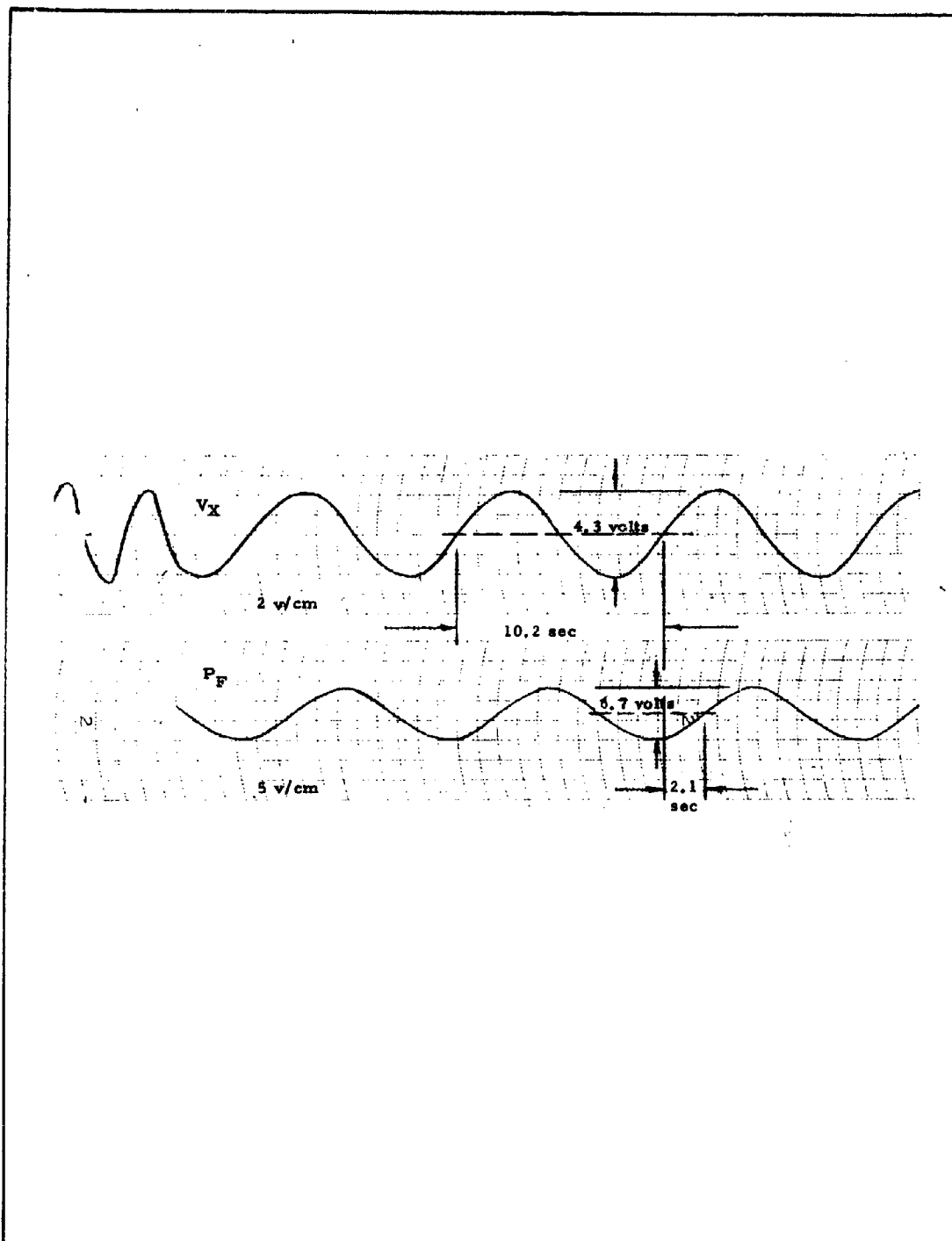


Figure B-42 - Example of Frequency Response Data Reduction

**CONFIDENTIAL**

B-77

	<u>Actual System</u>	<u>Computer Simulation</u>
$V_X$	10V = 1 inch	100V = 1 inch
$V_S$	3V = 5000 psi	100V = 5000 psi

Now the desired frequency response data can be calculated:

$$\begin{aligned}
 K &= 20 \log_{10} \frac{6.7V \times 50 \text{ psi/V} \times 0.0006 \text{ V/psi}}{4.37V \times 0.01 \text{ in/V} \times 10 \text{ V/in.}} \\
 &= 20 \log_{10} \frac{0.201}{0.437} \\
 &= -6.76 \text{ db} \\
 \theta &= \frac{2.1 \text{ seconds}}{10.2 \text{ seconds}} \times 360^\circ \\
 &= 74^\circ.
 \end{aligned}$$

The above frequency data points can be found in Figure B-25 with the initial free-volume for a frequency of 1 cps.

APPENDIX C - DESIGN ANALYSIS FOR NOZZLE NO. 1 (2-TO-1 EXPANSION)

1. INTRODUCTION

This appendix presents the design analysis data for the first stop-start test nozzle. Heat transfer, materials analysis, and design are discussed herein. This nozzle is the first in a series of six test nozzles which will be used for altitude testing.

The materials laboratory test results are presented in paragraph 2, below.

2. ANALYSES

a. Materials Evaluation

(1) Introduction

The refractory materials used for the nozzle throat area are exposed to severe heat flux conditions and represent a critical problem area from the standpoint of maintaining dimensional stability and structural integrity. In single-pulse firings, the throat life is controlled by:

1. Melting temperature,
2. Thermal shock resistance, and
3. Chemical reactivity and erosion resistance.

In the case of nozzles to be used for start-stop applications, additional factors such as thermally-induced, low-cycle fatigue, and the effects of recrystallization and grain growth on thermal shock resistance must also be considered. It is well known that materials subjected to pulsed thermal exposure will undergo cracking, which depends upon the magnitude of the temperature differential and the number of exposure cycles. Although extensive effort in the area of thermal fatigue has been devoted to evaluating turbine alloys and brittle refractory ceramics, relatively little information exists on tungsten or graphite, the materials being considered for restartable nozzles. In the case of tungsten when multiple firings occur, recrystallization may take place after the first firing cycle and

continued grain growth may result during subsequent pulses. The beneficial effects of the worked structure are, therefore, lost and the nozzle insert may be susceptible to thermal shock at some subsequent stage of the duty cycle.

The purpose of this investigation was to examine the susceptibility of tungsten and pyrolytic graphite to thermal fatigue under conditions which may involve up to 20 cycles and temperature differentials approaching 5000° F. In addition, attempts have been made to evaluate the influence of high-temperature exposure on grain growth in tungsten. The ultimate aim is to obtain sufficient data to allow satisfactory material selection for restartable rocket nozzle structures.

(2) Experimental Procedures

(a) Materials

Unalloyed tungsten, tungsten-1% thoria, and pyrolytic graphite were the three refractory materials studied. These materials were selected on the basis of their high-temperature capability, along with adequate thermal shock and erosion resistance when exposed to single-pulse duty cycles.

Tests were conducted to determine thermal fatigue resistance, grain growth under cyclic and constant-temperature exposure, and variations in transition temperature produced by grain size changes. The thermal fatigue studies were conducted on 1/4- and 1/8-in. diameter rods of tungsten and tungsten-1% thoria alloys. The pyrolytic graphite was obtained in the form of discs, 3 in. in diameter and 1/2 in. thick. The "C" axis of this highly anisotropic material was oriented perpendicular to the faces of the disc. Rods (3 in. long by 1/4 in. diameter) with the "C" axis perpendicular to the rod axis were fabricated from these discs for the low-cycle thermal fatigue studies. Coupons from unalloyed tungsten sheet in two conditions, as-received-recrystallized and hot-cold-worked 75%, were included to determine the effects of prior micro-structure on the constant-temperature, grain-growth behavior of tungsten.

Specimens of tungsten-1% thoria could be readily obtained only as 1/8 or 1/4 in. diameter rods. The former, which had a partially wrought case and a fully recrystallized core, was used to determine effects of thermal cycling on grain growth. The latter was fully wrought material used for constant-temperature studies and transition temperature determination.

(b) Thermal Fatigue Testing

To determine the relative susceptibility of the three materials to low-cycle thermal fatigue, rod specimens were heated by self-resistance and cycled a minimum of 25 times between room temperature and 5000° F in the apparatus shown in Figure C-1. The test cycle consisted of applying the power for 30 seconds, then force-cooling the specimen with a dry nitrogen gas jet for 150 seconds. The rods used were 1/4 in. in diameter by 3 in. long with a 2.3 in. distance between grips. Both smooth and notched specimens were cycled. The notched specimens consisted of a 60° V notch machined to a depth of 0.016 in. with a maximum radius of 0.005 in. at the root. The maximum test temperature in all cases was determined using a two-color pyrometer. A chromel-alumel thermocouple was placed at the bottom of the specimen to insure that this section of the specimen was below 400° F (the assumed minimum ductile-to-brittle transition temperature for tungsten) before the next cycle was started.

(c) Grain Size Studies

The effects of various thermal environments on the recrystallization and grain growth characteristics of unalloyed tungsten and tungsten-1% ThO<sub>2</sub> were studied using several techniques. To evaluate the influence of cumulative time at the temperature maximum in a particular duty cycle, constant temperature tests were employed. Coupons 3/4 by 1/8 in. of unalloyed tungsten with two different processing histories and 1/4 in. diameter by 1 in. rods of tungsten

**CONFIDENTIAL**

AFRPL-TR-65-209, Vol I

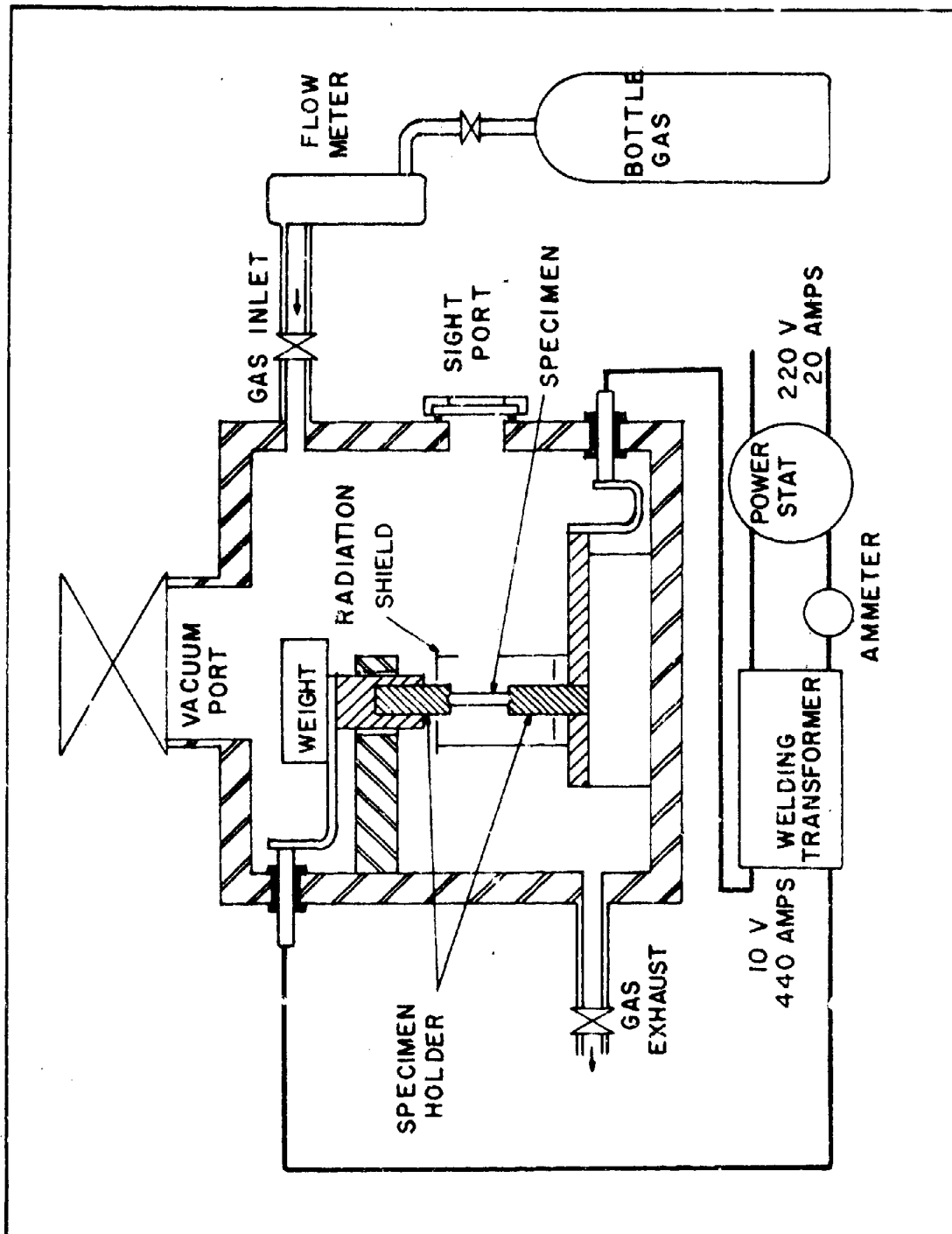


Figure C-1 - Schematic Diagram of Equipment Used for Low Cycle Thermal Fatigue Evaluation

C-4

**CONFIDENTIAL**

-1% ThO<sub>2</sub>, were heated in a vacuum (Brew furnace) for varying lengths of time (5 hours, 1 hour, 20 minutes and 5 minutes) at constant temperature.

Test temperatures of 3000, 3500 and 3900<sup>o</sup>F were employed. The extent of recrystallization and amount of grain growth were determined both metallographically and with hardness measurements. The grain boundary intercept method was used to measure grain dimensions with the final values representing the average of at least five separate readings.

Rod specimens of both unalloyed tungsten and tungsten-1% ThO<sub>2</sub> heated by self-resistance were used to study the variation in microstructure produced by constant and cyclic temperature exposure above 4000<sup>o</sup>F. The apparatus previously discussed for the thermal fatigue testing was used with 1/8 and 1/4 in. diameter by 3 in. long specimens. Both the maximum temperature and number of cycles were varied to determine their combined effect. Grain size and/or hardness values were measured on all specimens.

Variations in grain size produced by thermal exposure are significant only if they produce an increase in thermal shock susceptibility. On a comparative basis, bend ductility transition temperature represents a convenient laboratory method for rating the ability of tungsten nozzle inserts to resist thermal shock.

Bend specimens of unalloyed tungsten and tungsten-1% ThO<sub>2</sub> were subjected to two thermal environments which produced rather gross changes in microstructure. Flat bend specimens of unalloyed tungsten (2 by 0.340 by 0.080 in.) and round bend specimens of tungsten-1% ThO<sub>2</sub> (2 by 1/4 in. diameter) were prepared. A standard three-point bend test, 1-1/2 in. span, was used with a cross-head speed of 0.050 in./minute. The variation on bend angle with temperature was used to determine the ductile-to-brittle transition.

(3) Results and Discussion

(a) Low-Cycle Fatigue

None of the three materials -- unalloyed tungsten, tungsten-1% ThO<sub>2</sub> or pyrolytic graphite -- showed any indication of low-cycle fatigue failure after exposure to 20 cycles which involved temperature differences as high as 4600° F (400° F to 5000° F). Both notched and smooth rod specimens were heated for one hour in air at 1000° F following thermal cycling to heat-tint any possible crack. The specimens were fractured after heating. No sign of crack initiation was observed.

Pyrolytic graphite also appeared immune to thermal fatigue over the range of variables examined. In addition, no indication of dimensional change was present in the pyrolytic graphite specimens after heating 50 times to 5000° F.

(b) Grain Growth Characteristics

The influence of constant temperature exposure on the grain size of unalloyed tungsten is summarized in Tables C-I and C-II.

In general, there was relatively little grain growth at exposure temperatures to 3920° F. The tungsten which was initially in the wrought condition recrystallized after one hour at 3000° F and the resultant size was comparable to that obtained in the as-received, recrystallized sheet. At a temperature exposure of 5000° F for 20 minutes, the tungsten tended to exhibit a noticeable but uniform increase in grain size. The specimen, aged at 3920° F for a relatively long time (300 minutes), exhibited some tendency for discontinuous grain growth, with the resultant grains ranging in size from  $5.1 \times 10^{-2}$  to  $96 \times 10^{-2}$  mm.

Grain growth in thoriated tungsten showed the typical elongated recrystallized structure. As in the

TABLE C-I - EFFECT OF TIME AND TEMPERATURE ON THE GRAINSIZE OF TUNGSTEN SHEET (As-Received, Recrystallized Condition)

Specimen	Temperature (°F)	Time (Min)	Average Grain Diameter (10 <sup>-2</sup> mm)
. . .	5000	5	6.1*
18	3920	300	5.1 to 96.0 (discontinuous growth)
17	3910	60	3.6
16	3920	20	3.6
15	3920	5	3.0
14	3510	300	3.4
13	3510	60	3.2
22	3500	20	3.9
24	3500	5	3.6
28	3000	300	4.6
33	3000	60	3.6
As-received	. . .	. . .	3.5

\* Data for this sample obtained on rod specimens.

TABLE C-II - EFFECT OF TIME AND TEMPERATURE ON THE GRAINSIZE OF TUNGSTEN SHEET (Hot-Cold Worked 75% at 2300°F)

Specimen	Temperature (°F)	Time (Min)	Average Grain Diameter (10 <sup>-2</sup> mm)
12	3920	300	4.6
11	3910	60	3.4
10	3920	20	3.4
9	3920	5	3.9
8	3510	300	3.2
7	3510	60	4.5
20	3500	20	3.8
25	3500	5	4.6
30	3000	300	3.6
32	3000	60	3.2

case of unalloyed tungsten, the average grain cross-section was relatively insensitive to thermal exposure up to temperatures of 3920°F (Table C-III). Although the longitudinal grain dimensions were large, they also appeared to be relatively stable until temperatures approaching 5000°F were attained.

In contrast to the relatively uniform increase in grain size which took place as a result of constant-temperature exposure for times comparable to rocket nozzle applications, cyclic temperature exposures in the range between 4500°F and 5000°F produced discontinuous and exaggerated grain growth. The cyclic exposure involves a total cycle time of approximately 30 seconds and the specimen was held at maximum temperature for 15 seconds. The center of the specimen contained a single grain which virtually encompassed the entire cross-section. The discontinuous grain growth produced by the thermal cycling occurred with a high degree of reproducibility while a single exposure at a time comparable to the total cumulative time involved in the cyclic exposure at the maximum temperature produced only a uniform grain size increase. The relationship between the number of cycles and temperature required to produce the discontinuous grain growth in unalloyed tungsten is tabulated in Table C-IV and shown in Figure C-2, while the influence of temperature on grain size for a given number of cycles is presented in Figure C-3. Tungsten-1% ThO<sub>2</sub> specimens did not undergo discontinuous grain growth as a result of thermal cycling (see Table C-V).

The sharp increase in grain size in unalloyed tungsten in the 4500 to 5000°F temperature range is comparable to that reported previously by Jeffries in his pioneer work on tungsten sintering .

---

\* Z. Jeffries, Met. Chem. Engineering, 16, 503, (1917).

**TABLE C-III - EFFECT OF TIME AND TEMPERATURE ON THE GRAIN  
SIZE OF 1/4-INCH TUNGSTEN-1% THO<sub>2</sub> ROD (70-90% REDUCTION)**

Specimen	Temperature (°F)	Time (Min)	Average Grain Width* (10 <sup>-3</sup> mm)
A2	5000	5	6.1
A4	5000	1	12.7
C	3920	20	4.2
B	3920	5	6.1
A	3510	300	5.1
D	3510	60	4.2
19	3500	20	4.2
23	3500	5	4.6
27	3000	300	5.1
31	3000	60	3.9
As-received	...	...	4.2

\* Lengths of grain all greater than 75 mm at 100X, widths were arbitrarily chosen as index of grain growth.

TABLE C-IV - EFFECT OF TIME, TEMPERATURE AND THERMAL  
CYCLING ON THE GRAIN SIZE OF 1/8-INCH TUNGSTEN ROD

Temperature (°F)	No. of Cycles	Time per Cycle (Sec)	Average Grain Diameter (10 <sup>-2</sup> mm)
5000	2	600	5.5
5000	1	300	6.1
5000	10	30	Single crystal* (Discon- tinuous growth)
5000	5	30	6.3
5000	1	60	4.6
4750	17	30	4.8 (13) <sup>†</sup> (Discontinuous growth)
4500	20	30	3.9 (13) <sup>†</sup> (Discontinuous growth)
4500	10	30	3.9
4000	20	30	4.6
4000	10	30	4.2

\* Center section of rod one large grain, approximately 25 mm by 60 mm.

<sup>†</sup> Diameter of large grains.

**CONFIDENTIAL**

AFRPL-TR-65-209, Vol I

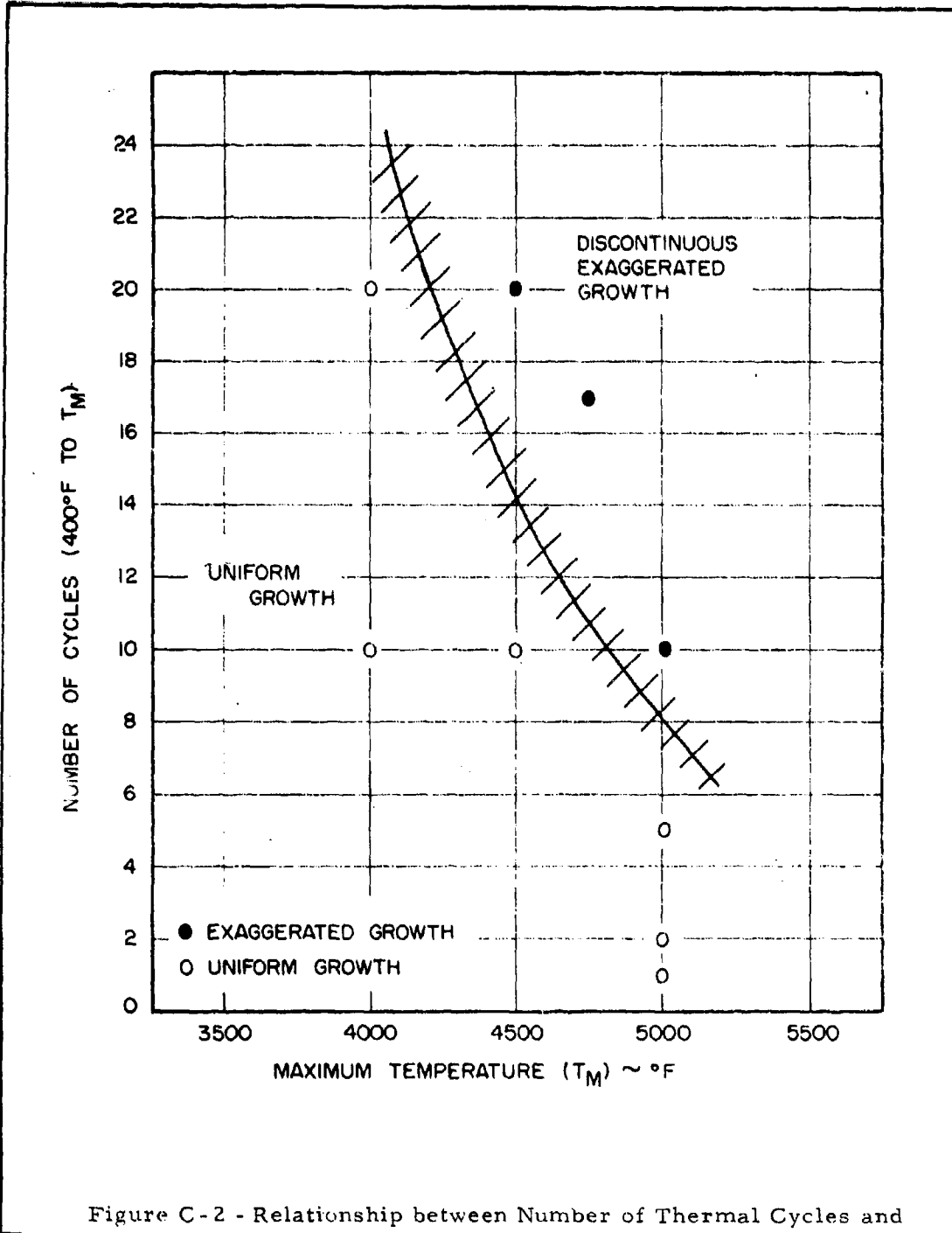


Figure C-2 - Relationship between Number of Thermal Cycles and Maximum Temperature Required to Produce Exaggerated Grain Growth in Unalloyed Tungsten Rod

**CONFIDENTIAL**

**CONFIDENTIAL**

AFRPL-TR-65-209, Vol I

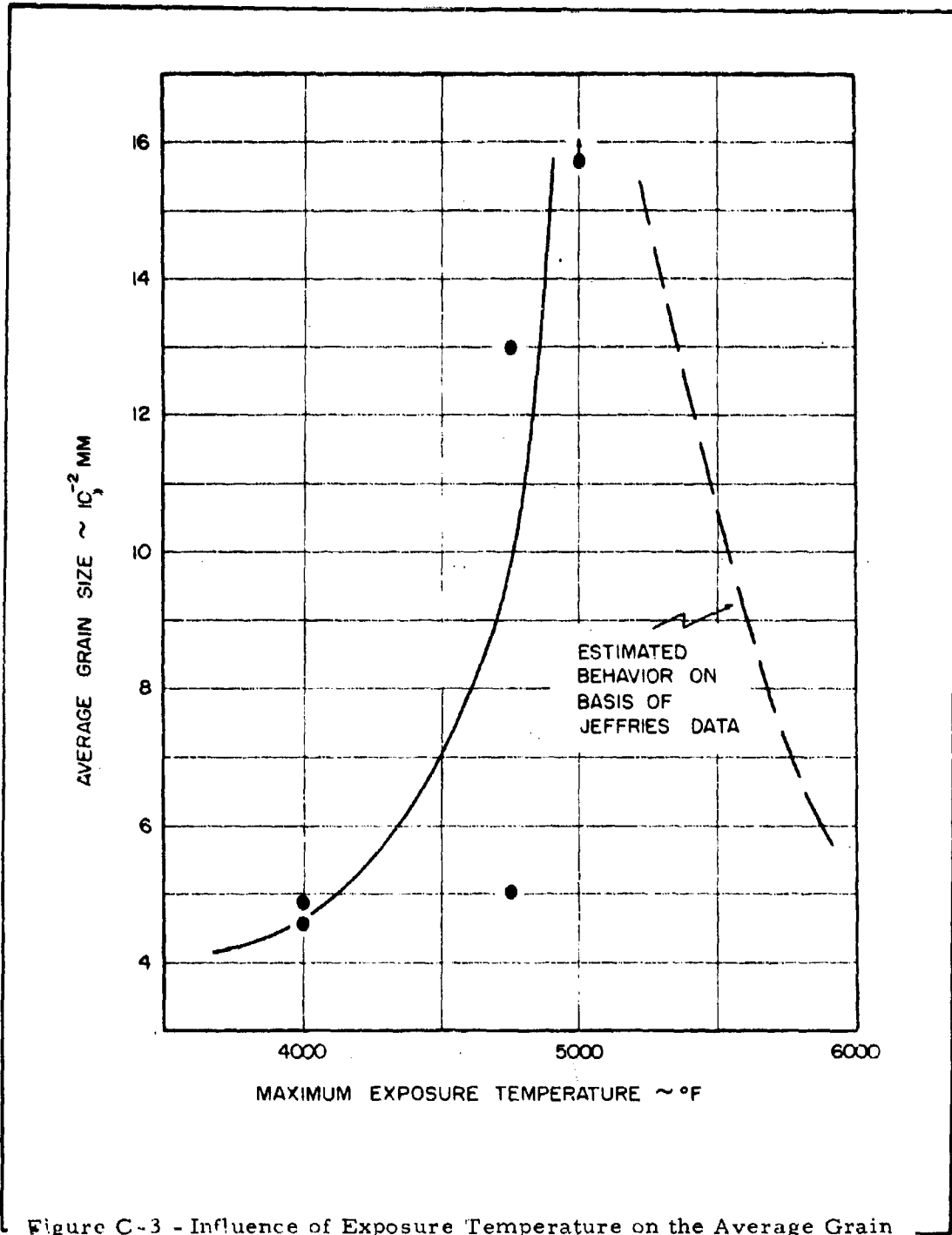


Figure C-3 - Influence of Exposure Temperature on the Average Grain Size Produced in Unalloyed Tungsten Subjected to Temperature Cycling (10 to 17 Cycles)

C-12

**CONFIDENTIAL**

TABLE C-V - EFFECT OF TIME, TEMPERATURE AND THERMAL CYCLING ON  
THE GRAIN SIZE OF 1/8-INCH TUNGSTEN - 1% THO<sub>2</sub>

Specimen	Temperature (°F)	Number of Cycles	Time Per Cycle (Sec)	Average Grain Length*	Average Grain Width
A1	5000	2	600	63.5	8.5
A2	5000	1	300	50.8	6.1
A3	5000	10	30	84.3	12.7
A4	5000	1	60	84.3	12.7
As-received	Surface	...	...	...	4.2
	Center	...	...	63.5	8.5

\* Due to high temperatures, grains coalesced sufficiently so lengths, as well as widths, could be measured.

In general, the tendency for discontinuous growth is a sensitive function of temperature gradients, degree of constraint, and impurity content. The mechanism presumably involves the production of a critical amount of plastic strain during the first thermal cycle. This strain results from thermal expansion and the presence of a suitable constraint on the material. Subsequent cycles in the 4500 to 5000° F range produce a few critical nuclei which grow very rapidly at the expense of the neighboring smaller grains. Jeffries has shown that exposure temperatures above approximately 5000° F may again produce a uniform grain size (similar to the dotted line in Figure C-3) because the nucleation rate increases so that many competing grains are formed.

(c) Bend Ductility Transition Temperature

The presence of very large grains as a result of thermal exposure for times and at temperatures comparable to the duty cycles in restartable nozzles raises the obvious question as to the effect of this microstructure on thermal shock susceptibility. Sheet bend specimens of unalloyed tungsten were exposed to thermal cycles which involve temperature differentials from 400 to 4500° F, and 400 to 5000° F. The resulting grain size was very large and somewhat heterogeneous. Rod bend specimens, 1/4 in. diameter of unalloyed tungsten and thoriated tungsten, were also thermally cycled to 5000° F. The bend ductility for the sheet specimens of unalloyed tungsten, shown in Figure C-4, indicate that the material after thermal cycling had a surprisingly low transition temperature (approximately 450 to 500° F), which was comparable to the materials which did not undergo the thermal exposure. The specimens exposed to 5000° F had a slightly higher transition temperature than the specimens treated to 4500° F. The results obtained for the thoriated tungsten rod bend specimens, shown in Figure C-5, indicate that the tungsten-1% ThO<sub>2</sub> alloy had a slightly lower transition temperature than the unalloyed tungsten.

---

\* Transition temperature is arbitrarily defined as minimum temperature at which specimens are capable of sustaining a 45° bend.

**CONFIDENTIAL**

AFRPL-TR-65-209, Vol I

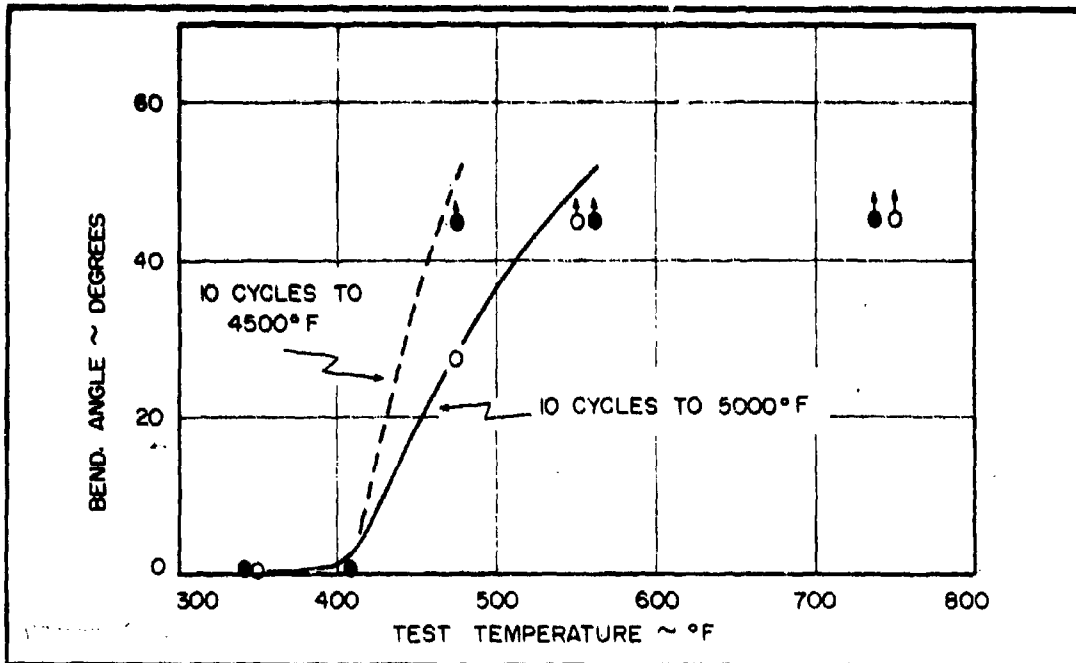


Figure C-4 - Bend Transition Temperatures for Sheet Specimens of Unalloyed Tungsten

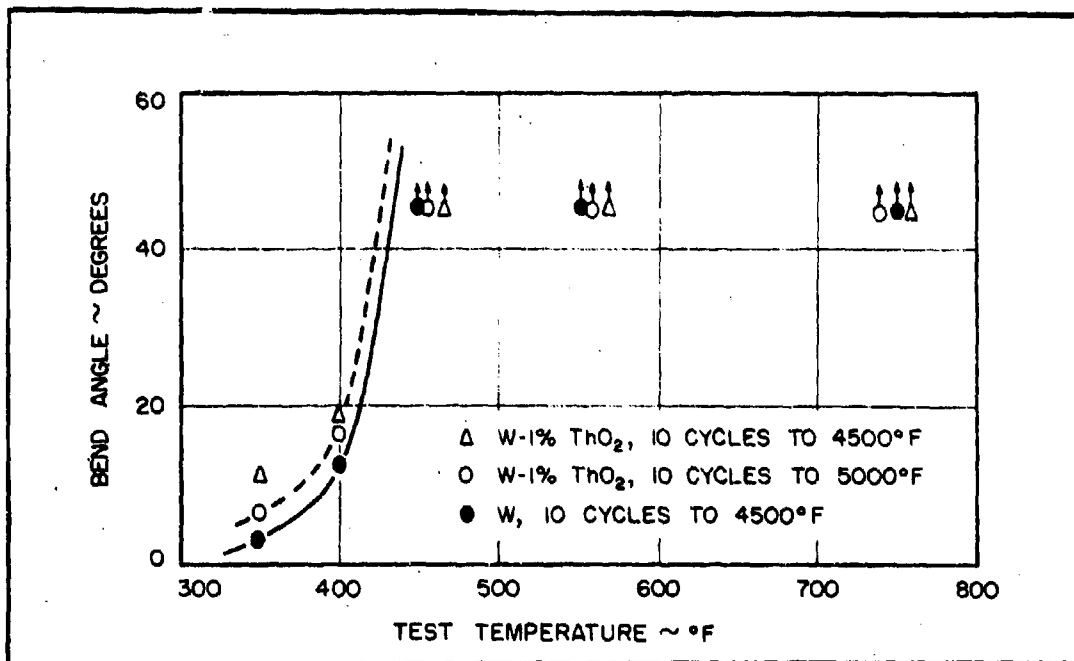


Figure C-5 - Bend Transition Temperatures for Rod Specimens of Unalloyed 1% Th O<sub>2</sub> Tungsten

**CONFIDENTIAL**

Previous firing experience has indicated that a bend ductility transition below 650° F was adequate to insure against thermal shock failure for the particular operating conditions and geometry of the first-stage Minuteman motor. Most current start-stop nozzles operate at conditions comparable to Minuteman and require even smaller throat diameters (less thermal shock susceptibility). On the basis of this background and the data presented in Figure C-4, the grain growth experienced under cyclic temperature exposure should not produce serious thermal shock problems in tungsten inserts for restartable nozzle structures.

(4) Conclusions

Tests were conducted to determine the susceptibility of tungsten, tungsten-1% thoria and pyrolytic graphite to low cycle, thermal fatigue. The results indicated that these materials did not sustain any crack initiation or significant dimensional change after exposures which involved up to 50 cycles at temperature differentials approaching 4600° F. Although the specimen size used in the thermal fatigue studies was relatively small by comparison to an actual nozzle insert, the combination of full restraint and a sharp notch introduced rather severe factors which tend to indicate that thermal fatigue would not be a problem in start-restart nozzles operating for comparable cycles.

Grain growth studies showed that cyclic exposure to temperatures in ranges between 4500 and 5000° F produced extremely large grains in unalloyed tungsten. Bend ductility transition tests indicated, however, that the extremely large grain sizes produced by this treatment did not significantly degrade the mechanical properties. The overall results were consistent with the conclusion that tungsten, tungsten-1% thoria, or pyrolytic graphite should be structurally reliable for use in current start-stop nozzle sizes. This conclusion must be tempered with the realization that large grain sizes can be a factor contributing to brittleness. Additional effort is required to further determine the microstructural factors which control the transition behavior in tungsten.

b. Heat Transfer

To establish limits for the operating requirements of the nozzle, steady-state analyses were made at the two extreme conditions. One limit, 80 lb/sec mass flow for 6 seconds, results in maximum surface temperature and very steep temperature gradients. The other limit, 4 lb/sec mass flow for 120 seconds, results in deeper heat penetration and lesser gradients. The data obtained from analyses of each major section of the nozzle were used to compute the thermal stresses existing in the component sections.

Transient analyses allowing for cyclic operation of pulses were made next to obtain the effects of heat soakback on insulation requirements. Since the greatest total heat input occurs for long-duration, low-mass-flow operation, a duty cycle was chosen which consists of 12 10.5-second pulses at 4 lb/sec flow rate, each followed by a cooldown of 10 minutes. The cooldown time was selected to provide restarting at the time instant when the supporting steel reached a maximum value due to heat soakback. While it is recognized that in actual operation the pulse and cooldown times will vary arbitrarily, this selected condition simulates the most severe heat soak within the operating envelope. Using as a baseline a maximum value of 200° F for the shell temperature, the analysis showed that a silica phenolic thickness of 2 inches is required at the throat.

A similar analysis was made to determine the expected temperature at the forward end of the nozzle. Based on preliminary selection of graphite as the hot-side material, the shell would reach 300° F under the influence of the selected duty cycle. This was deemed borderline, but acceptable. A change in material from graphite to carbon-cloth phenolic at this location was made as a result of preliminary stress calculations, and the difference in thermal diffusivity between these materials ( $2 \times 10^{-2}$  for graphite versus  $6 \times 10^{-4}$  for carbon-cloth phenolic) will provide considerable reduction in the expected temperature. Approximate calculations indicate maximum expected temperature at this location of 120° F.

The design criteria selected for the nozzle were very conservative for the first of the heavyweight test nozzles. Both the analytical methods and the boundary conditions selected were chosen to provide maximum thermal protection.

### 3. DESIGN

This nozzle, shown in Figure C-6, is designed as a test vehicle to obtain the maximum amount of data for design of a flightweight stop-start nozzle. The nozzle inlet is made of carbon cloth, which was selected for its erosion resistance and insulative properties. Fiber orientation is perpendicular to the nozzle centerline for minimum erosion considerations.

CGW monolithic graphite was selected for the nozzle throat because of its erosion resistance properties. Graphite is used to establish a base line and to determine the erosive properties of the motor. Tungsten and pyrolytic graphite throats will be evaluated in future firings.

RUD graphite is used in the nozzle exit for erosion control.

Silica is used for insulation in this nozzle, primarily for its char strength.

TX fiber is used as an insulator in the nozzle exit. Laboratory tests have shown this material to be a superior insulator. This test will evaluate its performance in a nozzle firing.

The nozzle support shell is 1020 steel.

Using graphite in this nozzle results in nozzle split line problems. To overcome this, Belleville springs are provided to accommodate graphite expansions and to close the resulting gaps that will occur during cooldown. These gaps would remain upon reignition if the Belleville springs were not used.

Initially, the springs are preloaded to provide a 38,000-pound load. They then are compressed further to accommodate expansion of the graphite. During cooldown, as gaps occur due to contraction of the graphite, the force provided by the compressed washers is sufficient to "close" the assembly and eliminate the gaps.

A detailed stress analysis was conducted for the nozzle (but not included here), which indicated that the design is conservative, and an adequate margin of safety exists.

**CONFIDENTIAL**

AFRPL-TR-65-209, Vol I

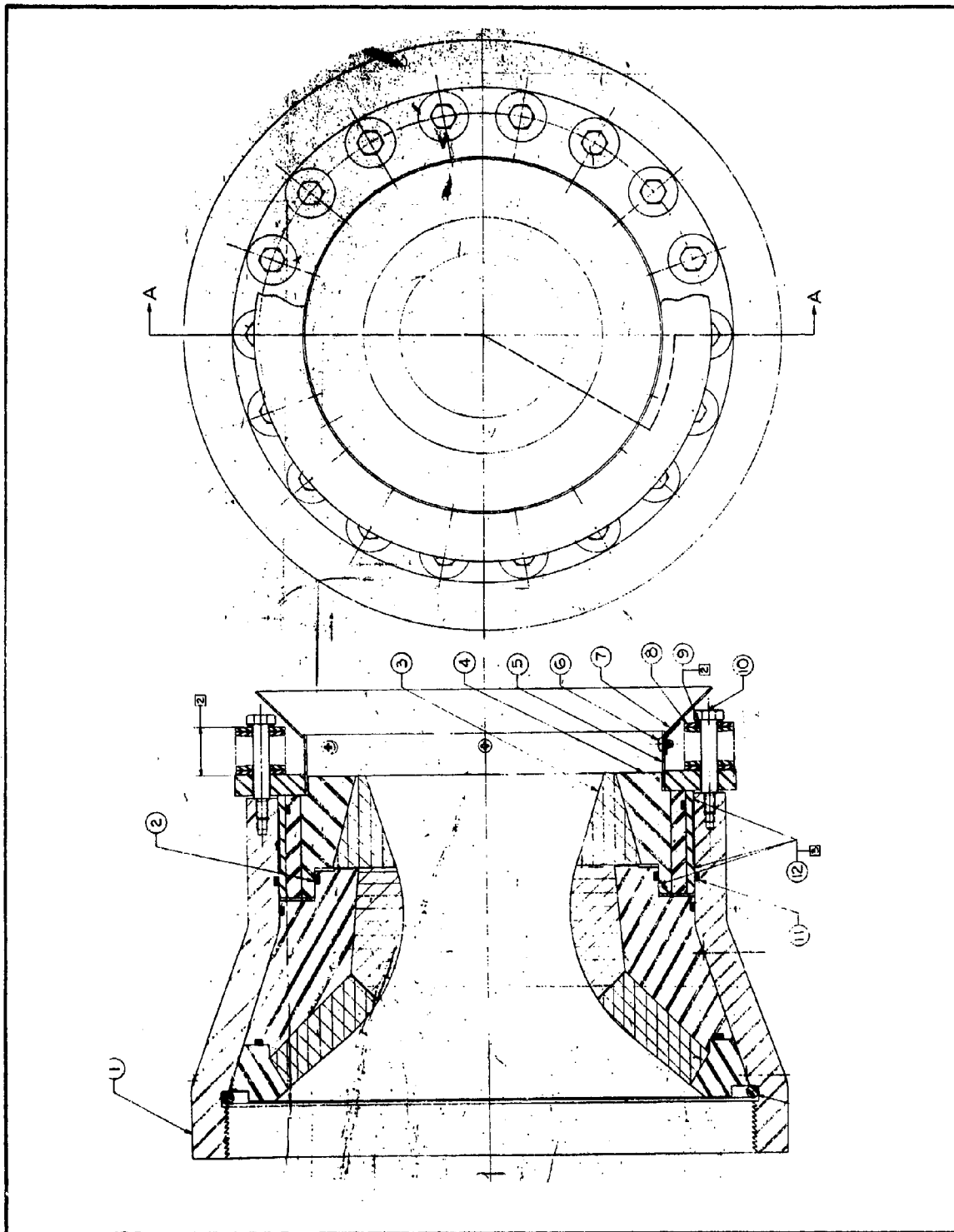


Figure C-6 - Design for Nozzle No. 1 (2-to-1 Expansion)

**CONFIDENTIAL**

4. FABRICATION

This nozzle incorporates components which require standard plastic molding and machining practices. The silica components will be match-metal die moldings. T-X fiber will be tape wrapped. The carbon phenolic component will be machined from a billet molded from a 12- by 12- by 3-in. high stack of plys in a hydroclave.

APPENDIX D - DESIGN ANALYSIS FOR NOZZLES NO. 2 AND 3  
(20-TO-1 EXPANSION)

1. INTRODUCTION

This appendix presents the design analysis data for the second and third stop-start test nozzles. These nozzles feature a 20:1 expansion ratio exit cone and will be fired in an altitude facility. Heat transfer, materials evaluation, and design are discussed herein.

The design criteria for these two nozzles was the same as the first nozzle (Appendix C), except for the addition of a 20:1 expansion cone. In order to increase the reliability of this nozzle, the monolithic graphite in the exit cone was replaced with carbon cloth. This minimizes the expansion forces in the nozzle and eliminates the requirement of the Belleville washers. A "slip joint" is provided to accommodate the expansion of the throat graphite and minimize flow to the silica.

2. ANALYSES

a. Materials Evaluation

Results of the materials evaluation program were presented in Appendix C. The materials selected for the second and third nozzles were based on those used in the first nozzle. The one exception is using carbon cloth in the throat extension rather than the monolithic graphite used in the first nozzle. Carbon cloth has a higher erosion rate than graphite; however, it is less prone to cracking and does not produce the expansion loads that exist with monolithic graphite.

b. Heat Transfer

(1) Theoretical Analysis

To establish limits for the operating requirement of the nozzle, steady-state analyses were made at the two extreme conditions. One limit, 80 lb/sec mass flow for 6 seconds, results in maximum surface temperature and very steep temperature gradients. The other limit, 4 lb/sec mass flow for 120 seconds, results in deeper heat

penetration and lesser gradients. The data obtained from these analyses were used to compute the thermal stresses existing in the component sections.

Downstream of the throat, at an area ratio of 2.3, the nozzle wall consists of 0.750 in. of carbon cloth, 1.12 in. of silica phenolic, and 0.32 in. of steel. In order to determine the maximum steel temperature, a duty cycle of a ten-second heat pulse, followed by a 10-minute cooldown, was imposed. The heating occurred at the lowest mass flow rate, since this leads to the worst conditions. The maximum steel temperature is about 220°F, extrapolated to the end of the twelfth cooldown. Similarly, the extrapolated char depth is about 0.2 inches. The actual calculations were carried out for only four cycles in order to conserve computer time. At this time, the slopes of the curves are fairly constant, allowing for a valid extrapolation.

At an area ratio of 5.0, the nozzle is composed of 1.0 in. of silica phenolic, 0.25 in. of steel, and 0.1 in. of glass overwrap. At the end of 12 duty cycles, the outer surface temperature reaches a maximum value of about 325°F, and the char depth is about 0.1 inches. Although these numbers represent extrapolated values from the end of the sixth cycle, they would be expected to be valid.

## (2) Experimental Analysis

A laboratory test was conducted to investigate the requirement for exit cone section thickness in a pulse firing operation. A section from a previously tested exit cone was used with an oxy-acetylene torch and plasma jet as heat sources. The heat flux provided by both sources was greater than would be experienced by the exit cone in actual firing.

In a pulse operation, the mass mean-temperature of an exit cone section is considerably greater than in a continuous single-pulse firing of equivalent duration. This fact was demonstrated in the laboratory test. There seem to be two factors which influence the increase in exit cone temperature in a pulse operation: (1) the heat

soakback, in effect, can initiate each succeeding pulse with an effectively increased ambient condition, depending on pulse timing; and (2) the total heat absorbed and stored can be significantly increased by virtue of the increased temperature difference between gas stream and liner wall surface temperature, when averaged over the total duty cycle.

(3) Comparison of Theoretical and Experimental Results

In the theoretical analysis for the heat pulse cycle, the silica thickness used was about one inch, and the backside temperature was approximately 325°F after 12 cycles. The silica thickness used for the experimental tests was 3/4 in. After 12 cycles with the plasma jet, the extrapolated backside temperature shown is 260°F. Also, the heating cycle used in the experimental test was comparatively more severe than that used for the theoretical case. Therefore, it is concluded that the theoretical analysis is quite conservative.

Based upon the theoretical heat transfer analysis and the experimental results, an exit cone thickness of one inch was used in the design. This thickness should provide an adequate margin of safety.

3. DESIGN

This nozzle, shown in Figure D-1, is designed as a test vehicle to obtain the maximum amount of data for design of a lightweight stop-start nozzle. The design was directed to be similar to the first nozzle, except for the addition of a 20:1 expansion cone for firing in an altitude facility.

The nozzle inlet is carbon cloth. This material was selected for its erosion resistance and insulative properties. Fiber orientation is perpendicular to the centerline for minimum erosion.

CGW monolithic graphite was selected for the nozzle throat because of its erosion resistant properties. Graphite is used to establish a base line and to determine the erosive properties of the motor.

**CONFIDENTIAL**

AFRPL-TR-65-209, Vol I

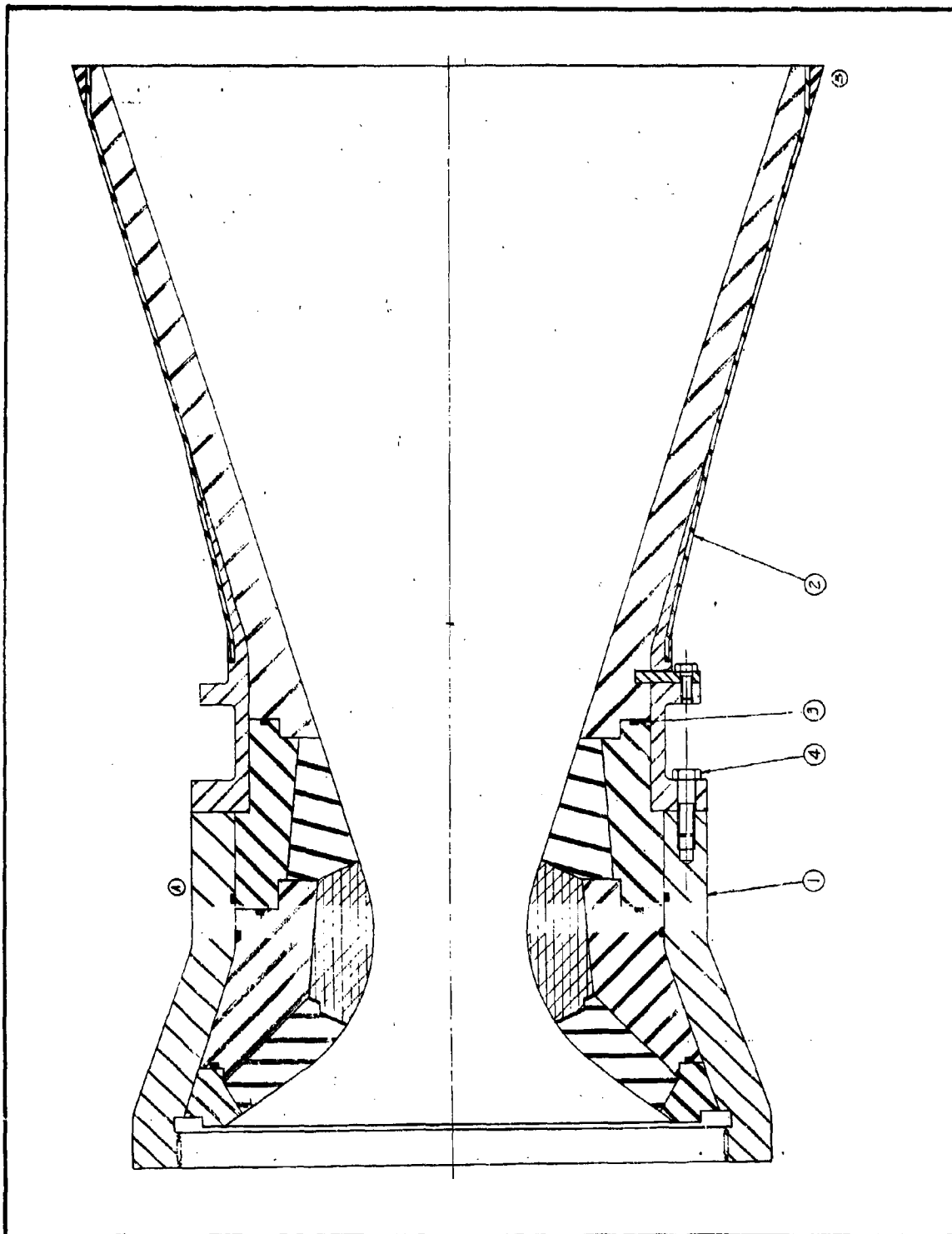


Figure D-1 - Design for Nozzles No. 2 and 3 (20-to-1 Expansion)

D-4

**CONFIDENTIAL**

The exit cone extension is carbon cloth. In order to increase the reliability of this nozzle, the monolithic graphite used in this area was replaced with carbon cloth. This minimizes the internal expansion forces in the nozzle and eliminates the requirement of Belleville springs to accommodate expansion. A slip joint is provided to accommodate expansion of the throat graphite and minimize direct flow to the silica.

Silica is used for insulation in this nozzle, primarily for its char strength.

The exit cone is silica. This material is chosen because of its satisfactory performance in this area of the nozzle. A glass overwrap is provided to carry the structural loads in the exit cone.

The support structure is made of 1020 steel for cost considerations. On a lightweight unit, a better grade steel would be used to minimize weight.

A "slip seal" is provided for the CGW graphite to grow axially. The diametral fit with the carbon cloth will prevent flow in the split line from reacting with the silica.

Retention of the silica exit cone is achieved primarily by the molded resin interface between the silica cone and the steel. A redundant tab retention arrangement is added to provide retention if the "bond line" temperature is excessive.

A detailed stress analysis was conducted for the nozzle (but not included here), which showed that the design is conservative, providing an adequate margin of safety.

#### 4. FABRICATION

This nozzle incorporates components which require standard plastic molding and machining practices. The silica insulation and carbon cloth components will be molded in a match metal die. Diced material will be used for the silica insulation and 120° segments will be used for the carbon cloth.

The exit cone will be a convolay layup. A pattern is developed and approximately 215 "plys" cut from this pattern will be "laid up" longitudinally on a male mandrel at a helix angle of 35° at the small

end of the cone. The component will then be hydroclave-cured at 1000 psi and 300<sup>o</sup>F. The O. D. of the cured cone will be machined and the steel ring bonded to it. A glass overwrap consisting of 120<sup>o</sup> "gore" segments will be "laid up" by hand over the silica cone and steel ring.

The overwrap will then be cured at 200 psi and 300<sup>o</sup>F in an autoclave. The component will then be finish-machined and bolted to the throat assembly.